

The Interplay of Structure and Reactivity in Ruthenium-catalysed Alkene Ring-closing Metathesis

David James Nelson

Department of Pure and Applied Chemistry

University of Strathclyde

Submitted in part fulfilment of the requirements
of the degree of **Doctor of Philosophy**

October 2012

Academic Supervisor: **Prof. Jonathan M. Percy** (Pure & Applied Chemistry)

Industrial Supervisor: **Dr. Ian W. Ashworth** (AstraZeneca)

Internal Examiner: **Prof. John A. Murphy** (Pure & Applied Chemistry)

External Examiner: **Prof. Guy C. Lloyd-Jones** (University of Bristol)

This thesis is the result of the author's original research. It has been composed by the author and has not been previously submitted for examination which has led to the award of a degree.

The copyright of this thesis belongs to the author under the terms of the United Kingdom Copyright Acts as qualified by University of Strathclyde Regulation 3.50. Due acknowledgement must always be made of the use of any material contained in, or derived from, this thesis.

Signed:

Date:

*“What you do in this world is a matter of no consequence,”
returned my companion, bitterly. “The question is, what can
you make people believe that you have done.”*

Sir Arthur Ignatius Conan Doyle

A Study in Scarlet

Acknowledgements

My thanks go first and foremost to Professor Jonathan Percy for his help and support during my PhD and, in particular, for teaching me to think carefully and critically about data and for providing a clean, safe and well-equipped laboratory in which to carry out research.

I am also indebted to Dr. Ian Ashworth (AstraZeneca, Macclesfield) for his help and advice throughout the project, and for providing a fresh look at results and data at numerous points.

I have had the pleasure of working within a friendly research group. Thanks go to all members of the Percy group past and present. In particular, thanks are due to Dr. Giuseppe Rinaudo, Dr. Davide Carboni and Dr. Sara Kyne, all of whom I have worked particularly closely with.

The work in this thesis was informed and supported by density functional theory calculations at a number of stages. In reactions where many processes are difficult or even impossible to observe, insight from computational work is invaluable. Professor Ian Hillier and Dr. Mark Vincent of the University of Manchester are thanked for providing their skills and computational firepower.

Much of this work, particularly with techniques such as NMR spectroscopy, mass spectrometry and Karl-Fischer titrimetry, would not have been possible without the aid of specialists and technical staff. Craig Irving and Dr. John Parkinson are thanked for their assistance with the NMR spectroscopy facilities, of which I have made considerable use. Pat Keating and Denise Gilmour are thanked for their assistance with mass spectrometry and UV/visible spectroscopy facilities, and Gavin Bain is thanked for his assistance with Karl-Fischer titrimetry. Dr. Alan Kennedy is thanked for X-ray crystallographic analysis. Bridget Stein and her team at the EPSRC national mass spectrometry service centre (NMSSC) are thanked for their assistance in acquiring GC-MS data with chemical ionisation at a time when we did not have the capability at Strathclyde.

Last and certainly not least, thanks are due to friends and family and especially Allyson for putting up with me during the past few years. In particular, she has endured my atypical definition of ‘five minutes’ remarkably well.

Abbreviations

ADMET	Acyclic diene metathesis
BHT	2,6-bis(1,1-dimethylethyl)-4-methylphenol
Bn	Benzyl (PhCH ₂)
BOC	<i>tert</i> -Butyloxycarbonyl
Brs	Brosyl (<i>p</i> -BrC ₆ H ₄ SO ₂)
Bz	Benzoyl (PhC(O))
CM	Cross metathesis
COSY	Correlation spectroscopy
DCM	Dichloromethane
DFT	Density functional theory
DMC	Dimethyl carbonate
EM	Effective molarity
EM _T	Thermodynamic effective molarity
ESI	Electrospray ionisation
FID	Flame ionisation detection
HCV	Hepatitis C virus
HSQC	Heteronuclear quantum correlation
IMes	bis(2,4,6-trimethylphenyl)imidazolium
IPr	bis(2,6-di- <i>iso</i> -propylphenyl)imidazolium
IR	Infra-red
IRC	Intrinsic Reaction Co-ordinate
MCB	Metallocyclobutane
MEM _T	Modified thermodynamic effective molarity

MS	Mass spectroscopy
MTBE	Methyl <i>tert</i> -butyl ether
NHC	<i>N</i> -heterocyclic carbene
NMR	Nuclear magnetic resonance
PES	Potential energy surface
PNB	<i>para</i> -nitrobenzyl (<i>p</i> -NO ₂ C ₆ H ₄ CH ₂)
RCM	Ring-closing metathesis
RRCM	Relay ring-closing metathesis
ROMP	Ring-opening metathesis polymerisation
SIMes	bis(2,4,6-trimethylphenyl)imidazolium
SIPr	bis(2,6-di- <i>iso</i> -propylphenyl)imidazolium
TEMPO	(2,2,6,6-Tetramethyl-piperidin-1-yl)oxyl
TES	Triethylsilyl
Tf	Triflate (F ₃ CSO ₂)
THF	Tetrahydrofuran
TON	Turnover number
UV	Ultraviolet

Abstract

Alkene ring-closing metathesis (RCM) has fundamentally changed the way that chemists consider the construction of molecules. However, quantitative understanding has not progressed at the same rate as synthetic application. There is still not a firm quantitative understanding of the relationship between pre-catalyst and diene structure and reaction rate or efficiency; measurements reported are typically yield measurements, which are sensitive to the work-up and isolation methods employed.

Work towards a detailed quantitative understanding of the interplay between structure and reactivity is presented. A variety of classical and modern physical organic chemistry tools such as spectroscopy, kinetic studies, density functional theory, and reaction simulation are employed.

Kinetic studies were applied to investigate the effect of ring size on RCM rate. The order of reactivity in prototypical dienes, in reactions shown to be under thermodynamic control, was established qualitatively and some quantification of this order of reactivity is presented. Attempts to quantify kinetic EMs were unsuccessful. Additionally, 1,5-hexadiene was revealed to be a metathesis inhibitor.

Reaction simulation approaches were explored for the quantification of outcomes from kinetic experiments and for comparison of substrates. An existing model for RCM was tested and several flaws were identified; overcoming these flaws allowed successful application of the model to substrate and pre-catalyst evaluation.

Significant substrate isomerisation encountered in small-scale reactions was probed using kinetic experiments under a number of reaction conditions. Benzoquinone suppressed this isomerisation but reduced the rate of productive RCM. A number of potential isomerisation agents were prepared and benchmarked, and one was detected in very small quantities in a metathesis reaction.

This work contributes to better quantitative understanding of RCM. In addition, the small-scale metathesis and reaction simulation approaches are excellent means by which to rapidly identify suitable reaction conditions for metathesis reactions.

Contents

Acknowledgements.....	iv
Abbreviations.....	v
Abstract.....	vii
1 Introduction.....	1
The Alkene Metathesis Reaction.....	1
The Need for Quantification in Alkene Metathesis	3
Important Processes in Alkene Metathesis Reactions.....	4
Pre-Catalyst Initiation.....	5
Alkylidene Transfer.....	13
Catalyst Decomposition.....	21
Non-productive Events in Metathesis	29
Substrate Structure and Reactivity.....	32
Functional Group Tolerance.....	32
Target Ring Size.....	32
Substitution Pattern of the Alkene Termini.....	60
Research Aims.....	69
2 Kinetic Studies of Ring-closing Metathesis Reactions	71
The Kinetics of Ring-closing Metathesis	71
Literature Studies of Ring-closing Metathesis Kinetics	71
New Studies of Ring-closing Metathesis Reactions	76
The Effects of Ring Size	77
Research Aims	77
Robust Kinetic Studies of Prototypical Substrates	79
Selecting a Model System.....	79
Requirements for a Kinetic Method.....	80
Selecting an Analytical Technique	81
Ensuring Robust Methodology.....	82
Results from Kinetic Studies.....	88

Ring Size and Reaction Rate.....	88
Quantifying Relative Rates.....	92
Comparison with the Ring-closing Literature.....	96
Comparison with a Literature Prototypical System.....	109
Diethyl Malonate Systems.....	109
Quantifying Kinetic Effective Molarities.....	119
The Utility of the Effective Molarity.....	119
1,5-Hexadiene Cross-Metathesis as a Model Intermolecular Reaction.....	120
1-Octene Metathesis as a Model Intermolecular Reaction.....	129
Evidence for Thermodynamic Control.....	132
Kinetic <i>versus</i> Thermodynamic Control in the Literature.....	132
Kinetic <i>versus</i> Thermodynamic Control in the Ring-closing Metathesis of Simple Prototypical α,ω -dienes.....	132
Perturbing the Reaction Equilibria.....	134
Approaching Reaction Equilibria.....	143
Conclusions.....	148
3 A Reaction Simulation Approach to Ring-closing Metathesis Kinetics.....	150
Reaction Simulation Approaches.....	150
Deconvolution of Complex Kinetic Behaviour.....	150
Reaction Simulation Approaches for Metathesis.....	150
A Study of the Adjiman Model for Ring-closing Metathesis Kinetics.....	154
Appraising the Published Model and Outcomes.....	154
Constraining the Model.....	164
Applications of the Modified Adjiman Model.....	177
Substrate Evaluation.....	177
Pre-catalyst Evaluation.....	183
Solvent Effects.....	224
Conclusions.....	233
4 Investigating Isomerisation Processes in Metathesis Reactions.....	235

Ruthenium-Catalysed Isomerisation Processes	235
Isomerisation Reactions as Deleterious Processes	235
Isomerisation Mechanisms	238
Isomerisation Under Mild Conditions	248
Research Aims	249
Benchmarking Isomerisation Agents.....	250
Kinetic Studies on Isomerisation.....	250
Monitoring the Rate of 1,8-Nonadiene Isomerisation	250
Hydridocarbonyl Complexes.....	253
Diruthenium Hydride Complex.....	258
Conclusions from Benchmarking Studies	262
‘On-pathway’ <i>versus</i> ‘Off-pathway’ Isomerisation	264
Kinetic Studies of Isomerisation in Metathesis Reactions	264
Exploring the Effects of Solvent.....	264
Exploring the Effects of Pre-catalyst.....	268
Isomerisation in ROMP <i>versus</i> RCM	277
Comparing Experimental Results with Density Functional Theory Calculations	288
Benzoquinone as an Isomerisation Suppressant.....	292
Suppressants for Isomerisation in Metathesis Reactions	292
Benzoquinone Applied to Simple Diene Metathesis	296
Probing the Mechanism of Action of Benzoquinone.....	300
Conclusions	310
5 Conclusions.....	313
Conclusions from Studies of Alkene Ring-closing Metathesis Reactions.....	313
Future Directions for Quantitative Studies.....	317
Experimental.....	320
Equipment.....	320
Materials	320
Preparations of Ruthenium Complexes	322
Ruthenium Alkylidene Complexes	322

Ruthenium Hydride Complexes.....	322
Typical Procedures	325
Metathesis Kinetics by ¹ H NMR Spectroscopy.....	325
Initiation Kinetics by UV/Visible Spectroscopy.....	326
Peer-Reviewed Publications.....	327
Chemical Physics Letters 2009	327
Tetrahedron 2009	327
Chemical Communications 2010.....	327
Chemical Communications 2011.....	327
The Journal of Organic Chemistry 2011	328
Chemistry – A European Journal 2011	328
European Journal of Organic Chemistry 2012.....	328
References	329

Chapter 1:

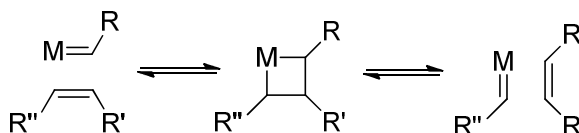
Introduction

The Alkene Metathesis Reaction

During the past two decades, the alkene metathesis reaction has developed from its early applications in large-scale processes with heterogeneous and ill-defined catalyst systems,¹ to a standard technique in synthetic chemistry and polymer laboratories.² The development of well-defined and often bench-stable pre-catalysts³ has been key to the widespread use of alkene metathesis in modern target synthesis projects. The impact of this useful reaction was recognised in 2005 by the award of the Nobel Prize in chemistry to Yves Chauvin, Robert Grubbs and Richard Schrock.⁴⁻⁶

In its simplest form, alkene metathesis is the transfer of groups between alkenes and metal carbenes, which proceeds *via* the formation of metallocyclobutane (MCB) species by [2+2]cycloaddition, followed by retro-[2+2]cycloaddition to yield different species (**Scheme 1.01**). Through this sequence of steps, new alkene and alkylidene species can be formed. Several types of metathesis reaction have been employed in various branches of chemistry; the most common reactions are cross-metathesis (CM), ring-closing metathesis (RCM) (in target synthesis), ring-opening metathesis polymerisation (ROMP) and acyclic diene metathesis (ADMET) (in polymer chemistry), although other variations and combinations of these processes are known (**Figure 1.01**).

Various metal carbene complexes are known to catalyse this reaction, including those based on metals such as rhenium, molybdenum, tungsten, tantalum, titanium and ruthenium.⁷ Well-defined and very active molybdenum catalysts such as **Mo1** and **Mo2** are known, but require careful handling in a glove-box; they are often intolerant of common functional groups in organic chemistry. Recently, Hoveyda *et al.* prepared well-



Scheme 1.01

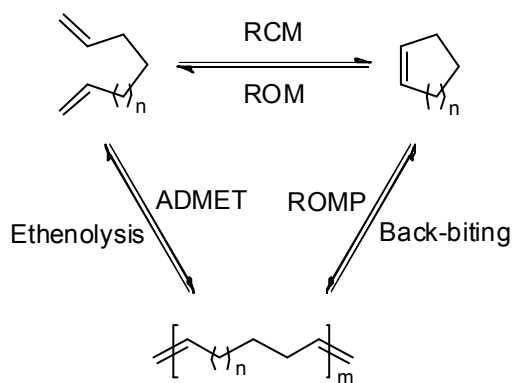
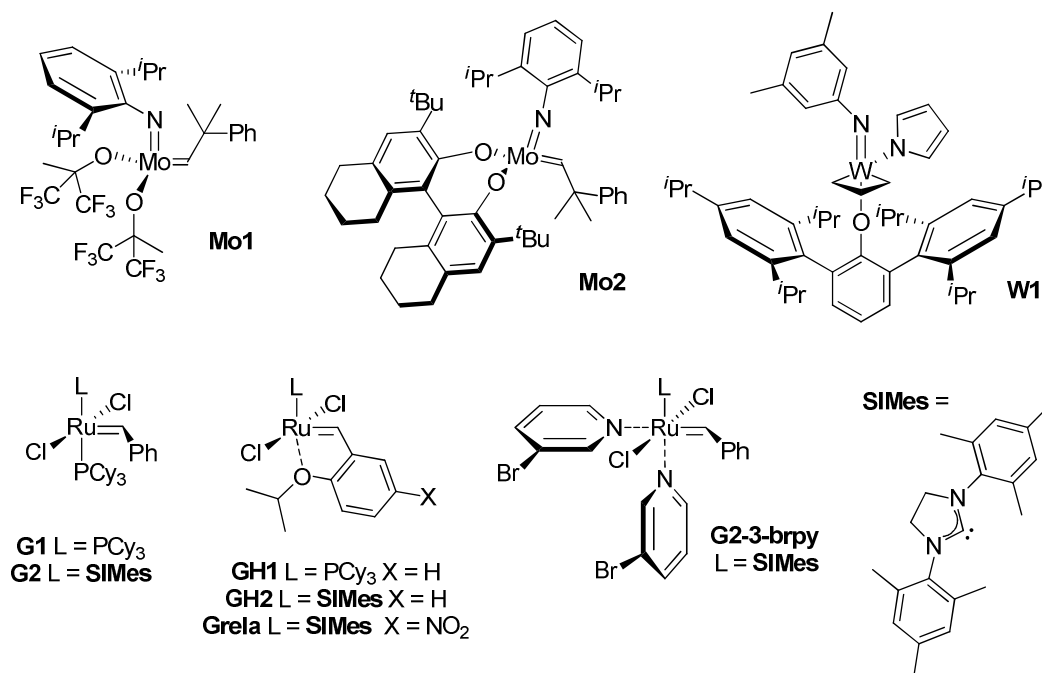


Figure 1.01. Common metathesis processes for α,ω -dienes and related compounds: ring-closing metathesis (RCM), ring-opening metathesis (ROM), acyclic diene metathesis (ADMET), ethenolysis, ring-opening metathesis polymerisation (ROMP) and oligomer back-biting.

defined and air-stable tungsten metallocyclic pre-catalyst **W1**,⁸ but this catalyst is not (at the time of writing) commercially available. The largest class of well-defined metathesis pre-catalysts feature a ruthenium centre, which typically bears phosphane and/or *N*-heterocyclic carbene (NHC) ligands. The two most common types of ruthenium-based metathesis pre-catalyst are phosphane-bound ‘Grubbs-type’ species such as **G1**⁹ and **G2**¹⁰ and chelated alkoxyarene ‘Hoveyda-type’ species such as **GH1**,¹¹⁻¹² **GH2**¹¹⁻¹² and **Grela**.¹³ Pyridine-ligated pre-catalysts such as **G2-3BrPy** have also been reported;¹⁴ while dinuclear metathesis catalysts and catalysts bearing other ligands are known, they are beyond the scope of this thesis. As a result of their activity, stability, relatively low cost, and ease of handling, the most commonly used pre-catalysts in target synthesis,



where very diverse functional groups are often involved, are **G2** and **GH2**. This thesis focuses exclusively on reactions catalysed by ruthenium, so systems based upon other metals are discussed here only very briefly.

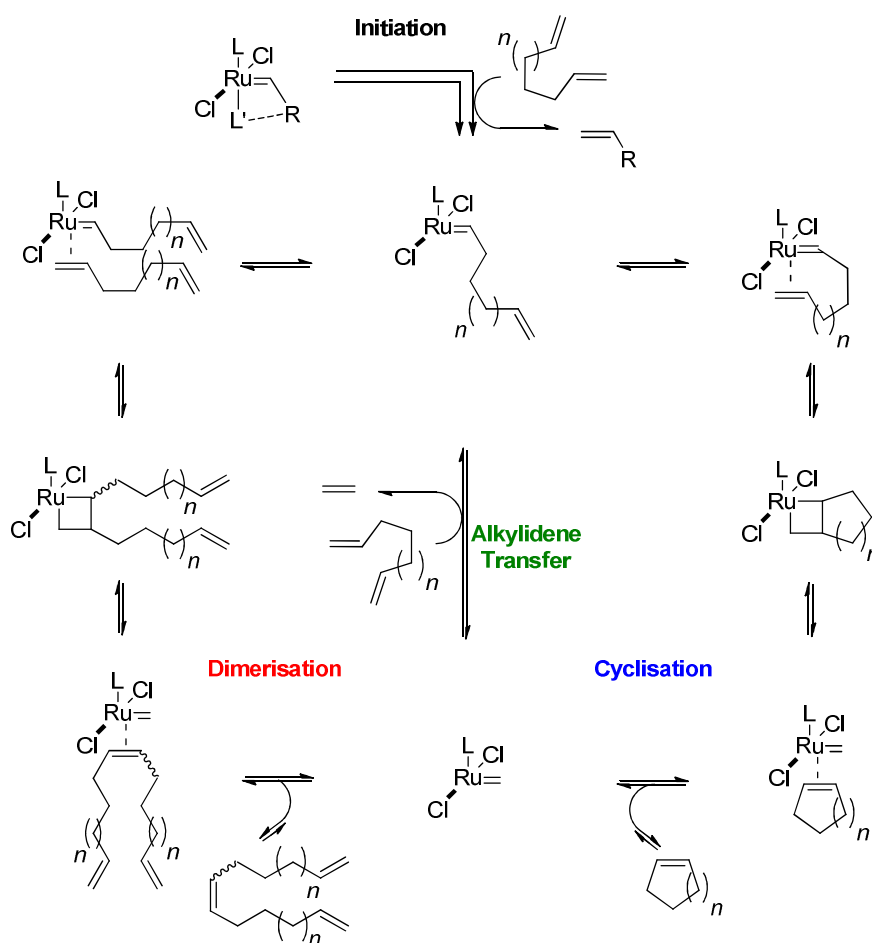
The Need for Quantification in Alkene Metathesis

The widespread use of the metathesis reaction has allowed many details to be elucidated about the effect of structure on reactivity. The majority of publications regarding alkene metathesis are derived from the synthetic chemistry literature and rely predominantly on yield measurements. Others typically detail the preparation of new metathesis pre-catalysts, usually with the aid of (purely qualitative) kinetic profiles. However, there are very few truly quantitative studies of alkene metathesis. Quantification is an important part of reaction optimisation, particularly when scaling up reactions for large scale synthesis.

A detailed understanding of the factors influencing ring-closing metathesis rate requires understanding of the key events that occur in metathesis reactions; of particular importance are processes associated with the initiation and decomposition of metathesis (pre-)catalysts. It is therefore interesting to survey the literature and understand how substrate structure is known to influence reactivity, before exploring useful metrics for cyclisation rate and efficiency (which can be used to select reaction conditions) and how they may be applied to the study of ring-closing metathesis.

Important Processes in Alkene Metathesis Reactions

An understanding of the processes involving ruthenium species that occur during metathesis reactions is of fundamental importance, and key to deconvolution of kinetic data from reactions. These processes include pre-catalyst initiation, alkylidene transfer, dimerisation and cyclisation (**Scheme 1.02**). This series of [2+2]cycloadditions and retro[2+2]cycloadditions proposed by Chauvin is the accepted mechanism for alkene metathesis.⁴ It successfully describes all forms of metathesis, although investigations into more detailed mechanistic aspects of metathesis chemistry continue, often driven by the ever-improving capabilities of multi-dimensional high field NMR spectroscopy¹⁵ and electrospray mass spectrometry (ESI-MS) techniques.¹⁶ It is of interest to consider the key steps in metathesis in order to understand, for example, where substrate structure may exert an influence on metathesis rate and efficiency. Key mechanistic details of alkene metathesis continue to be discussed, as current and future pre-catalyst



Scheme 1.02

development relies on understanding how the pre-catalyst enters the catalytic cycle and which structural features affect the activity of a ruthenium catalyst (discussed briefly below). However, from a synthetic chemistry point of view, important issues include: how diene substrates partition between cycloalkene and oligomer; how substrate structure affects RCM rate and efficiency; understanding the non-productive or deleterious side reactions that occur in metathesis; and how the catalytic species decompose, limiting their availability.

Pre-Catalyst Initiation

For a general mononuclear five-coordinate pre-catalyst bearing two (pseudo)-halide ligands, a non-dissociating ligand and a dissociating ligand, the overall reaction rate is determined by the activity of the species that performs catalytic turnovers (i.e. the rate of metathesis turnovers), how quickly this species is generated (i.e. the rate of pre-catalyst initiation), and how quickly this species decomposes (**Figure 1.02**). In the metathesis of α,ω -dienes, the catalytic species is predominantly a methyldiene ($\text{Ru}=\text{CH}_2$) complex. The dissociating ligand **L'** and alkylidene **R** determine the stability of the pre-catalyst and how fast the catalytic species enters and leaves the cycle; pre-catalysts that differ only in **L'** and/or **R** will converge upon the same intermediate after one turnover.¹⁴ Ligand **X** is most often a halide, and is typically chloride. Fogg *et al.* have pioneered the preparation of a class of pre-catalysts where the halide ligands are replaced with alkoxide or aryloxy ligands,¹⁷ which allows further fine-tuning of the pre-catalyst structure (and therefore, of its activity).¹⁸ Dissociating ligand **L'** is most often a phosphane¹⁰ or ether functional group,¹¹ but examples are known where this is a

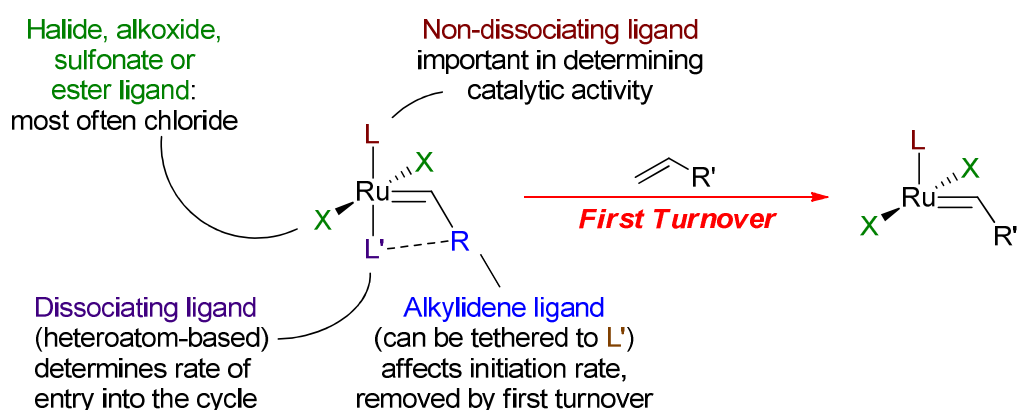
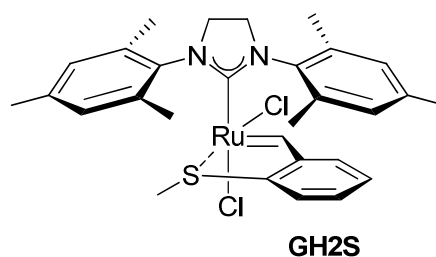


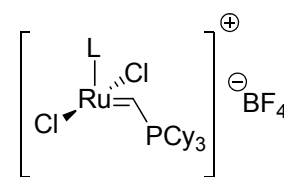
Figure 1.02. Key functional components of a metathesis pre-catalyst.

phosphite¹⁹⁻²⁰ or ketone,²¹ or a nitrogen-²² or sulfur-based ligand.²³ Phosphite ligands confer increased pre-catalyst stability at high temperatures, while strongly binding chelated ligands featuring Lewis basic heteroatoms are typically employed to generate latent pre-catalysts such as **GH2S**, which can be easily handled in the presence of metathesis substrates but respond to a stimulus (e.g. heat) in order to become active.²⁴⁻²⁵ In contrast, pyridine-ligated pre-catalysts are utilised when rapid initiation is desired, even at low temperatures.¹⁴ Initiation rates for some analogues of **G2** and **GH2** are presented in Chapter 3, where the rates of pre-catalyst initiation and metathesis are decoupled and quantified.

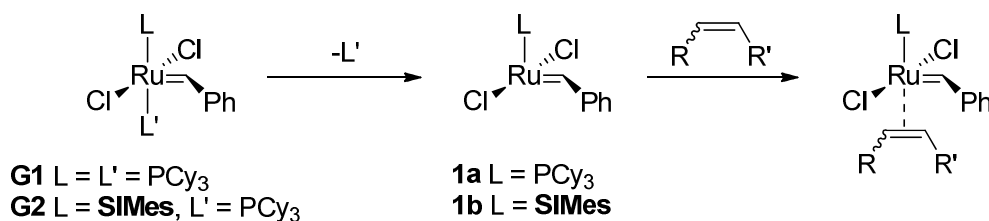


The initiation process is a key event in the metathesis cycle, due to its role in determining a large part of the overall reaction rate. For example, initiation of **G2** generates 14e catalytic species **1b**; alkenes bind to the vacant site on the metal to form η^2 -complexes which then lead to metathesis (**Scheme 1.03**).²⁶ The 14e alkylidene species are among the least stable of the ruthenium carbenes involved in metathesis, have not been observed by NMR, and are often implicated in decomposition pathways,²⁷⁻²⁸ so metathesis reactions are therefore conducted using pre-catalysts.

Ligand **L'** is typically removed during pre-catalyst initiation; however, pre-catalysts which do not feature an **L'** ligand and in which the alkylidene ligand (R in **Figure 1.02**) is a phosphonium salt are known. Pre-catalysts such as **Piers1** and **Piers2** initiate rapidly *via* cross-metathesis to (irreversibly) form a vinylphosphonium salt by-product (*vide infra*).²⁹⁻³¹ This class of pre-catalyst has enabled the rapid formation of significant concentrations of intermediate species such as MCBs. Fundamental processes in metathesis reactions have been explored in mechanistic studies that have employed this class of pre-catalyst.^{15,32-38}

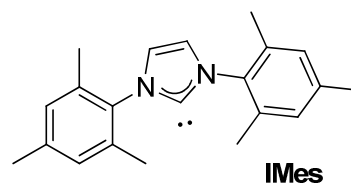


Piers1 L = PCy₃
Piers2 L = **SIMes**

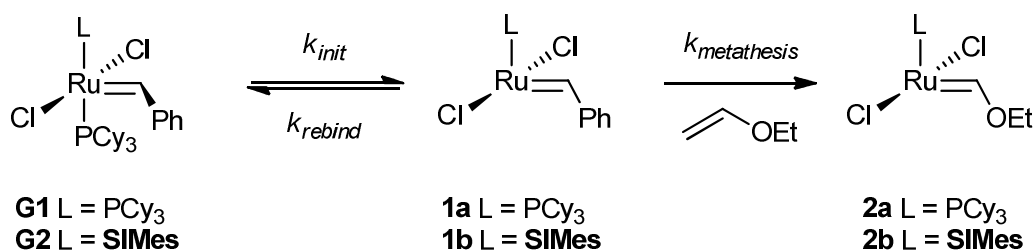


Scheme 1.03

Most ruthenium-based metathesis pre-catalysts are referred to as either first-generation or second-generation. The nature of the non-dissociating ligand **L** determines this classification: those pre-catalysts bearing a phosphane ligand are referred to as first-generation, while those that possess an NHC ligand are termed second-generation. Several researchers refer to those pre-catalysts where **L** is pyridine as third-generation catalysts, although this nomenclature is not as widespread as the first-generation/second-generation classification. NHCs often possess quite different properties from phosphanes.³⁹ While they have been found to possess similar proton affinities,⁴⁰ NHC ligands are more electron donating than phosphanes⁴¹ and form stronger ruthenium-ligand bonds; **IMes**, PCy₃ and PⁱPr₃ were found to have ruthenium-ligand bond strengths of 15.6, 10.5 and 9.4 kcal mol⁻¹ respectively.⁴² Differences between (and often within) these two classes of pre-catalyst arise both in their initiation behaviour and in the selectivity and reactivity of the 14e complexes that they generate (such as **1**).



The initiation of pre-catalysts such as **G1** and **G2** has been studied in considerable depth experimentally, in order to understand and fine-tune the delivery of active species into the catalytic cycle. Grubbs *et al.* have measured the rate of phosphane dissociation using ³¹P NMR experiments, in which excess free phosphane was added and the transfer of magnetisation between free and bound phosphane was monitored.^{26,43} For both of these pre-catalysts, Eyring-Polyani plots revealed large and positive values of ΔS^\ddagger , consistent with a dissociative mechanism for initiation (12 ± 2 cal K⁻¹ mol⁻¹ for **G1** and 13 ± 6 cal K⁻¹ mol⁻¹ for **G2**). It was also shown that the irreversible metathesis of vinyl ether substrates (which forms relatively inactive Fischer carbene species such as **2**)⁴⁴ was rate-limited by phosphane dissociation from **G2** (**Scheme 1.04**). Initiation rates for **G2** and analogues were obtained that were consistent with those



Scheme 1.04

Table 1.01. Initiation rates for pre-catalysts **G1** and **G2** measured *via* ^{31}P magnetisation transfer NMR spectroscopy and the metathesis of ethyl vinyl ether.

Pre-catalyst	T (K)	k_{init} / s^{-1} (^{31}P NMR) ^a	k_{init} / s^{-1} (Metathesis)
G1	283	$(3.8 \pm 0.6) \times 10^{-3}$	$(1.0 \pm 0.1) \times 10^{-3}$
G2	308	$(4 \pm 3) \times 10^{-4}$	$(4.6 \pm 0.4) \times 10^{-4}$

^a Determined by extrapolation of Eyring plots from magnetisation transfer experiments at higher temperatures

obtained *via* ^{31}P magnetisation transfer experiments; monitoring the decay of the pre-catalyst concentration in the presence of excess ethyl vinyl ether afforded the rate constants in **Table 1.01**. Under these conditions, for **G2**, $k_{metathesis} \cdot [\mathbf{1b}] \cdot [\text{ethyl vinyl ether}] \gg k_{rebind} \cdot [\mathbf{1b}] \cdot [\text{PCy}_3]$. Despite the demonstrated superior effectiveness of NHC-bearing pre-catalysts such as **G2** for metathesis reactions,^{10,45-46} the initiation rates of **G2** and analogues were found to be lower than the initiation rate of **G1**.^{43,45} Subsequent experiments, in which metathesis reactions with ethyl vinyl ether were conducted in the presence of excess PCy_3 , established that **1b**, derived from **G2**, was approximately equally selective for phosphane and alkene binding (**Equation 1.01** and **Figure 1.03**).²⁶

$$1/k_{obs} = (k_{rebind} \cdot [\text{PCy}_3]) / (k_{init} \cdot k_{metathesis} \cdot [\text{ethyl vinyl ether}]) + 1/k_{init} \quad (1.01)$$

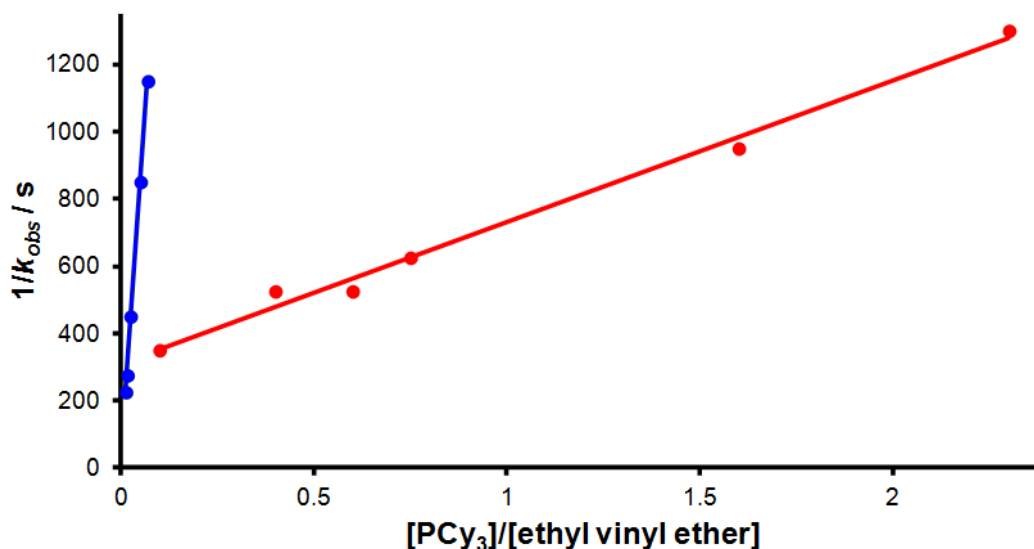


Figure 1.03. Plot of $1/k_{obs}$ versus $[\text{PCy}_3]/[\text{ethyl vinyl ether}]$ for the metathesis of ethyl vinyl ether with **G1** (blue) and **G2** (red) in the presence of added PCy_3 .²⁶

In contrast, **1a**, derived from **G1**, was found to be 1000-fold more selective for phosphane than alkene, which was proposed to account for its lower activity in metathesis reactions; while **1a** is generated more readily, it is less likely to undergo metathesis before becoming captured by phosphane.

Kennepohl *et al.* studied **G1** and **G2** using Ru K-edge X-ray absorption spectroscopy.⁴⁷ This technique allowed the electron density at the metal centre of each pre-catalyst to be evaluated. It was found that the ruthenium centre of **G2** was more electron deficient than that of **G1**, which arose as a consequence of back-bonding from the ruthenium centre into the Ru-NHC π^* -orbital. This was consistent with the lower observed rate constant for phosphane dissociation from **G2** than **G1**.

Various *in silico* studies have treated this phosphane dissociation event. Such studies are potentially very valuable as they can yield more insight into why specific pre-catalysts initiate faster than others, and therefore can influence the development of future metathesis pre-catalysts. Density functionals which do not account for dispersive interactions (such as B3LYP, PW91 and BP86) often treat metal-ligand binding incorrectly,⁴⁸ and tend to underestimate the barriers to phosphane dissociation.⁴⁹ Such functionals typically determine the correct *order* of energies, but will systematically underestimate the absolute values. For example, Cavallo *et al.* have calculated the energies of reaction for PCy₃ dissociation from a series of pre-catalysts (**Table 1.02**), and obtained values of *ca.* 7.9 to 14 kcal mol⁻¹ using the BP86 functional.⁵⁰ In addition, lower values were obtained when solvation was applied in the calculations, using a polarisable continuum model (PCM) which places the structures in an electronic field designed to emulate that of a solvent. These values are far lower than the *ca.* 20 – 25 kcal mol⁻¹ barriers measured experimentally for phosphane dissociation.²⁶

In recent years, density functionals such as the M06 suite pioneered by Truhlar *et al.* which account for dispersive interactions and metal-ligand bonding correctly have been developed.^{48,51-52} Truhlar *et al.* have shown that underestimation of phosphane dissociation barriers is due to the importance of attractive dispersive interactions in metathesis chemistry;⁴⁹ when they considered the phosphane dissociation event, the level of theory employed made a dramatic difference to the magnitude of the barrier (**Table 1.03**). Removal of the ruthenium and its two chloride ligands from the models allowed the impact of the non-covalent interactions to be isolated; M06-L/DZQ calculated contributions of 9.9 and 14.4 kcal mol⁻¹ (for **G1** and **G2** respectively), while

Table 1.02. ΔG° for phosphane dissociation from complexes featuring different alkylidene groups, calculated by Cavallo *et al.* using the BP86 density functional.⁵⁰

L = SIMes

3b R = R' = H
G2 R = Ph, R' = H
G2-ind R,R' = indenyl

4b R = R' = H
1b R = Ph, R' = H
5b R,R' = indenyl

Alkylidene	Solvent			
ΔG° (kcal mol ⁻¹)	None	-	12.2	-
	Toluene	-	9.8	-
	THF	-	8	-
	DCM	14.0	7.9	8.1
	Acetone	-	7.4	-
	Acetonitrile	-	7.3	-

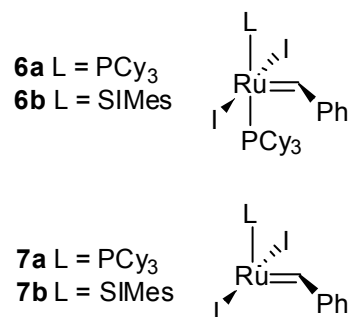
Table 1.03. Calculated bond dissociation energies (BDE) (kcal mol⁻¹) for the dissociation of PCy₃ from pre-catalysts **G1** and **G2**.

Functional	Basis Set	Counterpoise Correction	BDE (G1)	BDE (G2)
M06-L	TZQ	No	36.1	40.2
		Yes	34.2	38.2
	DZQ	No	41.7	45.2
		Yes	38.3	41.7
B3LYP	DZQ	No	19.0	17.4
		Yes	15.6	14.0
BP86	DZQ		20.0	18.8
PW91	DZQ		26.1	25.7
PBEh	BZQ	No	28.9	28.1
TPSSh	DZQ		24.6	23.5

B3LYP/DZQ calculated contributions of $-4.5 \text{ kcal mol}^{-1}$ and $-8.0 \text{ kcal mol}^{-1}$. Therefore B3LYP treats the interactions as *repulsive* rather than *attractive*. Similar conclusions were reached by Hillier *et al.* using the model system of methane and mesitylamine.⁵³ For these reasons, functionals such as BLYP-D and M06-L are favoured for the study of metathesis reactions.^{51,54}

Goddard *et al.* calculated ΔG^\ddagger for phosphane dissociation from **G2** in toluene at $23.4 \text{ kcal mol}^{-1}$ ($\Delta H^\ddagger = 28.4 \text{ kcal mol}^{-1}$) using the M06-L density functional;⁵⁵ this calculated barrier was in remarkably good agreement with the experimentally-determined value for ΔG^\ddagger of $23.0 \pm 0.4 \text{ kcal mol}^{-1}$ ($\Delta H^\ddagger = 27 \pm 2 \text{ kcal mol}^{-1}$) (from ^{31}P NMR spectroscopy methods),²⁶ but required the co-ordination of a molecule of toluene to the vacant site on the metal, suggesting that specific solvent interactions may be important in determining the initiation rate.

Chen *et al.* conducted detailed ESI-MS studies on metathesis reactions, and used these studies to quantify some of the barriers to steps in the reaction.⁵⁶ The results of their studies suggested that the reaction of the 14e methylidene **4b** with phosphane or alkene was effectively barrierless, and therefore that $\Delta G^\ddagger \approx \Delta G^\circ$ for phosphane dissociation (measured at $36.9 \text{ kcal mol}^{-1}$ experimentally). However, a later and detailed *in silico* study of the phosphane dissociation event has been carried out by Jensen *et al.*, employing the BLYP-D-CP functional (which features corrections for dispersive interactions, and counterpoise correction to reduce basis set superposition error) which was selected after a brief benchmarking study.⁵⁷ In this report, Jensen *et al.* stepped the ruthenium-phosphorus distance in complexes **6a** and **6b** along the intrinsic reaction coordinate (IRC), calculating single point energies at each step. Energy maxima were located at 3.945 \AA for complex **6a** and at 3.971 \AA for complex **6b**, followed by a decrease in energy upon further increasing the Ru-P distance (**Figure 1.04**); the energy of the infinitely separated 14e species **7** plus PCy_3 were found to be *larger* than these barriers, showing that the energetics of the two separated species do not accurately reflect the barrier to dissociation, and therefore that $\Delta G^\ddagger \neq \Delta G^\circ$. For example, for **G2** analogue **6b**, $\Delta E^\ddagger = ca. 17 \text{ kcal mol}^{-1}$ while $\Delta E = ca. 18 \text{ kcal mol}^{-1}$. Even when the ruthenium-phosphorus bond had been cleaved (i.e. the Ru-P distance was $>4\text{\AA}$), there were still long-range



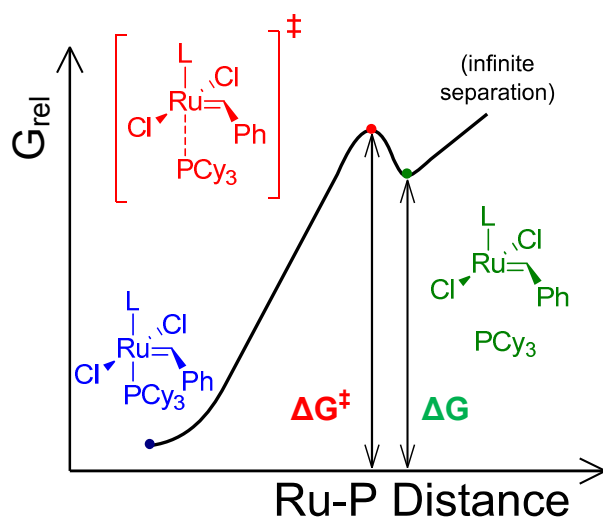
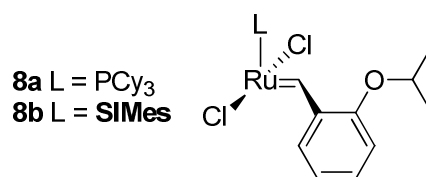


Figure 1.04. The relationship between Ru-P bond length and free energy as calculated by Jensen *et al.* (at the BLYP-D-CP level of theory).⁵⁷

interactions between the phosphane and the ruthenium centre.

While the dissociative mechanism is well accepted for phosphane-bound pre-catalysts such as **G1** and **G2**, the initiation reactions of pre-catalysts such as **GH2** and catalysts such as **G1** and **G2**, the initiation reactions of pre-catalysts such as **GH2** and **Grela** have been the subject of recent studies. Initially, **GH2** was thought to initiate in a manner analogous to **G2**, *via* rotation of the alkoxy styrene moiety around the Ru=C and C-C linkages, with scission of the Ru-O bond, to yield an active 14e species **8**.⁵⁸ However, later work by Grubbs *et al.* suggested an associative mechanism on the basis of experimentally determined activation parameters, with ΔS^\ddagger determined to be *ca.* $-20 \text{ cal K}^{-1} \text{ mol}^{-1}$ (*cf.* $13 \pm 6 \text{ cal K}^{-1} \text{ mol}^{-1}$ for **G2**).⁵⁹ More recently, Plenio *et al.* found that the initiation rates of **GH2** and **Grela** changed in the presence of various concentrations of alkene, and suggested an interchange mechanism based on their observations;⁶⁰ a follow-up study suggested that *both* dissociative and interchange mechanisms were in operation, due to nonlinear behaviour in detailed plots of k_{obs} *versus* [alkene] when **GH2** and analogues were exposed to various alkenes in huge excess (up to *ca.* 3×10^5 equivalents).⁶¹ The topic of initiation in Hoveyda-type pre-catalysts is discussed more fully in Chapter 3, including a more detailed discussion of the literature and new results in this field.

Pre-catalysts featuring a phosphonium alkylidene moiety (such as **Piers1** and **Piers2**) initiate *via* reaction with alkene and release of the corresponding vinylphosphonium salt.²⁹ The rapid and irreversible nature of the initiation event in



these pre-catalysts has rendered them ideal for the generation and study of metallocyclobutanes at low (*ca.* 200 – 230 K) temperatures.^{32,36} Pre-catalyst **G2-3BrPy** initiates so rapidly that an exact initiation rate could not be measured by Grubbs *et al.* using UV/visible spectroscopy;¹⁴ initiation was complete within *ca.* 0.5 seconds. Detailed discussion of these rapidly-initiating pre-catalysts are beyond the scope of this thesis, so are not discussed further. However, it is important to note that the mechanism of pre-catalyst initiation varies depending on pre-catalyst structure, underlining the importance of understanding the reactions that the pre-catalyst undergoes during the reaction.

Alkylidene Transfer

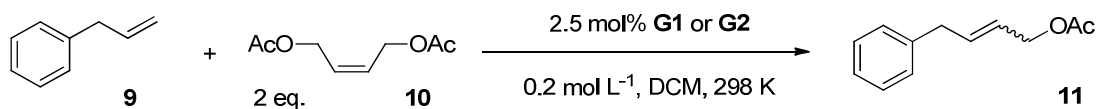
The alkylidene transfer step generates new ruthenium alkylidene complexes during metathesis reactions, as the 14e species that are generated from pre-catalyst initiation undergo reaction with alkene substrates to yield new alkylidene complexes. While the rate of pre-catalyst initiation has an impact on how the solution concentration of active 14e catalyst species will vary with time, the activity and selectivity of this active species will affect the overall performance of the catalytic system significantly.

First *versus* Second Generation Pre-catalysts

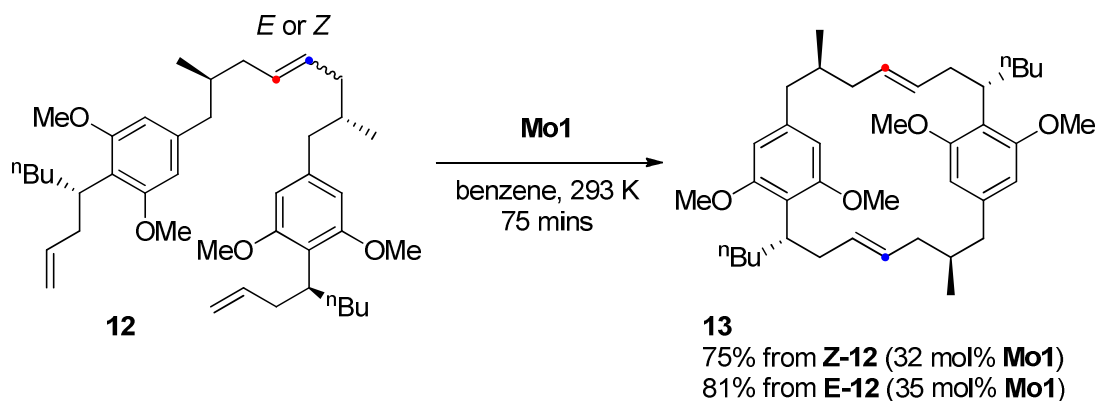
Second generation pre-catalysts tend to operate in the thermodynamic regime, while first generation pre-catalysts yield the kinetic products (*vide infra*).⁴⁵ Differences in reactivity have also been established in the synthetic chemistry literature. Grubbs *et al.* have classified alkenes as Types I to IV, which exhibit different reactivity in metathesis reactions (*vide infra*).⁶² A key outcome of the study was that different pre-catalyst systems exhibit different reactivity towards each functional group or alkene substitution pattern. These key differences between first and second generation alkylidenes have a considerable impact on reaction outcomes. For example, while **G2** will catalyse the reactions of 1,1-disubstituted alkenes and alkenes with quaternary-substituted allylic positions, **G1** will not. Second generation alkylidenes are less selective and will react with reactants *and* products. As the steps that comprise alkene metathesis are all formally reversible, the final product mixtures can often be expected to reflect the expected thermodynamic mixture of products. However, the degree to which the thermodynamic mixture is obtained depends heavily on the pre-catalyst selected for the metathesis transformation. First generation pre-catalysts such as **G1** are known to react more slowly

with the acyclic and cyclic 1,2-disubstituted alkenes found in metathesis products, and will therefore take much longer to establish equilibrium.⁶² Kinetic control is therefore the usual consequence when **G1** is employed in a metathesis reaction. This thermodynamic *versus* kinetic control has been found to be reflected in the *E/Z* selectivity of cross metathesis reactions. In the prototypical cross metathesis reaction between allylbenzene **9** and but-2-ene-1,4-diol derivative **10** (Scheme 1.06), the *E/Z* ratio of product **11** and its time dependence were found to be dependent on the pre-catalyst; **G1** resulted in a slower reaction and lower *E/Z* ratios, while **G2** was more than ten-fold faster, yielding a higher *E/Z* ratio in the products due to faster secondary metathesis processes (Figure 1.05);⁴⁵ while the differences in outcomes with **G1** *versus* **G2** are significant, differences in the structures of NHC-bearing pre-catalysts exert only modest effects on *E/Z* selectivity.⁶³⁻⁶⁴

This behaviour can affect the outcomes of synthetic RCM reactions. Various manifestations of thermodynamic *versus* kinetic control have been reported in the literature, a selection of which are discussed here. Smith *et al.* have studied the synthesis of cyclophane natural products *via* RCM of **12**; thermodynamic product **13** was favoured, regardless of the configuration of the substrate (Scheme 1.07).⁶⁵ Reaction did not occur solely at the monosubstituted termini, as this would have yielded a different product. Instead, the catalyst must also have reacted with the 1,2-disubstituted alkene,



Scheme 1.06⁴⁵



Scheme 1.07⁶⁵

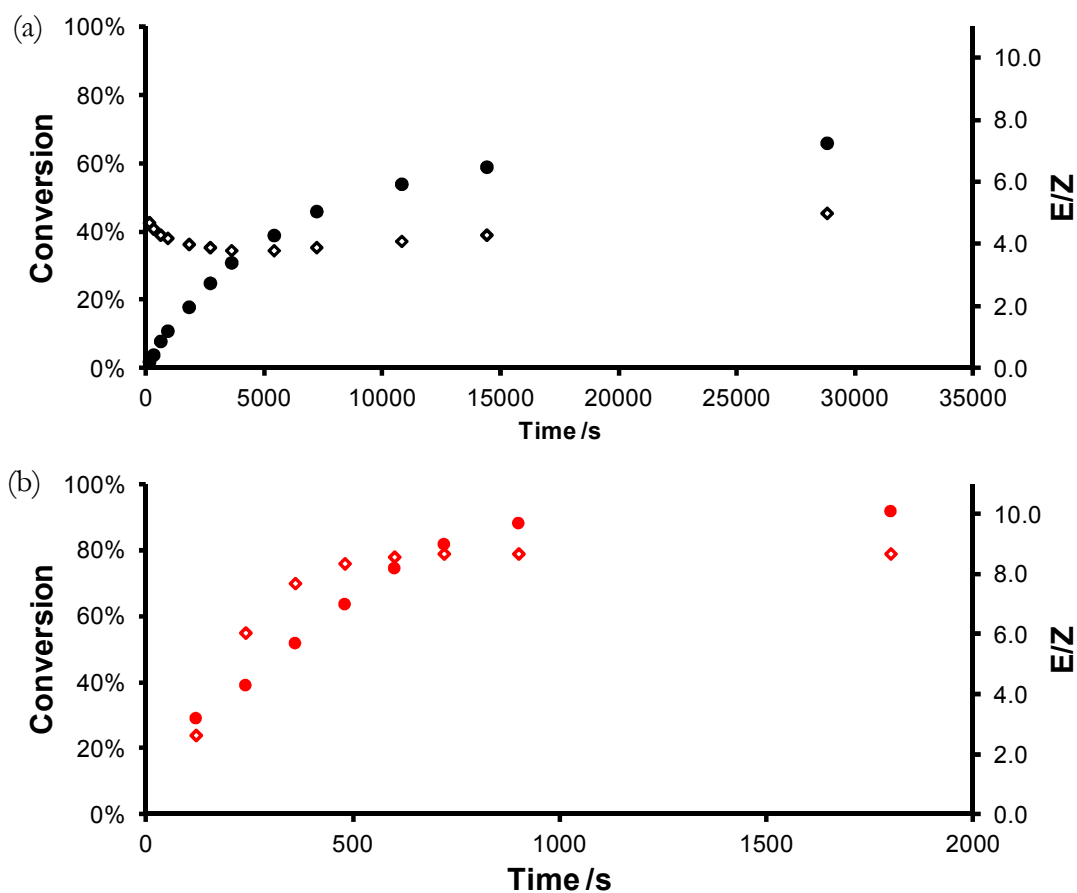
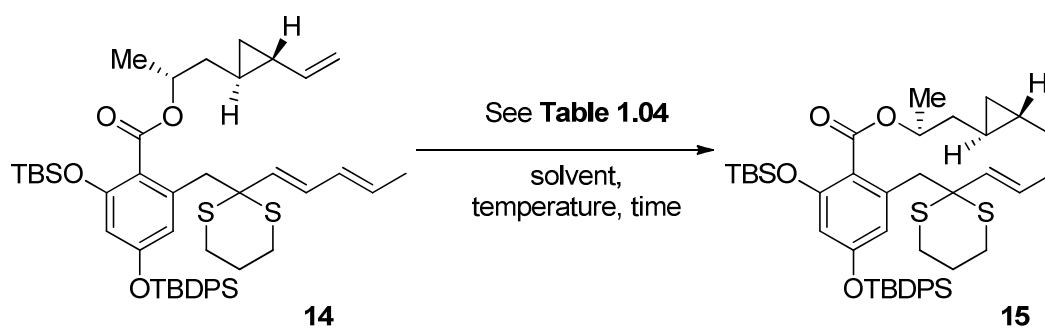


Figure 1.05. Conversion (closed circles) and *E/Z* ratio (of **11**, open diamonds) versus time for the reaction in Scheme 1.06 with (a) 2.5 mol% **G1** or (b) 2.5 mol% of **G2**.⁴⁵

leading to a different product to that expected.

Danishefsky *et al.* recovered mixtures of target cycloalkene and oligomers from the dilute RCM reactions of compound **14** (Scheme 1.08 and Table 1.04). The spread of yields of **15** (16 to 55%) was attributed to the reaction times; the best outcome was obtained from a rapid, hot RCM followed by quenching of the active species and work-



Scheme 1.08⁶⁶

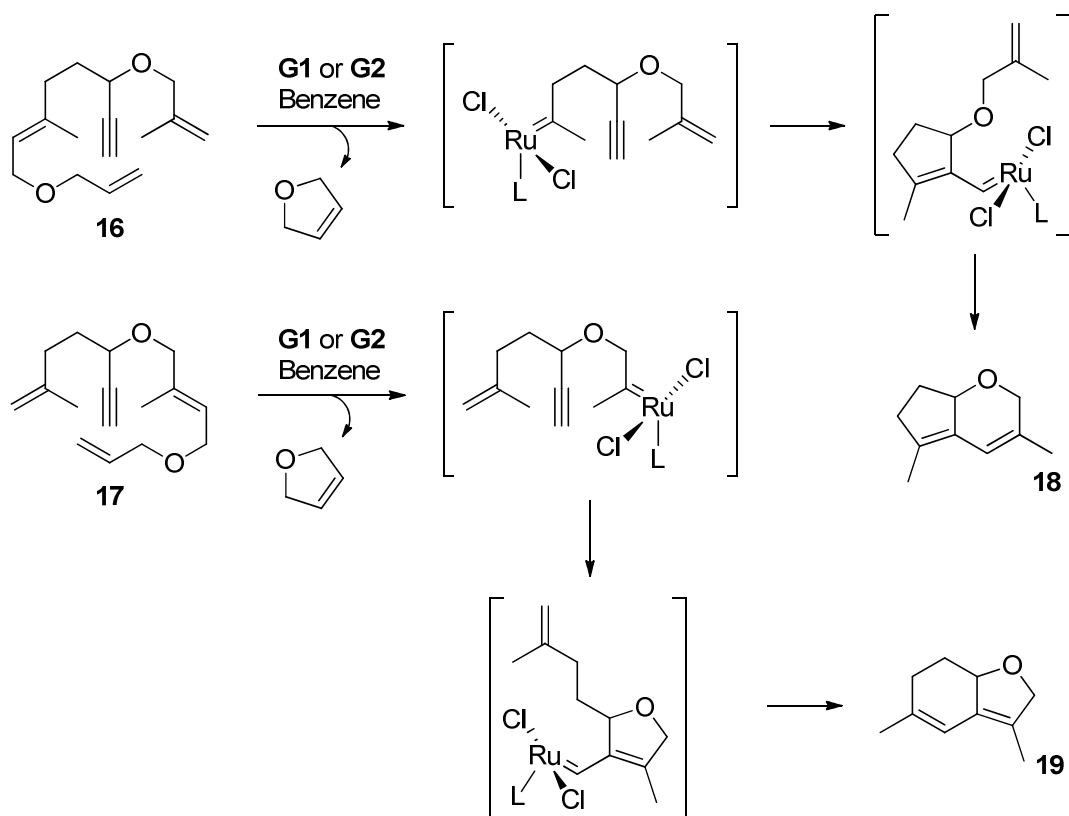
Table 1.04. Conditions screened for the synthesis of **15** by RCM.⁶⁶

Solvent	T (°C)	Reaction Time	[14] ₀ (mmol L ⁻¹)	15	Oligomers
DCM	42	19 h	0.5	16%	30%
Toluene	42	19 h	0.5	27%	48%
Toluene	110	10 min	0.2	55%	0%
Benzene	80	35 min	0.5	33%	36%

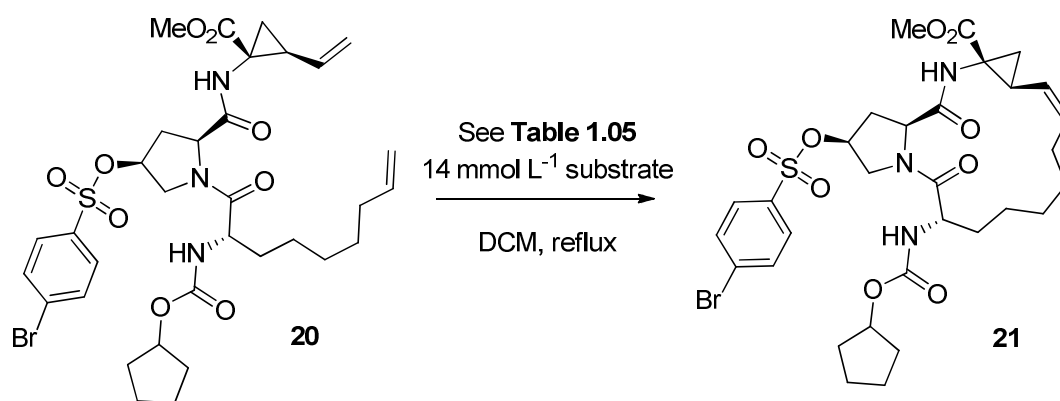
up. Ring-opening to form a cyclic dimer was found to occur if the reaction was conducted over longer periods, as tested by re-exposing the product to the reaction conditions. This suggested that secondary metathesis events caused the erosion of yield. Hoyer *et al.* used relay ring-closing metathesis (RRCM) to direct the formation of ruthenium carbenes in the metathesis reactions of triene-yne substrates.⁶⁷ In substrates **16** and **17**, the catalyst would be expected to react first with the mono-substituted terminus, then undergo RCM to yield a molecule of 1,4-dihydrofuran and place the carbene in position to react with the alkyne; substitution of the appropriate terminus with the ether unit directs the carbene throughout the sequence and leads to the synthesis of the desired product (**Scheme 1.09**). Metathesis of substrate **16** with **G1** (at 50°C) and **G2** (at room temperature) yielded isomeric dihydropyran and dihydrofuran products **18:19** in ratios of 26:1 and 4.7:1 respectively. Metathesis of **17** was 45-fold selective with **G1** and 7-fold selective with **G2** for the dihydrofuran isomer. In both cases, **G1** was five-fold more selective for the desired product than **G2**, which was most likely because RRCM induces selectivity through a *kinetic* effect, by rendering one terminus more attractive to a metal carbene catalyst. Second-generation pre-catalysts such as **G2** can react competently with multiply-substituted alkenes and so selectivity is not enforced as strongly by the substrate structure.

The consequences of this difference in activity was encountered by chemists at Boehringer-Ingelheim when scaling up the RCM of **20** to form **21** *en route* to macrocyclic hepatitis C virus (HCV) NS3 protease inhibitor (**Scheme 1.10**).⁶⁸ The use of first generation pre-catalyst **GH1** resulted in a slower reaction but formed less dimeric (or oligomeric) by-products than the second-generation species **G2** and **GH2** (**Table 1.05**).

Similar reactivity differences were reported by Nolan *et al.* in the RCM reaction of **22**;⁶⁹ **G1** produced dienes **23**, while **G2-unsat** yielded cycloalkenes **24** (**Scheme 1.11**).



Scheme 1.09⁶⁷

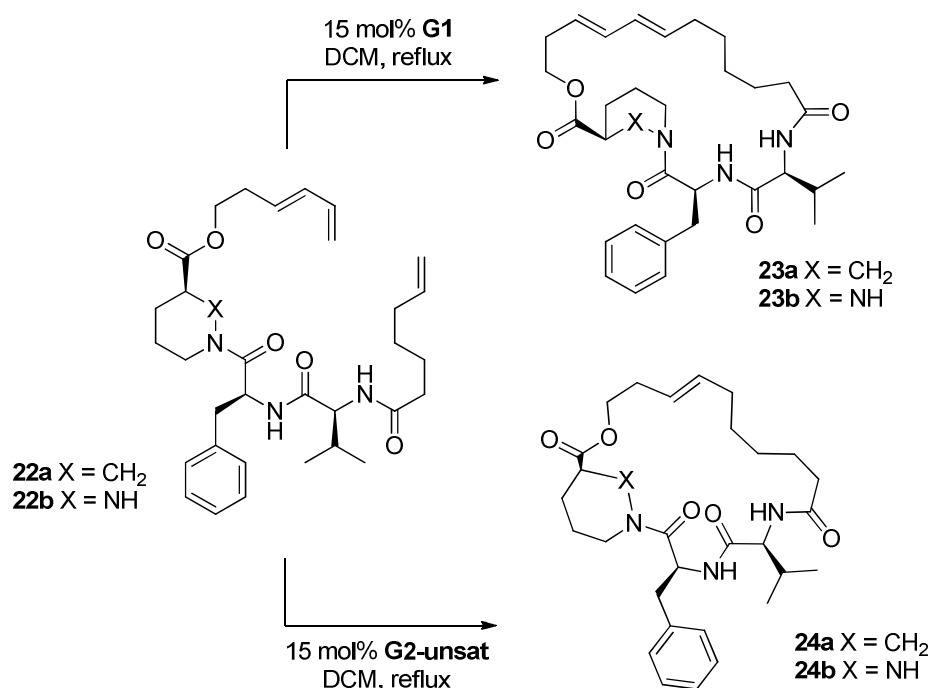


Scheme 1.10⁷⁰

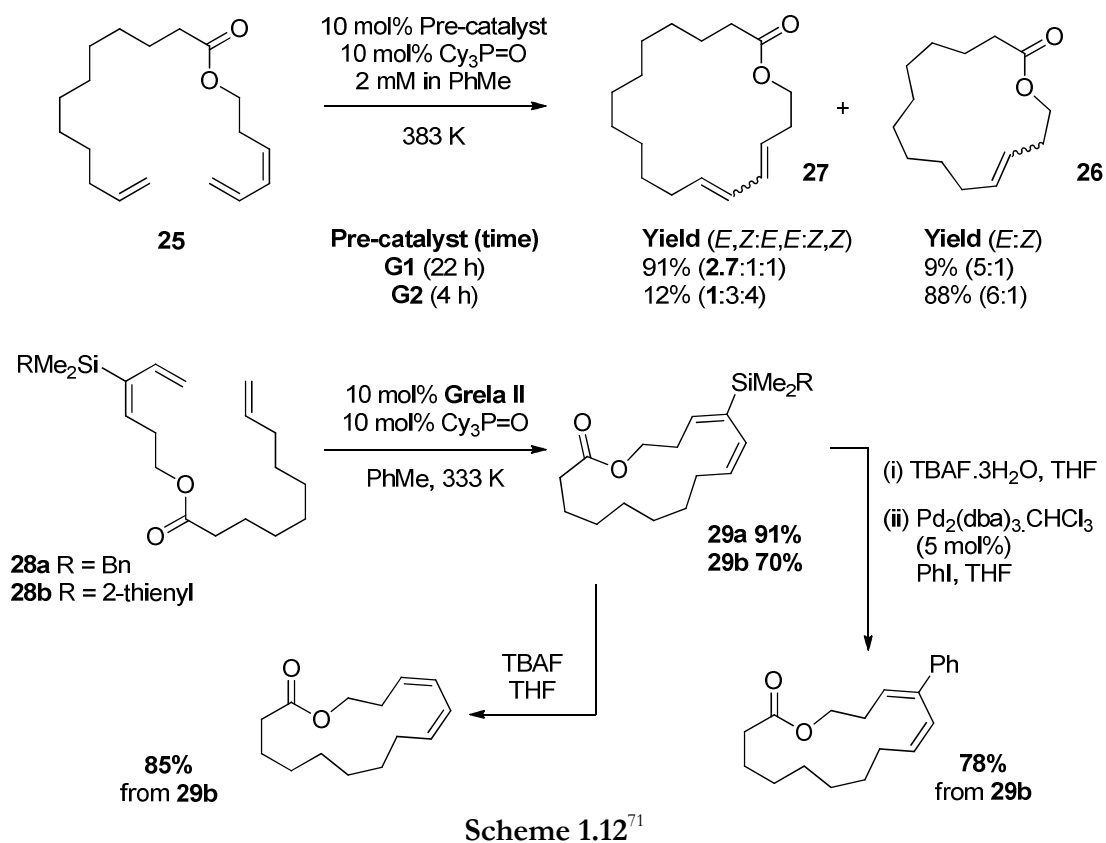
In this example, the NHC-bearing pre-catalyst formed a macrocyclic product that was two atoms smaller than the desired one, and produced a different alkene (butadiene) as a by-product; the 23 membered ring is therefore likely to be the kinetic product and the 21 membered ring the thermodynamic product, so the reaction equilibrates over time to the smaller product. More detailed studies and/or thermochemical calculations would be required to confirm if this is the case.

Table 1.05. Catalyst screening in the scale-up of the RCM reaction in **Scheme 1.10**.⁶⁸

Pre-catalyst (loading)	Solvent	Temperature (°C)	Time (h)	HPLC Yield	Dimer Content
GH1 (5 mol%)	CH ₂ Cl ₂	40	24	90%	< 0.5%
GH1 (3.5 mol%)	PhMe	60	20	90%	< 0.5%
G2 (0.5 mol%)	PhMe	60	4	87%	8%
GH2 (1 mol%)	PhMe	55	1	85%	10%

**Scheme 1.11**⁶⁹

In order to avoid this behaviour, substantial structural modifications are necessary such as the use of trialkylsilyl substitution to block metathesis at the internal alkene, as employed by Fürstner *et al.* (**Scheme 1.12**).⁷¹ Without the aid of the bulky silyl substituent, RCM of **25** with **G2** was selective for the ring-contracted product **26** instead of the desired cyclodiene **27**. The trialkylsilyl-bearing substrates **28** were used to achieve selectivity for products **29**, but the silyl group was easily removed, or utilised in a subsequent palladium-catalysed coupling step to elaborate the core structure. The issue of thermodynamic *versus* kinetic control is discussed and investigated more fully in Chapter 2, and is shown to be in operation in a prototypical ring-closing metathesis



reaction. These examples serve to illustrate that the outcomes of metathesis reactions cannot always be predicted from the substrate structure alone, and are also a function of the catalyst system employed; different catalyst systems can potentially result in different products from the same substrate.

The underlying origins of this selectivity have been probed, in order to obtain better understanding of the reactions between ruthenium alkylidenes and alkenes. As described above, it was discovered by Grubbs *et al.* that second-generation 14e species are approximately equally as selective for phosphane as for alkene.²⁶ The corresponding first-generation pre-catalysts were found to be 10³-fold more selective for phosphane.

Straub has investigated the difference in reactivity of 14e methylidene complexes derived from **G1** and **G2** with alkenes using DFT methods (at the B3LYP/LACV3P**+ level of theory) by modelling the potential conformers for the methylidene-ethene η^2 -complexes (**Figure 1.06**). Of the four possible conformers, only one is reactive and can lead on to a MCB. In this reactive conformer, the methylidene protons are in the Cl-Ru-Cl plane, and the ethene is aligned parallel to the methylidene for reaction to occur. Straub *et al.* discovered *via* DFT calculations that the energetics of these η^2 -complexes

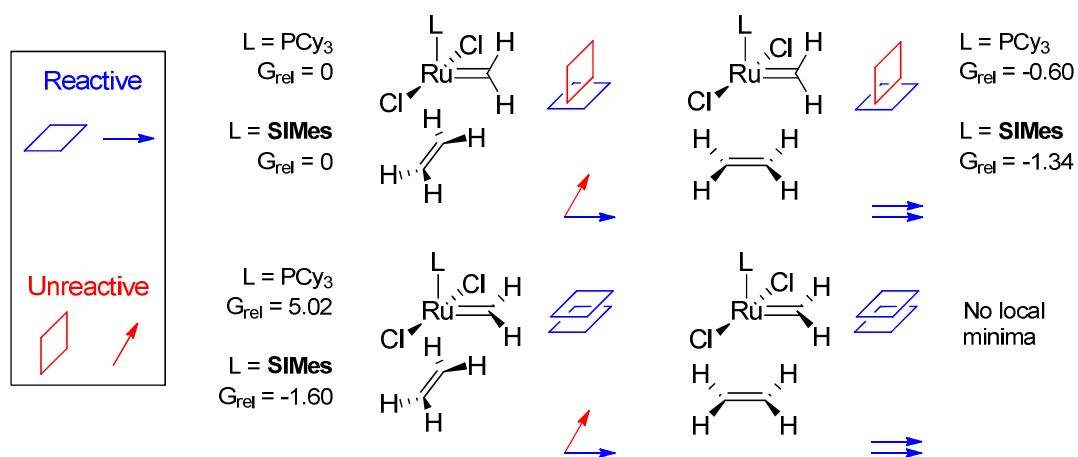


Figure 1.06. The four conformers of the complex between methyldiene and ethene;⁷² relative energies are in kcal mol⁻¹ using the B3LYP density functional.

were quite different in first- (L = PCy₃) and second-generation (L = **SIMes**) systems; the latter system favoured the reactive conformer more than the former. This is in agreement with the known greater reactivity of **G2** with alkenes compared to **G1**,²⁶ if the binding of alkene to the metal centre is more likely to result in metathesis, then this would manifest as a change in the apparent selectivity for alkene over phosphane.

Other researchers have also discussed the issue of active *versus* inactive conformers of metathesis intermediates. Truhlar *et al.* have studied the energy profiles of active *versus* inactive ruthenium carbene complexes (using the M06-L density functional).⁷³ Through DFT studies, they have suggested that the differences between both the initiation rates of **G1** and **G2** and the metathesis activity of the corresponding 14e electron species can be explained through calculation of the barriers to the active rotamer. During the initiation event, the carbene moieties in pre-catalysts **G1** and **G2** must first rotate to dissociate phosphane (**Figure 1.07**); barriers to these rotations were calculated to be 10.1 kcal mol⁻¹ and 16.8 kcal mol⁻¹ respectively, consistent with the faster initiation rate of **G1**. However, carbene rotation in the 14e species to bring the carbene substituents (e.g. H and Ph in the case of 14e complexes **1a** and **1b**) into the Cl-

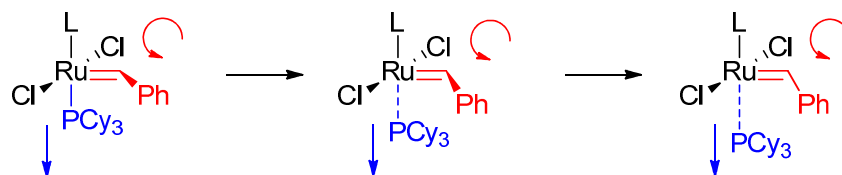


Figure 1.07. Coupling of alkene rotation to phosphane dissociation.

Ru-Cl plane and therefore into a reactive form proceeds *via* a lower barrier for **G2** (4.8 kcal mol⁻¹) than for **G1** (13.3 kcal mol⁻¹), consistent with the superior activity of **G2**.

Fernández *et al.* have proposed that there is a specific interaction between the *ipso*-carbon of the NHC aryl groups and the ruthenium carbene, on the basis of DFT calculations (at the BP86/def2-SVP level of theory);⁷⁴ this interaction was proposed to stabilise the active conformation of η^2 -complexes, rendering them lower in energy than the inactive conformations, and therefore to lead to increased catalytic activity.

Catalyst Decomposition

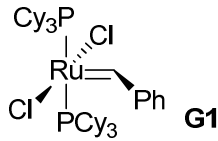
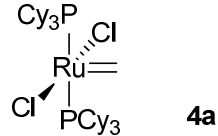
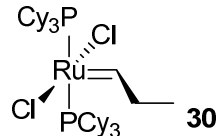
Catalyst decomposition is a significant problem in metathesis chemistry. By understanding when and why decomposition occurs, efforts can be made to avoid it through pre-catalyst design and the control of reaction conditions. Just as pre-catalyst initiation rate determines how quickly the population of active catalyst is built up, the decomposition rate determines how quickly this reservoir is depleted and therefore can significantly affect the overall reaction rate.

The decomposition pathway(s) active in a given reaction will depend on the pre-catalyst employed. Rapidly initiating pre-catalysts such as **G2-3-brpy** will quickly generate large quantities of 14e species such as benzylidene **1b** and methylidene **4b**, which are more susceptible to decomposition than phosphane-bound species such as **G2** in which the otherwise vacant site is occupied by a ligand. For this reason, it was found that **G2-3-brpy**, while reacting more rapidly at first, failed to achieve complete conversion in the otherwise trivial metathesis reactions such as diethyl diallylmalonate.⁴⁵ Decomposition can occur at various stages of the reaction and can include pre-catalyst decomposition, decomposition of the methylidene species that are present in the reaction, and decomposition promoted by certain functional groups.

Pre-catalyst Decomposition

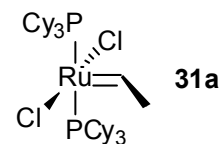
The earliest studies of pre-catalyst stability were conducted by Grubbs *et al.*, in which **G1** and derivatives were thermolysed at 328 K and their decrease in concentration was monitored (**Table 1.06**).⁷⁵ Methylidene species (such as **4a**) were identified to be the least stable phosphane-bound species ($t_{1/2} = 40$ min, *cf.* $t_{1/2} = 8$ days for **G1**). Decomposition of these complexes yielded a number of products; various species were observed by ³¹P NMR spectroscopy, including free PCy₃. Propylidene **30**, which is most

Table 1.06. Selected decomposition rates (from thermolysis at of a 23 mmol L⁻¹ solution in benzene at 328 K) for complexes **G1**, **4a** and **30**.²⁸

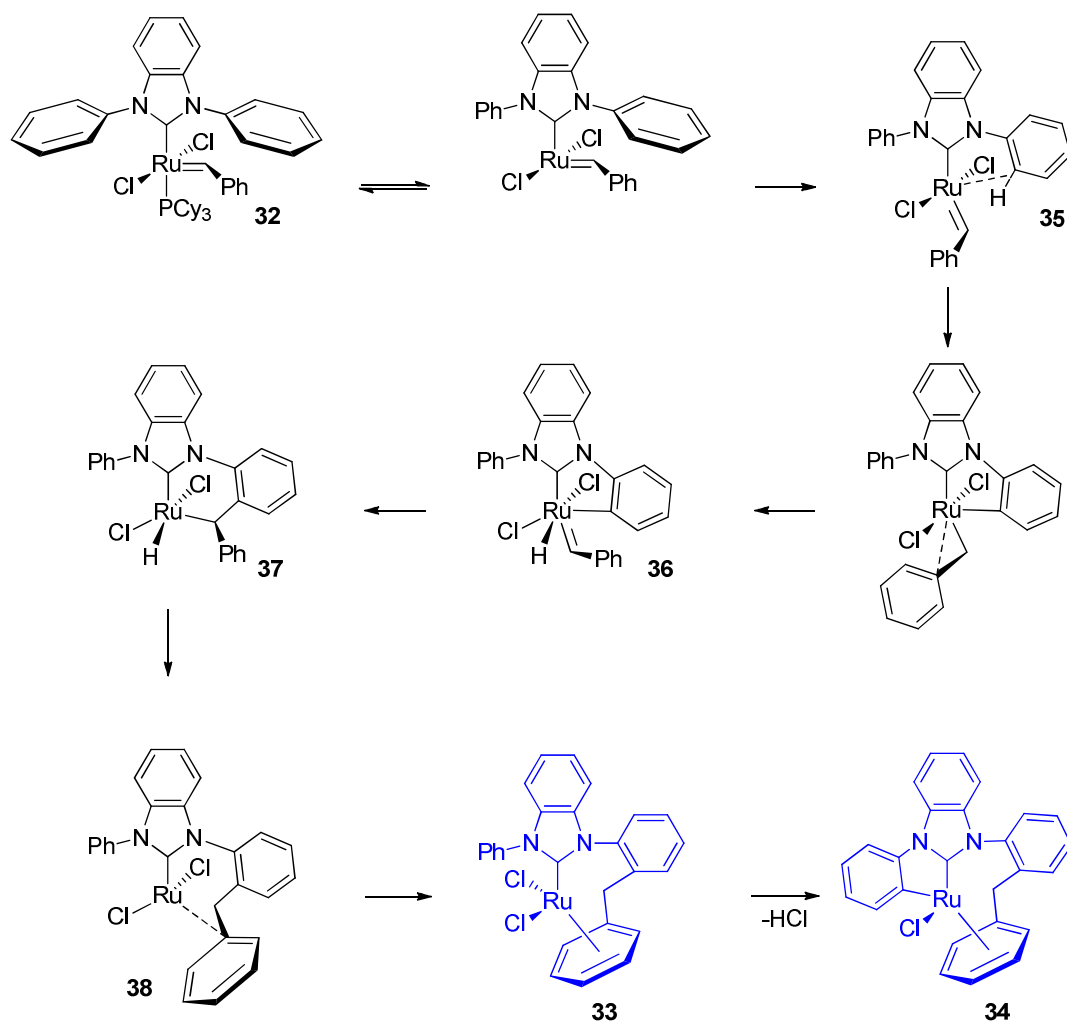
Complex	k_{decomp} (s ⁻¹)	Decomposition $t_{1/2}$
	1.0×10^{-6} ^a	8 days
	2.9×10^{-4} ^a	40 min
	2.4×10^{-5} ^a	8 h

^a Calculated from $t_{1/2}$.

representative of ruthenium carbene complexes present during metathesis reactions, yielded *trans*-3-hexene upon decomposition, suggesting the involvement of two molecules of this species in the decomposition mechanism. Traces of ruthenium hydride complexes ($\delta_{\text{H}} \sim -7$ ppm) and ethylidene **31a** were detected; the latter complex could arise from metathesis of alkene (generated during decomposition) that had been isomerised by the ruthenium hydride complexes. Notably, the rate of decomposition decreased in the presence of added phosphane, suggesting that decomposition proceeded *via* monophosphane 14e complexes such as **1a** (for **G1**).



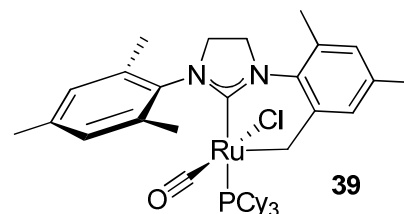
Pre-catalysts featuring different NHC ligands can decompose *via* other reactions with the substituents on the ligand. Complex **32** decomposed *via* insertion of the ruthenium centre into an aromatic *ortho*-carbon-hydrogen bond on the NHC ligand (**Scheme 1.13**);⁷⁶⁻⁷⁷ the products in blue were obtained from experimental studies by Grubbs *et al.*,⁷⁶ while the mechanism presented is that proposed by Cavallo *et al.* on the basis of density functional theory calculations.⁷⁷ When heated to 333 K in benzene for three days, 58% conversion of **32** to η^6 -complex **33** was obtained, plus traces of the double insertion product **34**. When pre-catalyst **32** was heated to 313 K in DCM for 12 h, significant quantities of **33** (24% conversion) and **34** (38% conversion) were obtained. Decomposition was proposed to proceed *via* an agostic interaction between the



Scheme 1.13⁷⁶

ruthenium centre and the *ortho*-carbon-hydrogen bond (complex **35**); insertion of the ruthenium into this bond would yield complex **36** which then can rearrange to form ruthenium hydride complex **37**. In this way, the benzylidene moiety effectively acts as a shuttle to deliver the *ortho*-hydrogen to the ruthenium centre. Rearrangement then β -hydride elimination would yield complex **38** in which the ruthenium centre can interact with the *ipso*-carbon of the benzylidene-derived phenyl ring, which then can rearrange to form η^6 -complex **33**; interaction of the ruthenium centre with another *ortho*-hydrogen on the NHC ligand would lead to complex **34** plus HCl. The pre-catalysts utilised in the studies in this thesis do not feature *ortho*-hydrogen atoms on the NHC ligand, but it is important to note that ruthenium hydride complexes have frequently been implicated as intermediates during catalyst decomposition, as these species are known to isomerise alkenes (see Chapter 4). The pathway proposed by Grubbs proceeds from the

benzylidene *pre-catalyst* and not the methylidene catalyst; the latter may decompose in a very different manner (*vide supra*), but could not form an aryl η^6 -complex as obtained from the pre-catalyst.



However, the products of ruthenium C-H insertion have also been isolated during the preparation of pre-catalysts such as **G2**. Grubbs *et al.* reported the isolation (and X-ray crystal structure) of complex **39**,⁷⁸ isolated when the preparation of **G2** from **G1** was conducted under conditions that were not rigorously free of air. When the reaction was carried out in a sealed Schlenk flask, this species was not detected.

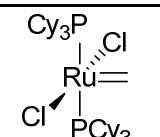
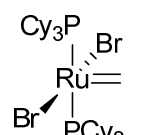
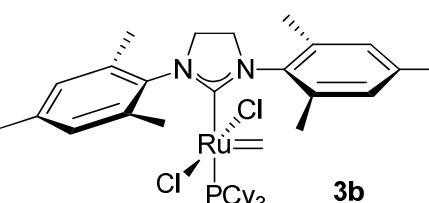
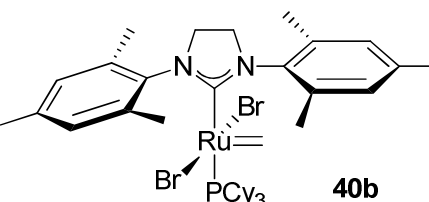
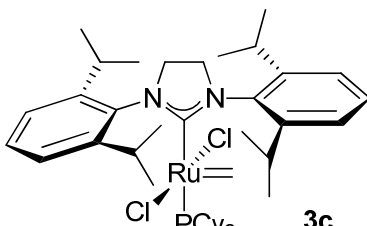
While pre-catalysts for metathesis are typically very robust, the potential exists for species such as ruthenium hydride complexes to be present either in the pre-catalyst batch itself, or as decomposition products.

Methylidene Decomposition

As discussed above, methylidene complexes are often the most sensitive and fragile species present in metathesis reactions (see **Table 1.06** above). Grubbs *et al.* carried out detailed decomposition studies with a range of phosphane-bound methylidene complexes.²⁸ Methylidene complexes are key intermediates as they are formed by the turnover of α,ω -dienes and are therefore present in most synthetic metathesis reactions. Thermolysis in benzene-*d*₆ allowed decomposition rates to be measured by NMR spectroscopy (**Table 1.07**); NHC complexes were more stable than bis(phosphane) complexes, while replacement of the chlorides with bromide ligands yielded slightly less stable complexes.

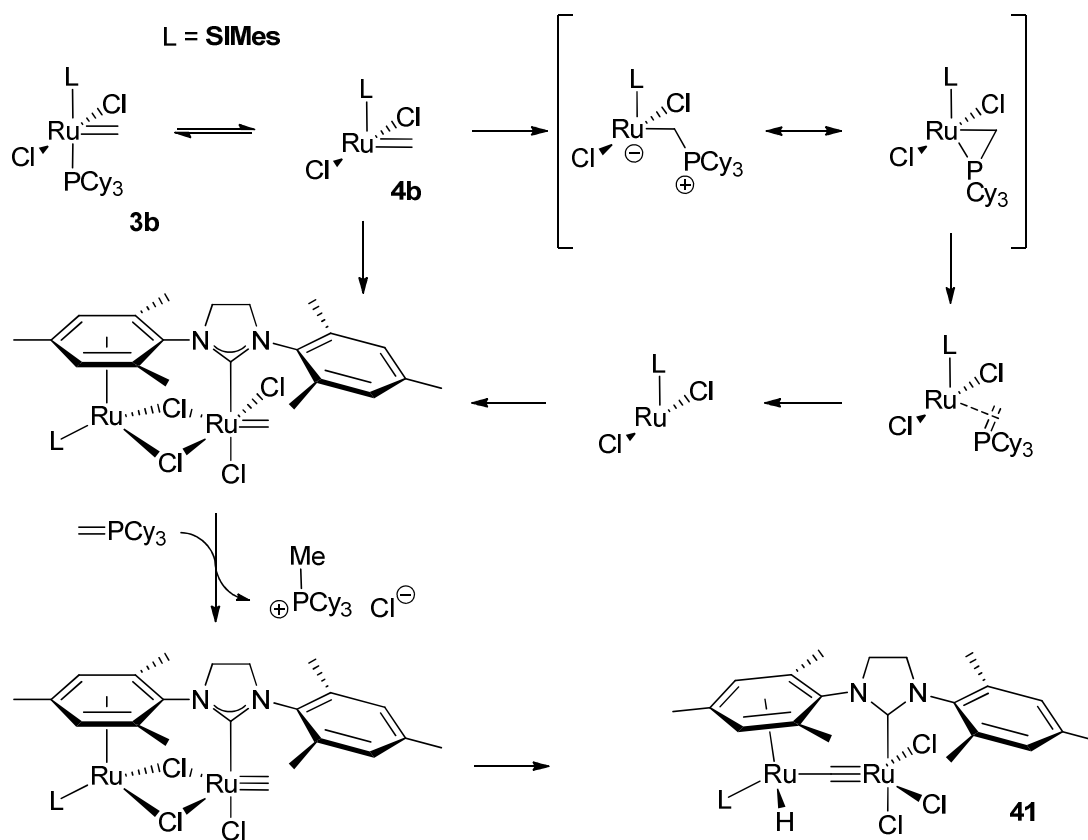
Diruthenium hydride **41** was obtained when **G2**-derived methylidene **3b** was thermolysed in this manner; this complex was isolated and characterised by NMR spectroscopy, mass spectrometry and X-ray crystallography.²⁷ A characteristic ¹H NMR signal (δ_{H} (DCM-*d*₂) = -8.6 ppm) indicated that a ruthenium hydride complex was present. A mechanism has been proposed for this decomposition pathway, in which PCy₃ dissociates from the metal centre before performing nucleophilic attack on **4b** (**Scheme 1.14**). The first step of this mechanism is significant, because the dissociation rate of PCy₃ from **3b** is known to be very slow;²⁶ in addition, the formation of a diruthenium complex in solution requires reaction between two 14e species that will be present in very low concentrations. [MePCy₃]Cl was also isolated from the

Table 1.07. Selected decomposition rates (from thermolysis at of a 23 mmol L⁻¹ solution in benzene at 328 K) for ruthenium methyldene complexes.²⁸

Methyldene complex	k_{decomp} (min ⁻¹)	Decomposition $t_{1/2}$
 3a	0.016	40 min
 40a	0.018	35 min
 3b	0.0021	5 h 40 min
 40b	0.0024	5 h 15 min
 3c	0.011	1 h

^a Calculated from $t_{1/2}$.

decomposition reaction, as well as from the decomposition reactions of complexes **3a** and **3c**. The decomposition of **SIPr**-bearing complex **3c** yielded the chloride salt of the NHC in addition, but the fate of the ruthenium was not identified. Complex **41** has been shown to be active for alkene isomerisation; the isomerisation performance of this complex is assessed in Chapter 4. The identification of a well-defined ruthenium hydride complex as a decomposition product of a complex known to be present in metathesis reactions was an important outcome. Pre-catalysts such as **G2** are the most commonly used ruthenium carbene complexes in synthesis, so understanding of their decomposition is very valuable. Previous studies that have generated ruthenium hydride

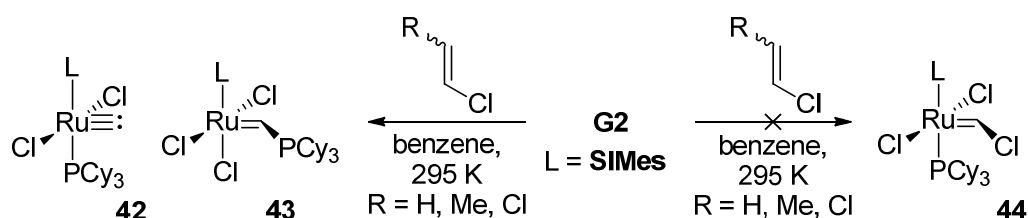


Scheme 1.14²⁸

complexes from ruthenium carbene species have typically relied on the use of reagents that would be unlikely to be present during synthetic metathesis reactions in concentrations sufficient to effect transformation to hydride complexes on the reaction timescale;⁷⁹⁻⁸¹ for example, ruthenium hydride complexes can be generated from thermolysis of metathesis pre-catalysts in the presence of alcohol and base. The conditions used for the decomposition studies by Grubbs *et al.* are still quite forcing, requiring prolonged thermolysis of purified methyldiene complexes. For example, the generation of **3** with a solution concentration of 23 mmol L^{-1} would require a 0.46 mol L^{-1} metathesis reaction with 5 mol% pre-catalyst or a 2.3 mol L^{-1} metathesis reaction with 1 mol% pre-catalyst. This perhaps explains why there have been no reports of the detection of this species in synthetic metathesis reactions, although synthetic chemists do not tend to analyse the high field of the ^1H NMR spectra of product mixtures. Straightforward RCM reactions are often run at concentrations of *ca.* $10^{-1} \text{ mol L}^{-1}$, but challenging reactions require high dilution to overcome competing oligomerisation (*vide infra*) and therefore reaction concentrations can be as low as 10^{-3} - $10^{-4} \text{ mol L}^{-1}$.

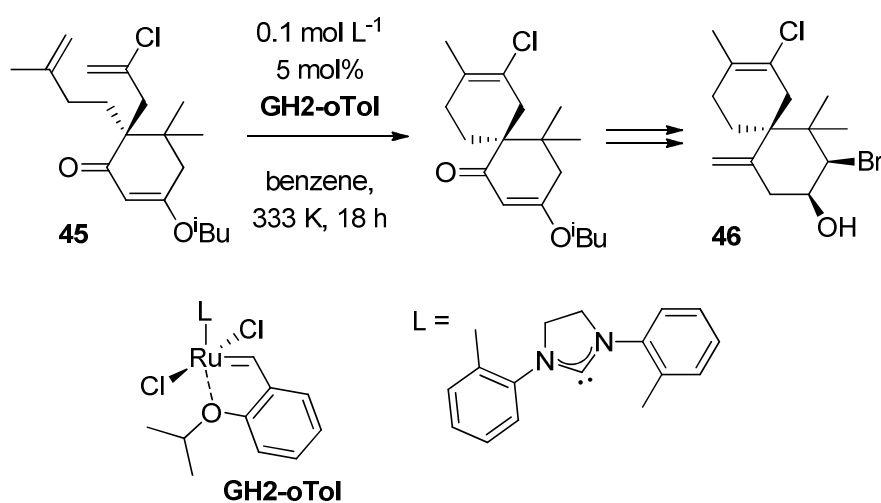
Decomposition Promoted by Functional Groups

Certain functionality is not well tolerated by ruthenium metathesis catalysts. For example, carbenium species **42** and phosphonium alkylidene **43** were obtained from the reaction mixture when **G2** was exposed to vinyl chloride compounds in benzene at room temperature, rather than species **44** (Scheme 1.15).

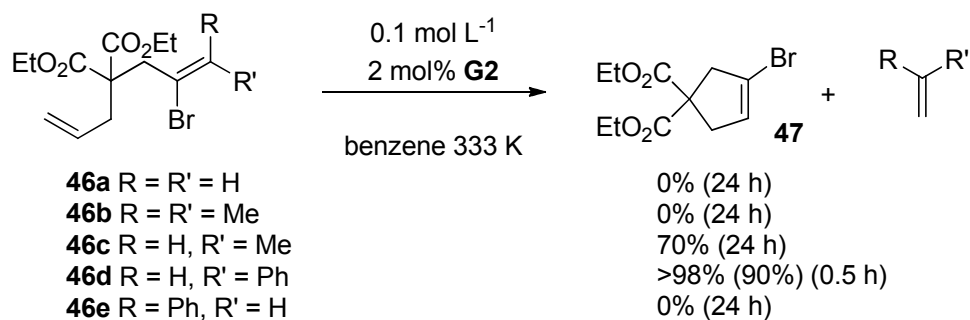


Scheme 1.15⁸²

The metathesis of vinyl halides is possible⁸³ but does not always proceed smoothly due to the potential for the formation of by-products from the intermediate carbene species. While examples of successful metathesis reactions of vinyl chloride substrates are known, these do not require formation of an α -chloro alkylidene. Stoltz *et al.* have successfully conducted RCM of dienyl chloride **45** *en route* to the natural product elatol **46** (Scheme 1.16),⁸⁴ while Dorta *et al.* have reported the ring-closing metathesis of vinyl bromides, provided that a phenyl moiety is also present *cis*- to the bromide (Scheme 1.17; results listed as conversion after (time period), with only one isolated yield reported);⁸⁵ substrates **46a-e** were all tested, but only diene **46d** achieved complete

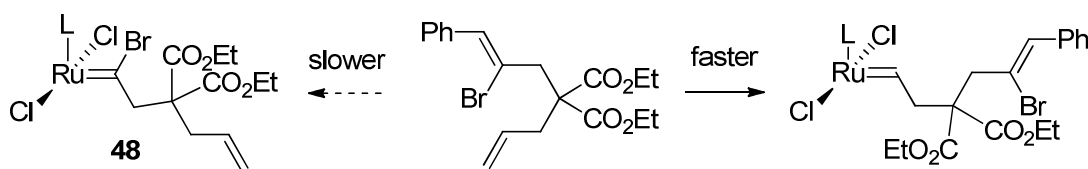


Scheme 1.16⁸⁴



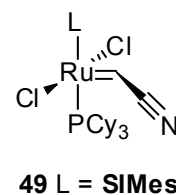
Scheme 1.17⁸⁵

conversion to product **47**. However, in both of these examples the formation of halomethylidene complexes such as **48** might be avoided if the ruthenium alkylidene reacts with the alternative terminus first (Scheme 1.18).

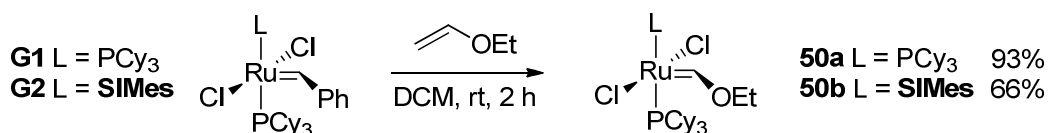


Scheme 1.18

The metathesis of acrylonitrile has been reported, but typically requires more active pre-catalyst systems; Grubbs *et al.* reported that phosphane-free pre-catalyst **G2-3BrPy** was an effective pre-catalyst for acrylonitrile metathesis, as the formation of (poorly active) phosphane-bound ruthenium carbene species **49** was avoided.¹⁴

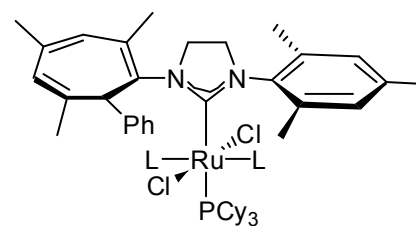


The metathesis of vinyl ethers yields low energy Fischer carbene species such as **50** (Scheme 1.19). Such complexes are not metathesis active unless heated to temperatures of *ca.* 323 K, at which point decomposition can compete with metathesis.⁴⁴ In contrast, some molybdenum pre-catalyst systems can effect cross-metathesis between alkenes and vinyl ethers.⁸⁶



Scheme 1.19⁴⁴

Strongly co-ordinating groups, such as carbon monoxide and isocyanates, have been found to trigger decomposition of metathesis catalysts. Diver reported that exposing **G2** to carbon monoxide caused insertion of the carbene moiety into the aromatic ring of the NHC.⁸⁷



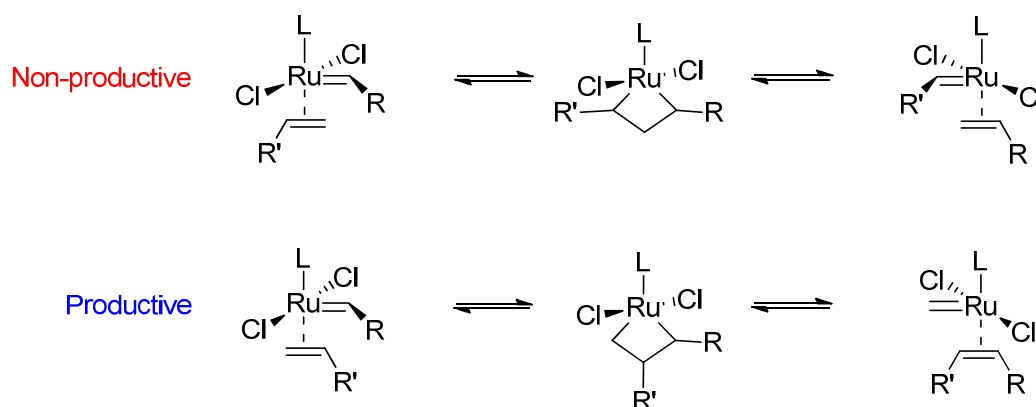
51a L = CO
51b L = CNCH₂CO₂K

Complexes **51** has been isolated and characterised. Isocyanates have been utilised to remove metathesis catalysts from solution to enable kinetic studies; complexes such as **51** can be removed from reaction mixtures by column chromatography.⁸⁸

Non-productive Events in Metathesis

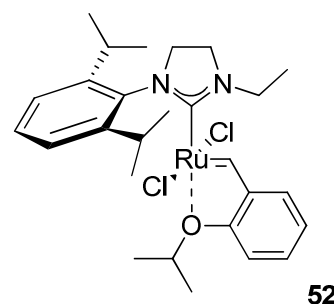
The two pathways in **Scheme 1.02** result in the synthesis of either a cycloalkene or an oligomeric species. However, non-productive metathesis pathways are available which do not yield metathesis products, but which may affect the rate of reaction by sequestering active catalyst. Metallocyclobutanation can occur in two different ways (**Scheme 1.20**); one η^2 -complex can undergo metallocyclobutanation to result in productive metathesis (i.e. a new product), while the other cannot. However, this will only have an effect on the rate of metathesis if the equilibrium constant for non-productive MCB formation is large enough to sequester quantities of active catalyst. If the equilibrium constant for this MCB formation is small, the non-productive cycles will have little or no effect on the overall reaction rate.

A detailed study of different pre-catalysts by Grubbs *et al.* has revealed that the relative numbers of productive *versus* non-productive catalytic cycles are highly pre-



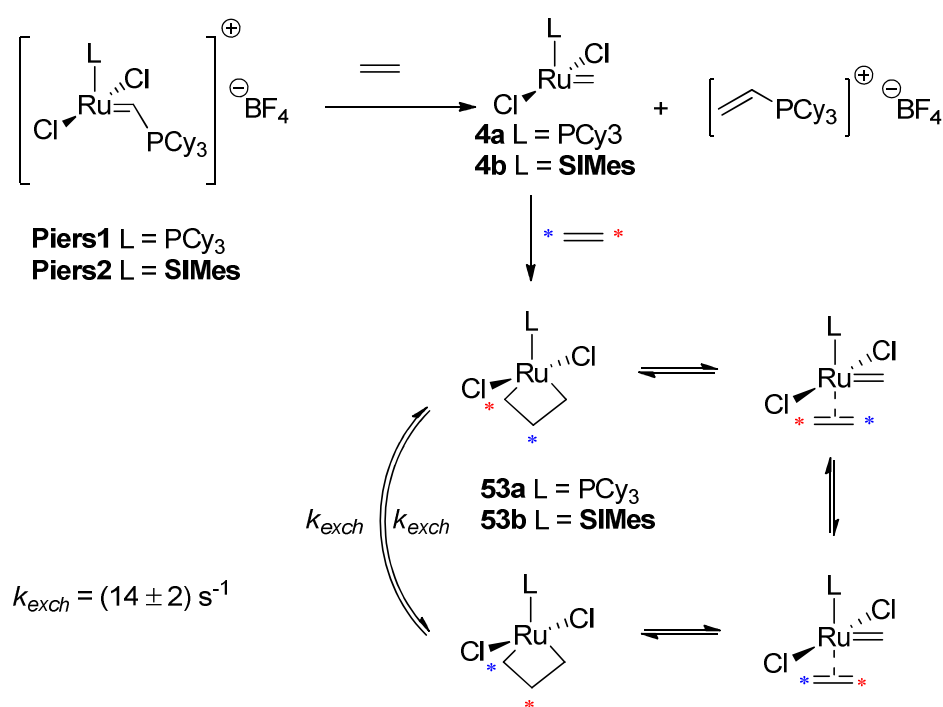
Scheme 1.20

catalyst dependent, with pre-catalysts bearing asymmetric NHC ligands, such as **52**, often performing as many non-productive cycles as productive cycles.⁸⁹ Pre-catalysts such as **G2** and **GH2** typically performed 10 productive turnovers per non-productive turnover. Non-productive cycles can also occur off the pathway of the desired



metathesis transformation. Piers *et al.* reported the formation of MCB **53b** at low temperatures (223 K) from the reaction of pre-catalyst **Piers2** and approximately 2 equivalents of ethene (**Scheme 1.21**); analogous MCB **53a** could not be observed.

Using ¹H EXSY experiments, the rate of the degenerate exchange of ethene at 223 K was quantified at $(14 \pm 2) \text{ s}^{-1}$.³³ In addition, later work has allowed the measurement of approximate relative energies, revealing that MCB **53b** is considerably lower on the PES than most other species.¹⁵ While pre-catalysts are typically still *ca.* 10 kcal mol⁻¹ lower on the PES than MCBs,⁵³ phosphane species are present in relatively low concentrations in metathesis reactions; the maximum concentration of phosphane present in metathesis reaction mixtures depends on the proportion of the pre-catalyst that has undergone initiation at that time. In contrast, the metathesis of α,ω -dienes produces up to one equivalent of ethene, which can then potentially sequester active



Scheme 1.21

Substrate Structure and Reactivity

While the choice of catalyst system can influence the reaction outcome, substrate structure also exerts an effect. The scope and limitations of the alkene ring-closing metathesis reaction can be divided broadly into three categories: functional group tolerance, alkene substitution pattern, and target ring size. The former two of these are typically determined by the catalyst system employed, while the latter can be considered in the context of general ring-closing chemistry.

Functional Group Tolerance

The functional group tolerance of ruthenium carbene (pre)-catalysts is excellent when compared to alternative systems, leading to their application in the syntheses of various interesting and useful compounds, including heterocycles containing oxygen,⁹² sulfur,⁹³ nitrogen⁹² and phosphorus.⁹³ The use of metathesis in natural product synthesis, often applied to intermediates that are densely functionalised, is widespread.^{3,94-95} While few specific functional groups can completely halt metathesis (*vide supra*), the substitution pattern of metathesis substrates can result in challenging reactions (*vide infra*).

Target Ring Size

Before considering the synthetic literature, which provides insight into the relative ease with which different ring sizes can be prepared, it is important to consider both how cyclisation efficiency can be best measured, and what outcomes a theoretical treatment of cycloalkene thermodynamic data would predict.

Intra- versus Inter-molecular Metathesis

While all metathesis reactions consist of a series of [2+2]cycloadditions and retro[2+2]cycloadditions, the metathesis of diene substrates can follow parallel pathways (**Scheme 1.02** on page 4); both pathways proceed *via* a formally reversible series of steps. After one turnover, both pathways start *via* the cross-metathesis of the catalyst species (methylidene **4** when the common case of α,ω -diene metathesis is considered) with a molecule of diene to yield a new alkylidene, referred to herein as the propagating carbene, plus a by-product alkene. This by-product is typically a small volatile alkene such as ethene (during α,ω -diene metathesis) which usually has the opportunity to egress

a refluxing reaction solution, and that will be removed easily during the work-up and purification of the reaction mixture. However, ethene does accumulate in solution at 298 K⁹⁶ and egresses slowly⁹⁷ so is available in solution, enabling the reverse reaction to occur. In target synthesis, it is usually the cycloalkene that is desired, but it is the fate of the propagating carbene that determines the mixture of cycloalkene and oligomer that is obtained from the reaction.

Two pathways are possible in the metathesis of α,ω -dienes. The *intramolecular* pathway proceeds *via* cyclic η^2 -complex formation with the alkene terminus of the propagating carbene, with rate constant k_{intra} . This rate constant will be a function of the chain length, as this dictates both the enthalpic and entropic cost of intramolecular η^2 -complex formation and the overall thermodynamics of cycloalkene formation.⁵³ The rate will also depend on the propagating carbene concentration (**Equation 1.02**). The rate of *intermolecular* metathesis will depend on the rate constant k_{inter} , which should be the same for α,ω -dienes with a similar substitution pattern but differing chain length.⁹⁸ The rate will also depend on the propagating carbene concentration and, crucially, the diene concentration (**Equation 1.03**).

$$v_{intra} = k_{intra} \cdot [\text{propagating carbene}] \quad (1.02)$$

$$v_{inter} = k_{inter} \cdot [\text{propagating carbene}] \cdot [\text{diene}] \quad (1.03)$$

High diene concentrations will favour the intermolecular pathway over the intramolecular pathway, because the rate expression for the latter does not include a diene concentration term, and will therefore shift the ratio of products towards oligomer. It is for this reason that ADMET reactions are often conducted neat by polymer chemists, because the oligomers (or larger polymers) are the desired products from these reactions.⁹⁹ However, a bimolecular reaction is required to form the propagating carbene initially, so if the reaction is conducted under conditions which are too dilute, the overall conversion of diene will be low.¹⁰⁰

The partitioning of the propagating carbene between intra- and inter-molecular metathesis pathways is quantifiable using the concept of effective molarity (EM) (*vide supra*).

Measuring Cyclisation Efficiency using the Effective Molarity

Yield measurements, based on the recovery of purified products, are the most commonly reported indicator of the success of synthetic reactions, and provide a good guide as to the overall efficiency and effectiveness of a synthetic procedure. However, the yield will be affected by factors at a number of stages of the reaction, including the quality of the reagents, solvents, vessels and catalysts employed, the effectiveness of the actual chemical reactions that occur, and the isolation and purification of the reaction product(s). Hudlicky *et al.* have shown that losses upon work-up and purification can introduce significant errors into yield determinations.¹⁰¹ In addition, methods commonly used to assess purity in synthetic organic chemistry laboratories (e.g. ¹H and ¹³C NMR spectroscopy or mass spectroscopy) will not detect all possible contaminants such as inorganic salts. Therefore, techniques which require minimal work-up and purification, and which include quantification using an internal standard, are optimal when seeking to interrogate reaction outcomes quantitatively.⁹⁶ The development and application of a method for studying RCM kinetics is documented in Chapter 2.

Intramolecularity can accelerate chemical reactions by bringing the reacting groups together. The entropic cost of an intramolecular reaction is often less than that of the corresponding intermolecular reaction; if the loss of rotational entropy for the (otherwise free to rotate) bonds frozen is less than the translational and rotational entropy of a molecule of substrate, the intramolecular reaction is entropically favourable. The enthalpic implications of cyclisation can be favourable (if strain in the acyclic compound is relieved) or unfavourable (if strain is introduced). The advantage of intramolecularity therefore depends on the entropic and enthalpic costs of cyclisation *versus* oligomerisation.

The yield of a reaction such as RCM, in which the partitioning between intra- and inter-molecular pathways depends acutely on the reaction concentration, will vary depending on the concentration that the reaction was conducted at. A better metric for cyclisation efficiency is the effective molarity (EM), which is concentration-independent and therefore can be used to predict the outcome of a reaction conducted at a given concentration (*vide infra*). Kirby describes the EM as “*formally the concentration of the catalytic group required to make the intermolecular reaction go at the observed rate of the intramolecular process*”.¹⁰² In the context of metathesis, the effective molarity is the concentration of diene at which cyclisation and oligomerisation will occur at the same rate, and therefore

give a 1:1 mixture of the target cycloalkene and oligomeric material. Two forms of the effective molarity have been explored in ring-closing chemistry.¹⁰² The kinetic EM (**Equation 1.04**) is a ratio of the *rate constants* for intra- and inter-molecular reaction, while the thermodynamic EM (or EM_T) is a ratio of the corresponding *equilibrium constants* (**Equation 1.05**).¹⁰² A suitable intermolecular reaction must occur *via* the same mechanism and result in the same overall chemical change.

$$\text{(kinetic)} \quad \text{EM} = k_{\text{intra}}/k_{\text{inter}} \quad \text{(1.04)}$$

$$\text{(thermodynamic)} \quad \text{EM}_T = K_{\text{intra}}/K_{\text{inter}} \quad \text{(1.05)}$$

While the effective molarity has units of mol L⁻¹, the EM is not always a physically attainable concentration. In terms of metathesis chemistry, the EM represents the reaction concentration at which a 1:1 mixture of cycloalkene and oligomer would be expected; i.e. the concentration at which the intra- and intermolecular reactions occur at the same rate (for EM) or with the same equilibrium position (for EM_T). Therefore, in order to avoid deleterious oligomerisation processes, metathesis reactions should be conducted at a concentration of *ca.* a tenth to a hundredth of EM (or EM_T).

Although the kinetic and thermodynamic effective molarities can be quite similar for a given cyclisation, they are often very different.¹⁰² The EM and EM_T for a given cyclisation are related to the free energy changes (and therefore the enthalpy and entropy changes) incurred when progressing from the starting material to the cyclisation transition state (**Equation 1.06**) and the final product respectively (**Equation 1.07**).¹⁰³ In this way, the EM can be separated into contributions from enthalpy (EM_H) and entropy (EM_S) (**Equations 1.08** and **1.09**). EM is a useful descriptor because the actual chemical process is factored out. Ruzicka has hypothesised that the probability of end-to-end reactions in a bifunctional monomer and the ring strain introduced by that

$$k_{\text{intra}} = (\kappa_B T/h) \cdot \exp(-\Delta G^\ddagger/RT) \quad \text{(1.06)}$$

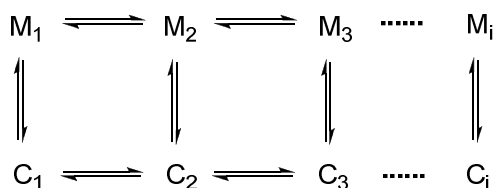
$$K_{\text{intra}} = \exp(-\Delta G^\circ/RT) \quad \text{(1.07)}$$

$$\begin{aligned} \text{EM} &= \exp(-(\Delta G^\ddagger_{\text{intra}} - \Delta G^\ddagger_{\text{inter}})/RT) &= \exp(-\Delta\Delta G^\ddagger/RT) \\ &= \exp(-\Delta\Delta H^\ddagger/RT) \cdot \exp(\Delta\Delta S^\ddagger/R) &= \text{EM}_H^\ddagger \cdot \text{EM}_S^\ddagger \end{aligned} \quad \text{(1.08)}$$

$$\begin{aligned} \text{EM}_T &= \exp(-(\Delta G^\circ_{\text{intra}} - \Delta G^\circ_{\text{inter}})/RT) &= \exp(-\Delta\Delta G^\circ/RT) \\ &= \exp(-\Delta\Delta H^\circ/RT) \cdot \exp(\Delta\Delta S^\circ/R) &= \text{EM}_H^\circ \cdot \text{EM}_S^\circ \end{aligned} \quad \text{(1.09)}$$

reaction are independent.⁹⁸ Therefore, when comparing the rates of intra- and intermolecular reaction, the bond-breaking and bond-forming steps are the same and so cancel out. The thermodynamics of these bond-breaking and bond-forming reactions do not contribute to the thermodynamic values ($\Delta\Delta H$ and $\Delta\Delta S$) which determine EM.

Ercolani *et al.* considered a more complex case (which is relevant to metathesis chemistry), in which the monomer M_1 can undergo oligomerisation to $M_2, M_3 \dots M_i$, and where each chain can cyclise to form a corresponding cyclic species C_i (**Scheme 1.23**).¹⁰⁴



Scheme 1.23

The equilibrium between linear M_i and the corresponding cyclic species C_i can be described using EM_i (**Equations 1.10** and **1.11**). The intermolecular reaction is based upon the analogous intermolecular reaction involving the same reacting groups. If the activity of the end groups is independent of the length of the chain (as hypothesised by Ruzicka)⁹⁸, then the reaction of iM_1 to form a linear species M_i can be related to the intermolecular reaction equilibrium (**Equation 1.12**); there is an equilibrium between iC_1 and C_i (**Equation 1.13**) and hence K_{ci} can be expressed in terms of two effective molarities (**Equation 1.14**); this ratio is known as the modified thermodynamic effective molarity (MEM_T). This allows quantification of the equilibrium position between C_1 and C_i using a metric that is independent of the reaction concentration and that does not require the concentrations of other species present to be quantified. However, MEM_T is far harder to relate to a practical meaning; while EM_T effectively allows the chemist to

$$EM_i = [K_{(intra)i}] / K_{inter} \quad (1.10)$$

$$K_{(intra)i} = [C_i] / [M_i] \quad (1.11)$$

$$K_{1i} = [M_i] / [M_1]^i = (K_{inter})^{i-1} \quad (1.12)$$

$$K_{ci} = [C_i] / [C_1]^i \quad (1.13)$$

$$\begin{aligned}
 K_{ci} &= (K_{inter})^{(i-1)} \cdot (K_{(intra)i}) / (K_{(intra)1})^i = EM_i' (EM_1)^i \\
 &= MEM_T \quad (1.14)
 \end{aligned}$$

choose the most appropriate initial reaction concentration, MEM_T does not relate so easily to the optimum reaction concentration. The EM or EM_T for the specific target compound of interest is far more useful.

Mandolini *et al.* have studied the topic of EM extensively, and have analysed a wide range of data from the literature. Through these empirical studies, they have shown that EM_T can be estimated in a relatively straightforward manner from the strain energy of the product cycloalkene (the enthalpic consequences, **Equation 1.15**) and the number of rotors frozen (the entropic consequences).¹⁰³

$$\Delta\Delta H^\circ = -(\Delta H^\circ_{\text{intra}} - \Delta H^\circ_{\text{inter}}) \approx H_{\text{strain}} \quad (1.15)$$

Ring strain is typically introduced during cyclisation due to three effects: angle strain, torsional strain and transannular interactions. Angle strain results when the bond angle is forced away from the lowest energy angle. For example, in methane, the bond angles are approximately 109.5° (the favoured bond angle for sp^3 centres), but if two substituents on an sp^3 centre are tethered by a ring, this angle may be perturbed (**Figure 1.07 (a)**). Torsional strain occurs when a molecule cannot, due to being tethered in a ring, adopt a conformation that allows it to avoid unfavourable eclipsing interactions (**Figure 1.07 (b)**); the eclipsed conformation is the most strained, followed by the *gauche* conformation, unless a specific effect relieves some of this strain. The third contribution to ring strain comes from transannular interactions, where substituents that are not on

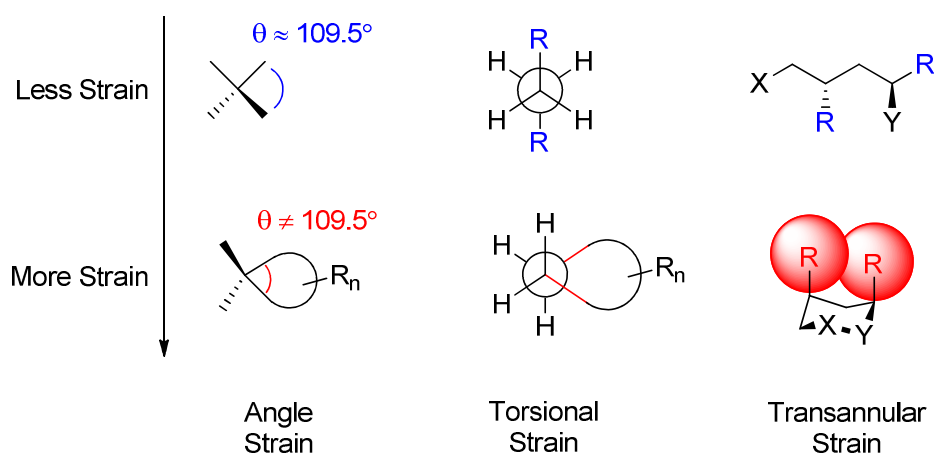
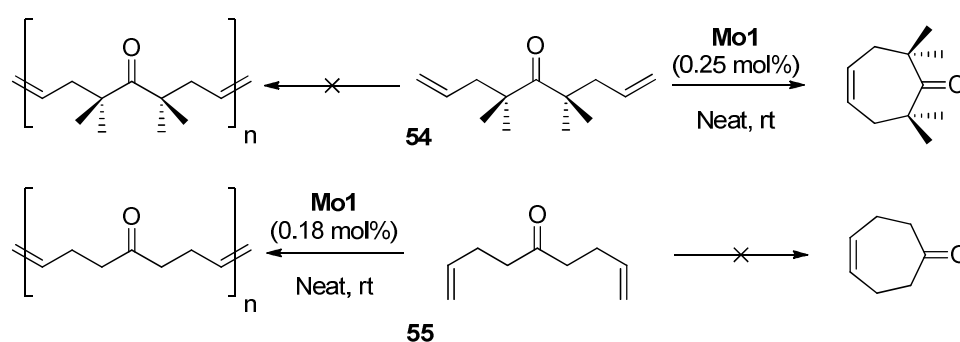


Figure 1.07. The three effects that contribute to ring strain: (a) angle strain, (b) torsional strain, and (c) transannular interactions.

adjacent ring atoms are forced into van der Waals contact due to the conformation of the ring (**Figure 1.07 (c)**). The relative influence of these factors will depend on the substitution pattern and size of the ring. In small rings (3-4 membered), bond angle distortion dominates, while eclipsing interactions dominate in common rings (5-7 membered) and transannular interactions dominate in medium rings (8-10 membered).

Cyclisations do not necessarily always *introduce* strain; in some cyclisations, strain can be relieved so that $\Delta\Delta H < 0$. For example, Forbes *et al.* reported the complete cyclisation of dienone **54** when a neat sample was exposed to a molybdenum-based metathesis catalyst, but complete oligomerisation of analogous **55** was obtained (**Scheme 1.24**). Relief of strain in the acyclic form is likely a driving force for cyclisation.



Scheme 1.24¹⁰⁵

The entropic cost of ring closing depends on how many rotors are frozen upon cyclisation; the entropy of rotation around the σ -bonds will be lost in small (three- and four-membered), common (five- to seven-membered) and medium (eight- to ten-membered) rings. In the formation of such rings, the entropic cost of cyclisation is *ca.* 4 cal K⁻¹ mol⁻¹ per rotor. Macrocycles do not suffer such an entropic penalty per rotor, as the less rigid structure retains more of the rotational entropy (**Figure 1.08**); the entropic cost per rotor in such cyclisations is *ca.* 1 cal K⁻¹ mol⁻¹. Mandolini *et al.* have shown empirically that for ring-closing reactions where fewer than eight rotors (rotatable bonds, denoted r) are frozen upon cyclisation, the value of $\Delta\Delta S^\circ$ (in cal K⁻¹ mol⁻¹) can be calculated from **Equation 1.16**. Taking into account **Equations 1.15** and **1.16**, **Equation 1.09** can be rewritten as **Equation 1.17**, for ring formation where fewer than eight rotors are frozen. Therefore, the advantage of intramolecularity in the metathesis of diene substrates lies in the difference in the entropic cost of cyclisation *versus* the

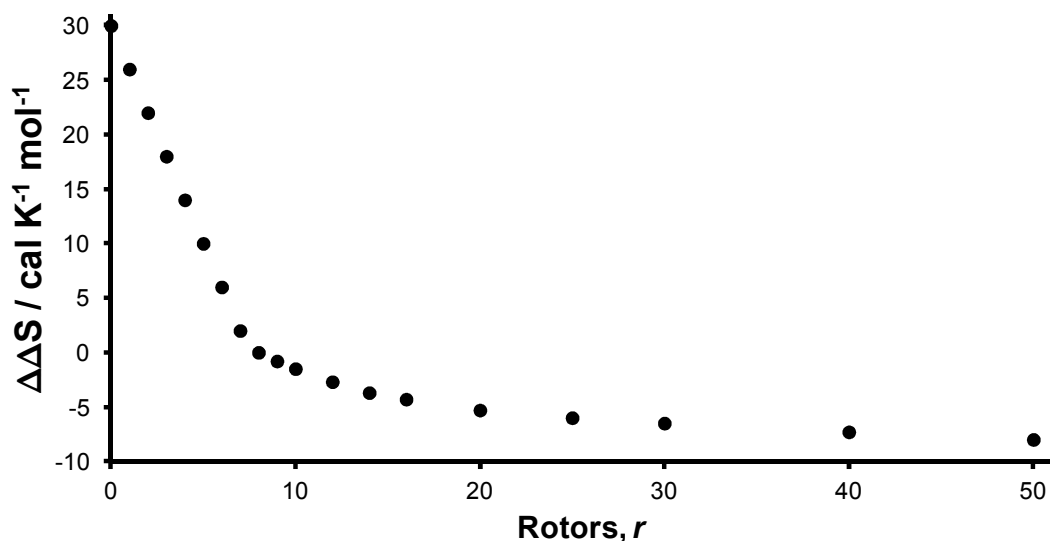


Figure 1.08. Entropic benefit of intramolecular reaction ($\Delta\Delta S$) *versus* number of rotors (rotatable bonds) frozen upon cyclisation.¹⁰³

$$\Delta\Delta S^\circ = 30 - 4r \quad (1.16)$$

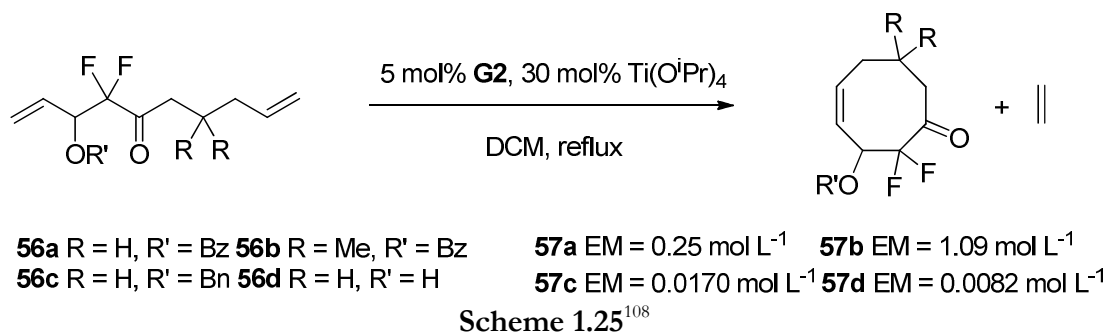
$$\ln EM_T = (H_{\text{strain}}/RT) \cdot ((30 - 4r)/R) \quad (1.17)$$

entropic cost of oligomerisation. The latter is *ca.* 30 - 50 cal K⁻¹ mol⁻¹ and therefore the entropic advantage of cyclisation is diminished with increasing ring size.^{103,106} For most cyclisations, there is a maximum (entropy-limited) EM where, if $H_{\text{strain}} = 0$ and therefore $EM_H = 1$, EM would equal EM_S , which is determined by the entropic cost of ring-closing alone. Cyclisations in which strain in the acyclic form is relieved (*vide infra*) are an exception to this; $\Delta\Delta H$ will then depend on the strain *relieved* by cyclisation and may therefore yield EM_H greater than unity.

Effective Molarity in Metathesis Chemistry

Quantification of reaction outcomes using metrics such as EM could allow a vast number of RCM reactions, with different substrates, catalyst systems and solvents, to be compared using the same scale. EM_T is a quantity that is intrinsic to a given cyclic molecule, and should be completely independent of the reaction used to create it,¹⁰⁷ while the kinetic EM of a cyclic compound *will* depend on the reaction that is used to create it. The quantification of EM and EM_T values allows the effects of changing substrate structure to be surveyed in different ways.

There are very few measured EMs for RCM reactions. Percy *et al.* quantified EM for the RCM of substrates **56** to form cyclooctenones **57** using a series of synthetic experiments, in which the RCM reactions of several substrates were conducted at a range of initial substrate concentrations for a fixed period of time (**Scheme 1.25**).¹⁰⁸



Careful quenching of the active ruthenium complexes was followed by accurate quantification of cyclic product and oligomer using gas chromatography (GC). The same method was used to allow the relative rates of RCM of each substrate to be determined from aliquots taken from a reaction mixture at different time points (**Figure 1.09**). A range of EMs was obtained, covering two orders of magnitude. Rate differences

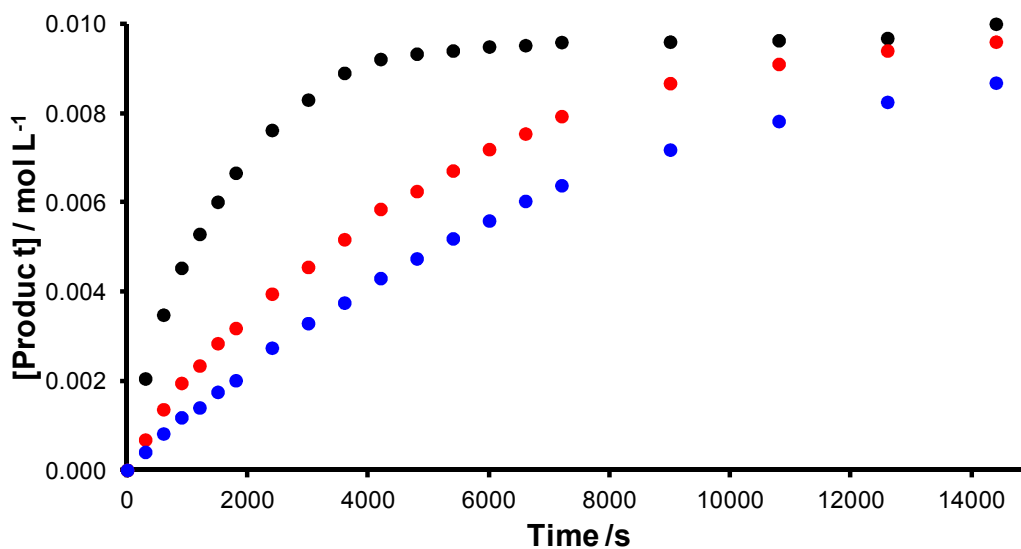


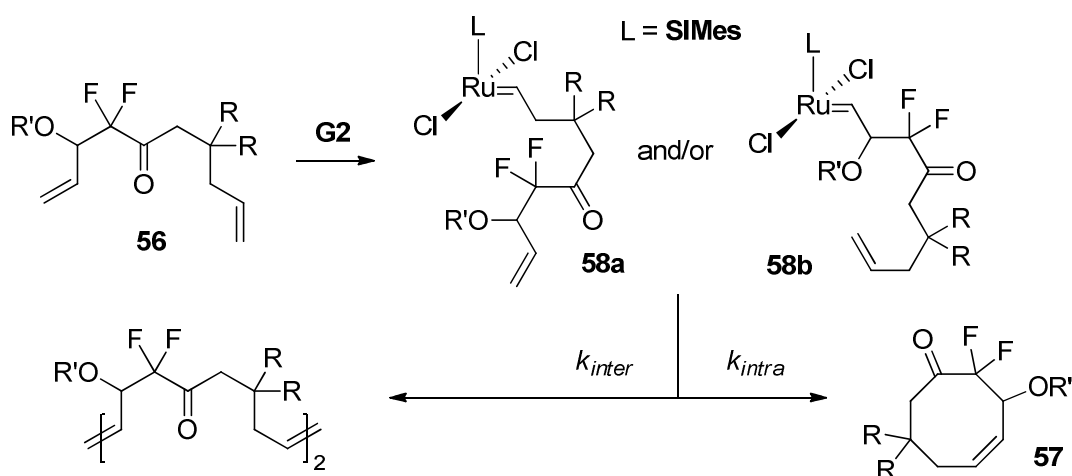
Figure 1.09. Concentration/time data for the production of products **57d** (R = H, black circles), **57a** (R = Bz, red circles) and **57c** (R = Bn, blue circles) from the three diene RCM reaction of **56d**, **56a** and **56c**, with 30 mol% Ti(OⁱPr)₄ and 6 mol% **G2** in DCM at reflux.¹⁰⁸

were more modest, with a *ca.* six-fold spread of $t_{1/2}$. Importantly, protecting groups provide an opportunity to improve cyclisation efficiency without altering the structure of the final target compound. For this reason, increased understanding about the effects protecting groups can exert on EM is very valuable to the synthetic chemist.

Kinetic EMs were quantified from the ratio of cyclic product to cross-metathesis product over a range of concentrations which allowed the evaluation of the kinetic *efficiency* of these reactions (i.e. the rate at which cyclisation occurs with respect to cross-metathesis). Two key conditions were met: the reactions were shown to be effectively irreversible, as exposing the eight-membered ring products to the reaction conditions did not result in ring-opening to form oligomeric material; it is known that all steps up to propagating carbene formation are common to both the cyclisation and oligomerisation pathways (see the mechanism in **Scheme 1.02**) and so the reaction of the propagating carbene is product-determining, although two different propagating carbenes can form which may have different reactivity. The ratio of intra- to intermolecular product yields an expression which can be rearranged to allow EM to be determined from a linear plot of [cyclic product]/[oligomer] *versus* the reciprocal of initial diene concentration (**Scheme 1.26** and **Equation 1.18**; $[58] = [58a] + [58b]$).

These data show that the protecting group can have a profound effect on the

$$\begin{aligned}
 [\text{cycloalkene}]/[\text{oligomer}] &= k_{\text{intra}} \cdot [58] / k_{\text{inter}} \cdot [58][\text{diene}] \\
 &= k_{\text{intra}} / (k_{\text{inter}} \cdot [\text{diene}]) \\
 &= \text{EM} / [\text{diene}] \qquad (1.18)
 \end{aligned}$$



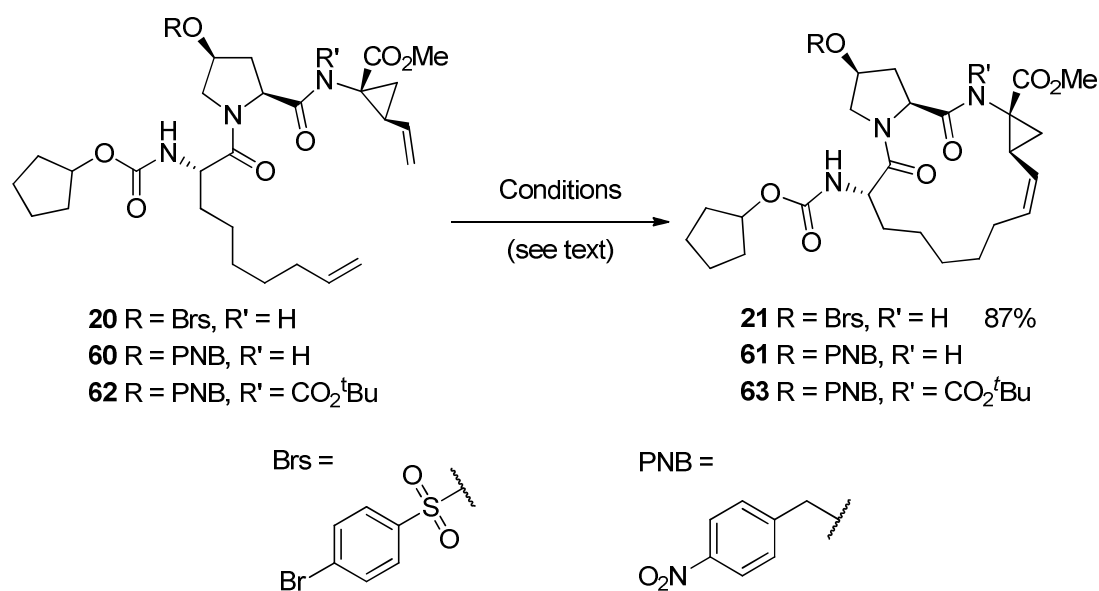
Scheme 1.26

reaction rate and efficiency and, importantly, that these two outcomes may be affected differently. Protecting group selection that may otherwise seem trivial may well prove important when considering the RCM step.

This treatment of data is not universally applicable, as it requires that the observed product ratio is the *kinetic* ratio of products, not the *thermodynamic* ratio; if there is inter-conversion between reaction products then the observed product distribution does not reflect $k_{intra}/(k_{inter}[\text{diene}])$ and the treatment does not hold.

For reactions that are under thermodynamic control, alternative approaches must be used. Chemists at Boehringer-Ingelheim have prepared HCV protease inhibitor **59**, using an RCM reaction as a key step (Scheme 1.27).^{68,109-111} The first generation process involved RCM of substrate **20** (at *ca.* 14 mmol L⁻¹) using 3 mol% **GH1** in toluene at 353 K,^{68,109} but the high dilution rendered this process difficult to scale up.

The EM of analogous substrate **60** was quantified using the method of Percy *et al.* described above,¹⁰⁸ and was found to be 46 mmol L⁻¹ (for reaction at 313 K in DCM).¹¹¹ Quantification was achieved by analysis of the crude reaction mixture after work-up, but the results were sufficient to establish that reaction conditions well below 50 mmol L⁻¹

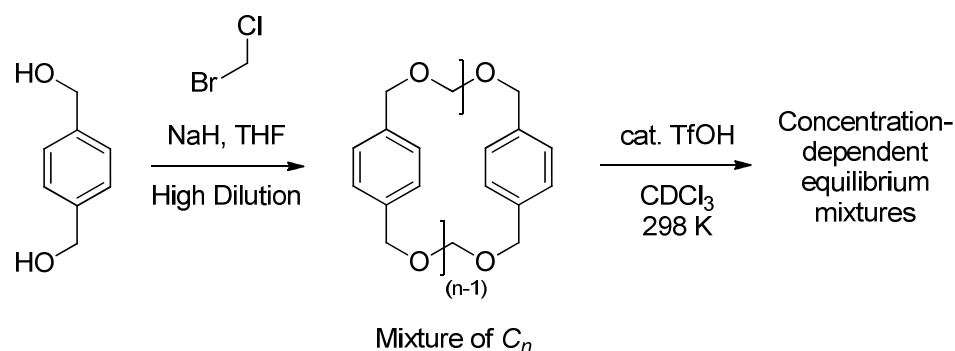


Scheme 1.27^{68,109-111}

were needed to obtain the desired macrocyclic product **61** selectively. Changes to the metathesis step could not be assessed by quantifying the EM, as the pre-catalyst was changed to **Grela**, which operates in the thermodynamic regime rather than the kinetic regime. Instead, MEM_T was quantified, providing a quantitative metric for cyclisation efficiency. The cyclisation of substrate **60** proceeded in toluene at 333 K (with 3 mol% **GHI**) with MEM_T of 0.096 mol L⁻¹. Substrate **62**, in which the cyclopropylamide functionality was protected as the corresponding *tert*-butyl carbamate (BOC), underwent RCM (at a concentration of 0.2 mol L⁻¹ in toluene) at 60°C with 0.1 mol% **Grela** to form product **63**; MEM_T was found to be 1.85 mol L⁻¹. A further increase in the reaction temperature (to 383 K) increased MEM_T further, to 2.56 mol L⁻¹. The considerable difference in MEM_T between substrates was attributed to the calculated reduced strain energy of the BOC-protected product, with respect to the diene;¹¹⁰ i.e. protection of the nitrogen decreases H_{strain} and therefore increases the MEM_T of the desired product.

From a process chemistry perspective, quantitative understanding of reaction efficiency is critical to enable meaningful and straightforward comparisons of reaction conditions. Particularly on a large scale, where techniques such as column chromatography would render a process prohibitively expensive, the formation of side products must be minimised to aid expeditious purification of reaction products. For the pharmaceutical industry, the presence of even small levels of impurities poses serious safety and toxicity issues for patients and therefore regulatory controls on pharmaceutical materials are very stringent. It should be noted that, while some studies show high turnover numbers with low catalyst loadings but not necessarily complete conversion, the resulting mixtures of starting materials and products can complicate purification.

As discussed previously, MEM_T lacks a clear practical meaning for synthetic chemists, and therefore the use of EM_T is preferable. Few MEM_T values have been measured, making it difficult to put these measured values into context. A method for determining EM_T from reactions under thermodynamic control has been developed by Mandolini *et al.*. Cyclophane syntheses were carried out under kinetic control (under anionic conditions) (**Scheme 1.28**); the acetal products were then equilibrated under acid catalysis. The acid-catalysed equilibration was conducted with various initial effective monomer concentrations (4.35 to 82.2 mmol L⁻¹), and the concentration of each size of product ring was determined by integration of the ¹H NMR spectra; species



Scheme 1.28

up to tetramer could be identified as discrete products in the mixture. A plot of the concentration of each product *versus* the initial effective monomer concentration ($\sum(iC_i)$, where C_1 is monomer, C_2 is dimer, etc.) yielded a curve which reached a maximum at EM_T , so a parabolic function could be used to estimate this value (**Figure 1.10**). Some scatter was obtained, presumably due to difficulty in integrating signals that were close together on the ^1H NMR spectra.

We have used this method to quantify the EM_T of the cyclisations of prototypical dienes.⁹⁶ In two cases, EM_T could be obtained using this method. The concentrations of cyclopentene and cycloheptene from the metathesis reactions of 1,6-heptadiene and 1,8-nonadiene respectively were measured by integration of the ^1H

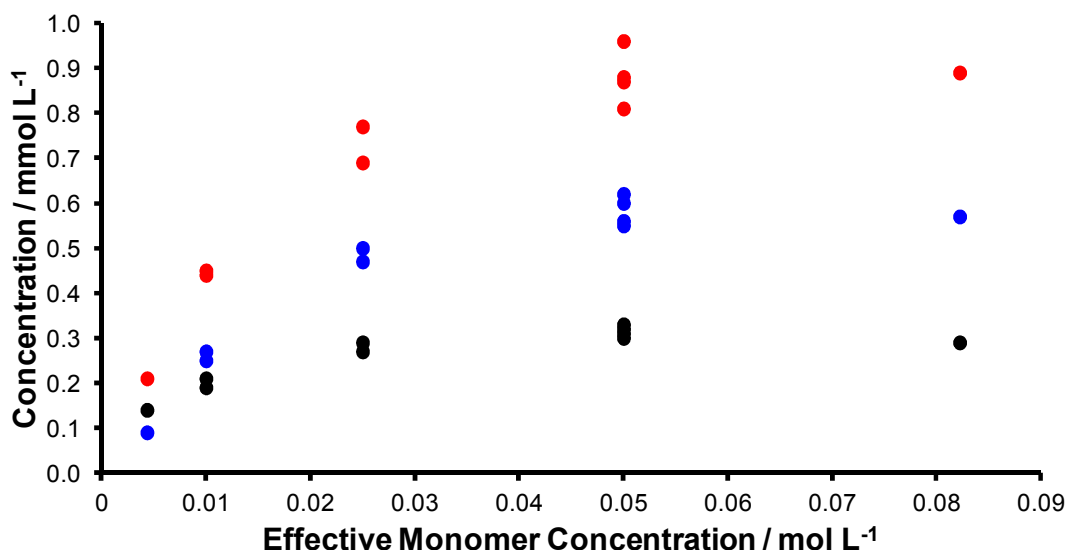


Figure 1.10. Concentrations of C_2 (black), C_3 (red) and C_4 (blue) obtained from the treatment of C_n at different concentrations with catalytic triflic acid (see **Scheme 1.28**).

NMR spectra of reactions conducted at a range of initial diene concentrations.⁹⁶ In the latter case, isomerisation-RCM processes (see chapter 4) removed material from the equilibrium due to the formation of cyclohexene, which does not undergo ring-opening in metathesis reactions.⁹⁰ Therefore, a plot of [cyclopentene] *versus* [1,6-heptadiene]₀ yielded EM_T (cyclopentene) = 538 mmol L⁻¹, while a plot of [cycloheptene] *versus* ([1,8-nonadiene]₀ - [cyclohexene]) yielded EM_T (cycloheptene) = 53 mmol L⁻¹ (**Figure 1.11**). This method for quantifying EM_T therefore has potential benefits in metathesis chemistry: if a series of RCM reactions are carried out at different concentrations, the maximum practical reaction concentration can be identified; if a synthetic preparation of cyclopentene or cycloheptene was desired, the reaction should be conducted at *ca.* 5 mmol L⁻¹ or 0.5 mmol L⁻¹ respectively, to ensure 100:1 selectivity for the cycloalkene over oligomer. Often, during synthetic campaigns, the reaction concentration is selected by trial and error, rather than being selected from consideration of measured EMs. In addition, if EM_T determination (or, at least, estimation) were to become routine in ring-closing metathesis studies, quantitative insight into the effect of different substrate structural features could be accumulated.

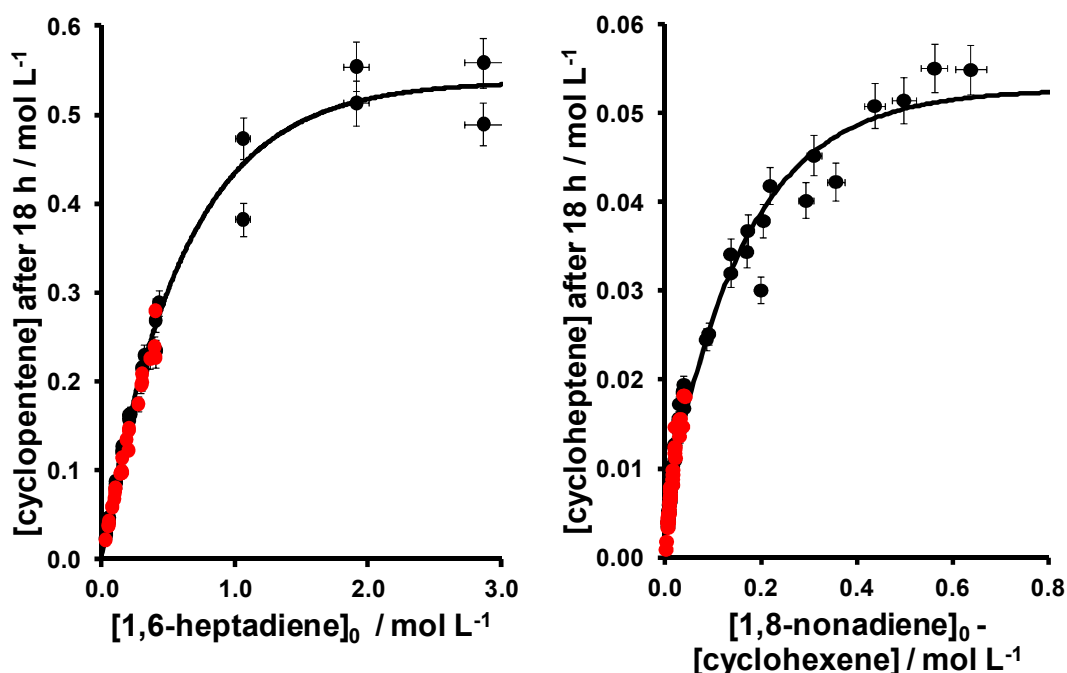


Figure 1.11. Concentrations of (a) cyclopentene in the RCM reactions of 1,6-heptadiene (0.025 – 3 mol L⁻¹) and (b) cycloheptene in the RCM reactions of 1,8-nonadiene after 18 hours at 298 K with 3 mol% **G2** in chloroform-*d* (**black**) or DCM-*d*₂ (**red**).⁹⁶

The quantification of reaction efficiency in metathesis chemistry is effectively limited to three examples, leaving considerable scope for further research in this area.

Prediction of EM_T from Thermodynamic Quantities

A theoretical treatment of literature data for the simplest possible cycloalkene compounds, which feature no additional functional groups, allows the investigation of the effect of ring size alone;⁹⁶ this approach requires calculation of EM_T for these species. As the strain energies of all of the products are known in the literature,¹¹² the calculation is straightforward, employing the method of Mandolini *et al.* whereby EM_H and EM_S are separated.¹⁰³ There is no relief of substrate strain upon cyclisation because all substrates are linear α,ω -dienes, therefore the approximation in **Equation 1.15** holds and H_{strain} can be used in place of $\Delta\Delta H^\circ$ (**Table 1.08**).

Cyclohexene is the least strained simple cycloalkene, and therefore has by far the largest EM_H . Cyclopentene, cycloheptene, *cis*-cyclooctene and *cis*-cyclodecene have similar strain energies, while *cis*-cyclononene is considerably more strained (due to transannular interactions). The *trans*-isomers of cyclooctene, cyclononene and cyclodecene are far more strained than the *cis*-isomers; under thermodynamic control, these would be equilibrated to the corresponding *cis*-stereoisomers.

The entropic cost of ring-closing to form these species can be evaluated by considering the number of rotors frozen upon cyclisation. The alkene bonds are not

Table 1.08. Calculation of EM_H for cyclopentene, cyclohexene, cycloheptene, *cis*- and *trans*-cyclooctene, *cis*- and *trans*-cyclononene and *cis*- and *trans*-cyclodecene.

Product Cycloalkene	$\Delta\Delta H^\circ \approx H_{\text{strain}}$ (kcal mol ⁻¹) ^a	EM_H (at 298 K)
Cyclopentene	5.0	2.15×10^{-4}
Cyclohexene	0.9	0.219
Cycloheptene	5.2	1.54×10^{-4}
<i>cis</i> -Cyclooctene	5.1	1.82×10^{-4}
<i>trans</i> -Cyclooctene	14.1	4.56×10^{-11}
<i>cis</i> -Cyclononene	8.5	5.83×10^{-7}
<i>trans</i> -Cyclononene	11.4	4.36×10^{-9}
<i>cis</i> -Cyclodecene	4.5	5.01×10^{-4}
<i>trans</i> -Cyclodecene	9.0	2.51×10^{-7}

^a From reference.¹¹²

free to rotate so for cyclisation to form an n -membered ring, $r = (n-1)$. EM_S can be evaluated from r using **Equation 1.16** above (**Table 1.09**). This results in a considerable spread of values, with EM_S decreasing by 7.4-fold for each additional rotor frozen upon cyclisation; the assumption is made in this calculation that *all* of the rotational entropy around the carbon-carbon single bonds is lost.

The EM_H and EM_S values can then be used to calculate EM_T (**Table 1.10** and **Figure 1.12**); plotting EM_H , EM_S and EM_T *versus* ring size n allows the effects of ring size to be understood graphically. The parent cycloalkenes are considered so that the differences in EM_T should be attributable to the ring size alone; the EM_T of substituted cycloalkenes will depend on the effects that the substitution patterns exert on the ring strain and the entropic contributions arising from rotation around σ -bonds. The values in **Table 1.10** for EM_T can provide estimates of the maximum concentration at which

Table 1.09. Predicting EM_S for cyclopentene, cyclohexene, cycloheptene, cyclooctene, cyclononene and cyclodecene.

Product Cycloalkene	Ring Size n	Rotors r	$\Delta\Delta S^\circ$ (cal K ⁻¹ mol ⁻¹) ^a	EM_S
		b		
Cyclopentene	5	4	14	1.1×10^3
Cyclohexene	6	5	10	1.5×10^2
Cycloheptene	7	6	6	20
Cyclooctene	8	7	2	2.7
Cyclononene	9	8	0	1.0
Cyclodecene	10	9	-0.8	0.67

^a From reference.¹⁰³ ^b Rotors frozen upon cyclisation.

Table 1.10. Predicting EM_T for cyclopentene, cyclohexene, cycloheptene, *cis*-cyclooctene, *cis*-cyclononene and *cis*-cyclodecene.

Product Cycloalkene	EM_H	EM_S	EM_T (mol L ⁻¹)	$\log_{10}(EM_T)$
Cyclopentene	2.15×10^{-4}	1.1×10^3	0.237	-0.63
Cyclohexene	0.219	1.5×10^2	32.9	1.52
Cycloheptene	1.54×10^{-4}	20	3.08×10^{-3}	-2.51
<i>cis</i> -Cyclooctene	1.82×10^{-4}	2.7	4.91×10^{-4}	-3.31
<i>cis</i> -Cyclononene	5.83×10^{-7}	1.0	5.83×10^{-7}	-6.23
<i>cis</i> -Cyclodecene	5.01×10^{-4}	0.67	3.36×10^{-4}	-3.47

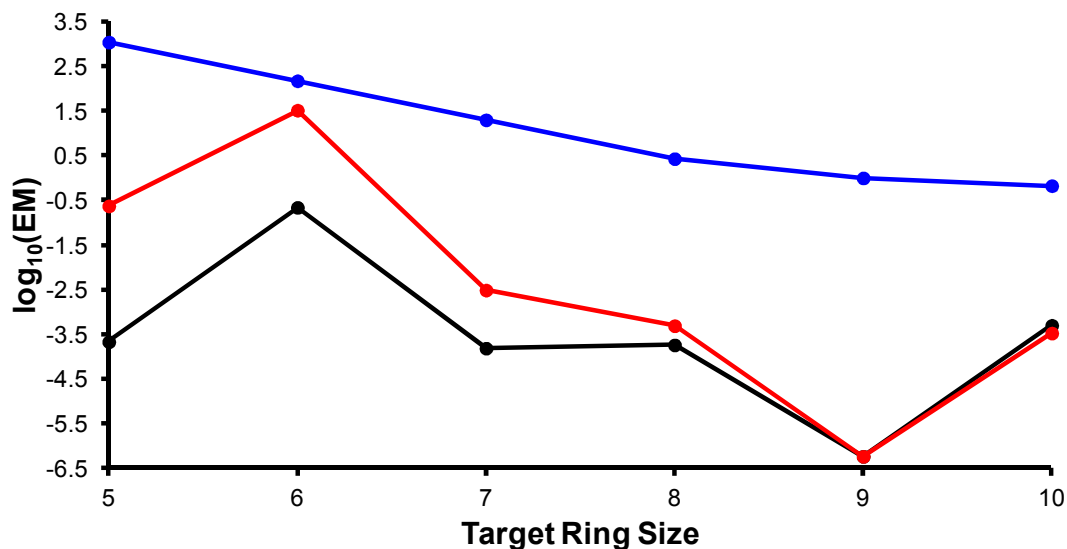


Figure 1.12. EM_H (black), EM_S (blue) and EM_T (red) for cyclopentene, cyclohexene, cycloheptene, *cis*-cyclooctene, *cis*-cyclononene and *cis*-cyclodecene.

Table 1.11. Maximum RCM concentrations at which 10:1 and 100:1 selectivity for cycloalkene over oligomer should be obtained, estimated from EM_T values in **Table 1.10**; units are mol L^{-1}

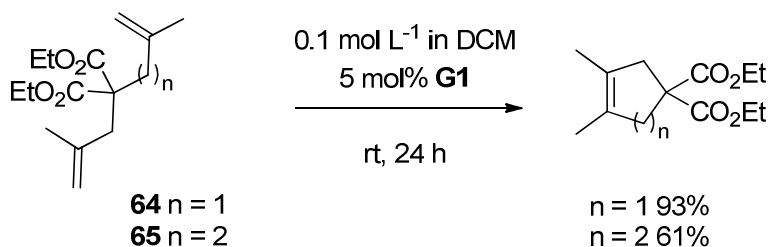
Ring Size	5	6	7	8	9	10
$[\text{diene}]_0$ (10:1)	0.024	3.3	3.1×10^{-4}	4.9×10^{-5}	5.8×10^{-8}	3.4×10^{-5}
$[\text{diene}]_0$ (100:1)	0.0024	0.33	3.1×10^{-5}	4.9×10^{-6}	5.8×10^{-9}	3.4×10^{-6}

the RCM reaction to form each product should be run (**Table 1.11**); values are calculated for 10:1 and 100:1 selectivity for cycloalkene over oligomer. The most straightforward metathesis reactions ought to be those that form six-membered rings, while it should be possible to prepare five-membered rings at practical concentrations (i.e. without high dilution conditions). Seven-, eight- and ten-membered rings would be expected to be challenging, while nine-membered rings should require very high dilution conditions.

Ring Size and Metathesis Efficiency in the Literature

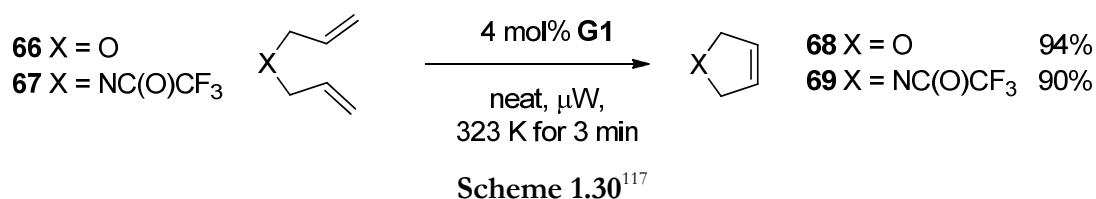
A survey of the literature rapidly highlights clear differences in the ease of formation of target cycloalkenes of different sizes that are qualitatively in agreement with the calculated EM_T values presented in the previous section. However, the selected examples presented below are typically taken from the synthetic chemistry literature, so are densely functionalised. In addition, the choice of pre-catalyst will influence the reaction outcome; first generation pre-catalysts operate in the kinetic regime and therefore should yield products that depend on the *kinetic* EM, while second-generation pre-catalysts should yield products consistent with EM_T . While the substitution pattern of the cyclic products can be decisive in the success or failure of RCM reactions (*vide infra*), the size of the ring itself still clearly exerts a significant effect. Macrocyclic formation by RCM is not considered here, although the topic has been reviewed recently.¹¹³ As discussed previously, yield measurements do not describe the efficiency of metathesis reactions well, and it is important to take into account the concentration regime required to obtain practical yields; the concentration at which a cyclisation *via* RCM is conducted is often a good indicator of the magnitude of the effective molarity.

Syntheses of five- and six-membered rings by RCM are typically straightforward, with most early studies of ruthenium-catalysed ring-closing metathesis reporting the syntheses of primarily five- and six-membered products¹¹⁴ using early pre-catalysts such as **G1** at relatively high concentrations (*ca.* 10^{-1} mol L⁻¹).¹¹⁵ Even substrates with more challenging substitution patterns (*vide infra*), such as **64** and **65**, undergo cyclisation catalysed by 5 mol% **G1** in moderate to excellent yields in 24 h at room temperature (**Scheme 1.29**).¹¹⁶ Stolz *et al.* have achieved RCM of a substrate with a challenging substitution pattern *en route* to the natural product Elatol; the six-membered spirocyclic product is obtained in excellent yield with 5 mol% of pre-catalyst **GH2-oTol** (**Scheme 1.16** above) when conducted with an initial substrate concentration of 0.17 mol L⁻¹.⁸⁴

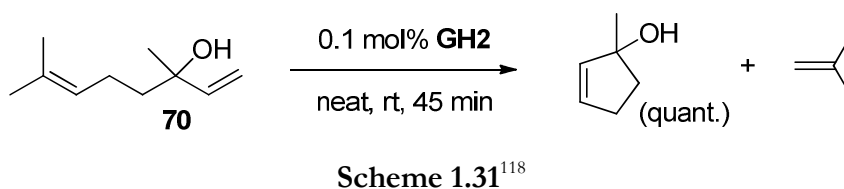


Scheme 1.29¹¹⁶

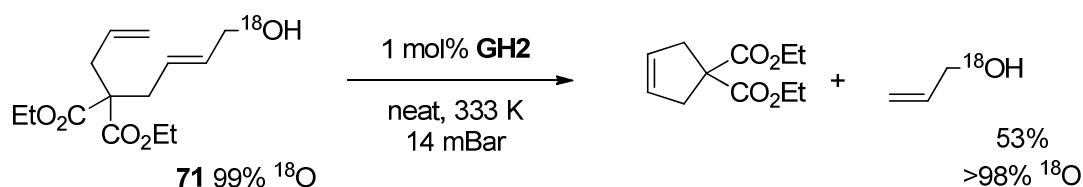
The typically very efficient synthesis of five- and six-membered rings has allowed a number of solvent-free syntheses to be conducted. Vo Thanh *et al.* reported the solvent-free microwave-heated RCM reactions of **66** and **67**, with high to excellent conversion for all of the five- and six-membered ring syntheses studied;¹¹⁷ excellent isolated yields of **68** and **69** were reported (**Scheme 1.30**). The EM_T values presented above suggest that 1,6-heptadiene RCM would not succeed under neat conditions, so the substitution pattern must also aid cyclisation, or the high selectivity for cycloalkene may be a consequence of kinetic rather than thermodynamic control (*vide supra*).



Cyclisation of Linalool **70** to yield 2-methylcyclopenten-2-ol has also been achieved under solvent-free conditions with **GH2**, yielding isobutene as a by-product (**Scheme 1.31**).¹¹⁸ Both metathesis products were then converted to useful fuel compounds. **GH2** should operate in the thermodynamic regime, so the smooth cyclisation obtained is surprising given the low calculated EM_T for cyclopentene. The efficiency is perhaps due to the *gem*-disubstitution of the cyclopentene product.

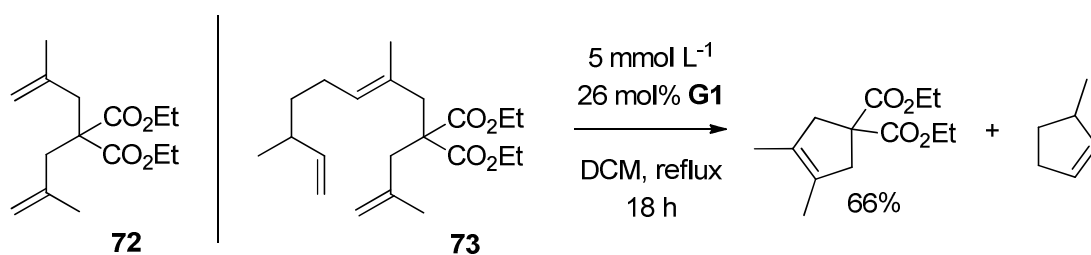


Lloyd-Jones *et al.* used a solvent-free RCM of labelled substrate **71** when preparing [¹⁸O]allyl alcohol; while the by-product was desired here, the metathesis reaction itself proceeds smoothly and efficiently, allowing the allyl alcohol to be collected by distillation from the reaction mixture (**Scheme 1.32**);¹¹⁹ removal of one of the reaction products in this manner will effect a higher degree of *conversion* (according to Le Chatelier's principle) but not a different ratio of products, as the release of allyl alcohol is common to both the cyclisation and oligomerisation pathways.



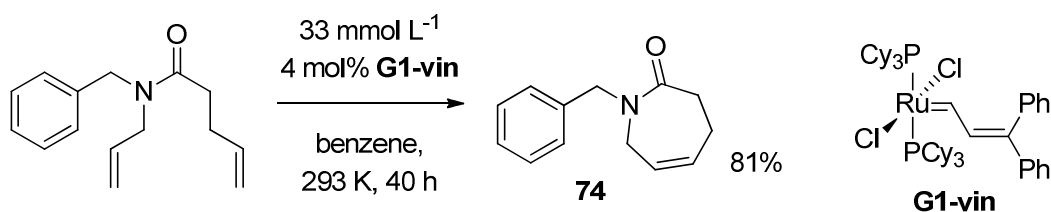
Scheme 1.32¹¹⁹

Similarly, five-membered ring formation drives RRCM, which allows the synthetic chemist to influence where on the substrate the catalyst reacts first.⁶⁷ RRCM has also been used to overcome the problematic RCM of sterically hindered substrates such as **72** (**Scheme 1.33**); analogue **73** undergoes RCM mediated by **G1**, while the parent compound is unreactive under these conditions. Relatively high dilution (5 mmol L⁻¹) was employed for this transformation, although the use of **G1** and the formation of a tetrasubstituted product mean that the outcome was not likely to be determined by thermodynamics. RRCM tethers based on allyl ether, 1,6-heptadiene¹⁰⁰ and diethyl diallylmalonate¹²⁰ motifs have also been reported.



Scheme 1.33⁶⁷

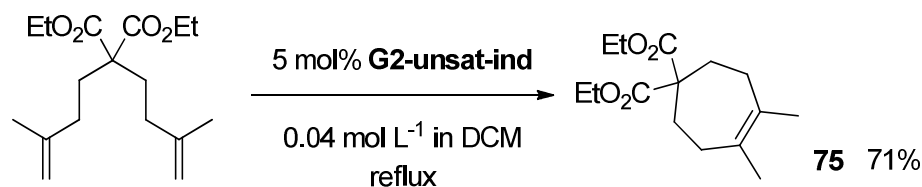
The synthesis of seven-membered rings is more difficult, with early examples of seven-membered heterocycle formation proceeding in up to *ca.* 70% yield, and few reports of the formation of simple cycloheptenes. Wagener reported the RCM of 1,8-nonadiene derivative **54** but this is an exceptional example where tetramethylation of the backbone drives the cyclisation (*vide infra*) (**Scheme 1.24** above).¹⁰⁵ The preparation of seven-membered cyclic amides such as **74** has been reported, where the conformational restriction afforded by the amide functional group likely aids cyclisation by reducing the entropic penalty of cyclisation and therefore facilitates cyclisation at a relatively high reaction concentration (**Scheme 1.34**).¹¹⁴ Tertiary amides can adopt two different conformations, one of which holds the two alkene termini apart and thereby *disfavours*



Scheme 1.34¹¹⁴

cyclisation. However, extended reaction times are required to obtain 81% yield and the use of a first-generation pre-catalyst means that ring-opening of the product is unlikely to occur quickly, placing the reaction under kinetic control.

Cycloheptenes have been prepared by RCM, with a challenging 1,2-dimethylated cycloheptene product **75** prepared *via* RCM of the corresponding α,ω -diene in 71% yield using pre-catalyst **G2-unsat-ind** (Scheme 1.35).¹²¹ The yield at a reaction concentration of 0.04 mol L^{-1} suggests that $EM \approx 10^{-1} \text{ mol L}^{-1}$ or greater, two orders of magnitude higher than the EM_T calculated for cycloheptene. This could be due to a decrease in $\Delta\Delta H$ of *ca.* $2.7 \text{ kcal mol L}^{-1}$, an increase in $\Delta\Delta S$ of $2.7 \text{ cal K mol}^{-1}$ or a combination of changes in $\Delta\Delta H$ and $\Delta\Delta S$. Bulky *gem*-diester functionality may potentially destabilise the acyclic form with respect to the cyclic product, or restrict rotation around the rotors closest to the *gem*-diester position (*vide infra*).



Scheme 1.35¹²¹

Higher reaction temperatures and lower substrate concentrations are often required to achieve cyclisation to form seven-membered rings compared to those used to prepare five- and six-membered targets. Syntheses of seven-membered rings are therefore achievable *via* RCM but present more of a challenge than five- or six-membered ring syntheses and typically result in lower yields.¹¹⁶

Eight-membered rings are less commonly prepared by RCM, with a number of reports of failure. Medium ring synthesis by RCM is often challenging, and has been the topic of a number of reviews.¹²²⁻¹²³ Grubbs *et al.* reported the failure of dienes **76a-b** to

undergo ring-closing metathesis when conducted at an initial substrate concentration of 10 mmol L⁻¹ (**Scheme 1.36**);¹¹⁶ the *gem*-diester functionality does not therefore provide the *ca.* 200-fold increase in EM_T necessary to achieve selective cyclisation at this reaction concentration (if the reaction were completely under thermodynamic control). Instead, dimeric species **77a-b** were isolated and characterised, indicating that the effective molarity was very low; the EM is likely to be below 1 mmol L⁻¹ as the desired cyclooctene products were not detected in the reaction mixture. This is in stark contrast to the five-, six- and seven-membered ring analogues, which underwent RCM smoothly. Undheim *et al.* reported the RCM of **78a-e** in yields from 53 – 99%, but could not prepare the cyclooctene analogue from **78f** (**Scheme 1.37** and **Table 1.12**). Yield differences were obtained between different isomers which cyclise to form the same ring size. Substrates in which a diene terminus was only three bonds from the dihydropyrazine nitrogen atom required more forcing conditions to achieve cyclisation. Reactions were typically conducted at *ca.* 50 mmol L⁻¹. The ease of RCM of **78d**, even at 40 mmol L⁻¹, suggests that the spirocyclic substituent perhaps aids cyclisation, either through restricting rotation of the alkenyl moieties, or by influencing the angle between the two alkene tethers.

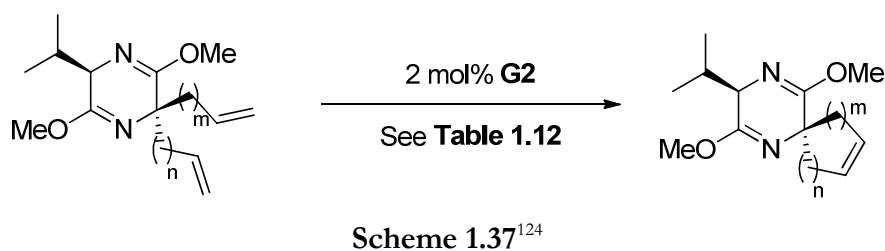
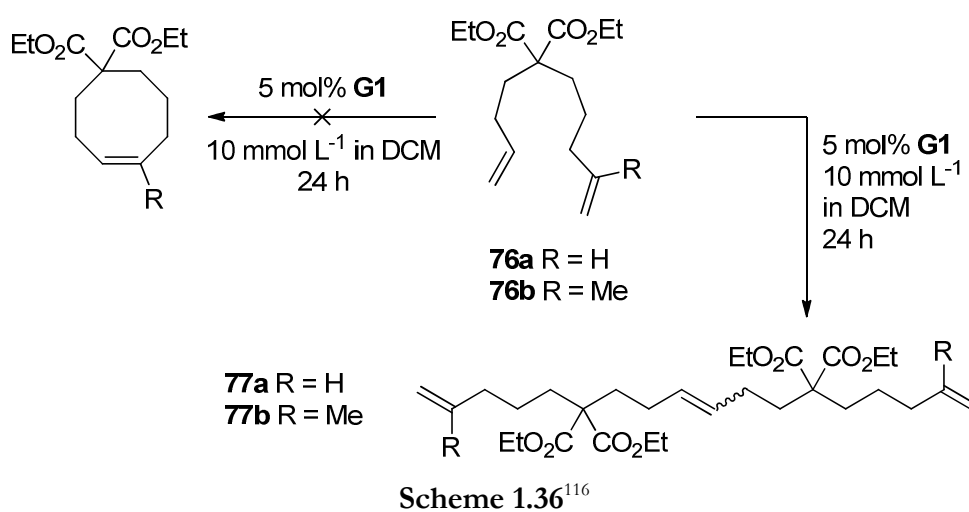


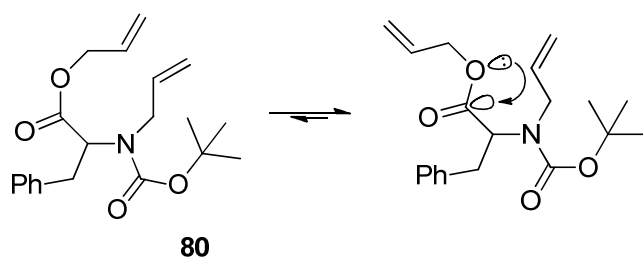
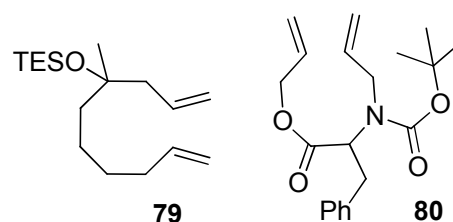
Table 1.12. RCM substrates utilised by Hammer and Undheim.¹²⁴

Substrate	<i>m</i>	<i>n</i>	Ring Size	Solvent	[diene] ₀ ^a	T /K	Time	Yield
78a	1	1	5	Toluene	73	373	18 h	53%
78b	1	2	6	Benzene	35	333	5 h	95%
78c	2	1	6	Benzene	42	293	23 h	99%
78d	2	2	7	Benzene	40	293	23 h	90%
78e	3	1	7	Toluene	64	353	8 h	60%
78f	3	2	8	Toluene	- ^b	353	24 h	0%

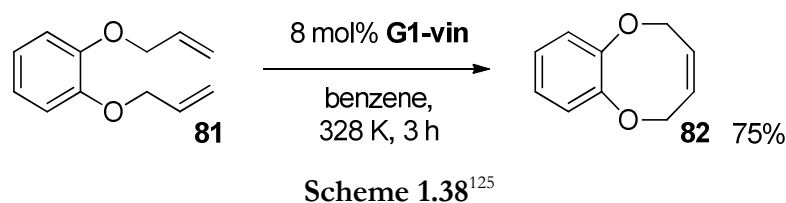
^a Units: mmol L⁻¹.^b Not stated.

The outcomes of eight-membered ring syntheses by RCM are often very sensitive to the substitution pattern. Grubbs *et al.* were unable to cyclise dienes **79** and **80** using pre-catalyst **G1-vin**.¹²⁵ The bulky disubstitution of

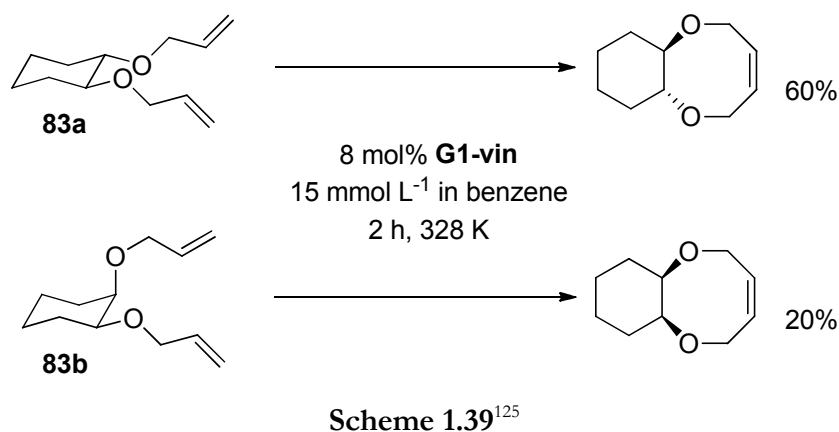
79 did not provide enough of a driving force for cyclisation, while **80** is likely to adopt a conformation that hinders cyclisation; donation of electron density from the oxygen lone pairs into the carbonyl σ^* -orbital means that the favoured conformation (by *ca.* 4 kcal mol⁻¹) is not conducive to cyclisation and therefore presents an additional enthalpic barrier to cyclisation that is not present for oligomerisation (**Figure 1.13**).

**Figure 1.13.** Esters favour conformations where the oxygen lone pair can donate electron density into the carbonyl σ^* orbital.

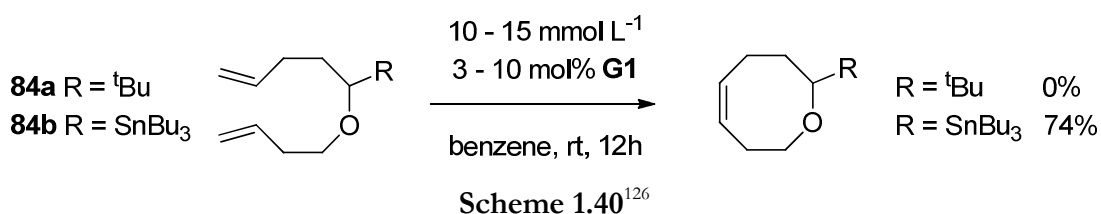
Annulative cyclisations, such as the RCM of diene **81** (which will have most likely proceeded under kinetic control) have been found to proceed more smoothly than annulative ones; diene **81** underwent RCM in good yield at 15 mmol L⁻¹ (**Scheme 1.38**).¹²⁵ In this example, the rigid aromatic ring reduced the entropic penalty of cyclisation (i.e. six rotors were frozen rather than seven; EM_S is therefore 7.4-fold higher)¹⁰³ and enabled product **82** to be obtained in 75% yield.



Annulative syntheses are not always a guarantee of success, as the alkene termini are not always moved into proximity by the presence of an existing cycle. While *trans*-(S,S)-configured **83a** underwent RCM with **G1-vin** in 60% yield, the yield from the RCM of *cis*-(R,S)-configured **83b** was poor at 20% (**Scheme 1.39**).¹²⁵ In addition, the two products will have different degrees of ring strain, so there may be additional enthalpic penalties for ring closing despite any entropic benefit. Calculations carried out on this system (using MM3) showed that $\Delta\Delta G = 0.44 \text{ kcal mol}^{-1}$ in favour of the (S,S)-product, which corresponds to a modest difference in equilibrium constant but is sufficient to explain the three-fold yield difference.

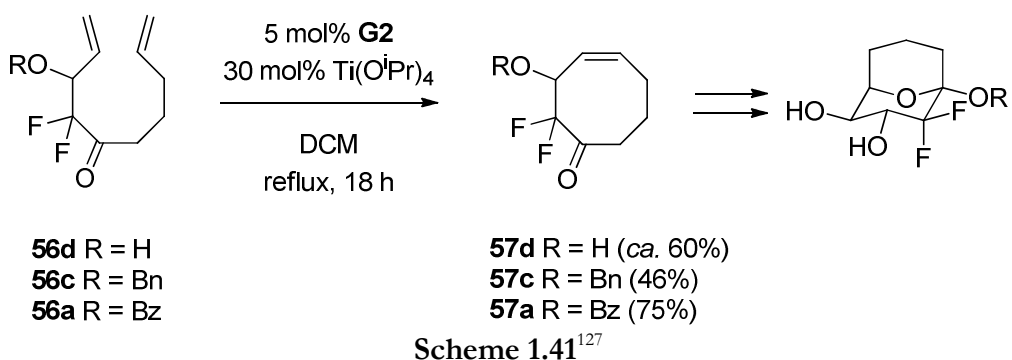


Linderman used trialkylstannyl-substitution to drive the cyclisation of dienes that would not otherwise undergo RCM.¹²⁶ Substrate **84a** did not undergo RCM with **G1** in 12 hours, yet trialkylstannyl-substituted substrate **84b** gave the desired product in 74% yield (12% of **84b**) (**Scheme 1.40**). The effective steric bulk of the tributyltin group (i.e. that which might affect the $\text{CH}_2\text{-CH(R)-O}$ angle or the $\text{CH}_2\text{-CH(R)-O-CH}_2$ dihedral angle) is unlikely to be significantly more than a *tert*-butyl group, and therefore there must also be a contribution from the interactions of the oxygen atom with the C-Sn molecular orbitals. The trialkylstannyl group could be elaborated further *via* tin-lithium exchange and reaction with electrophiles, so provided a useful functional group handle



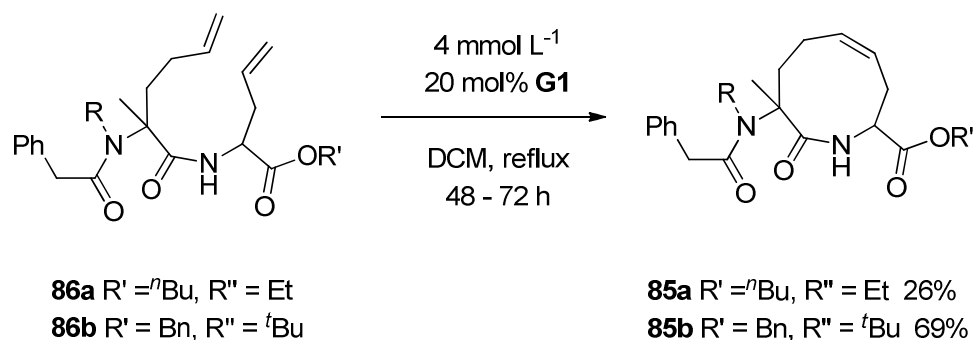
as well as a cyclisation aid.

More recent examples of cyclooctene formation have been reported where cyclisation was achieved without the need for annelation; for example, Percy *et al.* have reported the syntheses of difluorinated cyclooctenones *en route* to conformationally-locked sugar mimics (**Scheme 1.41**).¹²⁷ These cyclisations were aided by a judicious choice of protecting group; RCM of benzyl-protected **56c** proceeded at 2.2 mmol L⁻¹ in 46% yield, while the benzoyl-protected substrate **56a** underwent RCM at 10 mmol L⁻¹ in 75% yield. All of these concentrations are much higher than the calculated EM_T for cyclooctene (0.5 mmol L⁻¹); the products did not undergo ring opening when re-exposed to the reaction conditions, although higher concentrations triggered ROMP processes.¹²⁸ Therefore, these results appear to be the thermodynamic outcome at these concentrations, and the EM_T values of these products are considerably higher than that of cyclooctene. Subsequent studies by Percy *et al.* showed that the choice of alcohol protecting group greatly influenced both the rate and EM of the RCM reaction (*vide supra*).¹⁰⁸ This outcome is particularly important in the context of synthetic chemistry; protecting groups can often be altered without altering the final target compound, so optimisation of a reaction *via* selection of a protecting group is often a viable strategy.



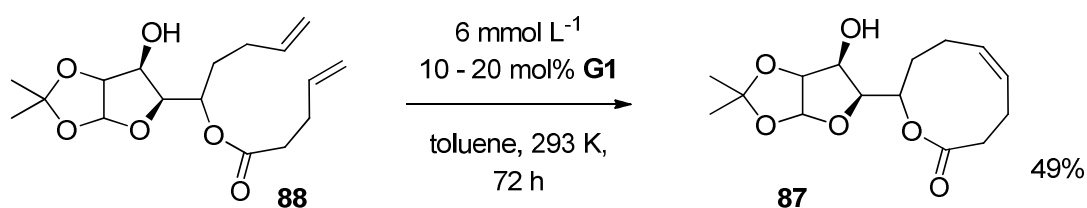
These results illustrate that synthesis of cyclooctenes can be challenging, and that the outcome of such reactions can acutely depend on substrate structure.

Reports of cyclononene syntheses by RCM are less common. As revealed by a theoretical treatment of EM_T (*vide supra*), cyclononene is the most strained unsubstituted Z-cycloalkene. In addition, up to eight rotors must be fixed in cyclononene synthesis, which carries a corresponding entropic cost. Banfi *et al.* reported the synthesis of **85a-b** from substrates **86a-b** (Scheme 1.42). However, 20 mol% pre-catalyst loadings and long reaction times (2 – 3 days) were required to obtain yields of 26 – 69% (thus TON $\approx 1 - 2.5$). This reaction was likely aided by *gem*-substitution (see Chapter 2).



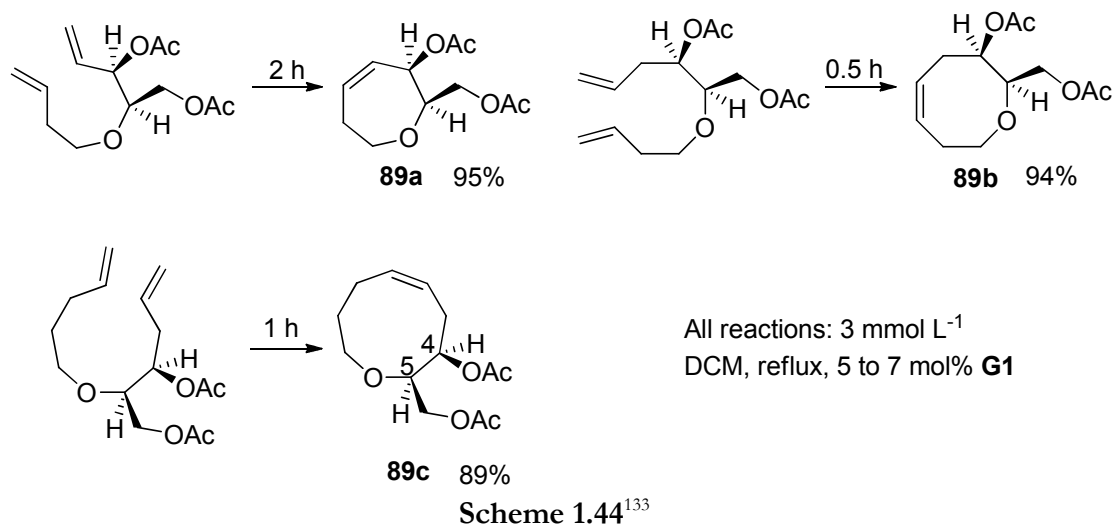
Scheme 1.42¹²⁹

Gesson *et al.* prepared **87** from **88** *via* RCM (Scheme 1.43). The pre-catalyst loading was high (10 – 20%), and only 58% conversion was achieved after three days in toluene at room temperature. However, this represents one of the few successful non-annulative cyclononene syntheses by RCM in the literature. Other examples of nine-membered ring synthesis have typically involved annelation rather than annulation.¹³¹⁻¹³²



Scheme 1.43¹³⁰

Crimmins *et al.* have prepared seven-, eight- and nine-membered oxacycles **89a-c** in excellent yields (Scheme 1.44). In these examples, the substitution pattern favoured a *gauche* arrangement between C4 and C5, allowing donation of electron density from the



σ_{CH} orbital into the σ^*_{CO} orbital (**Figure 1.14**). The *gauche* conformation favours cyclisation more than the *anti* conformation, so a substitution pattern that favours the *gauche* conformation will reduce both the entropic and enthalpic penalties of cyclisation.

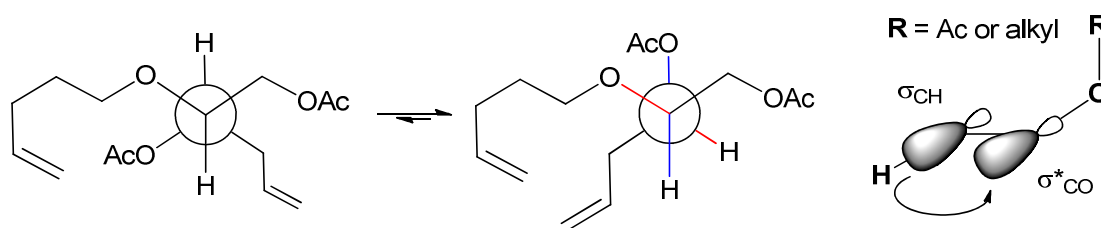
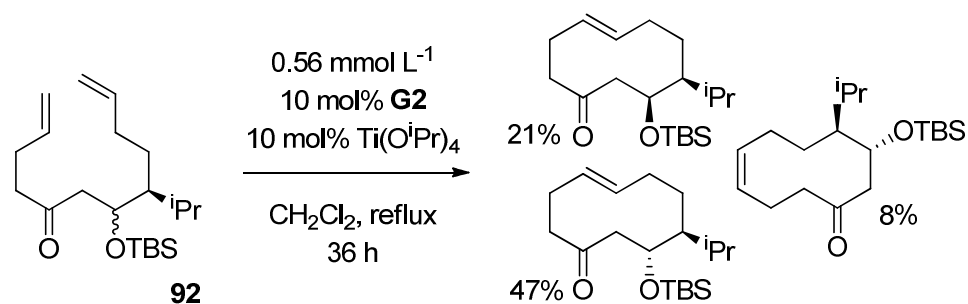


Figure 1.14. Electron donation from the σ_{CH} -bond to the σ^*_{CO} -bond stabilises a C4-C5 *gauche* arrangement, which would bring the alkene termini closer together in space.

Cyclodecene synthesis by RCM is rare, and typically requires high dilution conditions. Rychnovsky *et al.* have prepared cyclodecene **90** by exposing a 1 mmol L⁻¹ solution of diene **91** to 20 mol% **G2** (**Scheme 1.45**).¹³⁴ This cyclisation will have been assisted by the bulky *gem*-diester substitution pattern, although the high dilution



conditions were necessary to avoid competing cross-metathesis. Similarly, Koskinen *et al.* achieved RCM of substrate **92** under high dilution conditions, isolating a mixture of the *E*- and *Z*-isomers (Scheme 1.46).¹³⁵



Scheme 1.46¹³⁵

This brief summary of the literature serves to highlight the relative ease with which different target cycloalkenes can be prepared by RCM. While five- and six-membered rings can often be prepared smoothly under very concentrated (or solvent-free) conditions by RCM, seven-membered rings are less straightforward to prepare. Eight-membered ring synthesis poses a bigger challenge, and is acutely sensitive to the substitution pattern of the substrate. Nine- and ten-membered rings are rarely prepared, with most literature examples requiring very high dilution and proceeding with often very modest yield and TON. The ring size not only affects RCM but also ROMP behaviour,¹³⁶ as ROMP releases ring-strain and allows the rotation of bonds that are otherwise restricted, although the topic of ROMP is beyond the scope of this thesis.¹³⁷

Links between calculated EM_T values and the reaction outcomes discussed here are not particularly easy to draw. In most cases, synthetic reactions have been found to proceed more smoothly and at higher concentrations than the thermodynamic quantities of the parent systems would suggest. This is likely to be due in part to the difference between *thermodynamic* and *kinetic* EM; the former can be calculated from relatively easy to obtain quantities while the latter is determined by the properties of unobservable transition states *en route* to cycloalkene and oligomer. The substitution pattern of the diene substrate can also influence the outcome of the reaction; the effects of some substituent effects are assessed in the following sections, while a study of the effect of ring size alone on metathesis rate can be found in Chapter 2.

Substitution Pattern of the Alkene Termini

The RCM rate depends on the alkene substitution pattern at two steps during the reaction; the influence this exerts will depend considerably on the pre-catalyst employed (*vide supra*). The catalyst reacts with the least hindered alkene¹³⁸ first, as the rate of cross metathesis is sensitive to substitution at and around the alkene, to yield the propagating carbene. This intermediate carbene complex then reacts with the alkene at the other end of the chain; this process is intramolecular so will tolerate more steric hindrance.¹⁰⁰ The alkene substitution pattern at both ends will exert an effect on the rate of reaction.

Grubbs *et al.* conveniently classified various alkene termini according to their metathesis activity,⁶² taking into account the dependence of such classifications on the catalyst system employed. The four classifications for alkenes are:

- **Type 1:** Rapidly homodimerises, but reversibly. Alkenes that are typically sterically unhindered and/or electron rich, rendering them the most reactive. Homodimers form during metathesis reactions, but the homodimers will also undergo metathesis.
- **Type 2:** Homodimerises slowly; homodimers are only sparingly consumable. Alkenes that are less reactive than Type I alkenes, due to steric and/or electronic effects. Homodimers do not form as quickly, and those that form undergo metathesis slowly.
- **Type 3:** Alkene does not homodimerise. Alkenes that are less reactive again, and will not homodimerise in metathesis reactions.
- **Type 4:** Alkene is inert to metathesis but will not deactivate the catalyst.

Using these classifications, the outcome of a cross-metathesis reaction can be anticipated by referring to **Table 1.13**. Four outcomes can result:

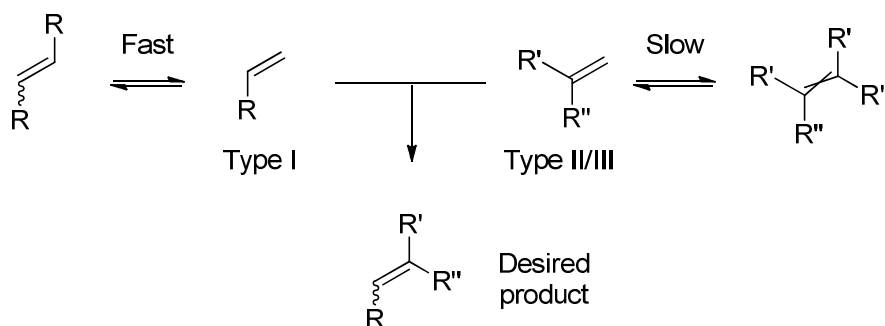
- **No CM:** No metathesis reaction occurs.

Table 1.13. Expected cross-metathesis outcomes as a function of the classifications of the alkenes employed.⁶²

	Type I	Type II	Type III	Type IV
Type I	Statistical CM	Selective CM	Selective CM	No CM
Type II	Selective CM	Non-selective CM	Selective CM	No CM
Type III	Selective CM	Selective CM	Non-selective CM	No CM
Type IV	No CM	No CM	No CM	No CM

- **Non-selective CM:** A mixture of homodimers and the desired cross-metathesis product will be obtained.
- **Statistical CM:** The yield of the desired cross-metathesis product will depend on the relative concentrations of each alkene that were added at the start of the reaction.
- **Selective CM:** The reaction will be selective for the desired product.

Cross-metathesis outcomes are therefore dependent on the rate of secondary metathesis processes; for example, in the reaction of a Type I with a Type II (or III) alkene, dimerisation of the Type I alkene will occur but the dimers are consumable, while dimerisation of the Type II (or III) alkene will be much slower (**Scheme 1.47**). In this case, productive metathesis to yield the desired product should dominate.



Scheme 1.47

This system of classification is quite broad, and does not describe quantitative differences between different alkene substitution patterns. The reactivity of alkenes covers a continuum from the very reactive to the unreactive, but the classifications described by Grubbs *et al.* are a convenient way in which to describe alkene substrates. In addition, the cross-metathesis focus of the study means that the effects on the cyclisation step (i.e. second metathesis step) have not been elucidated.

Examples of alkenes of each type can be found in **Table 1.14**, based on a literature survey by Grubbs *et al.*⁶² These classifications demonstrate the superior reactivity of the second-generation pre-catalysts; substrates that react slowly with **G1**, such as 1,1-disubstituted alkenes, will undergo metathesis mediated by **G2**, for example.

Often, a potentially detrimental alkene substitution pattern can be mitigated when the RCM reaction is otherwise straightforward; for example, Grubbs *et al.* have

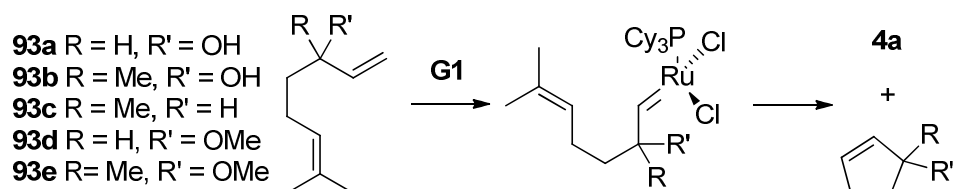
Table 1.14. Examples of Type I, II, III and IV alkenes, with respect to **G1** and **G2**.⁶²

Alkene	G1	G2
Type I	Terminal alkenes, allyl silanes, primary allylic alcohols, ethers, esters, allyl boronate esters, allyl halides	Terminal alkenes, primary allylic alcohols, esters, allyl boronate esters, allyl halides, styrenes (without large <i>ortho</i> -substituents), allyl phosphonates, allyl silanes, allyl phosphane oxides, allyl sulfides, protected allyl amines
Type II	styrene, secondary allylic alcohols, vinyl dioxolanes, vinyl boronates	styrenes (with large <i>ortho</i> -substituents), acrylates, acrylamides, acrylic acid, acrolein, vinyl ketones, unprotected tertiary allylic alcohols, vinyl epoxides, secondary allylic alcohols, perfluoroalkyl alkenes
Type III	vinyl siloxanes	1,1-disubstituted alkenes, non-bulky trisubstituted alkenes, vinyl phosphonates, phenyl vinyl sulfone, tertiary allylic carbons (all alkyl substituents), protected tertiary allylic alcohols
Type IV	1,1-disubstituted alkenes, disubstituted α,β -unsaturated carbonyls, tertiary allylic carbon-containing alkenes, perfluoroalkyl alkenes, protected tertiary allylamines	vinyl nitro alkenes, protected trisubstituted allyl alcohols

obtained excellent yields of cyclopentene and cyclohexene products featuring tetrasubstituted alkenes.¹¹⁶ In these examples, while reaction between the pre-catalyst and alkene termini will be slow, once the reaction takes place the cyclisation event should still occur fast enough that catalyst decomposition should not render the reaction a failure. In addition, strategies such as RRCM have been employed to enable ruthenium carbene species to react with hindered termini that would otherwise be poorly reactive,⁶⁷ although this typically requires planning preparing the metathesis substrate.

Substitution at the Allylic Position

Allylic functionality is suitably close to the alkene termini to exert a considerable effect on the outcomes of metathesis reactions.



It is generally accepted that an allylic hydroxyl group accelerates the rate of metathesis.¹³⁹ This effect was discussed by Hoye *et al.*, who monitored a series of binary competition reactions between dienes **93a-e** which differed only in their allylic substitution pattern. The alternative alkene terminus was trisubstituted in order to ensure that reaction proceeded *via* initial cross-metathesis at the desired terminus.¹³⁸ The reactions of these substrates should then have proceeded as per **Scheme 1.48**, with the allylic substitution pattern influencing primarily the rate of initial cross-metathesis. Relative rates for the RCM of **93a-e** were determined from their relative conversions once the most reactive substrate had achieved *ca.* 50 to 100% conversion (**Table 1.15**). While these results clearly demonstrated that **93b** underwent RCM faster than **93c**, the relative rate was modest (*ca.* 1.5-fold). Crucially, a key experiment (R = R' = H) was not conducted; therefore, while an allylic hydroxyl group resulted in faster metathesis than the analogous substrate with an allylic *methyl* group, it is not possible to infer the rate difference between the simplest systems. The data obtained were still valuable, showing that allylic methyl and methoxy functionality are both detrimental to metathesis rate.

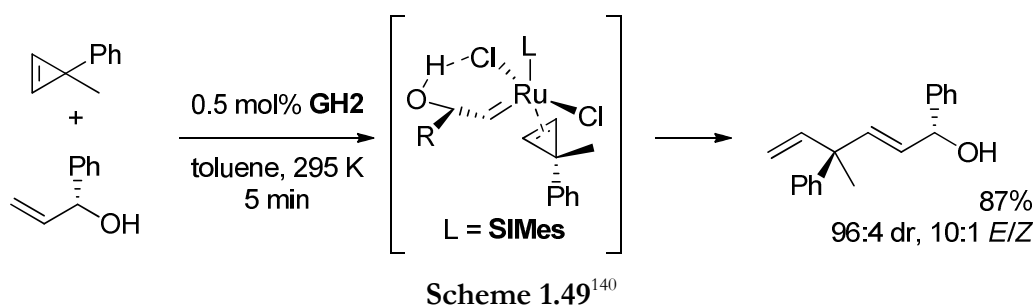
As described above, Percy *et al.* observed a rate difference in favour of a substrate with an unprotected allylic alcohol, but this was compared to two protected alcohols;¹⁰⁸ therefore, while these protecting groups slowed metathesis, no conclusions

Table 1.15. Relative rates for a series of RCM substrates that differ only in the allylic substitution pattern.¹³⁹

Substrate	R	R'	Relative RCM rate
93a	H	OH	60
93b	Me	OH	12
93c	Me	H	8
93d	H	OMe	1
93e	Me	OMe	~0

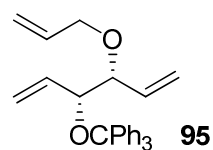
can be drawn on the effect of an allylic alcohol *versus* a dihydro-allylic position.

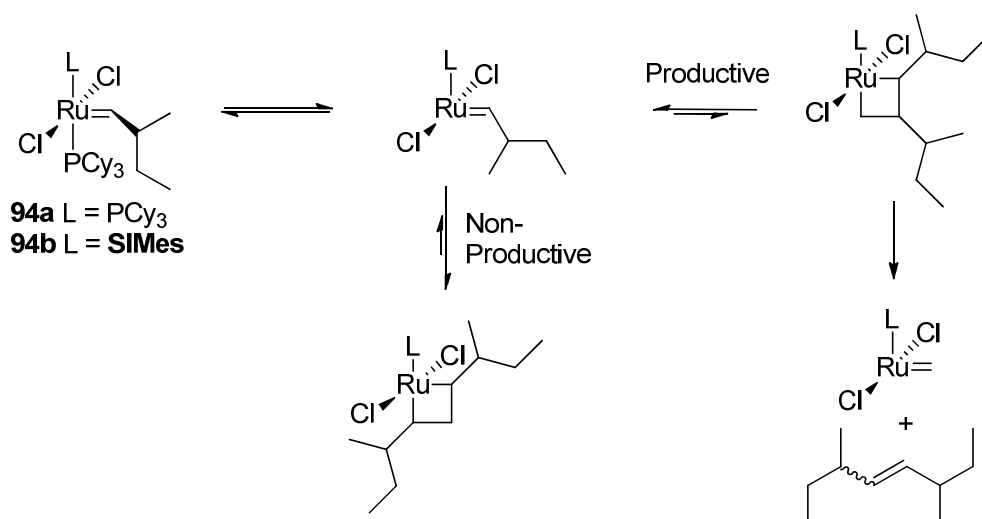
The origin of the allylic hydroxyl effect could potentially be the co-ordination of the hydroxyl group to the chloride ligand, directing it to the alkene terminus. This explanation was invoked to explain the diastereoselectivity of the cross-metathesis reaction between enantiomerically enriched 3-phenylprop-1-en-3-ol and 2-methyl-2-phenylcyclopropene conducted by Hoveyda *et al.*;¹⁴⁰ hydrogen bonding of the alcohol to the chloride ligand present on the metathesis catalyst was proposed to induce diastereoselectivity, as the cyclopropene substrate would be expected to co-ordinate the ruthenium centre placing the largest ligand towards the bottom (**Scheme 1.49**).



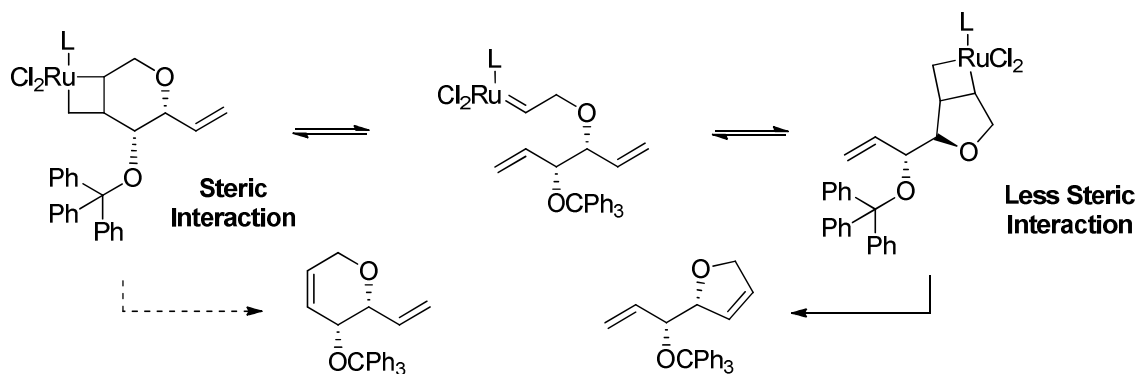
Wagener *et al.* investigated the effects of allylic methylation with pre-catalysts **G1** and **G2**.¹⁴¹ Each pre-catalyst was in turn exposed to *ca.* 3 equivalents of 3-methylpent-1-ene in benzene-*d*₆ at 318 K. The ¹H NMR spectra were checked periodically, showing clearly the pre-catalyst, methylidene **3**, ethylidene **31b** (for **G2** only) and phosphane-bound carbene **94**. The presence of methylidene indicated that at least two turnovers had been completed, while propagating carbene was formed from the reaction of methylidene **4** or benzylidene **1** with the alkene substrate. The metathesis reaction was very slow, which was attributed to the steric bulk of the substrate. This was believed to lead to the substrate partitioning in favour of MCBs that result in non-productive metathesis, rather than those that favour productive metathesis (**Scheme 1.50**).

Bulky allylic substituents have been used to direct metal carbene movement during a metathesis reaction. For example, Schmidt *et al.* used a bulky trityl (triphenylmethyl) protecting group to promote selectivity for a specific ring size in the RCM of **95** (**Scheme 1.51**).¹⁴² Use of the trityl group yielded 20:1 selectivity for the five-membered ring with **G1** (L = PCy₃), 12:1 with a benzyl group instead, or 1:1 with no protecting





Scheme 1.50¹⁴¹



Scheme 1.51¹⁴²

group. This presumably occurred due to steric interaction between the trityl group and the MCB, disfavoring formation of the six-membered ring. Lower (or no) selectivity was obtained with **G2** (3:1 and 1:1 for trityl and benzyl respectively), due to the fact that steric control is a kinetic effect, and that **G2** operates in the thermodynamic regime.

Co-ordinating Functionality

Various functional groups have been proposed to co-ordinate to the metal centre in intermediates on metathesis pathways. It has been proposed in different studies in the literature that the co-ordinating effects of functionality that might form a 1,5-chelate or a 1,6-chelate (**Figure 1.15**) with the metal centre are both detrimental *and* beneficial to synthetic RCM experiments.

Researchers at Boehringer-Ingelheim studied the effects of amide protecting group on the RCM reactions of **60**, **62**, **96** and **97** (Figure 1.16).¹¹⁰ Exposure of **60** to 30 mol% **G1** in DCM-*d*₂ allowed the relative proportions of carbene at each terminus to be evaluated by ¹H NMR. The catalyst underwent metathesis with the unprotected amide **60** or *N*-benzylated amide (**96**) at terminus A preferentially, while BOC protection (**62**) or *N*-acylation (**97**) favoured initiation at terminus B. Protection of the amide was proposed to disrupt 1,6-chelation of the metal centre by the ester through A^{1,3} strain.

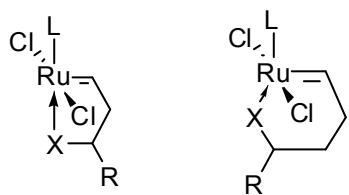


Figure 1.15. Potential chelate formation in metathesis reactions, referred to here as (a) 1,5-chelate formation and (b) 1,6-chelate formation.

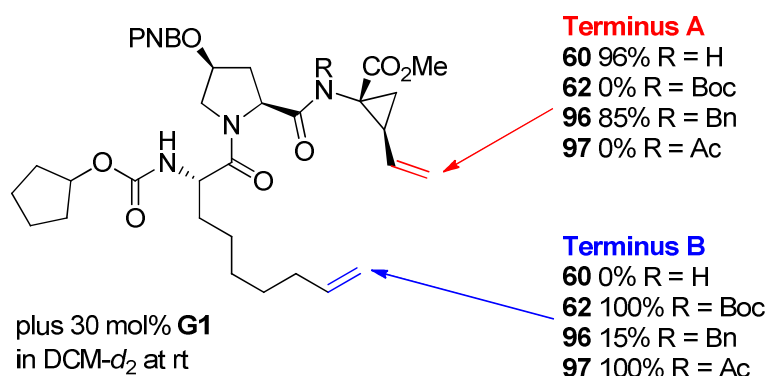
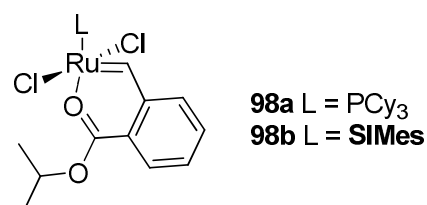
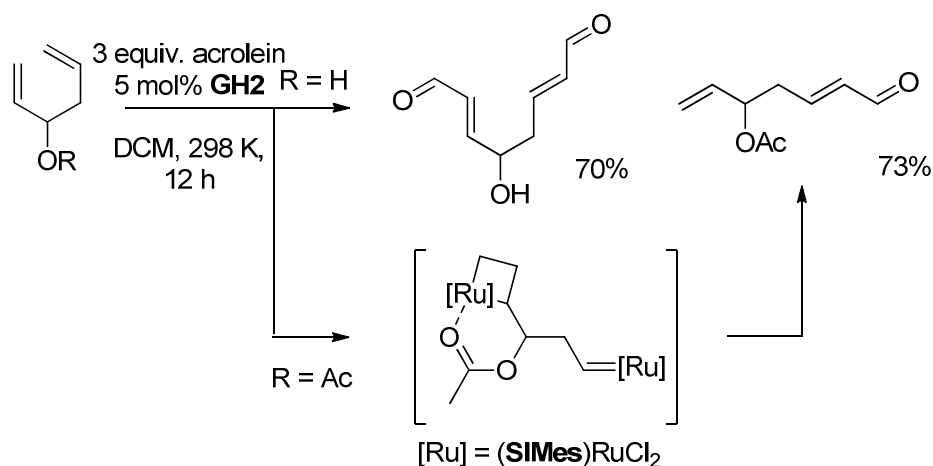


Figure 1.16. Probing the selectivity of the initial cross-metathesis event.¹¹⁰

Stable chelates of these types have been isolated from metathesis reactions, and have in one case spawned an entire classification of pre-catalysts;¹¹⁻¹² in species such as **GH2**, **98a** and **98b**,²¹ co-ordination of an oxygen *via* the lone pair has yielded stable and isolable complexes.

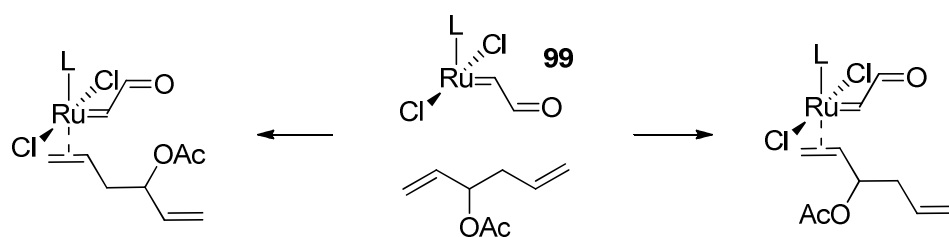


The effect of allylic chalcogen groups has been proposed to be beneficial in a number of syntheses; Davis *et al.* have reviewed this area recently.¹⁴³ The effects of allylic chalcogens are not necessarily clear-cut, however. Cossy *et al.* proposed that co-ordination of an allylic acetate group effectively protected one terminus from reaction and allowed chemoselective cross-metathesis at the other (Scheme 1.52);¹⁴⁴ the proposed mechanism suggested that the ester group chelated the MCB that would be formed if reaction occurred at the terminus closest to this group, preventing it from



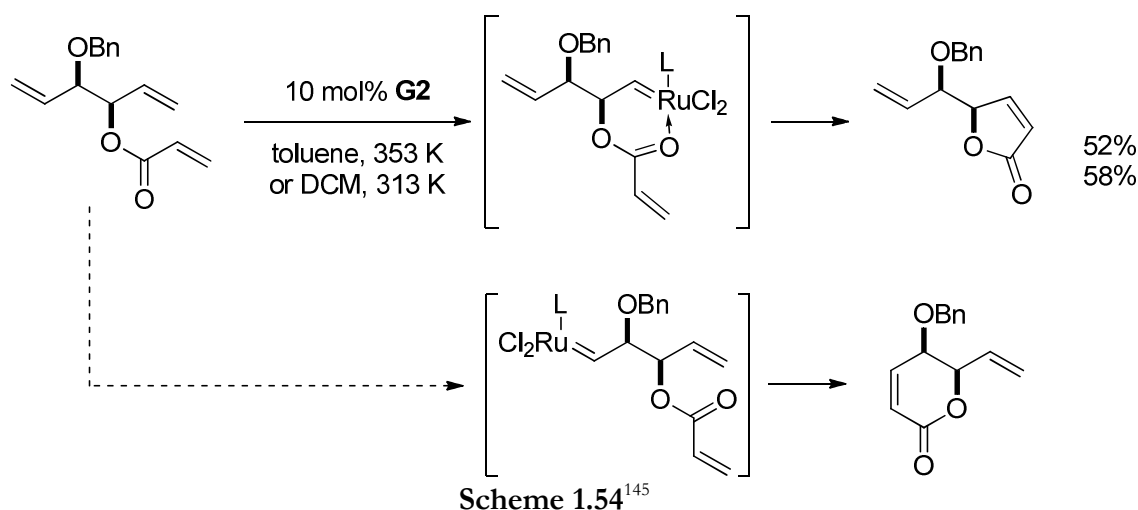
Scheme 1.52¹⁴⁴

forming a ruthenium carbene here. In contrast, a ruthenium carbene at the alternative terminus would be able to undergo cross metathesis unimpeded. However, the explanation presented in the original paper would require the reaction of a molecule of diene with two molecules of active catalyst; diene is present in 20-fold excess over pre-catalyst so the presence of two ruthenium centres on a single molecule of diene seems unlikely. Another explanation might be that **GH2** reacts with acrolein first, as it is present in three-fold excess over the diene; the reactivity of the intermediate species **99** might then influence selectivity (Scheme 1.53). The ester is much bulkier than the alcohol so may promote cross-metathesis at the less hindered end of the molecule. Alternatively, the cross-metathesis reaction at the position bearing an allylic ester may simply be slower than at the less hindered end.



Scheme 1.53

Quinn *et al.* proposed that co-ordination of the metal centre *promotes* metathesis at sites that possess co-ordinating functionality in the allylic position (Scheme 1.54).¹⁴⁵ However, this selectivity could be explained by the larger size of the benzyl ether group,



which is a steric reason for preferential reaction at the site bearing the allylic ester.

Substitution of the Substrate Backbone

Substitution elsewhere on the substrate can also exert an effect on both the rate and efficiency of RCM. Several of these effects have already been discussed previously; all reduce the entropic and/or enthalpic penalty of cyclisation.

The *gem*-disubstitution of the alkene backbone can aid cyclisation. For example, Wagener *et al.* reported the considerable effect of di-*gem*-dimethylation of 1,8-nonadiene-5-one on the metathesis outcome (see **Scheme 1.24** previously); the heavily-alkylated substrate most likely undergoes *relief* of strain upon cyclisation. The topic of *gem*-disubstitution is discussed in chapter 2.

The conformation of the acyclic form is important; Crimmins *et al.* have achieved RCM to form seven-, eight- and nine-membered rings, which was most likely due to the substitution pattern favouring a *gauche* conformation which would bring the alkene termini closer together (see **Scheme 1.44** and **Figure 1.14** previously).¹³³

Annulative strategies have also enabled RCM of otherwise difficult substrates. Some of the earliest examples of medium-ring formation feature annulative syntheses which reduce the entropic penalty of ring closing.¹²⁵ For example, RCM of a 1,9-decadiene motif requires seven rotors to be frozen, while if one rotor is already fixed the entropic penalty of cyclisation is decreased and EM_s increases 7.3-fold.¹⁰³

The effects of such substitution patterns are not always particularly obvious, but can determine the success or failure of RCM reactions.

Research Aims

While the mechanism, scope and limitations of metathesis are well established, the effect of substrate structure on reactivity has not been quantitatively investigated in detail. Some quantitative details of metathesis reactions have been established, but such studies are few and far between. A detailed quantitative study of alkene metathesis has the potential to aid in the optimisation of metathesis reactions, especially those that may be conducted on a large scale in industrial scenarios.

The effect of substrate structure on reactivity in metathesis reactions can be dramatic, but the choice of catalyst system also plays a considerable role. Therefore, in order to understand metathesis reactions fully, it is necessary to consider and quantify the rates of the key processes occurring in these reactions.

The aims of the work reported in this thesis were therefore three-fold.

The effect of ring size on reaction outcome can be considerable, and there exist mature methods by which to estimate and quantify cyclisation efficiency. However, no previous study has sought to isolate the effect of ring size from the clearly complex interplay of substrate structure and reactivity. The relative rates of cyclisation to form simple prototypical cycloalkenes were desired; a kinetic method that could be used to assess these rates was therefore necessary. The synthetic literature contains a large number of examples of RCM reactions, but most substrates are densely functionalised and will, as established in the preceding sections of this chapter, exert considerable influence on the outcomes of the reactions. A suitable prototypical system was required that isolated the effects of ring size from those of functional group pattern as far as possible; comparisons could then be made with more functionalised prototypical systems. In addition, it was of interest to explore whether these cyclisations are under kinetic or thermodynamic control, and quantify the relevant effective molarities (kinetic or thermodynamic) for these cyclisations. These topics are investigated in Chapter 2.

Kinetic studies yield concentration/time data for those components that are monitored, but traditional interpretation of such data often requires simplifying the reaction to fit a kinetic order, or running a series of reactions under different (and not always synthetically relevant) conditions. Reaction simulation methods were therefore explored, with the aim of developing, understanding and applying a kinetic model for RCM reactions that could allow more detailed quantitative insight into both the effect of

substrate structure on RCM rate, and the effect of other processes occurring in the reaction (such as pre-catalyst initiation). Reports of new pre-catalysts are frequently accompanied only by qualitative kinetic comparisons with existing catalysts, rather than measured initiation and/or decomposition rates, and so the reaction simulation approach could potentially be applied to the assessment of new metathesis pre-catalysts.

During the course of this work, deleterious isomerisation side reactions were observed to take place under remarkably mild conditions, often consuming considerable quantities of diene substrate. There have been a number of studies in which various agents have been proposed to account for isomerisation in RCM reactions, but a detailed study was required to conclusively identify the source of the isomerisation in our reactions, and to understand the effects of various experimental variables on the rate of isomerisation.

Together these aims represent a drive to further develop quantitative knowledge of metathesis, using simple systems and carefully considered experiments to isolate and quantify specific effects.

Chapter 2:

Kinetic Studies of Ring-closing Metathesis Reactions

The Kinetics of Ring-closing Metathesis

Literature Studies of Ring-closing Metathesis Kinetics

Kinetic studies quantify the behaviour of reactions with respect to real time. By following the concentrations of various species and their evolution over time, the chemist can gain greater understanding of the behaviour of the reaction by identifying, for example, when a particular by-product is formed, or if there is a time at which product formation reaches a plateau. Through more detailed studies, derivation of rate laws and quantification of rate constants allow understanding of reaction mechanism. In reactions where competing processes occur, the relative competencies of product and by-product forming processes can be assessed.

There are few rigorous kinetic studies of metathesis reactions in the literature. The majority of experiments are qualitative and used to compare pre-catalysts; in these studies, such as the one by Ritter *et al.*, a series of prototypical substrates were exposed to a palette of different pre-catalysts and the concentration/time profiles for the reactions were overlaid.⁴⁵ In this manner, qualitative information about the relative activities of common ruthenium-based pre-catalysts has been obtained. These experiments provide a quick overview of the relative activity of metathesis pre-catalysts, and particularly of initiation rate when a very simple reaction is undertaken. However, very little in the way of quantitative information has been obtained from this study. No rate constants are reported in the publication itself; those recorded in the supporting information typically required some editing of the dataset as the reactions did not fit a first-order treatment well. The complexity of the reaction mechanism has most likely dissuaded many researchers from tackling detailed kinetic studies of RCM; *a priori* studies of metathesis are difficult, and often make approximations necessary (*vide infra*).

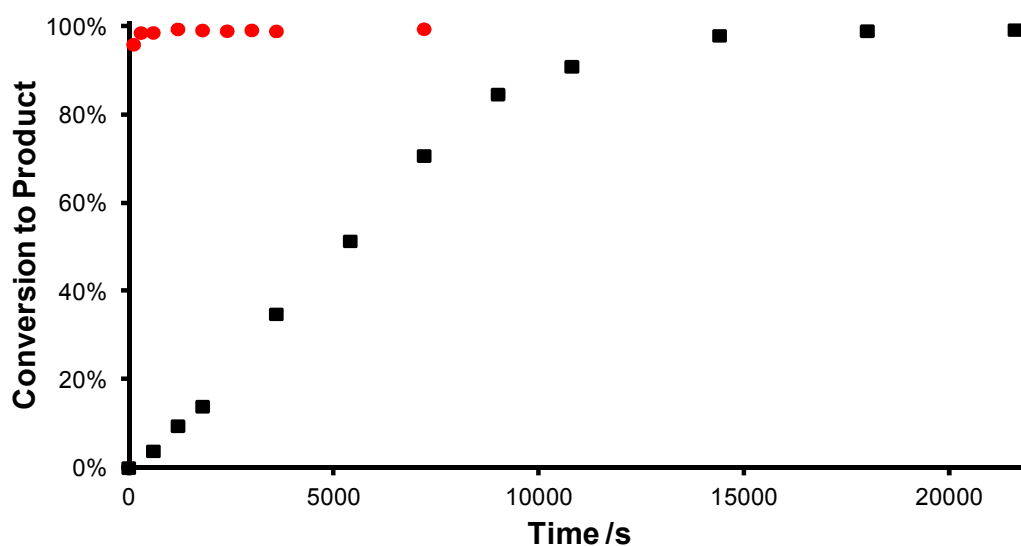


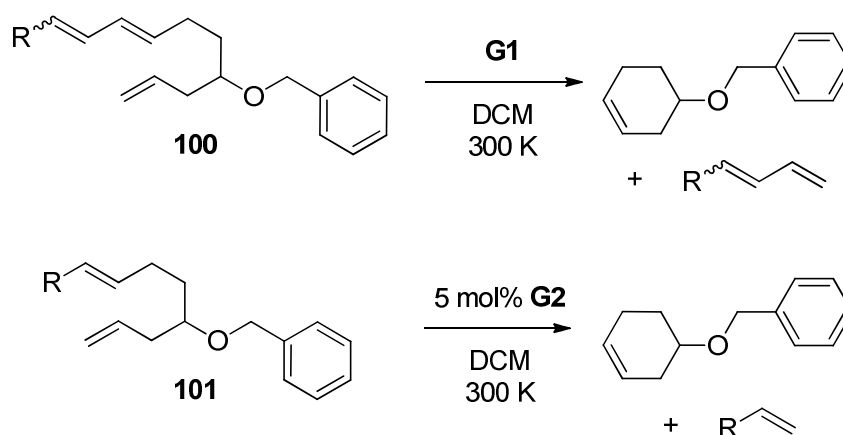
Figure 2.01. Conversion/time profile for the RCM of **56c** with (black points) and without (red points) (pre-)catalyst quenching before analysis.¹⁰⁸

rate constants were obtained due to the complexity of the concentration/time profiles.¹⁰⁸ The nature of the moiety used to protect the allylic hydroxyl functionality was found to exert an effect on both the rate and EM of the RCM reaction (**Scheme 1.25** and **Figure 1.09** in the introduction); *gem*-dimethylation was also found to increase the rate and EM of RCM by a factor of *ca.* four-fold (by comparing reaction $t_{1/2}$). The range of substrates considered in this study is rather small, but the kinetic study is used effectively to illustrate the effects of protecting group choice.

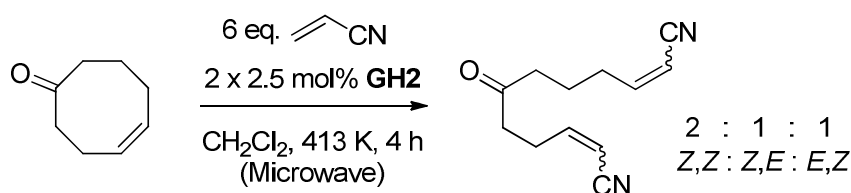
Quantitative kinetic studies of RCM, where rate constants are quantified, are rare. Ratios of conversion at time points have been used employed by Hoye *et al.* to investigate the effects of allylic hydroxyl functionality on RCM rate. Linalool and analogues were exposed to pre-catalyst **G1** and relative reactivities were evaluated.¹³⁹ In a series of reactions, pairs of substrates (from **93a-e**) were exposed to **G1** and the conversion/time profile was obtained for each by monitoring the reaction using ¹H NMR spectroscopy. Typically only 50% to 80% of the faster RCM reaction of the pair was monitored, and the relative ratio of each product was used to determine an approximate relative reactivity (**Table 1.15** in the introduction). For example, in the reaction where a mixture of linalool **93b** and citronellene **93c** were exposed to the same charge of pre-catalyst **G1**, a relative reactivity of 1.5x (in favour of linalool) was arrived at from the relative mole fraction of each cyclic product when linalool had undergone

approximately 50% conversion to the corresponding cyclopentene compound. The relative reactivities are therefore only very approximate, as in many cases very little of the slower reaction will have been recorded.

Paquette *et al.* have conducted some kinetic studies to evaluate the electronic effects on the RCM reactions of trienes **100a-h** with **G1**¹⁴⁹ and dienes **101a-i** with **G2** (**Scheme 2.03**).¹⁴⁸ Reactions were monitored by ¹H NMR spectroscopy and the resulting concentration/time data were fitted to a first order expression to yield rate constants (**Table 2.01**). Substrates featuring cyano or phenylthio groups (**100g** and **100h**) were reported to poison the catalyst system and no conversion was obtained. Alkenes such as acrylonitrile have been known to be reluctant metathesis substrates;¹⁵⁰ Grubbs *et al.* have shown that highly active, rapidly initiating pre-catalysts are required to achieve useful yields,¹⁴ while Stockman *et al.* successfully achieved ring-opening of cycloocten-4-one followed by double cross metathesis with acrylonitrile using two 2.5 mol% portions of pre-catalyst **GH2** and prolonged microwave heating (**Scheme 2.04**).¹⁵¹ In all reports, acrylonitrile cross-metathesis is selective (but not specific) for the *Z*-isomer. It is possible that the substrate does not poison the catalyst but that **G1** is simply not active enough to effect the reaction. Unfortunately the studies of Paquette *et al.* suffer from



Scheme 2.03¹⁴⁸⁻¹⁴⁹



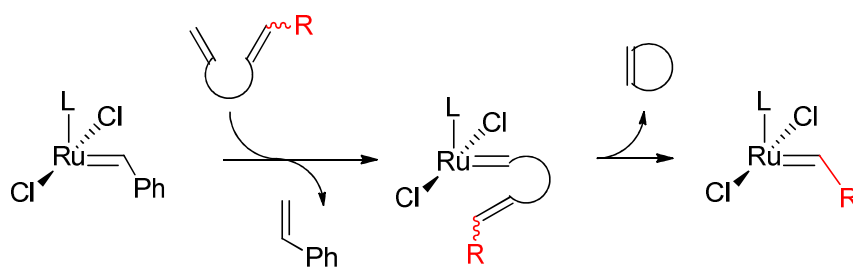
Scheme 2.04.¹⁵¹

Table 2.01. Rate constants and half-lives ($t_{1/2}$) for the reactions in **Scheme 2.03**.¹⁴⁸⁻¹⁴⁹

Entry	Substrate	R	k (s ⁻¹)	$t_{1/2}$ (s)
A1 ^a	100a	MeO	1.03 x 10 ⁻⁴	6.71 x 10 ³
A2 ^a	100b	C(O)Me	2.57 x 10 ⁻⁴	2.70 x 10 ³
A3 ^a	100c	SO ₂ Ph	2.97 x 10 ⁻⁴	2.34 x 10 ³
A4 ^a	100d	CH ₂ OH	3.58 x 10 ⁻⁴	1.93 x 10 ³
A5 ^a	100e	CO ₂ Et	4.35 x 10 ⁻⁴	1.59 x 10 ³
A6 ^a	100f	H	1.12 x 10 ⁻³	6.19 x 10 ²
A7 ^a	100g	SPh	- ^b	- ^b
A8 ^a	100h	CN	- ^b	- ^b
B1 ^c	101a	Me	2.2 x 10 ⁻²	3.14 x 10 ¹
B2 ^c	101b	CO ₂ Et	2.2 x 10 ⁻²	3.22 x 10 ¹
B3 ^c	101c	H	1.9 x 10 ⁻²	3.56 x 10 ¹
B4 ^c	101d	C(O)Me	1.7 x 10 ⁻²	4.02 x 10 ¹
B5 ^c	101e	SO ₂ Ph	4.8 x 10 ⁻³	1.45 x 10 ²
B6 ^c	101f	<i>p</i> -MeC ₆ H ₄	1.4 x 10 ⁻³	5.11 x 10 ²
B7 ^c	101g	Ph	1.1 x 10 ⁻³	6.58 x 10 ²
B8 ^c	101h	<i>p</i> -(CF ₃)C ₆ H ₄	7.2 x 10 ⁻⁴	9.63 x 10 ²
B9 ^c	101i	<i>p</i> -(NO ₂)C ₆ H ₄	4.7 x 10 ⁻⁴	1.49 x 10 ³

^a Reference¹⁴⁹ ^b No reaction ^c Reference¹⁴⁸

some flaws. Reactions often have very short half-lives, with the shortest $t_{1/2}$ reported to be only 30 s. It is difficult to use a technique such as ¹H NMR spectroscopy to monitor such fast reactions: the acquisition of an NMR spectrum typically requires at least one minute and therefore it would be difficult to gather data quickly enough to construct a concentration/time profile from which to obtain reliable rate constants for these reactions. Secondly, and most importantly, the substrate substitution pattern will fundamentally change the nature of the propagating carbene species in each example, and therefore the different reaction half-lives reported represent an aggregate of the effects of the different substrate *and* of the different catalytic species (**Scheme 2.05**). The ruthenium species that performs the majority of turnovers derives from the first turnover of the pre-catalyst, which in turn depends upon the terminal substitution of the RCM substrate. It has been established that the rate of the initial alkylidene transfer, in which the pre-catalyst reacts with the substrate to form the propagating carbene, is



Scheme 2.05

inversely dependent upon the degree of alkene substitution,¹³⁸ in the simplest examples of α,ω -diene RCM where both termini are mono-substituted, the initial alkylidene transfer may occur on *either* terminus. However, for **100a-h** and **101a-i**, one terminus is 1,2-disubstituted. The initial cross metathesis would therefore be expected to occur at the mono-substituted terminus, followed by RCM onto the second alkene resulting in the generation of a new carbene species. This new species carries the ω -substitution pattern and is therefore *different* in the RCM reactions of each of the different substrates. It is then impossible to determine if the trends identified result from the electronic effects on the ring-closing step, or from the different properties of the propagating carbene species in each reaction that carries out most of the turnovers. A further set of experiments, in which each potential ruthenium carbene product is tested with the same metathesis substrate, would be required to deconvolute the results of this study and quantify the effects of the different ruthenium carbene structure.

With kinetic studies on RCM rare and often inconclusive, there is a need to develop a method for, and carry out, a series of careful and precise kinetic studies to assess the effects of substrate structural features quantitatively.

New Studies of Ring-closing Metathesis Reactions

There is a need for rigorous quantification of the effects of substrate structure on RCM rate and efficiency, as the success or failure of an RCM reaction is often acutely dependent on the substrate structure. Often referred to as ‘gearing’ in the synthetic chemistry literature,¹⁵² structural features of RCM substrates can augment the enthalpic or entropic change upon the cyclisation of a diene to yield cyclic product. In this manner (as discussed in the introduction), the entropy decrease upon cyclisation can be reduced, for example, by restricting the conformational freedom of the substrate.¹⁵³ The enthalpic penalty of cyclisation (i.e. introduction of ring strain) can be reduced in some

cases by, for example, replacing sp^3 centres with sp^2 centres, reducing the transannular strain in the product. Strain is not always necessarily *introduced* in the cyclisation; for example, the RCM of 4,4,6,6-tetramethylnona-1,8-dien-5-one, relief of strain in the acyclic precursor drove the cyclisation reaction towards the product (**Scheme 1.24**).¹⁰⁵

The understanding and quantification of the effects of substrate structure on reactivity are important in the successful planning of synthetic reactions; a rigorous and quantitative knowledge of structural effects allows for less ‘trial and error’. If the EM¹⁰² for a given cyclisation is known then the optimal concentration range for that reaction can be selected in a straightforward manner.

The Effects of Ring Size

A key issue in RCM is that of the effect of target ring size on RCM rate and efficiency, which has been reviewed in the introduction. This review of the literature revealed that five- and six-membered rings are typically formed quickly, in high yields and under very mild conditions. In contrast, seven- and eight-membered¹²³ rings are less common products of RCM, with higher dilutions often required to achieve successful reactions. Nine- and ten-membered ring syntheses by RCM are very rare, due to both ring strain induced by transannular interactions¹¹² and the requirement to restrict a large number of otherwise rotatable bonds.¹⁰³ Macrocyclic formation is well explored in the literature,¹¹³ but considerable dilution of the reaction (frequently to *ca.* ≤ 5 mmol L⁻¹) is usually required to avoid competing cross-metathesis processes, unless the substitution pattern of the substrate is particularly favourable.¹¹⁰

Research Aims

This work was undertaken to fulfil two primary aims: to develop a robust and general protocol to study the kinetics of RCM reactions, and to use this protocol to evaluate quantitatively the effect of ring size alone on RCM rate and efficiency. Two important pieces of information were desired from a study of the effects of target ring size.

Firstly, rate constants were sought to allow quantitative comparisons between the rates of different reactions. When conducted at scale, the length of time a reaction requires to reach completion has significant cost implications; in addition, a slow primary reaction may allow side-reactions to consume significant quantities of substrate

and/or product material. The rate constants obtained can also be used to draw inferences about mechanistic aspects of the reaction.

A second key piece of information is cyclisation efficiency. Cross-metathesis processes can compete with the desired ring-closing reaction, which results in a loss of product yield and introduces complications during work-up and product isolation. The most appropriate metric for assessing the competition between intra- and intermolecular reactions is the effective molarity (EM),¹⁰² as this allows the use of a single number to compare the relative rates of cyclisation and oligomerisation; a discussion of EM and its applications in metathesis chemistry can be found in the introduction. The EM has important practical consequences: when a reaction is conducted with a substrate concentration equal to the EM, a 1:1 mixture of cyclic target and cross-metathesis product should result. To ensure greater than 90% selectivity for the cyclic target, the initial substrate concentration must be one tenth (or less) of the EM. While the *thermodynamics* of ring-closing can be assessed in a somewhat straightforward manner (*vide infra*),¹⁰³ the kinetic EM is not so easy to predict, and depends on the enthalpy and entropy changes from substrate to transition state as opposed to the entropy and enthalpy differences between substrate and product. Measurement of the EM may therefore allow insight into the nature of the transition state.

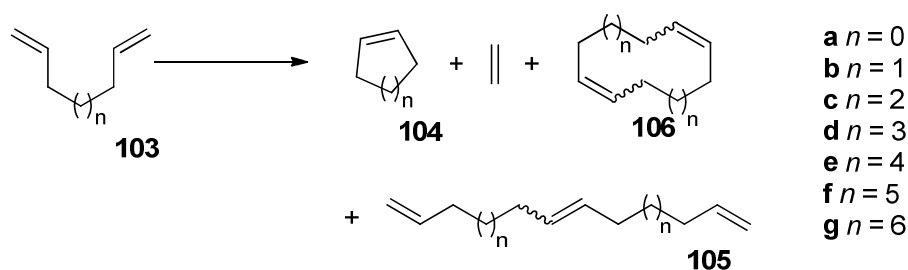
Robust Kinetic Studies of Prototypical Substrates

Selecting a Model System

As has been established from the survey of the literature in the introduction, even substrate structural features that are remote from the reacting alkenes can exert a considerable influence on the outcome of RCM reactions. It was therefore important that the model system selected to evaluate the effects of ring size isolated the effect of ring size.

Substrates such as diethyl diallylmalonate **102** (and various analogues) are favoured in the literature for pre-catalyst evaluation (see, for example, the pre-catalyst benchmarking study by Ritter *et al.*).⁴⁵ These compounds can be prepared cheaply and in a straightforward manner *via* alkylation of diethyl malonate.¹¹⁶ However, the presence of functionality and (in some cases) the lack of symmetry may bias or complicate results.

A simpler series of substrates was selected for this study (**Scheme 2.06**). 1,6-Heptadiene **103b**, 1,7-octadiene **103c**, 1,8-nonadiene **103d**, 1,9-decadiene **103e**, 1,10-undecadiene **103f** and 1,11-dodecadiene **103g** are all commercially available, symmetrical and free from extra functionality. All six α,ω -dienes can undergo RCM to form cycloalkenes with ring sizes from five to ten (cycloalkenes **104b-g**), cross-metathesis to form linear dimers **105b-g**, or cross-metathesis followed by RCM to form cyclic dimers **106b-g**. The production of larger linear and cyclic species (trimer, tetramer and so on) is also possible. The RCM products of all reactions except that of 1,11-undecadiene (cyclopentene **104b**, cyclohexene **104c**, cycloheptene **104d**, *cis*-cyclooctene **104e**, and *cis*- and *trans*-cyclodecene **104f**) are also commercially available. Some other species, such as 1,6,11-dodecatriene **105b** (the cross-metathesis product of 1,6-heptadiene) and cyclic dimers **106b-g**, have been reported previously in the literature,^{136,153-155} although the



Scheme 2.06

former was prepared using a non-metathesis route. Many of the substrates, products and by-products are volatile, which presented some handling difficulties, and rendered reaction mixtures very difficult to work up using traditional synthetic organic chemistry methodology. However, these points were considered when devising a method for carrying out kinetic studies.

Pre-catalysts **G2** and **GH2** are most commonly employed in synthetic RCM reactions, so **G2** was selected for this study initially. Comparisons with some results obtained with **GH2** can be found in Chapter 3.

Evaluating the effects of target ring size in the RCM reactions of this series of simple prototypical substrates should therefore provide information about cyclisation rates and the effectiveness of cyclisation compared to oligomerisation (measured using the kinetic EM) which is a function of target ring size only. Any effects brought about by diene functionalisation or substitution pattern can therefore be introduced carefully and systematically once the parent system is understood.

Requirements for a Kinetic Method

A method which seeks to quantify the effects of substrate structure on RCM rate and efficiency using kinetic experiments must fulfil several requirements:

- The method must measure solution concentrations accurately, with suitable precision to allow the construction and analysis of detailed concentration/time profiles; in RCM reactions, the rate of the competing cross-metathesis process is dependent on the concentration of diene, so it is critical that this concentration is known accurately
- Data collection must allow for suitable data density in concentration/time profiles, with enough data points to allow for meaningful treatment and interpretation of the kinetic data, particularly within the first reaction half-life ($t_{1/2}$)
- The method must be reproducible; the initial concentrations of diene and pre-catalyst must be charged and known accurately
- The method must not perturb the reaction outcome; for example, aqueous work-up and removal of the solvent under reduced pressure could potentially remove volatile products from the reaction mixture

Pre-catalysts frequently employed for alkene metathesis reactions, such as **G2** and **GH2**, are reported to be air- and moisture-stable.¹⁰⁻¹¹ However, reaction mixtures containing these pre-catalysts (and related ruthenium species that comprise reaction intermediates)

may be more sensitive and must therefore be treated with care. As this project aimed to inform synthetic chemistry projects, the conditions used for these studies reflected (at worst) those used by synthetic chemists. Such synthetic work would typically be conducted under a dry atmosphere of nitrogen or argon, and with dried solvents. Glove box conditions are useful for pre-catalyst preparation or manipulation of particularly sensitive organometallic side products or intermediates, but do not reflect the conditions under which the vast majority of RCM reactions are conducted.

Selecting an Analytical Technique

The choice of analytical method was a key decision to make during the design of these studies. Various methods have been reported in the literature for the monitoring of metathesis reactions. Grubbs *et al.* (and many others) have employed ^1H NMR spectroscopy routinely to monitor reactions of new pre-catalysts with prototypical substrates,^{45,156} while both Grubbs *et al.* and Fogg *et al.* favour gas chromatography with mass spectrometry (MS) or flame ionisation (FID) detection for high-throughput studies.^{147,157-158} However, the latter class of analyses typically focus simply on identifying 'hits' (where *any* conversion is obtained) rather than on constructing detailed concentration/time profiles. Percy *et al.* have employed GC-FID in their study of RCM reactions, both for the profiling of reactions and for accurate conversion measurements at the end of reactions.¹⁰⁸ Diver *et al.* have applied infrared (IR) spectroscopy to their studies on alkyne metathesis;¹⁵⁹ the decrease of the signal corresponding to the terminal alkyne was monitored. Verpoort *et al.* have employed Raman spectroscopy to monitor some ring-closing metathesis reactions.¹⁶⁰ Electrospray ionisation-mass spectrometry (ESI-MS) is gaining popularity as a technique for the study of metal-catalysed reactions,¹⁶ and has been applied to the study of ruthenium carbene species in RCM reactions.^{56,161-165} Plenio *et al.* have used UV/visible spectroscopy to monitor the initiation reactions of **GH2** and **Grela** with different substrates.⁶⁰⁻⁶¹

Each method has advantages and disadvantages. GC analyses require sample processing which can perturb the reaction outcome, especially given the volatility of the substrates studied herein. Reaction monitoring *via* ESI-MS requires dedicated and specialist equipment, and focuses primarily on catalyst-derived species. While UV/visible spectroscopy can be used to monitor the concentrations of ruthenium species in the reaction, the substrates and products do not feature suitable

chromophores and cannot typically be followed using this technique. The use of mid-IR spectroscopy for the analysis of reaction mixtures was explored briefly, but even relatively concentrated solutions of alkene (*ca.* 500 mmol L⁻¹ 1-octene) did not yield a detectable signal in the IR spectrum between 500 cm⁻¹ and 1800 cm⁻¹, so this technique was not suitable for monitoring the metathesis reactions of interest.

¹H NMR spectroscopy was selected as the analytical method for these studies. Despite the relatively high cost of instrument time, the need for deuterated solvents and the limited throughput of this technique, it is the most appropriate for this study. All dienes **103**, products **104** (and byproducts **105** and **106**) have ¹H nuclear magnetic resonances that can be used to measure solution concentration. In addition, the concentrations of pre-catalyst and related species can be measured by integration of the corresponding ¹H NMR resonances between approximately 17 and 21 ppm, which yields additional useful information about the metathesis reaction.¹⁰

Ensuring Robust Methodology

¹H NMR spectra of authentic samples of dienes **103** and cycloalkenes **104** were collected. An internal standard (1,3,5-trimethoxybenzene, which has been employed previously in metathesis chemistry)¹⁶⁶ was employed so that solution concentrations could be quantified for each component. Other internal standards have been employed for the study of metathesis reactions such as anthracene, which is only sparingly soluble in solvents such as benzene and DCM (≤ 10 mg/mL).

The integral of each signal on the ¹H NMR spectrum is proportional to the concentration of that species present within the solution. However, the response is also heavily dependent on the relaxation time (T_1) of the nucleus that it represents. If too short a delay is employed between the radiofrequency (RF) pulses, part of the population will not have relaxed fully, and the integral of the resonance will under-represent the population of that species. To avoid this problem, T_1 was measured for each signal in a number of representative substrates and products (1,7-octadiene **103c**, cyclopentene **104b**, cyclohexene **104c**, cycloheptene **104d** and *cis*-cyclooctene *cis*-**104e**) were measured. The ¹H NMR spectrum of each of these substrates or products (an authentic commercial sample in chloroform-*d*) was acquired a number of times, with different interpulse delays from *ca.* 0.01 to 45 seconds (termed D_1 on the Bruker instruments employed) for each acquisition. Data were fitted to the function in

Table 2.02. Longitudinal relaxation delays (T_1) of **103c** and **104b-e** in chloroform-*d*.

Compound	δ_H (ppm)	T_1 (s)	δ_H (ppm)	T_1 (s)	δ_H (ppm)	T_1 (s)	δ_H (ppm)	T_1 (s)
1,7-Octadiene	5.82	5.94	4.97	5.08	2.06	3.73	1.41	3.49
Cyclopentene	5.76	6.93	2.33	5.42	1.84	5.46	-	-
Cyclohexene	5.75	6.84	2.00	4.89	1.62	5.00	-	-
Cycloheptene	5.81	6.54	2.14	4.82	1.74	4.50	1.52	4.66
<i>cis</i> -Cyclooctene	5.64	6.05	2.16	4.16	1.51	4.08	-	-

Equation 2.01 (using the T_1/T_2 relaxation module of Bruker Topspin 2.1)¹⁶⁷ to yield the values recorded in **Table 2.02**; I_τ is the integral of the signal when delay τ is employed between pulses, P is a constant and T_1 is the longitudinal relaxation time of that signal.

$$I_\tau = I_0 + P \cdot \exp(-\tau/T_1) \quad (2.01)$$

The longest T_1 measured was 7 seconds, so the interpulse delay was set to 35 s for all subsequent kinetic experiments (unless otherwise stated).

Two instruments were employed for all in-magnet kinetic studies: an Avance 400 equipped with a BBFO- ζ -ATMA probe (^1H observation at 400 MHz), and an Avance II+ 600 equipped with either a BBO- ζ -ATMA probe or a TBI- ζ probe (^1H observation at 600 MHz). A number of technical differences between the two instruments resulted in superior results on the 600 MHz equipment: the higher magnetic field strength improved signal dispersion, while the self-levelling feet reduced the baseline noise. When running experiments on the 400 MHz equipment, four scans per spectrum were necessary to ensure an adequate signal to noise ratio. Similar quality spectra could be obtained using the 600 MHz apparatus with two scans per spectrum, and zero dummy scans (with the BBO- ζ -ATMA probe). Use of the TBI- ζ probe at 600 MHz yielded excellent quality spectra; the inverse arrangement of the probe, whereby the ^1H channel is closer to the sample, resulted in clear and sharp spectra, even at low concentrations and with only two scans (**Figure 2.02**).

RCM reactions can often be conducted under very mild conditions, which has been a factor in its rise to widespread use within synthetic chemistry laboratories. Reactions

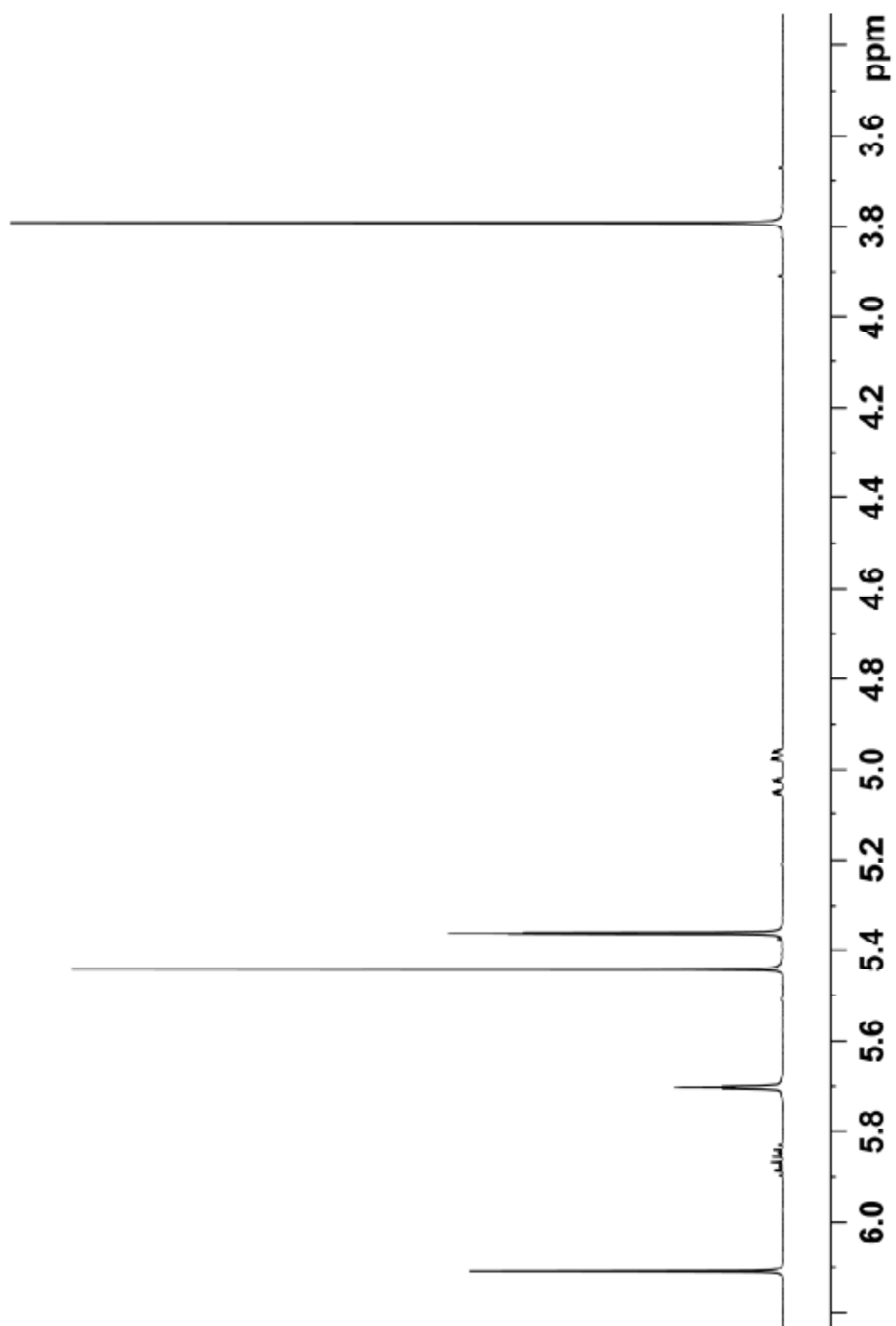


Figure 2.02. Partial 600 MHz ^1H NMR spectrum from the RCM of 1,7-octadiene (10 mmol L $^{-1}$ in DCM- d_2 with 1 mol% **G2**); this spectrum was acquired with two scans.

conducted here were carried out close to room temperature (298 K) unless otherwise stated, which provided benefits in terms of the ease of handling and preparation of reaction samples. It is not possible to reflux reactions within the magnet of the spectrometer due to the release of solvent vapour and the resulting change in volume (and hence concentration) and the potential for pressurisation of the NMR tube.

All reactions were performed in clean, dry NMR tubes, manufactured from an appropriate grade of glass. This avoided the introduction of artefact from the transfer of a reaction that was in progress from a separate vessel to an NMR tube. The NMR tube cap was pierced to allow the egress of ethene and to avoid the build-up of pressure within the thin-walled tube. Dried syringes and volumetric glassware (dried in a vacuum desiccator or in an oven, respectively) were used to manipulate and prepare solutions to ensure accurate and reproducible charging of reaction components. RCM reaction outcomes are, due to the competition between *intra*- and *inter*-molecular processes, heavily dependent on substrate concentration, so it was imperative that this critical parameter was known and set accurately and precisely.

Deuterated solvents were purchased from commercial sources, dried overnight on freshly-activated 4 Å molecular sieves, and sparged with dry oxygen-free nitrogen or argon before use. Karl Fischer titration of commercial chloroform-*d* and DCM-*d*₂ revealed that the drying procedure had reduced the water content from *ca.* 30 ppm to *ca.* 7 ppm,¹⁶⁸ similar to that found in solvents purchased as anhydrous, or in solvents obtained from the in-house solvent purification system; this therefore represents the level of water found in reaction solvents in typical synthetic metathesis reactions. Dienes were passed through activated alumina before use to remove polar impurities; in some cases this treatment stained the alumina yellow. The NMR spectra of treated dienes were checked to ensure that they did not contain organic impurities.

The solid pre-catalysts (purchased from commercial sources) and all solutions of them were handled under a flow of dry oxygen-free nitrogen or argon. Glove box conditions were not employed for the reasons discussed previously.

For each reaction, a *t*₀ sample (without pre-catalyst) was prepared that matched the concentration of the reaction mixture. This sample was used to tune, match, lock and shim the NMR spectrometer before starting the experiment, and to allow careful inspection of the stock solution and measurement of the initial diene concentration.

Experiments were conducted in duplicate to ensure that the protocol was a

reproducible means of acquiring kinetic data for RCM reactions. The reactions of 1,7-octadiene **104c** (at 10 mmol L⁻¹ and 100 mmol L⁻¹ in chloroform-*d*) were carried out with 1 mol% **G2**. Smooth concentration/time profiles were acquired (**Figures 2.03** and **2.04**). The material balance, defined here as the sum of the number of moles of substrate and product, was also quantified at each time point. The flat line obtained in all four reactions showed that the reaction components were accounted for correctly; if a slope had been obtained, this would have suggested that either the T_r measured for the substrate and/or product was wrong (and that the nuclei were not fully relaxing between RF pulses), or that substrate or product was being lost, for example, to a deleterious side reaction. Close inspection of the NMR spectra confirmed that only cyclohexene was generated as a product in this RCM reaction. The material balance showed that the sum of substrate and product was typically within *ca.* 3% of the initial charge of diene, and that any further deviation from this value was only obtained when the reaction had reached complete conclusion. When the concentration of diene is zero, integration of the baseline will still yield a (small) integral which may lead to this effect. The material balance therefore allows the error bars for NMR integration to yield the concentration of each component in the reaction to be estimated at *ca.* 1.5%.

These results demonstrated that this method was capable of generating

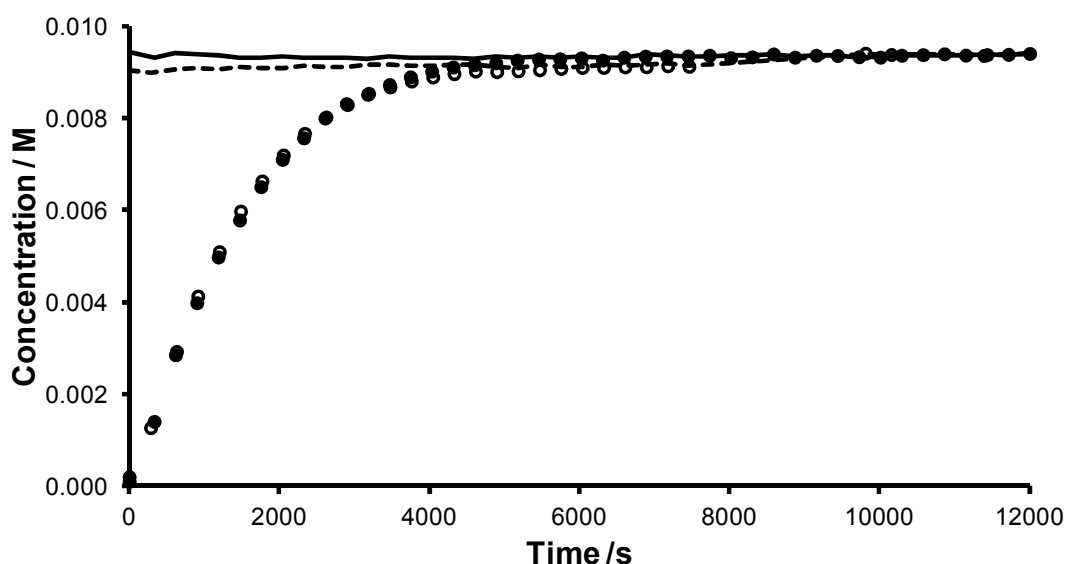


Figure 2.03. Concentration/time profiles showing the concentration of cyclohexene (solid and open circles) plus material balance (solid and dashed lines) in the RCM reactions of 1,7-octadiene (10 mmol L⁻¹ in chloroform-*d* with 1 mol% **G2**).

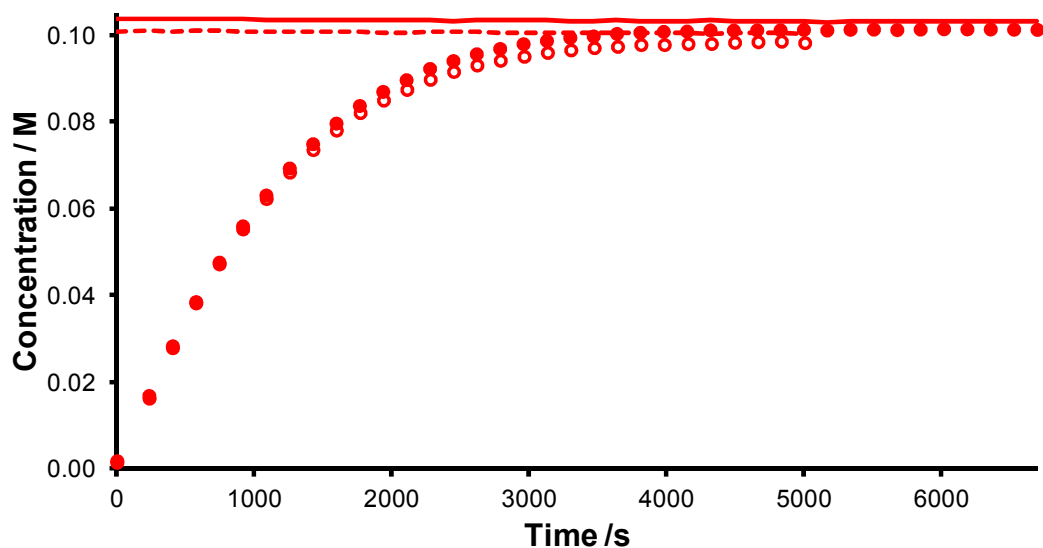


Figure 2.04. Concentration/time profiles showing the concentration of cyclohexene (solid and open circles) plus material balance (solid and dashed lines) in the RCM reactions of 1,7-octadiene (100 mmol L^{-1} in chloroform-*d* with 1 mol% **G2**).

reproducible and high-quality NMR data, with sufficient data density (*ca.* 4 points in the first $t_{1/2}$) to construct smooth concentration/time profiles.

With a suitable method in place, the protocol was applied to the acquisition of a large number of datasets in order to achieve the greater aims of the work.

Results from Kinetic Studies

Ring Size and Reaction Rate

A series of experiments was carried out to assess the effect of ring size on RCM rate, using 1,6-heptadiene, 1,7-octadiene and 1,8-nonadiene, in the first instance. These substrates were selected as they form five-, six- and seven-membered rings, and therefore represent the most common ring sizes prepared by RCM. Experiments were carried out using the method described above, with **G2** and in chloroform-*d* or DCM-*d*₂.

Multi-substrate experiments are an important way in which to establish relative orders of reactivity, as they ensure that all substrates undergo reaction under exactly the same conditions. Any impurities present, for example, traces of water, alcohol or dissolved oxygen in the solvent, or impurities from the pre-catalyst, can potentially interact with all reactions. However, the *degree* to which the components present in solution interact with intermediates during the reaction will depend on how sensitive various intermediates are to those components, as well as the concentrations of those intermediates that are present. RCM reactions where cyclisation is rate determining may lead to the accumulation of propagating carbene, for example, while those reactions where another step is rate determining might not; therefore, if this species was sensitive to a specific impurity, the reactions for which cyclisation is rate determining may be affected to a greater extent than those where it is not.

The concentration *versus* time profiles for experiments containing three diene substrates (*ca.* 3.3 mmol L⁻¹ each of **103b-d**) with 1 mol% **G2** in each solvent (**Figures 2.05** and **2.06**) clearly showed that cyclohexene formed fastest, followed by cyclopentene; cycloheptene formed slowest and did not reach completion in the timeframe studied. This order of reactivity was confirmed using reproducible single diene reactions in each solvent (**Figures 2.07** and **2.08**). Small solvent effects on the rate of reaction were observed.

While the RCM reactions of 1,6-heptadiene and 1,7-octadiene produced the target cycloalkenes exclusively, the RCM of 1,8-nonadiene produced small quantities of 1,7-tetradecadiene **106d**, which is the cyclic dimer derived from the RCM of 1,8,15-hexadecatriene **105d** (**Scheme 2.07**). This species has been reported previously, and characterised by ¹H and ¹³C NMR spectroscopy and mass spectrometry;^{136,154-155} it was

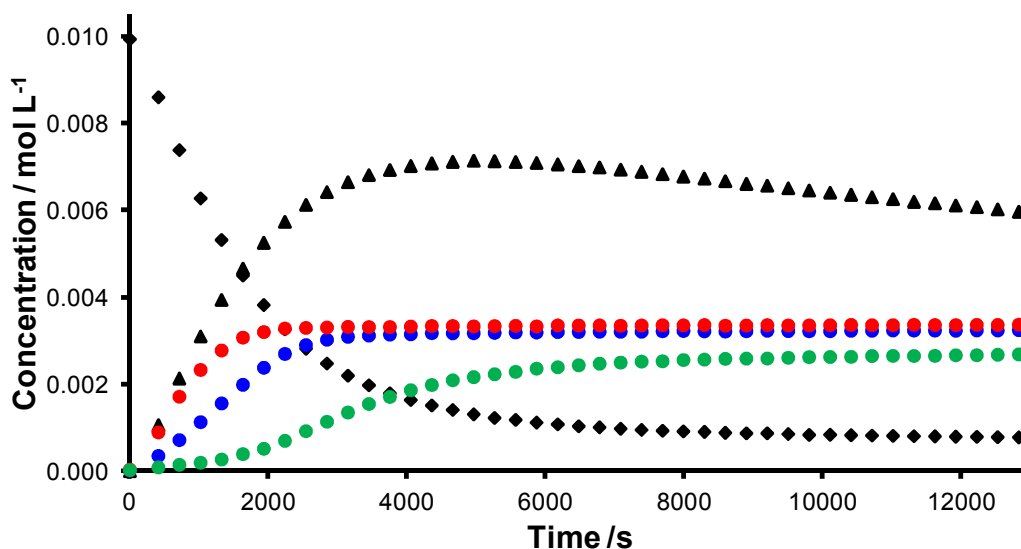
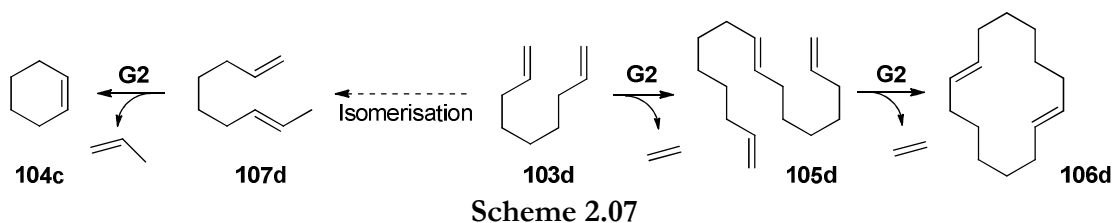


Figure 2.05. RCM of 1,6-heptadiene **103b**, 1,7-octadiene **103c** and 1,8-nonadiene **103d** to produce cyclopentene (**blue circles**), cyclohexene (**red circles**), cycloheptene (**green circles**) and ethene (**black triangles**) in chloroform-*d* (*ca.* 3.3 mmol L⁻¹ in each diene, 0.1 mmol L⁻¹ **G2**); the total diene concentration is also plotted (**black rhombi**).

identified here from its characteristic resonance at *ca.* 5.25 ppm in the ¹H NMR spectrum, which is distinct from the resonances found at *ca.* 5.5 ppm for larger oligomers.⁹⁶ In addition, the RCM of 1,8-nonadiene produced small quantities (*ca.* 0.2 mmol L⁻¹) of cyclohexene *via* RCM of 1,7-nonadiene **107d** (see chapter 4 for investigations into the isomerisation side reaction). Interestingly, 1,8-nonadiene RCM reactions exhibited a latency period before product formation and did not proceed to completion, with the cycloheptene concentration/time profile reaching a plateau. Either the catalyst system had expired and the reaction had simply stopped, or the reaction was approaching equilibrium. The former explanation can be ruled out, as the ¹H NMR resonance for the α -proton of pre-catalyst could be clearly identified in kinetic experiments (*ca.* 19-20 ppm, depending on solvent).¹⁰ Later experiments have shown

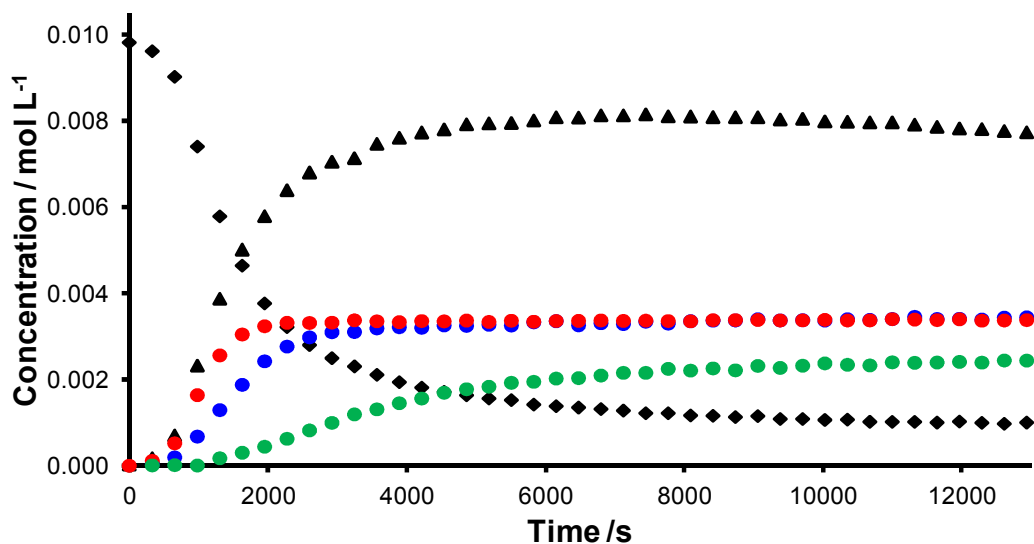


Figure 2.06. RCM of 1,6-heptadiene **103b**, 1,7-octadiene **103c** and 1,8-nonadiene **103d** to produce cyclopentene (blue circles), cyclohexene (red circles), cycloheptene (green circles) and ethene (black triangles) in DCM-*d*₂ (ca. 3.3 mmol L⁻¹ in each diene, 0.1 mmol L⁻¹ **G2**); the total diene concentration is also plotted (black rhombi).

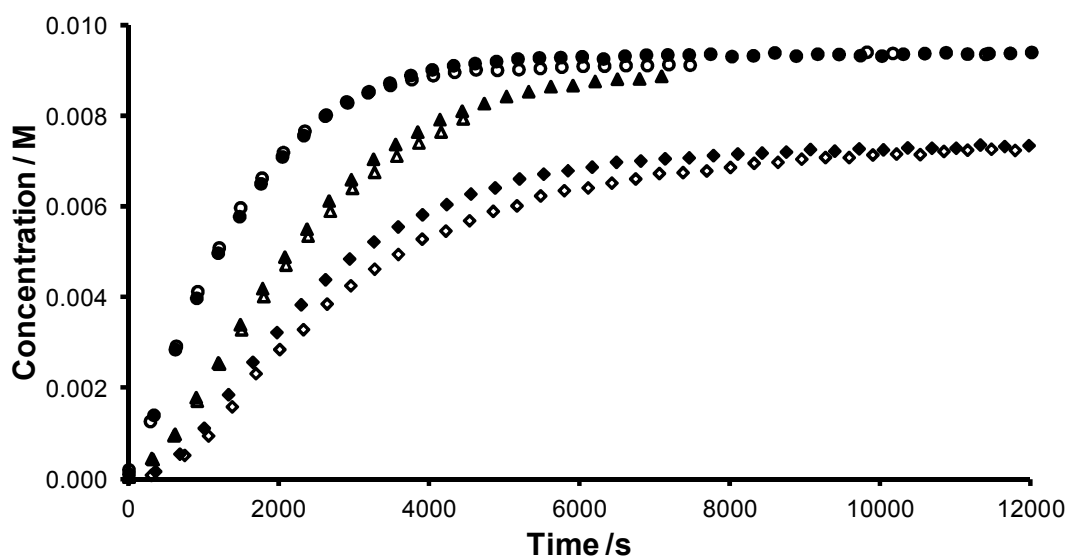


Figure 2.07. Concentration/time profiles for the RCM reactions of 10 mmol L⁻¹ of 1,6-heptadiene **103b**, 1,7-octadiene **103c** and 1,8-nonadiene **103d** in chloroform-*d* (in duplicate: open and closed shapes) with 0.1 mmol L⁻¹ **G2**, showing the production of cyclopentene (triangles), cyclohexene (circles) and cycloheptene (rhombi) respectively.

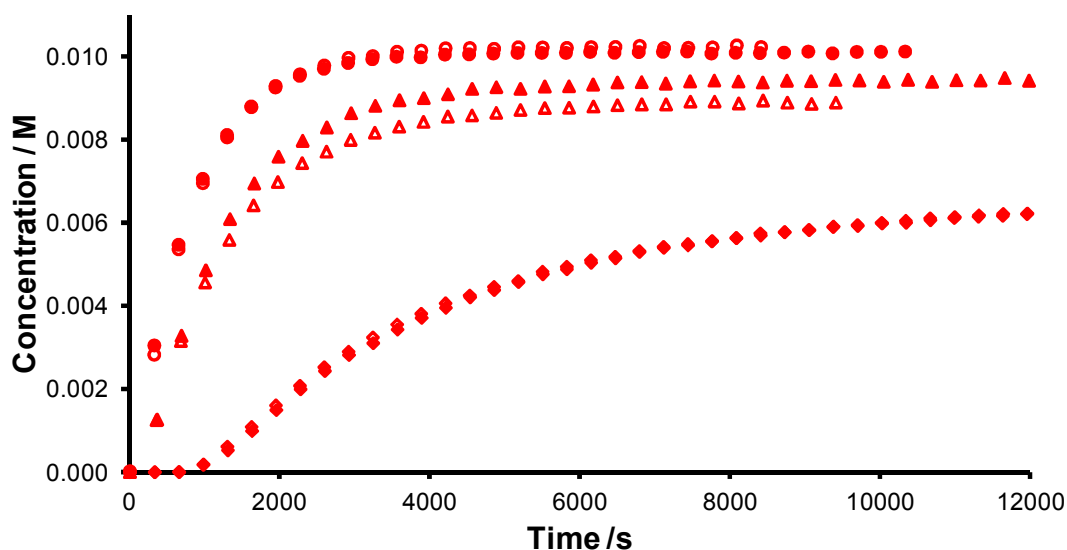


Figure 2.08. Concentration/time profiles for the RCM reactions of 10 mmol L⁻¹ of 1,6-heptadiene **103b**, 1,7-octadiene **103c** and 1,8-nonadiene **103d** in DCM-*d*₂ (in duplicate: open and closed shapes) with 0.1 mmol L⁻¹ **G2**, showing the production of cyclopentene (triangles), cyclohexene (circles) and cycloheptene (rhombi) respectively.

that this system is indeed under thermodynamic control (*vide infra*).⁹⁶

Attempts to monitor the RCM reaction of 1,9-decadiene **103e** (10 mmol L⁻¹ in chloroform-*d*) in the same manner were less successful. Only *ca.* 5% conversion (entirely to oligomeric material, $\delta_{\text{H}} = \text{ca. } 5.5$ ppm, confirmed by GC-MS with chemical ionisation (methane)) was obtained after 4 hours. All ethene had left the system, and no *cis*-cyclooctene was obtained. Conversion did not improve after 24 hours, in marked contrast to the other cyclisations which all resulted in greater than 50% conversion of diene after 4 hours. The reaction was repeated with a solid cap in case air and/or moisture had infiltrated the previous reaction. Conversion was improved (*ca.* 35% after 8 hours), but notably *cis*-cyclooctene *was* detected in this reaction mixture *via* the characteristic ¹H NMR resonance (δ_{H} (chloroform-*d*) = 5.63 ppm (*ca.* 2% conversion, **Figure 2.09**)). This assignment was confirmed by analysis of a commercial sample. Oligomers still comprised most of the products, with small quantities of cycloheptene and cyclohexene detected (*vide infra*). Unfortunately, the study of 1,9-decadiene RCM rate is not feasible using this method due to the low conversion obtained.

In all of the reactions, the accumulation of ethene in solution could be followed by ¹H NMR (*via* the resonance at $\delta_{\text{H}} =$ (chloroform-*d*) 5.43 ppm, (DCM-*d*₂) 5.46 ppm)

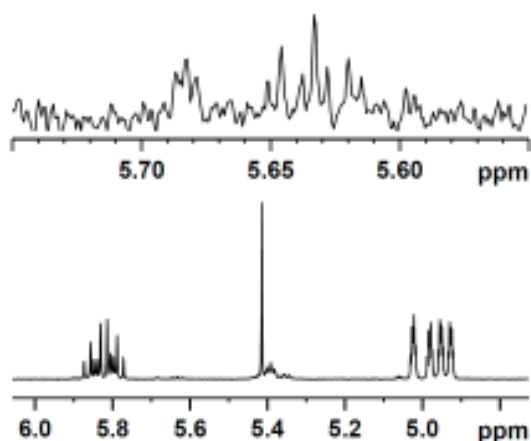


Figure 2.09. Partial ^1H NMR (400 MHz) from the RCM of 1,9-decadiene (10 mmol L^{-1}) with **G2** (1 mol%) in chloroform-*d* after 8 hours.

which increased to a maximum concentration of typically *ca.* 9 mmol L^{-1} (in samples where the total initial diene concentration was 10 mmol L^{-1}), then decreased slowly.

Ethene was not confined in these reactions, as the NMR tube cap was pierced to prevent pressurisation of the tube. For synthetic RCM experiments, reaction mixtures are typically heated to reflux and so ethene is driven from the system. The solubility of ethene in some organic solvents is known to decrease with increasing temperature¹⁶⁹ so higher temperatures favour ethene egress, even if the reaction is not heated to reflux.

The presence of small quantities of cyclohexene in 1,8-nonadiene RCM, and cyclohexene and cycloheptene in 1,9-decadiene RCM is was interesting, as these must have arisen from isomerisation followed by RCM. The topic of isomerisation side reactions is discussed and investigated more fully in Chapter 4.

In summary, these concentration/time profiles show that the order of RCM rate varies with target ring size as $6 > 5 > 7 \gg 8$. In addition, slower and less thermodynamically favourable RCM reactions are found to produce oligomers and isomerisation-RCM products.

Quantifying Relative Rates

Concentration/time profiles are of limited utility; while they can illustrate a clear rate difference (e.g. during pre-catalyst evaluation),⁴⁵ they are not a quantitative means of comparison. Rate constants were sought from the kinetic data in order to allow a quantitative comparison.

The use of a first-order kinetic treatment was attempted first (**Equations 2.02** and **2.03** are the rate law and integrated rate law, respectively). Implicit in this treatment

are the assumptions that the concentration of active catalyst (methylidene **4b**) remains constant (**Equation 2.04**) and that the rate determining step involves the diene. However, only 1,7-octadiene RCM in DCM fits a first order treatment well, with moderate fits obtained for 1,6-heptadiene in DCM- d_2 and 1,7-octadiene in chloroform- d (**Figure 2.10**). None of the 1,8-nonadiene RCM reactions fitted a first-order expression. While reaction simulation can obtain rate constant data from complex concentration/time data, the approach requires considerably more work to develop, so is explored fully in chapter 3.

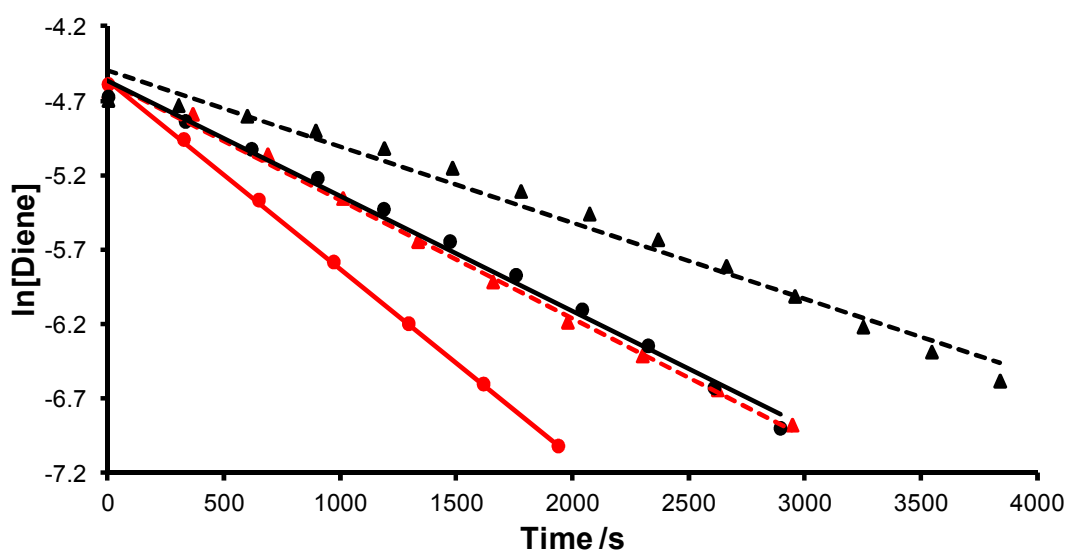


Figure 2.10. First-order treatment of concentration/time data for 1,6-heptadiene (triangles, dashed lines) and 1,7-octadiene (circles, solid lines) in chloroform- d (**black**) and DCM (**red**); lines represent a linear fit to the first three half lives of the reaction.

$$d[A]/dt = k_{obs} \cdot [A]_t \quad (2.02)$$

$$[A]_t = [A]_0 \cdot \exp(k_{obs}t) \quad (2.03)$$

$$k_{obs} = k \cdot [4b] \quad (2.04)$$

A semi-quantitative approach, in which a selected (linear) portion of the $\ln[\text{diene}]$ versus time plot was used to obtain a pseudo first-order rate constant, was adopted here instead (**Figure 2.11** shows the results of applying this treatment to data obtained from reactions in DCM- d_2). Treatment of all the data in this manner yields the rate constants and, from those, relative rates in **Table 2.03**. This treatment allowed the

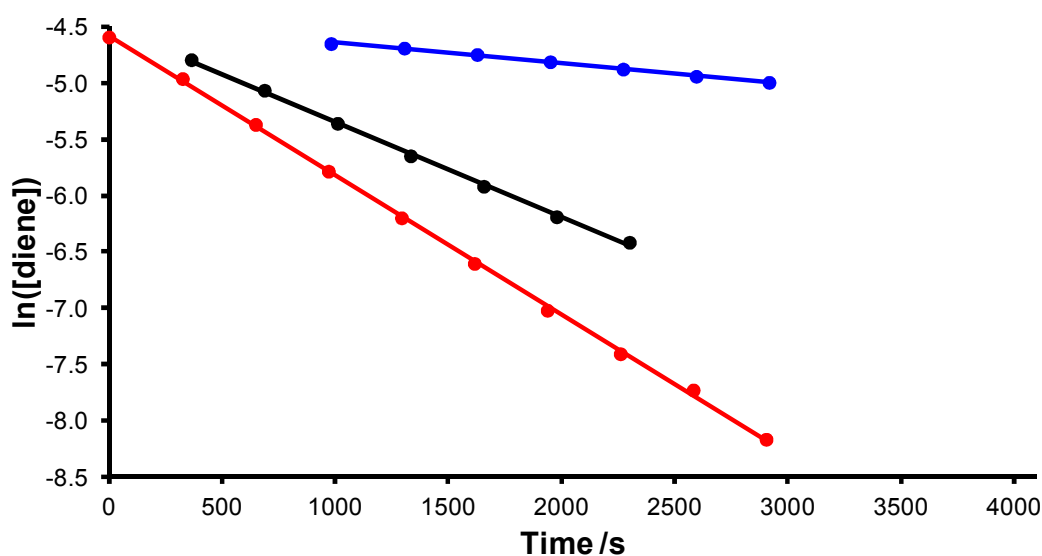


Figure 2.11. Use of a semi-quantitative approach to obtain pseudo-first-order rate constants for the RCM reactions of 1,6-heptadiene (**black points**), 1,7-octadiene (**red points**) and 1,8-nonadiene (**blue points**) in DCM- d_2 (10 mmol L $^{-1}$, 1 mol % **G2**).

Table 2.03. Rate constants (units s $^{-1}$) and relative rates (where 1,7-octadiene RCM in DCM- d_2 has $k_{rel} = 1$) from the RCM reactions of 1,6-heptadiene, 1,7-octadiene and 1,8-nonadiene in chloroform- d and DCM- d_2 with 1 mol% **G2**; each rate constant is the average from two experiments.

Substrate	mmol L $^{-1}$	Chloroform		DCM	
		k_{obs}	k_{rel}	k_{obs}	k_{rel}
1,6-Heptadiene	10	5.6×10^{-4}	0.47	8.2×10^{-4}	0.68
1,7-Octadiene	10	8.4×10^{-4}	0.70	1.2×10^{-3}	(1.00)
1,8-Nonadiene	10	2.8×10^{-4}	0.23	1.9×10^{-4}	0.16
1,7-Octadiene	100	1.1×10^{-3}	0.92	-	-

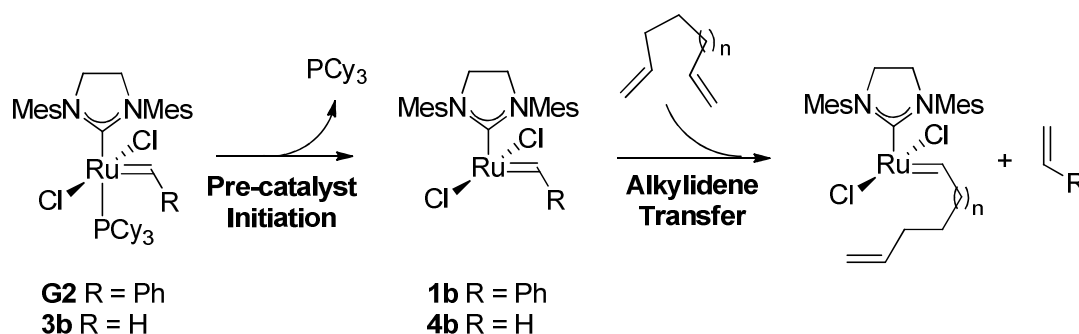
approximate relative rates of each reaction to be assessed. However, as only part of the profile was used in some cases (*ca.* $1t_{1/2}$ for 1,8-nonadiene, $2t_{1/2}$ for 1,6-heptadiene), these relative rates must be regarded as only a semi-quantitative measurement of RCM rate. This is especially true given the very narrow (8-fold) spread of values obtained.

The RCM reactions of 1,6-heptadiene and 1,7-octadiene proceeded approximately 1.5-fold faster in DCM- d_2 than in chloroform- d . This was a rather modest

solvent effect so it was clear that these reactions were not significantly affected by solvent choice. The relative rates of 1,6-heptadiene RCM and 1,7-octadiene RCM were the same in each solvent, but there was a switch in the relative rate of 1,8-nonadiene RCM, which occurs *faster* in chloroform-*d*. As these effects are modest, there is potential to explore less conventional solvents for metathesis; if RCM proceeds at approximately the same rate in all solvents (that are tolerated by the metathesis catalyst system) then solvents can be selected more on the basis of their safety, toxicity or environmental profiles or general acceptability for scale-up within industry.¹⁷⁰

These data show that 1,7-octadiene RCM was approximately 1.5-fold faster than 1,6-heptadiene RCM and approximately 4-6 times faster than 1,8-nonadiene RCM; 1,9-decadiene RCM proceeded far more slowly and with poor conversion (*vide supra*) so relative rates for this reaction have not been calculated.

Some mechanistic inferences can be drawn from these relationships, if one assumes that alkylidene transfer (**Scheme 2.08**) occurs at the same rate, regardless of n , in the case of the simple dienes **103** studied here. If, for example, pre-catalyst initiation or alkylidene transfer were rate determining in all three reactions, all reactions would proceed at the same rate (**Scheme 2.08**), therefore the rate-determining step is not the same in each reaction, or is a step that is dependent on the value of n .⁹⁸ 1,7-Octadiene RCM reactions produce cyclohexene, freezing relatively few rotors and introducing almost no strain into the product.¹¹² Therefore, the good fit of 1,7-octadiene RCM reactions to a first order reaction model may be indicative of fast cyclisation and therefore of rate-limiting alkylidene transfer. The rate expression for this step is first order in both catalyst (*not* pre-catalyst) and 1,7-octadiene **103c** (**Equation 2.05**); if the concentration of methylene **4b** in solution remains approximately constant, which is

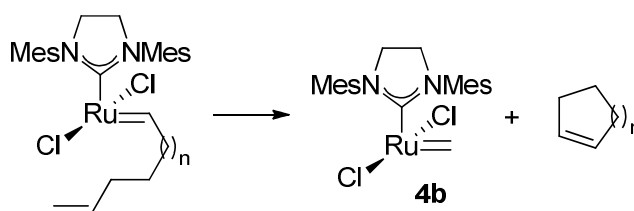


Scheme 2.08

$$d[103c]/dt = k \cdot [103c] \cdot [4b] \quad (2.05)$$

$$d[103c]/dt = k_{obs} \cdot [103c] \quad (\text{where } k_{obs} = k \cdot [4b]) \quad (2.06)$$

possible given the slow initiation rate of **G2**,²⁶ then this can be approximated to the expression in **Equation 2.06** which would explain the good first order behaviour. As all three cyclisation rates are different, the rate-determining step for 1,6-heptadiene **103b** and 1,8-nonadiene **103d** RCM reactions must involve events after alkylidene transfer, i.e. must involve the cyclisation itself. This is consistent with the distinct latency period before cycloheptene production in the RCM reaction of 1,8-nonadiene, suggesting a build-up of a species due to the cyclisation being rate determining (**Scheme 2.09**).



Scheme 2.09

While interpretation of reaction outcomes is somewhat complicated by the appearance of oligomeric material and isomerisation-RCM side products, the order of reactivity in the simplest prototypical systems is clear: six-membered rings form fastest, *ca.* 1.5-fold faster than five-membered rings, which in turn form *ca.* 2-4 times faster than seven-membered rings; eight-membered rings form an order of magnitude slower. None of these systems is conformationally restricted, and therefore these results represent the effect of target ring size *alone*. This is an important outcome, as there has been very little study of the rates of cyclisation reactions which form π -bonds rather than σ -bonds.

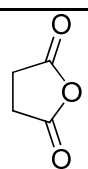
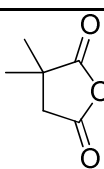
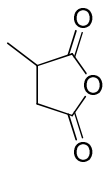
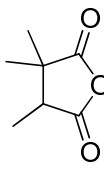
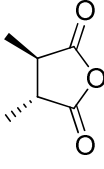
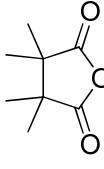
Comparison with the Ring-closing Literature

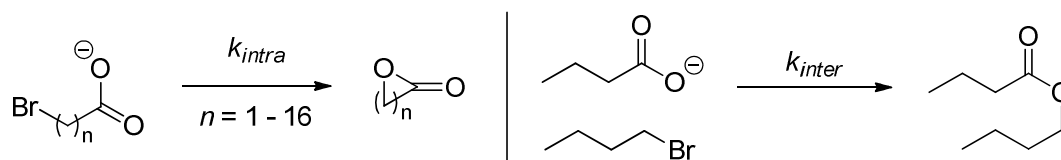
In classic ring-closing literature, which typically considers ring-closing *via* creation of σ -bonds, the ease of formation of different ring sizes is generally in the order $3 > 4 < 5 > 6 > 7$.¹⁰² Where a series of similar reactions is considered (i.e. where the corresponding intermolecular reaction with rate constant k_{inter} is the same) this manifests as a rate difference in the same order. Therefore it would be expected that the five-membered ring (cyclopentene) should form faster than the six-membered ring (cyclohexene), if the

ring were to be formed *via* σ -bond creation in a classic nucleophilic substitution at an sp^3 centre or *via* an acid- or base-catalysed ring-closing reaction at a carbonyl group. Both types of ring-closing reactions have been well studied in the literature, particularly by Kirby¹⁰² and Mandolini,^{103,171} and mechanistic differences can be identified between these classes. Nucleophilic ring-closing reactions typically have kinetic EMs of 10^4 - 10^8 mol L⁻¹ *versus* less than 10 mol L⁻¹ for acid- or base-catalysed ring-closing; product formation *via* looser transition states in the latter class of reactions results in lower kinetic EMs.¹⁰² For example, Kirby has presented data for the ring-closing reactions of a series of succinamic acid analogues to form products **108a-f** (Table 2.04), in which the ratio of kinetic EM to thermodynamic EM typically decreases as hydrogen atoms on the backbone are replaced with methyl groups. This was attributed to methylation of the backbone leading to gradually looser (and hence less sterically-demanding) transition states and therefore a lower ratio of kinetic to thermodynamic effective molarity.

For a series of ring-closing reactions in which different ring sizes are formed, but with the same pattern of functionality (e.g. the S_N2 lactone-forming reactions in

Table 2.04. Thermodynamic and kinetic effective molarities for the cyclisations of succinamic acids to the corresponding succinamic anhydrides **108** at 333 K,¹⁰² all EM values are recorded in mol L⁻¹.

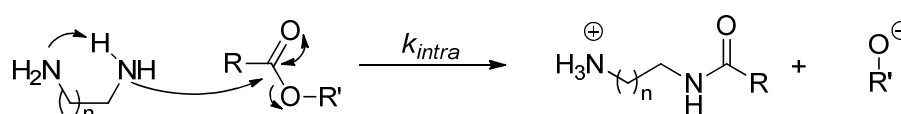
Product	Kinetic EM	EM _T	Product	Kinetic EM	EM _T
	5.1 x 10 ⁴	1.9 x 10 ⁵		1.2 x 10 ⁶	6.7 x 10 ⁶
108a			108d		
	1.3 x 10 ⁵	1.1 x 10 ⁶		6.6 x 10 ⁶	3 x 10 ⁸
108b			108e		
	5.9 x 10 ⁵	2.7 x 10 ⁶		2.0 x 10 ⁷	4.6 x 10 ⁹
108c			108f		



Scheme 2.10¹⁰³

Scheme 2.10),¹⁰³ the same intermolecular reaction can be used to obtain k_{inter} when calculating kinetic EMs. Therefore, the relative kinetic EM and relative k_{inter} are the same, and the kinetic EMs yield information about the relative rates and efficiencies of formation of rings of different sizes. The relative cyclisation rates for this series of reactions depended acutely on n : formation of the five-membered ring ($n = 3$) proceeded 10^2 -fold faster than that of the six-membered ring ($n = 4$), 10^4 -fold faster than that of the seven-membered ring ($n = 5$), and 10^6 -fold faster than that of the eight- or nine-membered ring ($n = 6$). These are far larger differences than those encountered between the relative RCM rates above.

Much smaller differences in kinetic EM were encountered in the intramolecular general base catalysis of aminolysis by a series of diamines of varying chain length (**Scheme 2.11** and **Table 2.05**), as this reaction occurred *via* a much looser transition state. The magnitude of the dependence of the reaction rate on ring size was found to be sensitive to the structure of the ester that underwent aminolysis; phenyl acetate hydrolysis was insensitive to the diamine chain length, while a modest (2-4 fold) spread of rate constants were obtained for acetyl imidazole hydrolysis. The intermolecular reaction in both cases was the hydrolysis of the ester by a monoamine of the same pK_a , and therefore relative kinetic EM is the same as relative rate as described above.



Scheme 2.11¹⁰²

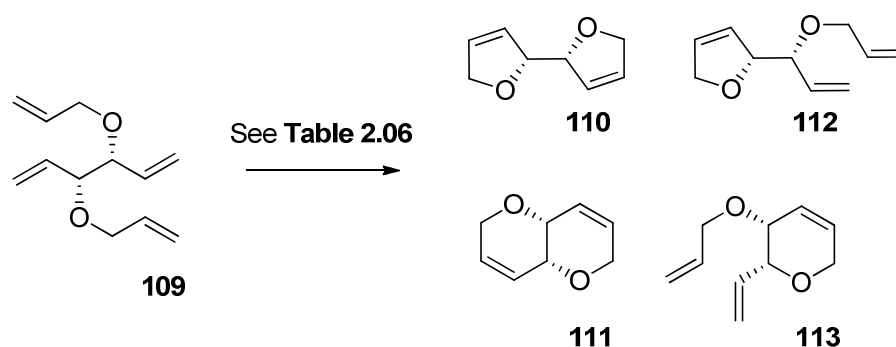
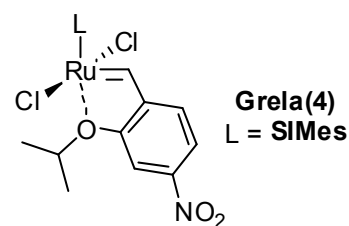
These examples from the literature differ from RCM in that nucleophilic ring-closing does not involve a catalyst, while the intramolecular acid- or base-catalysed reactions rely on catalysis of the process by the bifunctional chain itself. RCM requires the use of a metal carbene pre-catalyst in order to effect the reaction.

Table 2.05. Kinetic EMs for the intramolecular general base-catalysed reaction in **Scheme 2.11**.¹⁰²

	<i>n</i>	1	2	3	4	5
EM (mol L ⁻¹) for R = Me, R' = Ph		<i>ca.</i> 1	<i>ca.</i> 1	<i>ca.</i> 1	1	<i>ca.</i> 1
EM (mol L ⁻¹) for R = imidazole, R' = Et		0.55	0.94	0.20	0.25	-

The calculation of kinetic EMs for RCM is relatively unexplored. Fogg *et al.* attempted to collect EM data for a number of RCM reactions, but the quoted values are not from the syntheses of the products *via* RCM, while most are for slightly different compounds (such as saturated analogues) than those presented;¹⁴⁶ quoted EMs are obtained from a variety of different reactions. To date, the only true measured kinetic EMs for RCM reactions are those reported by Mitchell *et al.* for the RCM reactions to form a series of difluorinated cyclooctenone products with various protecting groups, with and without *gem*-disubstitution;¹⁰⁸ the relatively low kinetic EMs (*ca.* 10⁻² to 10⁰ M) allowed the quantification of the products of the kinetically-controlled cyclisation *and* oligomerisation in the same reactions. This study is discussed in the introduction.

The modern metathesis literature does contain some discussions of ring-size effects on selectivity. Schmidt has studied the RCM reaction of compound **109**, which can undergo RCM to form four different products with various combinations of ring-sizes, with pre-catalysts **G1**, **GH1**, **G2**, **GH2**, **Grela** and **Grela(4)** (**Scheme 2.12**).¹⁷² This substrate can in principle undergo cyclisation to yield bicyclic products **110** and/or **111**, featuring either two five-membered rings or two six-membered rings, or only one RCM reaction



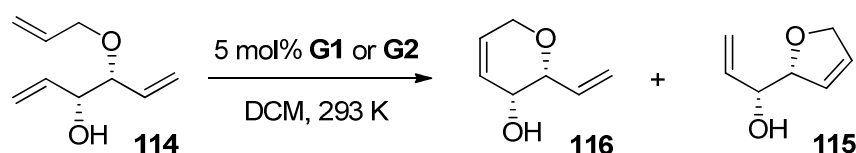
Scheme 2.12¹⁷²

Table 2.06. Product mixtures from the metathesis reactions of **109**.¹⁷²

Entry	Solvent	Pre-Catalyst (5 mol%)	P (bar)		Conv. (%)	Product Ratio		
			Ar	C ₂ H ₄		111	110	112+113
1	DCM ^a	G1	1	-	99	Only 110		
2	DCM ^a	G2	1	-	99	1.0	1.7	-
3	Toluene ^b	G1	1	-	99	1.0	11.0	-
4	Toluene ^b	G2	1	-	99	1.0	1.4	-
5	Toluene ^b	G1	-	12	99	1.0	8.0	0.2
6	Toluene ^b	G2	-	12	80	1.0	1.5	0.4
7	Toluene ^b	Grela(4)	-	12	85	1.0	0.8	0.2
8	Toluene ^b	G1	30	12	95	1.0	5.0	0.3
9	Toluene ^b	G2	30	12	99	1.0	1.4	-

^a $T = 20^{\circ}\text{C}$ ^b $T = 110^{\circ}\text{C}$

to yield products **112** and/or **113**. Various pre-catalysts and reaction conditions were explored for the metathesis of **109**, resulting in various mixtures of the four possible products (**Table 2.06**). Pre-catalyst **G1** does not react as rapidly with disubstituted olefins as second-generation pre-catalysts such as **G2**,⁶² providing lower *E:Z* selectivities in cross- metathesis reactions, for example.⁴⁵ In addition, **G1** is less capable of reacting with RCM products¹³⁸ and therefore typically yields the *kinetic* rather than *thermodynamic* product of RCM. Schmidt *et al.* postulate that as **G1** yields exclusively the bis(dihydrofuran) product **110**, that **110** is therefore the kinetic RCM product. Conducting the metathesis reaction either at higher temperatures (therefore making ring-opening of the product more competitive) or under an atmosphere of ethene (which disfavours product formation by driving the reaction equilibrium back towards products) resulted in a higher proportion of the bis(dihydropyran) product **111**. These outcomes are consistent with the presumption that **111** was the thermodynamic product. Metathesis of the simpler triene **114** (**Scheme 2.13**) with **G1** resulted in a 1:1 mixture of

**Scheme 2.13**¹⁷²

with our results that six-membered ring formation is fastest in the simplest diene systems, but do not discriminate between the five- and seven-membered ring products. It is important to note, however, that these results are obtained with the first-generation pre-catalyst **G1**, and that gas-phase and solution-phase reactivity may differ.¹⁶ More recent studies by Metzger *et al.* have shown that **G2** and **GH2** can in principle be studied by forming the alkali metal adduct in the mass spectrometer, but no studies on metathesis reactions with **G2** or **GH2** have been reported yet.¹⁷³

Given the different chain lengths attached to the alkylidenes in **Scheme 2.14**, larger differences in the ratios of **117:118** would be expected. DFT calculations (M06-L/6-311G*) conducted by Hillier *et al.* on the alkylidenes derived from second-generation pre-catalyst systems suggest that differences should be larger.⁵³ Evaluation of the energies of **119** and **120** (**Scheme 2.15**) for the alkylidenes derived from dienes **103b-g** (**Table 2.07**) resulted in equilibrium constants K_{alkene} that varied by several orders of magnitude. The phosphane-binding step in all reactions (with equilibrium constant K_{phos}) should be independent of the length of the alkylidene chain, and the equilibrium constant for the formation of phosphane-bound alkylidenes **121** from the pre-catalyst ought to be independent of chain length as well, by analogy with the findings of Schore *et al.* (*vide infra*).¹⁶⁵ Expressions for K_{alkene} and K_{phos} led to **Equation 2.07**, which

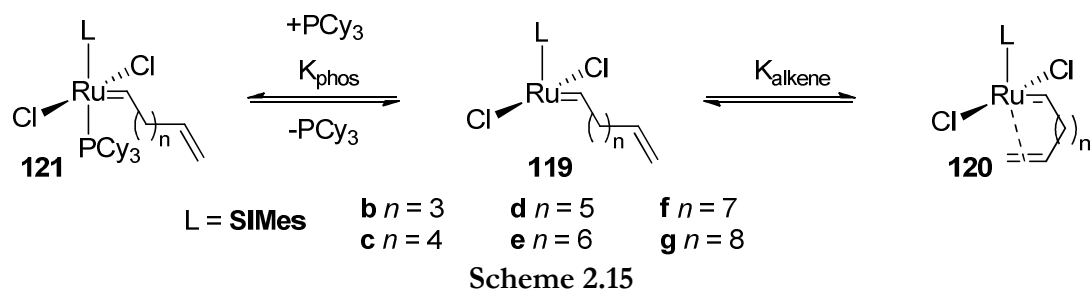


Table 2.07. Evaluation of K_{alkene} (in **Scheme 2.15**) for the alkylidenes **120** *versus* **119**, derived from simple dienes **103b-g**.⁵³

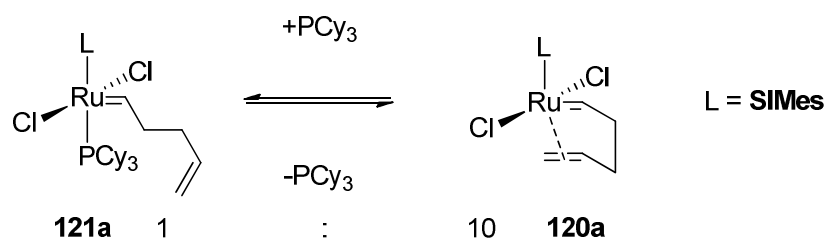
Alkylidenes	b	c	d	e	f	g
Target ring size	5	6	7	8	9	10
ΔG (kcal mol ⁻¹) ^a	-11.48	-6.59	-7.66	-5.15	-0.75	-4.44
K_{alkene}	2.6×10^8	6.8×10^4	4.2×10^5	6.0×10^3	3.6×10^0	1.8×10^3
K_{rel} (relative to b)	(1.0)	2.6×10^{-4}	1.6×10^{-3}	2.3×10^{-5}	1.4×10^{-8}	6.9×10^{-6}

^a Calculated free energies, including solvation.

demonstrated that the relative ratios of alkylidene **120** to phosphane-bound **121**, in the presence of a given concentration of PCy₃, ought to depend only on the equilibrium constants K_{alkene} and K_{phos}, of which only K_{alkene} varies between alkylidenes. Findings based on DFT calculations yield very different results to those reported by Metzger *et al.*, perhaps due to the different pre-catalyst systems (second *versus* first generation).

$$[\mathbf{121}]/[\mathbf{120}] = K_{\text{alkene}} \cdot ([\text{PCy}_3]/K_{\text{phos}}) \quad (2.07)$$

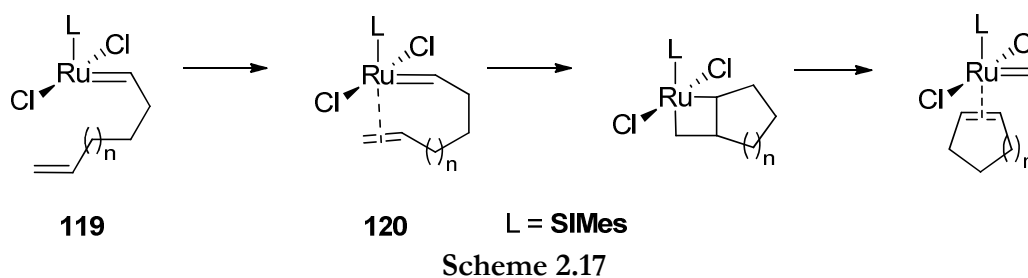
Metzger *et al.* found that η^2 -complex **120a** derived from 1,5-hexadiene **103a** was far more favoured than **121a**, more so than for the corresponding complexes derived from 1,6-heptadiene; phosphane-bound complex **121a** was detected at levels ten-fold *lower* than the corresponding chelated alkylidene **120a** (Scheme 2.16). The interesting case of 1,5-hexadiene is discussed more fully in a subsequent section of this chapter.



Scheme 2.16¹⁶⁴

While it is interesting to probe the behaviour of different intermediate species *en route* to metathesis products with different target ring sizes, it is important to note that the RDS on the PES lies beyond this point,⁵³ so the calculated relative chelation equilibrium does not translate directly into an overall calculated relative RCM rate.

The slow and incomplete RCM of 1,8-nonadiene was of interest. While the strain energy of cycloheptene **104d** is similar to that of cyclopentene **104b** (5.2 kcal mol⁻¹ *versus* 5.0 kcal mol⁻¹, respectively)¹¹² the value of EM_s is *ca.* 10-fold lower (2.7 *versus* 20)¹⁰³ due to the two extra rotors which must be frozen upon cyclisation. It is important to note, however, that these values represent *thermodynamic* efficiency and that the effect of this extra entropy loss (with respect to 1,6-heptadiene RCM) on the *kinetics* of the reaction will depend on which step is rate-determining and on the entropy loss in the transition state(s) *en route* to the product from the alkylidene **119** (Scheme 2.17).



Detailed calculations of the PESs for the RCM reactions of dienes **103b-g** (M06-L/6-311G*) suggest that the MCB retro-[2+2]cycloaddition steps have the highest barrier in the cycles and are therefore the rate determining steps for the RCM of 1,6-heptadiene – 1,10-undecadiene;⁵³ MCB formation was identified as rate determining instead for 1,11-dodecadiene. Comparing the calculated overall free energy change for cyclisation to the barrier for MCB formation for each cyclisation does not reveal a clear trend (**Figure 2.12**). However, for the formation of ring sizes from seven to ten (inclusive), there is a clear correlation between the free energy for the overall RCM reactions and the free energy differences between alkyldienes **119** and cyclic η^2 -complexes **120**. The product cycloalkenes from these RCM reactions are both strained and involve the freezing of a number of rotors (six to nine); some of the enthalpic and entropic effects of this overall cyclisation appear to be felt at this stage in the reaction.

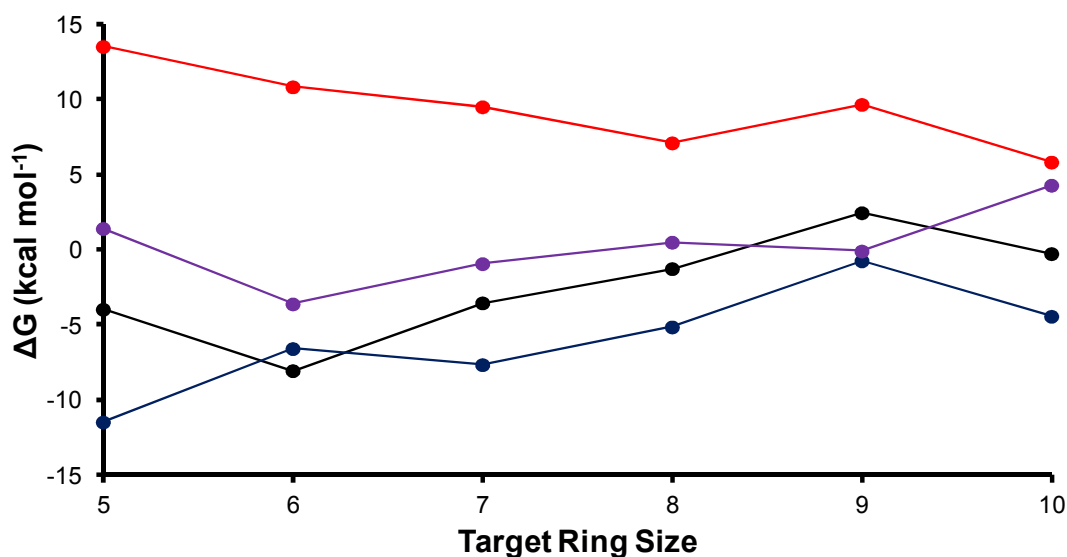


Figure 2.12. Calculated free energies for RCM (**black**),⁹⁶ alkyldiene to cyclic η^2 -complex (**blue**), η^2 -complex to metalocyclobutane (**purple**) and free energy barrier to metalocyclobutane breakdown (**red**) *versus* target ring size (M06-L/6-311G*).⁵³

In the RCM reactions of 1,8-nonadiene under more concentrated conditions (see Chapter 4), a signal in the ^1H NMR spectrum is attributed to the phosphane-bound propagating carbene, which is consistent with the calculations discussed here.⁹⁶ A similar (though less clear) trend appears between the five- and six- membered ring free energies of RCM and the corresponding metallocyclobutanation free energy differences.

Linking calculated and experimental relative rates is not trivial. There are no clear correlations between a single free energy difference or barrier and the overall reaction rate. Thermodynamic control in these RCM reactions (*vide infra*) complicates interpretation of DFT calculations on catalytic intermediates. An alternative approach to identifying a single rate-determining step in the sequence is to use the energetic span model developed by Kozuch *et al.*, in which the lowest energy intermediate (the TOF determining intermediate, TDI) and highest energy transition state (the TOF determining transition state, TDTS) in the cycle are considered (**Equation 2.08**).¹⁷⁴

$$\begin{aligned} \text{TOF} &= (k_{\text{B}}T/h)\exp(-\delta E/RT) \quad \text{where} \\ \delta E &= E_{\text{TDTS}} - E_{\text{TDI}} \quad (\text{if TDTS occurs after TDI}); \text{ or} \\ &E_{\text{TDTS}} - E_{\text{TDI}} + \Delta G^\circ \quad (\text{if TDTS occurs before TDI}) \end{aligned} \quad (2.08)$$

For the metathesis reactions of the simple diene substrates considered here, the TDI is the MCB for 1,7-octadiene, 1,8-nonadiene and 1,10-undecadiene, while for 1,6-heptadiene, 1,9-decadiene and 1,11-dodecadiene the TDI is the cyclic η^2 -complex. The TDTS is less obvious; for 1,10-undecadiene and 1,11-dodecadiene it may be the breakdown of this MCB, but for the other systems methylenide **4b** plus diene is of higher energy (**Figure 2.13**). There may be additional, higher barriers on the PES, for example, for the reaction of **4b** plus diene. Straub has calculated the barrier for **4b** plus ethene to be only 1 kcal mol⁻¹,⁷² albeit using the B3LYP/LACV3P**+ level of theory which is not ideal for these systems.⁵⁴ In addition, the reaction of **4b** with alkene has been shown to be close to barrierless.^{56,72} For the systems studied here, the energy of **4b** plus diene can be considered as a lower limit for the TDTS; the barriers that are encountered *en route* to the propagating carbenes **119** should be essentially the same, as the reactivity of the alkene terminus should be independent of the length of the chain. As the TDTS occurs before the TDI for these four systems, ΔG° must be included in the calculation; $\Delta G_{\text{RCM}}^\circ$ was used for this purpose.⁹⁶ The relevant values were tabulated

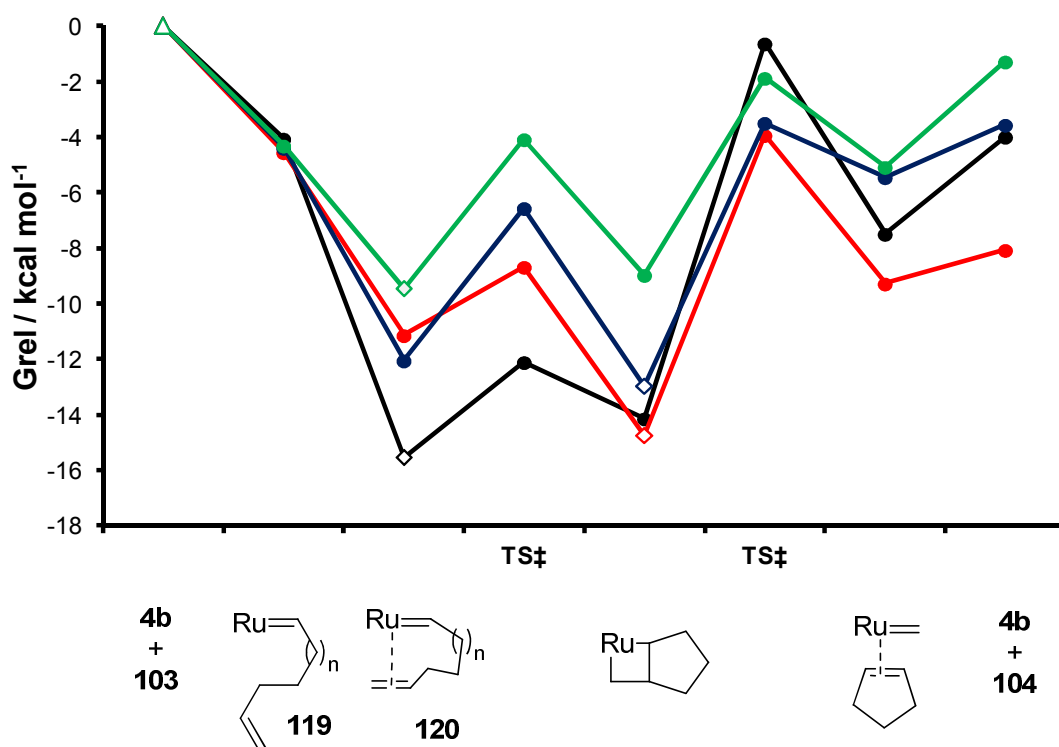


Figure 2.13. Partial PESs (G_{rel}) for the RCM reactions of 1,6-heptadiene (**black**), 1,7-octadiene (**red**), 1,8-nonadiene (**blue**) and 1,9-decadiene (**green**) calculated at the M06-L/6-311G* level of theory, normalised to methyldiene **4b** plus diene, the TDI is indicated by a rhombus and the TDTS (**4b** + **103**, as a lower limit) by a triangle.⁵³

Table 2.08. Applying the energetic span model to the RCM reactions of 1,6-heptadiene, 1,7-octadiene, 1,8-nonadiene and 1,9-decadiene; free energies are in kcal mol⁻¹.

Target Ring Size	ΔG_{RCM}° (corr.) ^a	G_{TDTS}^b	G_{TDI}^b	δE	Rel. TOF ^c
5	2.02	0	-15.53	17.55	2.7×10^{-4}
6	-2.06	0	-14.75	12.69	1
7	2.45	0	-12.98	15.43	9.8×10^{-3}
8	4.73	0	-9.45	14.18	8.1×10^{-2}

^a From reference⁹⁶ ^b Relative to **4b** plus diene ^c Relative to 1,7-octadiene RCM

and δE and therefore TOF were calculated using this methodology (**Table 2.08**). This treatment suggested that 1,7-octadiene ought to undergo RCM fastest by orders of magnitude, whereas experimentally the reaction only occurred approximately two-fold faster than the RCM of 1,6-heptadiene. Also, the order of TOF for 1,6-heptadiene, 1,8-

nonadiene and 1,9-decadiene was predicted to be the *opposite* of what is experimentally observed. Therefore, this approach cannot reliably be used to calculate TOF for the six RCM reactions explored using free energies from DFT calculations by Hillier *et al.* The ΔG° for cycloalkene formation ranks the three systems correctly (6 > 5 > 7; -8.06, -3.98 and -3.55 kcal mol⁻¹ respectively) but the particularly low energy of the cyclic η^2 -complex derived from 1,6-heptadiene increases the energetic span of the PES for this cyclisation and suggests that cyclopentene ought to be formed *slower* than cycloheptene. Further work to develop computational methods and approaches is necessary before DFT calculations can be used to predict the relative rates of RCM; current DFT methods that use implicit solvation models (such as the SM8 model developed by Cramer and Truhlar)¹⁷⁵ do not deal properly with the entropic effects of solvation.⁹⁶ In addition, the reversible nature of each of the steps (as opposed to the palladium-catalysed coupling chemistry to which the energetic span model has been successfully applied) may go some way to explaining the discrepancy between experimental and DFT outcomes.

The observation of *cis*-cyclooctene as a product in the RCM reaction of 1,9-decadiene was surprising in the context of previous RCM literature. Grubbs *et al.* postulated that only systems that are ‘conformationally predisposed for ring formation’, such as catechol derivatives **81** (Scheme 1.38) can successfully form eight-membered rings;¹²⁵ RCM of malonate derivatives **76** (10 mmol L⁻¹ at room temperature in DCM) yielded only an acyclic dimer when exposed to **G1** (Scheme 1.36).¹¹⁶ It is important to note that conclusions in the literature are based almost exclusively on *yield* measurements and/or inspection of the ¹H NMR spectra of worked-up reaction mixtures. Artefacts may be introduced in preparing the sample for analysis; the cyclisations examined alongside those of malonate derivatives **76** were concentrated and purified by column chromatography before analysis and so the reduction of the solvent volume with active ruthenium species still present may have led to the ROMP reaction of the product.^{68,108} When optimising the RCM reaction *en route* to macrocycle **59**, chemists at Boehringer-Ingelheim noted that: ‘...when some of the solvent was distilled off, the HPLC yield [of product] dropped with time ... the presence of a still active catalytic species at the end of the RCM was a major hurdle toward the isolation of our product, and it became imperative to devise a means for catalyst inactivation’.⁶⁸ In kinetic reactions, where work-up and processing are avoided, very small quantities of *cis*-cyclooctene were produced, agreeing to some extent with the literature precedent that eight-membered rings are more challenging RCM

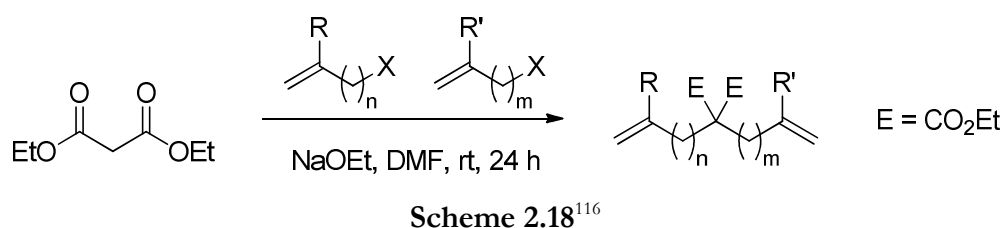
targets. Our methodology (which avoids perturbation of the reaction as far as is possible) is crucial to the clear identification of *cis*-cyclooctene in the reaction. Had this reaction been worked-up and purified before analysis, ROMP processes or losses during work-up may have yielded a negative result. The ‘conformational predisposition’ that was proposed by Grubbs *et al.* to account for the limited success of eight-membered ring syntheses refers to the reduced entropy or enthalpy loss upon cyclisation of substrates which already have rotors restricted or in which cyclisation will relieve strain. The catechol derivative **81** has six rotors frozen during cyclisation, as opposed to seven for 1,9-decadiene RCM; the corresponding entropy loss upon cyclisation is therefore *ca.* 2 – 4 cal K⁻¹ mol⁻¹ less.¹⁰³ In addition, the replacement of two CH₂ units with ether linkages, plus the sp² hybridisation of two carbon atoms in the chain (*versus* sp³ hybridisation in 1,9-decadiene) may reduce ring-strain contributions from transannular interactions. Stereochemical effects on eight-membered ring formation *via* RCM have also been reported, due to the differing strain energies of the diastereomeric products.¹²⁵

While the relative rates of RCM established here (6 > 5 > 7 >> 8) are not the same as those established for classical nucleophilic, acid- or base-catalysed ring-closing (5 > 6 > 7 > 8),¹⁰² the results presented here provide robust verification of the trend apparent within literature studies of more functionalised systems. There are only modest differences between RCM *rates* of different systems, but multi-diene experiments presented above have confirmed the order of reactivity. The distinction between common and medium rings is clear, both from the literature and from results presented here in which 1,8-nonadiene RCM reactions do not reach completion (at 10 mmol L⁻¹) and 1,9-decadiene RCM is too slow to follow at 298 K. The modest difference observed between the rates of RCM of 1,6-heptadiene and 1,7-octadiene present no basis for any considerable selectivity between the ring sizes under kinetic control, despite the suggestions from theory that quite large differences should be evident. These results shed further light on the results of Schmidt *et al.*, who obtained various outcomes when tetraene **109** was exposed to different metathesis pre-catalysts under a variety of reaction conditions. In contrast, little or no ring-size selectivity was observed for simpler triene **114** (Scheme 2.13 above); the 1:1 mixture of five- and six-membered ring obtained with **G1** is most likely a result of purely kinetic control, while the 3:1 mixture of six-:five-membered obtained with **G2** is further evidence of this pre-catalyst operating in the thermodynamic regime.

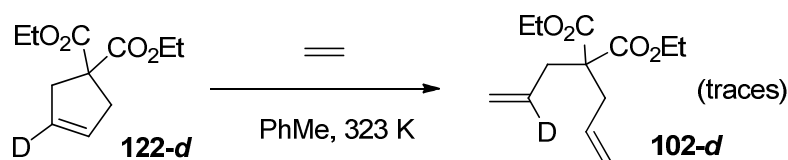
Comparison with a Literature Prototypical System

Diethyl Malonate Systems

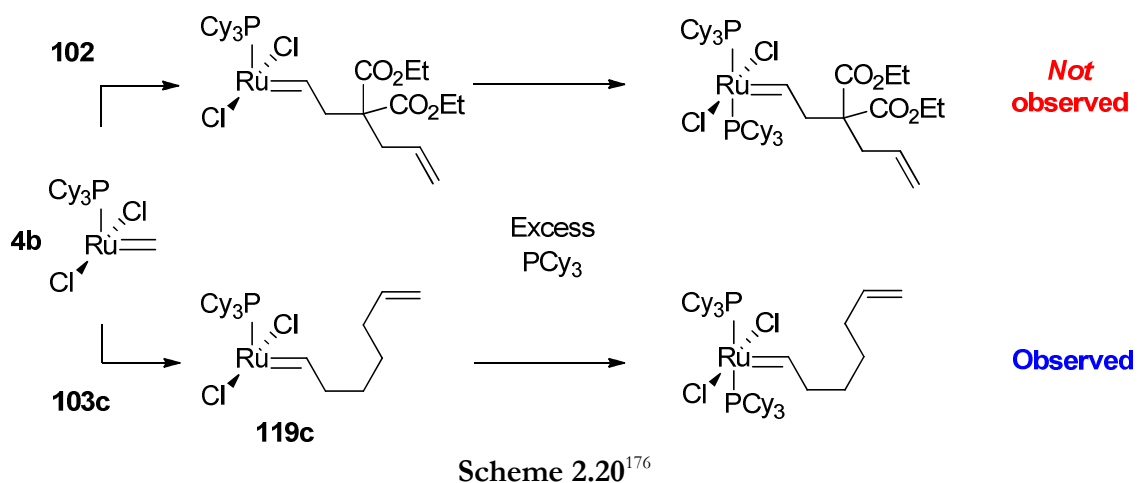
Prototypical systems reported in the literature are most commonly either a diethyl malonate compound or an *N*-tosylamine with pendant alkenes; the length of the chain between the core unit and the alkene can be varied to vary the product ring size, or the substitution pattern can be altered. This approach was used by Grubbs *et al.* when exploring the scope and limitations of RCM using pre-catalyst **G1** (Scheme 2.18).¹¹⁶



RCM substrates prepared using this approach tend to be relatively involatile oils which are easier to handle than the volatile and low-boiling liquids that have been used for the studies documented in this thesis. Reaction mixtures can be worked-up using traditional methods and purified using column chromatography to obtain isolated yields. Diethyl diallylmalonate **102** is believed to cyclise irreversibly, based on deuterium labelling studies by Grubbs *et al.* in which ring-opening of **122-d** occurred very slowly at 323 K (Scheme 2.19);⁸⁹ only traces of product **102-d** were detected by MS. The RCM of **102** is believed to proceed *via* rate-limiting alkylidene transfer and not rate-limiting cyclisation, as proposed by Grubbs *et al.* during early studies on the activity of pre-catalysts such as **G1** (Scheme 2.20):¹⁷⁶ ‘... the second metathesis step, the intramolecular reaction to form the cyclised product is faster than the first, intermolecular metathesis, due to the decreased activation entropy. This is evidenced by the fact that we never observe the intermediate that precedes the cyclisation step even when



Scheme 2.19⁸⁹



excess phosphine is added, as opposed to the cyclisation of 1,7-octadiene to cyclohexene, during which this intermediate is observed by ¹H NMR in the presence of excess phosphine.

The effect of the bulky *gem*-disubstitution pattern in **102** was evaluated. Diethyl diallylmalonate can be considered as a functionalised analogue of 1,6-heptadiene **103b**. Any difference in the rate or EM (kinetic or thermodynamic) of the RCM of this substrate must therefore be as a result of this functionality; this might, for example, affect the number and energies of accessible diene conformations and/or have an impact on the strain present in the cyclic product. The presence of this functionality ought to accelerate cyclisation, either *via* the Thorpe-Ingold effect¹⁷⁷⁻¹⁷⁸ or the reactive-rotamer effect.¹⁷⁹ There are key differences between these two theories. The Thorpe-Ingold effect is brought about by a change of angle between the reacting termini due to a corresponding change in bond angle caused by disubstitution (**Figure 2.14 (a)**); the presence of bulky substituents is proposed to reduce angle θ , bringing the reacting centres X and Y closer together. An alternative explanation is the reactive-rotamer theory, whereby the bulky substituents reduce the energy difference between the *gauche* and *anti* forms, effectively lowering the relative energy of the rotamer where the reacting

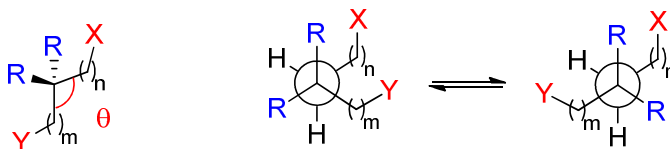
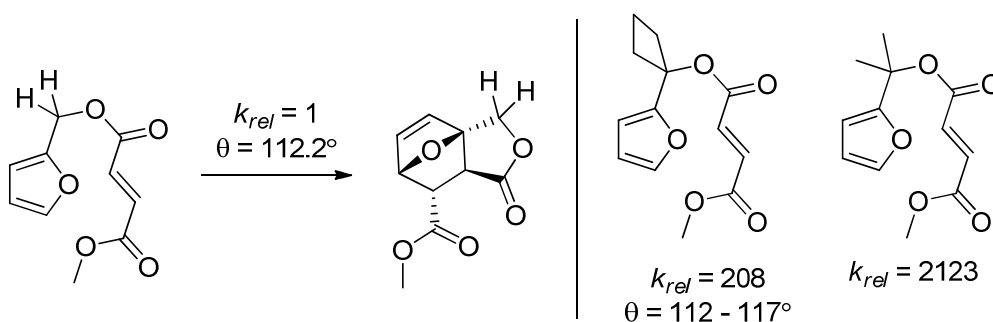


Figure 2.14. (a) The Thorpe Ingold effect, where the increasing size of R decreases angle θ ; (b) the reactive-rotamer effect where, as R increases, the energy of the *anti*- and *gauche*-conformations become closer.



Scheme 2.21¹⁸⁰

end groups are closest together (**Figure 2.14 (b)**). This effect has been shown to predominate in some intramolecular Diels-Alder reactions where backbone substitution patterns with similar steric impact but different angle θ were both found to cyclise faster than the parent dihydro compound (**Scheme 2.21**).¹⁸⁰ If angle compression were the only factor that determined the rate of reaction, then the cyclobutane-substituted compound would be expected to undergo cyclisation *more slowly* than the corresponding dihydro compound. Instead, a significant rate *increase* was obtained.

Regardless of the exact mode of action, it is accepted that *gem*-disubstitution typically increases the rate of cyclisation. The rate of cyclisation of **102** was examined by exposing the substrate (10 mmol L⁻¹ in DCM-*d*₂) to **G2** (0.1 mmol L⁻¹) using the method detailed previously. The concentration/time profile was compared to the analogous reaction of 1,6-heptadiene (**Figure 2.15**). Surprisingly, the rate of diethyl diallylmalonate RCM ($t_{1/2} = ca. 2000$ s) was *half* that of 1,6-heptadiene ($t_{1/2} = ca. 1000$ s), despite the presence of a quaternary centre that would typically be expected to accelerate the cyclisation compared to the parent system. This order of reactivity was confirmed using a multi-component kinetic experiment in which each substrate (5 mmol L⁻¹ in each in DCM-*d*₂) was exposed to the same charge of **G2** (0.1 mmol L⁻¹). When these RCM reactions were conducted at higher (*ca.* 1 mol L⁻¹) substrate concentrations, a second key difference was revealed between the two systems: while diethyl diallylmalonate underwent complete RCM, 1,6-heptadiene metathesis formed considerable quantities of oligomeric material. Therefore, while 1,6-heptadiene metathesis is *faster*, the effective molarity of 1,6-heptadiene is far lower than that of **102**.

A first-order treatment of the concentration/time data from the RCM reaction of diethyl diallylmalonate was attempted (**Figure 2.16**). The reaction behaviour is close to first order, but a linear section covering approximately two half-lives was selected for

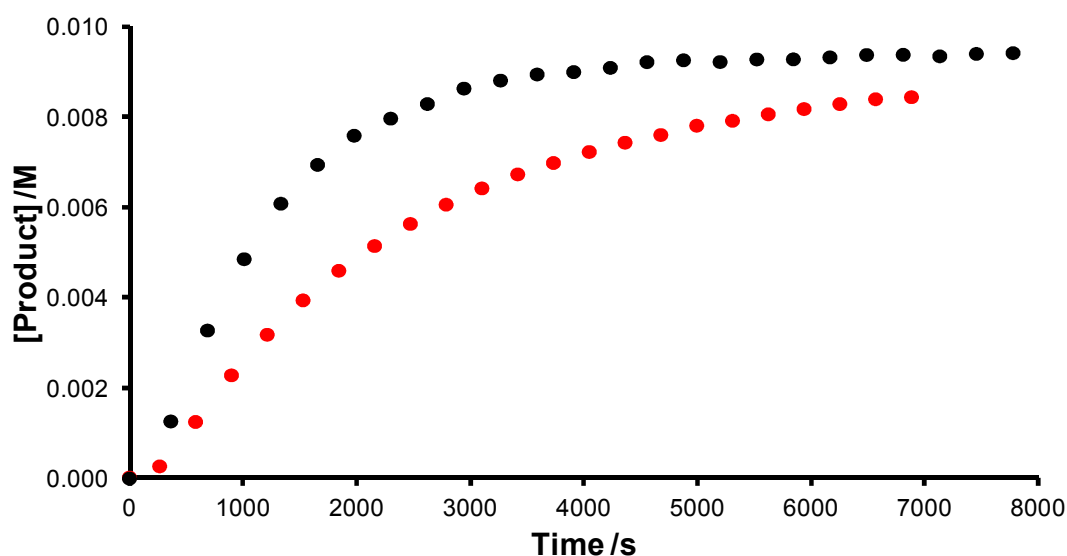


Figure 2.15. Concentration/time profiles for product formation from (i) the RCM of diethyl diallylmalonate **102** (red) and (ii) the RCM of 1,6-heptadiene **103b** (black); both reactions were carried out with 10 mmol L^{-1} substrate plus 0.1 mmol L^{-1} **G2** in $\text{DCM-}d_2$.

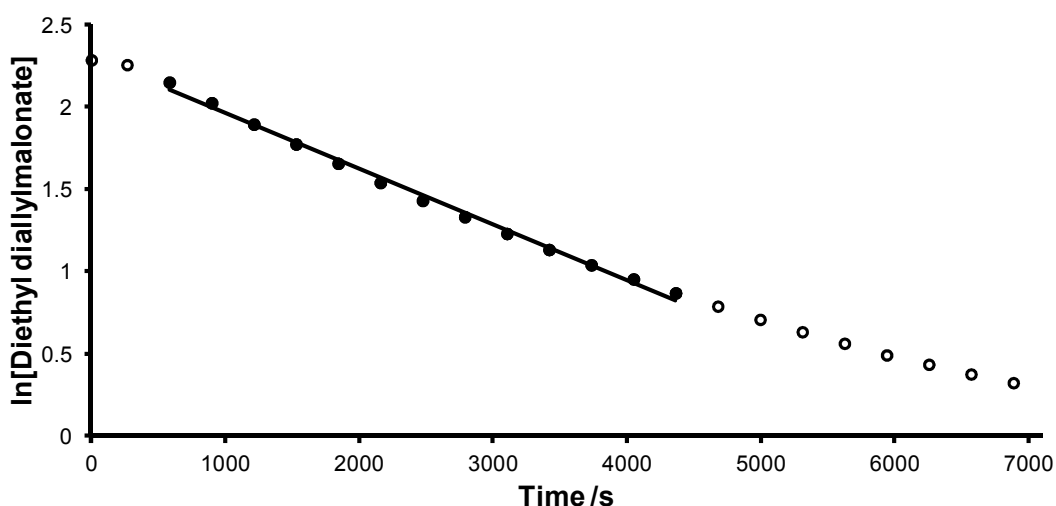
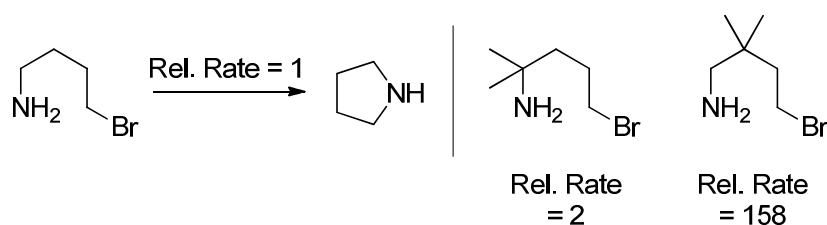


Figure 2.16. First-order treatment of the kinetic data in **Figure 2.15** using (i) all data points (open circles, $k_{obs} = 3.0 \times 10^{-4} \text{ s}^{-1}$, $R^2 = 0.988$) or (ii) selected data points from a linear portion of the plot (closed circles, $k_{obs} = 3.4 \times 10^{-4} \text{ s}^{-1}$, $R^2 = 0.996$).

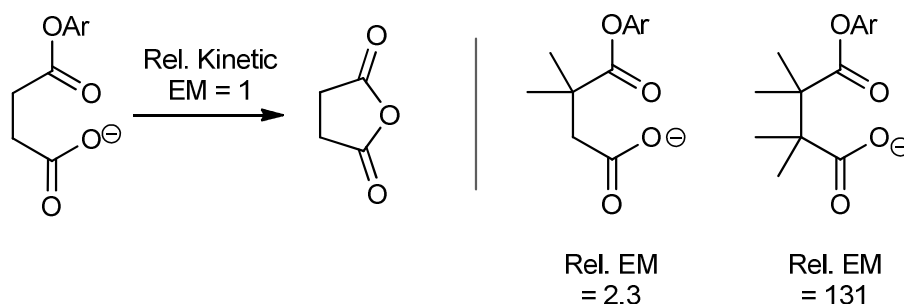
calculation of an approximate pseudo first-order rate constant, in the same way as rate constants have been calculated previously. Comparing the rate constant obtained ($3.4 \times 10^{-4} \text{ s}^{-1}$) with those obtained for the simple α,ω -diene substrates (**Table 2.03** above) allows relative rate constants (in $\text{DCM-}d_2$) to be compared; diethyl diallylmalonate RCM

has $k_{rel} = 0.28$, compared to 0.68 for 1,6-heptadiene, 1.00 for 1,7-octadiene and 0.16 for 1,8-nonadiene. Despite the bulky *gem*-substitution, RCM of diethyl diallylmalonate proceeded at approximately *half* the rate of the parent 1,6-heptadiene system.

When considering existing literature on the *gem*-disubstituent effect (typically *gem*-dimethyl, rather than *gem*-diester), an accelerating effect would be expected and both the kinetic EM and thermodynamic EM_T would be expected to exceed those of an unsubstituted substrate. For example, in the cyclisations of a series of succinamic acids to the corresponding anhydrides an increase in both EM and EM_T was obtained upon successive methylation of the backbone (**Table 2.04** above);¹⁰² while EM and EM_T both increased, the latter increased much more quickly. The effects in **Table 2.04** are large, with a 20-fold increase in kinetic EM and a 30-fold increase in EM_T from *gem*-dimethylation alone (**108a** versus **108d**). However, rate and efficiency differences are not always so large. In two other literature examples, the nucleophilic ring-closing of bromoalkylamines to form pyrrolidines and the anhydride-forming reactions of aryl succinamates, the relative rates and kinetic EMs are more modest (**Schemes 2.22** and **2.23**). The pyrrolidine-forming reactions are of particular note: the rate enhancement obtained was highly sensitive to the placement of the *gem*-dimethyl substituents. Placement of the *gem*-dimethyl substituent close to the reacting centres resulted in steric



Scheme 2.22¹⁰²



Scheme 2.23¹⁰²

hindrance offsetting the benefit of strain relief, while placement mid-chain revealed relative rates that showed clear strain relief upon cyclisation.

Similar trends were obtained from the ring-closing metathesis literature, as discussed in the introduction. Wagener *et al.* reported that metathesis of neat nona-1,8-dien-5-one yields exclusively oligomeric material, while metathesis of the 4,4,6,6-tetramethyl analogue yields only 3,3,5,5-tetramethylcyclohepten-4-one (**Scheme 1.24**).¹⁰⁵ Percy *et al.* recorded a four-fold increase in rate for the RCM of **56b** *versus* **56a** and a four-fold kinetic EM increase for the RCM of **56b** *versus* **56a** (**Scheme 1.25**).¹⁰⁸ Cyclisation would not be expected to be rate-determining in the RCM of diethyl diallylmalonate **102**, as the cyclisation event should be accelerated by the presence of *gem*-disubstitution. Therefore the alkylidene transfer step (see **Scheme 2.08** above) must be rate determining for this substrate. The bulky diester functionality might retard the alkylidene transfer rate, resulting in a slower overall rate of reaction compared to the RCM of 1,6-heptadiene, due to the steric impact of the *gem*-diester. This may result in steric repulsion between methyldiene **4b** and **102**, despite the diester being located quite far from the alkene terminus; visualisation of the optimised geometry of **4b** (M06-L/6-311G*) using a space-fill model shows how congested the metal centre is (**Figure 2.17**).

A second possibility is that the ester functionality chelates the metal centre, in a manner analogous to **GH2**, in which the electron-rich heteroatom occupies the vacant site *trans* to the N-heterocyclic carbene *in lieu* of a phosphane ligand.

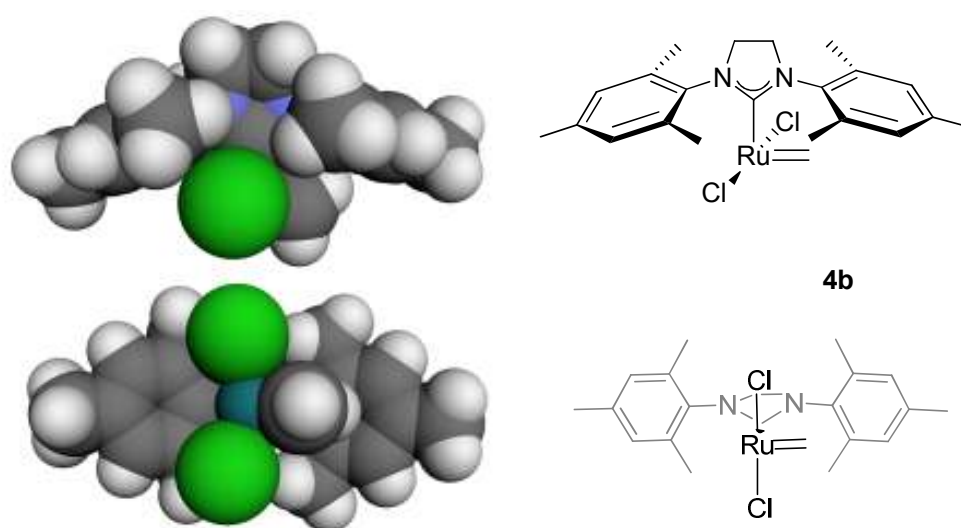
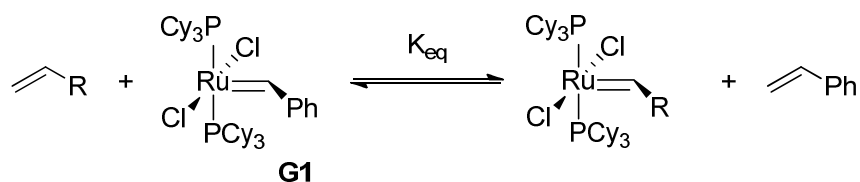


Figure 2.17. Space-fill model of the optimised geometry of methyldiene **4b** (at the M06-L/6-311G* level of theory).⁹⁰



Scheme 2.24¹⁸¹

Schore *et al.* have studied the equilibria that exist when **G1** is exposed to a series of alkenes (Scheme 2.24).¹⁸¹ The equilibrium constant was found to vary considerably (from *ca.* 2×10^{-3} to *ca.* 1×10^1) depending on the substitution pattern of the alkene introduced (Table 2.09); while most simple alkenes (1-butene to 1-decene) resulted in $K_{\text{eq}} \approx 0.3$, malonate derivatives yielded K_{eq} from *ca.* 0.002 to 0.2 depending on the length of the alkyl chain. The most dramatic difference was obtained upon moving from **102** to diethyl methyl(allyl)malonate, which features a quaternary centre. Further

Table 2.09. Equilibrium constants (and ΔG°) for the reactions between pre-catalyst **G1** and various alkenes, as measured by NMR integration by Schore *et al.*.¹⁸¹

Substrate	K_{eq}^a	ΔG° (kcal mol ⁻¹)	Substrate	K_{eq}^a	ΔG° (kcal mol ⁻¹)
	8.7 ^b	-1.25		0.0019	3.69
	1.8	-0.33		0.13	1.21
	0.34	0.62		0.015	2.47
	0.29	0.73		0.036	1.93
	0.32	0.66		0.17	1.03
	0.30 ^c	0.69		0.0046	3.14
	0.30	0.70		0.0021	3.60
	0.30	0.69		0.0019	3.79

^a Average of 10 runs unless otherwise stated.

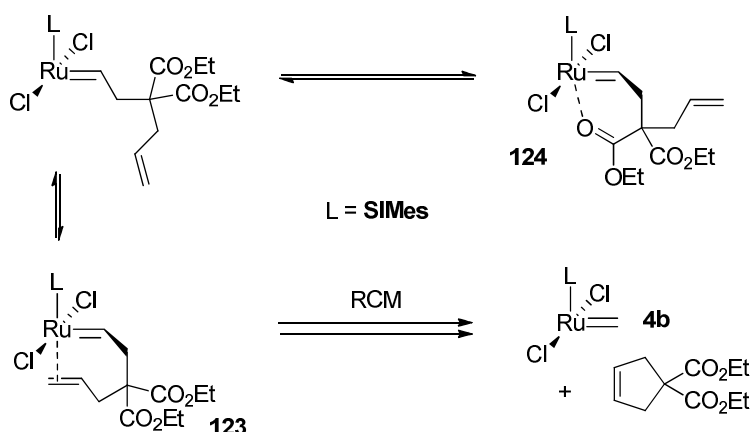
^b 8 runs.

^c 9 runs.

increases in the steric bulk of the malonate by adding successive methylene units had less of an effect, but reduced K_{eq} further. The equilibrium constants for reaction of **G1** with the malonate derivatives are two orders of magnitude lower than those for reactions with simple linear alkenes; this may explain, at least in part, the low rate of diethyl diallylmalonate RCM. Notably, these results suggest that there is no chelation of the ester to the metal centre, otherwise formation of a chelate complex would be expected to shift the equilibrium towards the substituted carbene and *increase* K_{eq} .

Chelation of the catalyst species to chalcogen moieties, typically present at the allylic position on the alkene, has been proposed numerous times to modulate the rate and efficiency of RCM reactions.¹⁴³ A discussion of the effects of allylic functionality can be found in the introduction, but it can be seen that the ester carbonyl group in the propagating carbene derived from diethyl diallylmalonate is positioned so that it can potentially chelate the metal centre *via* a six-membered arrangement. The possibility of ester chelation to the metal centre of **G2** (or analogues, such as **GH2**) was briefly investigated using density functional theory calculations using the M06-L density functional. Two competing intermediates can be envisaged: one in which the alkene is co-ordinated to the metal centre (η^2 -complex **123**) and one in which the ester carbonyl functionality is co-ordinated to the ruthenium centre (chelate complex **124**). If the chelated ester complex is significantly lower in energy than the productive η^2 -complex **123** then this could reduce the rate of reaction as ruthenium species are sequestered in the form of a non-productive low energy species (**Scheme 2.25**).

Calculations were carried out using Wavefunction Spartan '10¹⁸² on model *dimethyl* diallylmalonate-derived complexes **125** and **126**, in order to reduce the



Scheme 2.25.

conformational complexity of the ruthenium carbene complexes without significantly changing the behaviour of the system. First, the diester functionality was built onto the 1,6-heptadiene-derived cyclic η^2 -complex **120b** taken from the literature,⁵³ and all atoms except the diester and the diene backbone were frozen before a conformer distribution routine (MMFF94) was run to select the five lowest energy conformers ($E_{\text{rel}} = 0, 0.13, 0.74, 0.89$ and 2.89 kcal mol⁻¹). These conformers were all optimised using DFT (M06-L/6-31G*; $E_{\text{rel}} = 0, 0.30, 0.42, 0.84, 0.89$ kcal mol⁻¹) and the lowest energy conformer was selected. The lowest energy conformer was used to construct **126**; the eight lowest energy conformers were built by hand and optimised using DFT (M06-L/6-31G*; $E_{\text{rel}} = 0, 1.25, 1.58, 2.02, 3.78, 4.01, 4.39, 4.79$ kcal mol⁻¹). The lowest energy conformer of the η^2 -complex was found to be 3.6 kcal mol⁻¹ lower in energy (ΔE) than the chelate complex (**Figure 2.18**). Chelation is therefore unlikely to account for the lower reaction rate of diethyl diallylmalonate with respect to 1,6-heptadiene; in terms of equilibrium constants, 3.6 kcal mol⁻¹ translates to a 436:1 ratio of the η^2 -complex **125** to the ester-chelated complex **126**. Given the results of Schore *et al.*, the low rate of diethyl diallylmalonate RCM is most likely due to unfavourable alkylidene transfer to form the

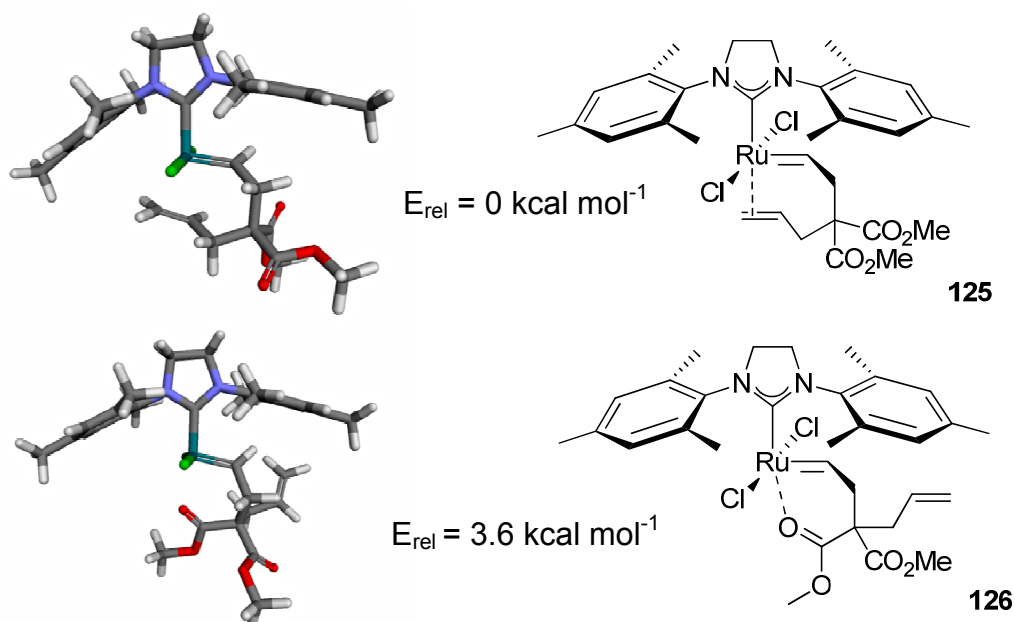
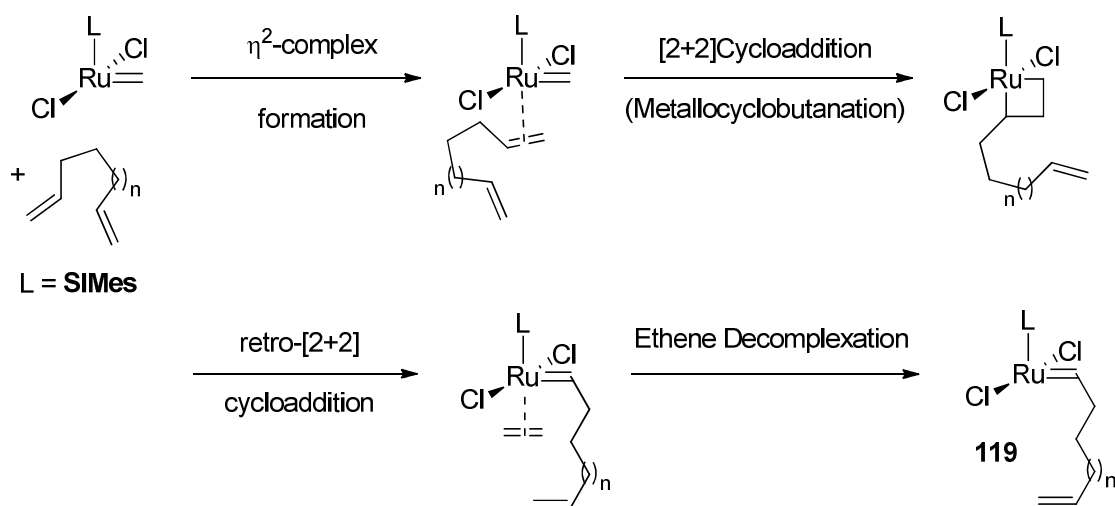


Figure 2.18. Optimised structures (at the M06-L/6-31G* level of theory) for complexes (i) **125**, in which the pendant alkene is co-ordinated to the metal centre and which can proceed to metallocyclobutane and (ii) **126**, in which the carbonyl group of the ester functionality is co-ordinated to the metal centre.



Scheme 2.26

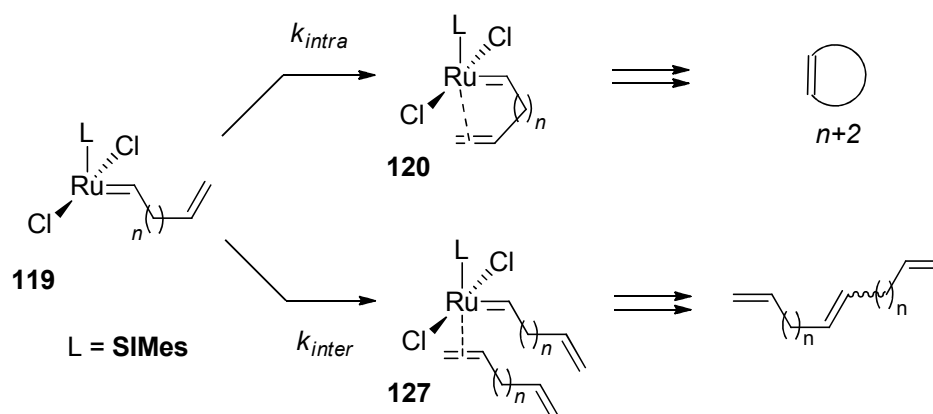
propagating carbene.¹⁸¹ Alkylidene transfer is itself a series of steps (**Scheme 2.26**), and so the rates of diethyl diallylmalonate and 1,7-octadiene RCM may be limited by different steps within this sequence.

Quantifying Kinetic Effective Molarities

The Utility of the Effective Molarity

The EM is a useful way in which to quantify the efficiency of an intramolecular reaction with respect to the corresponding intermolecular alternative. For alkene metathesis, RCM represents the former (with rate constant k_{intra}) and cross-metathesis represents the latter (with rate constant k_{inter}). The rate-determining step must be different in each reaction in order to calculate a kinetic EM, and therefore for RCM must involve reaction of the intermediate alkylidene **119** generated in both pathways and how it partitions between cyclic η^2 -complex **120** and η^2 -complex **127** (Scheme 2.27). In some cases, both rate constants can be measured from the same reaction.¹⁰² This approach has been applied only three times to RCM reactions. Percy *et al.* have measured EMs for some RCM reactions (using **G2**) to form difluorinated cyclooctenone products which ranged from 0.017 mol L⁻¹ to 1.09 mol L⁻¹,¹⁰⁸ and later measured the EM for formation of a trisubstituted alkene analogue.¹⁰⁰ Researchers at Boehringer-Ingelheim have measured the kinetic EM for the formation of macrocyclic intermediate **61** (*en route* to kilogram quantities of a HCV protease inhibitor) using pre-catalyst **GH1** (EM = 0.046 mol L⁻¹).¹¹¹ In all cases these values were arrived at from a plot of 1/[diene]₀ versus the ratio of intra- to intermolecular reaction products (Equation 1.18).

However, in all of these examples the intra- and inter-molecular products can be obtained from the same series of reactions. This requires the reaction to be under purely *kinetic* control, because if the products interconvert then the product ratios at a single



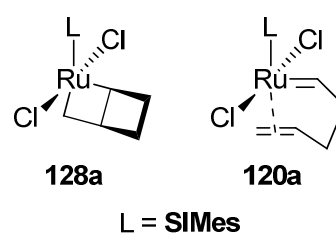
Scheme 2.27

point in time will not reflect the relative rates of intra- and inter-molecular reaction. In these cases, appropriate rate constants must be determined from separate reactions. As these reactions are known to be under thermodynamic control (*vide infra*),⁹⁶ the products will interconvert to reach the thermodynamic ratio of products. The intra- and inter-molecular rate constants k_{intra} and k_{inter} must be determined from separate experiments in order to separate the kinetic and thermodynamic product ratios. This required identification of a suitable model intermolecular reaction from which to obtain k_{inter} , and calculation of a rate constant under the same conditions used for the RCM reactions.

1,5-Hexadiene Cross-Metathesis as a Model Intermolecular Reaction

The reactivity of end groups on a chain are independent of the length of the chain,⁹⁸ so the rate of a suitable model cross-metathesis reaction would provide an appropriate value of k_{inter} for use in the calculation of the kinetic EM for the RCM reactions described above. In his seminal paper on effective molarities, Kirby states that, when choosing an intermolecular reaction with which to measure k_{inter} : ‘... the mechanisms of both intermolecular and intramolecular reactions must be known and have been shown to be the same. The acceptable rate measurements must be carried out under the same conditions for both reactions.’¹⁰² Cross metathesis proceeds with the same mechanism as RCM, with the exception that in RCM the two alkene moieties are linked by a chain of covalent bonds. Both cross-metathesis and RCM can be studied under the same conditions, and therefore the criteria described by Kirby can be fulfilled.

While the RCM reaction of 1,5-hexadiene would formally produce cyclobutene **104a**, the considerable ring strain in this product renders this reaction pathway incompetent. An energy minimum for MCB **128a** could not be located using DFT calculations (M06-L/6-311G*¹⁸³). Instead, the attempted optimisation yielded cyclic η^2 -complex **120a**.



As RCM is not possible, cross-metathesis is the only metathesis reaction that can occur if 1,5-hexadiene is exposed to pre-catalysts such as **G2**. 1,5-Hexadiene is a simple and symmetrical α,ω -diene and a homologue of the dienes which have undergone RCM as described in the preceding sections. Analysis of the reaction rate can be complicated by the formation of linear and cyclic trimers, tetramers and larger species. However,

following the rate of decrease of 1,5-hexadiene in the metathesis reaction ought to provide an estimate of k_{inter} . The rate of cross-metathesis between, for example, linear dimer **105** and **103** should be the same as that between two molecules of **103**.

Unfortunately, cross-metathesis of 1,5-hexadiene could not be followed under the conditions that were used for study of the RCM reactions of dienes **103b-d**. Exposure of a 10 mmol L⁻¹ solution of 1,5-hexadiene (in chloroform-*d*) to 1 mol% **G2** yielded no conversion within 22 hours (**Figure 2.19**). Reasoning that the reaction may simply have been very slow, the concentration of 1,5-hexadiene was increased; however, conversion was still poor. The cross-metathesis reaction of 1,5-hexadiene at 2.5 mol L⁻¹ (1 mol% **G2**) achieved only *ca.* 40% conversion after 2 hours.

The rate of the cross-metathesis reaction would be expected to be second order in 1,5-hexadiene if considered as a single step reaction between catalyst **4b** and two molecules of 1,5-hexadiene (**Equation 2.09**). However, considering the reaction as a sequence of two irreversible steps (**Scheme 2.27** above) leads to an expression for the rate of 1,5-hexadiene consumption (**Equation 2.10**); applying the steady state approximation to the intermediate carbene **119a** (**Equation 2.11**) leads to a simplified

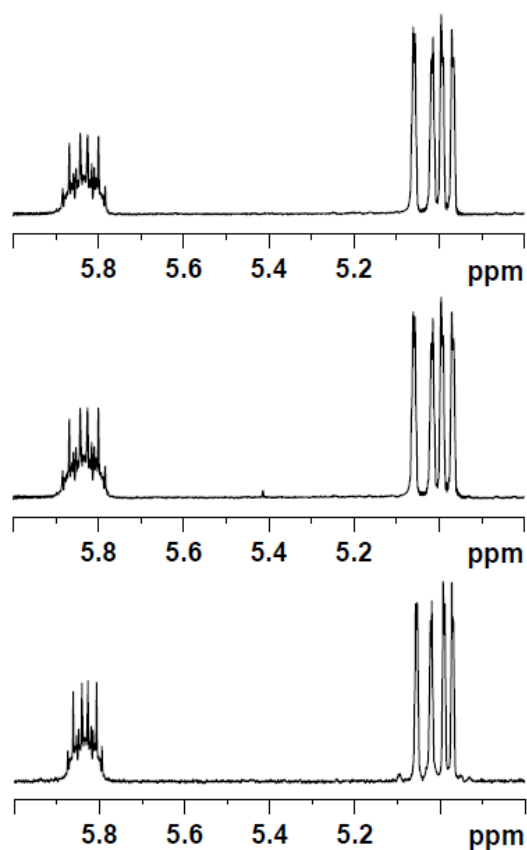


Figure 2.19. Partial ¹H NMR spectra from the cross-metathesis reaction of 1,5-hexadiene (10 mmol L⁻¹) with **G2** (1 mol%) in chloroform-*d* (i) before pre-catalyst addition, (ii) after 2.5 hours and (iii) 22 hours.

rate expression that is first order in both catalyst and 1,5-hexadiene (**Equation 2.12**).

$$d/dt[103a] = k_1[4b] \cdot [103a]^2 \quad (2.09)$$

$$d/dt[103a] = -k_1[4b] \cdot [103a] - k_2[119a] \cdot [103a] \quad (2.10)$$

$$k_1[4b] = k_2[119a] \quad (2.11)$$

$$\begin{aligned} d/dt[103a] &= -k_1[4b] \cdot [103a] - k_1[4b] \cdot [103a] \\ &= -2k_1[4b] \cdot [103a] \end{aligned} \quad (2.12)$$

The data from the 2.5 mol L⁻¹ 1,5-hexadiene cross-metathesis is not well behaved first or second order, but approximate observed rate constants can be obtained in both cases (**Figure 2.20**). It is not possible to quantify [4b] in these reactions, as it cannot be detected spectroscopically,¹⁵ and therefore it is not possible to compare reaction rates between reactions with different **G2** concentrations.

The RCM reaction of 1,5-hexadiene was also conducted with a high pre-catalyst loading (0.3 mol L⁻¹, 15 mol% **G2**), which increased conversion but led to a complex mixture of products (**Figure 2.21**). The low-field region of the ¹H NMR was also very complex; various phosphane-bound ruthenium species were identified, including

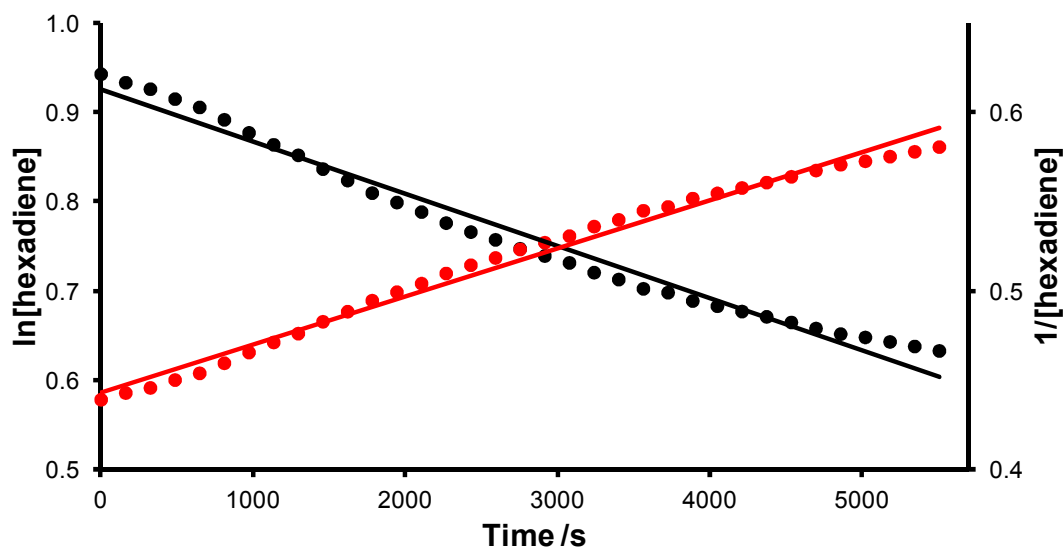


Figure 2.20. Attempted fitting of the concentration/time data from the RCM of 1,5-hexadiene (2.5 mol L⁻¹) with **G2** (1 mol%) in chloroform-*d* using (i) a first-order treatment ($k_{obs} = 5.8 \times 10^{-5} \text{ s}^{-1}$, $R^2 = 0.9777$) and (ii) a second-order treatment ($k_{obs} = 2.7 \times 10^{-5} \text{ L mol}^{-1} \text{ s}^{-1}$, $R^2 = 0.9872$).

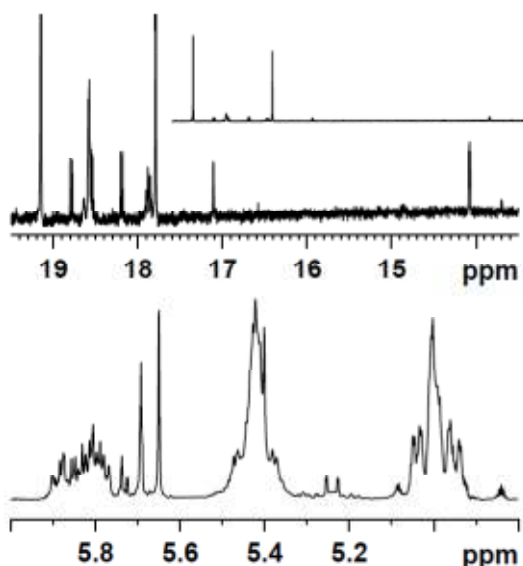
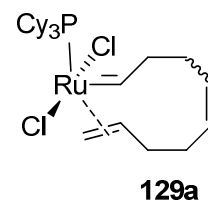


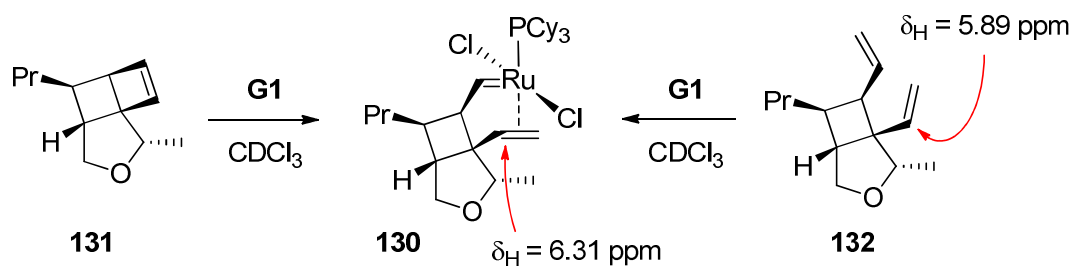
Figure 2.21. Partial ^1H NMR spectrum from the cross-metathesis of 1,5-hexadiene (300 mmol L^{-1}) with **G2** (15 mol%) in chloroform-*d* after 14 hours showing the (i) low field region and (ii) alkene region.

unreacted pre-catalyst, methyldiene and alkylidene. In addition, ethylidene was detected, suggesting that isomerisation processes were occurring in the reaction (the topic of isomerisation is discussed in more detail in chapter 4). Unfortunately, distinguishing between phosphane-bound alkylidene **121a** and chelate η^2 -complex **120a** is not trivial; the $^3J_{\text{H-P}}$ couplings are only rarely observed in ruthenium alkylidenes and the complex mixture obtained renders isolation of the chelate complex extremely difficult.⁴⁴

The low metathesis rate of 1,5-hexadiene is not without precedent. Wagener *et al.* have noted the rate difference between the cross-metathesis reactions of 1,5-hexadiene and 1,9-decadiene, postulating that the rate difference may be due to formation of cyclic η^2 -complex **129a**;¹⁸⁴⁻¹⁸⁵ this species is also a chelate but is likely less stable than **120a** characterised by Metzger *et al.* due to the need to freeze additional rotors.¹⁶⁵



Snapper *et al.* isolated complex **130** from the **G1**-catalysed ring-opening metathesis of cyclobutene **131** (Scheme 2.28).¹⁸⁶ This alkylidene complex was also



Scheme 2.28¹⁸⁶

obtained from the metathesis of the corresponding 1,5-hexadiene **132**, resulting in a downfield shift of *ca.* 0.4 ppm upon complexation for the ¹H NMR signal corresponding to the vinylic proton, which in turn indicated that complexation of the alkene to the ruthenium centre resulted in the deshielding of the alkene proton nuclei.

As discussed previously, Wang *et al.* noted that chelate complexes **120** are formed from alkylidene complexes **119** during ESI-MS studies of the RCM reactions of substrates **103a-103d**. While the productive RCM reactions yield equilibria between phosphane-bound alkylidene and cyclic η^2 -complexes that prefer the phosphane-bound species (in a ratio of 3-7:1), the corresponding cyclic η^2 -complex derived from 1,5-hexadiene was instead favoured over the phosphane-bound alkylidene (10.2:1). However, these studies all concern first generation pre-catalyst **G1**, and no metathesis reactions with second generation complexes such as **G2** have been reported.¹⁷³

Experimental evidence and literature precedent suggested that the low metathesis rate was due to the formation of a stable η^2 -complex, so **120a** was characterised using DFT calculations (M06-L/6-311G*).¹⁸⁷ The free energy of this complex was found to be 10.6 kcal mol⁻¹ lower than the propagating carbene, rendering it energetically competitive with MCBs, which tend to be low (*ca.* -10 to -15 kcal mol⁻¹) on the PES.^{15,53} The low energy of **120a** is due at least in part to attractive dispersive interactions. These interactions are important in metathesis chemistry, both with regard to the metal-ligand binding energy⁴⁸ as well as interactions between the alkylidene α -proton and the *ipso*-carbon on the aromatic ring above it.^{49,53} The latter interaction is highly dependent on the structure of the pendant alkylidene for example, **120a** features a close contact (*d* = 2.39 Å) while 1,7-octadiene-derived **120c** does not (**Figure 2.22**).¹⁸⁷

The potential consequences of a stable η^2 -complex intermediate in the system studied here were tested experimentally; concentration/time profiles were collected for two multi-diene metathesis reactions with 1,7-octadiene (5 mmol L⁻¹ of each diene, 0.1 mmol L⁻¹ **G2** in chloroform-*d*): one with 1,5-hexadiene and one with 1,6-heptadiene. These were compared to the concentration/time profiles for 1,7-octadiene RCM in **Figure 2.07** (10 mmol L⁻¹, with 0.1 mM **G2**, **Figure 2.23**). These profiles showed that 1,5-hexadiene had an inhibitory effect on the otherwise more rapid RCM of 1,7-octadiene: the approximate *t*_{1/2} for 1,7-octadiene RCM was typically *ca.* 1000 s in the absence of 1,5-hexadiene, but increased to *ca.* 2000 s when 1,5-hexadiene was present. Despite 1,7-octadiene undergoing RCM faster than any other substrate studied here, the presence of

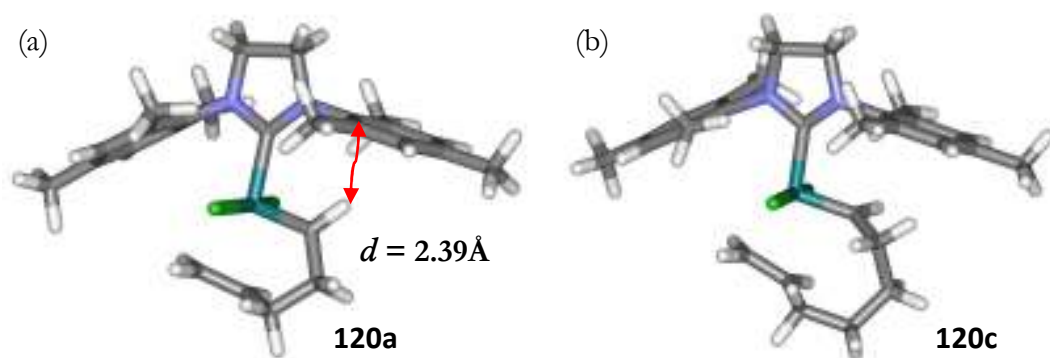


Figure 2.22. Optimised geometries (at the M06-L/6-311G* level of theory) for **G2**-derived propagating carbenes (a) **120a**, from 1,5-hexadiene and (b) **120c**, from 1,7-octadiene; the α -proton on alkylidene **120a** features an attractive dispersive interaction with the *ipso*-carbon on the aromatic ring above.¹⁸⁷

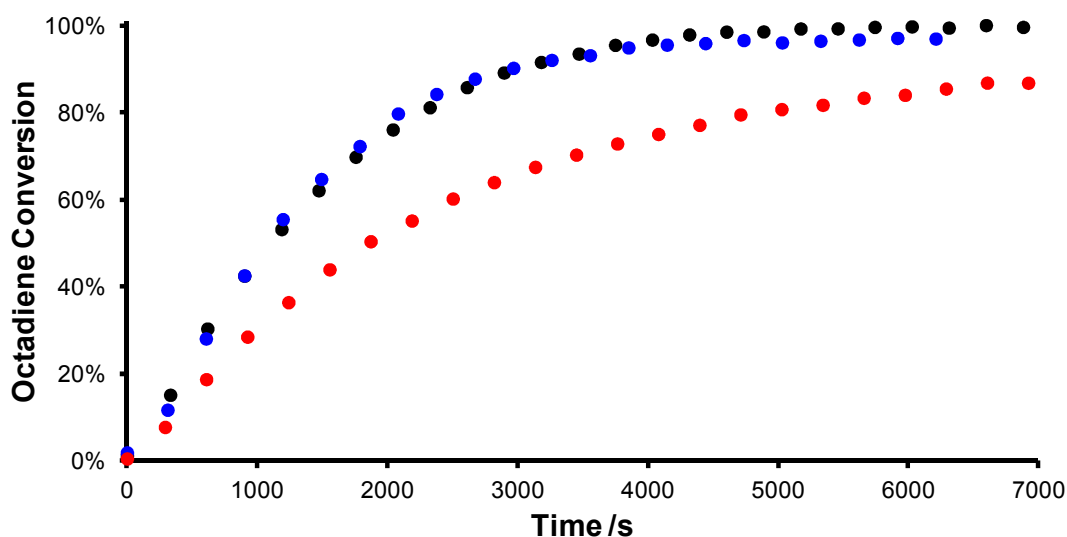
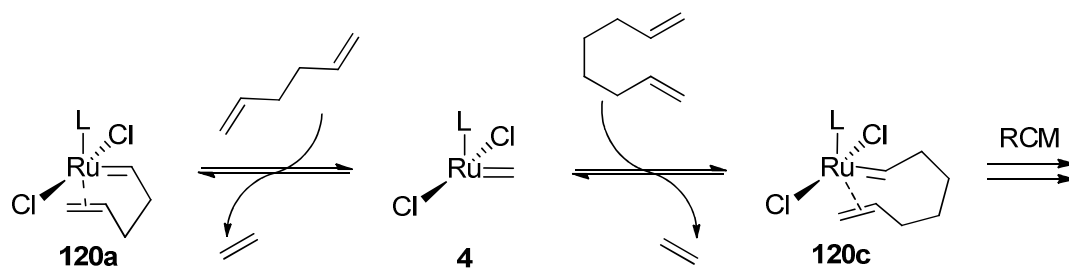


Figure 2.23. Conversion/time profiles for the reactions (with 0.1 mmol L⁻¹ **G2**) of (i) 10 mmol L⁻¹ 1,7-octadiene (**black**), (ii) 5 mmol L⁻¹ 1,7-octadiene and 5 mmol L⁻¹ 1,6-heptadiene (**blue**) and (iii) 5 mmol L⁻¹ 1,7-octadiene and 5 mmol L⁻¹ 1,5-hexadiene (**red**).

1,5-hexadiene considerably retarded the reaction rate, presumably due to formation of a stable chelate η^2 -complex sequestering a proportion of the active catalyst. The effect of 1,5-hexadiene was most pronounced towards the end of the reaction, which was likely due to the increasing ratio of 1,5-hexadiene to 1,7-octadiene. The latter is consumed in the (effectively irreversible)⁹⁰ RCM reaction, while there was negligible 1,5-hexadiene consumption during the course of the experiment. If the equilibria in **Scheme 2.29** are



Scheme 2.29

in operation, then this would explain the slower rate of RCM in the presence of 1,5-hexadiene plus the slowing of the RCM as conversion increased.

To establish if this behaviour extends to other productive α,ω -diene RCM reactions, a reaction was conducted in which 1,5-hexadiene and 1,6-heptadiene (5 mmol L⁻¹ of each) were exposed to **G2** (0.1 mmol L⁻¹). The conversion/time profiles in **Figure 2.24** show that 1,5-hexadiene still exerts a detrimental effect on RCM rate.

The observation that 1,5-hexadiene behaves as a metathesis inhibitor is important for synthetic chemists; while the diene RCM reactions studied here are very simple systems, more complex systems such as those encountered *en route* to complex natural products may contain 1,5-diene units. Evidence presented here implicates this motif in the retardation of metathesis rate.

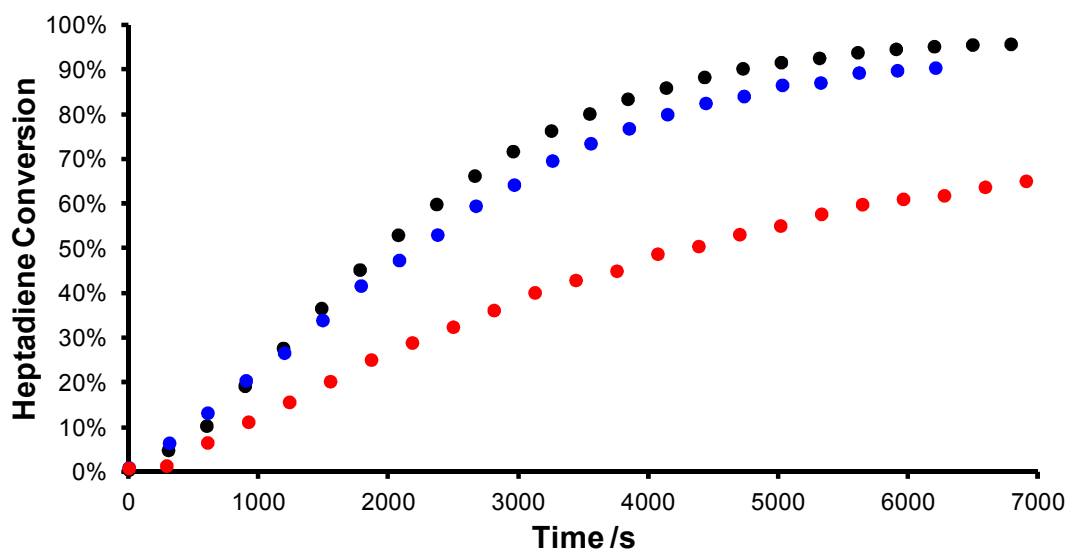


Figure 2.24. Conversion/time profiles for the reactions (with 0.1 mmol L⁻¹ **G2**) of (i) 10 mmol L⁻¹ 1,6-heptadiene (**black**), (ii) 5 mmol L⁻¹ 1,7-octadiene and 5 mmol L⁻¹ 1,7-octadiene (**blue**) and (iii) 5 mmol L⁻¹ 1,5-hexadiene and 5 mmol L⁻¹ 1,6-heptadiene (**red**).

In order to understand this effect more fully, DFT calculations (M06-L/6-311G*)¹⁸⁷ of the PESs for the RCM reactions of 1,6-heptadiene and 1,7-octadiene (reported previously) were investigated.⁵³ The η^2 -complex **120c**, formed during the RCM of 1,7-octadiene, lacks the dispersive interaction found in complex **120a** and is only 6.6 kcal mol⁻¹ lower in energy than the propagating carbene (*cf.* -10.6 kcal mol⁻¹ for **120a**; **Figure 2.25**); MCB **128c** is similar in energy (with respect to **119c**) to **120a** (with respect to **119a**). The analogous alkylidene complex **120b**, derived from 1,6-heptadiene, is of a similar energy (with respect to the propagating carbene **119b**) as that derived from 1,5-hexadiene (**Figure 2.26**). However, 1,5-hexadiene reduces the rate of 1,6-heptadiene RCM, as described above, as the 1,5-hexadiene-derived η^2 -complex is still energetically competitive with the productive 1,6-heptadiene-derived complex ($\Delta G = 0.9$ kcal mol⁻¹, which is within the margin of error of the calculations; $K \approx 4.5$). In addition, the cyclic η^2 -complex derived from 1,6-heptadiene faces a 3.4 kcal mol⁻¹ barrier to metallocyclobutanation *versus* 2.5 kcal mol⁻¹ for 1,7-octadiene plus a much higher barrier to metallocyclobutane retro[2+2]cycloaddition, and therefore will progress through the catalytic cycle more slowly.

To identify if the low energy of **120a** is directly responsible for the rate decrease,

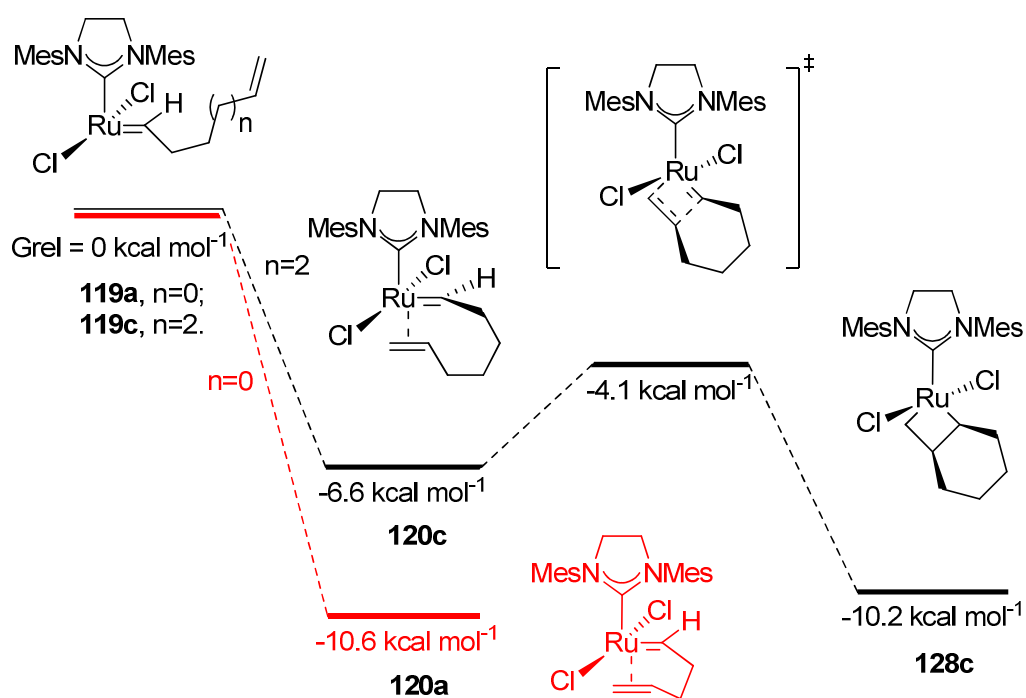


Figure 2.25. Partial potential energy surfaces for the metathesis of 1,5-hexadiene and 1,7-octadiene at the M06-L/6-311G* level of theory.^{53,90,187}

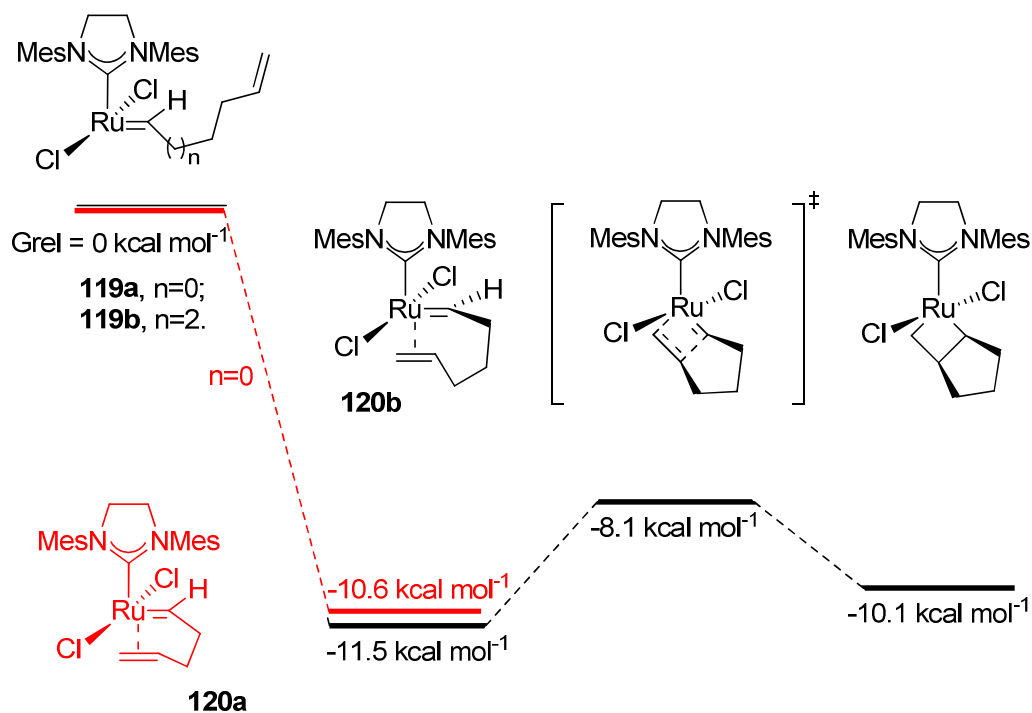
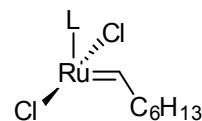


Figure 2.26. Partial potential energy surfaces for the metathesis of 1,5-hexadiene and 1,6-heptadiene at the M06-L/6-311G* level of theory.^{53,187}

a subsequent experiment with 1-octene and 1,7-octadiene was performed (5 mmol L⁻¹ of each in chloroform-*d*, with 0.1 mmol L⁻¹ **G2**). This represents a control reaction, as 1-octene will compete for catalyst but cannot form a chelate η^2 -complex. The concentration *versus* time profile was of a different shape, but reached 100% conversion far more quickly than the reaction containing 1,5-hexadiene (**Figure 2.27**). The different reaction profile is likely due to cross-metathesis with 1-octene yielding a species that is still active for metathesis (i.e. 14e heptylidene complex **133**). The latency period before cyclisation is suggestive of an initiation period; further studies of this reaction, perhaps involving a reaction simulation study (see Chapter 3), would be necessary to establish what events are occurring that lead to this shape of conversion/time profile. Notably, **133** is metathesis active, while **120a** is considerably lower in energy than **119a**, and therefore events occurring in the reaction are likely to be very different.



133 L = SIMes

After encountering difficulties in quantifying k_{inter} using this system, alternative model intermolecular reactions were sought.

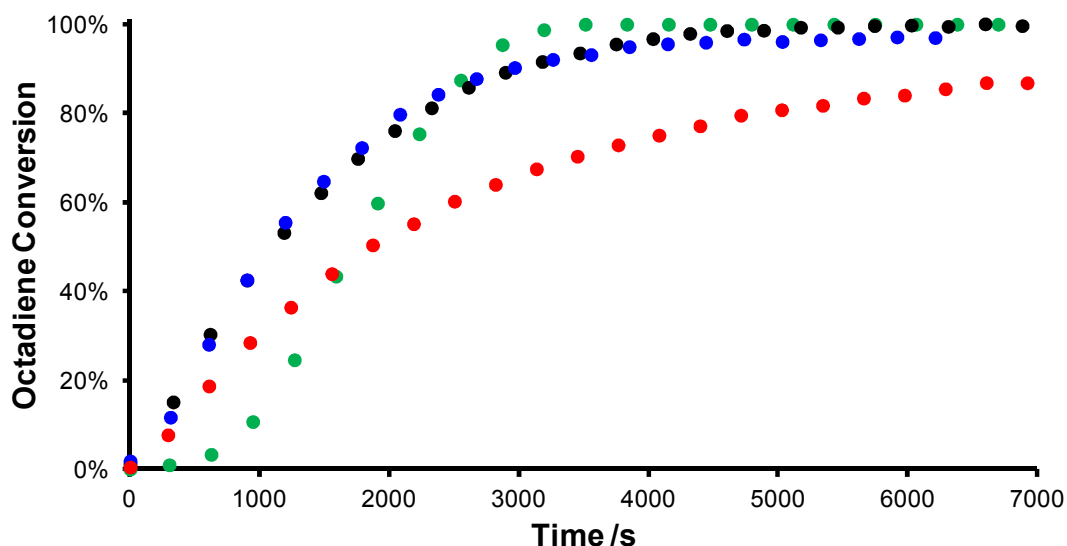
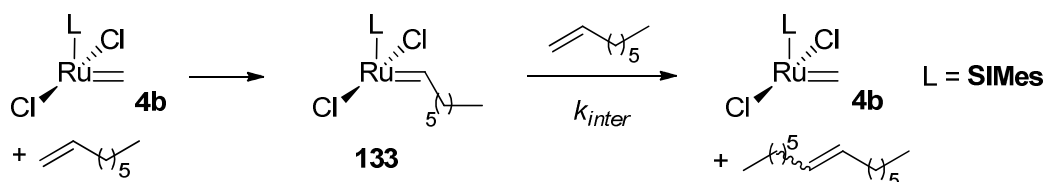


Figure 2.27. Conversion/time profiles for the reactions (with 0.1 mmol L^{-1} **G2**) of (i) 10 mmol L^{-1} 1,7-octadiene (**black**), (ii) 5 mmol L^{-1} 1,7-octadiene and 5 mmol L^{-1} 1,6-heptadiene (**blue**), (iii) 5 mmol L^{-1} 1,7-octadiene and 5 mmol L^{-1} 1,5-hexadiene (**red**) and (iv) 5 mmol L^{-1} 1,7-octadiene and 5 mmol L^{-1} 1-octene (**green**).

1-Octene Metathesis as a Model Intermolecular Reaction

1-Octene is similar to 1,5-hexadiene in that it is a simple alkene which possesses no backbone functionality. However, 1-octene cannot form a cyclic η^2 -complex, and can only dimerise; the formation of trimers or larger species is not possible (**Scheme 2.30**).

The metathesis of 1-octene was carried out (10 mmol in chloroform- d , $1 \text{ mol}\%$ **G2**) in the NMR spectrometer in the same manner as the previous experiments. Conversion was negligible after 5 hours, with only a very small signal for ethene obtained. The reaction of a sample containing a higher concentration of 1,5-hexadiene (0.4 mol L^{-1}) with a higher pre-catalyst loading ($4.5 \text{ mol}\%$ of **G2**) in DCM- d_2 resulted in *ca.* 25% turnover to the dimer after 4 hours at 298 K (**Figure 2.28**). A build-up of alkylidene **134** was observed, along with traces of ethylidene **31b** which indicated that



Scheme 2.30

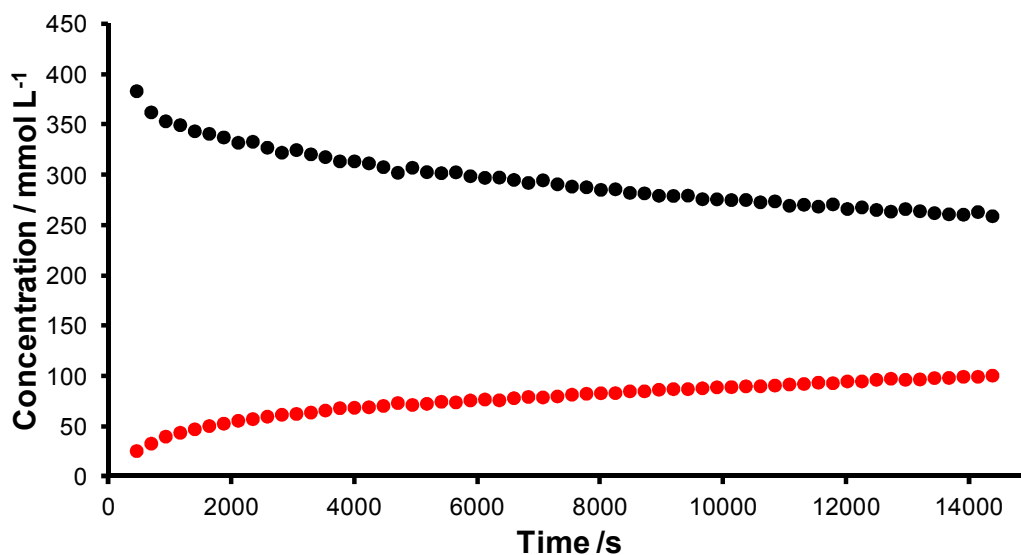


Figure 2.28. Concentration/time profiles for 1-octene (**black**) and 7-tetradecene (**red**) in the metathesis of 1-octene (0.4 mol L^{-1}) with **G2** ($4.5 \text{ mol}\%$) in $\text{DCM-}d_2$.

isomerisation processes were also occurring (**Figure 2.29**).

While approximate (first and second order) rate constants could be obtained from the concentration/time profile (**Figure 2.30**), translating these numbers into usable rate constants for **134** $L = \text{SiMes}$ effective molarity calculations is not possible due to the aforementioned issues with

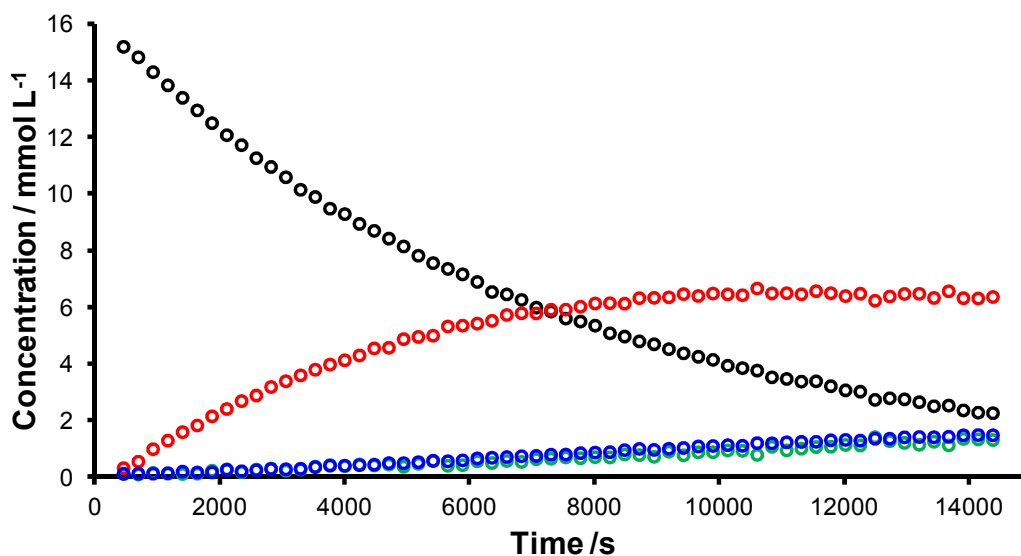
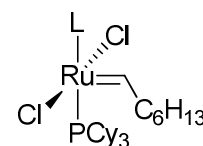


Figure 2.29. Concentration/time profiles for pre-catalyst (**black**), alkylidene **134** (**red**), methyldiene **3b** (**blue**) and ethylidene **31b** (**green**).

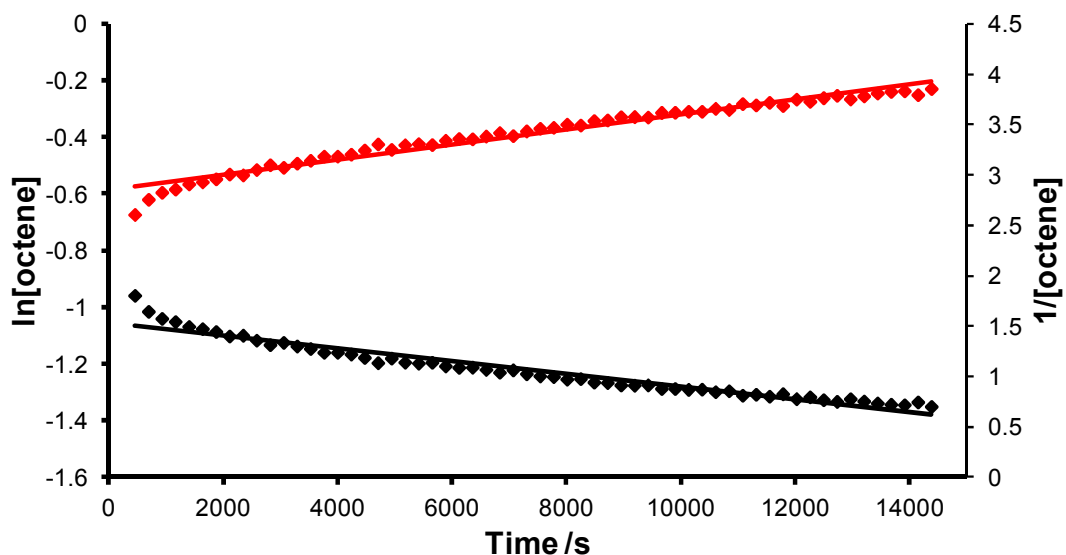


Figure 2.30. Attempted fitting of the concentration/time data from the metathesis of 1-octene (0.4 mol L^{-1}) with **G2** (4.5 mol%) in chloroform-*d* using (i) a first-order treatment ($k_{obs} = 2.3 \times 10^{-5} \text{ s}^{-1}$, $R^2 = 0.9414$; **black** points) and (ii) a second-order treatment ($k_{obs} = 7.5 \times 10^{-5} \text{ L mol}^{-1} \text{ s}^{-1}$, $R^2 = 0.9622$; **red** points).

quantifying **[4b]**. It was not possible, therefore, to obtain an accurate value for k_{inter} from these data. Due to the complexity of the kinetic data (i.e. lack of adherence to a simple kinetic order), only a value for k_{inter} obtained at the same concentration of pre-catalyst can be used to calculate a kinetic EM (**Equation 2.13**).

$$\text{EM} = k_{intra}/k_{inter} = k_{intra} \cdot [\mathbf{4b}] / k_{inter} \cdot [\mathbf{4b}] \quad (2.13)$$

Separation of the pre-catalyst initiation from the cross-metathesis reaction would allow quantification of the cross-metathesis rate, as the concentration of active catalyst could be accounted for during the reaction. Chapter 3 details the interrogation and development of a kinetic model for alkene ring-closing metathesis; a logical extension to the simple model presented would potentially allow for quantification of cross-metathesis rate, and allow the topic of kinetic effective molarity in these systems to be revisited. However, as the reactions were found to be under thermodynamic control (*vide infra*), later work focussed on the quantification of EM_T instead.⁹⁶

Evidence for Thermodynamic Control

Kinetic *versus* Thermodynamic Control in the Literature

The concept that alkene metathesis reactions are under *thermodynamic* control rather than *kinetic* control has been discussed in some detail in the literature.^{2,188} This behaviour arises due to the formal reversibility of each step in the alkene metathesis mechanism, as both cross-metathesis and RCM are series of reversible [2+2]-cycloadditions and retro-[2+2]-cycloadditions. The degree of thermodynamic control is also to some extent a function of pre-catalyst: **G1** and analogues such as **GH1** tend to result in reactions under *kinetic* control, due to their slow reaction with disubstituted alkenes.⁶² In contrast, **G2** and analogues such as **GH2** most often yield the *thermodynamic* products. This difference can be seen in typical cross-metathesis reactions; **G1** and analogues yield lower *E:Z* ratios than second-generation pre-catalysts such as **G2** as discussed in the introduction.⁴⁵

Kinetic *versus* Thermodynamic Control in the Ring-closing Metathesis of Simple Prototypical α,ω -dienes

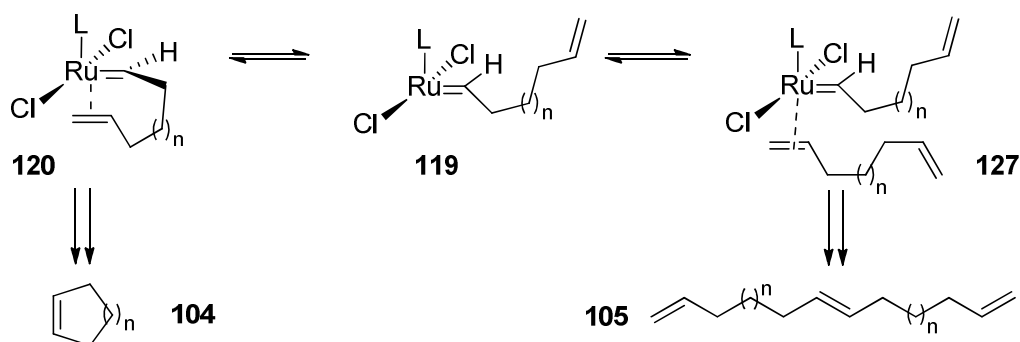
While the selected examples discussed above illustrate that metathesis reactions catalysed by second generation (NHC-bearing) complexes can be under some degree of thermodynamic control, it was of interest to explore whether the RCM reactions studied in this thesis were under thermodynamic or kinetic control. The RCM reactions of 1,8-nonadiene (10 mmol L⁻¹) failed to reach completion in the timeframe studied, and also formed oligomeric and isomerisation-RCM products, so this reaction was therefore studied in more detail to identify if the system was under thermodynamic control.

Reactions under thermodynamic control exhibit a number of behaviours:

- The product-determining step of the reaction must be formally reversible; irreversible reactions cannot equilibrate
- Substrates and products must all be present, plus any catalytic species required to perform the transformation; if the products completely egress or precipitate from solution then an equilibrium will not be reached
- The system, once at equilibrium, should re-adjust if perturbed by factors such as substrate concentration and temperature

- The system should approach the same equilibrium position from different directions: exposing the products to the reaction conditions should yield the same mixture of reactants and products as the original reaction

The product-determining step is the reaction of the alkylidene **119**, which can either coordinate the pendant alkene (**120**) or bind a second molecule of diene (**127**), yielding the target cycloalkene or the cross-metathesis product respectively (**Scheme 2.31**).



Scheme 2.31

Examination of reaction mixtures (such as from the RCM of 10 mmol L⁻¹ 1,8-nonadiene) revealed the presence of unreacted diene, target cycloalkene, oligomeric material (*vide infra*) and ethene, confirmed *via* detailed 1D and 2D NMR analyses and GC-MS analysis.⁹⁶ Ethene accumulated in the kinetic reactions conducted at 298 K even when the reaction was conducted in a vessel that was not closed, such as an NMR tube with a pierced plastic cap. While a detailed study of the behaviour of ethene in metathesis reactions remains to be conducted, it was clear that ethene was available in solution in these experiments to facilitate the reverse reaction. Pre-catalyst **G2** persisted in reaction solutions for considerable periods of time (hours, even when charged at 1 - 3 mol%), so incomplete conversion was not due to catalyst death. Reactions therefore possess the necessary components to allow for the reverse reaction to occur.

The third and fourth points required further experimental exploration. The RCM reaction of 1,8-nonadiene was used to investigate the issue of thermodynamic control; later work has established that this system has EM_T = 53 mmol L⁻¹ so a wide variety of outcomes (i.e. differing degrees of oligomerisation *versus* cyclisation) can be obtained over a practical range of concentrations (*ca.* 10 mmol L⁻¹ to 100 mmol L⁻¹).⁹⁶ In contrast, the RCM reaction of 1,7-octadiene proceeds to completion, even with initial

concentrations of 4 mol L⁻¹,⁹⁰ so this is not a good substrate with which to evaluate thermodynamic control in RCM. If this reaction is under thermodynamic control, the equilibrium position greatly favours cyclohexene over oligomer, i.e. $K_{\text{intra}} \gg K_{\text{inter}}$. At the other end of the reactivity scale, the RCM reactions of 1,9-decadiene, 1,10-undecadiene and 1,11-dodecadiene are too slow to monitor using kinetic experiments.

Perturbing the Reaction Equilibria

Reactions were carried out in chloroform-*d* at 298 K unless stated otherwise. The choice and loading of pre-catalyst varied amongst these experiments, but if these reactions are under thermodynamic control then many outcomes are independent of the pre-catalyst and depend only on the *substrate* structure.

Various metrics are used here to describe the reaction mixture composition. The ratio of [cycloalkene]:[oligomer] is the simplest measure of the effectiveness of the system for cyclisation *vs.* oligomerisation, but is dependent on the reaction concentration. The modified thermodynamic effective molarity (MEM_T) (equal to [cycloalkene]²/[cyclic dimer]),^{104,111} as discussed in the introduction, is another term that has been used to compare reaction under different conditions. The utility of this metric is that, like EM_T, the value of MEM_T is independent of the initial reaction concentration (or total effective monomer concentration), and therefore can be compared across reactions at different initial substrate concentrations.

Changes in Substrate Concentration

A reinoculation experiment was carried out to identify if and how the reaction mixture changes as additional substrate is charged to the reaction. A solution of **G2** (1.2 mmol L⁻¹) was treated with 1,8-nonadiene (10 mmol L⁻¹) and the reaction was monitored by ¹H NMR spectroscopy until the spectrum of the reaction mixture did not change. At this point, a further charge of 1,8-nonadiene was added to bring the total effective diene concentration to 20 mmol L⁻¹. The system responded, moving to a new equilibrium position with a higher ratio of cyclic dimer **106d** (quantified by integration of the resonance with $\delta_{\text{H}} = ca. 5.25$ ppm) to cycloheptene. This confirmed that the pre-catalyst/catalyst system was still active. The reaction was inoculated a further two times (to yield diene concentrations of 30 mmol L⁻¹ and 40 mmol L⁻¹), which yielded smooth concentration/time profiles that showed equilibrium being reached after each addition

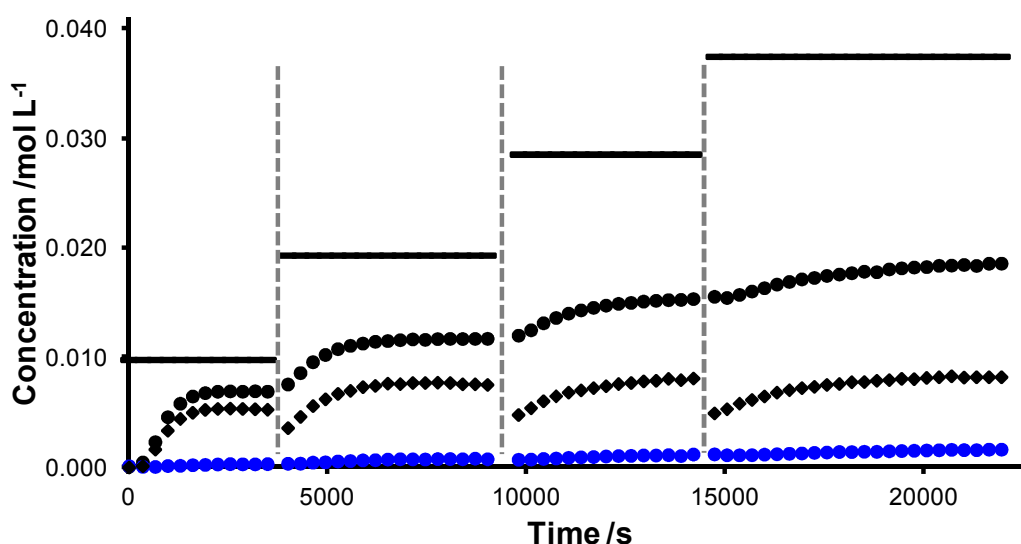


Figure 2.31. Concentration/time profiles for cycloheptene (**black circles**), ethene (**black rhombi**), cyclic dimer **106d** (**blue circles**) from a reinoculation experiment with 10, 20, 30 and 40 mmol L⁻¹ 1,8-nonadiene and the same 1.2 mmol L⁻¹ charge of **G2**; bold black lines represent the total 1,8-nonadiene charge at that time.

of 1,8-nonadiene (**Figure 2.31**). MEM_T was calculated immediately before each reinoculation (**Table 2.10**); the value obtained was approximately the same each time, tending to *ca.* 0.2. The fact that a similar value was obtained at various initial reaction concentrations is in agreement with the theoretical work of Ercolani *et al.*,¹⁰⁴ as the value of MEM_T is a function of the thermodynamics of cycloheptene and cyclic dimer **106d** alone. There is less confidence in the value obtained at the first equilibrium position, due to difficulties in accurately measuring the very small integral of the ¹H NMR signal for cyclic dimer. The ethene concentration decreased slightly after each charge due to the tube being opened briefly, which may have perturbed the equilibria within the

Table 2.10. Values for [cycloheptene]²/[cyclic dimer] at each equilibrium position during the reinoculation experiment with 1,8-nonadiene.

Time (s)	[104d] ₀ /mol L ⁻¹	[104d] ² /[106d] /mol L ⁻¹
3483	0.0098	0.1511
9013	0.0193	0.1816
14189	0.0286	0.1981
21935	0.0375	0.2115

reaction slightly. However, the overall equilibrium between cycloheptene and cyclic dimer does not involve ethene; the balance between the two species can be considered as an equilibrium between two equivalents of cycloheptene and one of cyclic dimer.

The ratio of [cycloheptene]/[cyclic dimer] also changed at each equilibrium position, as would be expected from increasing the effective monomer concentration in a thermodynamically-controlled cyclisation reaction. When the effective monomer concentration was increased, the intermolecular reaction was pushed further towards oligomer at the expense of cycloalkene formation (**Figure 2.32**).

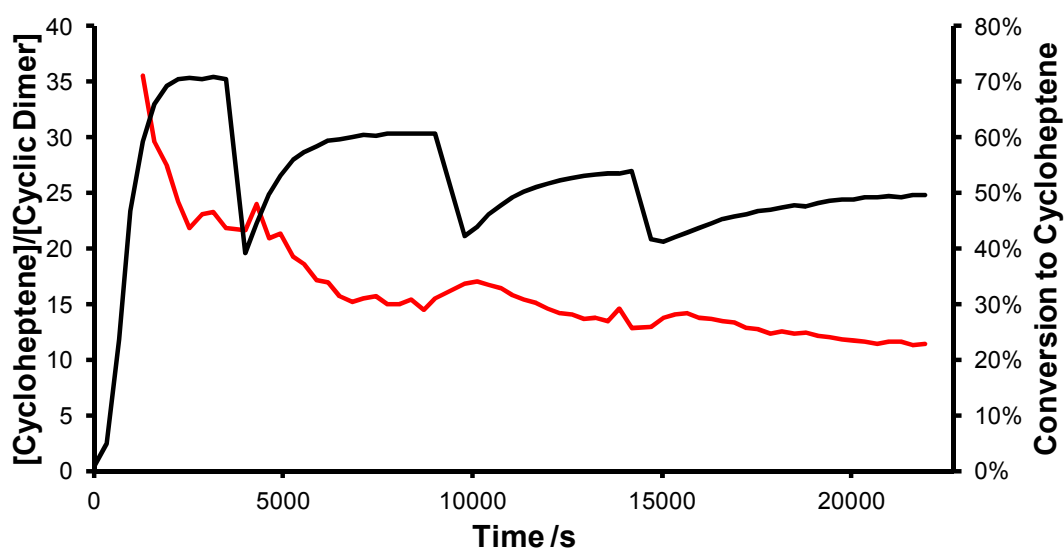


Figure 2.32. Profiles from the reinoculation experiment in **Figure 2.31**, showing how (i) [cycloheptene]/[cyclic dimer] (**red**, primary axis) and (ii) conversion to cycloheptene (**black**, secondary axis) change over time.

Changes in Temperature

A reaction that is under thermodynamic control should respond to changes in temperature, as the constant K for any equilibrium depends both on the free energy difference and on the temperature (**Equation 2.14**). In metathesis reactions, common- and medium-ring formation is typically driven by the entropic benefit of cyclisation over oligomerisation, as ring strain is introduced and therefore $\Delta\Delta H$ is typically > 0 .¹⁰³ Some exceptions to this exist, such as the relief of strain in the acyclic form,¹⁰⁵ or the

$$K = \exp(-\Delta G^\circ/RT) = \exp(-\Delta H^\circ/RT) \cdot \exp(\Delta S^\circ/R) \quad (2.14)$$

formation of products with little or no ring strain, such as cyclohexene.¹¹²

To assess the effects of temperature on the RCM of 1,8-nonadiene, a solution of 1,8-nonadiene (40 mmol L^{-1}) was exposed to **G2** (4 mmol L^{-1}) at 278 K in the magnet of the NMR spectrometer and ^1H NMR spectra were acquired over time. The concentration *versus* time profiles obtained showed the system slowly approaching equilibrium (**Figure 2.33**). The temperature was increased to 298 K and the reaction approached a second equilibrium position after a brief period of rapid reaction. Finally, the reaction was warmed to 318 K, at which point the rate of RCM and of cyclohexene production (*via* isomerisation-RCM, see chapter 4) increased.

The concentration of **G2** present in the reaction could be monitored by ^1H NMR spectroscopy, which revealed very slow pre-catalyst initiation (**Figure 2.34**); the solution concentration of active catalyst must therefore have been low, even though 10 mol% of pre-catalyst was charged. Pre-catalyst initiation was faster at 298 K, and rapid and almost complete within 2 h at 318 K. Rate constants could be obtained at each temperature (**Figure 2.35**) and, from these, values for thermodynamic parameters (ΔH^\ddagger , ΔS^\ddagger and ΔG^\ddagger) could be obtained (**Figure 2.36**). These values are only approximate as only a very small part of the initiation reaction (less than $t_{1/2}$) was monitored, except at 318 K. Despite the poor data density, the estimated parameters for ΔH^\ddagger ($29.9 \text{ kcal mol}^{-1}$

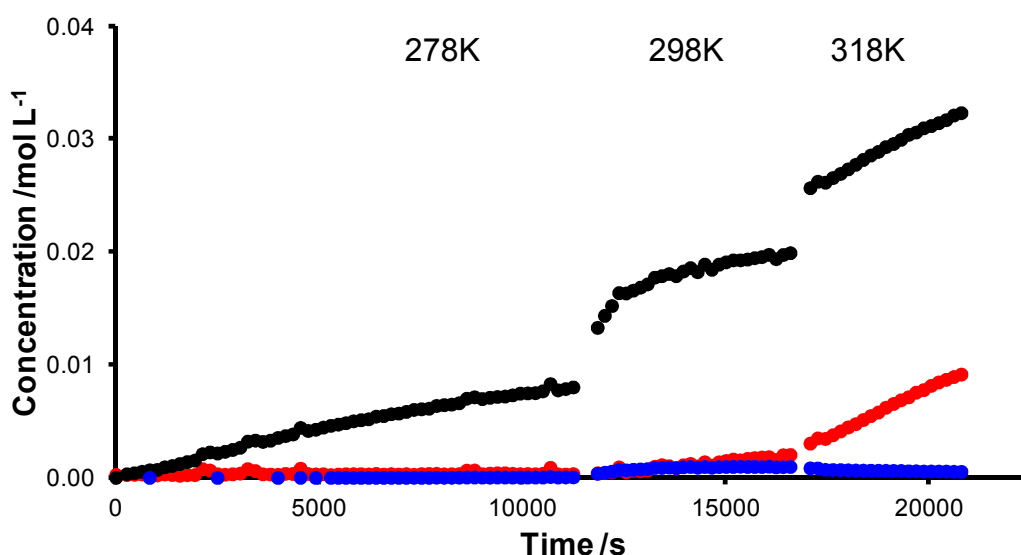


Figure 2.33. Concentration/time profiles for cycloheptene (**black**), cyclohexene (**red**) and cyclic dimer (**blue**) in the variable temperature RCM of 1,8-nonadiene (40 mmol L^{-1}) with **G2** (4 mmol L^{-1}) at 278 K, 298 K and 318 K.

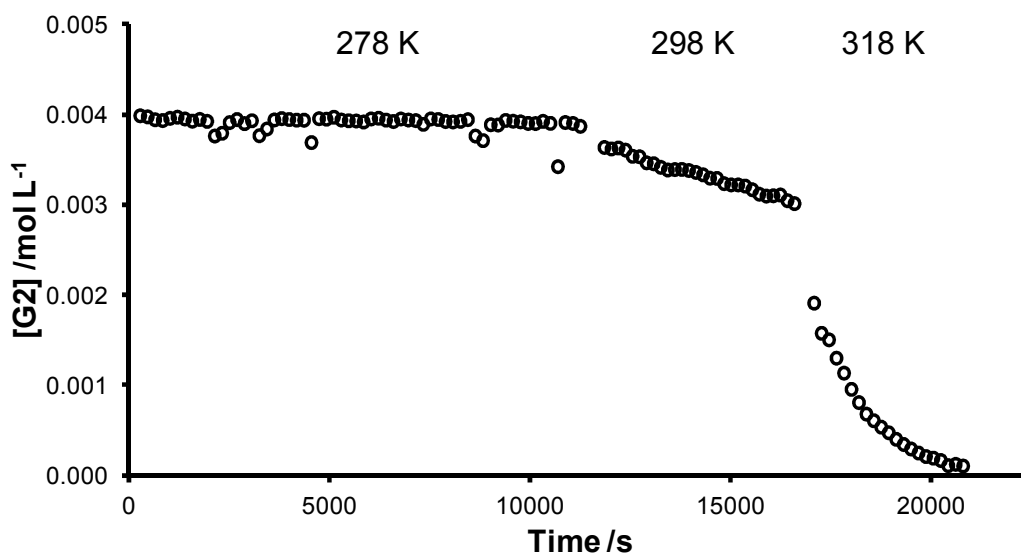


Figure 2.34. Pre-catalyst concentration/time profile for the RCM of 1,8-nonadiene (40 mmol L⁻¹) with **G2** (4 mmol L⁻¹) at 278 K, 298 K and 318 K.

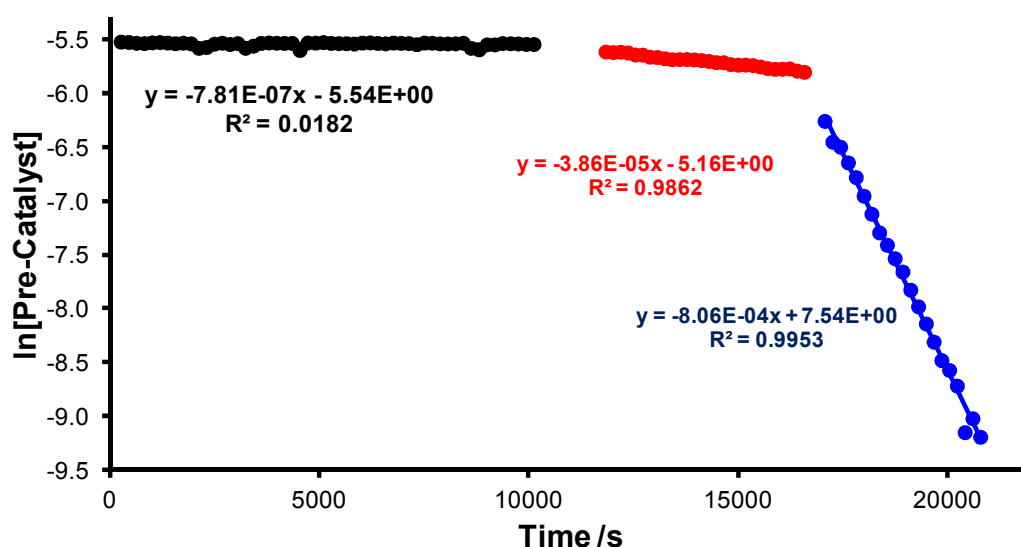


Figure 2.35. A first-order treatment of pre-catalyst concentration in the variable temperature RCM of 1,8-nonadiene (40 mmol L⁻¹) with **G2** (4 mmol L⁻¹) at 278 K (black), 298 K (red) and 318 K (blue).

¹), ΔS^\ddagger (21 cal K⁻¹ mol⁻¹) and ΔG_{298}^\ddagger (23.5 kcal mol⁻¹) were in agreement with those reported by Grubbs *et al.* from variable temperature ³¹P magnetisation transfer experiments in toluene ($\Delta H = 27 \pm 2$ kcal mol⁻¹, $\Delta S = 13 \pm 6$ cal K⁻¹ mol⁻¹, $\Delta G_{298K} = 23.0 \pm 0.4$ kcal mol⁻¹).²⁶ The event that this pre-catalyst decay represents is most likely to

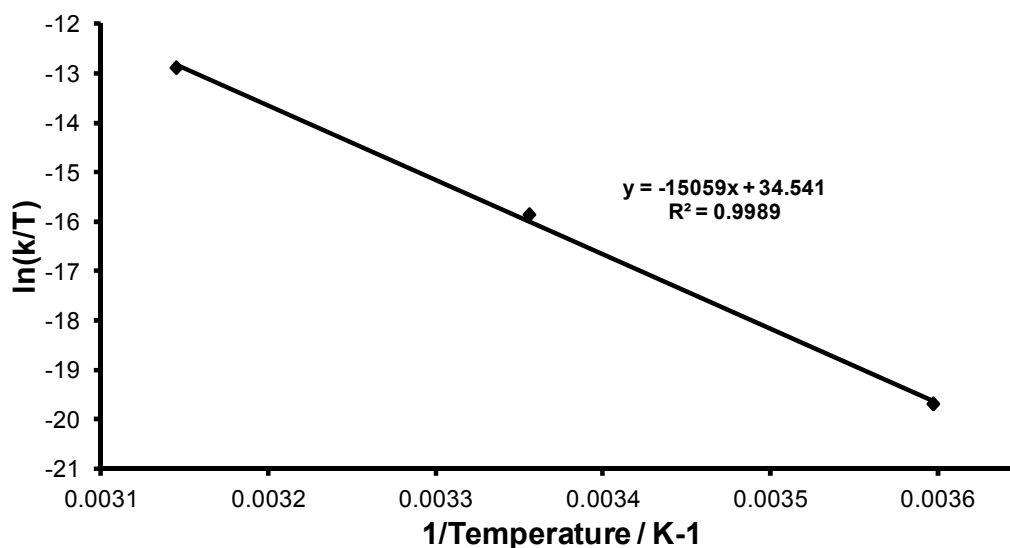


Figure 2.36. Eyring treatment of the rate constants obtained from **Figure 2.35**.

be the initiation event and not, for example, decomposition of **G2**.

Inspection of the alkyldiene region of the ^1H NMR spectrum revealed quantifiable levels of ruthenium carbene species at 318 K. A signal at $\delta_{\text{H}} = 18.6$ ppm appearing as a broad apparent triplet was assigned to propagating carbene **119c**, correlated to a signal at *ca.* 1.5 ppm in the [^1H , ^1H] COSY spectrum.⁹⁶ A singlet at $\delta_{\text{H}} = 17.8$ ppm was assigned to methyldiene **3b** (by comparison with an authentic sample) and a quadruplet at $\delta_{\text{H}} = 18.4$ ppm was assigned to phosphane-bound ethyldiene **31b** (**Figure 2.37**).¹⁴¹ Propagating carbene species **119c** is an intermediate *en route* to both cycloheptene and oligomer, and the fact that it is found to accumulate in solution shows that cyclisation must be slower than alkyldiene transfer. Methyldiene **3b** is believed to be catalytically inactive,²⁶ while metathesis-active ethyldiene **31b** is a known by-product from the isomerisation-RCM sequence (see Chapter 4).¹⁸⁹

A second experiment was designed to overcome the issues introduced by the slow initiation rate of **G2**. The EM_{T} of a cyclic compound is an intrinsic property of that compound and independent of the reaction (whether real or virtual)¹⁷¹ used to create it, so the same equilibrium positions ought to be reached in 1,8-nonadiene metathesis regardless of the pre-catalyst employed. The mechanism of the initiation of **GH2** has been studied in some detail recently (see chapter 3);^{60-61,190-191} the initiation is (at least partly) dependent on the concentration of the alkene substrate, and is usually much more rapid than the initiation of **G2**. 1,8-Nonadiene (40 mmol L^{-1}) was exposed to **GH2**

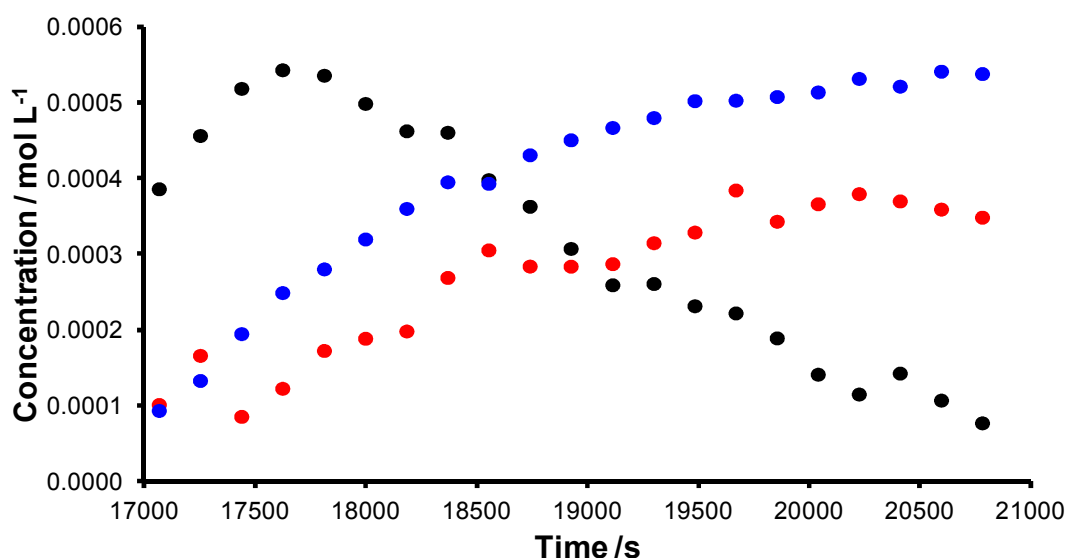


Figure 2.37. Concentration/time profiles for propagating carbene **119c** (black), methylenide **3b** (blue) and ethylenide **31b** (red) in the RCM of 1,8-nonadiene (40 mmol L⁻¹) with **G2** (4 mmol L⁻¹) at 318 K in chloroform-*d*.

(4 mmol L⁻¹) and the reaction temperature was stepped from 278 K to 318 K in 10 K increments. Different equilibrium positions were reached at each temperature. The formation of cyclohexene (*via* isomerisation-RCM) was faster in this experiment, and occurred even at 278 K. The concentrations of cycloheptene, cyclohexene, cyclic dimer and pre-catalyst were profiled (**Figure 2.38**). Equilibrium was clearly reached at each temperature in this experiment due to the superior activity of **GH2** at low temperatures.

In order to understand the effect of changing temperature on the RCM of 1,8-nonadiene, the MEM_T was quantified at each temperature (**Figure 2.38**). The increase of this value with increasing temperature is qualitatively consistent with the behaviour of thermodynamically-controlled cyclisations: the TΔS component of the Gibbs free energy expression (**Equation 2.15**) is most strongly affected by temperature (ΔH and ΔS vary relatively little with temperature).

$$\Delta G = \Delta H - T\Delta S \quad (2.15)$$

For the dimerisation reaction, two molecules are brought together to form one molecule and so the rotational and translational entropy of one molecule is lost. Therefore, for dimerisation, ΔS ≈ -30 to -40 cal K⁻¹ mol⁻¹ so this process is most disfavoured with

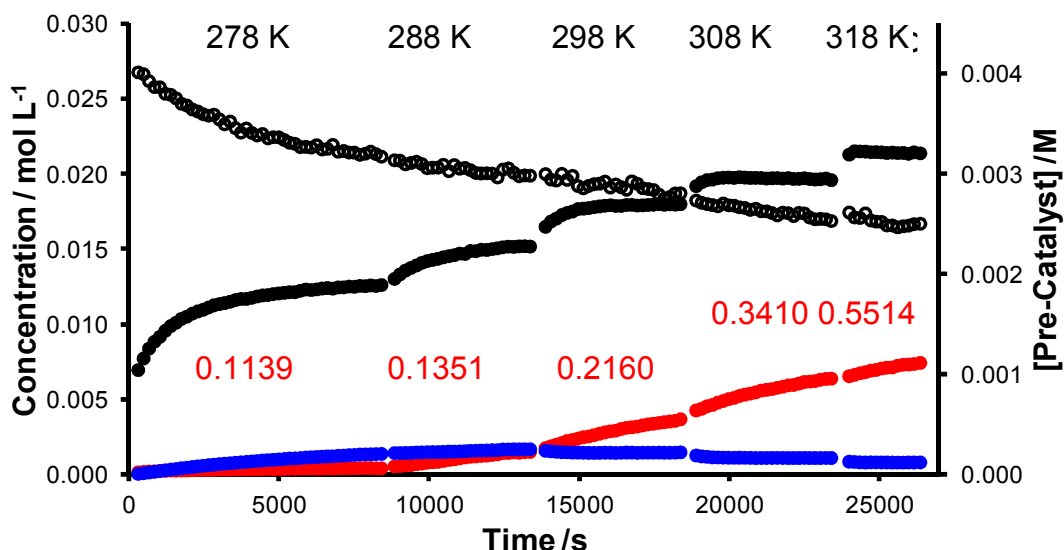


Figure 2.38. Concentration/time profiles for cycloheptene (closed **black** points), cyclohexene (**red**), cyclic dimer (**blue**) and pre-catalyst (open **black** points) in the variable temperature RCM of 1,8-nonadiene (40 mmol L^{-1}) with **GH2** (4 mmol L^{-1}) at 278 K, 288 K, 298 K, 308 K and 318 K; the red numbers refer to the MEM_T at the last data point at that temperature.

increasing temperature. Cyclisation to form cyclic dimer **106d** requires limiting the rotation around twelve (otherwise unrestricted) rotors, while cyclisation to form cycloheptene requires the restriction of only six. Therefore, while an increase in temperature changes the free energy in the same direction for all three processes (i.e. $T\Delta S$ decreases and so ΔG increases), the formation of linear or cyclic dimer is disfavoured *more* than cyclisation to form cycloheptene due to the magnitudes of the relevant ΔS terms (i.e. $\Delta S_{\text{inter}} > \Delta S_{\text{intra},2} > \Delta S_{\text{intra},1}$). This relationship can also be considered algebraically: the ratio of EM_T (**Equation 2.16**, where $\text{EM}_{T,1} = \text{EM}_T$ of cycloheptene and $\text{EM}_{T,2} = \text{EM}_T$ of the cyclic dimer) can be written as an expression involving the appropriate thermodynamic parameters (**Equation 2.17**).

$$\frac{(\text{EM}_{T,1})^2}{\text{EM}_{T,2}} = \frac{(\text{EM}_{H,1} \cdot \text{EM}_{S,1})^2}{\text{EM}_{H,2} \cdot \text{EM}_{S,2}} = \exp\left(\frac{2\Delta\Delta S_1}{R} - \frac{2\Delta\Delta H_1}{RT}\right) / \exp\left(\frac{\Delta\Delta S_2}{R} - \frac{\Delta\Delta H_2}{RT}\right) \quad (2.16)$$

$$\ln\left(\frac{(\text{EM}_{T,1})^2}{\text{EM}_{T,2}}\right) = \frac{2\Delta\Delta S_1 - \Delta\Delta S_2}{R} - \frac{2\Delta\Delta H_1 - \Delta\Delta H_2}{RT} = \frac{2\Delta S_{\text{intra},1} - \Delta S_{\text{intra},2} - \Delta S_{\text{inter}}}{R} - \frac{2\Delta H_{\text{intra},1} - \Delta H_{\text{intra},2} - \Delta H_{\text{inter}}}{RT} \quad (2.17)$$

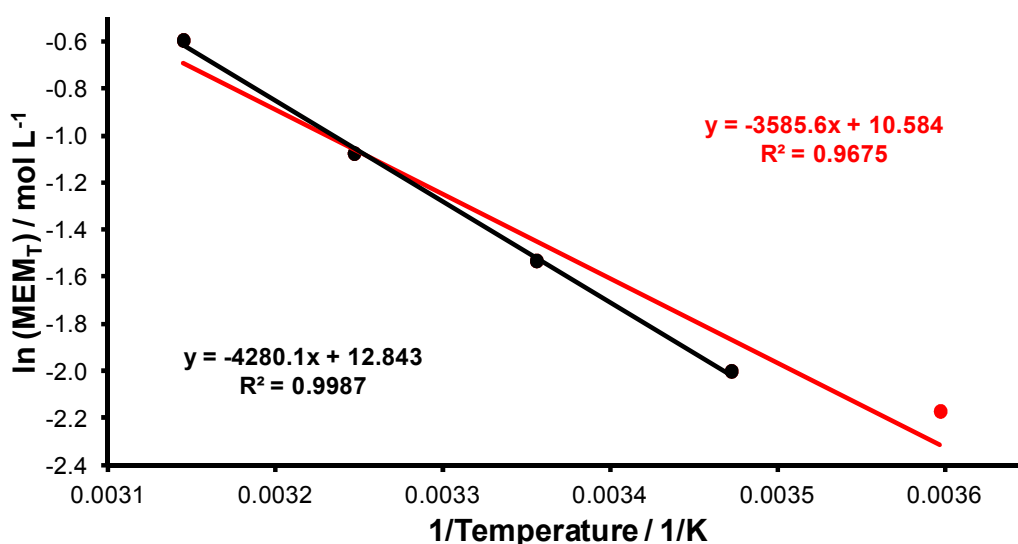


Figure 2.39. Plot of $\ln(\text{MEM}_T)$ versus $1/T$ for cycloheptene with (i) data points from 278 K – 318 K (red and black points, red line) and (ii) 288 K – 318 K only (black points only, black line).

This expression confirms algebraically that as temperature increases, MEM_T increases exponentially, and also suggested that a plot of $\ln(\text{MEM}_T)$ versus $1/T$ ought to yield a straight line. A plot was constructed using the values in **Figure 2.38**. While the values obtained at 288 K to 318 K lie on an excellent straight line (**Figure 2.39**), the data point at 278 K lies off of this line. The low temperature point may not be entirely reliable if the system has not properly reached equilibrium; the reaction is slow at this temperature, despite the high loading of **GH2**, and may have not reached equilibrium.

While this result was further proof of thermodynamic control in this RCM reaction, these data also presented an opportunity to derive data about the thermodynamics of ring-closing versus oligomerisation. The enthalpic and entropic advantages of cyclisation (to form cycloheptene) can be obtained from the gradient and intercept of the straight line, respectively. These values were calculated from the straight line encompassing the four good fit points (**Equations 2.18** and **2.19**). The large and positive entropy difference ($\approx 25 \text{ cal K}^{-1} \text{ mol}^{-1}$) is close to Mandolini's estimate of the entropy loss upon bringing two molecules together in solution,¹⁰⁵ which suggested that

$$2\Delta S_{\text{intra},1} - \Delta S_{\text{intra},2} - \Delta S_{\text{inter}} = 25.5 \text{ cal K}^{-1} \text{ mol}^{-1} \quad (106.6 \text{ J K}^{-1} \text{ mol}^{-1}) \quad (2.18)$$

$$2\Delta H_{\text{intra},1} - \Delta H_{\text{intra},2} - \Delta H_{\text{inter}} = 8.5 \text{ kcal mol}^{-1} \quad (35.5 \text{ kJ mol}^{-1}) \quad (2.19)$$

the cyclisation reaction to form cycloheptene was entropically favoured over the alternative oligomerisation-cyclisation process by the entropy loss of the oligomerisation step alone. This was a sensible result, given that the same number of rotors is frozen in both cases (i.e. two cyclisation reactions to form cycloheptene *versus* one to form cyclic dimer **106d**). The corresponding enthalpy expression reveals that the cyclisation to form (two molecules of) cycloheptene is enthalpically disfavoured (by *ca.* 8.5 kcal mol⁻¹) *versus* the dimerisation-RCM route to **106d**. Given that $\Delta H_{\text{inter}} \approx 0$,¹⁹² this represents the extra strain energy introduced when forming two molecules of cycloheptene *versus* a molecule of **106d**, suggesting that **106d** is not particularly strained.

These values can be tested *versus* the DFT calculations on the hydrocarbon species alone; calculation of **Equations 2.18** and **2.19** using DFT data reveal values for entropy and enthalpy of -32.3 cal K⁻¹ mol⁻¹ and 12.5 kcal mol⁻¹ respectively. The enthalpy calculation is relatively close to the experimentally determined value, especially given the use of five separate DFT-calculated terms which each have potential uncertainty of ± 0.5 kcal mol⁻¹, which would result in an uncertainty in this calculation of ± 7 kcal mol⁻¹. The entropy calculation is far less accurate, resulting in a value of approximately the correct magnitude, but predicting a *favourable* entropy difference. The issues with entropy calculations using these DFT methods have already been discussed;⁹⁶ corrections based on empirical evidence are necessary to bring the calculations into agreement with experiment.

Approaching Reaction Equilibria

A reaction under thermodynamic control will approach the same equilibrium position from any mixture of substrate and product, provided that the total effective monomer concentration is the same.¹⁰⁴ Initial effective monomer concentrations were selected that would allow the observation of both cycloheptene and oligomers. In reactions where metathesis products were exposed to the reaction conditions, the solution was sparged with ethene to make sure that all pathways available in the metathesis of the α,ω -dienes were also available in the metathesis of the products.

Three experiments were conducted:

- The cyclisation of 1,8-nonadiene (40 mmol L⁻¹) with 1 mol% **G2**, which should yield a thermodynamic mixture of 1,8-nonadiene, cycloheptene, cyclic dimer and ethene

- The cyclisation of 1,8-nonadiene (40 mmol L⁻¹) with 3 mol% **G2**, which should yield the *same* thermodynamic mixture, but approach it *more quickly*
- The ROMP of cycloheptene (40 mmol L⁻¹) with 1 mol% **G2** in the presence of ethene (40 mmol L⁻¹) should approach the same mixture as the RCM experiments, but from the opposite direction

The concentration/time profiles for each reaction, in which cycloheptene, ethene and cyclic dimer can be speciated, show that each reaction results in the same equilibrium position (**Figure 2.40**). The RCM reaction with a higher pre-catalyst loading reached the same position, but more quickly. The values of MEM_T and [cycloheptene]/[cyclic dimer] were quantified at each time point, and were found to converge upon similar values (**Table 2.11**). Traces of cyclohexene were detected in each reaction. These reactions are clearly under thermodynamic control; the composition of the reaction products depends on temperature and substrate concentration and is not a function of the pre-catalyst loading. This series of experiments is the first example of a study where kinetic experiments have been used to show that RCM reactions with ruthenium-based pre-catalysts are under thermodynamic control. The RCM reactions of 1,8-nonadiene described here show that the reaction responds to changes in concentration and temperature, and metathesis of cycloheptene (in the presence of ethene) results in the same mixture of products as the corresponding RCM reaction.

These outcomes are similar to those reported by Kress, who studied the ROMP of a series of cycloalkenes (cyclopentene, cycloheptene and *cis*-cyclooctene, in the absence of ethene) with tungsten-based metathesis catalysts in DCM-*d*₂.¹³⁶ ROMP of cyclopentene (0.3 mol L⁻¹) was rapid at 210 K, and slower at 225 K. When the mixture

Table 2.11. Initial reaction conditions and conversion to cyclopentene (in mol L⁻¹ and %), [cycloheptene]:[cyclic dimer] and MEM_T at equilibrium for reactions in **Figure 2.41**.

	1,8-Nonadiene	1,8-Nonadiene	Cycloheptene
[Substrate] ₀	0.0405	0.0382	0.0364
Loading of G2	1 mol%	3 mol%	3 mol%
[Cycloheptene]	0.0199	0.0216	0.0195
Conversion to Cycloheptene	49.1%	56.5%	53.6%
[cycloheptene]:[cyclic dimer]	12.2	12.7	10.4
MEM _T	0.241	0.275	0.203

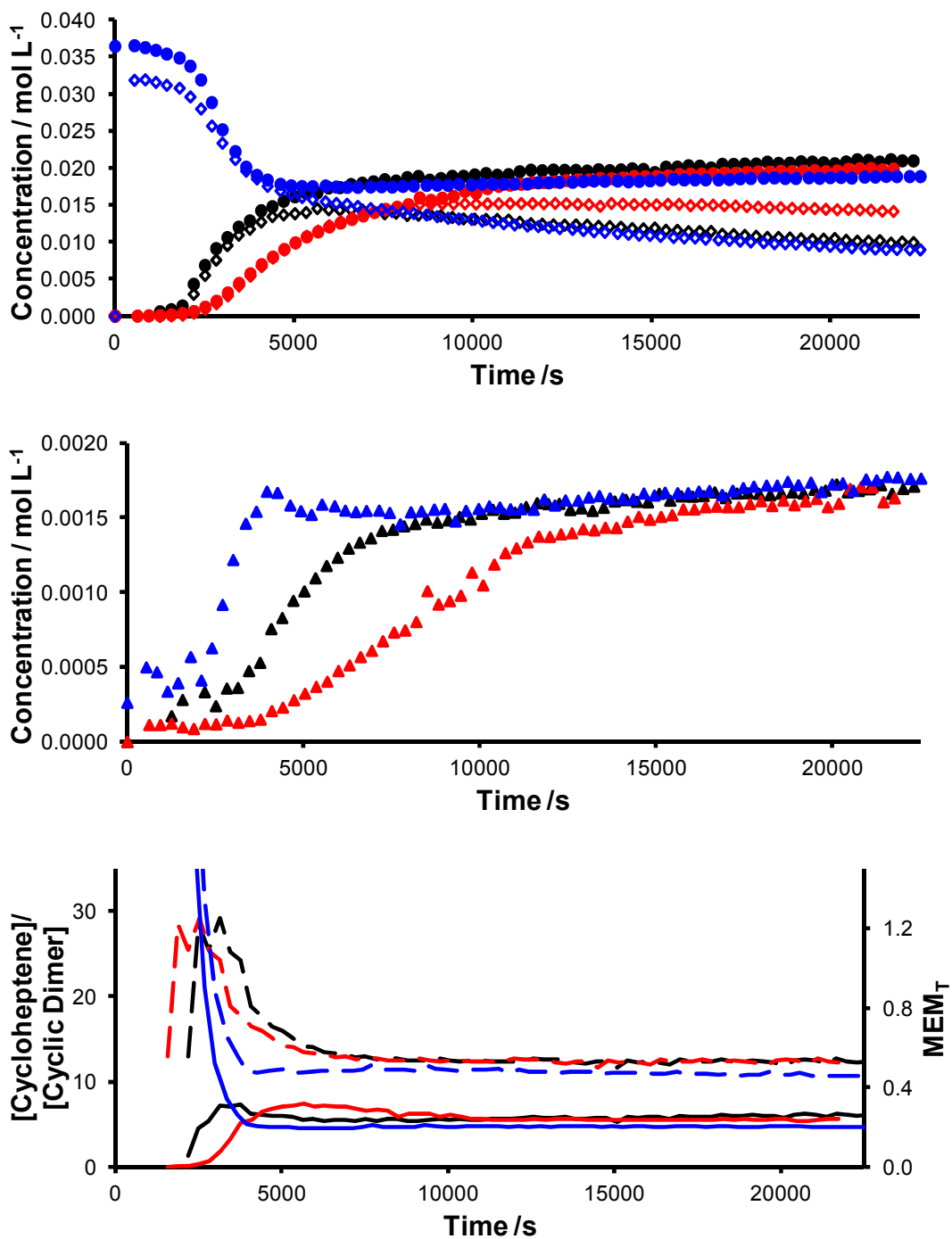


Figure 2.40. (a) and (b): Concentration/time profiles for cycloheptene (closed circles), cyclic dimer (closed triangles) and ethene (open rhombi) in (i) the RCM reaction of 1,8-nonadiene (40 mmol L⁻¹) with 3 mol% **G2** (black), (ii) the RCM reaction of 1,8-nonadiene (40 mmol L⁻¹) with 1 mol% **G2** (red) and (iii) the ROMP reaction of cycloheptene (40 mmol L⁻¹) with 3 mol% **G2** (blue); (c): MEM_T (solid line) and [cycloheptene]/[cyclic dimer] (dashed line) *versus* time in the same experiments.

was warmed to 240 K and then 260 K, the reverse reaction occurred and cyclopentene was re-formed. Cooling the mixture to 235 K resulted in ROMP once more. When cycloheptene (0.275 mol L^{-1}) was exposed to the metathesis catalyst at 270 K, rapid polymerisation occurred, followed by a slower back-biting process to yield cyclic dimer **106d**. This suggested that the kinetic and thermodynamic products were different; while the initial reaction produced long chains, these equilibrated to form molecules of cyclic dimer. As the cyclic dimer is not particularly strained,⁹⁶ the entropic benefit of dividing a chain up into a number of discrete molecules drives the reaction. *cis*-Cyclooctene (0.2 mol L^{-1}) was found to polymerise rapidly at 250 K and yield a white precipitate.

The ROMP reaction was repeated in the absence of ethene, to evaluate the effect this had on the equilibrium position. The concentration/time profile showed, after a short latency period, the establishment of equilibrium between cycloheptene and cyclic dimer **106d**, without the formation of oligomers (**Figure 2.41**). MEM_T was determined to be 0.215 at the end of the experiment, in agreement with the values obtained in the presence of ethene. As expected no diene, ethene or linear oligomers were detected in the reaction mixture; unexpectedly, no cyclohexene was detected. This outcome was important, as it confirmed experimentally that MEM_T can be applied in the absence *and* in the presence of ethene. This would be expected because both the

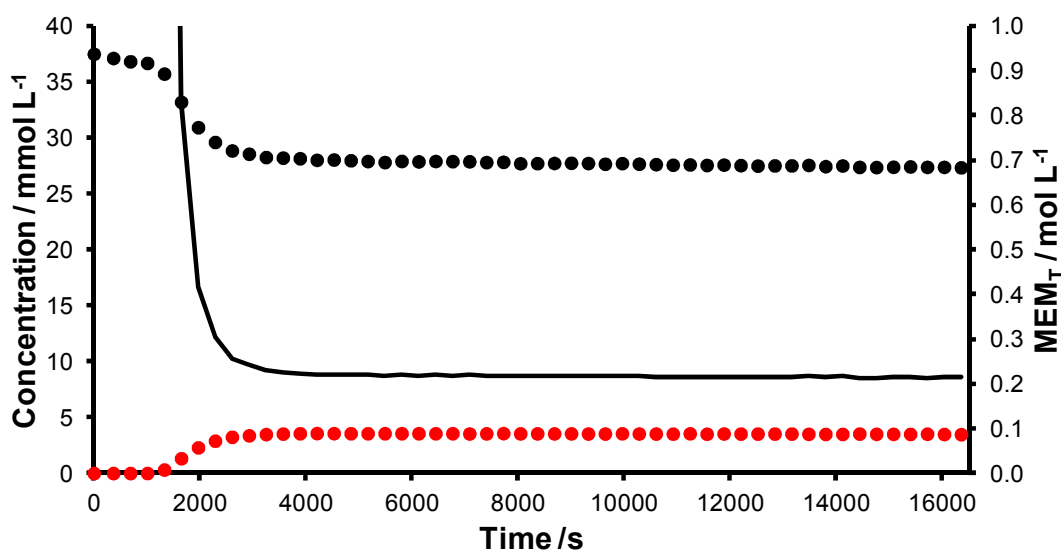


Figure 2.41. Concentration *versus* time profiles for cycloheptene (**black points**) and cyclohexene (**red points**) and MEM_T (**black line**) in the ethene-free ROMP reaction of 1,8-nonadiene (40 mmol L^{-1} with 3 mol% **G2** at 298 K in chloroform-*d*).

formation of two equivalents of cycloheptene and the formation of one equivalent of cyclic dimer (from two equivalents of 1,8-nonadiene) would liberate two equivalents of ethene.

As well as proving that these reactions are under thermodynamic control, these experiments are consistent with experimentally measured EM_T for cyclopentene, cycloheptene and *cis*-cyclooctene (*ca.* 0.5 mol L⁻¹, 0.05 mol L⁻¹ and 0.1 – 1 mmol L⁻¹ respectively).⁹⁶ This study also represents the first example of conclusive kinetic experiments showing an RCM reaction to be under thermodynamic control.

Conclusions

This chapter documents the development and use of a method for acquiring high quality kinetic data for the RCM reactions of a small series of prototypical α,ω -dienes using ^1H NMR spectroscopy. The method allows reproducible collection of datasets for reactions that contain species that are potentially sensitive to oxygen, water and other contaminants. Importantly, this method perturbs the reaction minimally, as all chemistry occurs within an NMR tube in the magnet of the spectrometer, without work-up, transfer, processing or purification.

The method has been used to investigate the effects of ring size on the rate of RCM of a series of simple α,ω -dienes that do not feature any functionality that may otherwise influence the reaction outcome. The order of reactivity has been clearly established as 1,7-octadiene > 1,6-heptadiene > 1,8-nonadiene \gg 1,9-decadiene. These results differ from the usual order of reactivity with respect to target ring size exhibited in nucleophilic or acid- or base-catalysed ring-closing reactions ($5 > 6 > 7 > 8$).¹⁰² Diethyl diallylmalonate was found to undergo RCM more slowly than 1,6-heptadiene, despite the presence of *gem*-disubstitution, which was attributed to the unfavourable and/or slow formation of the intermediate carbene species.

Comparison with data obtained from DFT calculations on the reaction does not provide a clear link between calculated barriers and relative rates; while metallocyclobutane breakdown typically presents the largest barrier on the potential energy surface, the order of the sizes of these barriers do not reflect the order of reactivity determined experimentally. Instead, the kinetic order of reactivity is the same as the thermodynamic order of reactivity.

1-Octene and 1,5-hexadiene cross metatheses were both explored as potential model reactions, with hopes of ultimately quantifying kinetic EMs for cyclisations studied. Unfortunately, a suitable value of k_{inter} could not be obtained from either reaction, due to the slow and poor conversion under the conditions used for the corresponding RCM reactions. 1,5-Hexadiene was found to inhibit metathesis reactions *via* formation of a stable cyclic η^2 -complex; this complex was found to be lower on the PES (with respect to the intermediate carbene) than any intermediate on the PES of 1,7-octadiene RCM.

Unfortunately, results were typically at best semi-quantitative, due to the fact that most of the reactions studied do not correspond to a simple kinetic order (the use of reaction simulation approaches to overcome this problem is discussed in Chapter 3). As an additional complication, these reactions have been shown to be under thermodynamic control. This outcome means that kinetic EMs cannot be obtained from a series of RCM reactions using the method described by Percy *et al.*, but has allowed quantification of the *thermodynamic* effective molarities.⁹⁶

Chapter 3:

A Reaction Simulation Approach to Ring-closing Metathesis Kinetics

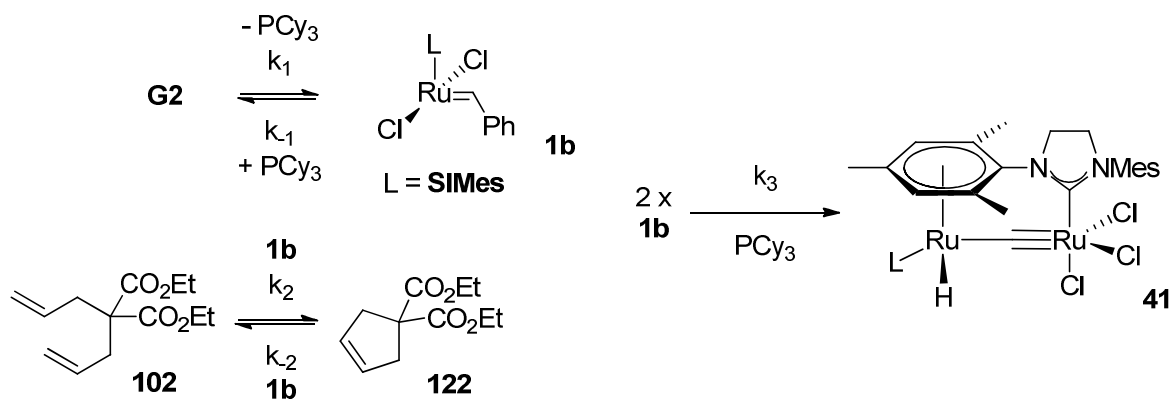
Reaction Simulation Approaches

Deconvolution of Complex Kinetic Behaviour

As discussed in Chapter 2, RCM reactions rarely behave in a simple first-order manner. Reaction simulations, in which series of differential equations describe how the concentrations of reaction substrates, intermediates and products change with respect to time, offer an approach to the analysis of reaction kinetic data. For complex multi-step reactions, this is often far simpler and easier than deriving a complicated rate expression which may require assumptions and simplifications. Such an approach was sought for RCM. Commercial software such as Berkeley Madonna¹⁹³ or Micromath Scientist¹⁹⁴ can be used to construct and use such models. Various other packages are also available but Madonna and Scientist were used throughout the course of this work; Madonna was used to obtain the rate constants and simulated concentration/time profiles in this chapter unless stated otherwise.

Reaction Simulation Approaches for Metathesis

There are very few examples of these approaches being used in metathesis chemistry, with the only detailed study carried out by Adjiman *et al.*¹⁶⁶ Adjiman *et al.* constructed a simple model to describe the RCM reaction of diethyl diallylmalonate **102**, in which the initiation event (phosphane dissociation, represented by k_1 and k_{-1}) is separated from the RCM reaction itself (represented by k_2 and k_{-2}) and a decomposition event (according to the mechanism presented by Grubbs *et al.*,²⁸ represented by k_3) (**Scheme 3.01** and **Equations 3.01-3.05**).¹⁶⁶ This model was used to study the effect of solvent on the RCM of **102** (0.12 mol L⁻¹) with pre-catalyst **G2** (6.7 mmol L⁻¹, except in cyclohexane and acetic acid, acid, in which the maximum concentration of **G2** was 0.4 mmol L⁻¹ due



$$d[\mathbf{G2}]/dt = -k_i \cdot [\mathbf{G2}] + k_i \cdot [\mathbf{1b}] \cdot [\text{PCy}_3] \quad (3.01)$$

$$d[\mathbf{1b}]/dt = k_i \cdot [\mathbf{G2}] - k_i \cdot [\mathbf{1b}] \cdot [\text{PCy}_3] - k_3 \cdot [\mathbf{1b}]^2 \quad (3.02)$$

$$d[\text{PCy}_3]/dt = k_i \cdot [\mathbf{G2}] - k_i \cdot [\mathbf{1b}] \cdot [\text{PCy}_3] - 2k_3 \cdot [\mathbf{1b}]^2 \quad (3.03)$$

$$d[\mathbf{102}]/dt = -k_2 \cdot [\mathbf{102}] \cdot [\mathbf{1b}] + k_2 \cdot [\mathbf{122}] \cdot [\mathbf{1b}] \quad (3.04)$$

$$d[\mathbf{122}]/dt = k_2 \cdot [\mathbf{102}] \cdot [\mathbf{1b}] - k_2 \cdot [\mathbf{122}] \cdot [\mathbf{1b}] \quad (3.05)$$

to solubility) at 298 K in each of six solvents (acetone- d_6 , acetic acid- d_4 , chlorobenzene- d_5 , cyclohexane- d_{12} , DCM- d_2 and toluene- d_6); rate constants for each of initiation, ring-closing, and catalyst decomposition were obtained (**Table 3.01**). Simulations of active catalyst and product concentration (from a simulated 0.1 mol L⁻¹ **102**, 0.42 mmol L⁻¹ **G2** reaction) were also presented, which suggested rapid and complete pre-catalyst initiation in all cases (**Figures 3.01** and **3.02**). The simulated profiles that were presented suggested that acetic acid was a far more efficacious solvent for this reaction than DCM

Table 3.01. Rate constants obtained by Adjiman *et al.* from fitting RCM concentration/time data to the model in **Scheme 3.01**.¹⁶⁶

Solvent	k_i (s ⁻¹)	k_{-i} (L mol ⁻¹ s ⁻¹)	k_2 (L mol ⁻¹ s ⁻¹)	k_{-2} (L mol ⁻¹ s ⁻¹)	k_3 (L mol ⁻¹ s ⁻¹)
Acetone	0.0146	2.434	1.676	0.231	3.000
Acetic Acid	0.527	0.00808	1.412	0.00872	0.029
Chlorobenzene	0.239	0.405	0.301	0.0197	0.0344
Cyclohexane	0.241	0.0363	0.523	0.0123	0
DCM	0.0617	0.373	0.137	0.00775	0
Toluene	0.159	0.0159	0.195	0.0128	0.0207

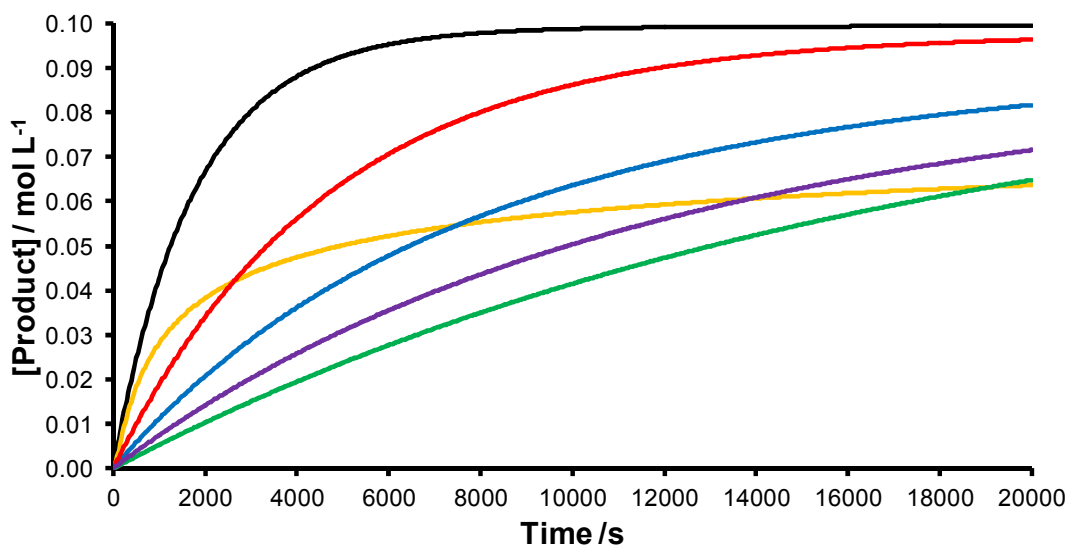


Figure 3.01. Simulated product concentration/time profiles from the RCM of **102** (0.1 mol L^{-1}) with **G2** (0.4 mmol L^{-1}) in **acetic acid**, **acetone**, **chlorobenzene**, **cyclohexene**, **DCM** and **toluene**.¹⁶⁶

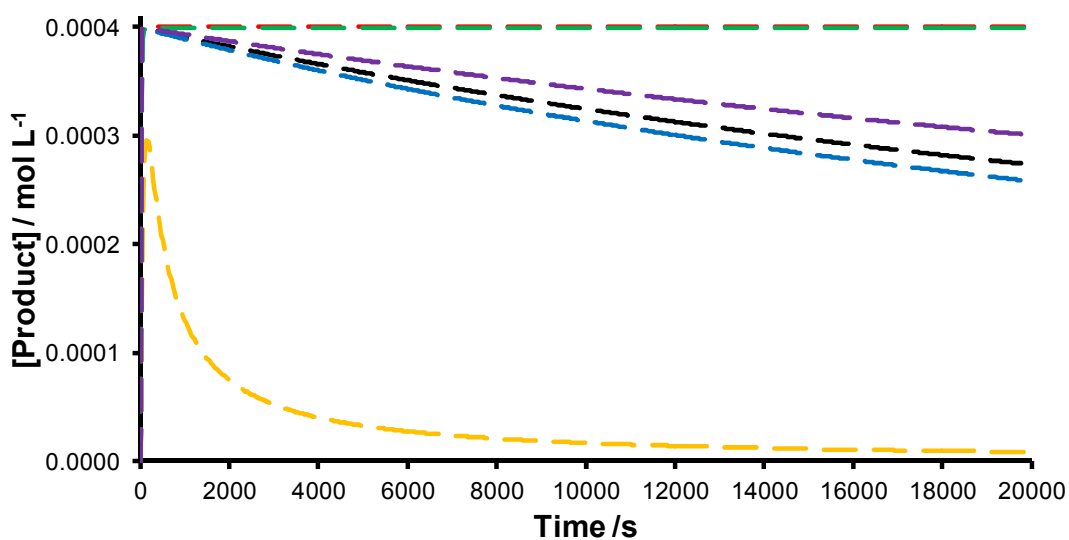


Figure 3.02. Simulated active catalyst concentration/time profiles from the RCM of **102** (0.1 mol L^{-1}) with **G2** (0.4 mmol L^{-1}) in **acetic acid**, **acetone**, **chlorobenzene**, **cyclohexene**, **DCM** and **toluene**.¹⁶⁶

or toluene, which are the usual solvent choices for metathesis reactions. The utility of acetic acid as a solvent for RCM was probed further by conducting a synthetic RCM reaction (83.3 mmol L^{-1} **102** with $0.25 \text{ mol}\%$ **G2**) at room temperature in which a better

result was achieved in acetic acid (complete conversion after 3 h and 82% isolated yield) than in DCM (80% conversion after 5 h). The rate constants in **Table 3.01** were processed further; rate constants were fitted to the expression in **Equation 3.06** in an attempt to probe the relative effects of different solvent properties on each step of the reaction. A , B and S are solvatochromic parameters¹⁹⁵ that measure the hydrogen bond acidity, hydrogen bond basicity and dipolarity/polarisability respectively, δ is a polarisability correction factor (1 for aromatic solvents, 0.5 for polyhalogenated aliphatic solvents, 0 for other solvents) and δ_{H}^2 is the cohesive energy density (in MPa).¹⁹⁶

$$\log k_{i,j} = c_{0,i} + c_{A,i}A_j + c_{B,i}B_j + c_{S,i}S_j + c_{\delta,i}\delta_j + (c_{\delta\text{H},i}/100)\cdot\delta_{\text{H},j}^2 \quad (3.06)$$

Values of the co-efficients for these solvent property parameters were obtained for each rate constant (**Table 3.02**). On the basis of these calculations, it was proposed that the solvent hydrogen bond acidity A influenced the rate of the RCM step itself, while a high value for the polarisability S of the solvent should limit the rate of catalyst deactivation.

Despite the simplifications and approximations required to express the complex metathesis mechanism in three steps (*vide infra*), the outcomes from this study are potentially very valuable. The identification of alternative solvents for metathesis is useful, as DCM is not acceptable on large scale synthetic projects and the use of toluene is discouraged.¹⁷⁰ Solvents such as acetic acid, dimethyl carbonate¹⁹⁷ and methyl *tert*-butyl ether¹⁵⁷ are far more appropriate for industrial large-scale metathesis. The topic of solvent selection is discussed in more detail in a subsequent section of this chapter.

It was hoped that this model would provide a means by which to quantitatively evaluate the effects of substrate structure.

Table 3.02. Solvatochromic coefficients for the five rate constants in the kinetic model published by Adjiman *et al.*¹⁶⁶

Rate Constant	$C_{0,i}$	$C_{A,i}$	$C_{B,i}$	$C_{S,i}$	$C_{\delta,i}$	$C_{\delta\text{H},i}$ (MPa)
k_1 ($i = 1$)	-16.888	3.097	4.039	-15.129	2.225	6.304
k_{-1} ($i = -1$)	-0.4720	-4.237	-0.3051	4.496	-1.922	-0.5062
k_2 ($i = 2$)	-17.555	2.239	5.151	-15.634	1.733	6.707
k_{-2} ($i = -2$)	-17.833	-0.1985	4.876	-15.372	1.188	6.570
k_3 ($i = 3$)	-95.272	11.196	35.701	-81.849	14.621	34.707

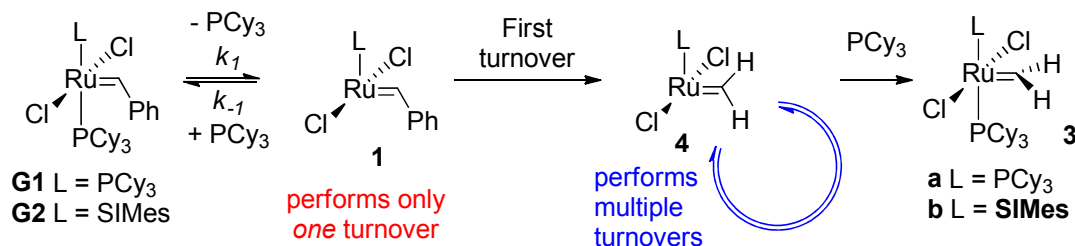
A Study of the Adjiman Model for Ring-closing Metathesis Kinetics

Appraising the Published Model and Outcomes

The Adjiman Model in the Context of Previous Literature

The model proposed by Adjiman *et al.* attempts to describe the complex series of steps and equilibria that comprise metathesis reactions (see **Scheme 1.02** in the introduction) with five rate constants in five differential equations;¹⁶⁶ the model must therefore significantly simplify the mechanism. It is useful to first appraise these simplifications and understand how they compare to what has been established in the literature about the processes that comprise the alkene metathesis reaction.

The initiation of the pre-catalyst is a key event in metathesis reactions.²⁶ Both the rate constant k_1 and equilibrium constant K_1 will have considerable impact on the overall RCM reaction rate. As discussed in the introduction, pre-catalyst **G2** initiates to form benzylidene **1b**, which is catalytically active (**Scheme 3.02**). However, the ruthenium carbene product of this first turnover of an α,ω -diene (such as **102**) is the 14e methylidene **4b** which binds phosphane *irreversibly*.²⁶ Grubbs *et al.* attempted to measure the rate of PCy_3 dissociation from **3b** at 353 K using ^{31}P NMR magnetisation transfer experiments in the presence of added PCy_3 , but decomposition precluded measurement of the initiation rate in this manner.²⁶ While phosphane-bound species **3b** is effectively inactive for metathesis, 14e methylidene **4b** is responsible for almost all metathesis turnovers. A metathesis reaction of an α,ω -diene to which x mol% of pre-catalyst is added will be catalysed by benzylidene **1b** for up to $x\%$ of the turnovers, with the remainder catalysed by methylidene **4b**. While Adjiman *et al.* have approximated the



Scheme 3.02.

behaviour of the catalyst in the model to that of the *benzylidene*, it would be far more appropriate to instead approximate this to the behaviour of the *methylidene* and therefore consider phosphane binding to be irreversible.

Adjiman *et al.* obtained a wide range of values for k_i and K_1 from fitting studies (**Table 3.03**);¹⁶⁶ the values of k_i obtained differ significantly from those obtained experimentally by Grubbs *et al.* (in toluene, THF and DCM) and Moore *et al.* (in benzene).^{26,198} The order of magnitude of the fitted (Adjiman) *versus* experimental (Grubbs, Moore) k_i values is very different; Adjiman *et al.* obtain values of *ca.* 0.01 to *ca.* 0.5 s⁻¹ from fitting concentration/time data (for RCM at 298 K), but Grubbs *et al.* and Moore *et al.* have measured values of *ca.* 10⁻³ s⁻¹ (at 296 or 308 K) directly from the reaction of **G2** with ethyl vinyl ether. This represents a difference of one to three orders of magnitude, which is a considerable discrepancy. In addition, equilibrium constant K_1 varied considerably amongst solvents. The reaction of 14e species **4b** was thought to be effectively barrierless,⁵⁶ and so it had been assumed that, for phosphane dissociation, $\Delta G^\circ \approx \Delta G^\ddagger$. However, Jensen *et al.* have recently conducted detailed studies on the modelling of the phosphane dissociation event, and have found that the barrier is in fact slightly lower than the free energy difference between 14e **1b** plus PCy₃ and **G2**.⁵⁷ Jensen *et al.* calculated ΔG^\ddagger for phosphane dissociation (at the BYLYP-D-CP level of theory, which includes a correction for dispersive interactions and a counterpoise correction to

Table 3.03. Rate constants for initiation of **G2** in various solvents, obtained from data fitting by Adjiman *et al.* and from experiment by Grubbs *et al.* and Moore *et al.*.^{26,166,198}

Solvent	From Data Fitting (at 298 K) ¹⁶⁶			From Experiment ^a		
	k_i (s ⁻¹)	k_i (L mol ⁻¹ s ⁻¹)	K_1	k_{init} (s ⁻¹)	T (K)	Ref.
Acetic acid	0.527	0.00808	63.4	-	-	-
Acetone	0.0146	2.434	0.00600	-	-	-
Benzene	-	-	-	8.6 x 10 ⁻⁴	296	198
Chlorobenzene	0.239	0.405	0.590	-	-	-
Cyclohexane	0.241	0.0363	6.64	-	-	-
DCM	0.0617	0.373	0.165	(6.1 ± 0.2) x 10 ⁻⁴	308	26
THF	-	-	-	(1.0 ± 0.1) x 10 ⁻³	308	26
Toluene	0.159	0.0159	10	(4.6 ± 0.4) x 10 ⁻⁴	308	26

^a From the reaction of **G2** with ethyl vinyl ether

overcome basis set superposition error) from **G2** to be 23.7 kcal mol⁻¹, in excellent agreement with the experimentally-determined value of 23.0 ± 0.4 kcal mol⁻¹.²⁶ A barrier for the reverse reaction was also discovered, as opposed to the barrierless re-binding of phosphane that had been assumed previously (see **Figure 1.04**). Therefore, $\Delta G^\ddagger \neq \Delta G^\circ$ and ΔG^\ddagger provides only a very approximate estimate of ΔG° . Assuming an uncertainty of *ca.* 5 kcal mol⁻¹ allows the use of **Equation 3.07** to estimate the approximate order of magnitude of K_1 at 10⁻¹³ to 10⁻²⁰ mol L⁻¹ ($\Delta G^\circ = 17$ to 28 kcal mol⁻¹).

$$K = \exp(-\Delta G^\circ/RT) \quad (3.07)$$

While this range is wide, K_1 is at most 10⁻¹³, far smaller than the *ca.* 10⁻² to 10² values derived by Adjiman *et al.*, which are therefore clearly not consistent with the known energetics of phosphane dissociation. Simulations presented in the publication suggested rapid and complete phosphane dissociation (**Figure 3.02**) yet this was not interrogated *via* inspection of the low field region of the ¹H NMR spectrum (lit. δ_H (DCM-*d*₂) = 19.16 ppm for **G2**).¹⁰ During experiments in deuterated solvents with 3 mol% **G2**, the pre-catalyst is found to persist at detectable levels for over 18 hours.⁹⁶

The decomposition of the active catalyst species was modelled according to the work of Hong *et al.*, in which two molecules of **4b** decompose to yield one molecule of diruthenium hydride complex **41** *via* attack of PCy₃ on methyldiene **4b**, as discussed in the introduction.²⁷⁻²⁸ However, this process occurred when a purified sample of phosphane-bound methyldiene **3b** was thermolysed in benzene at 333 K for 72 hours; **41** has not been reported as a by-product from synthetic metathesis reactions in the literature. This pathway may be limited to reactions carried out under conditions less mild than the quick (*t*_{1/2} < 2 h) and complete room temperature metathesis of **102**. Signals consistent with **41** have only been identified in studies conducted with high pre-catalyst concentrations over extended periods of time (for example, ≥ 0.25 mol L⁻¹ 1,8-

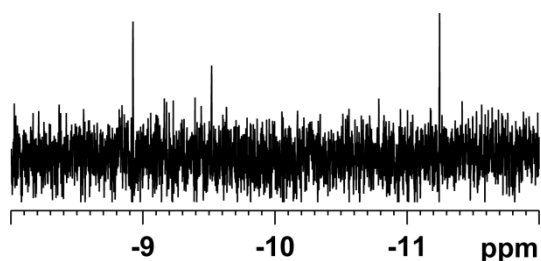


Figure 3.03. Partial ¹H NMR spectrum of the reaction mixture from the RCM of 1,8-nonadiene (0.25 mmol L⁻¹) in chloroform-*d* with 3 mol% **G2**; the signal at *ca.* -8.9 ppm is consistent with hydride complex **41**.¹⁹⁹

nonadiene, 3 mol% **G2**, 18 h at room temperature) (**Figure 3.03**).⁹⁶ While **41** can be observed by ¹H NMR (lit. δ_{H} (DCM-*d*₂) = -8.6 ppm), Adjiman *et al.* did not inspect this region of the spectrum, and so the decomposition rate in this manner is not calibrated against experiment. The reported values of k_3 in solvents such as acetone predict that **41** ought to be present in detectable quantities in these reaction mixtures after a few hours.

The equilibrium between substrate **102** and product **122** is also approximated in this model. In reality, the product *and ethene* are in equilibrium with the substrate, yielding an expression for K_2 (**Equation 3.08**). In contrast, the model considers only substrate and product, and therefore k_{-2} contains an implicit ethene concentration term (**Equation 3.09**). The concentration of ethene present in solution changes considerably over time, from zero to approximately 90% of the initial substrate concentration,¹⁸⁷ despite the fact that Adjiman *et al.* assert that “*..there is always a sufficient amount of ethylene in solution (confirmed by NMR spectroscopy), so that the concentration of ethylene is not included in the rate expression for the reverse metathesis reaction.*” Therefore, the value of k_{-2}^{model} will also change over time and K_2^{model} in the model is not a true reflection of the actual, very large,⁸⁹ equilibrium constant $K_2^{\text{mech'm}}$.

$$K_2^{\text{mech'm}} = k_2^{\text{mech'm}} / k_{-2}^{\text{mech'm}} = ([\mathbf{122}] \cdot [\text{ethene}] / [\mathbf{102}]) \quad (3.08)$$

$$K_2^{\text{model}} = k_2^{\text{model}} / k_{-2}^{\text{model}} = [\mathbf{122}] / [\mathbf{102}] \\ = k_2^{\text{mech'm}} / (k_{-2}^{\text{mech'm}} \cdot [\text{ethene}]) \quad (3.09)$$

Despite these simplifications and inconsistencies, the model was thoroughly tested using kinetic data acquired using the method developed in Chapter 2. Simplifications and approximations are necessary in order to reduce the considerable complexity of the full metathesis mechanism (**Scheme 1.02**), but the impact of these simplifications and approximations on the performance of the model should be systematically investigated.

Reproducing the Published Simulation

Before the model was applied to new reactions, attempts were made to reproduce the published dataset in DCM-*d*₂. The RCM of **102** (0.12 mol L⁻¹ with 6.7 mmol L⁻¹ **G2**) was carried out using the method and precautions outlined in Chapter 2; the 600 MHz NMR spectrometer was employed in the first instance to ensure the

Table 3.04. Relaxation times (T_1 , in seconds) measured for each ^1H NMR signal (with chemical shift δ_{H} , in ppm) for diethyl diallylmalonate **102** and RCM product **122**.

	δ_{H}	T_1								
102	5.70	4.65	5.17-5.10	2.64	4.18	3.51	2.64	1.21	1.26	3.14
122	5.63	6.81	4.19	4.45	3.01	2.30	1.26	3.70		

maximum number of data points was collected for fitting. Longitudinal relaxation times (T_1) were measured for **102** and **122** (Table 3.04) to ensure accurate quantification of concentrations; based on these data, an interpulse delay of 35 seconds was selected.

The experimental concentration *versus* time profile was compared with a simulated profile generated using the rate constants in Table 3.01. Unfortunately, the two profiles were different (Figure 3.04).

While care was taken to ensure that the DCM- d_2 used for this study was dry, it was reasoned that water in the solvent used by Adjiman *et al.* may have led to a different overall rate of reaction. As discussed in chapter 2, Karl Fischer titrimetry revealed that solvents dried using activated 4 Å molecular sieves contained *ca.* 7 ppm water. This is similar to that present in solvents from commercial solvent purification systems. In

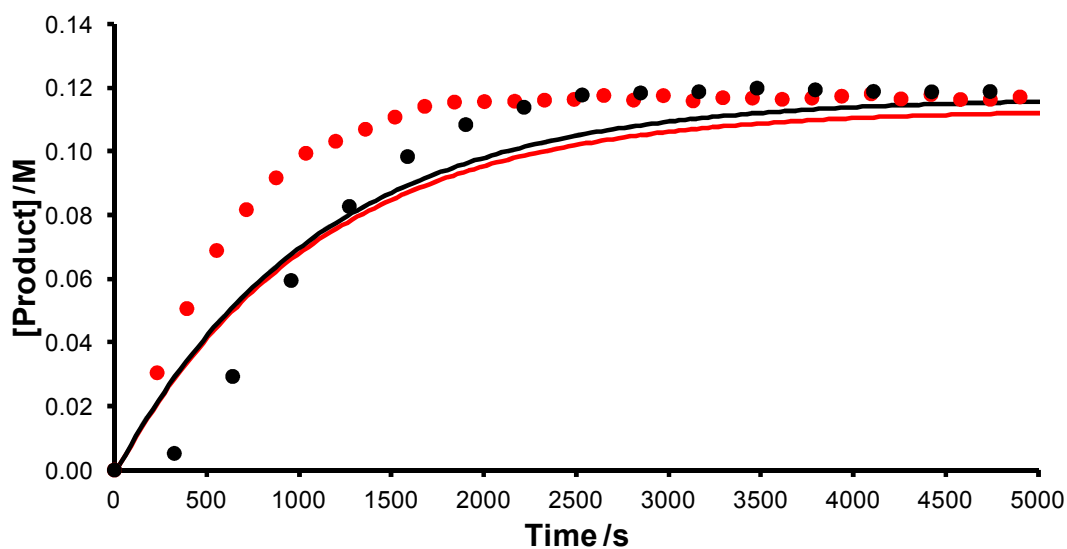


Figure 3.04. Simulated (lines) *versus* experimental (points) concentration/time profiles for the RCM of 0.12 mol L⁻¹ diethyl diallylmalonate in (i) dried DCM- d_2 (red) and (ii) undried DCM- d_2 (black).

contrast, undried commercial deuterated solvents contained water at *ca.* 30 ppm. When untreated solvents were used the reaction was slower, but the experimental concentration *versus* time profile still did not agree with the corresponding simulated profile (**Figure 3.04**).

Assessing the Flexibility of the Model

The flexibility of the model was explored next, because if the model can generate a number of different good fits to the experimental concentration *versus* time profiles with different values for the five rate constants in each case, then the model is poorly constrained and will yield *local* best fits rather than the single *global* best fit. A ‘good fit’ is defined here as a fit with a low root mean squared error of fit, in which the simulated profile intersects the majority of the experimental data points. Concentration/time data for the RCM reaction of **102** (**Figure 3.04** above, in dry DCM-*d*₂) was imported into Berkeley Madonna and a model was constructed according to Adjiman *et al.*¹⁶⁶ Fitting the data yielded the rate constants in **Table 3.05**; initial values for each rate constant of 0.01 and 100 were used in the data fitting routine for this and, unless stated otherwise, all other fits in this chapter.

Very different values for each of the five rate constants are obtained, particularly for k_1 and k_{-1} , yet an excellent fit to the experimental data was obtained (**Figure 3.05**). The potential flexibility of the model was therefore explored in a more systematic manner. As **102** cyclises irreversibly *via* rate limiting alkylidene transfer, the rate at which pre-catalyst enters (and stays in) the catalytic cycle is important. It follows from this that the correct values for k_1 and K_1 are critical to a successful modelling approach to this reaction, so a study was undertaken to explore whether the success of the fit was dependent on the correct value for k_1 . The rate constant k_1 was fixed at a series of

Table 3.05. Rate constants obtained from unconstrained fitting of the experimental profile in dry DCM-*d*₂ (in **Figure 3.04**) to the model in **Scheme 3.01**.

Entry	k_1 (s ⁻¹)	k_{-1} (L mol ⁻¹ s ⁻¹)	k_2 (L mol ⁻¹ s ⁻¹)	k_3 (L mol ⁻¹ s ⁻¹)	k_4 (L mol ⁻¹ s ⁻¹)
1	3.94 x 10 ⁻⁴ s ⁻¹	19.8	5.39	0.0529	3.28 x 10 ⁻⁶
2 ¹⁶⁶	0.0617	0.373	0.137	0.00775	0

^a Units s⁻¹

^b Units L mol⁻¹ s⁻¹

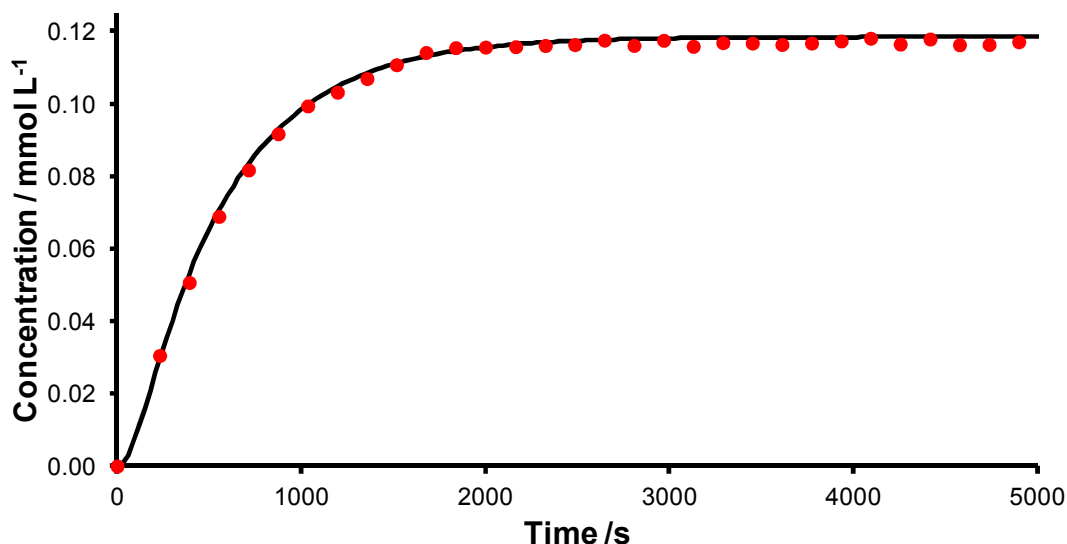


Figure 3.05. Simulated (using the rate constants in **Table 3.05**, Entry 1) (line) and experimental (points) concentration/time profiles for the RCM of diethyl diallylmalonate (0.12 mol L^{-1} with 6.7 mmol L^{-1} **G2** in $\text{DCM-}d_2$ at 298 K).

values (10^n , where n is an integer from -10 to 0 inclusive), and the rest of the rate constants were obtained from fitting (**Table 3.06**). Good fits were obtained for $n = -10$ to -2 (inclusive) (sample fits can be found in **Figure 3.06**). There were clear trends in the values of other rate constants as k_1 was varied. This suggested that when k_1 was

Table 3.06. Rate constants obtained when exploring the flexibility of the model in **Scheme 3.01**. k_1 was fixed and other rate constants were obtained from fitting.

$\log_{10}(k_1)$	k_1 ($\text{L mol}^{-1} \text{ s}^{-1}$)	k_2 ($\text{L mol}^{-1} \text{ s}^{-1}$)	k_2 ($\text{L mol}^{-1} \text{ s}^{-1}$)	k_3 ($\text{L mol}^{-1} \text{ s}^{-1}$)	RMS ^a
-10	2.81×10^{-2}	9.91×10^6	4.90×10^5	2.76×10^6	0.0090203
-9	1.72×10^{-6}	1.78×10^6	1.02×10^4	1.39×10^6	0.00345043
-8	7.64×10^5	2.06×10^5	2.20×10^3	1.60×10^{-2}	0.00284699
-7	2.20×10^4	1.77×10^4	9.72×10^1	1.12×10^4	0.00347453
-6	1.13×10^4	2.41×10^3	1.82×10^1	1.31×10^{-4}	0.00280632
-5	1.00×10^{-4}	2.29×10^2	2.00×10^0	4.96×10^2	0.00280791
-4	5.64×10^1	1.84×10^1	2.04×10^{-1}	2.44×10^{-1}	0.00301891
-3	7.57×10^1	5.86×10^0	2.47×10^{-2}	2.00×10^{-7}	0.00365562
-2	5.86×10^1	1.67×10^0	4.53×10^{-3}	4.38×10^{-8}	0.00423124

^a Error of fit; lower is better.

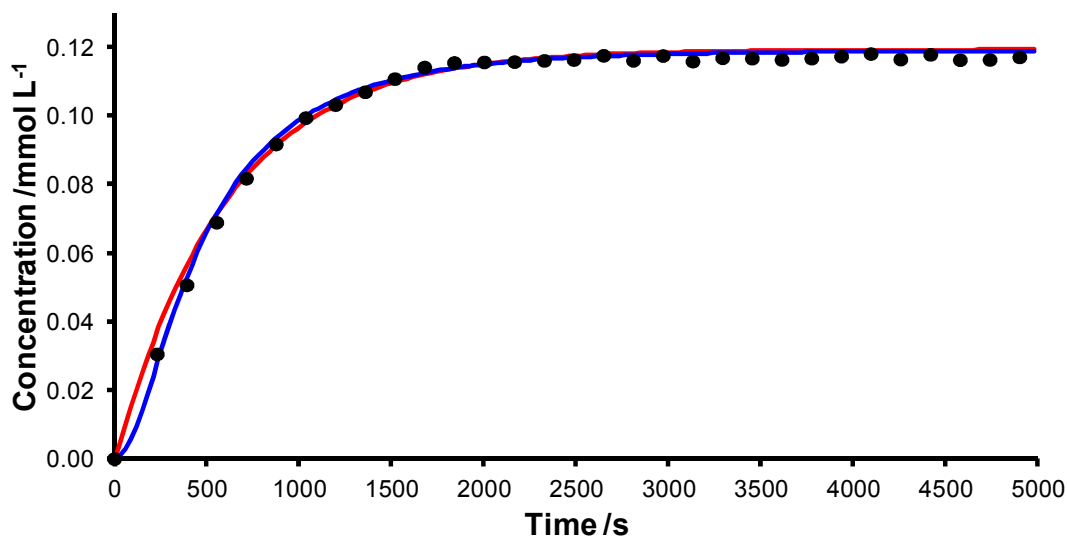


Figure 3.06. Sample fits from **Table 3.06**, where (i) $n = -2$ (**red**) and (ii) $n = -7$ (**blue**).

changed, the values of other rate constants changed in line with it and therefore the rate constants are correlated (**Figure 3.07**). The model is clearly very flexible, because all thirteen values of k_i generate good fits to the experimental concentration/time profile. Because none of the rate constants are calibrated to an experimentally-determined value, a large number of sets of rate constants will generate good fits to the experimental data.

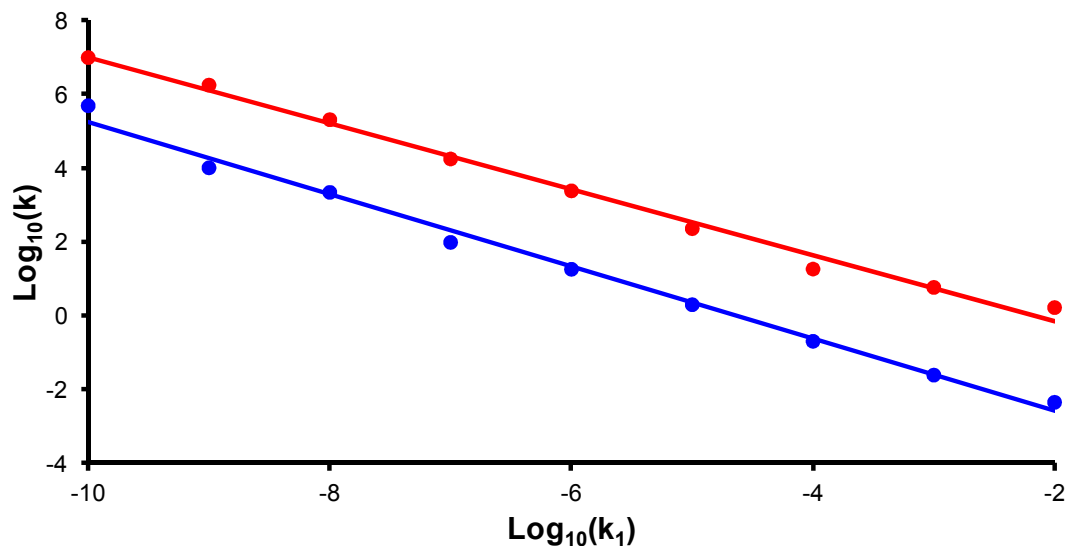


Figure 3.07. Plot of $\log_{10}(k_2)$ (**red**) and $\log_{10}(k_{-2})$ (**blue**) *versus* $\log_{10}(k_1)$ obtained from the fitting results in **Table 3.06**.

To explore if the model could be better constrained, this process was repeated with k_3 set to zero. Adjiman *et al.* reported that catalyst decomposition (to yield diruthenium hydride **41**) was negligible in DCM; no decomposition product **41** was observed in any of the RCM reactions reported here despite close inspection of the appropriate region of the 600 MHz ^1H NMR spectrum ($\delta_{\text{H}} = ca. -8$ to -9 ppm). As no **41** is detected, this decomposition process cannot occur at a significant rate in these reactions.

Good fits to the experimental concentration/time data were obtained over a slightly narrower range of values for k_i (10^n ; where n is an integer from -8 to -4 inclusive) (**Table 3.07**); rate constants were observed to be correlated strongly again, with clear relationships between k_i and each of k_{-1} , k_{-2} , and k_{-2} (**Figure 3.08**). Of particular note was K_2 (i.e. k_{-2}/k_{-2}) in each of the fits, both with k_3 free to fit and fixed to zero. The ratio was the same in each fit (**Figure 3.09**), resulting in an estimate for K_2 of 114. This occurred, despite the fact that the absolute values of k_{-2} and k_{-2} varied considerably, because this ratio is set by the relative concentrations of **102** and **122** present at the *end* of the reaction. In contrast, the absolute values of the rate constants depend on the shape of the profile to reach that end point.

It was clear from this series of fitting experiments that the model was not well constrained, and would yield a large number of local minima that are highly dependent on the initial values employed, rather than the global minimum. Relying upon rate constants obtained from unconstrained fitting of a single dataset can therefore generate misleading results, with potential consequences if these rate constants are analysed further, e.g. by applying quantitative methods to explore solvent effects.

Table 3.07. Rate constants obtained when exploring the flexibility of the model published by Adjiman *et al.*; k_1 was fixed, k_3 was fixed at zero, and other rate constants were obtained through fitting.

$\log_{10}(k_i)$	k_{-1} (L mol $^{-1}$ s $^{-1}$)	k_{-2} (L mol $^{-1}$ s $^{-1}$)	k_{-2} (L mol $^{-1}$ s $^{-1}$)	RMS ^a
-8	1.04 x 10 ⁶	2.38 x 10 ⁵	2.08 x 10 ³	0.00279605
-7	1.04 x 10 ⁵	2.38 x 10 ⁴	2.08 x 10 ²	0.00279605
-6	1.04 x 10 ⁴	2.38 x 10 ³	2.08 x 10 ¹	0.00279604
-5	1.04 x 10 ³	2.38 x 10 ²	2.08 x 10 ⁰	0.00279602
-4	1.03 x 10 ²	2.39 x 10 ¹	2.09 x 10 ⁻¹	0.00279578

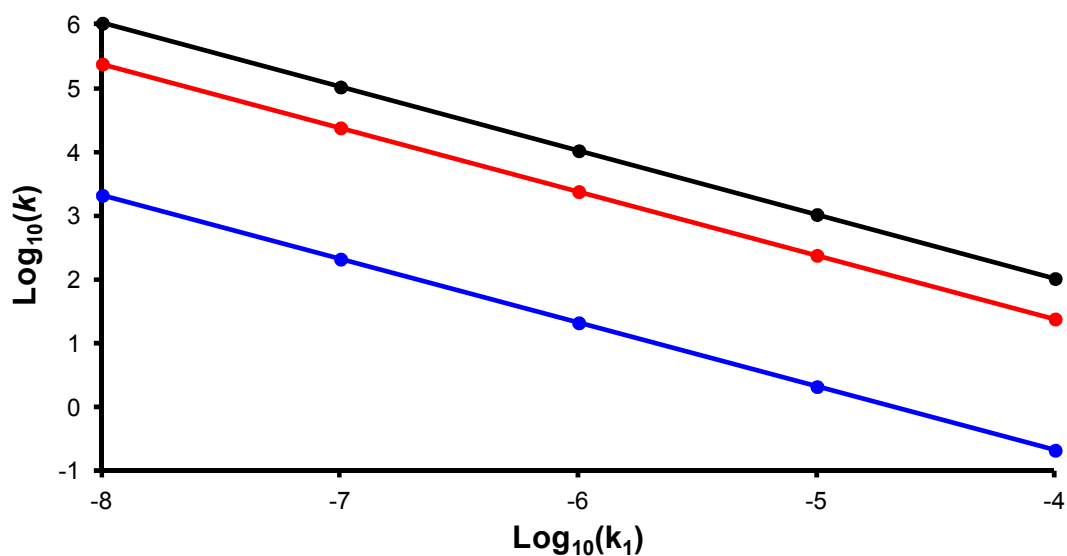


Figure 3.08. Plot of $\log_{10}(k_{.1})$ (**black**), $\log_{10}(k_{.2})$ (**red**) and $\log_{10}(k_{.3})$ (**blue**) versus $\log_{10}(k_{.1})$ obtained from the fitting results in **Table 3.07**.

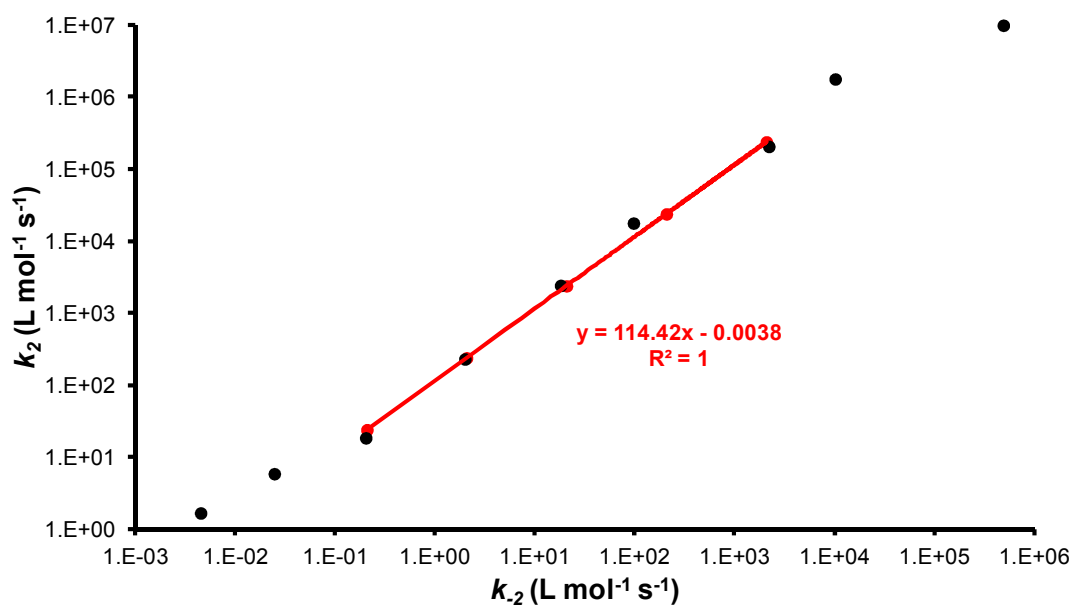


Figure 3.09. Plot of $k_{.2}$ versus $k_{.2}$ from the fitting studies with $k_{.3}$ fitted (**black**) and $k_{.3}$ fixed to zero (**red**); a logarithmic scale is presented for clarity.

Constraining the Model

Extending the Concentration Range

Attempts were made to constrain the model by fitting kinetic data obtained over a wider range of conditions, as only one set of conditions was explored by Adjiman *et al.* (0.12 mol L⁻¹ **102** with 6.7 mmol L⁻¹ **G2**). The RCM of **102** was therefore carried out with various initial concentrations of substrate (0.01 to 0.5 mol L⁻¹) and **G2** (0.1 mmol L⁻¹ to 25 mmol L⁻¹; 1 to 10 mol%) in DCM-*d*₂ (**Table 3.08**); concentration/time profiles were collected using ¹H NMR (at 400 MHz). These experiments considerably increased the chemical space explored for this simulation approach, and represent typical

Table 3.08. Conditions explored for the RCM reaction of diethyl diallylmalonate **102** with **G2**; dataset 9 was used above to assess the flexibility of the model; measured concentrations (from ¹H NMR integration *versus* a known weight of internal standard) are reported, with nominal concentrations in brackets.

Dataset	[102] (mmol L ⁻¹)	[G2] (mmol L ⁻¹)	G2 Loading (mol%)
1	505.9 (500)	25.7 (25)	5.1 (5.0)
2	491.7 (500)	12.0 (12.5)	2.4 (2.5)
3	507.0 (500)	5.2 (5.0)	1.0 (1.0)
4	404.5 (400)	14.4 (14.0)	3.6 (3.5)
5	250.7 (250)	25.9 (25)	10.3 (10.0)
6	250.5 (250)	12.7 (12.5)	5.1 (5.0)
7 ^a	121.7 (120)	6.7 (6.7)	5.5 (5.6)
8 ^a	121.8 (120)	6.7 (6.7)	5.5 (5.6)
9 ^{a, b}	119.6 (120)	6.7 (6.7)	5.6 (5.6)
10	76.1 (75)	1.2 (1.1)	1.6 (1.5)
11	50.2 (50)	5.1 (5.0)	10.1 (10.0)
12	48.2 (50)	1.2 (1.3)	2.5 (2.5)
13	9.9 (10)	0.1 (0.1)	1.0 (1.0)

^a Conditions used by Adjiman *et al.*. ^b Collected using ¹H NMR at 600 MHz

concentration regimes for five- and six-membered ring formation in the synthetic literature. The various pre-catalyst concentrations (and loadings) are important also; while the concentration at which an RCM reaction should be conducted is determined by the thermodynamic effective molarity, the *rate* at which the equilibrium position is reached depends on the pre-catalyst loading.⁹⁶ The ability to use a reaction simulation approach to quantitatively assess the effect of pre-catalyst loading on reaction rate would be very useful, in order to balance the length of time required for the reaction (which will have considerable cost implications when running reactions on scale in the plant) and the charge required of (expensive) pre-catalyst.

Concentration/time data from all thirteen reactions were imported into Berkeley Madonna and fitted to the Adjiman model. The rate constants in **Table 3.09** were obtained; these differed significantly (often by orders of magnitude) from those obtained by fitting only a single concentration/time profile (0.12 mol L⁻¹ **102**, 6.7 mmol L⁻¹ **G2**) (**Table 3.05**). Although rate constants were obtained, only some of the simulated concentration/time profiles agreed well with the corresponding experimental data (**Figure 3.10**); reactions at 0.25 mol L⁻¹ fitted well, with acceptable fits for most 0.5 mol L⁻¹ and 0.12 mol L⁻¹ reactions (simulated $t_{1/2}$ within *ca.* $\pm 20\%$ of experimental $t_{1/2}$). However, the simulations did not fit for more dilute reactions (< 75 mmol L⁻¹ **102**). The model did not deal well with describing this range of reaction concentrations, even when a wide range of initial estimates were used for the fitting routine (10^{-5} , 10^{-1} for k_1 ; 10^1 , 10^3 for k_{-1} ; 10^{-3} , 10^2 for k_2 , k_{-2} and k_3). The simplifications used to convert a complex metathesis mechanism into a less detailed model therefore appear to compromise the ability of the model to describe reactions over a large concentration range.

Table 3.09. Rate constants obtained from fitting thirteen datasets in **Table 3.08** to the model in **Scheme 3.01**.

k_1 (s ⁻¹)	k_{-1} (L mol ⁻¹ s ⁻¹)	k_2 (L mol ⁻¹ s ⁻¹)	k_{-2} (L mol ⁻¹ s ⁻¹)	k_3 (L mol ⁻¹ s ⁻¹)
1.64 x 10 ⁻⁵	243	64.1	0.890	0.567

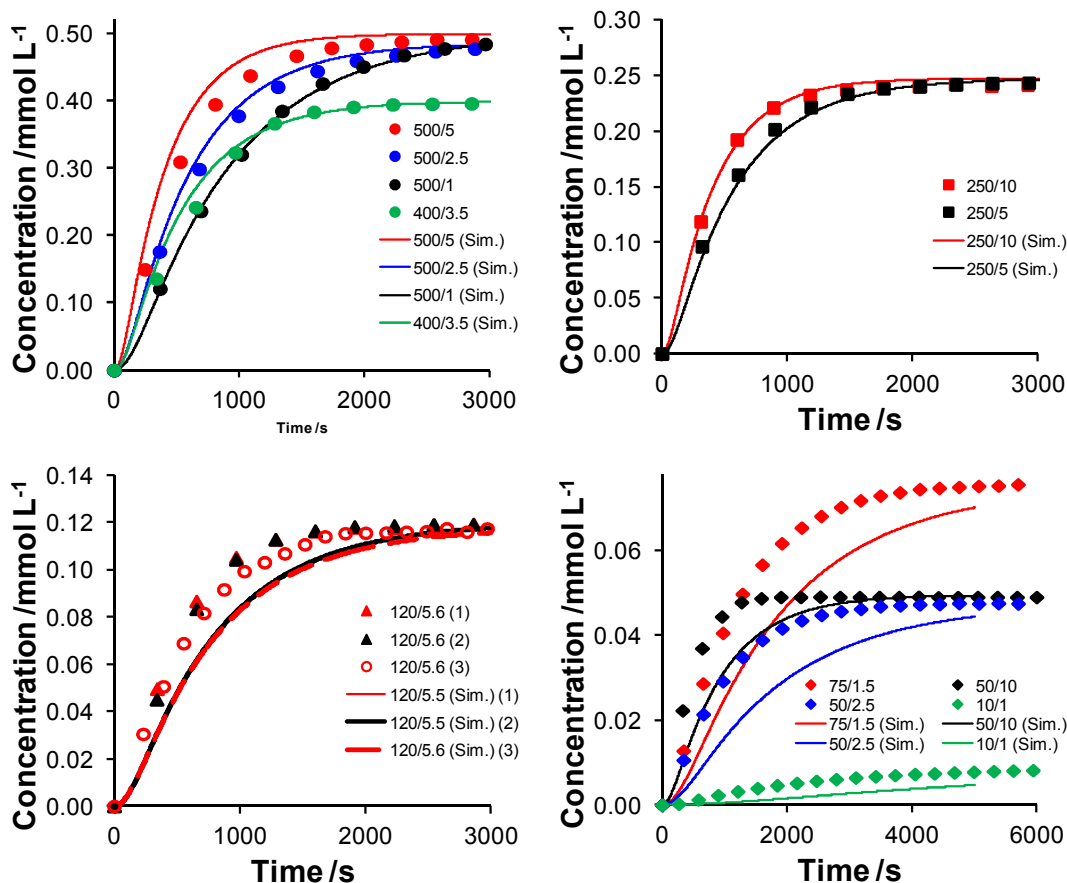


Figure 3.10. Simulated *versus* experimental concentration/time profiles for the RCM reactions in **Table 3.08**, with simulations generated using the rate constants in **Table 3.09**.

Fixing Rate Constants in the Model

Further constraint of the model was desired, reasoning that a better fit might be obtained if the absolute value of one of the rate constants was known and fixed in the fitting. The results in **Figure 3.07** and **3.08** above show that the rate constants in the model are all strongly correlated, and while some ratios (such as K_2) are constant throughout, the absolute value of rate constants such as k_2 can vary amongst the large number of good fits to the experimental concentration/time profile.

Each rate constant was considered in turn, to decide which (if any) rate constants could be obtained through experiment. Initiation rate constant k_i can be determined by measuring the rate of reaction of **G2** with ethyl vinyl ether.²⁶ The value of k_i cannot be measured directly, but Grubbs *et al.* have measured the ratio $k_{rebind}/k_{metathesis}$ at 323 K for **G1** and **G2** by measuring the initiation rate of these pre-catalysts in the

presence of added PCy₃ (**Scheme 1.04**, **Equation 1.01** and **Figure 1.03**).²⁶ The quantification of both k_{mit} ($\equiv k_1$) and $k_{rebind}/k_{metathesis}$ ($\equiv k_{-1}/k_2$) for **G1/1a** and **G2/1b** was a seminal advance in metathesis chemistry, but these values refer to the initiation rate of **G2** (the benzylidene) and the selectivity ratio of **1b**. As discussed previously, this model does not distinguish between benzylidene and methyldiene; methyldiene **3b** is effectively metathesis inactive while the selectivity of the corresponding 14e species **4b** is not known. Hypothetically, k_2 (in the model) could be obtained from the first-order treatment of RCM kinetic data in the presence of a constant and known concentration of active catalyst. However, the concentration of active catalyst is *not* constant in RCM reactions; it is in fact the *lack* of a clear kinetic order that stimulated the investigation into reaction simulation approaches initially. No diruthenium hydride species **41** was observed in these reactions (by close inspection of the high field region of the ¹H NMR spectrum), so a rate cannot be measured for the decomposition reaction (*vide supra*).

Of the rate constants in the kinetic model, k_1 best reflects the actual chemical process. This rate constant was measured experimentally and fixed to the appropriate value in subsequent fitting routines. The initiation rate of **G2** was measured in DCM-*d*₂ ([**G2**] = *ca.* 0.017 mol L⁻¹) by monitoring the reaction with ethyl vinyl ether (*ca.* 0.5 mol L⁻¹)²⁶ at 298 K by ¹H NMR spectrometry (**Figure 3.11**). A first order treatment of pre-

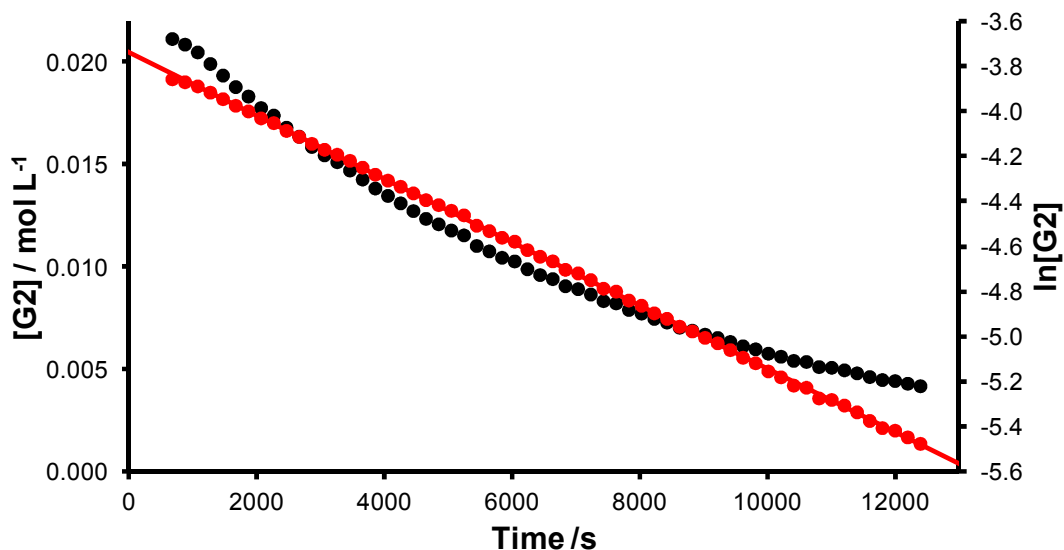


Figure 3.11. Concentration/time profile (**black**) and first order treatment (**red**) from the reaction of **G2** (0.017 mol L⁻¹) with ethyl vinyl ether (0.5 mol L⁻¹) in DCM-*d*₂ at 298 K; $k_{mit} = k_1 = 1.40 \times 10^{-4} \text{ s}^{-1}$ ($R^2 = 0.9998$).

catalyst concentration (measured by integrating the ruthenium carbene signal on the ^1H NMR spectrum *versus* 1,3,5-trimethoxybenzene as an internal standard) yielded $k_1 = 1.40 \times 10^{-4} \text{ s}^{-1}$. This rate constant was fixed in the subsequent fitting experiment to yield the rate constants in **Table 3.10** (Entry 1) when all thirteen datasets were fitted; k_3 was fixed to zero. Simulated and experimental concentration/time profiles can be found in **Figure 3.12**. Fixing k_1/k_2 to 1.25 in addition yielded the results in Entry 2, but the quality of the fit was inferior. As described above, the $k_{\text{rebind}}/k_{\text{metathesis}}$ ratio has been measured for the benzyldiene species **1b** only, so cannot be applied here. The electronic and steric demands of the methyldiene species **4b** and the benzyldiene species **1b** are likely to be different. While the rate constants from Entry 1 provide a better fit to the experimental data than those in **Table 3.09** (compare **Figures 3.10** and **3.12**), unfortunately the model still does not fit data over a wide range of conditions.

Table 3.10. Rate constants obtained from fitting all thirteen datasets in **Table 3.08** to the model in **Scheme 3.01** with (i) $k_1 = 1.4 \times 10^{-4} \text{ s}^{-1}$, $k_3 = 0$ and (ii) k_1/k_2 fixed to 1.25 in addition.

Entry	k_1 (L mol $^{-1}$ s $^{-1}$)	k_2 (L mol $^{-1}$ s $^{-1}$)	k_3 (L mol $^{-1}$ s $^{-1}$)
1	29.8	7.69	0.110
2	5.63	4.50	0.095

Possible causes of the continued discrepancy were investigated. An appropriate set of rate constants should model pre-catalyst concentration accurately, as well as substrate consumption and product formation. To investigate this, the low field region of the ^1H NMR spectrum was inspected. Two signals were observed during the course of the reaction: the pre-catalyst resonance at *ca.* 19.2 ppm¹⁰ and a second resonance at *ca.* 17.8 ppm which was assigned to phosphane-bound methyldiene **3b**.²⁶ The concentrations of these species were profiled in the RCM reaction of **102** (0.12 mol L $^{-1}$) with **G2** (5.6 mol%), showing a slow decay of pre-catalyst and a slow increase in **3b** (**Figure 3.13**). While the simulations presented by Adjiman *et al.* suggested rapid and complete initiation of **G2** (**Figure 3.02** previously), integration of the appropriate ^1H NMR resonances revealed considerable pre-catalyst concentrations and suggested that the process was in fact very slow, in agreement with the observations of Grubbs *et al.*⁴³

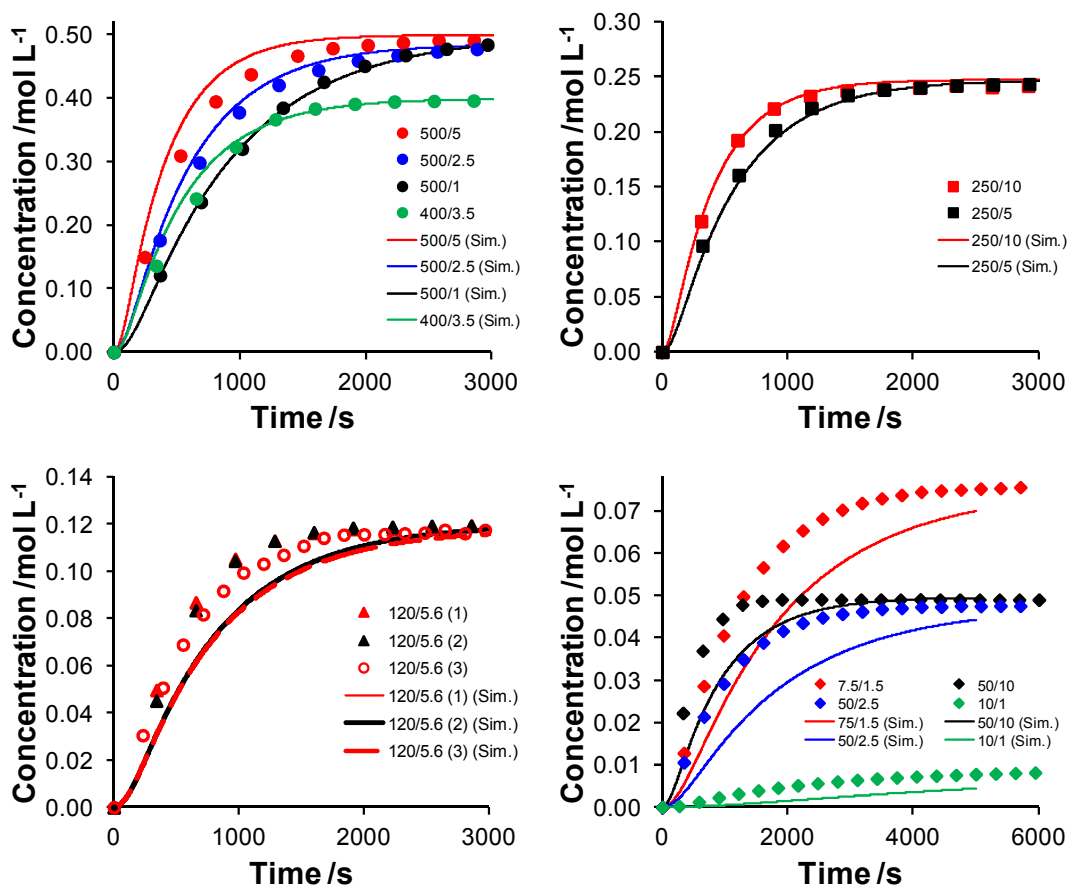


Figure 3.12. Simulated *versus* experimental concentration/time profiles for the RCM reactions in **Table 3.08**, with simulations generated using the rate constants in Entry 1 of **Table 3.10**.

The reaction of **102** (0.12 mmol L⁻¹) with **G2** (5.6 mol%) was complete before even one third of the charge of **G2** had initiated, with the remainder of the pre-catalyst charge effectively wasted. The rate constants obtained by Adjiman *et al.* (**Table 3.01**) and those obtained in this work (**Table 3.10**, Entry 1) yield quite different simulated pre-catalyst concentration/time profiles. Notably, the former set of rate constants vastly overestimated both the rate and the extent of initiation, while the latter significantly underestimated the extent of phosphane dissociation. This trend was apparent across all of the reactions studied here; a plot of simulated *versus* experimental **G2** concentrations at *ca.* 2000 s shows this trend graphically (**Figure 3.14**). Although the RCM reaction in **Figure 3.13** is complete after *ca.* 2000 s, the pre-catalyst concentration continued to decrease, despite the irreversible nature of the RCM step.⁸⁹ The possibility of pre-catalyst decomposition was considered, but the rate of this decrease throughout the

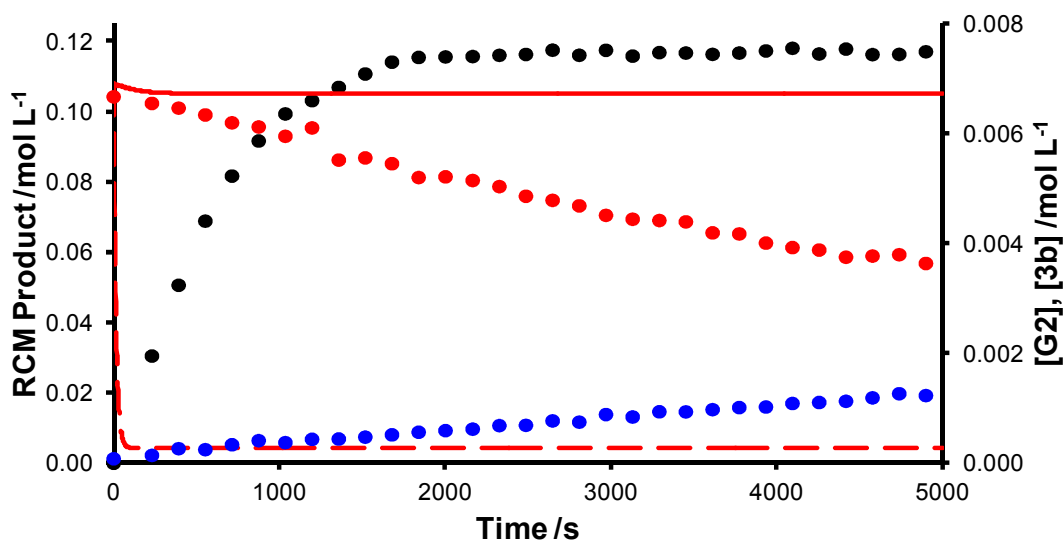


Figure 3.13. The concentration/time profiles from the RCM reaction of **102** (0.12 mol L^{-1}) with **G2** (5.6 mol%); **122** (black circles), **G2** (red circles) and **3b** (blue circles) are plotted, as well as the simulated **G2** concentrations obtained using the rate constants from Adjiman *et al.* (dashed red line) and **Table 3.10**, Entry 1 (solid red line).

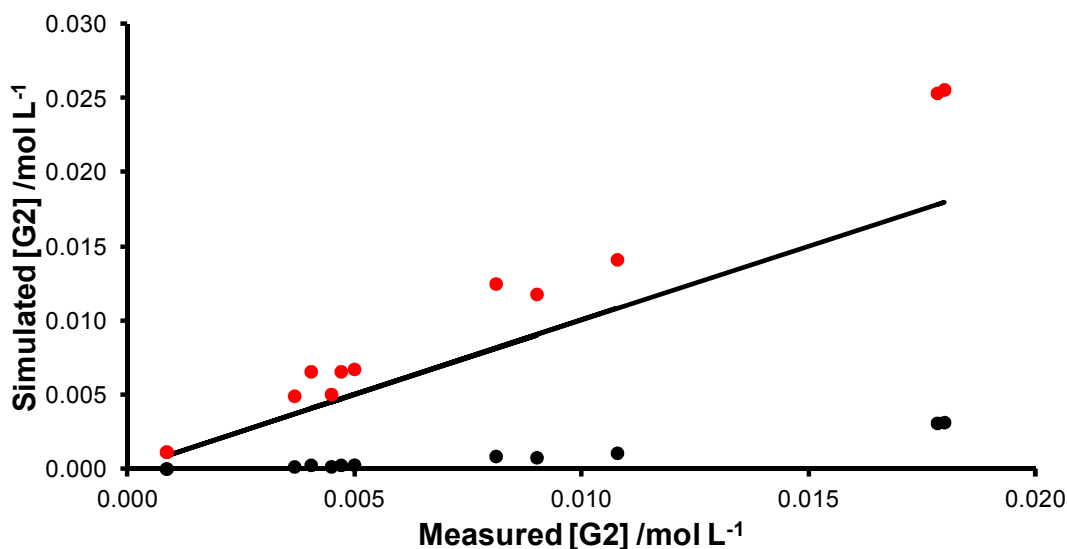


Figure 3.14. Simulated *versus* experimental concentrations of **G2** after *ca.* 2000 s in the reactions in **Table 3.08** (except Entry 13) using (i) the rate constants from by Adjiman *et al.*, **Table 3.01** (black) and (ii) the rate constants in **Table 3.10**, Entry 1 (red); the black line represents unity.

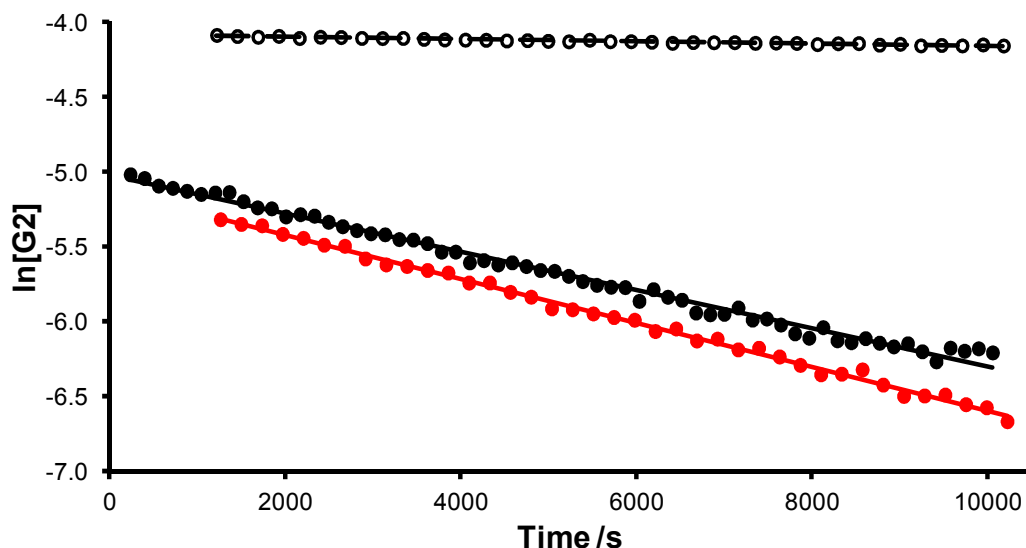


Figure 3.15. Plot of $\ln[\mathbf{G2}]$ versus time for the pre-catalyst decay in (i) the RCM of diethyl diallylmalonate (0.12 mol L^{-1}) with $\mathbf{G2}$ ($5.6 \text{ mol}\%$) (closed black circles), (ii) the reaction of ethene (26 mmol L^{-1}) with $\mathbf{G2}$ (5 mmol L^{-1}) (closed red circles) and (iii) the decomposition of 16.8 mmol L^{-1} $\mathbf{G2}$ in the absence of alkene (open black circles).

experiment ($k_{obs} = 1.28 \times 10^{-4} \text{ s}^{-1}$) was found to be almost equal to the measured initiation rate of $\mathbf{G2}$ with ethyl vinyl ether ($k_i = 1.40 \times 10^{-4} \text{ s}^{-1}$) (Figure 3.15).

At the end of the reaction, almost an equivalent of ethene (with respect to $\mathbf{102}$) was present in solution. Ethene can react with metathesis catalysts to yield (typically very low energy) MCB species,^{15,32-33,36-37} so it was proposed that it was the reaction of pre-catalyst with ethene that caused the sustained decrease in pre-catalyst concentration; i.e. the pre-catalyst is drawn through the reaction with ethene due to the irreversible formation of phosphane-bound methyldene. This hypothesis was confirmed by dissolving $\mathbf{G2}$ (*ca.* 5 mmol L^{-1}) in $\text{DCM-}d_2$ that had been sparged with ethene (to *ca.* 26 mmol L^{-1}) and monitoring the rate of pre-catalyst decay. This revealed a decay rate ($k_{obs} = 1.47 \times 10^{-4} \text{ s}^{-1}$) in agreement with the rate constants measured both with ethyl vinyl ether and with diethyl diallylmalonate (Figure 3.15 above). In addition, the rate of pre-catalyst decomposition (16.8 mmol L^{-1} $\mathbf{G2}$ in $\text{DCM-}d_2$) in the *absence* of alkene was found to be an order of magnitude less ($k_{obs} = 7.21 \times 10^{-6} \text{ s}^{-1}$) (Figure 3.15), so the decomposition of the pre-catalyst did not contribute significantly to its rate of disappearance in metathesis reactions. The data from this latter experiment was treated as first order, but the reaction was monitored only for 0.1 half-lives due to the very slow rate of $\mathbf{G2}$

initiation. While the rate constant is approximate, the data are sufficient to establish that **G2** decomposition is far slower than **G2** initiation with ethyl vinyl ether or ethene.

While the initiation rate fixed in the fitting was correct, secondary events that occur during metathesis reactions (such as formation of MCBs with ethene) were not considered in the kinetic model. In addition, because methyldene **4b** captures phosphane irreversibly, equilibrium between pre-catalyst and active catalyst is not reached; the active catalyst, if it undergoes reaction with terminal olefins, will eventually result in **4b** which does not exist in equilibrium with phosphane-bound species **3b**.

Micromath Scientist provides confidence limits for rate constants obtained through fitting,¹⁹⁴ so this software was applied to the study of three RCM reactions (Entries 3, 7 and 12 in **Table 3.08**) both separately and simultaneously, to explore the behaviour of each of the rate constants in the model. The data fitting was conducted with k_7 fixed to the experimentally-determined value of $1.4 \times 10^{-4} \text{ s}^{-1}$. As expected, different rate constants were obtained from each of the three experiments separately, with each set of rate constants yielding a good fit to the experimental concentration/time data for that dataset (**Table 3.11**, Entries 1-3). In contrast, the fitting of all three datasets simultaneously gave a fourth set of rate constants which did not agree well with the concentration/time data for any of the three experimental concentration/time profiles (**Table 3.11**, Entry 4). The 95% confidence intervals were typically very wide, and were often over 20% of the value of the rate constant itself. The confidence limits for k_3 were of particular note: in all four cases these encompassed zero, which suggested that k_3 has little or no bearing on the reaction. Such behaviour would be expected from a bimolecular reaction conducted under dilute conditions. The concentrations of active catalyst and PCy₃ in solution will be very low during most of

Table 3.11. Rate constants ($\text{L mol}^{-1} \text{ s}^{-1}$) obtained through fitting datasets 3, 7 and 12 in **Table 3.08** to the model in **Scheme 1.02** using Micromath Scientist, with k_7 fixed to $1.4 \times 10^{-4} \text{ s}^{-1}$. Uncertainties quoted are 95% confidence intervals.

Entry	Dataset(s)	k_1	k_2	k_2	k_3
1	3	23.4 ± 5.9	7.19 ± 0.525	0.0394 ± 0.0011	0.461 ± 0.501
2	7	28.8 ± 11.5	13.9 ± 1.95	0.213 ± 0.0797	$(1.42 \pm 94.1) \times 10^{-14}$
3	12	166 ± 61	35.9 ± 5.1	0.195 ± 0.118	0.0308 ± 2.3763
4	3, 7, 12	27.4 ± 14.5	7.99 ± 1.30	0.0452 ± 0.0271	0.621 ± 1.049

the RCM reaction, because **G2** initiates slowly. As previously established, detectable quantities of diruthenium hydride **41** were not obtained from these reactions; a study of this decomposition product can be found in Chapter 4.

Restricting the Concentration Range for Data Fitting

The model in its current form represents an approximation of the true metathesis mechanism, so it was of interest to find out if the model could be applied over a narrower range of concentrations and therefore applied to useful applications in metathesis chemistry. Twelve of the experiments listed in **Table 3.08** were divided into two groups based on initial diene concentration. One group contained reactions conducted with initial **102** concentrations between 0.05 and 0.12 mol L⁻¹ (inclusive) and one contained reactions conducted with initial **102** concentrations between 0.25 mol L⁻¹ and 0.5 mol L⁻¹ (inclusive); experiments within each group covered a range of pre-catalyst loadings. Each group was processed separately, with k_1 fixed in each case to 1.4 x 10⁻⁴ s⁻¹ and k_3 fixed to zero. Different rate constants were obtained from each fit: the lower concentration batch fitted with k_{-1} and k_2 larger and k_2 smaller than the higher concentration fit (**Table 3.12**). The quality of each fit was good, with simulations agreeing well with the experimental concentration/time data for reactions across the concentration and pre-catalyst loading range (**Figure 3.16**).

The value of k_1 ought to be independent of concentration, as it reflects the rate at which phosphane binds to the 14e species. However, as described above, the description of the ruthenium carbene species in the model is incorrect, and does not take into account the different reactivity of benzylidenes **1b** and **G2** compared to methyldiene species **4b** and **3b**. As **3b** is a very poor pre-catalyst, the model will overestimate the total catalytic effectiveness of the sum of the ruthenium species present in the reaction; for example, when 10% of **G2** has undergone initiation and performed turnover of diene, **4b** is rendered inactive. However, the model does not

Table 3.12. Rate constants (L mol⁻¹ s⁻¹) used to describe the RCM reaction of diethyl diallylmalonate across defined concentration ranges.

Entry	Concentration Range	k_{-1}	k_2	k_2
1	250 – 500 mmol L ⁻¹	26.6	6.90	0.103
2	50 – 120 mmol L ⁻¹	71.1	20.0	0.165

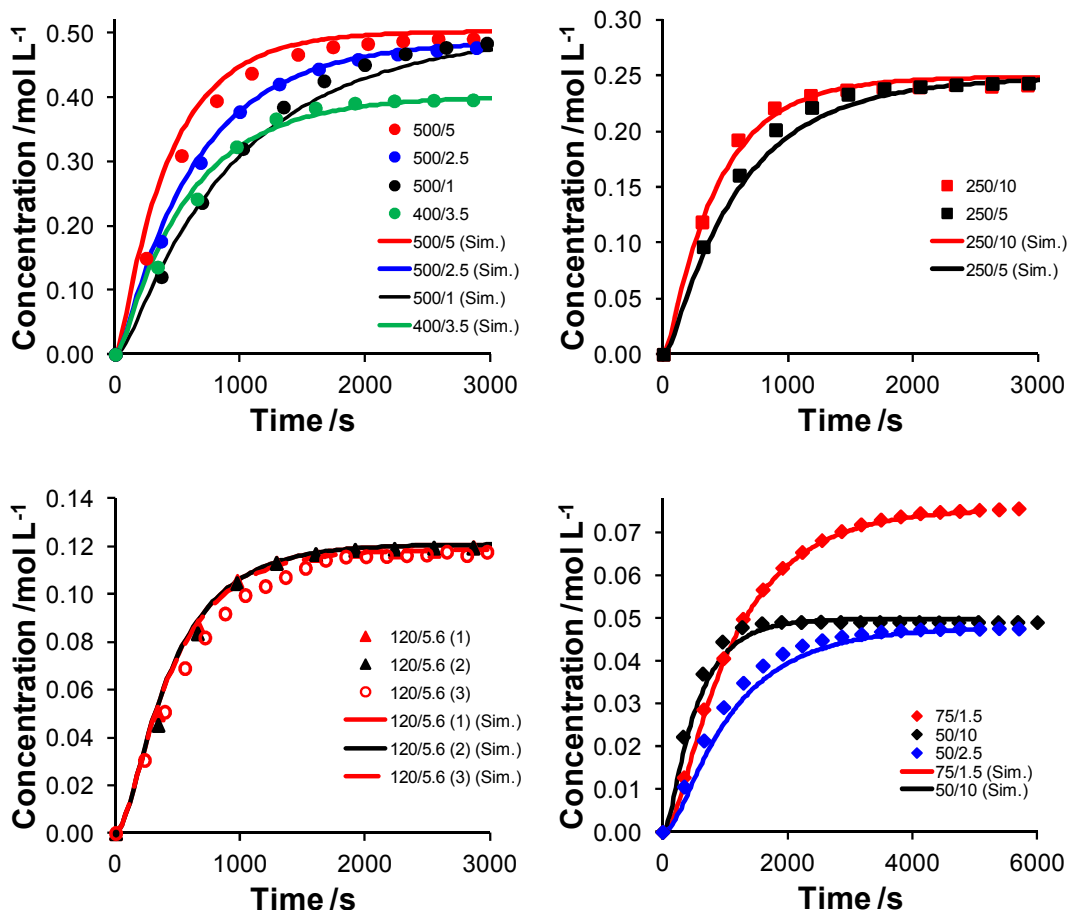


Figure 3.16. Simulated (lines) *versus* experimental (points) concentration/time profiles for the RCM reactions of diethyl diallylmalonate in **Table 3.08**, Entries 1 to 12; simulations are generated using rate constants obtained from fitting the experimental data to the model in **Scheme 3.01**, with $k_1 = 1.4 \times 10^{-4} \text{ s}^{-1}$ and $k_3 = 0 \text{ L mol}^{-1} \text{ s}^{-1}$.

differentiate between methylidene and benzylidene, overestimates the catalytic potential of the ruthenium carbene population, and increases k_1 to compensate. The model therefore believes there to be less 14e alkylidene species in solution than there is, and overestimates the activity of these species as a result. In addition, the absence of an ethene term in the model results in this concentration being embedded in the rate constant k_2 as described previously. Therefore, the effects of changing the behaviour of the phosphane rebinding were explored. The differential equations were modified to render the rebinding event irreversible (**Equation 3.08** replaced **Equation 3.01**). Rate constant k_1 was also renamed as k_3 ; the decomposition event (formerly represented by rate constant k_3) was not modelled in subsequent fitting. Fitting the thirteen datasets

(see **Table 3.08**) with initial values for each constant of 0.001 and 100 and k_f fixed to $1.4 \times 10^{-4} \text{ s}^{-1}$ gave a slightly better fit (**Figure 3.17**) and the rate constants in **Table 3.13**. While simulation of the concentration/time profile of **G2** was better (**Figure 3.18**), the model still did not fit all datasets simultaneously.

$$d[\text{G2}]/dt = -k_f \cdot [\text{G2}] \quad (3.08)$$

The values of these new rate constants do not differ significantly from those obtained with models that feature reversible phosphane dissociation. However, given the better treatment of pre-catalyst concentration with this modification, all further work was carried out with **Equation 3.08** in place of **Equation 3.01**.

Despite the inaccuracies introduced by the model due to the necessary simplification of the full metathesis mechanism, it is useful for predicting profiles for

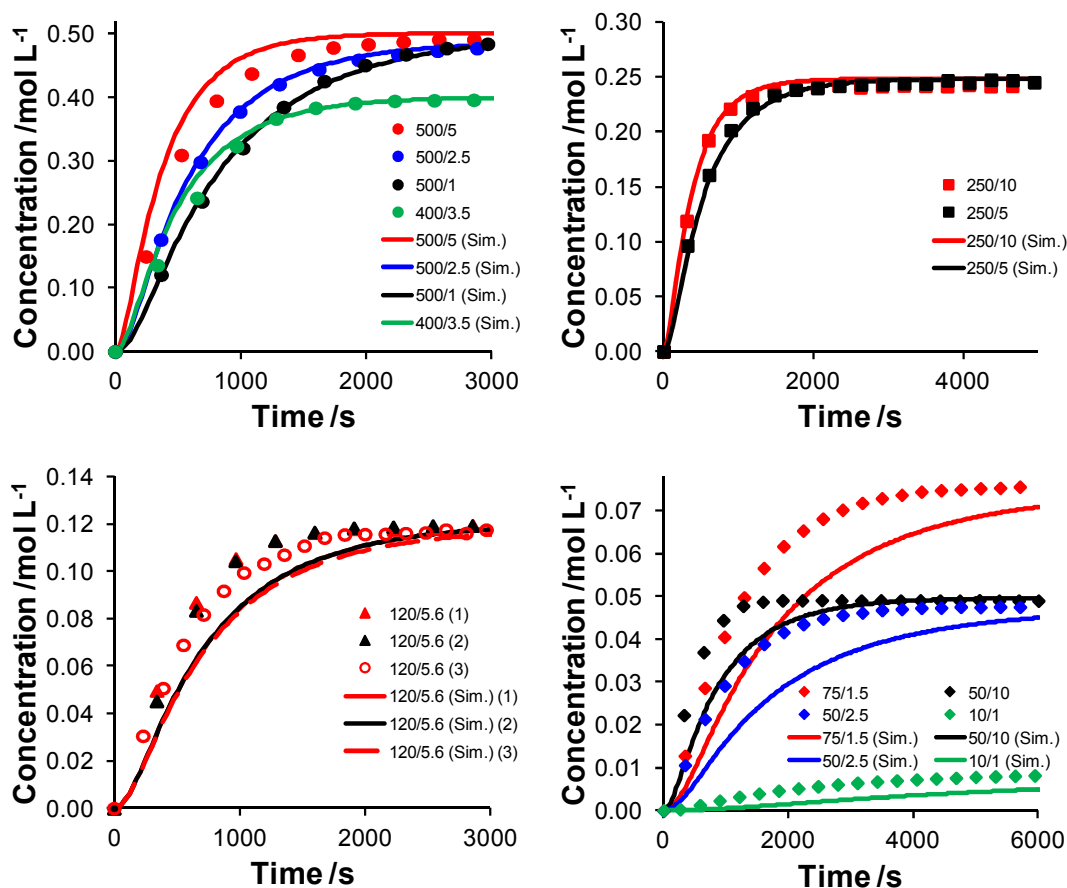


Figure 3.17. Simulated *versus* experimental concentration/time profiles for the reactions in **Table 3.08**, with simulations generated using the rate constants in **Table 3.13**.

Table 3.13. Rate constants obtained from fitting all thirteen datasets simultaneously, treating phosphane re-association as irreversible.

k_1 (s ⁻¹)	k_2 (L mol ⁻¹ s ⁻¹)	k_2 (L mol ⁻¹ s ⁻¹)	k_3 (L mol ⁻¹ s ⁻¹)
1.4×10^{-4} (fixed)	7.78	0.0788	28.0

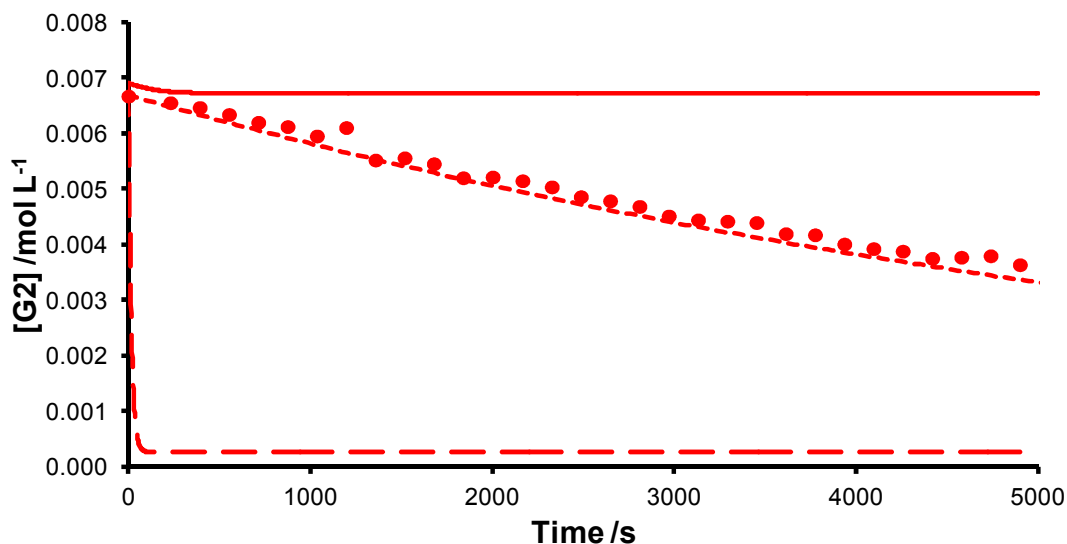


Figure 3.18. Simulated (lines) *versus* experimental (points) concentration/time profiles for **G2** in the RCM reaction of **102** (0.12 mol L⁻¹ in DCM-*d*₂ with 6.7 mmol L⁻¹ **G2**); simulations were generated using (i) the rate constants in Entry 1, **Table 3.10** (solid line), (ii) the rate constants obtained by Adjiman *et al.* (dashed line) and (iii) the rate constants in **Table 3.13** (dotted line).

reactions with a range of pre-catalyst loadings, and therefore represents a cost-effective means of identifying suitable reaction conditions for RCM. The application of this model towards assessing pre-catalysts and solvents, working around the concentration regime limitations, is therefore a potentially very valuable application of the model. Three key changes to the published model allow its applications to be explored: the fixing of k_7 to an experimentally-determined value; the removal of the decomposition event from the model; and the treatment of phosphane binding as irreversible. However, this model is limited to describing reactions that undergo RCM only, and can only describe reactions over limited concentration ranges.

Applications of the Modified Adjiman Model

Substrate Evaluation

The reaction simulation study was originally embarked upon due to the difficulty of extracting rate constants from the RCM reactions studied in Chapter 2, so the application of the modified model to the determination of relative rates for different substrates was explored. Use of the model to draw quantitative comparisons between substrates could be very useful, as it would allow the effects of different structural features to be interpreted in a detailed and rigorous manner, and aid in the optimisation of RCM reactions. Using the simple model described in this chapter, the pre-catalyst initiation can be separated from the RCM event itself. For example, Percy *et al.* have found that allylic protecting groups have a considerable effect on the reaction rate and EM,¹⁰⁸ while chemists working at Boehringer-Ingelheim identified that BOC-protection of amide functionality significantly improved the EM of the cyclisation and led to a far more cost-effective and environmentally-friendly process overall.¹¹¹ Quantitative insights often have direct application in the optimisation of synthetic metathesis reactions.

The effects of target ring size were studied in detail in Chapter 2. Attempts were made to calculate the relative rates of five- *versus* six-membered ring formation. While the concentration *versus* time profiles from kinetic experiments conducted with single and multiple dienes clearly showed a rate difference in favour of six-membered ring formation, only an approximate relative rate constant ($k_{obs}^5/k_{obs}^6 = 0.67$ (chloroform-*d*) or 0.68 (DCM-*d*₂)) could be obtained; this was extracted from a semi-quantitative first order treatment of the kinetic data (see **Table 2.03** in Chapter 2).

Substrate benchmarking was approached by fitting concentration/time data from multiple experiments simultaneously. Rate constants k_1 and k_3 are substrate independent, and should therefore be the same across reactions with different substrates; however, the necessary simplifications in the model render it applicable only over limited concentration ranges (see **Table 3.12** previously). Different k_2 and k_{-2} should be obtained for different substrates. If the reactions are carried out under similar conditions, then the pre-catalyst dependent rate constants should be identical and the relative values of k_2 should provide relative metathesis rates for each substrate.

To confirm that a large number of reactions conducted under similar conditions

can be fitted simultaneously, a series of reactions was conducted (in chloroform-*d* with 0.1 mmol L⁻¹ **G2**) with various ratios of 1,6-heptadiene to 1,7-octadiene (**Table 3.14**). Concentration/time profiles (from ¹H NMR spectra) were imported into Berkeley Madonna. The initial concentrations of each diene (typically *ca.* (9.5 ± 0.5) mmol L⁻¹ in total), measured by ¹H NMR spectroscopy before the addition of **G2**, were set in the Madonna model. The concentration and loading of **G2** was calculated from the weight of pre-catalyst that was used to make the stock solution before addition to the diene.

The initiation rate k_i of **G2** in chloroform-*d* was measured (by monitoring the reaction of **G2** with ethyl vinyl ether by ¹H NMR spectroscopy)²⁶ and revealed a rate ($k_i = 4.5 \times 10^{-5} \text{ s}^{-1}$) that was *ca.* three-fold slower than **G2** initiation in DCM-*d*₂ ($k_i = 1.4 \times 10^{-4} \text{ s}^{-1}$; *vide supra*) (**Figure 3.19**). This rate constant was fixed in all subsequent fitting of these datasets; the phosphane re-association was modelled as irreversible as before.

A simultaneous fitting experiment was carried out in Berkeley Madonna in

Table 3.14. RCM reactions conducted in chloroform-*d* to assess the suitability of the model for assessing substrate reactivity; nominal values are presented in brackets.

Entry	[103b] (mmol L ⁻¹) ^a	[103c] (mmol L ⁻¹) ^a	[G2] (mmol L ⁻¹) ^b	G2 Loading (mol%)
1	9.25 (10.0)	-	0.098 (0.10)	1.06 (1.0)
2	9.22 (10.0)	-	0.098 (0.10)	1.06 (1.0)
3	8.31 (9.0)	1.01 (1.0)	0.099 (0.10)	1.06 (1.0)
4	8.14 (9.0)	1.07 (1.0)	0.100 (0.10)	1.09 (1.0)
5	6.86 (7.5)	2.57 (2.5)	0.099 (0.10)	1.05 (1.0)
6	6.72 (7.5)	2.57 (2.5)	0.099 (0.10)	1.07 (1.0)
7	4.60 (5.0)	4.67 (5.0)	0.099 (0.10)	1.07 (1.0)
8	4.46 (5.0)	4.67 (5.0)	0.099 (0.10)	1.08 (1.0)
9	2.29 (2.5)	7.28 (7.5)	0.099 (0.10)	1.03 (1.0)
10	2.45 (2.5)	7.17 (7.5)	0.100 (0.10)	1.04 (1.0)
11	1.11 (1.0)	8.65 (9.0)	0.098 (0.10)	1.00 (1.0)
12	0.93 (1.0)	8.59 (9.0)	0.099 (0.10)	1.04 (1.0)
13	-	9.23 (10.0)	0.100 (0.10)	1.08 (1.0)
14	-	9.23 (10.0)	0.099 (0.10)	1.07 (1.0)

^a From integration of the ¹H NMR spectrum before pre-catalyst addition

^b From the mass of pre-catalyst used to prepare the stock solution

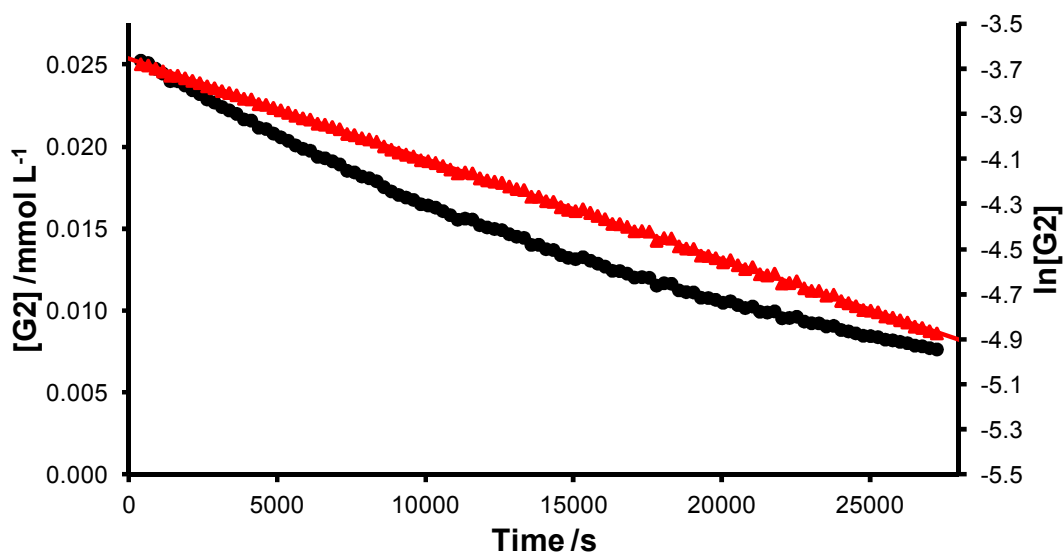
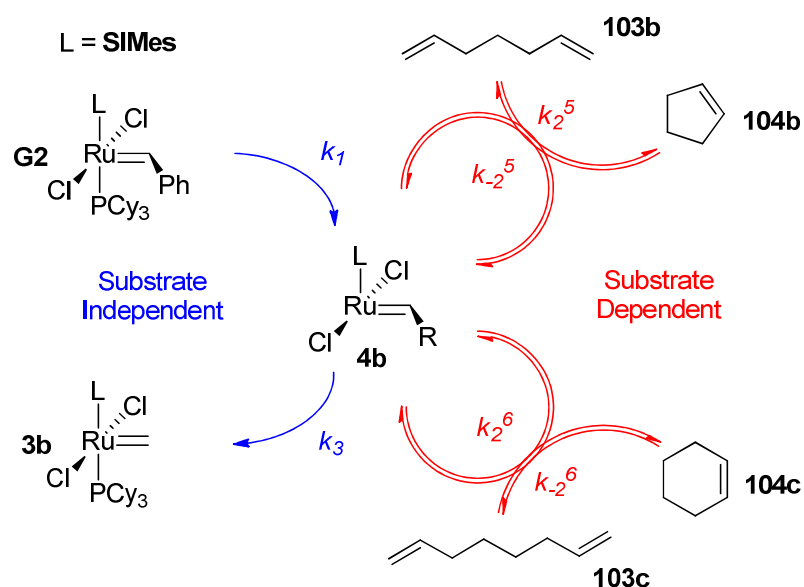


Figure 3.19. Measurement of the initiation rate of **G2** in chloroform-*d* at 298 K; the concentration/time profile (**black**) and $\ln[\mathbf{G2}]$ versus time (**red**) are presented.

which all experimental concentration/time data for dienes and cycloalkenes was fitted to the modified model. Different k_2 and k_2 rate constants were used to describe 1,6-heptadiene and 1,7-octadiene RCM reactions (referred to as k_2^5 , k_2^5 and k_2^6 , k_2^6 respectively); common values of k_1 and k_3 were used (**Scheme 3.03**). The rate constants in **Table 3.15** were obtained from fitting the concentration/time data, which yielded the fits in **Figure 3.20**. The quality of the fits was good across the range of concentrations studied, and the k_2^5/k_2^6 ratio (0.55), while close to the ratio obtained from a semi-quantitative treatment of RCM data (0.67), is a more accurate measure of the relative cyclisation rates because it was determined from multiple reactions simultaneously. Very different K_2 values were obtained for each of the substrates ($K_2^5 = ca. 10^8$, $K_2^6 = ca. 50$), most likely due to the inaccuracy of integrating very small signals; i.e. K_2 is determined by the end point of the reaction. This fitting experiment shows that substrates can be assessed using this model; the separation of pre-catalyst initiation and substrate RCM was important as the changing yet immeasurable concentration of active catalyst was

Table 3.15. Rate constants (in $\text{L mol}^{-1} \text{s}^{-1}$) obtained from simultaneous fitting of fourteen datasets, with $k_1 = 4.5 \times 10^{-5} \text{ s}^{-1}$.

k_2^5 ($\text{L mol}^{-1} \text{s}^{-1}$)	k_2^5 ($\text{L mol}^{-1} \text{s}^{-1}$)	k_2^6 ($\text{L mol}^{-1} \text{s}^{-1}$)	k_2^6 ($\text{L mol}^{-1} \text{s}^{-1}$)	k_3 ($\text{L mol}^{-1} \text{s}^{-1}$)
209	1.05×10^{-6}	380	7.65	795



Scheme 3.03

accounted for when considering the kinetics of the RCM step. If data for multiple reactions are fitted simultaneously, error due to the simplifications introduced into the model is systematic and *relative* values of k_2 can be compared. The step represented by k_2 does not have a single potential energy barrier, but represents a number of steps in the mechanism and therefore the absolute value of k_2 has limited physical meaning. However, relative values allow metathesis rates of different substrates to be compared.

The simultaneous fitting of concentration/time profiles for the RCM reactions of three different substrates was explored. Concentration/time data from kinetic studies of the RCM reactions of 1,6-heptadiene **103b**, 1,7-octadiene **103c** (each in duplicate) and diethyl diallylmalonate **102** (at 10 mmol L⁻¹ in DCM-*d*₂ at 298 K with 1 mol% **G2**) were imported into Berkeley Madonna and fitted to the model in **Scheme 3.03**. The value of k_7 was set to 1.4 x 10⁻⁴ s⁻¹. An excellent fit to the experimental concentration/time data was obtained, which described all five reactions well (**Table 3.16** and **Figure 3.21**). The rate of diethyl diallylmalonate RCM was already known to be lower than that of 1,6-heptadiene or 1,7-octadiene, presumably due to an unfavourable equilibrium for alkylidene transfer,¹⁸¹ which is in turn due to steric bulk (see the discussion in chapter 2). This fitting study allowed the quantification of relative rates for these RCM reactions (0.59:1.00:0.27 for 1,6-heptadiene:1,7-octadiene:diethyl diallylmalonate).

While this model was shown to be appropriate for the benchmarking of RCM substrates, it was important to appreciate its limitations. The model is the simplest

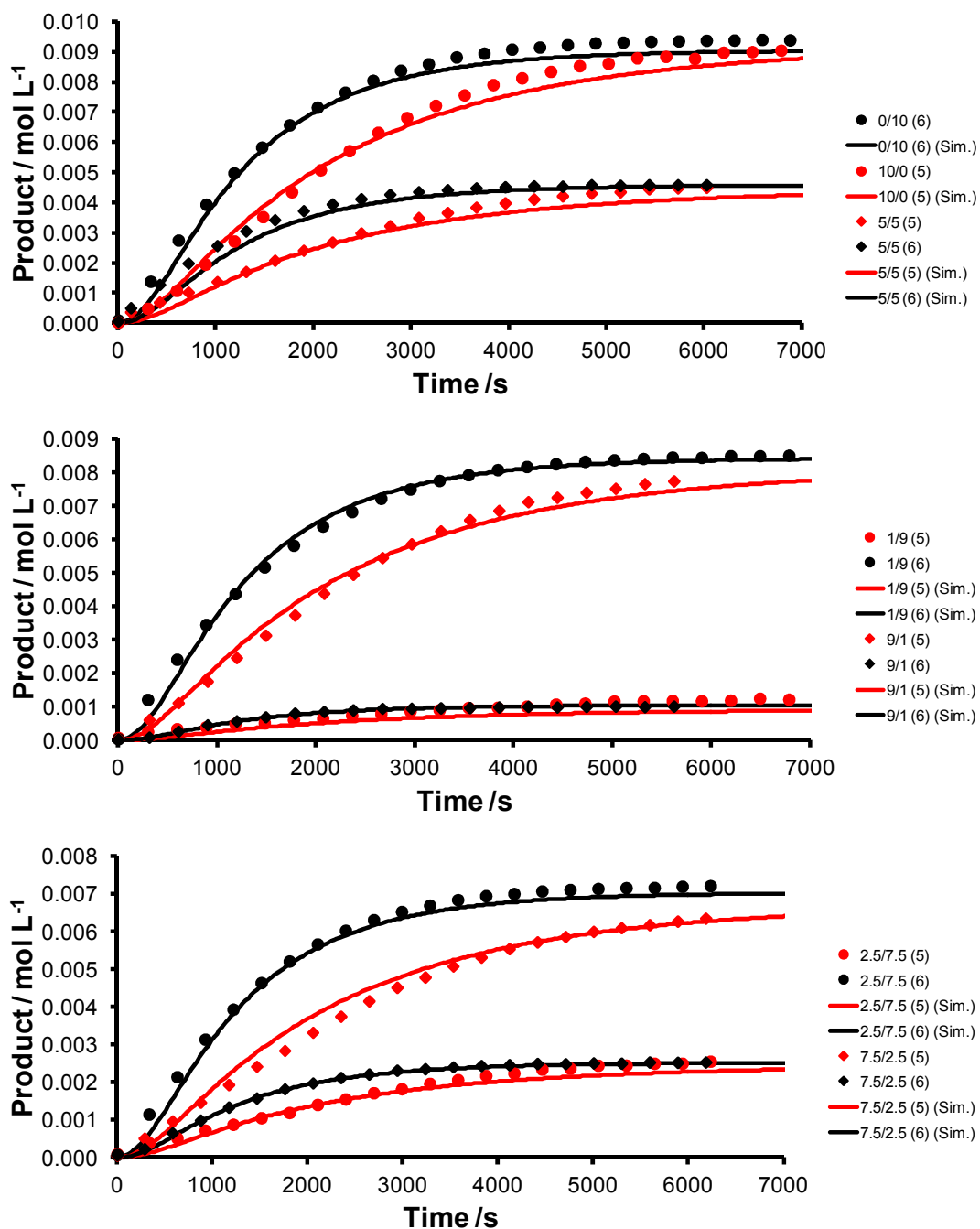


Figure 3.20. Simulated (lines) *versus* experimental (points) concentration/time profiles for the RCM reactions of 1,6-heptadiene (**red**) and 1,7-octadiene (**black**) in chloroform-*d* at 298 K. Only one reaction under each set of conditions is plotted for clarity.

possible representation of the complex mechanism for alkene ring-closing metathesis. As a result, the absolute values of almost all rate constants (except k_r) are not associated with specific single steps on the metathesis PES, and therefore do not represent barriers

Table 3.16. Rate constants obtained from the simultaneous fitting of concentration/time data for the RCM (10 mmol L⁻¹ substrate, 1 mol% **G2**, DCM-*d*₂ at 298 K) of 1,6-heptadiene, 1,7-octadiene (each in duplicate) and diethyl diallylmalonate.

Substrate	k_1 (L mol ⁻¹ s ⁻¹)	k_2 (L mol ⁻¹ s ⁻¹)	k_2 (L mol ⁻¹ s ⁻¹)	k_{rel}
Diethyl diallylmalonate		135	2.66	0.27
1,6-Heptadiene	1618	297	8.05	0.59
1,7-Octadiene		506	2.42	1.00

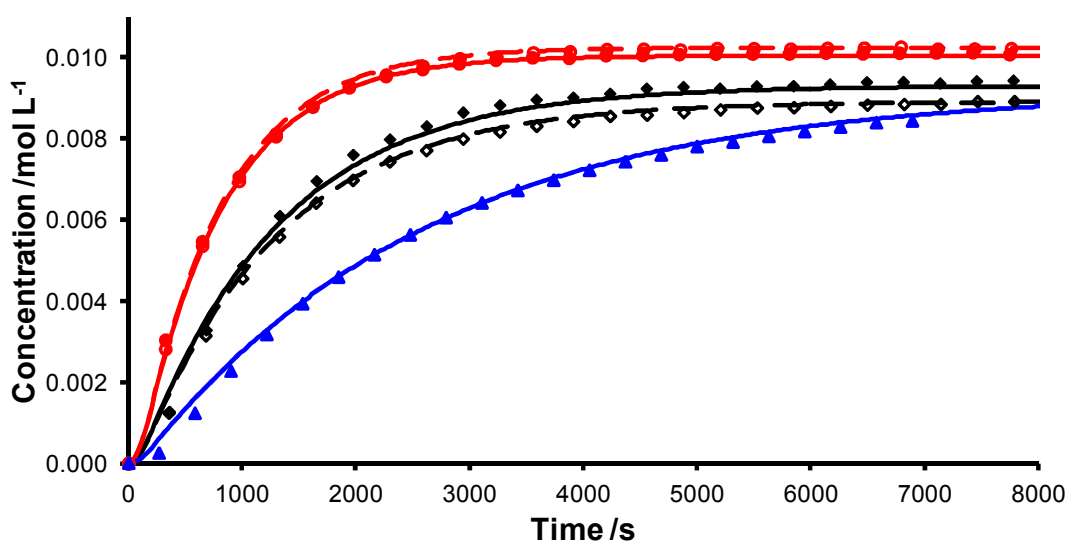


Figure 3.21. Simulated (lines) *versus* experimental (points) concentration/time data for the RCM reactions of 1,6-heptadiene (**black**) 1,7-octadiene (**red**) and diethyl diallylmalonate (**blue**) at 10 mmol L⁻¹ in DCM-*d*₂ at 298 K with 1 mol% **G2**; duplicate runs are displayed as open and closed points and solid and dashed lines.

in specific chemical processes occurring in solution. Several processes that have been documented to occur during metathesis reactions have not been accounted for, such as alkene dimerisation (or formation of trimers, tetramers and larger species),^{96,187} metallocyclobutane with ethene,³³ or non-productive catalytic cycles.⁸⁹ Therefore, this model in its current form should only be used to assess reactions over a restricted concentration range, and in which substrate smoothly cyclises to product, which limits the range of reactions to which it can be applied.

Pre-catalyst Evaluation

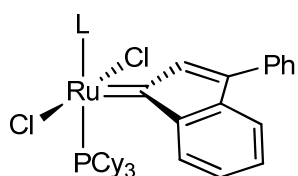
The assessment of new metathesis pre-catalysts is typically carried out by benchmarking using a series of prototypical metathesis reactions, from which concentration/time profiles are compared or single time-point yield measurements are made. The most extensive studies of this type have been carried out by Grubbs *et al.*⁴⁵ and Grela *et al.*,²⁰⁰ the former study compared (qualitatively) concentration/time profiles from a series of experiments, while the latter focussed primarily on yield measurements. Both concluded that there was not a single (pre-)catalyst that was superior overall, and that different applications require the use of different pre-catalysts. These studies only provide limited conclusions. While it can be said that, for example, **SIPr-G2** performs the RCM of **102** faster than **G2**, the *reason* for this difference is not known; this might be due to faster initiation, more active 14e species, or a combination of the two factors.

The model in **Scheme 3.03** separates pre-catalyst initiation from the RCM reaction itself, and is therefore a useful tool for evaluating the effect of pre-catalyst structural features more specifically; it can distinguish between systems where a large concentration of catalytic species is present and those where a smaller concentration of more active species results. Two series of NHC-bearing pre-catalysts were selected for this study: a series of Grubbs-type phosphane-bound complexes and a series of Hoveyda-type complexes which feature a chelating alkoxy-styrene ligand. DCM(*-d*₂) was used throughout as the reaction solvent, due to its ubiquity in metathesis chemistry.

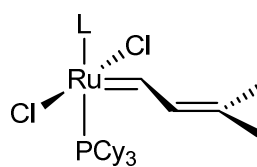
Phosphane-ligated Pre-catalysts

As discussed in the introduction, phosphane-bound pre-catalysts initiate *via* a dissociative mechanism, where the phosphane ligand dissociates from the 16e pre-catalyst to yield a 14e intermediate which then binds alkene before onward reaction;²⁶ in this sequence, the dissociation of the phosphane is the rate-limiting step.

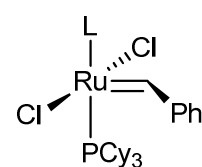
Pre-catalysts **G2**, **G2-ind**, **G2-ind-unsat**, **G2-vin** and **G2-SIPr** are known in the literature^{10,201-203} and are commercially available. The initiation rate of each pre-catalyst was measured using the method published by Grubbs *et al.*, whereby the pre-catalyst (*ca.* 10 – 15 mmol L⁻¹) was exposed to ethyl vinyl ether (0.5 mol L⁻¹) and the rate of the decrease in integral of the pre-catalyst ¹H NMR signal was monitored.²⁶ Fitting this decrease to a first-order expression (**Equation 3.09**) yielded the initiation rate. Indenylidene pre-catalysts **G2-ind** and **G2-ind-unsat** do not feature a proton α - to the



L = **SIMes G2-ind**
L = **IMes G2-ind-unsat**



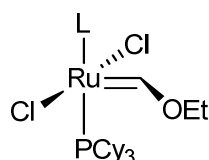
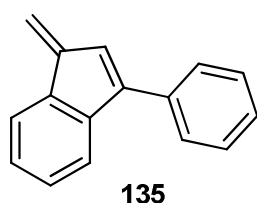
L = **SIMes G2-vin**



L = **SIPr G2-SIPr**

$$\ln[\text{pre-catalyst}] = \ln([\text{pre-catalyst}]_0) - k_t t \quad (3.09)$$

ruthenium centre, so the rate of pre-catalyst concentration decrease was measured by monitoring the ^1H NMR resonances corresponding to the free indene compound **135** and the relevant product Fischer carbene (complex **2b** or **2d**, respectively).^{44,204}



2b L = **SIMes**
2c L = **SIPr**
2d L = **IMes**

The five pre-catalysts studied feature three different NHCs and three different alkylidenes. The only structural features common to the entire set are the two chloride ligands, plus a PCy_3 ligand. The initiation rates for these pre-catalysts covered five orders of magnitude (*ca.* 10^{-7} s^{-1} to *ca.* 10^{-2} s^{-1}) (**Table 3.17**). The initiation of **SIPr-G2**

Table 3.17. Initiation rates and half-lives for pre-catalysts, determined by reaction with ethyl vinyl ether at 298 K in DCM-d_2 ; values in brackets are estimated.

Pre-catalyst	Rate k_{init} (s^{-1})	Half-life $t_{1/2}$ (h)	Approximate k_{rel} ^a
G2	$1.40 \times 10^{-4} \text{ s}^{-1}$	82.5 min	1.0
G2-vin	$1.62 \times 10^{-5} \text{ s}^{-1}$	11.9 h	1.2×10^{-1}
G2-SIPr	($> 6 \times 10^{-3} \text{ s}^{-1}$)	(< 2 min) ^b	($> 4.3 \times 10^2$)
Ind-Unsat	(< $3.2 \times 10^{-7} \text{ s}^{-1}$)	(> 600 h) ^c	(< 2.3×10^{-3})
Ind-Sat	(< $3.2 \times 10^{-6} \text{ s}^{-1}$)	(> 60 h) ^d	(< 2.3×10^{-2})

^a Relative to **G2**

^b Complete initiation in less than 10 mins

^c Achieved < 1% conversion to Fischer carbene after 12 h

^d Achieved *ca.* 10% conversion to Fischer carbene after 12 h

could not be accurately monitored using this method; the reaction was complete before the first ^1H NMR spectrum could be acquired (*ca.* 10 mins after the reaction had begun). No pre-catalyst could be detected in this first spectrum, therefore an approximate $t_{1/2}$ for initiation of less than 2 minutes (i.e. $< 3\%$ of the pre-catalyst remains) has been ascribed to this pre-catalyst, which is equivalent to an initiation rate $k_{obs} > 6 \times 10^{-3} \text{ s}^{-1}$. The Fischer carbene **2c** that resulted from this experiment had not been reported previously in the literature, so the product was characterised by multinuclear NMR spectroscopy. Characteristic chemical shifts were detected in the ^1H and ^{13}C NMR spectra (δ_{H} (DCM- d_2) = 13.90 ppm, d ($^3J_{\text{H,P}}$ = 1.0 Hz); δ_{C} (DCM- d_2) = 277.3 ppm). [^1H , ^{13}C] HSQC analysis revealed a clear correlation between the alkylidene ^1H signal and the ^{13}C NMR resonance (**Figure 3.22**). These chemical shifts were similar to those of the analogous complex **2b**, which exhibited characteristic ^1H and ^{13}C resonances at 13.63 ppm and 276.7 ppm respectively (in DCM- d_2), slightly upfield from this new species.⁴⁴

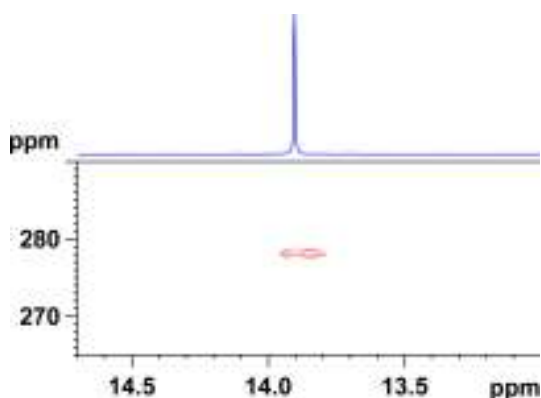


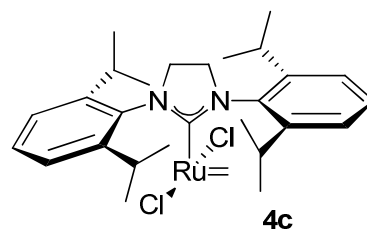
Figure 3.22. Partial [^1H , ^{13}C] HSQC spectrum of a solution of Fischer carbene **2c** in DCM- d_2 , showing a correlation between the alkylidene proton (δ_{H} (DCM- d_2) = 13.90 ppm) and the carbene carbon (δ_{C} (DCM- d_2) = 277.3 ppm).

At the opposite end of the reactivity scale, indenylidene-based pre-catalysts reacted very slowly with ethyl vinyl ether in DCM- d_2 . Very poor conversions to the corresponding Fischer carbenes **2b** and **2d** were obtained, so reliable rate constants could not be determined. Indenylidene pre-catalysts are generally employed when increased pre-catalyst stability for use at high temperatures and/or for long reaction times is required;¹²¹ initiation would occur more quickly at elevated temperatures.

The lack of precise k_i values for all but two of the pre-catalysts that were studied rendered quantitative insight into pre-catalyst performance limited. In addition, attempts to benchmark **G2-SIPr** by monitoring the metathesis of 1,7-octadiene (10 mmol L⁻¹)

with 1 mol% of pre-catalyst were unsuccessful. While the reaction of this substrate with 1 mol% of **G2** allows the collection of detailed concentration/time profiles for the smooth and complete RCM reaction that occurs,¹⁸⁷ the analogous reaction with **G2-SIPr** was complete before the first ¹H NMR spectrum could be acquired.

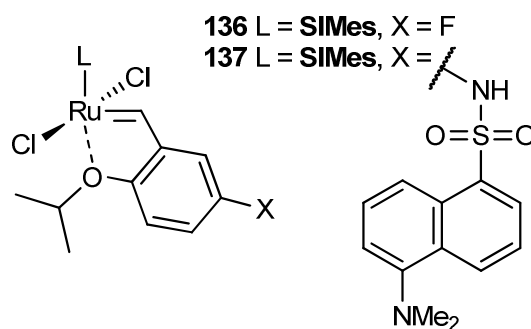
Comparisons between **G2** and **G2-SIPr** have been reported in the literature. Both pre-catalysts have been benchmarked by Ritter *et al.*, where the RCM of **102** (0.1 mol L⁻¹ in DCM-*d*₂ at 308 K with 1 mol% pre-catalyst) with **G2-SIPr** was found to occur faster than with **G2** (*t*_{1/2} = *ca.* 2.5 mins *versus ca.* 7 mins).⁴⁵ The difference was more pronounced with a more substituted substrate, diethyl allyl(methylallyl)malonate (*t*_{1/2} = < 1 min *vs.* 10 mins). In addition, Mol *et al.* have measured TON for **G2** and **G2-SIPr** in the solvent-free metathesis of 1-octene at various temperatures; **G2-SIPr** was shown to have far higher TON, particularly at temperatures below 323 K.²⁰³ While the superior performance of **G2-SIPr** in metathesis reactions may well have been due to the increased initiation rate alone, a different ruthenium carbene species (**4b** *versus* **4c**) was produced in each case, which may have considerably different metathesis activity.



Further studies, perhaps at lower temperatures or with lower pre-catalyst loadings, would be required to separate initiation rate and metathesis activity using kinetic experiments.

Alkoxy-styrene-ligated Pre-catalysts

The second of the two most popular classes of metathesis pre-catalysts are those that bear a chelating alkoxy-styrene ligand in place of a phosphane ligand; these species are typically referred to as ‘Hoveyda-type’ metathesis pre-catalysts, as the first examples were reported by



Hoveyda *et al.*¹¹⁻¹² While ethers are less Lewis basic than phosphanes and ligate metals less strongly, the chelate nature of the alkoxy-styrene ligand results in stable pre-catalysts.¹¹⁻¹² Originally, a ‘release-return’ mechanism, in which the chelating *isopropoxystyrene* ligand returns to the metal centre after the metathesis reaction is

complete, was proposed to be in operation, rendering ‘Hoveyda-type’ pre-catalysts recyclable.¹¹ However, Plenio *et al.* used fluorine-tagged and fluorescence-labelled pre-catalysts **136** and **137** to prove that the ligand did not return to the metal centre, even if the solution was concentrated or excess ligand was added.¹⁹⁰ Instances where recovery of the pre-catalyst is reported are therefore most likely due to recovery of pre-catalyst that has not reacted during short and straightforward metathesis reactions.

A variety of Hoveyda-type pre-catalysts have been reported, many of which are available commercially. In this course of work, a series of pre-catalysts (**GH2**, **Grela**, **Zhan1B**, **M7₁-SIMes**, **GH2-SIPr**, **Grela-SIPr**, **M7₁-SIPr**, **M8₃₂-SIPr**, **M8₃₃-SIPr**) were studied; initiation rates were measured and the kinetic model was used to quantify the metathesis activity of active catalyst species **3** bearing each NHC.

Attempts to obtain initiation rate data for the first generation pre-catalyst **GH1** were discontinued after UV/visible spectroscopy kinetic experiments revealed that initiation with ethyl vinyl ether (0.1 mol L⁻¹) at 293 K resulted in a measured $t_{1/2}$ of 15 hours. A first order treatment of the absorbance *versus* time data yielded $k_{obs} = 1.29 \times 10^{-5} \text{ s}^{-1}$ (**Figure 3.23**). This result may go some way to explaining the postulated ‘release-return’ mechanism¹¹ for Hoveyda-type pre-catalysts and is consistent with the results of Plenio *et al.*,¹⁹⁰ the particularly slow initiation rate of the pre-catalyst may have led to the isolation of *unreacted* pre-catalyst rather than *re-formed* pre-catalyst.

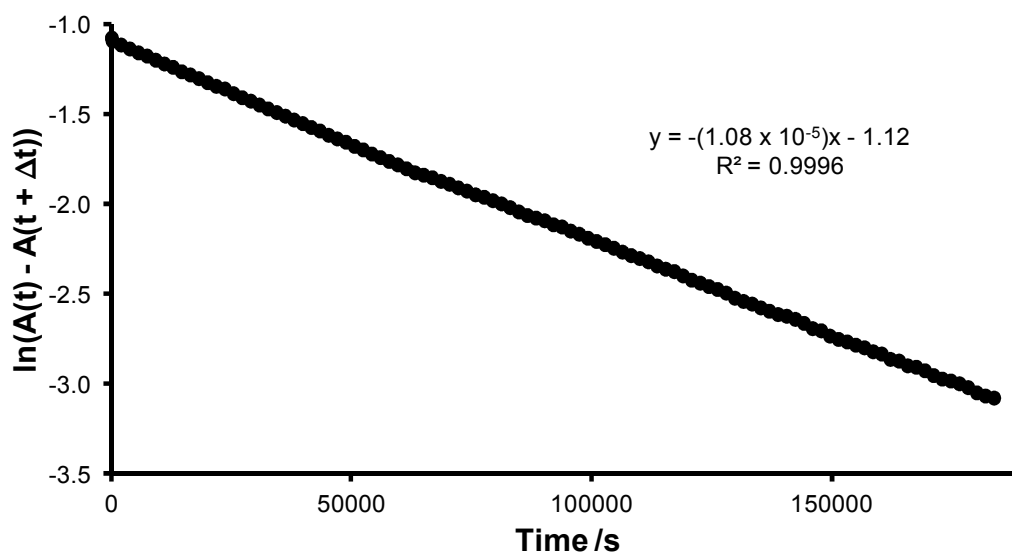
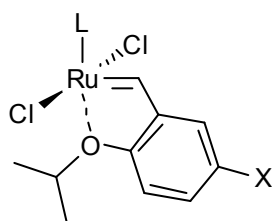


Figure 3.23. First-order treatment of data for the initiation of **GH1** (0.1 mmol L⁻¹) with ethyl vinyl ether (0.1 mol L⁻¹) at 293 K in DCM.



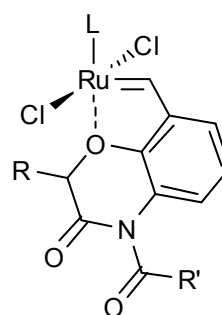
Zhan1B L = **SIMes**, X = SO₂NMe₂

M7₁-SIMes L = **SIMes**, X = NHC(O)CF₃

GH2-SIPr L = **SIPr**, X = H

Grela-SIPr L = **SIPr**, X = NO₂

M7₁-SIPr L = **SIPr**, X = SO₂NMe₂

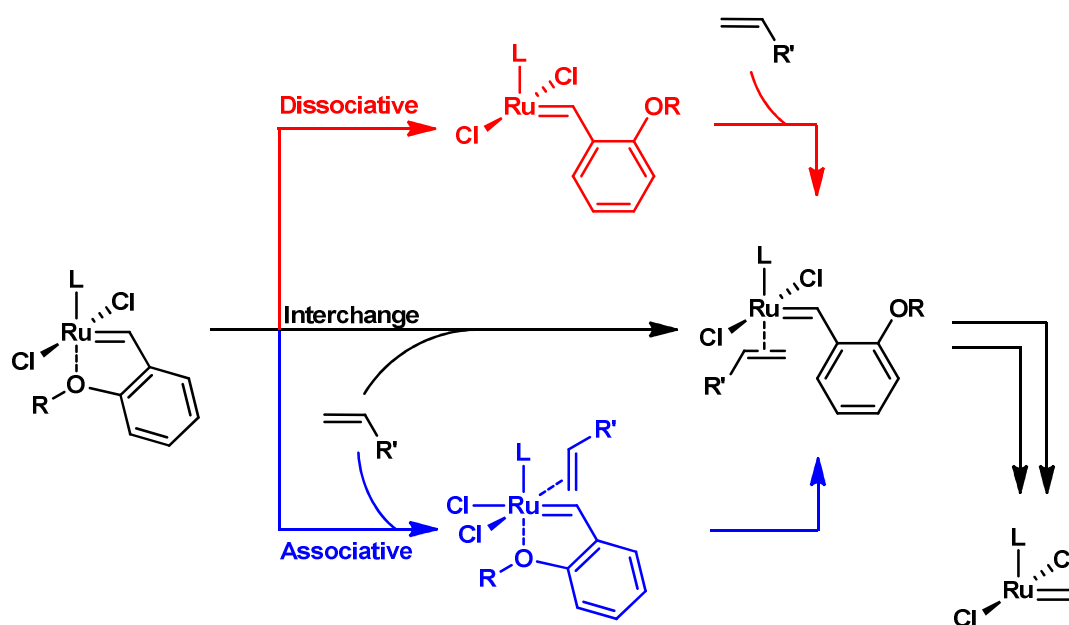


M8₃₂-SIPr L = **SIPr**, R = Et, R' = O^tBu

M8₅₃-SIPr L = **SIPr**, R = ⁱPr, R' = C₆F₅

Mechanistic Insights into the Initiation of Alkoxy-styrene-ligated Pre-catalysts

An understanding of the initiation mechanism of these Hoveyda-type pre-catalysts is necessary in order to be able to model the event correctly using reaction simulation approaches. Three potential mechanisms for the initiation step can be envisioned (**Scheme 3.04**): an associative mechanism, in which alkene associates to the pre-catalyst to yield a six-co-ordinate intermediate; a dissociative mechanism, analogous to the mechanism of **G2** initiation, in which the ether ligand dissociates before alkene coordination; and an interchange mechanism in which alkene binding and ether de-binding occur in the same step, *via* a transition state in which the alkene is incoming and the oxygen-ruthenium bond is elongated. In all three mechanisms, an intermediate η^2 -



Scheme 3.04

complex is formed *en route* to the methyldiene complex **4**, which is common to all pre-catalysts bearing that NHC ligand.

Hoveyda-type pre-catalysts were initially believed to initiate *via* a dissociative mechanism, analogous to that for phosphane-bearing pre-catalysts.⁵⁸ Activation parameters were obtained by Grubbs *et al.* for the reaction of **GH2** with ethyl vinyl ether in toluene ($\Delta H^\ddagger = 19.9 \pm 0.5 \text{ kcal mol}^{-1}$, $\Delta S^\ddagger = 1 \pm 2 \text{ cal K}^{-1} \text{ mol}^{-1}$, $\Delta G^\ddagger (298 \text{ K}) = 19.6 \pm 0.5 \text{ kcal mol}^{-1}$) which were consistent with a dissociative mechanism for pre-catalyst initiation. However, later work from the Grubbs group suggested that the entropy of activation for some Hoveyda-type pre-catalysts was in fact quite large and negative, with a different set of activation parameters measured for the reaction of butyl vinyl ether with **GH2** (in either benzene-*d*₆ or toluene-*d*₈; the literature is unclear) ($\Delta H^\ddagger = 15.2 \pm 0.8 \text{ kcal mol}^{-1}$, $\Delta S^\ddagger = -19 \pm 3 \text{ cal K}^{-1} \text{ mol}^{-1}$, $\Delta G^\ddagger (298 \text{ K}) = 20.69 \pm 0.02 \text{ kcal mol}^{-1}$).⁵⁹ No detailed mechanistic analysis was presented, but these parameters are consistent with a loss of the translational and rotational entropy of approximately one molecule,²⁰⁵ so could indicate either an associative or an interchange mechanism.

Recent studies by Plenio *et al.* using pre-catalysts **GH2** and **Grela** have shown that the rate of pre-catalyst initiation is dependent on the identity and concentration of the alkene present in solution (**Figure 3.24**).⁶⁰ These results were proposed to be inconsistent with a dissociative mechanism, where the alkene identity or concentration should not affect the rate of initiation; the barrier to alkene association to a 14e ruthenium carbene species is known to be negligible,⁵⁶ so the ether dissociation event would be expected to be rate determining. Due to the sterically crowded environment around the metal centre, an associative mechanism was ruled out, and an interchange mechanism was proposed instead. In isolation, a rate of initiation that was dependent on alkene concentration and identity would be consistent with a dissociative mechanism in which dissociation and reassociation of the ether ligand was very fast, followed by rate determining reaction of the 14e species with alkene. If such a mechanism was in operation, the ether dissociation ought to become rate determining at low alkene concentrations. Further investigations into the different possibilities were necessary.

This influences the way in which the pre-catalyst initiation event must be modelled using reaction simulation software, as the substrate concentration must be included in the expression. While the initiation rate does depend on the substrate structure, a measured rate constant for initiation will at the very least allow some

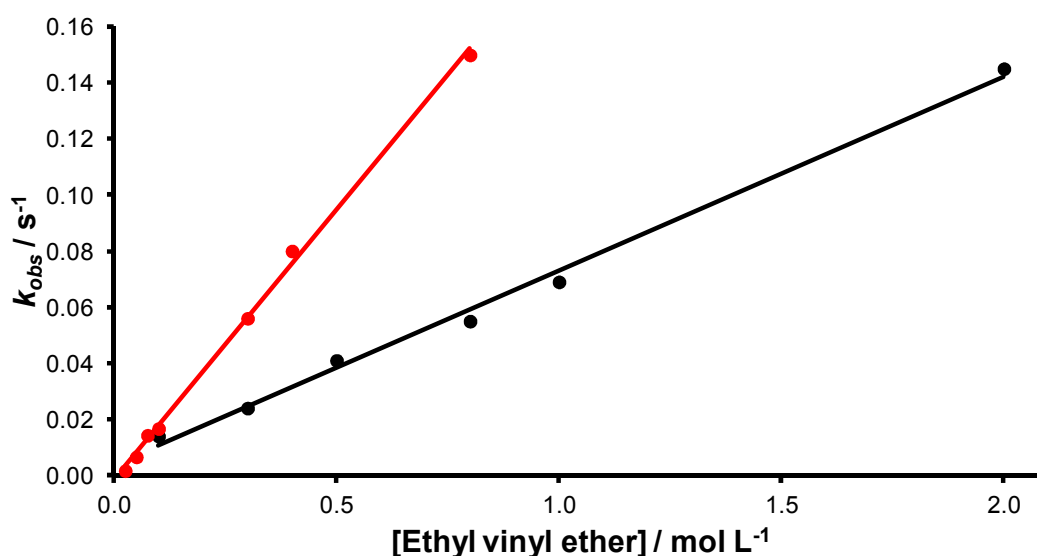
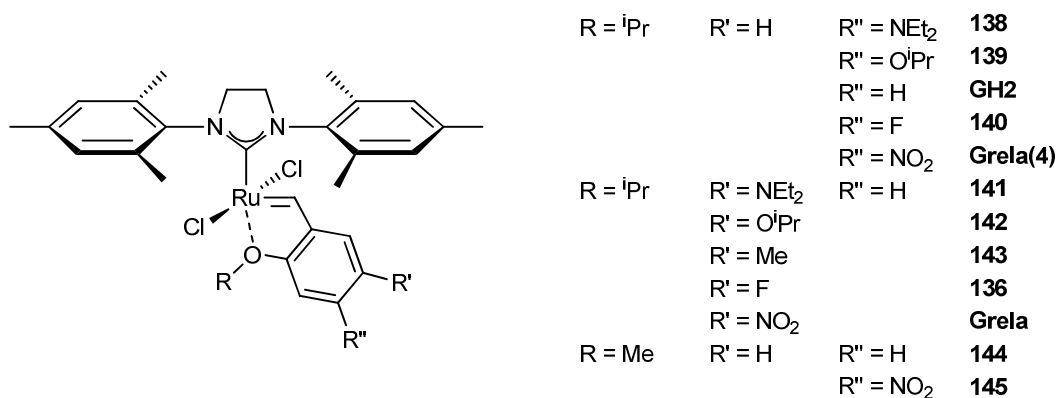


Figure 3.24. Initiation rate at 40°C in toluene *versus* ethyl vinyl ether concentration for pre-catalysts **GH2** ($k_{init} = 0.0691 \text{ L mol}^{-1} \text{ s}^{-1}$, **black**) and **Grela** ($k_{init} = 0.192 \text{ L mol}^{-1} \text{ s}^{-1}$, **red**), determined by Plenio *et al.*⁶⁰

constraint in the fitting routine.

A subsequent and detailed study by Plenio *et al.* has since been published, in which a large number of pre-catalysts (**GH2**, **Grela**, **Grela(4)**, **136** and **138-145**) were prepared and studied.⁶¹ Cyclic voltammetry experiments were used to quantify the oxidation potentials of these species, showing that the substitution pattern of the alkoxy-styrene ligand had an effect on the electron density at the metal centre. This effect was communicated *via* the ruthenium carbene moiety, as shown by a good Hammett correlation when the carbene moiety was connected to the *ipso*-carbon of the aromatic ring and a poor Hammett correlation when the alkoxy-substituent was connected to the



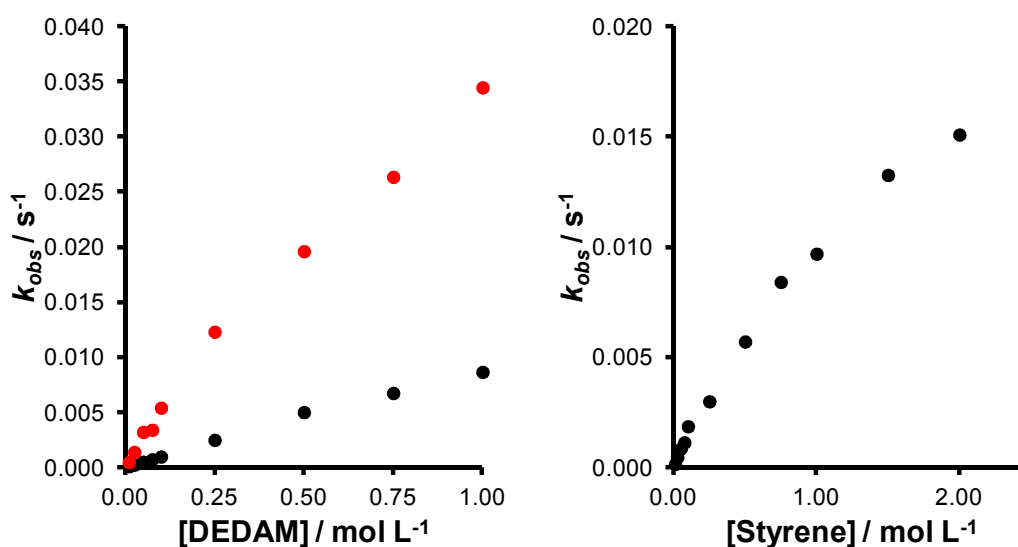


Figure 3.25. Rate constants k_{obs} for the reaction of **GH2** (black) and **Grela** (red) with (a) diethyl diallylmalonate **102** and (b) styrene in toluene at 303 K.⁶¹

ipso-carbon. Plots of k_{obs} versus [alkene] exhibited a curve (**Figure 3.25**), attributed to a contribution from a (substrate-independent) dissociative pathway and a contribution from a (substrate and substrate concentration-dependent) interchange pathway. Diverse behaviour was exhibited by each pre-catalyst and with different substrates; initiation rates for pre-catalysts with electron-withdrawing substituents were insensitive to changes in substrate, while substrate structure was found to alter the relative contributions to the initiation rate from the dissociative and interchange pathways.

Before embarking on a study of Hoveyda-type pre-catalysts, investigations were conducted in order to decide how the pre-catalyst initiation event should be modelled using the reaction simulation approach. Most kinetic data acquired during the studies documented in this thesis were collected at 298 K in chlorinated solvents such as chloroform and DCM, while Plenio *et al.* favoured toluene (at 303 K or 313 K) for their studies, presumably due to the wider practical temperature range available.

Our investigations had two key aims. Firstly, it was important to identify if a linear relationship between k_{obs} for pre-catalyst initiation and [alkene] was obtained. Secondly, activation parameters for the initiation reaction of **GH2** and analogues were desired, to enable comparison with activation parameters derived from DFT calculations. Only the dissociative pathway for the initiation of Hoveyda-type pre-catalysts has been investigated using DFT methods (at the B3LYP/6-311G* level of

theory)²⁰⁶ so a DFT treatment of all three possible mechanisms would contribute a great deal to our understanding of the initiation event; detailed understanding may inform future pre-catalyst design.

UV/visible spectroscopy was used to monitor the reaction of **GH2** (0.1 mmol L⁻¹) with freshly distilled ethyl vinyl ether in dry DCM (obtained from the in-house solvent purification system). Reactions were conducted over a range of ethyl vinyl ether concentrations (25 – 200 mmol L⁻¹) at 298 K, during the course of which solutions turned from lime green to a deep red colour. Spectra were acquired at each time point, showing the decrease of the pre-catalyst signal ($\lambda_{\text{max}} = 375$ nm) and the appearance of a weak and broad signal at *ca.* 500 nm (in agreement with the results of Plenio *et al.*) (**Figure 3.26**).⁶⁰ Clear isosbestic points were observed in each reaction, indicating a smooth reaction of **GH2** to another, single, species. The decrease of the signal at 375 nm was monitored and found to decrease at a rate that was dependent on the ethyl vinyl ether concentration (**Figure 3.27**).

Rate constants were sought from this data so a Guggenheim approach was used, as the initial ($A(t_0)$) and final ($A(t_\infty)$) absorbances were not known. This approach can be derived as follows. The absorbances at times t and $(t + \Delta t)$ minus the absorbance at infinite time can be expressed as in **Equations 3.10** and **3.11**. The difference between these expressions yields the difference between the absorbances at times t and $(t + \Delta t)$ (**Equation 3.12**); taking the natural log of each side of the expression yields an expression that is linear in time (**Equation 3.13**).

$$A(t) - A(t_\infty) = (A(t_0) - A(t_\infty)) \cdot e^{-kt} \quad (3.10)$$

$$\begin{aligned} A(t + \Delta t) - A(t_\infty) &= (A(t_0) - A(t_\infty)) \cdot e^{-k(t + \Delta t)} \\ &= (A(t_0) - A(t_\infty)) \cdot (e^{-kt} \cdot e^{-k\Delta t}) \end{aligned} \quad (3.11)$$

$$\begin{aligned} (A(t) - A(t + \Delta t)) &= (A(t_0) - A(t_\infty)) \cdot [e^{-kt} \cdot e^{-k\Delta t} - e^{-kt}] \\ &= (A(t_0) - A(t_\infty)) \cdot [e^{-k\Delta t} - 1] \cdot e^{-kt} \end{aligned} \quad (3.12)$$

$$\ln(A(t) - A(t + \Delta t)) = \ln\{(A(t_0) - A(t_\infty)) \cdot [e^{-k\Delta t} - 1]\} - kt \quad (3.13)$$

Instead of plotting the natural log of absorbance *versus* time, the absorbance at a subsequent time point $A(t + \Delta t)$ is subtracted from the absorbance at each time point $A(t)$ first. Treatment of data from each experiment in this way showed that good first-order kinetic behaviour was exhibited by each reaction (**Figure 3.28**). Each experiment

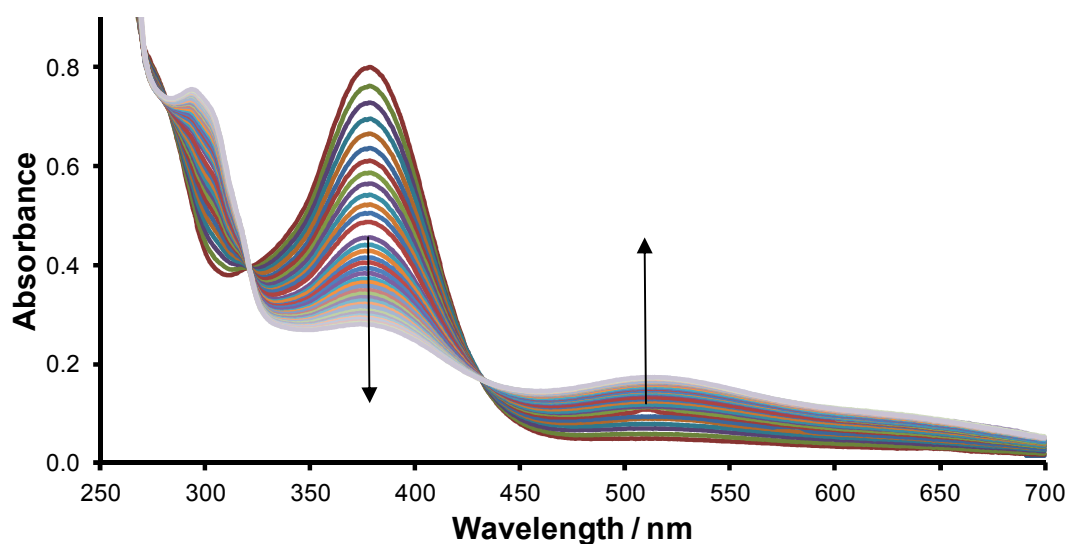


Figure 3.26. Sample UV/visible spectra from the reaction of **GH2** (0.1 mmol L^{-1}) with ethyl vinyl ether (200 mmol L^{-1}) in DCM at 298 K.

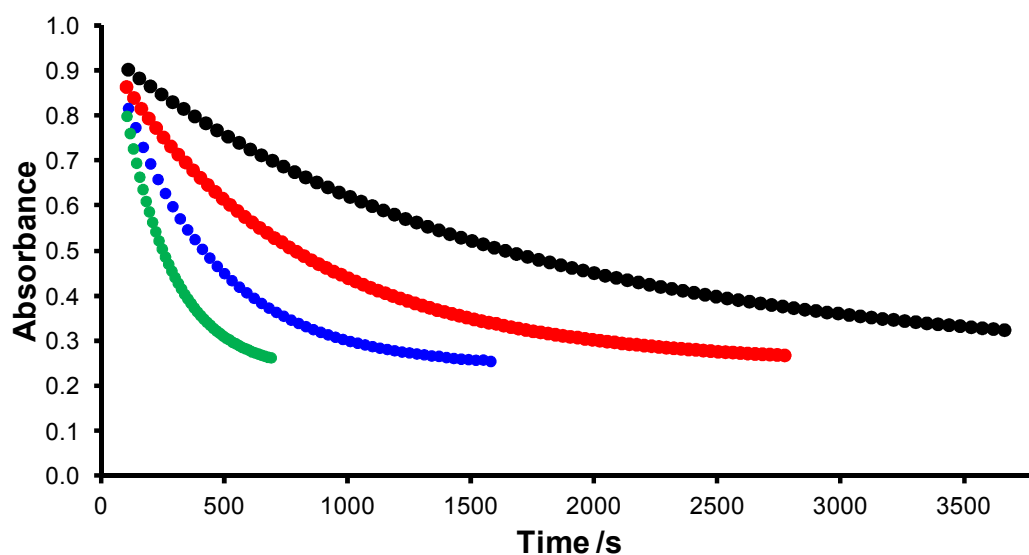


Figure 3.27. Absorbance *versus* time profiles for the reactions in DCM at 298 K of **GH2** (0.1 mmol L^{-1}) with ethyl vinyl ether at (i) 25 mmol L^{-1} (**black**), (ii) 50 mmol L^{-1} (**red**), (iii) 100 mmol L^{-1} (**blue**) and (iv) 200 mmol L^{-1} (**green**).

was conducted in triplicate or quadruplicate to ensure that the results were reproducible, with different ethyl vinyl ether and pre-catalyst stock solutions used each time. The second order rate constant for the initiation reaction ($k_{init} = 0.0264 \text{ L mol}^{-1} \text{ s}^{-1}$) was determined by plotting the rate constants k_{obs} obtained from the reactions at each ethyl vinyl ether concentration *versus* ethyl vinyl ether concentration (**Figure 3.29**). The best-

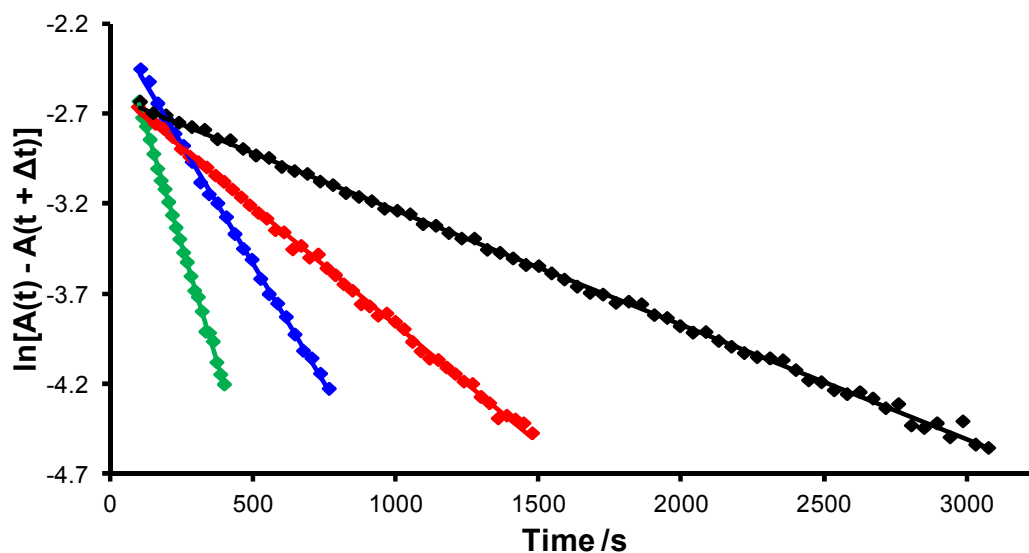


Figure 3.28. First-order treatment of the absorbance *versus* time data in **Figure 3.27** using the Guggenheim approach for the reactions with (i) 25 mmol L⁻¹ (**black**), (ii) 50 mmol L⁻¹ (**red**), (iii) 100 mmol L⁻¹ (**blue**) and (iv) 200 mmol L⁻¹ (**green**).

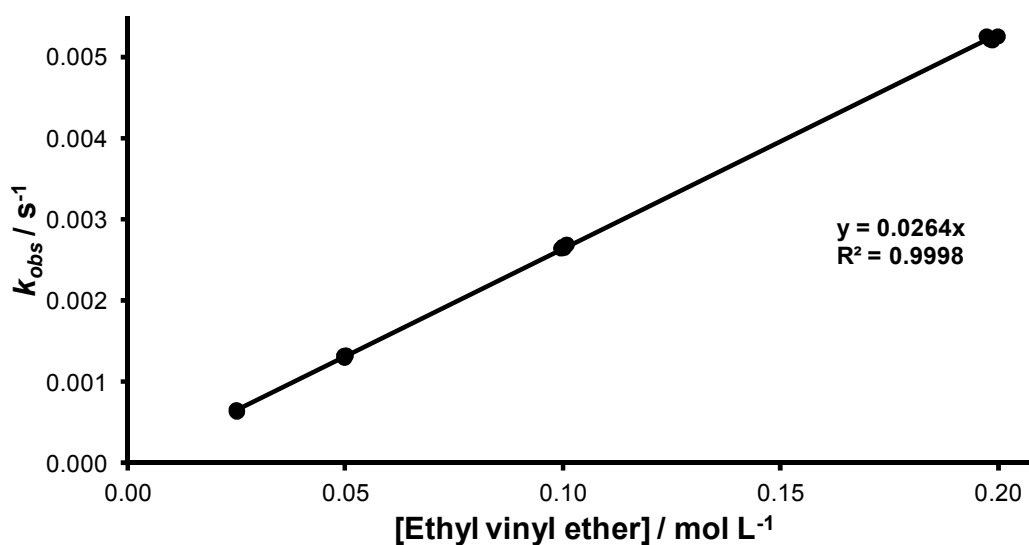


Figure 3.29. Derivation of a second order rate constant for the reaction of **GH2** with ethyl vinyl ether (in triplicate or quadruplicate).

fit straight line was forced through zero, as no reaction would be expected at zero ethyl vinyl ether concentration, yielding an excellent straight line fit that intersected each point. The curved plots reported by Plenio *et al.* were not observed here; this difference in behaviour is discussed later in this section (*vide infra*).

Activation parameters were determined for the reactions of **GH2** and **Grela** with ethyl vinyl ether in DCM by conducting the same four experiments at different temperatures in duplicate (283 K, 293 K, 298 K, and 303 K for **GH2** and 278 K, 283 K, 288 K, 298 K and 303 K for **Grela**); the available temperature range was restricted at one end by the limits of the Peltier cooling (*ca.* 278 K) and at the other end by the boiling point of DCM (*ca.* 313 K). In addition, the build-up of condensation on the cuvette surface at low temperatures led to practical difficulties on some occasions. Values for k_{init} at each temperature were obtained (**Table 3.18**); second-order plots were linear in each case, and forced through zero.

Activation parameters were extracted from these data in two ways. Firstly, an Arrhenius plot was constructed (**Equations 3.14** and **3.15**), which allowed quantification of the activation energy E_a . Secondly, an Eyring-Polanyi plot, which allowed calculation of ΔH^\ddagger , ΔS^\ddagger and ΔG^\ddagger , was constructed (**Equations 3.16** and **3.17**).

Table 3.18. Initiation rate constants for pre-catalysts **GH2** and **Grela**.

T (K)	GH2		Grela	
	k_{init} (L mol ⁻¹ s ⁻¹)			
278	-	-	0.06204	0.06057
283	0.00694	0.00704	0.09546	0.09729
288	-	-	0.13649	0.14265
293	0.01630	0.01625	-	-
298	0.02628	0.02634	0.32181	0.31103
298	0.02645	0.02611	-	-
303	0.03790	0.03871	0.41358	0.41989

$$k = A \cdot \exp(-E_a/RT) \quad (3.14)$$

$$\ln k = \ln A - (E_a/R) \cdot (1/T) \quad (3.15)$$

$$k = [(k_B \cdot T)/h] \cdot \exp(-\Delta G^\ddagger/RT)$$

$$= [(k_B \cdot T)/h] \cdot \exp(\Delta S^\ddagger/R) \cdot \exp(-\Delta H^\ddagger/RT) \quad (3.16)$$

$$\ln(k/T) = (-\Delta H^\ddagger/R) \cdot (1/T) + \ln(k_B/h) + (\Delta S^\ddagger/R) \quad (3.17)$$

The determination of ΔS^\ddagger from Eyring-Polanyi plots requires extrapolation over a long distance (i.e. to infinite temperature), and therefore often results in considerable error

bars. Errors were quantified for the gradient and intercept by calculating the error in k_{init} and then plotting $\ln(k/T)$ versus $1/T$ if the end points on the line were at the extremes of their error bars; i.e. k_{init} plus Δk_{init} at the lowest temperature and k_{init} minus Δk_{init} at the highest temperature and *vice versa* were plotted.

The thermodynamic parameters in **Table 3.19** were obtained from the Arrhenius and Eyring-Polanyi plots in **Figures 3.30** and **3.31** respectively. The parameters obtained for **GH2** differed from the first set obtained by Grubbs *et al.*;⁵⁸ the entropy change determined here is negative and relatively large, while Grubbs *et al.* obtained a value close to zero. However, the values are very close to those reported by Grubbs *et al.* for the reaction of **GH2** with butyl vinyl ether, with a similarly large and negative entropy of activation, a similar enthalpy of activation (14.1 kcal mol⁻¹ versus 15.2 kcal mol⁻¹) and similar Gibbs free energy of activation (19.6 kcal mol⁻¹ versus 20.1 kcal mol⁻¹; at 298 K).

DFT calculations were used to gain further insight into the initiation mechanism.^{183,191} Initially, all three potential mechanisms in **Scheme 3.04** were explored with **GH2** and ethene, while the interchange mechanism was also modelled with ethyl vinyl ether. It should be noted that both of these substrates are privileged in metathesis chemistry. Ethene is the least hindered alkene possible, and converts ruthenium carbene species to ruthenium methylidene complexes, which are among the least stable ruthenium carbene complexes²⁷⁻²⁸ and which can undergo degenerate metathesis with ethene to yield low energy metallocyclobutane species.³³ Ethyl vinyl ether is a very electron-rich alkene, and will convert ruthenium carbene species into Fischer carbene species that are typically metathesis-inactive at low (<323 K) temperatures. Calculated

Table 3.19. Activation energy E_a , pre-exponential factor A (from **Equation 3.15**) and ΔH^\ddagger , ΔS^\ddagger and ΔG^\ddagger (298.15 K) (from **Equation 3.17**).

Parameter	GH2	Grela
E_a	14.7 kcal mol ⁻¹	13.0 kcal mol ⁻¹
A	1.5×10^9	9.9×10^8
ΔH^\ddagger	(14.1 ± 1.2) kcal mol ⁻¹	(12.4 ± 1.0) kcal mol ⁻¹
ΔS^\ddagger	(-18.5 ± 4) cal K ⁻¹ mol ⁻¹	(-19.3 ± 3.5) cal K ⁻¹ mol ⁻¹
ΔG^\ddagger ^a	(19.6 ± 2.0) kcal mol ⁻¹	(18.2 ± 1.7) kcal mol ⁻¹

^a At 298.15 K

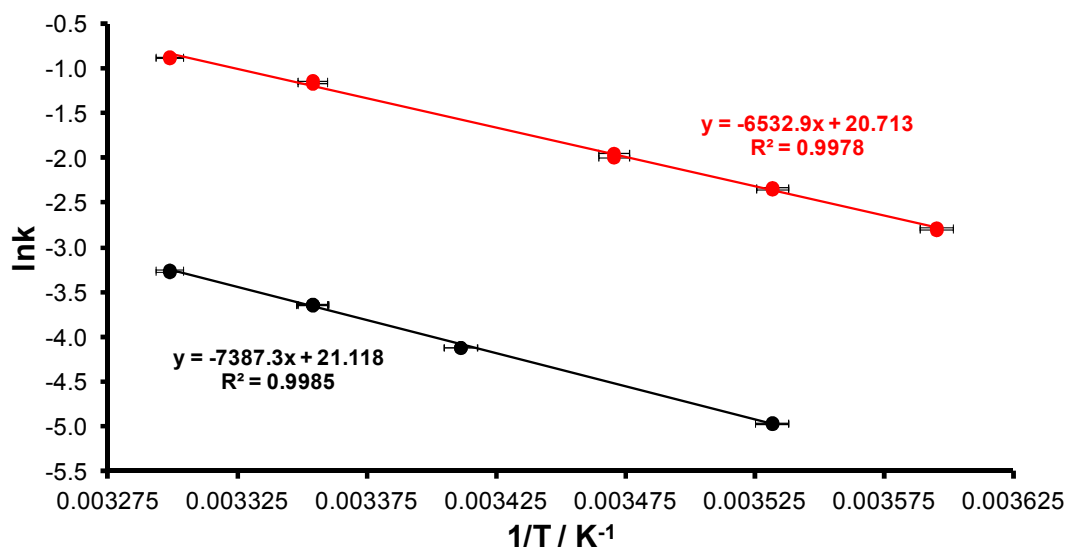


Figure 3.30. Arrhenius plot for the reactions of **GH2** (black) and **Grela** (red) with ethyl vinyl ether (25 – 200 mmol L⁻¹) in DCM; E_a and A are recorded in **Table 3.19**.

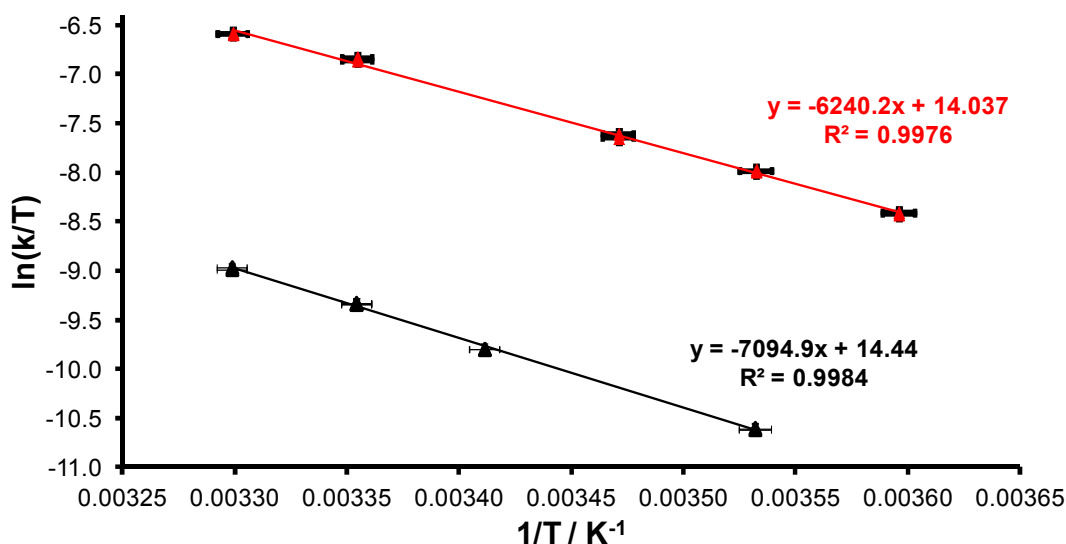


Figure 3.31. Eyring-Polyani plot for the reactions of **GH2** (black) and **Grela** (red) with ethyl vinyl ether (25 – 200 mmol L⁻¹) in DCM; thermodynamic parameters are recorded in **Table 3.19**.

parameters for all three mechanisms are recorded in **Table 3.20**, while transition states for each mechanism (with ethene) can be found in **Figure 3.32**. The calculated barrier for the dissociative mechanism is similar to that measured and calculated for the

Table 3.20. Calculated (using DFT at the M06-L/6-311G* level of theory) activation parameters for the initiation of **GH2** with ethene and ethyl vinyl ether in DCM at 298 K; values for ethyl vinyl ether are in brackets.¹⁹¹

Mechanism	ΔH^\ddagger (kcal mol ⁻¹)	ΔS^\ddagger (cal K ⁻¹ mol ⁻¹)	ΔG^\ddagger (at 298 K) (kcal mol ⁻¹)
Associative	19.5	-7.2	21.6
Dissociative	24.6	2.0	24.0
Interchange	13.9	-14.3	18.2
	(13.2)	(-8.5)	(15.8)

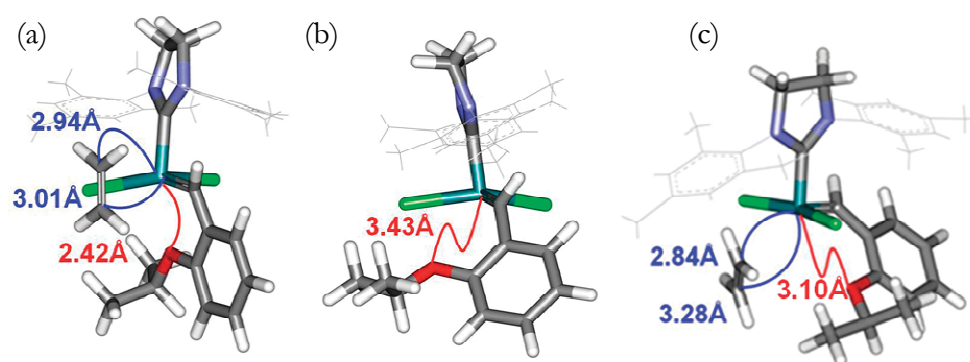
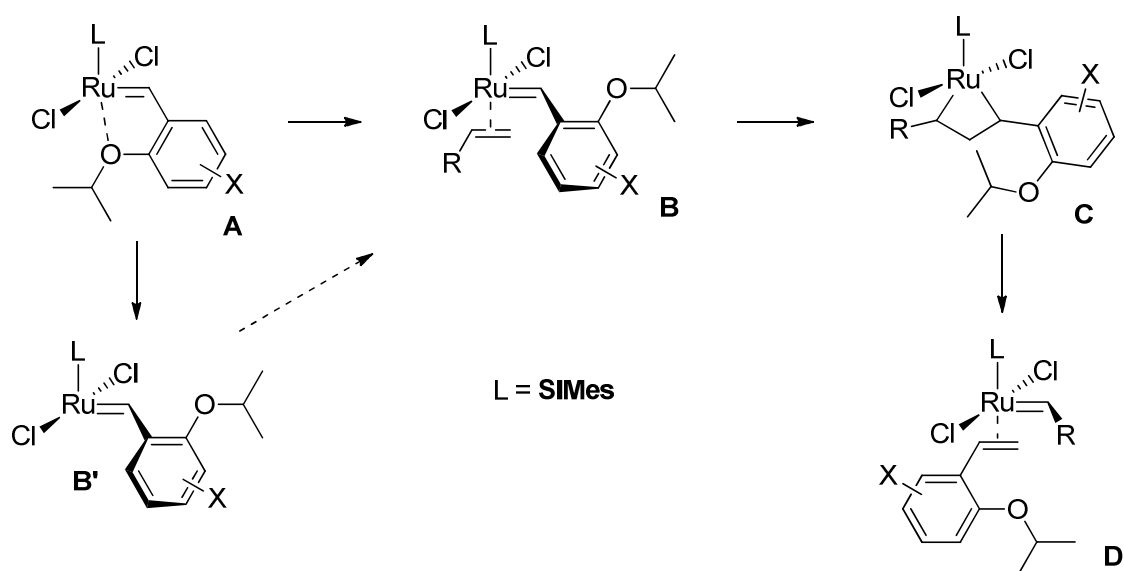


Figure 3.32. Transition state geometries for the initiation of **GH2** with ethene *via* (a) an associative mechanism, (b) a dissociative mechanism and (c) an interchange mechanism.

dissociation of phosphane from pre-catalyst **G2** (23.0 ± 0.4 kcal mol⁻¹).^{26,57} In the associative mechanism, the Ru-O bond distance is lengthened and the chloride ligands are perturbed as ethene is bound to the ruthenium centre. However, the molecule of ethene is not particularly close to the ruthenium centre, yet must perturb the ligand geometry considerably. This resulted in an increased barrier compared to the interchange mechanism, where the ethene approaches the ruthenium between the chloride ligands as the Ru-O distance increases. The interchange mechanism presents the lowest barrier of the three mechanisms. Notably, the experimentally-determined enthalpy of activation is within experimental error of the calculated value. Entropy values from both theory and experiment are less reliable; the implicit solvation model does not deal with entropy correctly in the calculations, while extrapolation over long ranges in Eyring-Polanyi plots is required to obtain experimental entropies of activation. This evidence strongly suggested that it was an interchange mechanism alone that was in

operation in these reactions, as the dissociative mechanism for **GH2** initiation is not energetically competitive with the interchange mechanism. The 3.4 kcal mol⁻¹ difference in Gibbs free energy of activation translates to a *ca.* 300-fold rate difference in favour of the interchange mechanism (in the presence of 1 mol L⁻¹ ethyl vinyl ether).

Further calculations were carried out to probe the effects of pre-catalyst and substrate structure on initiation rate more fully.¹⁸³ Complexes from pre-catalyst through to product η^2 -complex were modelled (**Scheme 3.05**). Calculations were carried out on pre-catalysts **GH2**, **Grela** and **GH2-OMe**; reaction with ethyl vinyl ether was considered for all three pre-catalysts, while the reaction of **GH2** with ethene was also considered. The latter substrate is rather small and so does not necessarily represent typical metathesis substrates, which will be (at minimum) monosubstituted and may be di-, tri- or tetra-substituted. Larger substrate molecules will require more space around the metal centre in the associative and interchange mechanisms. The PES for the dissociative mechanism was compared with that for the interchange mechanism for the initiation of **GH2** with ethyl vinyl ether (**Figure 3.33**). The barrier to initiation *via* the interchange mechanism ($\Delta G^\ddagger = 15.8$ kcal mol⁻¹) is lower than that to rotation of the alkoxy styrene and scission of the oxygen- ruthenium bond ($\Delta G^\ddagger = 24.0$ kcal mol⁻¹). However, both of these steps lead *reversibly* to an η^2 -complex which then must overcome a further barrier to form the MCB complex ($\Delta G^\ddagger = 11.4$ kcal mol⁻¹) which is considerably higher than the barrier to the reverse reaction for the interchange



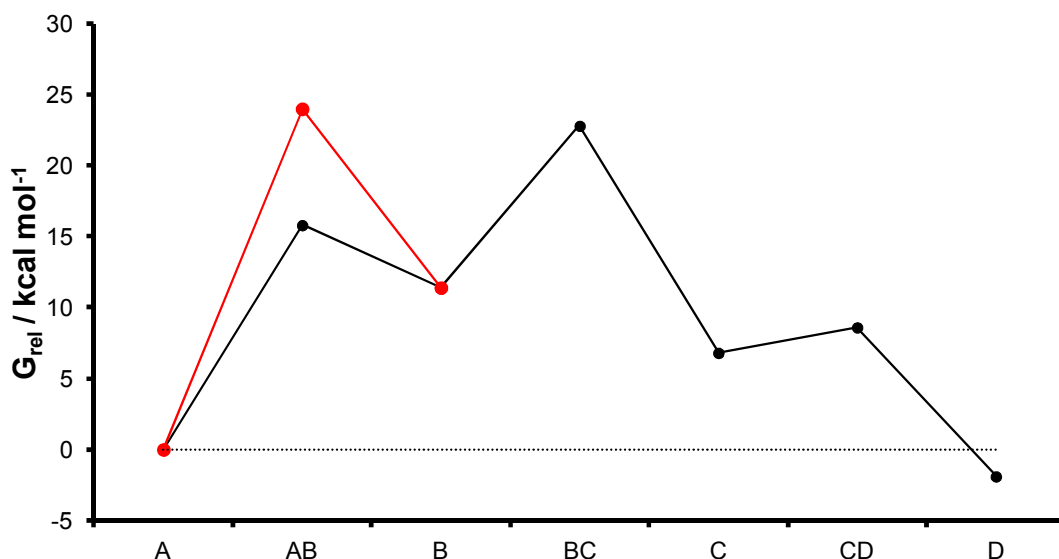


Figure 3.33. PES (at the M06-L/6-311G* level of theory) for the initiation of **GH2** with ethyl vinyl ether; the **black** series represents the interchange mechanism, while the **red** series represents the dissociative mechanism.¹⁸³

mechanism ($\Delta G^\ddagger = 4.4 \text{ kcal mol}^{-1}$). Subsequent steps present far lower energetic barriers and result in a product η^2 -complex that is $1.9 \text{ kcal mol}^{-1}$ lower in energy than the pre-catalyst plus ethyl vinyl ether.

Substitution of the alkoxy styrene ligand with electron-withdrawing groups reduced the barriers to both mechanisms; the barrier to the dissociative mechanism with **Grela** was $0.8 \text{ kcal mol}^{-1}$ lower in energy, while electron-rich **GH2-OMe** encountered a barrier that was $0.7 \text{ kcal mol}^{-1}$ higher in energy. Similar trends were uncovered for the interchange mechanism; however, a stronger effect was felt from the electron density of the alkoxy styrene ligand, lowering the initial barrier by $2.7 \text{ kcal mol}^{-1}$ for **Grela** with respect to **GH2** (Figure 3.34). Substrate structure was also found to exert an effect on the PES, in agreement with experimental observations (Figure 3.35); notably the major differences were encountered between product η^2 -complexes, with that derived from ethene $14.5 \text{ kcal mol}^{-1}$ higher in energy than the pre-catalyst complex plus ethene (*cf.* $-1.9 \text{ kcal mol}^{-1}$ for the corresponding reaction with ethyl vinyl ether).

The influence of the overall equilibrium on the initiation of **GH2** was tested experimentally by dissolving the pre-catalyst (*ca.* 2.5 mmol L^{-1}) in chloroform-*d* that had been sparged with ethene beforehand to a concentration of *ca.* 65 mmol L^{-1} ; in the analogous experiment with **G2**, a slow first-order decrease of [**G2**] was discovered. The

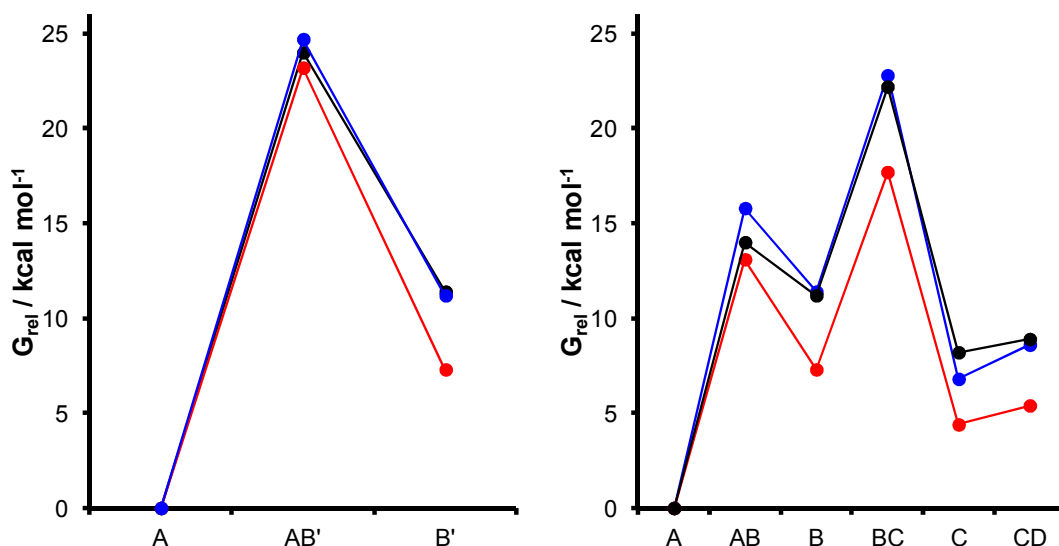


Figure 3.34. PES (at the M06-L/6-311G* level of theory) for the initiation of **GH2** (black), **Grela** (red) and **GH2-OMe** (blue) with ethyl vinyl ether, (a) *via* the dissociative mechanism or (b) *via* the interchange mechanism.¹⁸³

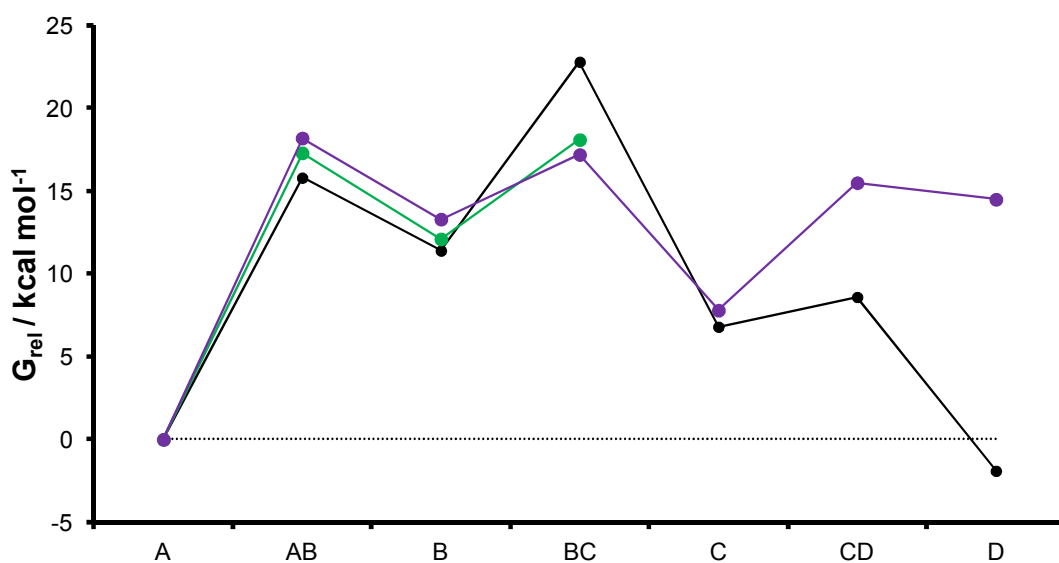


Figure 3.35. Potential energy surface (at the M06-L/6-311G* level of theory) for the initiation of **GH2** with ethyl vinyl ether (black), propene (green) and ethene (purple).¹⁸³

reaction was monitored at 293 K by ¹H NMR spectroscopy for 4.5 hours (**Figure 3.36**). During this experiment, only approximately 30% of the pre-catalyst was consumed. The decay of the pre-catalyst concentration did not fit first-order behaviour, unlike the

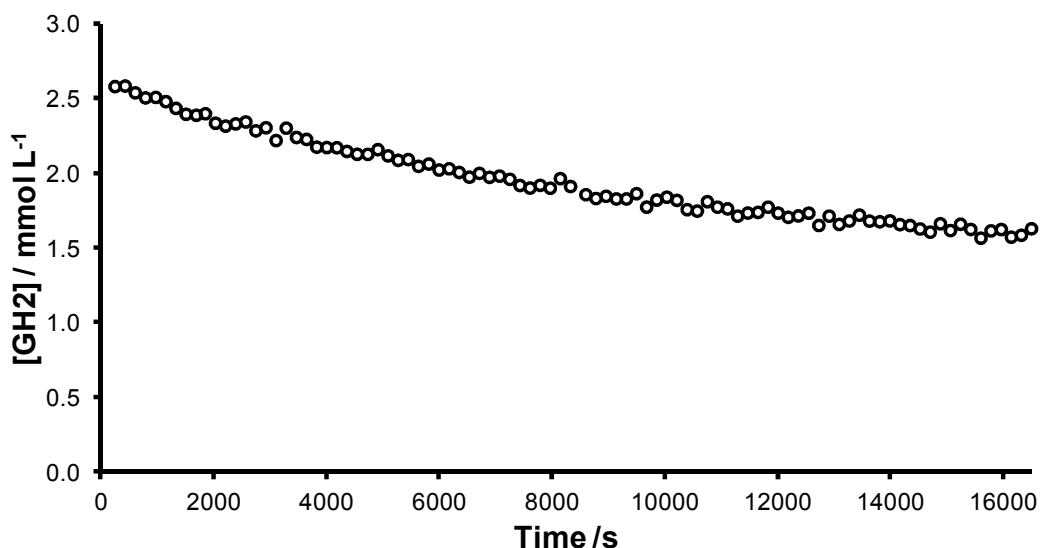
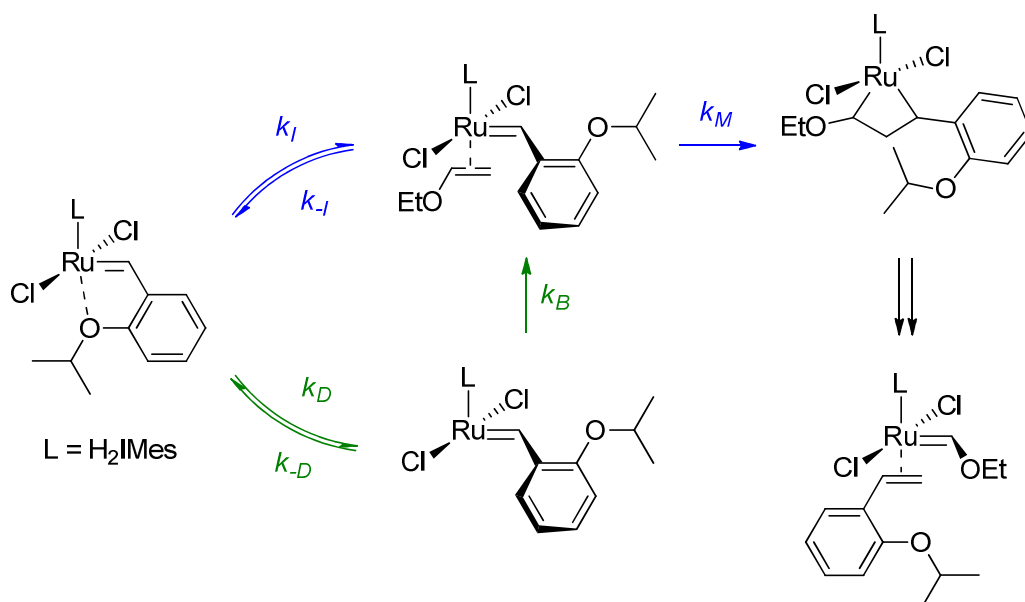


Figure 3.36. Concentration *versus* time profile for **GH2** when exposed to ethene (*ca.* 65 mmol L⁻¹) in chloroform-*d* at 293 K.

analogous experiment with **G2** (**Figure 3.15**, *vide supra*), and suggested that reaction with ethene was unfavourable. This result was consistent with the data obtained from DFT studies described above.

Interpreting the kinetic consequences of these potential energy surfaces and comparing them to experimental observations was challenging. Therefore, the rate expressions for the dissociative and interchange mechanism were considered. The first two steps of each mechanism were treated (**Scheme 3.06**).²⁰⁷

The interchange mechanism consists of a bi-molecular step to form an η^2 -complex (with forward and reverse rate constants k_f and k_r respectively), followed by a unimolecular reaction to form a MCB (with rate constant k_M). Therefore, the rate of reaction (equivalent to the rate of MCB formation) can be expressed as **Equation 3.18**. Applying the steady-state approximation to the η^2 -complex yields **Equation 3.19**, which can be rearranged to give an expression for η^2 -complex concentration (**Equation 3.20**). Substituting **Equation 3.19** into **Equation 3.18** gives **Equation 3.21**, and therefore an expression for k_{obs} (**Equation 3.22**). If k_f is much faster than k_2 (as suggested by the DFT calculations above), then the expression simplifies to **Equation 3.23**; if the opposite were true, then **Equation 3.24** would be obtained. Both of these limiting cases result in a linear relationship between k_{obs} and the alkene concentration. The only difference is what the gradient of a plot of k_{obs} *versus* [alkene] represents: $k_M \cdot K_I$ or k_f .



Scheme 3.06

$$v = d[\text{metallocyclobutane}]/dt = k_M \cdot [\eta^2\text{-complex}] \quad (3.18)$$

$$0 = k_I \cdot [\text{GH2}] \cdot [\text{alkene}] - k_{-I} \cdot [\eta^2\text{-complex}] - k_M \cdot [\eta^2\text{-complex}] \quad (3.19)$$

$$[\eta^2\text{-complex}] = (k_I \cdot [\text{GH2}] \cdot [\text{alkene}]) / (k_{-I} + k_M) \quad (3.20)$$

$$v = (k_I \cdot k_M \cdot [\text{GH2}] \cdot [\text{alkene}]) / (k_{-I} + k_M) \\ = k_{obs} [\text{GH2}] \quad (3.21)$$

$$k_{obs} = (k_I \cdot k_M \cdot [\text{alkene}]) / (k_{-I} + k_M) \quad (3.22)$$

$$k_{obs} \approx k_M \cdot K_I \cdot [\text{alkene}] \quad (3.23)$$

$$k_{obs} \approx k_I \cdot [\text{alkene}] \quad (3.24)$$

The alternative, dissociative mechanism can be considered as a unimolecular equilibrium between pre-catalyst and 14e catalyst where the alkoxy-styrene ligand has rotated (with rate constants k_D and k_{-D} and equilibrium constant K_D), followed by a bimolecular reaction where alkene binds to the 14e complex (with rate constant k_B). The rate of reaction is therefore **Equation 3.25**. The steady state approximation yields an expression for the concentration of 14e complex (**Equations 3.26 and 3.27**), which can be inserted into **Equation 3.25** to yield **Equation 3.28**, which in turn yields an expression for k_{obs} (**Equation 3.29**). The two limiting cases, (i) if $k_D \gg k_B \cdot [\text{alkene}]$ (**Equation 3.30**) and (ii) if $k_B \cdot [\text{alkene}] \gg k_D$ (**Equation 3.31**) result in alkene concentration-dependent behaviour at low [alkene], tending to a maximum value

$$d[\eta^2\text{-complex}]/dt = k_B \cdot [14e] \cdot [\text{alkene}] \quad (3.25)$$

$$0 = k_D \cdot [\mathbf{GH2}] - k_{-D} \cdot [14e] - k_B \cdot [14e] \cdot [\text{alkene}] \quad (3.26)$$

$$[14e] = (k_D \cdot [\mathbf{GH2}]) / (k_{-D} + k_B \cdot [\text{alkene}]) \quad (3.27)$$

$$\begin{aligned} \nu &= (k_D \cdot k_B \cdot [\mathbf{GH2}] \cdot [\text{alkene}]) / (k_{-D} + k_B \cdot [\text{alkene}]) \\ &= k_{obs} [\mathbf{GH2}] \end{aligned} \quad (3.28)$$

$$k_{obs} = (k_D \cdot k_B \cdot [\text{alkene}]) / (k_{-D} + k_B \cdot [\text{alkene}]) \quad (3.29)$$

$$k_{obs} \approx k_B \cdot K_D \cdot [\text{alkene}] \quad (3.30)$$

$$k_{obs} \approx k_D \quad (3.31)$$

independent of [alkene].

While the way in which the two mechanisms are considered is not completely consistent with the mechanism, i.e. the formation of the η^2 -complex is not irreversible, DFT calculations suggest that the barrier to the reverse reaction is larger (by at least 1 kcal mol⁻¹)¹⁸³ than the forward reaction to form the MCB complex.

The kinetic analysis is consistent with the conclusion that both mechanisms are in operation (as proposed by Plenio *et al.*),⁶¹ but the same behaviour was not observed in the experiments conducted here in DCM. Alternative explanations for the curved k_{obs} *versus* [alkene] plot were considered.

The concentration range covered by Plenio *et al.* is vast, typically from *ca.* 0.01 mol L⁻¹ to 3 mol L⁻¹.⁶¹ Interestingly, the authors note that the reaction of **GH2** with diethyl diallylmalonate at 4 mol L⁻¹ results in a value for k_{obs} that deviates from the trend observed at concentrations of *ca.* 2 mol L⁻¹ and lower; this was attributed to the fact that in the experiment the solvent was composed of 96% diethyl diallylmalonate and 4% toluene. This raises two possibilities for the observed shape of the k_{obs} *versus* [alkene] plots. Firstly, the different solvent composition will alter the properties of the solvent. Plenio *et al.* suggest that a change in dielectric constant ϵ is not the source of the curvature, from comparing the profiles of plots for alkenes with different dielectric constants. No link between dielectric constant and initiation rate has been established, but Grubbs *et al.* have postulated that such a link might exist on the basis of three initiation rate measurements.²⁶

To evaluate the effects of solvent on **GH2** initiation, the initiation rates with ethyl vinyl ether were measured in benzene, chloroform, dimethyl carbonate (DMC), 1,2-difluorobenzene, hexafluorobenzene, methyl *tert*-butyl ether (MTBE), toluene and

trifluorotoluene (Figures 3.37 and 3.38 and Table 3.21) in triplicate. Differences between the initiation rates in various solvents were relatively modest, with a *ca.* 2.5-fold difference between the fastest (MTBE) and the slowest (chloroform). Reactions in aromatic solvents were typically faster than those in the non-aromatic solvents evaluated.

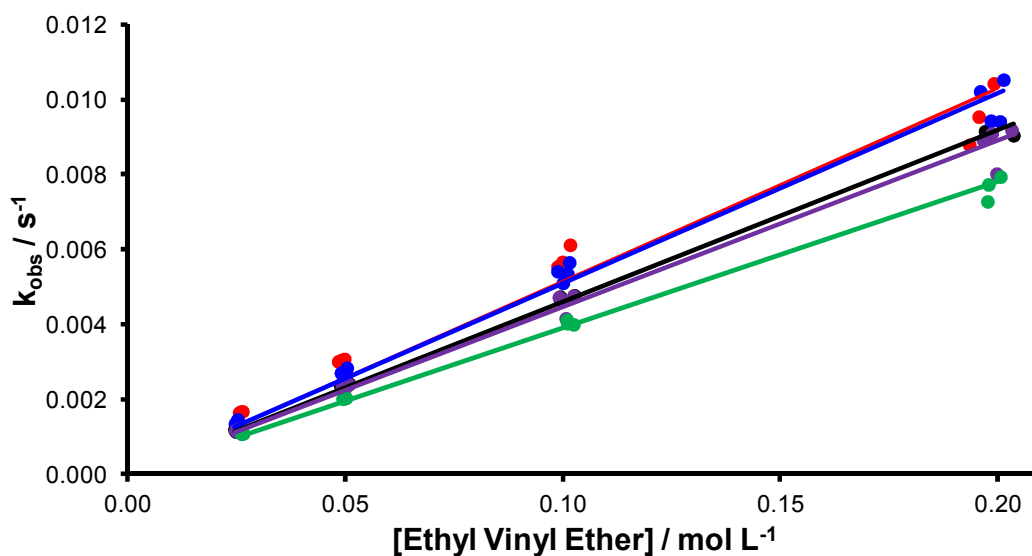


Figure 3.37. Plot of k_{obs} versus ethyl vinyl ether concentration for the reactions of GH2 with ethyl vinyl ether at 298 K in benzene, hexafluorobenzene, toluene, trifluorotoluene and 1,2-difluorobenzene.

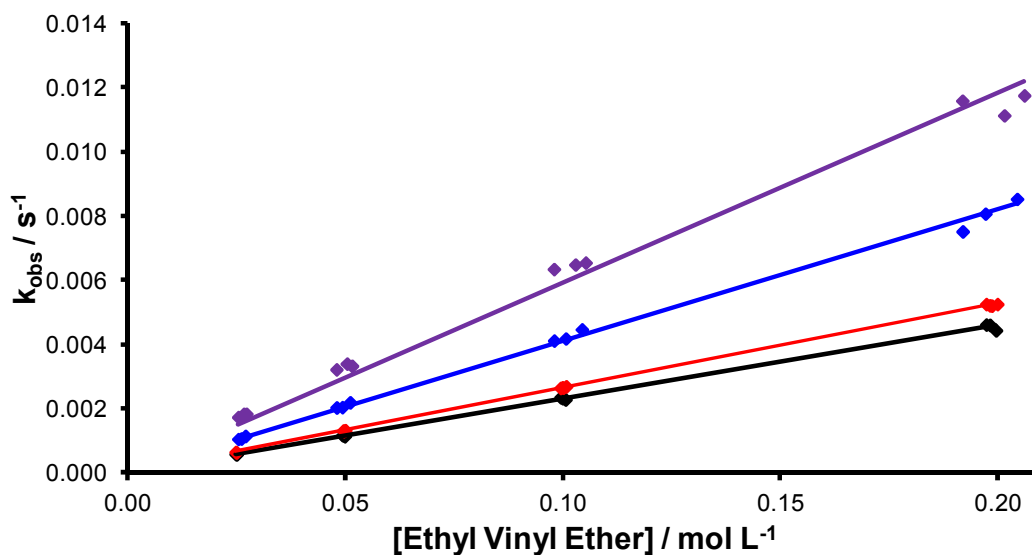


Figure 3.38. Plot of k_{obs} versus ethyl vinyl ether concentration for the reactions of GH2 with ethyl vinyl ether at 298 K in chloroform, DCM, DMC and MTBE.

Table 3.21. Initiation rates for **GH2** with ethyl vinyl ether in various solvents, measured by UV/visible spectroscopy at 298 K.

Solvent	Dielectric Constant ϵ (at temperature)	k_{init} ($L mol^{-1} s^{-1}$)
Benzene	2.28 (293) ²⁰⁹	0.0460
Chloroform	4.8 (293) ²⁰⁹	0.0231
DCM	9.1 (293) ²⁰⁹	0.0264
1,2-Difluorobenzene	13.8 (301) ²¹⁰	0.0390
DMC	3.09 (298) ²¹¹	0.0411
Hexafluorobenzene	2.03 (298) ²¹²	0.0515
MTBE	4.5 (293) ²⁰⁹	0.0592
Toluene	2.38 (293) ²⁰⁹	0.0509
Trifluorotoluene	9.22 ²¹³	0.0446

A plot of k_{init} versus dielectric constant revealed no trend (**Figure 3.39**). These results did not allow the effects of the specific solvent mixtures encountered by Plenio to be fully evaluated, but demonstrate that solvent has an effect on initiation rate which is not correlated to the dielectric constant alone. Further discussion of solvent effects can be

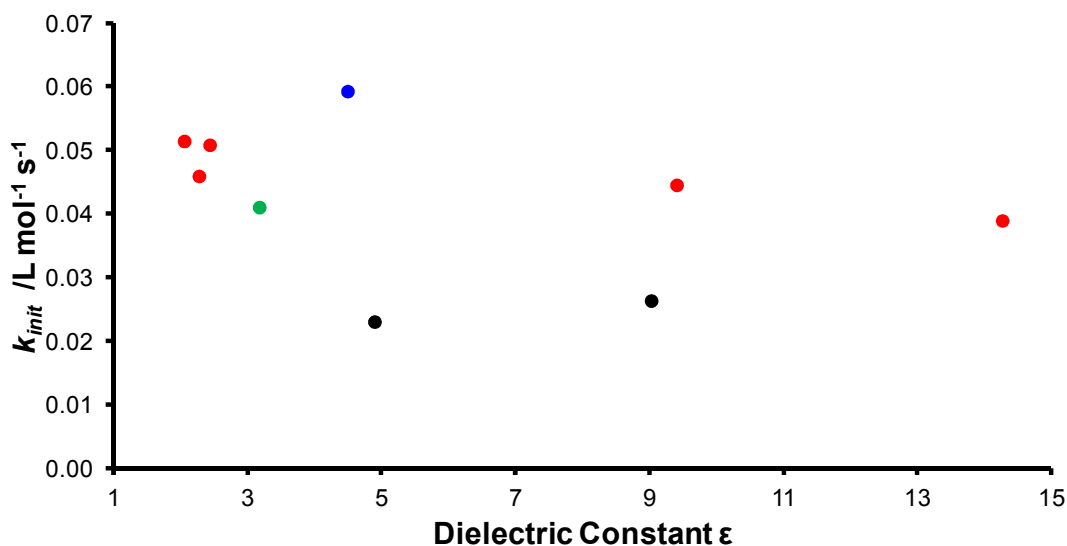


Figure 3.39. Second order initiation rate constant for the initiation of **GH2** with ethyl vinyl ether at 298 K versus solvent dielectric constant ϵ showing aromatic solvents in **red**, chlorinated solvents in **black**, MTBE in **blue** and DMC in **green**; dielectric constants were obtained from the literature.^{210,214}

found in a subsequent section of this chapter.

Most importantly, the activity of a solute is not the same in concentrated solution as in dilute solution; a solute deviates from ideal (approximately infinite dilution) behaviour as its mole fraction in solution increases.²⁰⁸ At low solute concentrations, solutes behave approximately like they would at infinite dilution but at high solute concentrations this approximation does not apply, and activity is not equal to concentration. Solute molecules can interact at high concentrations, thereby reducing their activity, when the molar ratio of solvent to solute is so low that solute molecules are not properly solvated. To illustrate this effect, the molar ratios of solute to solvent were calculated for solutions of diethyl diallylmalonate, ethyl vinyl ether, butyl vinyl ether, 1-hexene and styrene in toluene at various concentrations (**Table 3.22**). These calculations show that the mole fraction of substrate reaches *ca.* 0.2 to 0.5 for 2 mol L⁻¹ solutions of these substrates in toluene at 298 K. In contrast, if the solvent is DCM the molar ratio drops to only *ca.* 0.15 to 0.25 at 2 mol L⁻¹. This may explain (at least in part) why curved plots of k_{obs} versus [alkene] were not obtained from the work documented here in DCM. The possibility that the curved plots obtained by Plenio *et al.* were a result of non-ideal behaviour of alkene solutions was investigated briefly by attempting to calculate approximate equilibrium constants for self-association of the substrate molecules in solution; the consequences of such self-association are a decreased

Table 3.22. Molar ratios of solute to solvent in the solutions of diethyl diallylmalonate, ethyl vinyl ether, butyl vinyl ether, styrene and 1-hexene in toluene at 298 K.

Concentration (mol L ⁻¹)	Diethyl diallylmalonate	Ethyl vinyl ether	Butyl vinyl ether	Styrene	1-Hexene
0.001	0.0001	0.0001	0.0001	0.0001	0.0001
0.005	0.0005	0.0005	0.0005	0.0005	0.0005
0.010	0.0011	0.0011	0.0011	0.0011	0.0011
0.050	0.0054	0.0053	0.0053	0.0054	0.0053
0.100	0.0109	0.0107	0.0107	0.0108	0.0107
0.500	0.0605	0.0547	0.0554	0.0559	0.0548
1.000	0.1399	0.1126	0.1155	0.1176	0.1130
2.000	0.4079	0.2390	0.2521	0.2626	0.2405
3.000	1.1275	0.3818	0.4164	0.4457	0.3856
4.000	9.5604	0.5444	0.6176	0.6844	0.5521

effective substrate concentration. Considering the equilibrium between alkene and non-covalent alkene dimer, referred to here as alkene₂, leads to an expression for the equilibrium constant for association of two molecules of alkene to form a non-covalently bonded dimer (**Equation 3.32**).

$$K = [\text{alkene}_2]/[\text{alkene}]^2 \quad (3.32)$$

The initial alkene concentration is equal to the sum of the alkene concentration and half of the dimer concentration (**Equation 3.33**), which can then be expressed in terms of the alkene concentration alone (**Equation 3.34**); rearrangement allows this to be expressed as a quadratic expression (**Equation 3.35**). The roots of this quadratic equation can be determined using **Equation 3.36**; solving for the positive root.

$$[\text{alkene}]_0 = [\text{alkene}] + 2[\text{alkene}_2] \quad (3.33)$$

$$= [\text{alkene}] + 2K[\text{alkene}]^2 \quad (3.34)$$

$$0 = (K[\text{alkene}]^2)/2 + [\text{alkene}] - [\text{alkene}]_0 \quad (3.35)$$

$$[\text{alkene}] = (-1 \pm \sqrt{1 + 2K[\text{alkene}]_0})/K \quad (3.36)$$

This expression can then be used to calculate the effective alkene concentration, assuming that the dimer does not undergo reaction (**Figure 3.40**).

This treatment was applied to the experimental data published by Plenio *et al.* for the initiation reactions of **GH2** with diethyl diallylmalonate and styrene and for **Grela** with diethyl diallylmalonate. Calculation of an effective alkene concentration using different values of K allowed an approximate equilibrium constant to be estimated that would render the k_{obs} versus [alkene] plot linear. Importantly, K should be dependent on substrate but not on pre-catalyst. A value of K = 1 rendered both of the diethyl diallylmalonate plots linear, while K = 4 was required to do so for styrene (**Figure 3.41**). This is consistent with stronger self-interactions between styrene molecules than diethyl diallylmalonate molecules. The former can undergo π -stacking²¹⁵ which would be expected to be a stronger than the dipole-dipole interactions in the latter compound.

Further investigation is necessary to confirm whether solvent effects and non-ideal behaviour are the source of curvature in the k_{obs} versus [alkene] plots presented by Plenio *et al.* However, as all plots of this type obtained from work reported here (which

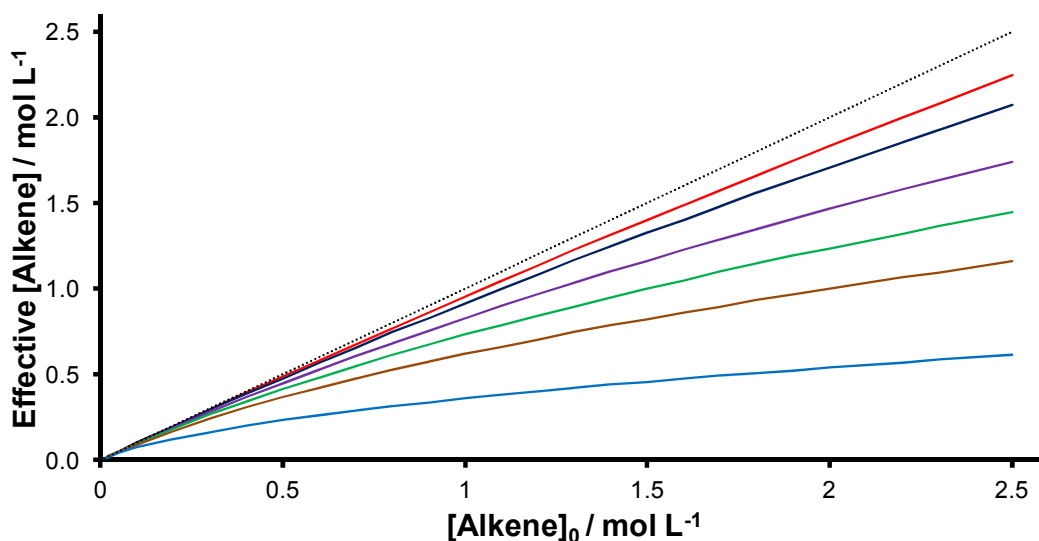


Figure 3.40. Effective alkene concentration calculated from **Equation 3.34** *versus* initial alkene concentration with $K = 0.1, 0.2, 0.5, 1, 2$ and 10 .

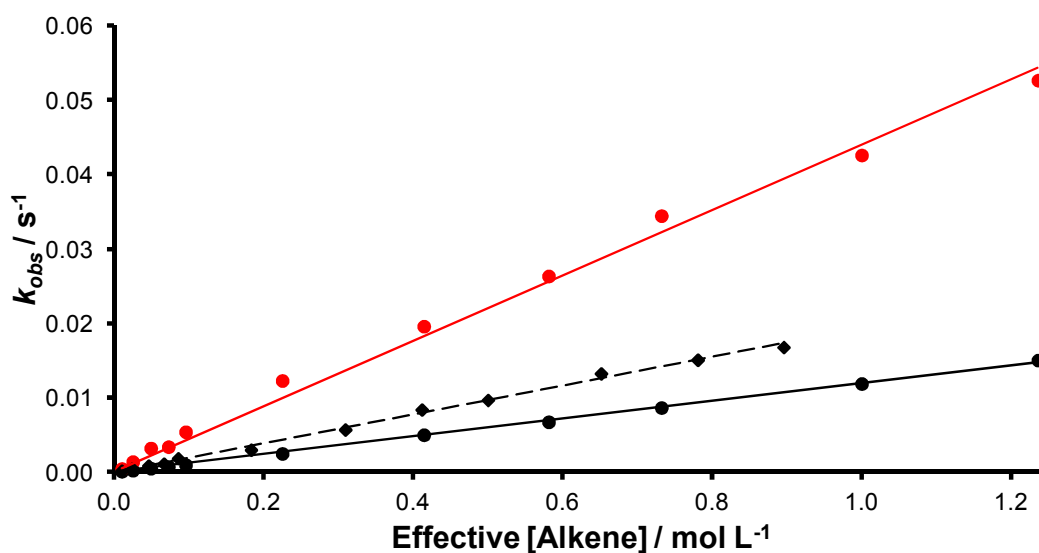


Figure 3.41. Plot of k_{obs} *versus* effective alkene concentration (see **Equation 3.34**) for the initiation of **GH2** with diethyl diallylmalonate (**black circles**) and styrene (**black rhombi**) and **Grela** with diethyl diallylmalonate (**red circles**); the original data were taken from reference.⁶¹

was conducted in DCM) were clearly linear, reaction simulation models where **GH2** and analogues were used as pre-catalysts were all constructed using the interchange model.

Measuring Initiation Rates for a Series of Pre-catalysts

Hoveyda-type pre-catalysts typically feature structural differences that fall into two categories. Firstly, the NHC ligand differs; while pre-catalysts bearing the **SIMes** and **SIPr** ligands are studied here, metathesis pre-catalysts bearing various other NHC ligands are known.^{156,216} Recently, ruthenium carbene metathesis pre-catalysts featuring asymmetrical NHCs have been advocated for selective ethenolysis⁹¹ and *Z*-selective metathesis,²¹⁷ while asymmetric *tert*-butyl-substituted NHCs are latent pre-catalysts.²¹⁸⁻²¹⁹

Secondly, the chelating alkoxy styrene ligand can be altered. Typical modifications to this ligand usually involve the substitution of the aromatic ring with an electron-withdrawing group in order to weaken the Ru-O bond.¹³ Plenio *et al.* have shown that the substituents on the aromatic ring can considerably alter the electron density of the ruthenium centre, and that good Hammett correlations can be obtained if the substituents are considered relative to the carbene rather than the ether;⁶¹ i.e. the electron density on the metal is affected *via* the carbene functionality, not the ether functionality. Solans-Monfort *et al.* have also highlighted the importance of π -electron density in the alkoxy styrene aromatic system when considering the activity of pre-catalysts using *in silico* methods.²⁰⁶ While not studied here, a further set of modifications is possible. Substitution of a chloride ligand with an alkoxide (or other ionic) ligand is possible;^{18,220} such modifications are typically introduced *via* a corresponding silver salt.

Initiation rates were measured for **GH2**, **GH2-SIPr**, **Zhan1B**, **Grela**, **Grela-SIPr**, **M71-SIMes**, **M71-SIPr**, **M8₃₂-SIPr** and **M8₅₃-SIPr** by monitoring the reaction with ethyl vinyl ether (at various concentrations) in dry DCM at 298 K using UV/visible spectroscopy. Plots of k_{obs} versus ethyl vinyl ether concentration were all forced through zero and were linear (**Figure 3.42**); measured initiation rates varied over two orders of magnitude (**Table 3.23**). These data revealed some interesting trends. For pre-catalysts with the same NHC ligand, electron withdrawing substituents increased the initiation rate. This is in agreement with the results of Plenio *et al.*, who measured the initiation rates of a large number of bis(mesityl)imidazolium-bearing pre-catalysts.⁶¹ However, the NHC ligand was found to dramatically influence the initiation rate; pre-catalysts bearing a bulky **SIPr** ligand initiated *ca.* 6 – 9 times *slower* than the corresponding **SIMes**-bearing pre-catalysts. This is the opposite trend to that observed previously for the phosphane-bearing pre-catalysts, where **G2-SIPr** was found to initiate orders of magnitude *faster* than **G2**.

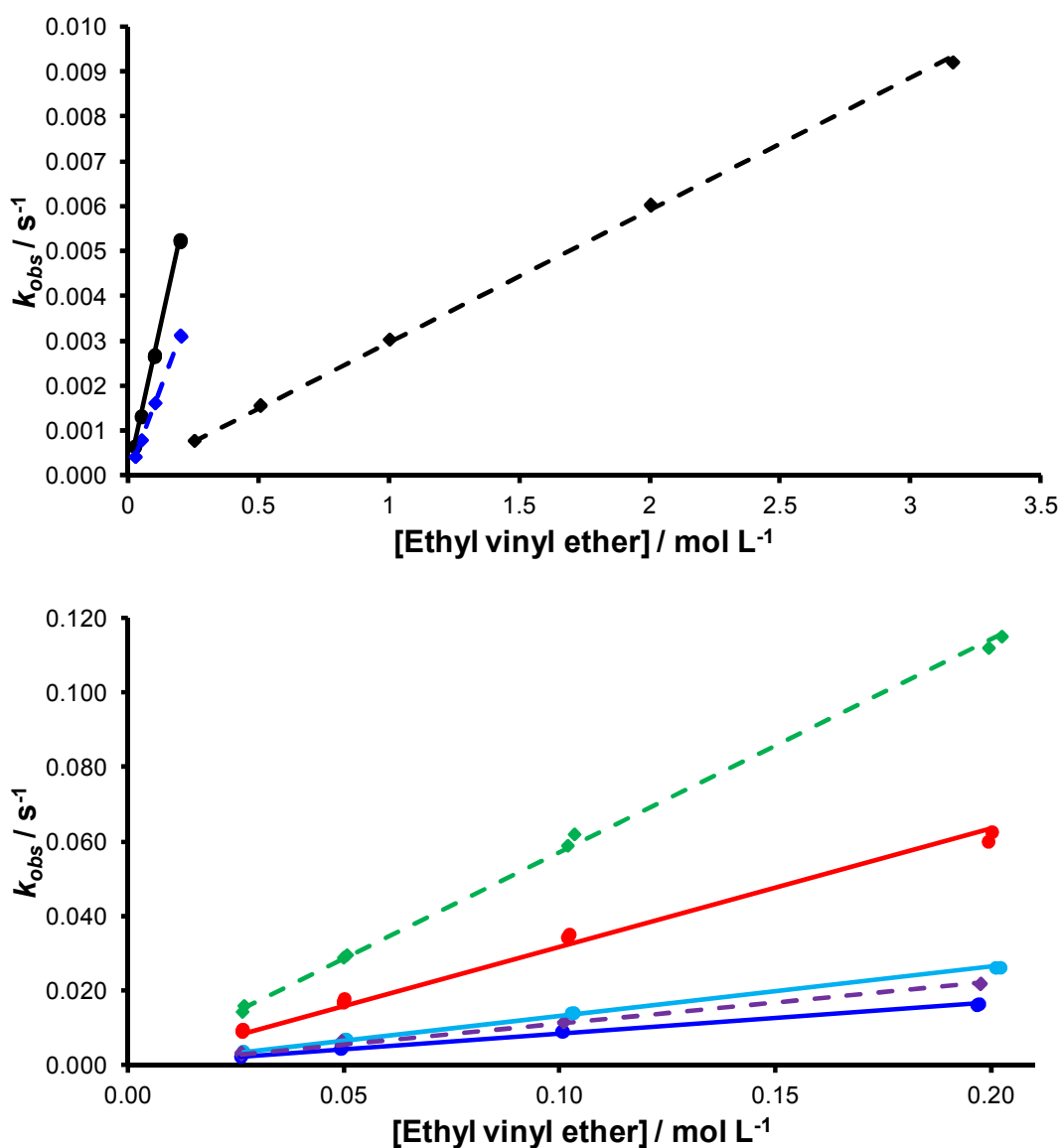


Figure 3.42. Initiation rates for pre-catalysts (i) GH2 (black circles), (ii) M71-SIPr (blue rhombi) (iii) GH2-SIPr (black rhombi), (iv) M853-SIPr (green rhombi), (v) Grela (red circles), (vi) Zhan1B (light blue circles), (vii) M831-SIPr (purple rhombi), (viii) M71-SIMes (blue circles), and (ix) Grela-SIPr (red rhombi).

NHCs can be compared on the basis of their size (and therefore steric effect on the metal centre) using the percent buried volume ($\%V_{bur}$) metric introduced by Nolan and Cavallo.²²¹ This means of measuring steric impact quantifies the percentage of the ligand volume that is located within a sphere of a chosen radius around the metal centre (typically 2.00 Å or 2.38 Å), thereby considering the proportion of the ligand that actually impacts upon the steric environment in which chemical reactions at the metal

Table 3.23. Initiation rates for pre-catalysts, measured by monitoring the reaction of each with ethyl vinyl ether in DCM at 298 K using UV/visible spectroscopy.

Pre-catalyst	NHC Ligand	k_{init} (L mol ⁻¹ s ⁻¹)	R ²
GH2	SIMes	0.02642	0.9998
GH2-SIPr	SIPr	0.002956	0.9991
Zhan1B	SIMes	0.1320	0.9982
Grela	SIMes	0.3172	0.9911
Grela-SIPr	SIPr	0.0368	0.9990
M71-SIMes	SIMes	0.08511	0.9945
M71-SIPr	SIPr	0.01560	0.9994
M831-SIPr	SIPr	0.1126	0.9955
M835-SIPr	SIPr	0.5711	0.9987

centre occur. This metric complements the Tolman cone angle, which is an existing metric for phosphane ligands.²²² The value of $\%V_{bur}$ has been shown to vary dramatically amongst different ligands. Gold chloride complexes with $\%V_{bur}$ from 23.5 to 51.2 and silver complexes with $\%V_{bur}$ from 26.1 to 46.5 have been identified (**Figure 3.43**);²²¹ these values were obtained with a metal-ligand bond length of 2.00 Å. Therefore, the spread of steric impact is typically 20 – 25 percentage points between the least and most bulky examples of NHC-metal complexes. However, no studies to date have established quantitative or semi-quantitative correlation between catalytic activity and $\%V_{bur}$.

$\%V_{bur}$ has been measured for various ruthenium-based metathesis pre-catalysts bearing the **SIMes** and **SIPr** ligands (**Table 3.24**). While **SIPr** is clearly bulkier, taking up *ca.* 0.5 to 1 percentage points more space around the metal centre, the trend for both the phosphane-bound and the Hoveyda-type pre-catalyst series was the same.

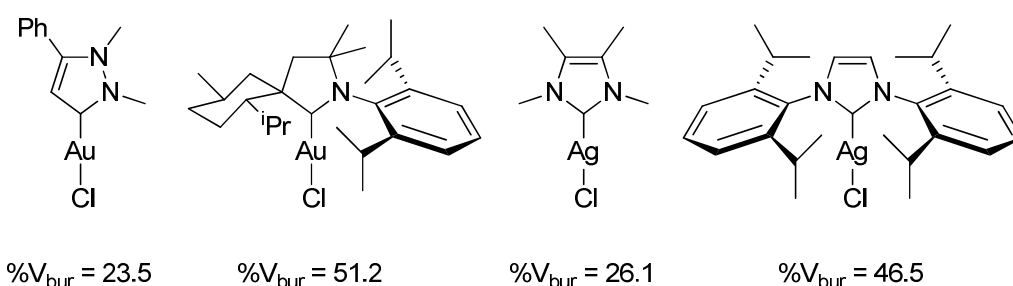
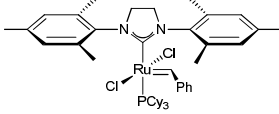
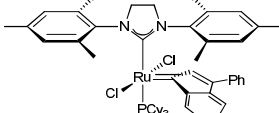
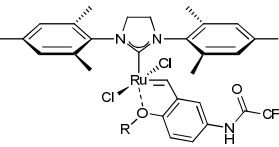
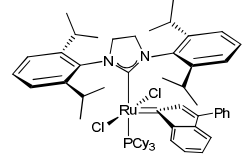
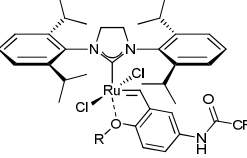


Figure 3.43. Examples of small and large *N*-heterocyclic carbenes.

Table 3.24. Selected examples of *N*-heterocyclic carbene-bearing ruthenium complexes and their corresponding % V_{bur} at 2.00 Å and 2.38 Å.²²¹

Complex	% V_{bur} (2.00 Å)	% V_{bur} (2.38 Å)	
	G2	32.8	27.8
	G2-ind	31.7	26.6
	M71-SIMes	35.0	29.9
	G2-SIPr-ind	32.8	27.6
	M71-SIPr	35.7	30.5

The comparisons in **Table 3.24** were drawn from X-ray crystallography data, but DFT-derived co-ordinates can also be used to calculate % V_{bur} . DFT calculations were used to obtain optimised geometries for pre-catalysts **GH2** and **GH2-SIPr**. The co-ordinates supplied by Solans-Monfort *et al.* were used as a starting point for both complexes.²⁰⁶ These co-ordinates were calculated for the methoxystyrene analogue of **GH2** (complex **144**) at the B3LYP/6-311G* level of theory, which does not treat important dispersive interactions and metal-ligand binding energies correctly,⁵¹ and will therefore miscalculate the shape (and hence the volume) of the ligand. Therefore, the additional two methyl groups were added and the structure was re-optimised using Wavefunction Spartan '10¹⁸² and the M06-L/6-31G* level of theory. This structure was then modified to remove the *para*-methyl groups, and to elaborate the *ortho*-methyl groups into *iso*-propyl groups. This structure was optimised again at the M06-L/6-31G* level of theory using Spartan '10. The optimised geometries were overlaid (**Figure 3.44**).

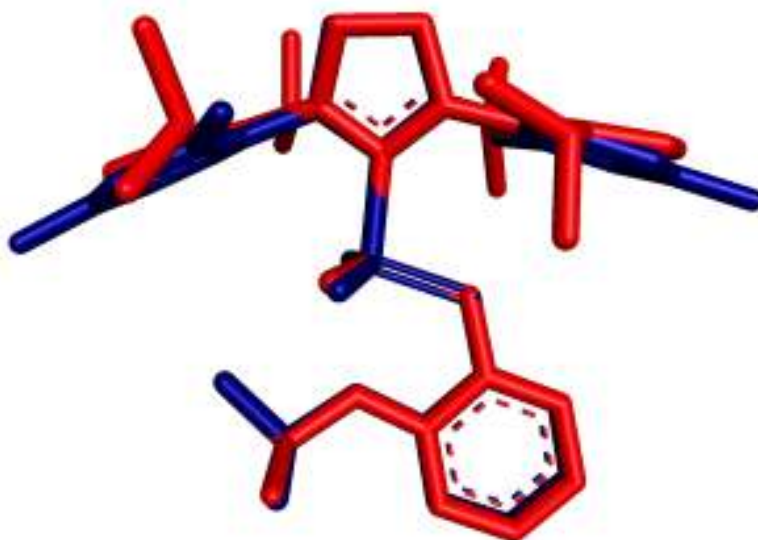


Figure 3.44. Overlaid optimised geometries (at the M06-L/6-31G* level of theory) for complexes **GH2** (blue) and **GH2-SIPr** (red).

The geometry of the lower half of each complex was very similar; the Ru-O distance was almost the same in both **GH2** (2.344 Å) and **GH2-SIPr** (2.350 Å), as was the C-Ru=C-C dihedral angle (175.97° versus 176.47° , respectively). In contrast, the conformation of the NHC ligand was quite different. The **SIMes** ligand sat lower, presumably due to less steric interaction between the *ortho*-methyl groups than between the *ortho-iso*-propyl groups in **GH2-SIPr**. In addition, the imidazolidinium ring was found to be more twisted in **SIPr** (Figure 3.45). The NHC is known to move in a way that is coupled to events occurring elsewhere around the ruthenium centre,^{53,57} so it is possible that steric bulk serves to limit this movement and perhaps increase the energies of intermediates and transition states along the potential energy surface for initiation.

The SambVca tool, developed by Cavallo *et al.*, was used to quantify $\%V_{bur}$ for these two complexes from the DFT data (Table 3.25).²²³ The values obtained suggest that, when the metal-ligand distance was set to the DFT calculated distance (as opposed to the default of 2 Å), the **SIPr** ligand exerted a far stronger steric influence on the metal centre; the difference between ligands grew to 2.7 percentage points (or 3.2 percentage points if hydrogen atoms are included) versus 0.7 to 1.1 percentage points at a metal-ligand distance of 2.00 Å for complexes **M7₁-SIMes** versus **M7₁-SIPr** and **G2-SIPr-ind** versus **G2-Ind** respectively (see Table 3.24 above). The more crowded steric environment was therefore most likely the source of the reduced initiation rate.

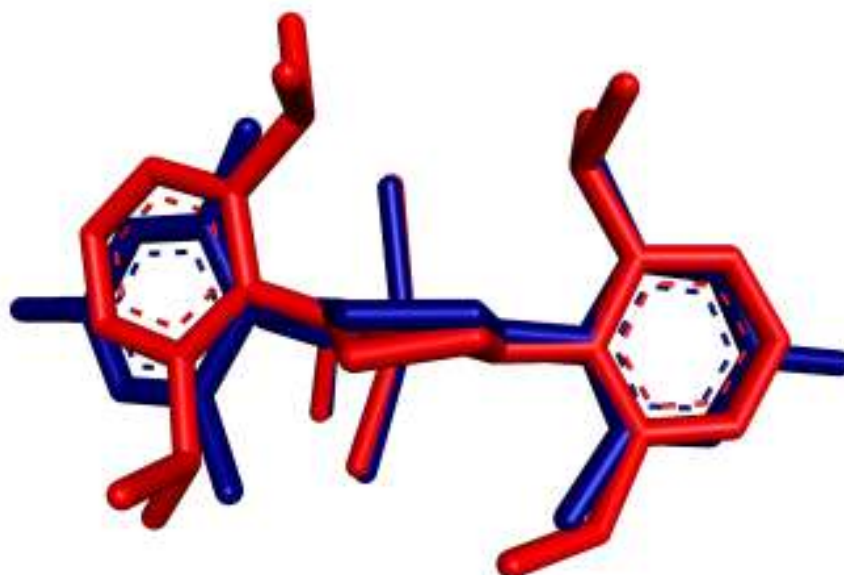


Figure 3.45. Overlaid optimised geometries (at the M06-L/6-31G* level of theory) for complexes **GH2** (blue) and **GH2-SIPr** (red).

Regardless of the mechanism(s) in operation for initiation, the steric environment would be expected to have an impact. A bulkier environment would obstruct the approach of the incoming alkene in the interchange mechanism, or disfavour the rotation of the ruthenium-carbene bond in the dissociative mechanism, where the alkoxy styrene ligand must be rotated up towards the NHC ligand. In contrast, in the analogous **G2-SIPr** pre-catalyst the phosphane dissociation occurs in a direction that is entirely away from the NHC ligand and therefore the increased initiation rate with respect to **G2** is consistent

Table 3.25. Calculated $\%V_{bur}$ values for complexes **GH2** and **GH2-SIPr**, based on density functional theory optimised geometries (M06-L/6-31G*).

Parameter	GH2		GH2-SIPr	
	H included	H excluded	H included	H excluded
Sphere radius ^a	3.5 Å	3.5 Å	3.5 Å	3.5 Å
Metal-ligand bond length ^b	1.963 Å	1.963 Å	1.957 Å	1.957 Å
Mesh size ^a	0.05 Å	0.05 Å	0.05 Å	0.05 Å
$\%V_{bur}$	36.8	35.5	40.0	38.2

^a Values recommended by Cavallo *et al.*

^b Values from DFT calculations

with a crowded steric environment around the metal centre.

DFT optimised geometries (M06-L/6-31G*) were calculated for each of the other seven pre-catalysts studied; structures for **GH2** and **GH2-SIPr** were used as a starting point, and additional functionality was built onto the ligands before re-optimisation. The values of $\%V_{bur}$ were calculated for the other seven pre-catalysts studied, and compared to their initiation rates (**Table 3.26**). Only small differences were obtained between complexes, and no trends were identified. Large differences in NHC were responsible for the difference between the two series of pre-catalysts, but the differences within those series were more likely to be due to the electronic characteristics of the chelating alkoxy styrene ligand.⁶¹ In addition, a larger basis set would better draw out smaller differences in ligand geometry between complexes.

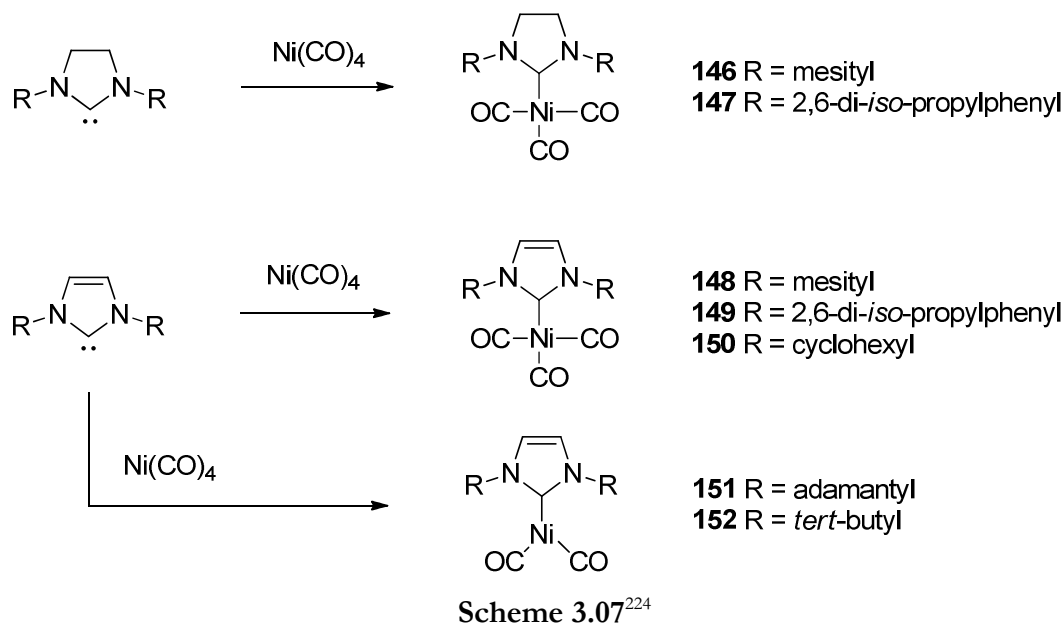
The electronic differences between the **SIMes** and **SIPr** ligands were investigated subsequently. The Tolman electronic parameter (TEP) was originally developed in order to evaluate the electronic effects that tertiary phosphane ligands exert upon metal centres;²²² using this method, complex $\text{LNi}(\text{CO})_3$ can be prepared from the ligand of interest L plus $\text{Ni}(\text{CO})_4$ and the infra-red spectrum can be acquired. While the carbonyl ligands are connected to the metal centre *via* a σ -bond, back-bonding *via* the carbonyl π^* -bond (the LUMO) can occur. Electron-rich metal centres therefore weaken the carbon-oxygen bond and lead to a corresponding decrease in the frequency

Table 3.26. Calculated $\%V_{bur}$ and Ru-C bond lengths (from the NHC ligand) from DFT-optimised geometries at the M06-L/6-31G* level of theory for pre-catalysts, and the corresponding experimentally-determined initiation rates.

Complex	k_{init} (L mol ⁻¹ s ⁻¹)	Ru-C (Å)	$\%V_{bur}$ ^a
GH2	0.0264	1.963	36.8
Grela	0.3172	1.967	37.0
Zhan 1B	0.1320	1.965	37.4
M71-SIMes	0.0851	1.964	37.0
GH2-SIPr	0.002956	1.957	40.0
Grela-SIPr	0.0368	1.965	40.4
M71-SIPr	0.0156	1.958	40.2
M831-SIPr	0.1126	1.956	40.4
M853-SIPr	0.5711	1.951	40.4

^a With sphere radius 3.5 Å, hydrogen atoms included and a mesh size of 0.05 Å

of the carbonyl vibration in the infra-red spectrum. The TEP has also been used to quantify the electronic properties of NHC ligands. Nolan *et al.* have prepared a series of (NHC)Ni(CO)₃ complexes (**146-150**) and measured their infra-red spectra, but attempts to prepare complexes based on particularly bulky NHC ligands were unsuccessful, yielding the (NHC)Ni(CO)₂ complexes (**151-152**) instead (**Scheme 3.07**).²²⁴



Subsequent studies by Nolan *et al.* have shown that (NHC)Ir(CO)₂Cl complexes can be prepared instead, which avoid the need for use of the volatile and toxic Ni(CO)₄ precursor complex.⁴¹ In addition, there was a linear correlation between the carbonyl stretching frequencies observed in the nickel and iridium complexes (**Table 3.27**, where **IPr** = bis(di-*iso*-propylphenyl)imidazolium).

In silico studies have also been carried out on these complexes. Gusev has shown that the frequency of the carbonyl stretching vibration can be obtained using density functional theory calculations (at the mPW1PW91/6-311+G(d,p) level of theory), provided the solvent is not changed.²²⁵ Notably, this approach allowed the calculation of stretching frequencies for nickel complexes that have not yet been prepared experimentally. Suresh *et al.* have shown that the molecular electrostatic potential (MEP) at the carbene carbon of NHC calculated using density functional theory (with B3LYP, BP86 and M05 functionals) is correlated to the TEP, allowing estimation of the TEP without modelling the complete metal complex itself.²²⁶

Table 3.27. Selected carbonyl ligand stretching frequencies in some $\text{LNi}(\text{CO})_3$ and $\text{LIr}(\text{CO})_2\text{Cl}$ complexes, where L is a tertiary phosphane or *N*-heterocyclic carbene;⁴¹ all IR spectra were recorded in DCM.

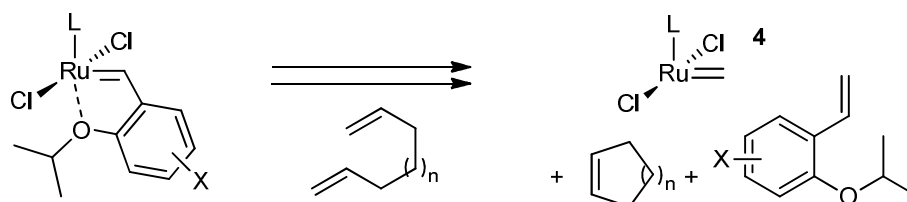
Ligand L	ν_{CO} (cm^{-1}) ($\text{LIr}(\text{CO})_2\text{Cl}$) ^a	TEP (cm^{-1}) ($\text{LNi}(\text{CO})_3$)
PPh_3	2043.5	2068.9
PEt_3	2037.5	2061.7
$\text{P}(\text{Pr})_3$	2031.5	2059.2
PCy_3	2028.0	2056.4
SIMes	2024.6	2051.5
SIPr	2024.9	2052.2
IMes	2023.1	2050.7
IPr	2023.9	2051.5

^a Average of the two carbonyl stretching vibrations

The electronic properties of the **SIMes** and **SIPr** are therefore well known, with the latter donating slightly less electron density onto the metal centre ($\Delta\text{TEP} = 0.7 \text{ cm}^{-1}$). This may strengthen the Ru-O interaction slightly, and therefore result in slower pre-catalyst initiation, during which this bond must be broken. DFT studies on the initiation event with both pre-catalysts could potentially yield better insight into exactly why the *ca.* ten-fold rate difference exists.

Initiation Rate *versus* Metathesis Activity

With initiation rates in hand for the pre-catalysts selected for this study, the effects of pre-catalyst structure on the rate of metathesis were explored. All of the pre-catalysts studied converge upon one of two intermediate methyldiene species; those pre-catalysts bearing a **SIMes** ligand will generate methyldiene **4b** after one turnover, while those bearing a **SIPr** ligand will generate the analogous methyldiene **4c** (Scheme 3.08). These



Scheme 3.08

two species possess different metathesis activity, so for a given NHC ligand the metathesis activity of the pre-catalyst should be directly related to the initiation rate.

The metathesis of 1,7-octadiene (10 mmol L⁻¹ in DCM-*d*₂ with 1 mol% pre-catalyst) was selected as a model reaction. This reaction proceeds smoothly to completion at 298 K to yield only cyclohexene and ethene as products.^{90,187} Concentration/time profiles for the RCM reactions with **GH2**, **GH2-SIPr**, **Grela**, **Grela-SIPr**, **Zhan1B**, **M8₃₂-SIPr** and **M8₃₃-SIPr** were collected by ¹H NMR spectroscopy using the method described in Chapter 2 (**Figure 3.46**). A 600 MHz NMR spectrometer was utilised to achieve maximum data density, as these reactions were typically quite fast; all reaction *t*_{1/2} were 20 minutes or less. These profiles show that for a given NHC ligand, the activity in the RCM reaction was determined by the initiation rate (**Grela** > **Zhan** > **GH2**; **M8₃₃-SIPr** > **M8₃₁-SIPr** > **Grela-SIPr** > **GH2-SIPr**).

This result was similar to that obtained by Grubbs *et al.* in their study of **G2** analogues.⁵⁸ When triarylphosphanes were functionalised with various groups and used to prepare pre-catalysts **153-158**, the initiation rate was found to change, with more electron-withdrawing groups accelerating the pre-catalyst initiation event. The ROMP of

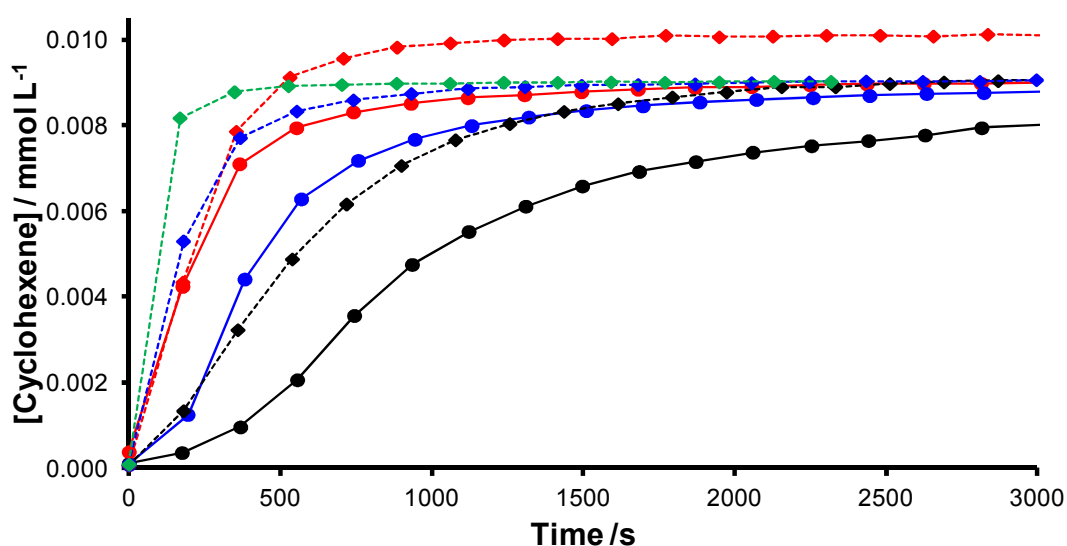


Figure 3.46. Concentration *versus* time profiles of the RCM of 1,7-octadiene (10 mmol L⁻¹ in DCM-*d*₂) with 0.1 mmol L⁻¹ of pre-catalysts **GH2** (black circles), **Zhan1B** (blue circles), **Grela** (red circles), **GH2-SIPr** (black rhombi), **Grela-SIPr** (red rhombi), **M831-SIPr** (blue rhombi), **M853-SIPr** (green rhombi). Lines are drawn only as a visual aid and do not represent data-fitting.

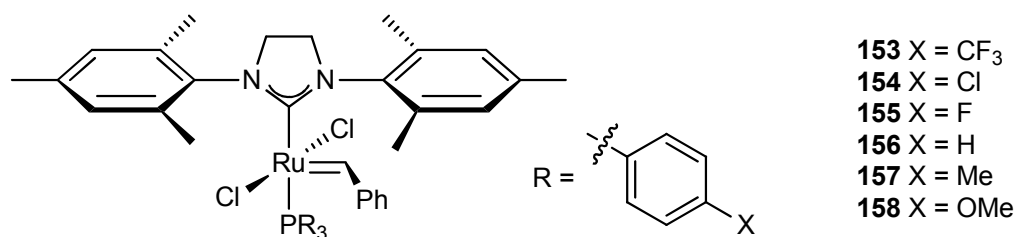


Table 3.28. Initiation rates at 353 K in toluene (from ^{31}P NMR magnetisation transfer experiments) and relative rates in the ROMP reaction of 1,5-cyclooctadiene for pre-catalysts **153-158**.⁵⁸

Complex	X	k_{init} (s ⁻¹) at 80 °C	rel. k_{init} at 80 °C ^a	rel. k_{ROMP} at 20 °C ^a
153	CF ₃	48 ± 2	6.40	6.8
154	Cl	17.9 ± 0.4	2.39	1.9
155	F	8.5 ± 0.2	1.13	1.0
156	H	7.5 ± 0.6	1.00	1.0
157	Me	4.1 ± 0.2	0.55	0.4
158	OMe	1.8 ± 0.1	0.24	0.2

^a Relative to **157** (X = H)

cyclooctadiene (COD) was used by Grubbs *et al.* as a test reaction for each of the pre-catalysts, which displayed ROMP activity proportional to the pre-catalyst initiation rate because the same alkylidene species is generated in each case (**Table 3.28**).

In the profiles in **Figure 3.46** that were acquired for the RCM of 1,7-octadiene with Hoveyda-type pre-catalysts, dramatic differences between **SIMes**-bearing and **SIPr**-bearing pre-catalysts were revealed. The latter species were far more active in this RCM reaction, despite the generally lower (by up to 9-fold) initiation rate when compared to their **SIMes**-bearing analogues. This is a considerable effect, resulting in order(s) of magnitude differences both in initiation rate and metathesis rate. While the precise origin of this effect is currently under investigation, it must arise from a reaction step common to all pre-catalysts, and is therefore most likely due to lower barrier(s) on the PES for the reaction of the corresponding methyldiene **4** with 1,7-octadiene. This difference in activity between complexes **4b** and **4c** could be probed using DFT, for example, as the reaction of methyldiene **4b** with 1,7-octadiene has already been explored in detail using the M06-L density functional.⁵³

These concentration/time profiles were used to quantify the different metathesis

rates for pre-catalysts bearing the two different NHC ligands. Modifications to the model were necessary to reflect the different initiation mechanism in operation. The initiation of **GH2** and analogues was modelled as a single-step, irreversible process that consumes one molecule of alkene and produces one molecule of product, therefore the model was constructed according to **Equations 3.37 – 3.40**.

$$d[\text{pre-catalyst}]/dt = -k_i \cdot [\text{pre-catalyst}] \cdot [\mathbf{103c}] \quad (3.37)$$

$$d[\text{catalyst}]/dt = k_i \cdot [\text{pre-catalyst}] \cdot [\mathbf{103c}] \quad (3.38)$$

$$d[\mathbf{103c}]/dt = -k_i \cdot [\text{pre-catalyst}] \cdot [\mathbf{103c}] - k_2 \cdot [\text{catalyst}] \cdot [\mathbf{103c}] + k_2 \cdot [\text{catalyst}] \cdot [\mathbf{104c}] \quad (3.39)$$

$$d[\mathbf{104c}]/dt = k_i \cdot [\text{pre-catalyst}] \cdot [\mathbf{103c}] + k_2 \cdot [\text{catalyst}] \cdot [\mathbf{103c}] - k_2 \cdot [\text{catalyst}] \cdot [\mathbf{104c}] \quad (3.40)$$

A different k_i was used for each pre-catalyst, while a common k_2 and k_2 were used for all reactions. The value of k_i will depend on the structure of the metathesis substrate. However, Plenio *et al.* have shown that the initiation rates of **GH2** with butyl vinyl ether and 1-hexene are very similar;⁶¹ larger alkenes such as diethyl diallylmalonate and styrene were found to initiate pre-catalysts more slowly. Therefore, ethyl vinyl ether and 1,7-octadiene ought to initiate these pre-catalysts at approximately the same rate, so the measured initiation rates were used to fix k_i values in the fitting unless stated otherwise.

The different metathesis rates with methyldiene complexes **4b** and **4c** were evaluated. Concentration/time data for the 1,7-octadiene RCM reactions with **GH2** and **GH2-SIPr** in DCM- d_2 were fitted separately, with fixed k_i values and fitted k_2 and k_2 values (**Figure 3.47** and **Table 3.29**). These results have quantified, for the first time, the difference in metathesis activity between methyldiene complexes **4b** and **4c**; the relative k_2 values allow a relative metathesis rate of 25.2 to be calculated. This difference

Table 3.29. Rate constants obtained from fitting concentration/time data for the RCM of 1,7-octadiene (10 mmol L⁻¹ with 1 mol% of either **GH2** or **GH2-SIPr** at 298 K in DCM- d_2) to the model described by **Equations 3.35 to 3.38**.

Pre-Catalyst	k_i (s ⁻¹) (fixed)	k_2 (L mol ⁻¹ s ⁻¹)	k_2 (L mol ⁻¹ s ⁻¹)	k_{rel}
GH2	0.0264	80.17	11.91	1.0
GH2-SIPr	0.002956	2022	91.46	25.2

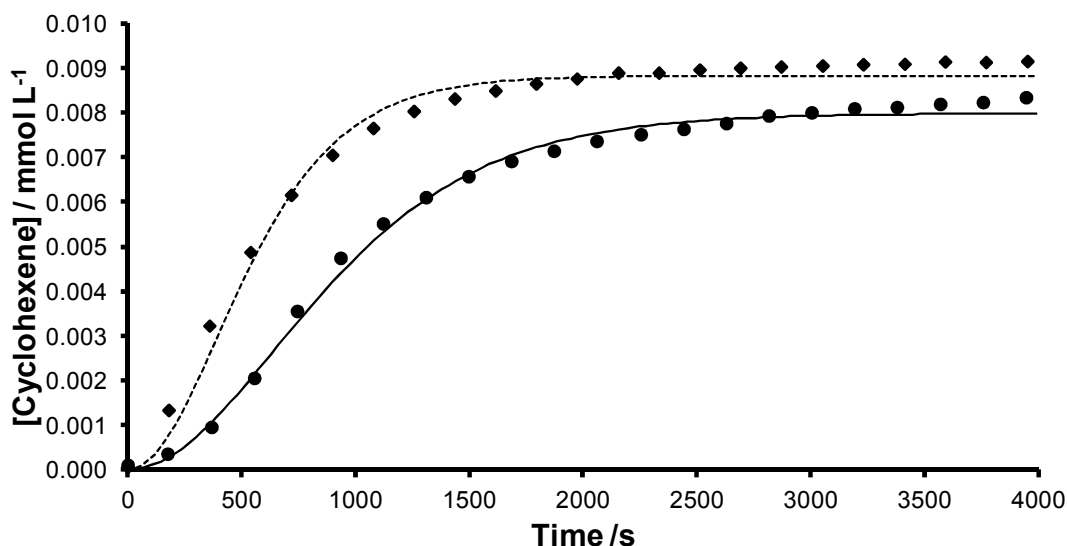


Figure 3.47. Experimental (points) and simulated (lines) concentration/time profiles for cyclohexene in the RCM of 1,7-octadiene (10 mmol L⁻¹) in DCM-*d*₂ at 298 K with 1 mol% of either (a) **GH2** (circles, solid line) or (b) **GH2-SIPr** (rhombi, dashed line).

was considerable, and suggested a *ca.* 1.9 kcal mol⁻¹ decrease in the energetic span of the catalytic cycle.¹⁷⁴ With this rate difference quantified, a second issue to address was whether the activity of a series of pre-catalysts bearing the same NHC exhibited relative activity that was dependent only on initiation rate. Qualitatively, the order of metathesis activity was the same as that of initiation rate, but decoupling of the initiation and metathesis rates was required to address the issue quantitatively. The kinetic data from all 1,7-octadiene RCM reactions were fitted to the kinetic model simultaneously; the value of k_7 for each pre-catalyst was fixed in the simulation, with shared rate constants k_2 and k_{rel} for each series of pre-catalyst (i.e. per NHC ligand). The rate constants in **Table 3.30** were obtained. This set of results suggested slightly different k_{rel} values than

Table 3.30. Rate constants for the metathesis event with **SIMes**-bearing and **SIPr**-bearing pre-catalysts, obtained from fitting concentration/time data for the RCM of 1,7-octadiene (10 mmol L⁻¹ in DCM-*d*₂ with 1 mol% pre-catalyst at 298K) with **GH2**, **Grela**, **Zhan**, **GH2-SIPr**, **Grela-SIPr**, **M8₃₂-SIPr** and **M8₅₃-SIPr**.

NHC	k_2 (L mol ⁻¹ s ⁻¹)	k_{rel} (L mol s ⁻¹)	k_{rel}
SIMes	83.67	6.337	1
SIPr	1160	33.30	13.9

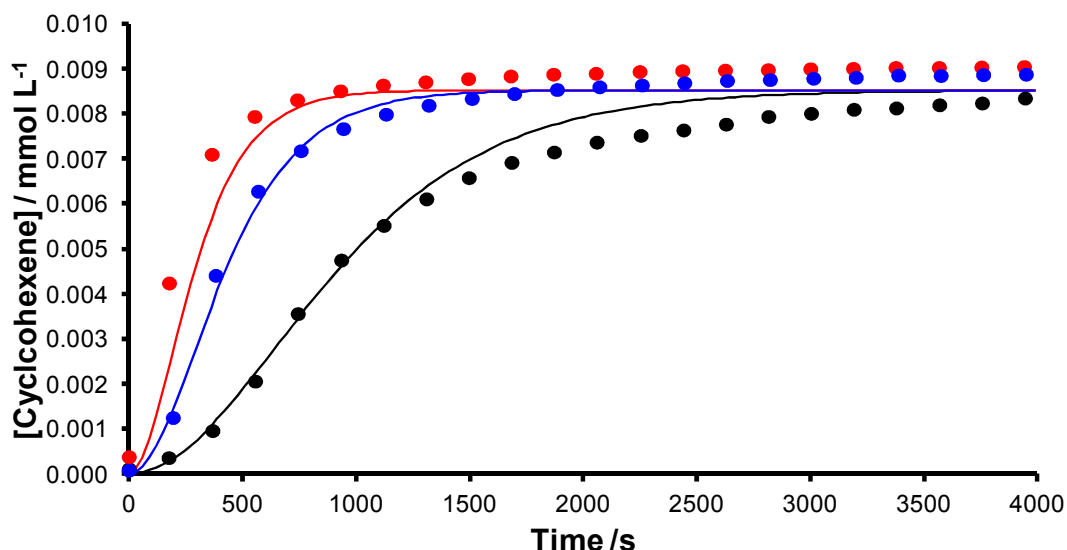


Figure 3.48. Experimental (points) and simulated (lines) concentration/time profiles for cyclohexene in the RCM of 1,7-octadiene (10 mmol L⁻¹) in DCM-*d*₂ at 298 K with either 1 mol% (a) **GH2**, (b) **Zhan1B** or (c) **Grela**.

the rate constants in **Table 3.29**, which were obtained by fitting concentration/time data obtained with **GH2** and **GH2-SIPr**. The rate constants in **Table 3.30** are effectively a multi-point determination of k_2^{SIMes} and k_2^{SIPr} ; pleasingly, the simulations for **SIMes**-bearing pre-catalysts yielded a good fit to the experimental concentration *versus* time data (**Figure 3.48**). The simulation correctly modelled the concentration/time profiles of reactions with all three pre-catalysts when the values of k_i were fixed, showing that the difference in overall reaction rate resulted only from the different initiation rates. The simulated reaction end points (i.e. the final concentrations of cyclohexene) underestimated the degree of overall conversion; K_2^{SIMes} was calculated to be 13.2. This most likely arose because the model is only a simplification of the full mechanism, so k_2 was used to fit the shape of the concentration/time profile, resulting in an under-estimate of final conversion.

The simulated profiles for 1,7-octadiene RCM with the SIPr-bearing pre-catalysts were not in as good agreement with the experimental data (**Figure 3.49**). The simulations for **M8₃₂-SIPr** and **M8₅₃-SIPr** slightly overestimated the rate of metathesis (simulated $t_{1/2} \approx 0.75 \times$ experimental $t_{1/2}$). As these pre-catalysts initiate rapidly ($k_i = 0.1126$ L mol⁻¹ s⁻¹ for **M8₃₂-SIPr** and $k_i = 0.5711$ L mol⁻¹ s⁻¹ for **M8₅₃-SIPr**), and lead to the most active methyldiene complex (**SIPr**-bearing **4c**) it is possible that a step on the

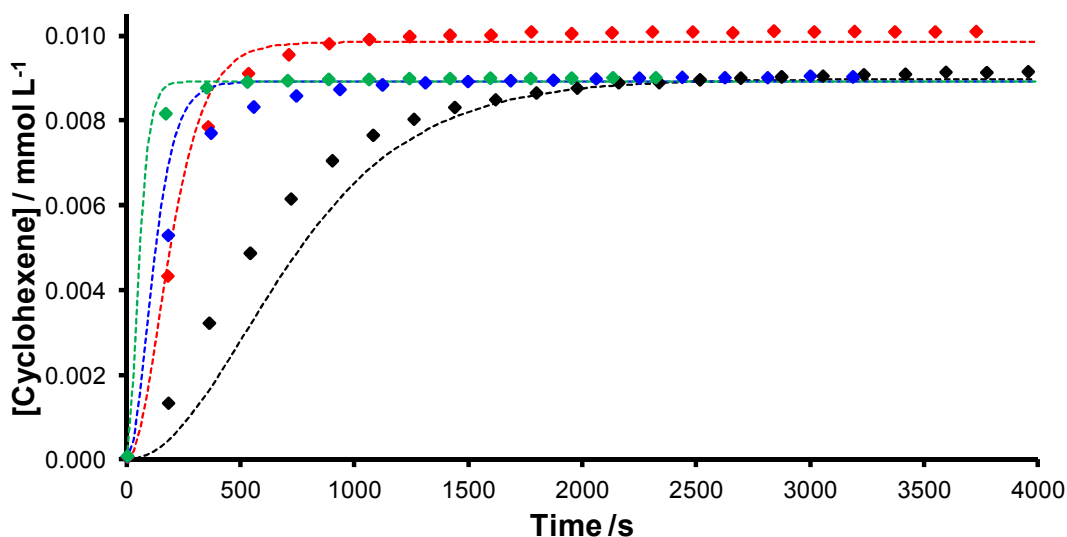


Figure 3.49. Experimental (points) and simulated (lines) concentration/time profiles for cyclohexene in the RCM of 1,7-octadiene (10 mmol L^{-1}) in $\text{DCM-}d_2$ at 298 K with either 1 mol% (a) **GH2-SIPr**, (b) **Grela-SIPr**, (c) **M8₃₂-SIPr** or (d) **M8₅₃-SIPr**.

metathesis pathway has become rate-determining. The model only considers two steps (pre-catalyst initiation and the metathesis step), so it cannot account for this difference.

These results demonstrated the utility of the kinetic model for pre-catalyst assessment, informed by only two experiments: the initiation rate measured by UV/vis spectroscopy, and an RCM concentration/time profile collected *via* ^1H NMR spectroscopy. Further use of this model can be envisioned for assessing the effects of different NHC ligands on catalytic activity, or for quantitatively assessing the effect of changing the pre-catalyst for a given RCM reaction.

Solvent Effects

Solvent choice is an important consideration for alkene metathesis, especially when reactions are to be conducted on a large scale. While toluene and DCM are favoured in the laboratory for relatively small (up to gram) scale syntheses, such solvents are unacceptable on a large (kilogram to ton) scale where safety, ecological and economic factors are important issues.¹⁷⁰ The use of different solvents for metathesis was explored using **G2** and **GH2**, which are the two most popular pre-catalysts in use currently.

DCM and toluene are most commonly employed for RCM reactions, although dichloroethane, chloroform and benzene are closely related analogues of these solvents

and have also been used. Grela *et al.* have investigated the effects of fluoroaromatic solvents on RCM reactions, reporting that metathesis proceeded more quickly and with higher isolated yields in perfluoroaromatic solvents than in aromatic or chlorinated solvents.²²⁷⁻²²⁸ Such perfluoroaromatic solvents are considerably more expensive, so solvent recycling would be a necessity: hexafluorobenzene is more than twenty-fold more expensive per litre than toluene at the time of writing. More environmentally acceptable yet still cost-effective solvents have been proposed in the literature for metathesis reactions. MTBE was used by Grubbs *et al.* in high-throughput studies of metathesis reactions using low loadings of pre-catalysts.¹⁵⁷ It was proposed that, at low catalyst concentrations, MTBE led to a reduced rate of catalyst decomposition compared to traditional metathesis solvents such as DCM and toluene. Dixneuf *et al.* have shown that dimethyl carbonate (DMC) can be used in place of DCM in metathesis reactions, resulting in similar RCM rates and yields.¹⁹⁷

Despite the use of various solvents in the literature, there has not yet been a robust and quantitative comparison of different solvents for alkene metathesis. Use of the reaction simulation approach should allow the solvent effects on the initiation step (with rate constant k_1) to be decoupled from those on the actual metathesis step (with rate constant k_2). A robust single study of solvents for alkene metathesis also provides an opportunity to probe more closely the actual solvent properties that determine pre-catalyst initiation rate and metathesis rate. Adjiman *et al.* used solvatochromic parameters in order to try to understand those solvent properties most important in metathesis.¹⁶⁶ As discussed in this chapter, the rate constants used in the published study were obtained from unconstrained fitting of data, and therefore are not reliable.⁹⁷

Several solvents were selected for this study. DCM and toluene were included, as these are most commonly used in metathesis and were available anhydrous from the in-house solvent purification system. Chloroform and benzene were also studied, although neither of these solvents is acceptable on scale. Environmentally friendly DMC was studied, as well as MTBE. Three fluorinated aromatic solvents were included: trifluorotoluene, hexafluorobenzene and 1,2-difluorobenzene; perfluoroaromatic solvents have been reported to improve reaction rate²²⁷⁻²²⁸ and 1,2-difluorobenzene has a high dielectric constant ($\epsilon = ca. 14$).^{210,214} The melting points, boiling points, dipole moments, dielectric constants and polarities are recorded in **Table 3.31**, along with the current regulatory and legislative status (for pharmaceutical syntheses). Only DMC and

Table 3.31. Solvents used in this study, plus selected physical properties and regulatory/legislative status.

Property	Benzene	Chloroform	DCM	1,2-Difluorobenzene	Dimethyl carbonate	Hexafluorobenzene	Methyl <i>tert</i> -butyl ether	Toluene	α , α -Trifluorotoluene
MP	6	-64	-95	-34	-1	5	-109	-95	-29
BP	80	61	40	92	91	80	55	111	102
ϵ_r ^a	2.27 ^b	4.89	9.02	14.26	3.17	2.05	4.5 ^c	2.43	9.40
Regulatory/ Legislative ^d	Not permitted	Not permitted	Not permitted	-	Permitted	-	Permitted	Future issues	Not permitted

^a From reference²¹⁴ at 293 K unless stated otherwise

^b At 298 K ^c From ref.²⁰⁹ ^d From ref.¹⁷⁰

MTBE are currently acceptable in large-scale synthetic projects, but no data is currently available for 1,2-difluorobenzene or hexafluorobenzene.

It has been suggested previously (by Grubbs *et al.*)²⁶ that initiation rate might be related to solvent dielectric constant. The solvents selected here cover a wide range of dielectric properties (from 2.05 to 14.26) and so allow this suggestion to be tested.

DCM and toluene were obtained from the in-house solvent purification system, while benzene, DMC, MTBE and trifluorotoluene were purchased as anhydrous. Chloroform was dried by passage through a column of activated alumina. 1,2-Difluorobenzene and hexafluorobenzene were distilled from calcium hydride onto activated 4 Å molecular sieves. Benzene-*d*₆, chloroform-*d*, DCM-*d*₂ and toluene-*d*₈ were dried overnight on activated 4Å molecular sieves before use.

Initiation rates were measured for each of **G2** and **GH2** in each of the solvents. For **G2**, rates were measured using the method described by Grubbs *et al.* as described previously; the reaction of *ca.* 15 mmol L⁻¹ pre-catalyst with *ca.* 0.5 mol L⁻¹ of freshly-distilled ethyl vinyl ether was monitored and the decay of the pre-catalyst ¹H resonance

at *ca.* 19.2 ppm¹⁰ was fitted to a first-order expression. Reactions were typically followed for *ca.* 3 $t_{1/2}$. Not all of the solvents studied were available as perdeuterated analogues, so 10% *v/v* chloroform-*d* was added to provide a lock signal for reactions in 1,2-difluorobenzene, DMC, hexafluorobenzene, MTBE and trifluorotoluene. The reaction in DCM was conducted twice in order to assess the effects of the presence of chloroform-*d*: once in DCM- d_2 and once in a 90/10 *v/v* mixture of DCM- d_2 /chloroform-*d*. Rate constants are recorded in **Table 3.32**. Poorer R² values were typically obtained for reactions in protonated solvents due to the need for manual locking and shimming of the instrument and the reduced receiver gain. The presence of 10% *v/v* chloroform-*d* appeared to significantly change the rate of initiation in DCM- d_2 ($1.1 \times 10^{-4} \text{ s}^{-1}$ *versus* $1.4 \times 10^{-4} \text{ s}^{-1}$ for neat DCM- d_2). Repeating these experiments with benzene- d_6 as the lock solvent would allow a lower proportion of deuterated solvent to be used, as it contains six moles of deuterium per mole of solvent rather than one, and the use of solvent suppression techniques would overcome the issue of sensitivity.

Initiation rates for **GH2** were measured by monitoring the reaction of 0.1 mmol L⁻¹ **GH2** with ethyl vinyl ether (at concentrations of 25 – 200 mmol L⁻¹) at 298 K according to the published procedure.¹⁹¹ Plots of k_{obs} *versus* [ethyl vinyl ether] forced

Table 3.32. Initiation rates for **G2** in various solvents measured by reaction of **G2** with ethyl vinyl ether at 298 K in the magnet of an NMR spectrometer.

Solvent	k_{init} (s ⁻¹)	rel. k_{init} ^a	R ²	$t_{monitored}/t_{1/2}$
Benzene- d_6	1.0×10^{-4}	0.71	0.9998	3.0
Chloroform- d^b	4.5×10^{-5}	0.32	0.9996	1.8
DCM- d_2^b	1.4×10^{-4}	1.00	0.9998	2.5
DCM- d_2^c	1.1×10^{-4}	0.79	0.9999	3.0
1,2-Difluorobenzene ^c	1.4×10^{-4}	1.00	0.9824	3.0
Dimethyl carbonate ^c	1.5×10^{-4}	1.07	0.9629	3.0
Hexafluorobenzene ^c	3.3×10^{-5}	0.24	0.9993	0.9
Methyl <i>tert</i> -butyl ether ^c	1.3×10^{-4}	0.93	0.9728	3.0
Toluene- d_8	9.2×10^{-5}	0.66	0.9995	3.0
Trifluorotoluene ^c	1.3×10^{-4}	0.93	0.9985	3.0

^a Relative to reaction in DCM- d_2 with no chloroform-*d* added

^b Reported in reference⁹⁷

^c Containing 10% *v/v* chloroform-*d* to enable a deuterium lock

Table 3.33. Initiation rates for **GH2** in various solvents at 298 K.

Solvent	k_{init} (L mol ⁻¹ s ⁻¹)	rel. k_{init} ^a	R ²
Benzene	0.0460	1.74	0.9982
Chloroform	0.0231 ^b	0.88	0.9985
DCM	0.0264 ^c	1.00	0.9998
1,2-Difluorobenzene	0.0390	1.48	0.9964
DMC	0.0411	1.56	0.9975
Hexafluorobenzene	0.0515	1.95	0.9631
MTBE	0.0592	2.24	0.9878
Toluene	0.0509	1.93	0.9887
Trifluorotoluene	0.0446	1.69	0.9910

^a Relative to DCM^b Reported in reference⁹⁷^c Reported in reference¹⁹¹

through zero were linear (see **Figures 3.37** and **3.38** previously in this chapter), and yielded the second-order rate constant k_{init} in each solvent (**Table 3.33**).

Only very modest differences in initiation rate for both **G2** and **GH2** were observed. For pre-catalyst **G2**, most solvents led to initiation rates of *ca.* 1.0 – 1.5 x 10⁻⁴ s⁻¹. Chloroform-*d* and hexafluorobenzene were the only solvents where a significant initiation rate difference was obtained. The particularly low initiation rate of **G2** in hexafluorobenzene is of note due to the claimed improved performance of metathesis reactions in this solvent.²²⁷⁻²²⁸ Any performance improvement must therefore arise from an increased rate for the metathesis step and/or a decreased rate of catalyst decomposition, or for practical reasons such as easier work-up and isolation. For pre-catalyst **GH2** a *ca.* 2-fold difference was obtained between chlorinated and aromatic solvents, but the overall range of reaction rates was very modest (0.0231 L mol⁻¹ s⁻¹ for chloroform to 0.0592 L mol⁻¹ s⁻¹ for methyl *tert*-butyl ether). These results show clearly that dielectric constant and pre-catalyst initiation rate are not correlated (**Figure 3.50**). In addition, different trends are revealed for each pre-catalyst, which is most likely a consequence of the different ways in which they must initiate.

Alternative methods were explored in order to probe the solvent effects quantitatively. Adjiman *et al.* fitted the rate constants in **Table 3.01** to a series of solvent properties (see **Equation 3.06**). Kamlet-Taft solvatochromatic parameters α , β and π^* (or A , B and S) represent the solvent hydrogen bond donor acidity, hydrogen bond

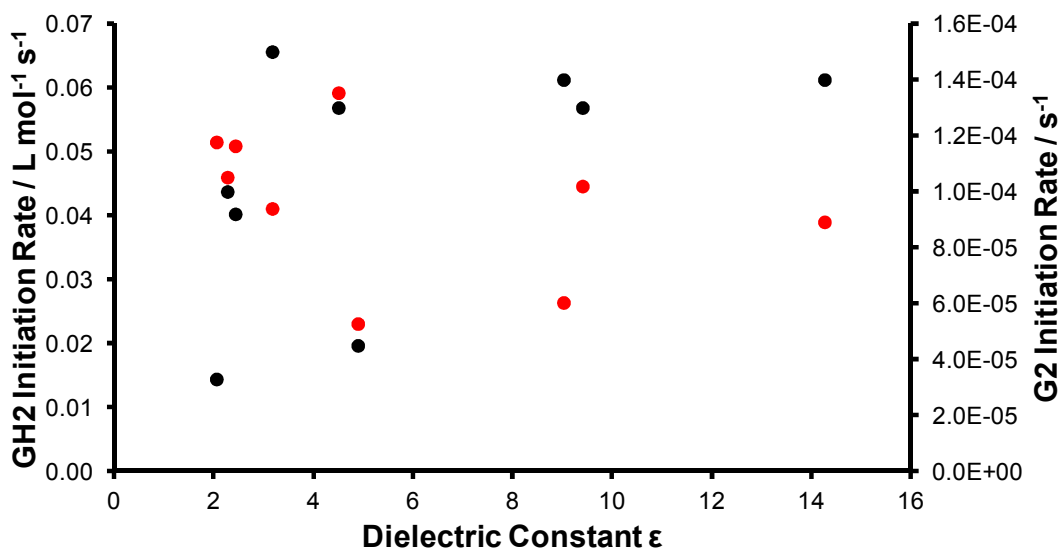


Figure 3.50. Initiation rates for **G2** (black) and **GH2** (red) *versus* dielectric constant ϵ (see **Tables 3.31, 3.32** and **3.33**).

acceptor basicity and solvent dipolarity/polarisability respectively.¹⁹⁵ The parameter δ is a solvent polarisability correction term, while δ_H^2 is the cohesive energy density (δ_H is also known as the Hildebrand solubility parameter).¹⁹⁶ Multiple linear regression can be used to assess the impact on the rate of each of these properties. Various data are available for the properties of a number of solvents, however α , β and π^* have only been reported for benzene, chloroform, DCM and toluene.^{195,214} As six parameters are required from a linear regression, six sets of data would be required to perform a multiple regression. Unfortunately, only four datasets are available (**Table 3.34**).

Various solvent polarity scales have been utilised other than the dielectric constant (or relative permittivity as it is also known).²²⁹ The concept of polarity is a complex one, and can represent various microscopic (hydrogen-bond acceptor and hydrogen-bond donor ability, for example) and macroscopic (dielectric constant, for example) solvent properties. However, data for all nine solvents used in this study are not available for most polarity scales and for this reason quantitative insights into the solvent effects on the initiation rate of **GH2** and analogues are somewhat limited.

Reichart's $E_T(30)$ scale, which employs the wavelength of the absorption maximum of dye **159** as an indicator of solvent polarity has been determined for a large number of solvents.²³⁰ This scale has been

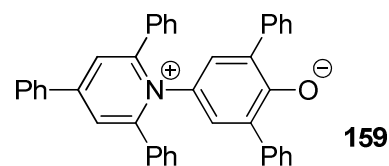


Table 3.34. Relative initiation rates for **GH2** in different solvents, plus some solvatochromic parameters and Hildebrand solubility parameter for those solvents.^{195,214}

Solvent	rel. k_{init} ^a	α	β	π^*	δ_H
Benzene	1.74	0.00	0.10	0.59	18.8
Chloroform	0.88	0.34	0.00	0.58	18.9
DCM	1.00	0.22	0.00	0.82	20.3
1,2-Difluorobenzene	1.48	-	-	-	18.4
DMC	1.56	-	0.38	-	19.5
Hexafluorobenzene	1.95	-	-	-	17.0
MTBE	2.24	-	-	-	15.2
Toluene	1.93	0.00	0.11	0.54	18.2
Trifluorotoluene	1.69	-	-	-	16.9

applied in analytical chemistry to describe the changes in retention time in chromatography, and as an indicator of solvent water content;²³¹ $E_T(30)$ is sensitive to the water content of aprotic solvents. In the context of chemical kinetics, the rate of the S_N2 reaction between 1,3-dimethylimidazole and benzyl bromide has been measured in various solvents, with correlations between rate and $E_T(30)$;²³² however, protic and aprotic solvents were considered separately. Correlations have been established between the rates of steps in ligand substitution processes in β -diketone iron complexes and $E_T(30)$.²³³ In both of the kinetics examples, the $E_T(30)$ range of the solvents studied was *ca.* 15 kcal mol⁻¹.

A plot of **GH2** initiation rate *versus* $E_T(30)$ shows a correlation (albeit it with considerable noise) (**Figure 3.51**) but no such correlation was obtained with pre-catalyst **G2**. This suggested that less polar solvents (according to this polarity scale) resulted in higher initiation rates. Measurement of initiation rate constants in a wider range of solvents would be necessary to confirm whether this trend holds across the range of $E_T(30)$, as the solvents studied here have $E_T(30)$ values of *ca.* 34-35 and 38-41 only, and cover only an 8 kcal mol⁻¹ range in total.

While the effect of different solvents on the rate of pre-catalyst initiation can be measured directly, the same cannot be achieved for the actual metathesis step, which is the reaction of the methyldene complex with the alkene substrate. Simulation experiments were carried out to explore whether the solvent effect on pre-catalyst

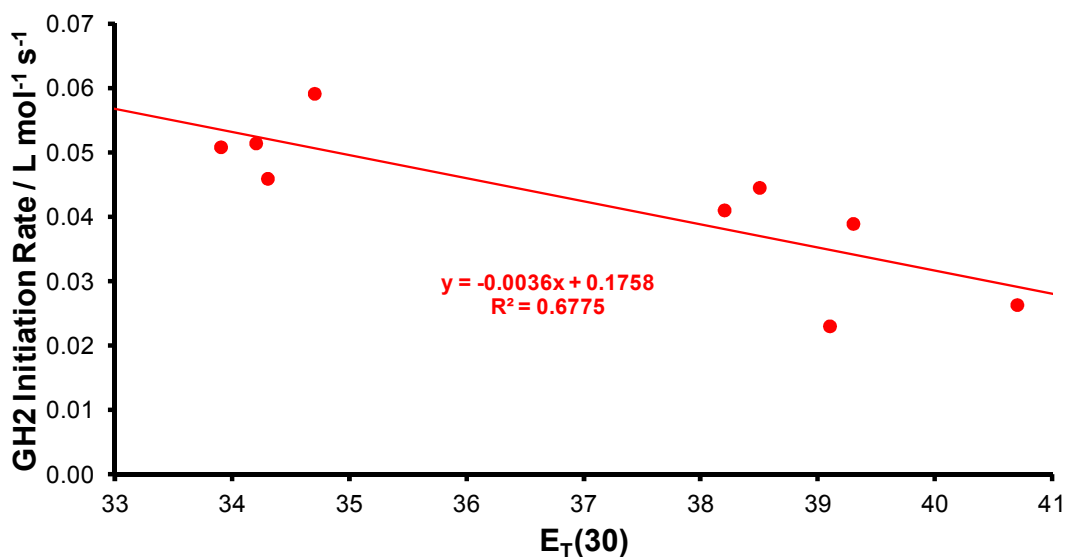


Figure 3.51. Initiation rate of **GH2** versus solvent $E_T(30)$.

initiation accounted for the overall difference in the rate of reaction.

The data above establish that there are modest solvent effects on the initiation rate of **G2** and **GH2**. However, once the pre-catalyst has turned over to methyldiene, do subsequent metathesis cycles occur at the same rate regardless of solvent? If so, then simulated profiles for the same reaction in different solvents should fit the experimental concentration/time data using common rate constants for the metathesis step (i.e. k_2/k_{-2}) but different values for rate constants that describe pre-catalyst initiation (i.e. k_1/k_{-1} for **G2** and k_1 for **GH2**). If not, then such a fit should not be possible.

Concentration versus time data for the reactions of 1,6-heptadiene and 1,7-octadiene (10 mmol L^{-1} with 1 mol% **G2**) in chloroform- d and DCM- d_2 were imported into Berkeley Madonna and fitted to the model in **Scheme 3.03**; each experiment was conducted in duplicate. The initiation rate k_1 for **G2** was fixed to the measured value for each solvent (see **Table 3.32**) and a different value of k_2 and k_{-2} were used for each substrate (denoted k_2^5 , k_{-2}^5 and k_2^6 , k_{-2}^6 for 1,6-heptadiene and 1,7-octadiene respectively). As described above, the same k_2 and k_{-2} constants were used in both solvents, reasoning that if the difference in overall reaction rate lay in the initiation rate alone then a good fit should be obtained. A good fit to the experimental concentration versus time profile was obtained (**Table 3.35** and **Figure 3.52**; only one replicate of each dataset is presented in **Figure 3.52** for clarity). This result suggests that any solvent effect on the metathesis step itself is very small. Accounting for the known (and

Table 3.35. Rate constants obtained from fitting experimental concentration *versus* time data for the RCM reactions of 1,6-heptadiene and 1,7-octadiene (with 1 mol% **G2** at 298 K) in chloroform-*d* and DCM-*d*₂ (each in duplicate) to the model.

Solvent	k_1 / s^{-1} (fixed)	k_{-1} ^a	k_2^5 ^a	k_{-2}^5 ^a	k_2^6 ^a	k_{-2}^6 ^a
Chloroform	4.5×10^{-5}	1262	258	3.93	473	1.49
DCM	1.4×10^{-4}	1278				

^a Units $\text{L mol}^{-1} \text{s}^{-1}$; values obtained through fitting and quoted to three significant figures

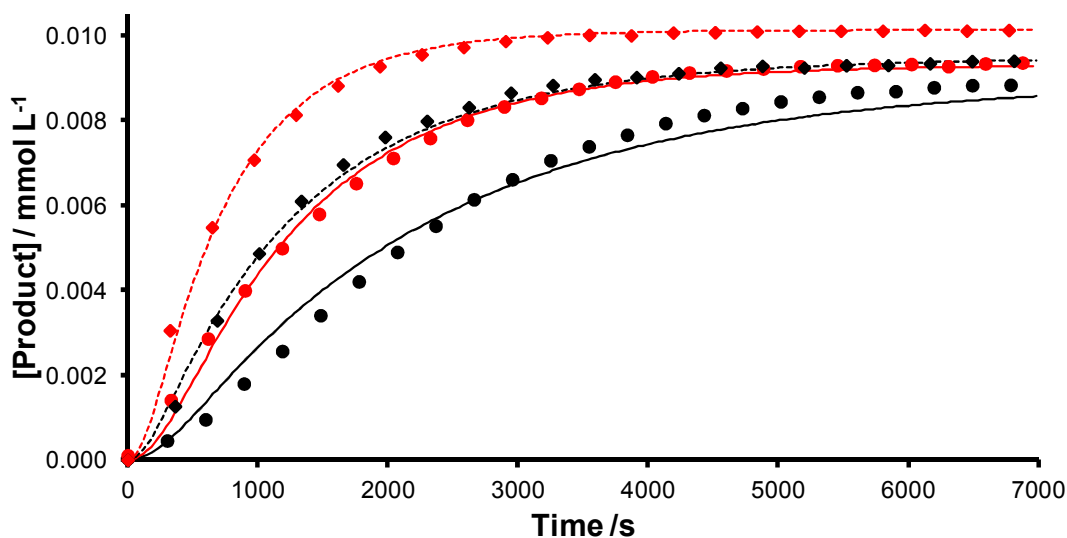


Figure 3.52. Simulated (lines) *versus* experimental (points) concentration *versus* time profiles for the products of the RCM reactions of 1,6-heptadiene (**black**) and 1,7-octadiene (**red**) (10 mmol L^{-1} with 1 mol% **G2** at 298 K) in (a) chloroform-*d* (circles) and (b) DCM-*d*₂ (rhombi); simulations were generated with shared k_2 and k_{-2} values for each substrate.

measured) difference in initiation rate successfully explains the overall difference in reaction rate. Chloroform and DCM are structurally quite similar so further comparisons, with reactions in benzene and/or toluene for example, would potentially yield further interesting insight into the effects of solvent on various stages of the reaction mechanism. However, if the metathesis rate is insensitive to the choice of solvent, large-scale metathesis reactions could potentially be carried out in more acceptable solvents (such as MTBE for example) without a significant impact on overall reaction rate and/or product yield.

Conclusions

A reaction simulation approach to the RCM reaction of model substrate diethyl diallylmalonate published in the literature has been thoroughly evaluated, and found to be unreliable due to a lack of constraint; for a given dataset, it was possible to obtain multiple sets of rate constants which yielded simulated concentration *versus* time profiles that were equally good fits to the experimental data. Fitting multiple datasets simultaneously, which were obtained from reactions conducted with various initial substrate concentrations and pre-catalyst loadings, did not allow suitable constraint of the model. A set of rate constants that described all of the datasets equally well was not obtained. Constraining the model using measured initiation rates (determined from the reaction of **G2** with ethyl vinyl ether) allowed a range of different reaction conditions to be described, provided that a suitably narrow concentration range was explored. This rendered the model suitable for evaluating changes to substrate concentration and/or pre-catalyst loading without the requirement to perform additional kinetic experiments.

The constrained model was then utilised in three applications. Firstly, relative rates were quantified for the RCM reactions of 1,6-heptadiene, 1,7-octadiene and diethyl diallylmalonate, despite the fact that only one of these reactions exhibited good first-order kinetic behaviour. It was shown that the relative rates of RCM for these substrates were 0.59:1.00:0.27, respectively, in agreement with the semi-quantitative relative rate determination discussed in chapter 2.

Secondly, the model was applied to evaluating the effects of a change of pre-catalyst. Initiation rates were measured for a number of different Hoveyda-type (alkoxystyrene-ligated) pre-catalysts, and their performance was tested for the RCM of 1,7-octadiene. The relative metathesis rates for SIMes-bearing methylenide **3b** and SIPr-bearing methylenide **3c** were quantified, with the latter system found to catalyse the RCM of 1,7-octadiene an order of magnitude faster. In addition, it was shown that the overall relative performances of a series of SIMes-bearing pre-catalysts and a series of SIPr-bearing pre-catalysts were a function of initiation rate; with these data in hand, the effect of new pre-catalysts from these series on the RCM of 1,7-octadiene could be simulated in the future using initiation rate data alone. This also represents the first quantitative determination of the effect of NHC structure on the rate of the actual metathesis reaction, by decoupling the initiation rate of the pre-catalyst.

Thirdly, solvent effects were explored on metathesis reactions catalysed by pre-catalysts **G2** and **GH2**. Solvent effects on initiation rate were modest, with only *ca.* 2 – 4 fold differences between the fastest and slowest initiation reactions of each pre-catalyst. This represents only a *ca.* 0.4 to 0.8 kcal mol⁻¹ difference in ΔG^\ddagger for initiation. It was established that there was no relationship between dielectric constant and initiation rate, although the $E_T(30)$ measure of polarity correlated with the initiation rate of **GH2**. The solvent effects on **G2** initiation are therefore perhaps more likely to be due to specific solvation interactions, rather than general descriptors of the bulk solvent polarity. The concept of polarity can vary depending on the scale employed, and there is scope to further explore effects on **G2** initiation. Interestingly, through use of the kinetic model, it was shown that the differences in the overall reaction rate in chloroform and in DCM could be explained quantitatively by the difference in initiation rate alone, suggesting that the metathesis rate is relatively insensitive to solvent choice.

In summary, the scope and limitations of a simple kinetic model for RCM have been explored. Small modifications have allowed this model to be employed for various interesting and useful applications. This model is still a simplification of the metathesis mechanism, but there is scope for further elaboration of this model, in order to apply it to different and more challenging purposes. In particular, the model could be modified to describe both intra- and inter-molecular metathesis reactions, and therefore allow the synthetic chemist to predict both the rate and efficiency of an RCM reaction under specific conditions. This work therefore provides the basis for a fuller, more detailed kinetic model in the future and, through this, more quantitative insight into alkene metathesis chemistry.

Chapter 4:

Investigating Isomerisation Processes in Metathesis Reactions

Ruthenium-Catalysed Isomerisation Processes

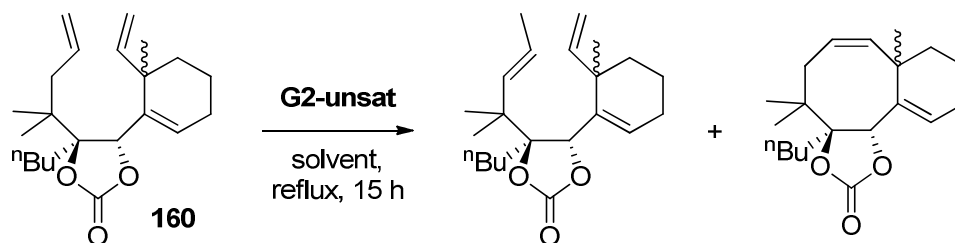
Isomerisation Reactions as Deleterious Processes

Isomerisation processes have been reported to occur during many ring-closing and cross-metathesis reactions. In these cases, one of three side-products is typically observed in the crude reaction mixture:

- Isomerised starting material, where a terminal (monosubstituted) alkene becomes an internal (disubstituted) alkene;
- Isomerised product where, for example, the desired ring size is obtained, but the alkene has moved to an unexpected position;
- Ring-contracted product where isomerised diene undergoes RCM to yield a product cycloalkene that is of a smaller ring size than desired.

There have been many literature reports of undesired isomerisation during metathesis, but only selected illustrative examples are discussed here. Isomerisation processes have been employed intentionally in a number of synthetic chemistry scenarios, but the synthetic usage of alkene isomerisation is beyond the scope of this thesis.²³⁴⁻²³⁵

Prunet *et al.* have described the isomerisation of diene **160** when it was exposed to **G2-unsat** in refluxing solvent (**Scheme 4.01** and **Table 4.01**).²³⁶

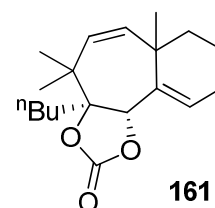


Scheme 4.01²³⁶

Table 4.01. Dependence of the degree of isomerisation in **Scheme 4.01** on solvent; product ratios were determined by ^1H NMR integration of crude reaction mixtures.²³⁶

Solvent	Boiling point (°C)	Cyclisation Yield	Isomerisation Yield
Benzene	80	50 – 70%	50 – 30%
Toluene	110	20%	80%
Dichloroethane	83	90%	10%
Dimethoxyethane	85	0%	100%

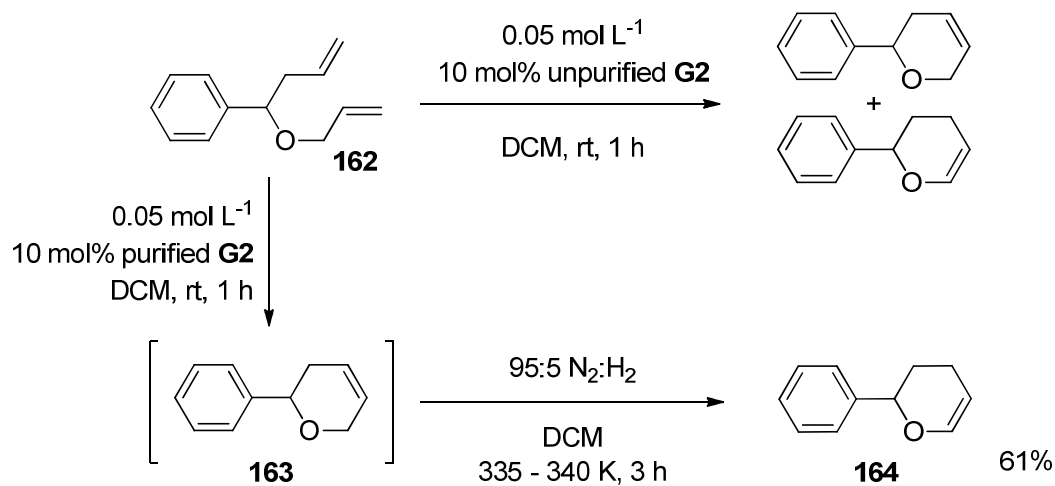
Ring-contracted product **161** was not detected, most likely due to steric effects, as both alkenes in the isomerised diene have quaternary allylic positions which are known to disfavour metathesis.^{62,141} Interestingly, there was a marked dependence of



the degree of isomerisation on the solvent employed, even when solvents with similar boiling points were used. Three of these solvents can co-ordinate to the metal centre, but would do so in different ways. Dichloroethane is a poorly co-ordinating solvent, while benzene and toluene would co-ordinate in an η^6 -manner. Dimethoxyethane features two ether groups which can co-ordinate to ruthenium *via* electron pairs in occupied orbitals on the oxygen atoms;¹¹ if a suitable number of co-ordination sites were available on the metal this might potentially bind to the catalyst in a bidentate fashion, which could explain the lack of metathesis activity. Coordination in an η^1 - or η^2 -fashion is also less sterically demanding on a metal centre than η^6 -coordination.

The identity of the isomerised side-product was determined by independent synthesis of the proposed structure. The co-ordinating ability of the solvent was proposed to influence the degree of isomerisation, with tricyclohexylphosphane oxide (but not triphenylphosphane oxide) reported to inhibit the isomerisation reaction.

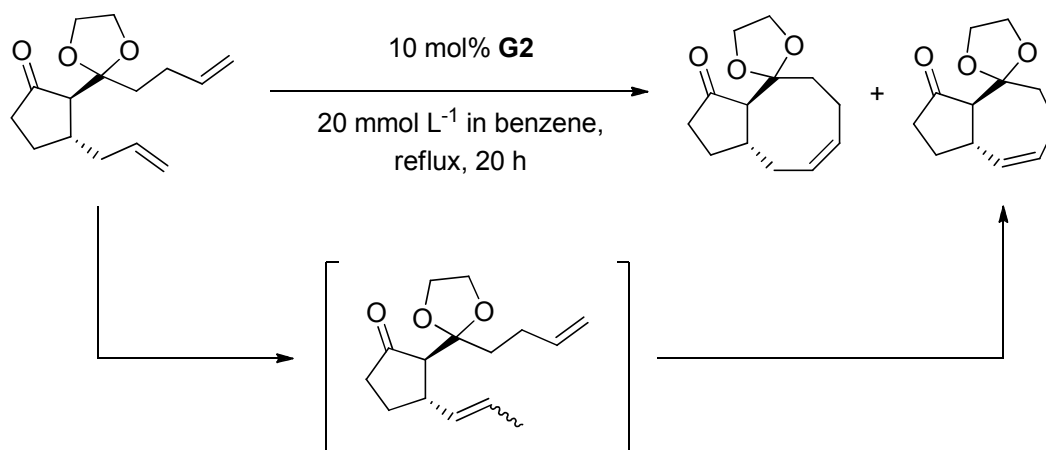
Snapper *et al.* reported isomerised products from the RCM reactions of substrates such as **162**, where product **163** underwent isomerisation to **164** (**Scheme 4.02**).²³⁷ The latter process was presumably driven by bringing the alkene into conjugation with the ether functionality. Snapper *et al.* attributed the undesired isomerisation to impurities present in the pre-catalyst; when the reactions were performed with purified pre-catalyst, isomerisation was suppressed. The isomerisation activity could be selectively switched on by exposing the metathesis reaction mixture to



Scheme 4.02²³⁷

a dilute atmosphere of hydrogen and then heating in a sealed tube, which was proposed to generate active ruthenium hydride species *in situ* (*vide infra*). Attempts to identify and characterise the species responsible for the isomerisation were unsuccessful. Exposure of a solution of **G2** to the dilute hydrogen mixture did not reveal the presence of hydride species that could be detected by ^1H or ^{31}P NMR spectroscopy. Prolonged exposure of **G2** to hydrogen generated a new signal at $\delta_{\text{p}} = 48 \text{ ppm}$, but no active isomerisation species. These results suggest that hydrogen may act upon an intermediate species, rather than **G2**, in order to generate the active isomerisation catalyst *in situ*.

Marko *et al.* have observed ring-contracted products from the RCM reactions of some substrates (Scheme 4.03);²³⁸ the desired eight-membered cycloalkene was obtained in addition to a cycloheptene product, in a ratio of 1.1:1. The seven-membered



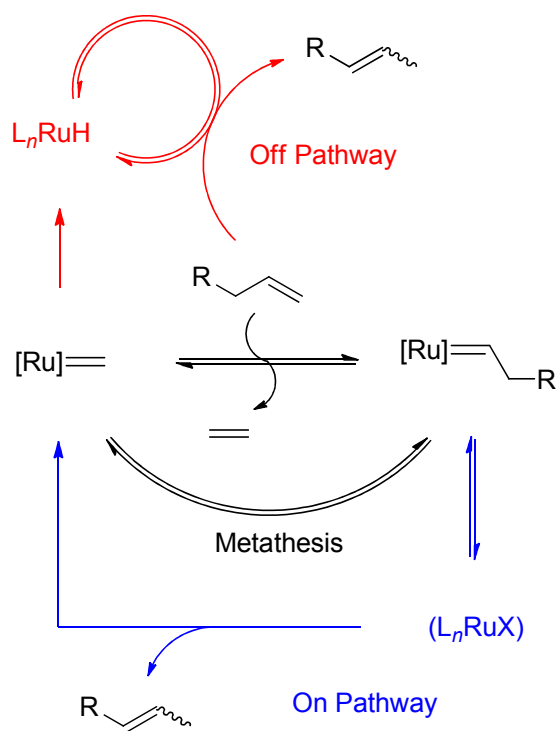
Scheme 4.03²³⁸

ring was obtained from an isomerisation side-reaction followed by RCM. As in the example reported by Prunet *et al.*, one of the terminal alkenes must isomerise to an internal alkene, followed by RCM.

All of these processes result in the recovery of material that is different from the target cycloalkene. Understanding these isomerisation side-reactions would therefore be very useful, and potentially widen the scope of the metathesis reaction, both in polymer chemistry and target synthesis.

Isomerisation Mechanisms

Various mechanisms for alkene isomerisation have been proposed in the literature, although only some of these are supported by theoretical and/or experimental studies. These mechanisms can be divided into two classes: on-pathway and off-pathway (**Scheme 4.04**). On-pathway processes are those that occur *via* intermediates on the metathesis pathway; species are formed *in situ* that can either catalyse isomerisation

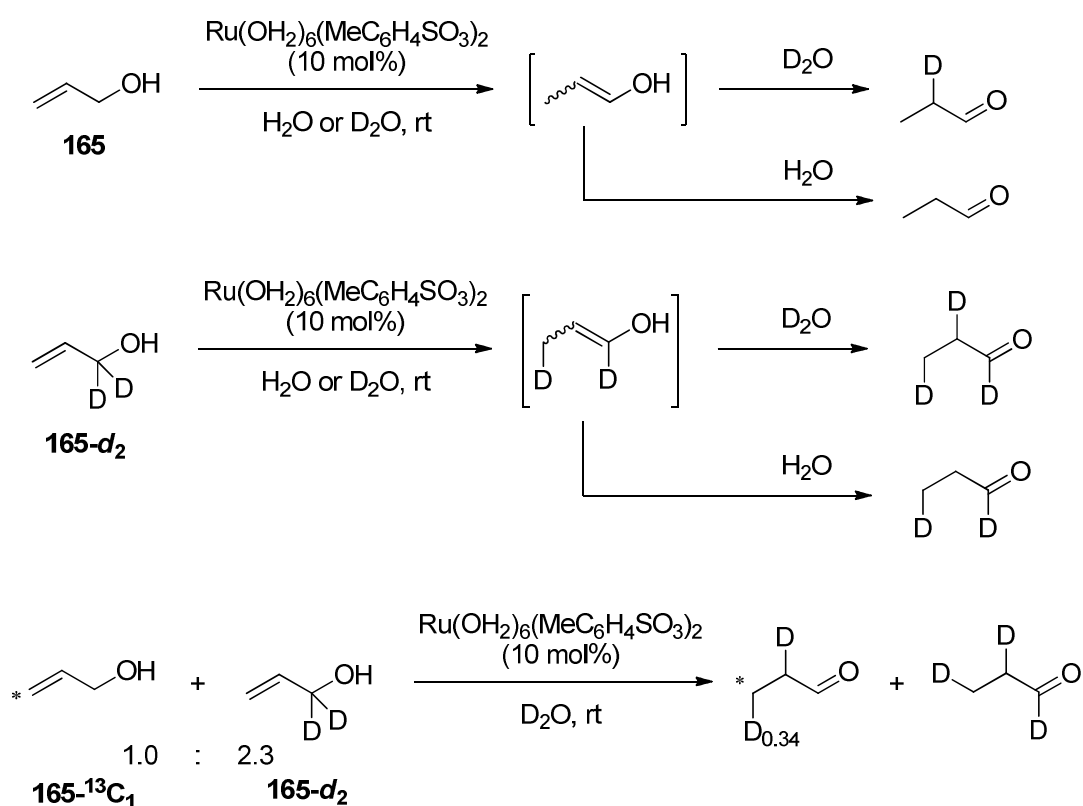


Scheme 4.04

reactions, or return to the metathesis pathway. Off-pathway processes rely on the *irreversible* generation of isomerisation catalysts (or reagents) *in situ* from side reactions involving the metathesis catalyst or intermediates, but that do not return the ruthenium species to a metathesis-active ruthenium carbene complex. The latter class of pathway is typically proposed to involve ruthenium hydride complexes as the active isomerisation species.²³⁴ Both types of pathway have been reported or proposed in the literature.

'Off-pathway' Isomerisation Processes

Ruthenium hydride complexes were implicated in isomerisation reactions, even before ruthenium-catalysed alkene isomerisation became a key topic in metathesis chemistry.²³⁹ Grubbs *et al.* studied the isomerisation of allyl alcohol **165** and isotopically-labelled analogues **165-*d*₂** and **165-¹³C₁** to propionaldehyde, catalysed by Ru(OH₂)₆(MeC₆H₄SO₃)₂ in aqueous solution (Scheme 4.05). The reaction of allyl alcohol **165** proceeded *via* enol **166**, which tautomerised to propionaldehyde-2-*d* in D₂O, or to propionaldehyde-*d*₀ in water. When **165-*d*₂** and **165-¹³C₁** (in a 2.3 to 1.0 ratio) were exposed to the catalyst, deuterium from the 1,1-*d*₂-labelled substrate was incorporated into the ¹³C-labelled substrate. This piece of evidence was used to rule out a π-allyl mechanism (Figure 4.01 (a)) which involved the entirely intramolecular transfer of hydrogen (or deuterium), and would not lead to cross-over. Instead, it was proposed that a metal hydride-mediated process was responsible (Figure 4.01 (b)), which would lead to transfer of deuterium from one molecule of substrate to another, *via* an *in situ* generated ruthenium hydride (or ruthenium deuteride) complex. Neither the exact identity nor precise origin of the ruthenium hydride complex responsible could be identified, in common with the reports



Scheme 4.05²³⁹

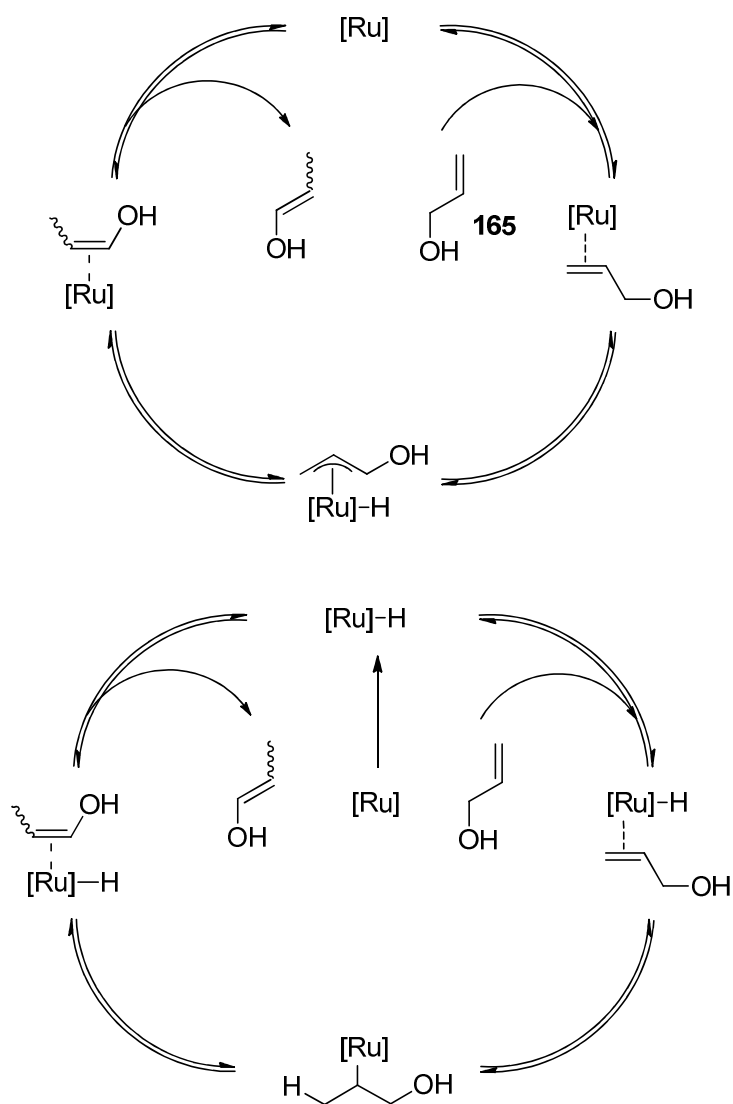
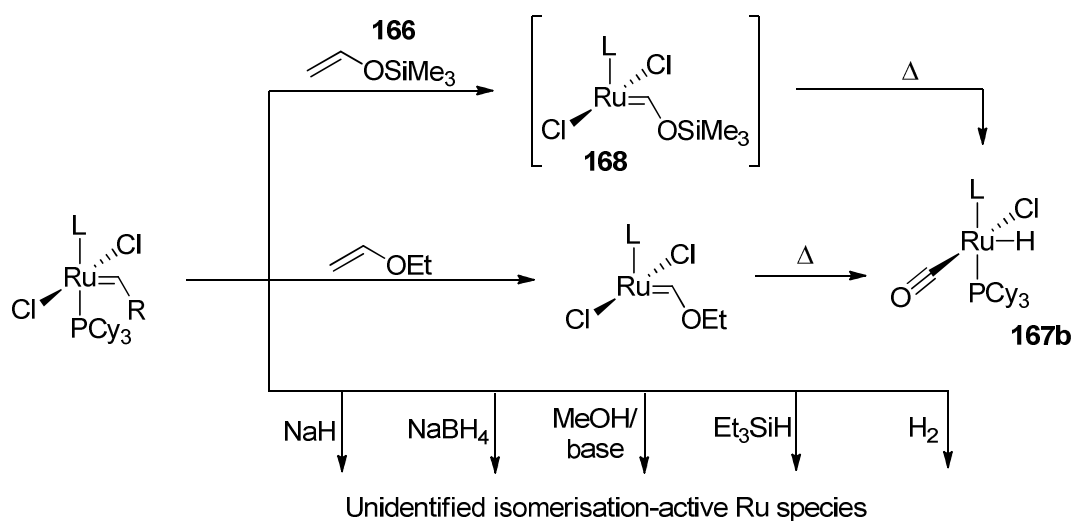


Figure 4.01. Two mechanisms for ruthenium-catalysed alkene isomerisation: (a) the π -allyl hydride mechanism and (b) the ruthenium-hydride mechanism.

of isomerisation side-reactions in metathesis reactions; protonation of the Ru^{II} complex was proposed to be a potential source of a Ru^{IV} hydride complex.

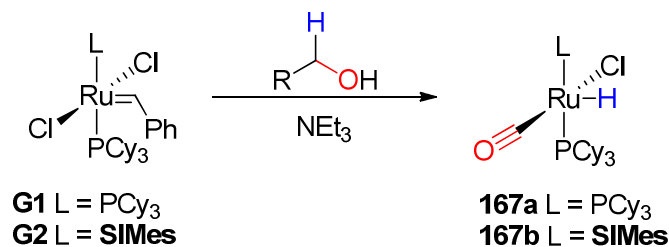
Most literature reports of the synthetic application of ruthenium-catalysed alkene isomerisation involve the *in situ* preparation of a ruthenium hydride complex. Hanessian *et al.* have achieved the isomerisation of a wide range of substrates in good to excellent yield by heating the substrate with **G1** in methanol for *ca.* 3 to 12 h.²⁴⁰ In tandem metathesis-isomerisation applications, Snapper *et al.* favour placing a metathesis reaction under an atmosphere of hydrogen,²³⁷ while Schmidt has utilised sodium borohydride,²⁴¹ sodium hydride,²⁴¹ triethylsilane²⁴² and ethyl vinyl ether,²⁴² the latter



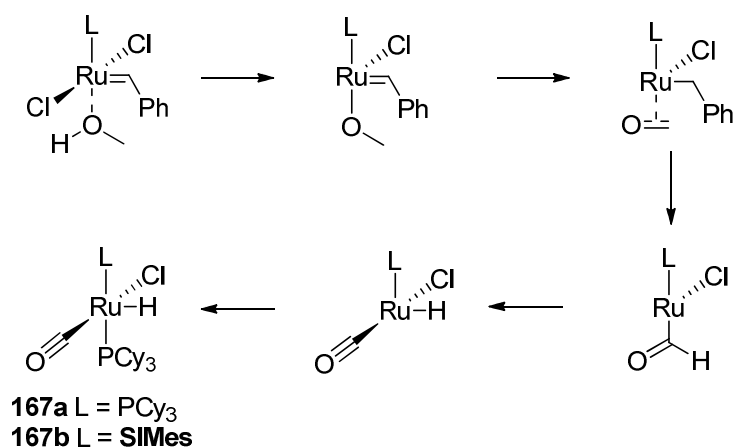
Scheme 4.06

reagent presumably forms the Fischer carbene which undergoes thermolysis to a ruthenium hydride complex, as reported by Grubbs *et al.*⁴⁴ Nishida *et al.* have used vinyloxytrimethylsilane **166** to generate **167b** *in situ* from **G2**, presumably due to the thermal decomposition of Fischer carbene **168**, to isomerise alkenes.²⁴³⁻²⁴⁴ These approaches are summarised in **Scheme 4.06**.

The alcoholyses of **G1** and **G2** have been investigated in detail by Mol *et al.* Heating **G1** and **G2** in the presence of primary alcohol and base was shown to generate hydridocarbonyl complexes **167a** and **167b** respectively (**Scheme 4.07**).⁷⁹⁻⁸⁰ Labelling studies with MeOD and ethanol-1-¹³C confirmed that the carbonyl ligand was obtained from the alcohol employed. The origin of the hydride was not from the acidic proton of the alcohol, but is proposed to come from the α -proton of the alcohol. Based on these observations, a tentative mechanism was proposed. In this mechanism, methanol coordinates to the 14e complex and yields a formyl complex (after elimination of HCl and toluene) which rearranges to the hydridocarbonyl complex (**Scheme 4.08**); further work



Scheme 4.07⁷⁹⁻⁸⁰



Scheme 4.08⁸⁰

would be necessary to confirm whether this was the mechanism in operation. This process was found to occur smoothly for **G1**, yielding known complex **167a** in 73% yield after a straightforward work-up. However, alcoholysis of **G2** yielded a mixture of hydrides, including complexes **167b** and **167a**; the latter complex must have arisen from the displacement of the *N*-heterocyclic carbene by PCy₃, either from **G2** or from **167b**.

Ruthenium hydrides have been reported as the products of the decomposition of metathesis catalysts and related complexes. As discussed in the introduction, Hong *et al.* studied the decomposition of a series of catalyst-derived methylidene complexes;²⁷⁻²⁸ the decomposition of **G2**-derived **3b**, *via* attack of the PCy₃ at the methylidene α -carbon, leads to diruthenium hydride complex **41** (Scheme 1.14 in the introduction). This complex was shown to be active for isomerisation, converting allylbenzene to phenylpropene in good yield but over relatively long reaction times (Scheme 4.09).²⁷



Scheme 4.09²⁷

While examples of well-defined ruthenium-hydride complexes prepared from metathesis pre-catalysts exist, it is important to note that the hydride complexes to which isomerisation activity is attributed are frequently generated *in situ*, and are rarely observed; it is rarer still that they are characterised in as much detail as complexes **167a**, **167b** and **41** have been.

Wagener *et al.* studied isomerisation side-reactions in metathesis in some detail. The metathesis reactions of 1-octene, 2-octene and 7-tetradecene at various temperatures were conducted using stringently purified solvents, substrates and **G2**, yet isomerisation was observed in all reactions.¹⁸⁹ GC analysis of the reaction mixtures showed that they were comprised of linear alkenes of various chain lengths (**Figure 4.02**). Higher temperatures were found to increase the degree of isomerisation in the metathesis experiments. While the decomposition products of methyldiene **4** have been implicated in isomerisation processes (*vide infra*), the results of Wagener *et al.* show that isomerisation occurs even in the metathesis of internal alkenes, where methyldiene cannot form. Reactions catalysed by **G1** resulted in far less isomerisation.

Later work by the same research group applied a deuterium-labelling approach to establish whether a metal hydride was present or a π -allyl metal hydride mechanism was in operation (similar to those considered by Grubbs *et al.*, see **Figure 4.01**). The former mechanism would result in both 1,2- and 1,3-hydrogen shifts while the latter would result in a formal 1,3-hydrogen shift. Exposure of allyl methyl ether- d_2 to **G2** resulted in isomerised products that were products of both 1,2- and 1,3-hydrogen shifts (**Scheme 4.10**). Deuteration of both positions suggested a metal hydride pathway was in operation, while the complete deuteration of the position α to the oxygen suggested that the isomerisation reaction was irreversible; if it were reversible, hydrogen-deuterium exchange would be expected to take place at this position. Crossover studies were not conducted – metathesis of a mixture of allyl methyl ether- d_2 and allyl methyl ether- d_0

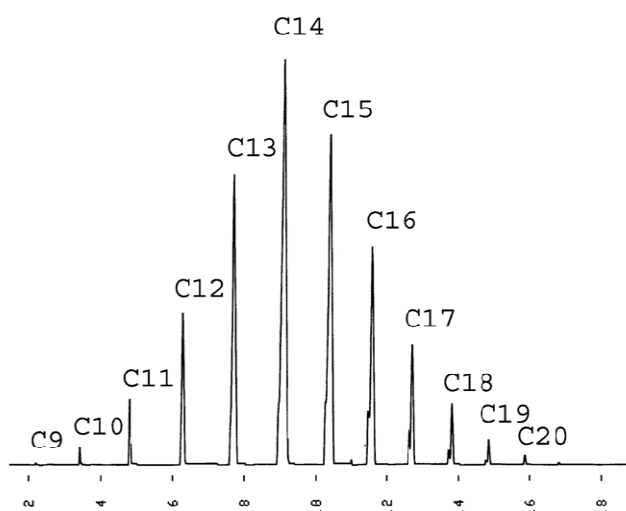
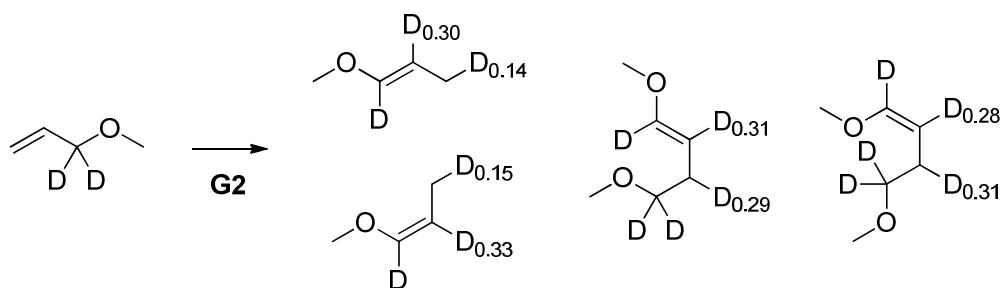


Figure 4.02. GC chromatogram from the metathesis reaction of 7-tetradecene with **G2** at 328 K.¹⁸⁹

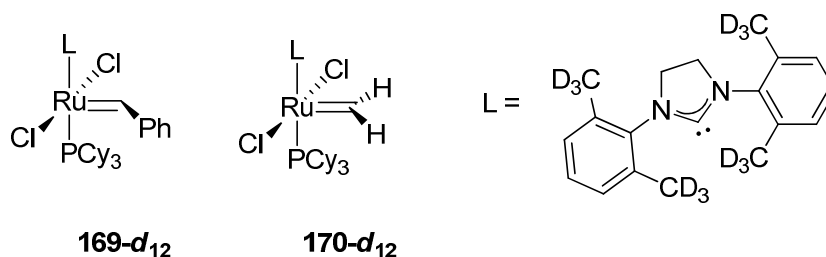


Scheme 4.10²⁴⁵

would have provided further insight into whether a metal hydride mechanism was in operation. Wagener *et al.* made several other key observations. A colour change from pink to bright yellow was observed, which was proposed to arise from the reaction of the vinyl ether products with the ruthenium carbene, which would yield a Fischer carbene complex that would then thermally decompose to produce a ruthenium hydride complex.⁴⁴ In addition, isomerisation was observed to occur after the system had reached equilibrium (at *ca.* 7% conversion; K for metathesis was estimated at 4.0×10^{-6}) with a pseudo-first order rate constant k_{obs} of $5.6 \times 10^{-6} \text{ s}^{-1}$ (at 308 K).

Selectively deuterated **169-d₁₂** was prepared and studied, to probe whether the hydride species responsible for isomerisation was catalyst-derived. Traces of hydride complexes were detected after thermolysis (343 K, 21 days), but no ruthenium deuteride was detected by ²H NMR spectroscopy. Importantly, the decomposed pre-catalyst solution was *less* active for alkene isomerisation than **G2**, ruling out pre-catalyst decomposition products as the sole source of isomerisation agents. The corresponding methylenide complex **170-d₁₂** was prepared and tested in the same manner; once again, the decomposition products were less active for isomerisation than **G2**.

Exposing 1-octene to complex **169-d₁₂** resulted in deuterium incorporation across many positions of the substrate and product, though primarily at the alkene terminus. This implicated C-H (or C-D) activation in the metathesis catalyst; traces of a



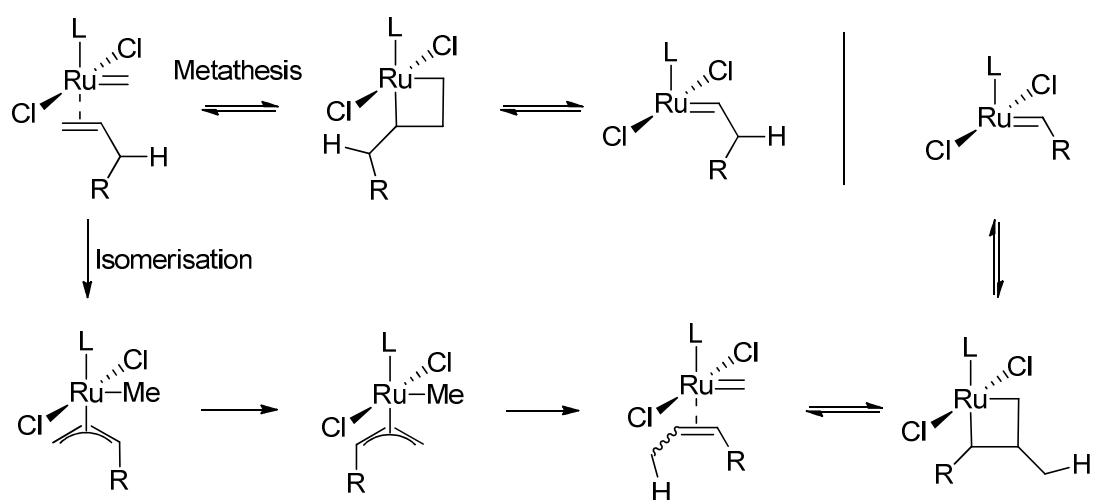
species consistent with a ruthenium hydride complex (δ_{H} (benzene- d_6) = -20.36 ppm, d ($^2J_{\text{H,P}}$ = 17.8 Hz)) were detected by ^1H NMR, but the identity and origin of this species were not established. Therefore the studies concluded that the isomerisation was due to metal hydride species, but only traces of hydride species were detected.

‘On-pathway’ Isomerisation Processes

In contrast to off-pathway processes, on-pathway processes are both derived from, and return to, an intermediate in the metathesis reaction. Some mechanisms of this type have been discussed in the literature.

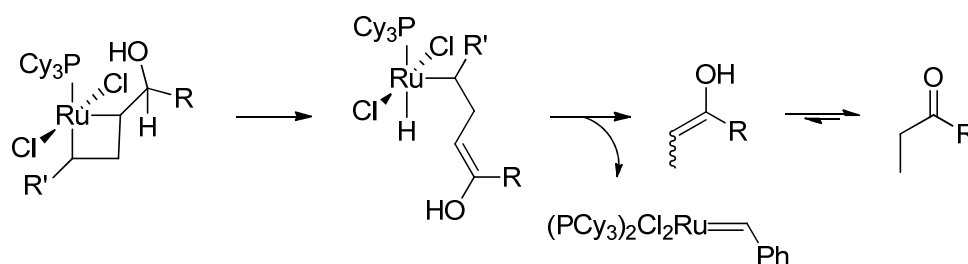
Nolan and Prunet proposed that isomerisation could result from the intramolecular reaction of the η^2 -complex between substrate and methyldiene; transfer of an allylic proton to the methyldiene might yield a ruthenium π -allyl complex. The proton could then be delivered to the terminus, yielding a new η^2 -complex (**Scheme 4.11**).²³⁶ The transfer step would compete with the productive metallocyclobutane step, but would return the ruthenium carbene species unchanged and so would not deplete the reservoir of active catalyst. This mechanism was consistent with the experimental finding that co-ordinating solvents increase the degree of isomerisation (**Table 4.01**, above), which was postulated to be due to such solvents competing with co-ordination of the second diene terminus to the ruthenium centre, therefore slowing the metathesis reaction and allowing isomerisation to become kinetically competitive.

Hydride transfer to ruthenium from MCB complexes has been discussed as a potential decomposition pathway. A mechanism was proposed by Paquette *et al.* for the



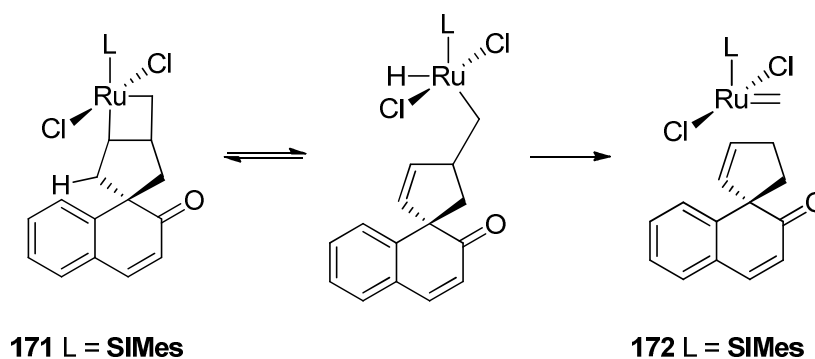
Scheme 4.11

decomposition of allyl alcohol substrates with **G1**, where a proton β - to ruthenium (but not on the metallocyclobutane itself) could be transferred to the ruthenium centre, opening the MCB and forming a ruthenium hydride intermediate (**Scheme 4.12**).²⁴⁶



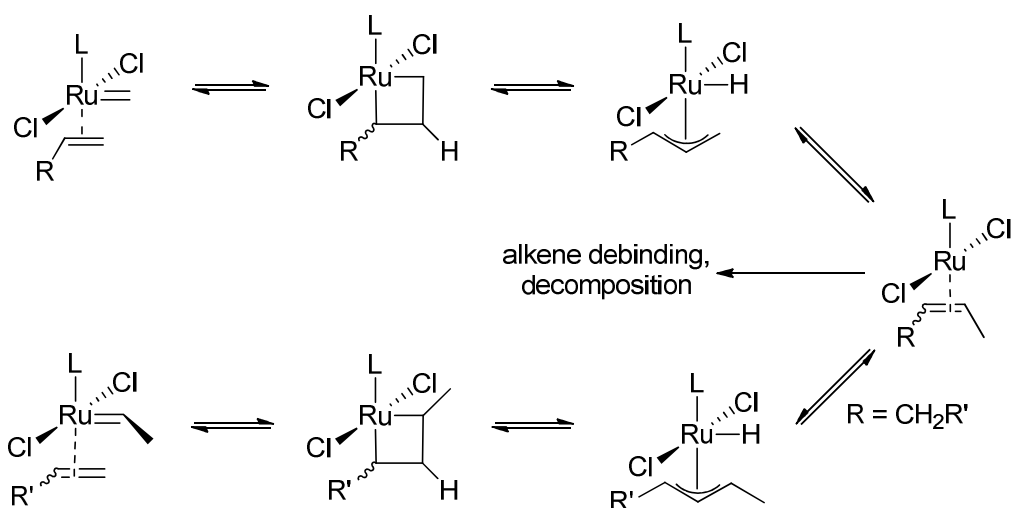
Scheme 4.12²⁴⁶

This intermediate could then undergo elimination of the ruthenium carbene fragment, releasing an enol species that would tautomerise rapidly to the corresponding ketone. Similarly, Kotha *et al.* proposed that hydride transfer in MCB **171** might be responsible for the appearance of isomerised product **172** (**Scheme 4.13**).²⁴⁷



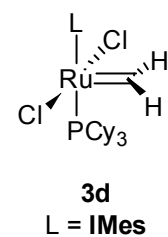
Scheme 4.13²⁴⁷

An alternative MCB-derived mechanism for isomerisation could result from the decomposition pathway investigated by van Rensburg *et al.*²⁴⁸ In this study, it was proposed that β -hydride transfer from the metallocyclobutane (derived from methyldiene **4b** plus ethene) to the metal should yield π -allyl ruthenium hydride (**Scheme 4.14**, where R = H); delivery of the hydride to the terminus of the allyl fragment would yield propene complexed to a four coordinate, metathesis-inactive complex. This pathway was investigated in some detail as a potential decomposition mechanism for metathesis catalysts using both experimental and theoretical (PW91



Scheme 4.14²⁴⁸

density functional) methods. Methylidene complexes **3a** and **3b**, derived from **G1** and **G2** respectively, were studied experimentally and calculations were carried out on complexes **3a** and **3d**, derived from complexes **G1** and **G2-unsat**. Electronic structure calculations predicted that the largest barriers on these PESs were for the β -hydride abstraction event (16.9 kcal mol⁻¹ for **G1**, 24.3 kcal mol⁻¹ for **G2-unsat**), followed by smaller barriers (≤ 3 kcal mol⁻¹) for the π -allyl to propene η^2 -rearrangement. These barriers are quite high, but are of similar size to those required for pre-catalyst initiation (*ca.* 20 – 25 kcal mol⁻¹).²⁶ In addition, MCBs are low energy species in alkene metathesis with respect to 14e complexes and η^2 -complexes,^{15,53} and would therefore be expected to comprise a significant proportion of the intermediates in solution during metathesis. Experimentally, the predicted decomposition products propene and 1-butene were detected by the GC-MS analysis of a reaction mixture from the metathesis of ethene by **G2** in benzene at 40°C for 16 hours. Propene resulted from the β -hydride transfer from the metalocyclobutane formed from methylidene plus ethene (R = H in **Scheme 4.14** above) to the metal centre, while 1-butene was obtained from the reaction of the metalocyclobutane derived from methylidene plus propene (R = Me in **Scheme 4.14**).



It could be envisaged that a modified version of this mechanism might form the basis of an isomerisation reaction mechanism. If β -hydride transfer occurred in an α -substituted metalocyclobutane (e.g. R = Me in **Scheme 4.14**), the hydride was delivered to the terminus and then the alternative hydride was abstracted, a metalocyclobutane

could be formed which then leads to an isomerised product. This process would deliver either the ethylidene complex **31** (observed in metathesis reactions where isomerisation occurs)^{96,141} plus isomerised alkene, or propene plus propagating carbene.

There has not yet been a study of alkene isomerisation side-reactions that considers and compares all of these potential mechanisms. With the exception of the van Rensburg mechanism there has been very little detailed study of the kinetics and mechanism of these processes, with mechanisms often proposed only on the basis of isolated products. All of the on-pathway mechanisms proposed regenerate ruthenium alkylidene species and therefore do not result in a net depletion of the active catalyst population and do not produce isolable new complexes.

Isomerisation Under Mild Conditions

When the metathesis reactions of 1,8-nonadiene and 1,9-decadiene were conducted in chloroform-*d* and DCM-*d*₂ at 298 K (with 3 mol% **G2**), smaller cycloalkenes were also obtained. 1,8-Nonadiene RCM produced significant quantities of cyclohexene when conducted at higher (>0.2 mol L⁻¹) concentrations (**Figure 4.03**), while 1,9-decadiene

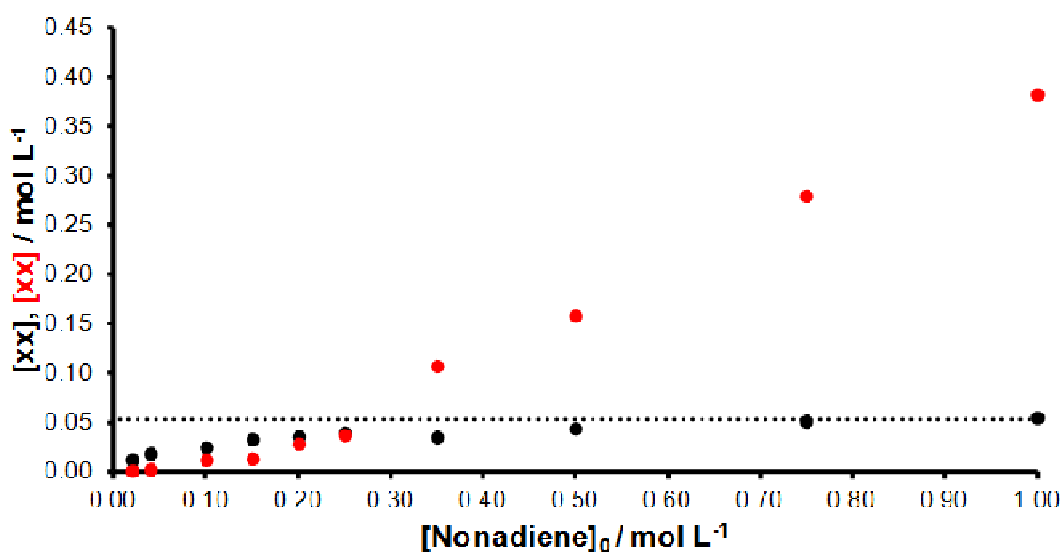


Figure 4.03. Concentrations of cycloheptene (**black**) and cyclohexene (**red**) obtained in small-scale metathesis reactions of 1,8-nonadiene in chloroform-*d* at room temperature after 18 h, quantified by ¹H NMR integration *versus* 1,3,5-trimethoxybenzene as an internal standard; each point is the average of two experiments and the dashed line represents the experimentally-determined EM_T for 1,8-nonadiene of 53 mmol L⁻¹.

RCM produced cyclohexene and cycloheptene.⁹⁶ Isomerisation of the α,ω -diene substrate followed by RCM yielded cyclohexene and cyclohexene plus cycloheptene, respectively, as by-products of the reaction. While at high initial diene concentrations the concentration of cycloheptene in 1,8-nonadiene RCM reaches a maximum at EM_T (53 mmol L⁻¹), the concentration of cyclohexene produced continues to increase.

Isomerisation processes are most often reported during metathesis reactions conducted under more forcing conditions, such as extended reaction times in refluxing solvents. These room-temperature isomerisation processes therefore occur under remarkably mild conditions, given the extent of isomerisation observed. A more detailed study was required to explore the source and rate of isomerisation in these RCM reactions of simple diene substrates more fully.

Research Aims

Investigations were carried out to achieve a number of key aims:

- Benchmark known ruthenium hydride complexes to assess their activity in alkene isomerisation reactions
- Identify if the appearance of isomerisation is an artefact of experimental conditions
- Identify if the isomerisation mechanism is on-pathway or off-pathway
- Explore the mode of action and effectiveness of known isomerisation suppressants

Achieving these aims should contribute to a more detailed understanding of alkene isomerisation side processes, and could potentially yield new methods for suppressing them.

Benchmarking Isomerisation Agents

Kinetic Studies on Isomerisation

The majority of these experiments were monitored using a 600 MHz NMR spectrometer, for four reasons. Firstly, the high magnetic field strength allows resolution of the components of typically very complex reaction mixtures. Secondly, the sensitivity (for ^1H) of the TBI- ζ inverse probe allows the detection of components that are present in relatively small concentrations, due to the ^1H detection coil being closest to the sample. Thirdly, the self-levelling feet result in the minimal amount of baseline noise (*vide supra*). Finally, the digital equipment allows a large dynamic spectrum width: sweep widths of *ca.* 50 ppm can be employed without baseline distortion.

This latter feature is particularly important: ruthenium hydride species tend to exhibit chemical shifts of *ca.* -8²⁷ to -25 ppm.⁷⁹⁻⁸⁰ All of the kinetic reactions documented here were monitored by ^1H NMR spectroscopy at 600 MHz, with a sweep width encompassing the chemical shift range from 22 ppm to -30 ppm.

Monitoring the Rate of 1,8-Nonadiene Isomerisation

Before considering the rate of alkene isomerisation by a series of known isomerisation agents, a metathesis reaction was conducted under conditions similar those used in metathesis reactions known to produce significant levels of isomerisation.⁹⁶ The relatively high concentration (0.5 mol L⁻¹) was selected for three reasons: it is above the EM_T of 1,8-nonadiene (53 mmol L⁻¹);⁹⁶ isomerisation happens at a rate such that it can be studied on a timescale of a few hours; and the effects of trace impurities in the solvents are reduced. The rate of cyclohexene production reflects the rate of isomerisation, because cyclohexene forms rapidly and irreversibly from 1,7-octadiene. Therefore the rate of cyclohexene appearance in the metathesis reaction provides a straightforward way to gauge the isomerisation rate. 1,8-Nonadiene (0.5 mol L⁻¹ in benzene-*d*₆) was exposed to **G2** (3 mol%) at 298 K in the NMR spectrometer (in an NMR tube fitted with a pierced cap), and concentration/time profiles for cycloheptene, cyclohexene and cyclic dimer **106d** were obtained (**Figure 4.04**). The equilibrium concentration of cycloheptene (*ca.* 40 mmol L⁻¹) was reached, in agreement with the results obtained from previous studies;⁹⁶ similarly, the concentration of cyclic dimer

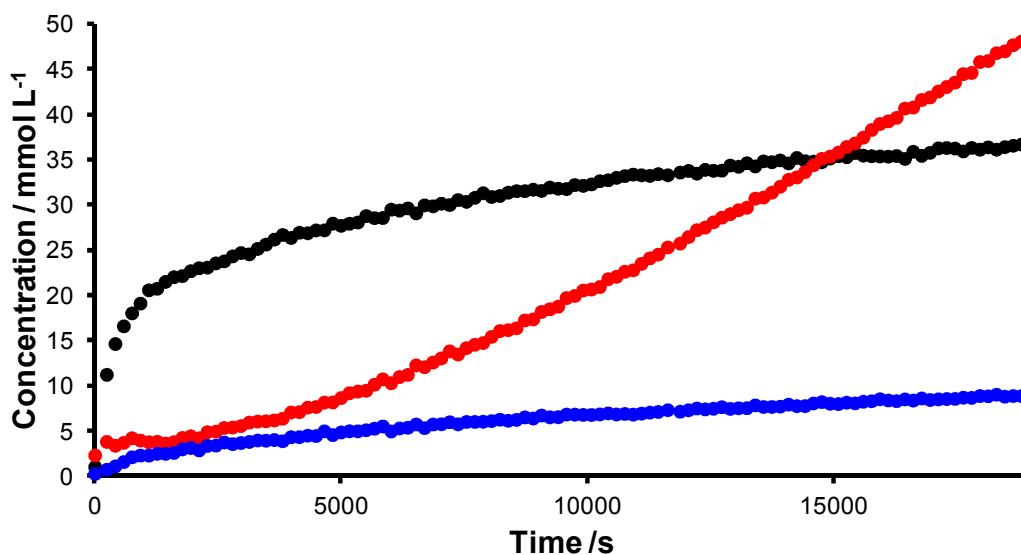


Figure 4.04. Concentration/time profiles for cycloheptene (**black**), cyclohexene (**red**) and cyclic dimer **106d** (**blue**) in the RCM reaction of 1,8-nonadiene (0.5 mol L^{-1}) in benzene- d_6 with 3 mol% **G2** at 298 K.

106d reached a maximum (at *ca.* 10 mmol L^{-1}). The concentration of cyclohexene slowly increased over the course of the experiment. The overall conversion of 1,8-nonadiene to cyclohexene (*ca.* 10%) rules out processes that would be stoichiometric in ruthenium and therefore produce one equivalent of cyclohexene per equivalent of pre-catalyst consumed; the loading in this case is 3 mol%, so only 3% conversion to cyclohexene could be obtained *via* a stoichiometric process. As a much higher conversion to cyclohexene is attained, a process must occur in which a species derived from a ruthenium species present in the reaction mixture *catalyses* the isomerisation reaction.

The low field region of the ^1H NMR spectrum was of particular interest, with various different species observable and quantifiable (**Figure 4.05**). These ruthenium carbene species were observable because they were phosphane-bound 16e species rather than 14e species with a vacant co-ordination site. The corresponding 14e ruthenium carbene species were not spectroscopically observable, because these species undergo reaction on a timescale much faster than that of ^1H NMR spectroscopy. Even at low temperatures (*ca.* 209 to 233 K), Piers *et al.* did not detect 14e ruthenium carbene species.¹⁵ This means that these species must be undergoing rapid exchange, even at low temperatures and therefore their ^1H NMR resonances are so broad as to be undetectable.

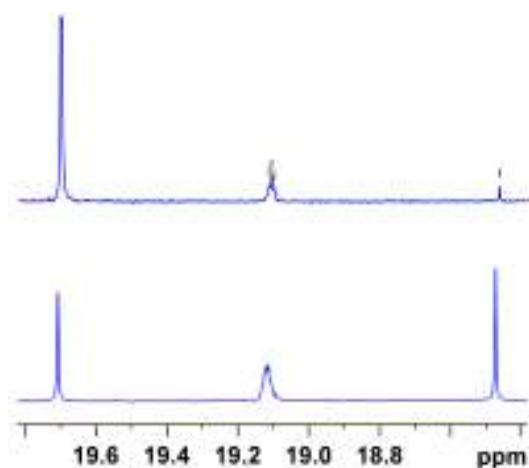


Figure 4.05. Low field region of the ^1H NMR spectrum of the RCM reaction of 1,8-nonadiene (0.5 mol L^{-1}) in benzene- d_6 with 3 mol% **G2** at 298K after (a) *ca.* 40 min and (b) *ca.* 5 h.

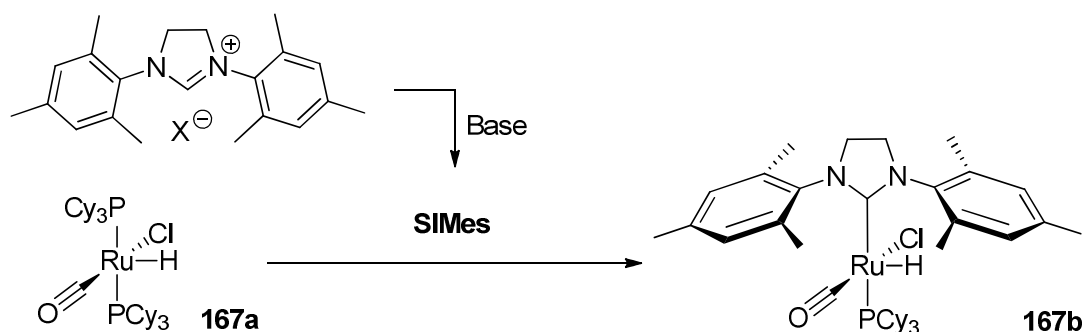
The concentration of the pre-catalyst (δ_{H} (benzene- d_6) = 19.7 ppm) decreased during the course of the experiment (with first order rate constant $k_{\text{obs}} = 9.2 \times 10^{-5} \text{ s}^{-1}$; *cf.* $1.0 \times 10^{-4} \text{ s}^{-1}$ measured for **G2** in benzene- d_6 by reaction with ethyl vinyl ether, see chapter 4). Methylidene **3b** (δ_{H} (benzene- d_6) = 18.5 ppm), which is known to be inactive for metathesis,²⁶ appeared in low (*ca.* 1.5 mmol L^{-1}) concentrations over the course of the experiment. The signal at $\delta_{\text{H}} = \text{ca. } 19.1 \text{ ppm}$ resulted from the overlapping signals of the propagating carbene(s) and (metathesis-active) ethylidene **31b**. In the early stages of the experiment, this signal was predominantly composed of propagating carbene and appeared as a well-defined triplet ($^3J_{\text{H,H}} = 4.3 \text{ Hz}$). Although the low field region of the ^1H NMR spectrum was rich in information, the low field region ($\delta_{\text{H}} = \text{ca. } -8 \text{ to } -25 \text{ ppm}$) revealed the absence of ruthenium hydride species.

The cyclohexene concentration/time profile in **Figure 4.04** was used to provide a frame of reference for the ruthenium hydride benchmarking reactions. The testing of potential isomerisation agents is useful, as it allows kinetically incompetent species to be ruled out. If one of the species examined is responsible for the isomerisation, then it should be able to generate the quantities of isomerised material that are obtained in the RCM experiments, within the same time frame. Importantly, inspection of the high field region of the ^1H NMR spectrum allowed the maximum concentration of hydride present in the reaction to be quantified. If isomerisation could be monitored using a known (and quantifiable) loading of ruthenium hydride, then this effectively sets a generous upper limit for the isomerisation activity of an undetectable quantity of that ruthenium hydride.

Hydridocarbonyl Complexes

Hydridocarbonyl complexes of the general form $(L)(PR_3)RuCl(CO)H$ (where L is a phosphane ligand or an *N*-heterocyclic carbene) have been reported frequently in the literature, since Moers *et al.* prepared $(P^iPr_3)_2RuCl(CO)H$.²⁴⁹⁻²⁵¹ Complexes of this form have been reported to catalyse reactions including alkene hydrovinylation²⁵² and hydrogenation,²⁵³⁻²⁵⁴ silylation of ketones²⁵⁵ and alkenes,²⁵⁶ and the cross-coupling of alkynes and carboxylic acids,²⁵⁷ as well as alkene isomerisation.⁷⁹⁻⁸⁰ Mol *et al.* obtained $(PCy_3)_2RuCl(CO)H$ **167a**, $(SIMes)(PCy_3)RuCl(CO)H$ **167b**, and $(SIPr)(PCy_3)RuCl(CO)H$ **167c** from heating the corresponding metathesis pre-catalysts **G1**, **G2** and **G2-SIPr** (respectively) in the presence of a primary alcohol and a base (Scheme 4.07 above).⁷⁹⁻⁸¹ Notably, alcoholyses of *N*-heterocyclic carbene-bearing complexes **G2** and **G2-SIPr** yield mixtures of products. When **G2** was exposed to *iso*-propyl alcohol and triethylamine in toluene, both the expected complex **167b** and the bis(tricyclohexyl)phosphane complex **167a** were obtained; the latter complex must arise due to displacement of the *N*-heterocyclic carbene by tricyclohexylphosphane.

While **G1** can be converted to **167a** in good yield, synthesis of the corresponding **G2**-derived complex is more difficult. This complex forms only part of the product mixture obtained from alcoholysis of **G2** and many reports detail its sensitivity to air and moisture. No crystal structure for **167b** has been reported, and the complex has been reported to decompose even when stored in the glove box. Both Mol *et al.* and Fogg *et al.* have prepared **167b** from the reaction of the corresponding first-generation hydridocarbonyl complex **167a** with carbene **SIMes**,^{79,251} which is typically prepared *in situ* by deprotonation of the corresponding salt (Scheme 4.15). Nishida *et al.* have prepared complex **167b** from the reaction of **G2** with vinyloxytrimethylsilane (see



Scheme 4.15^{79,251}

Scheme 4.06 above). These hydridocarbonyl complexes have been shown to be active for the isomerisation of 1-octene, although these reactions are typically carried out under bulk conditions and at elevated temperatures.⁷⁹⁻⁸¹ Benchmarking reactions were conducted under conditions more akin to those in the kinetic study of 1,8-nonadiene RCM where significant quantities of cyclohexene were produced. Reactions were conducted with 0.5 mol L⁻¹ 1-octene in dry solvent; different solvents were used across this series of reactions due to the need for specific solvents for *in situ* preparation of hydride complexes, or due to solubility issues.

Complex **167a** was studied here because Mol *et al.* obtained it from alcoholysis of the *second-generation* complex **G2**.⁷⁹ **167a** was prepared for these studies by heating a slurry of **G1** in dry methanol with a few drops of triethylamine to 343 K for 30 minutes; the methanol had been distilled from CaH₂ onto activated 4Å molecular sieves before use. The reaction changed colour from purple, through red and orange, to a mustard yellow colour. Once cooled, the suspension was filtered and washed with dry methanol and dry hexane to yield a bright yellow solid which slowly turned grey-brown on storage under nitrogen or argon over the course of a number of days. Analysis of the yellow solid by ¹H NMR (in benzene-*d*₆) revealed no ruthenium carbene species ($\delta_{\text{H}} = ca. 20$ ppm) but showed the presence of **167a** (δ_{H} (benzene-*d*₆) = -24.1 ppm, t ($^2J_{\text{H,P}} = 18.0$ Hz)) (**Figure 4.06**).⁸⁰ A freshly prepared sample of **167a** (*ca.* 1 mol%) was added to a solution of 1-octene (0.5 mol L⁻¹ in benzene-*d*₆) and the reaction was monitored by ¹H NMR at 298 K. The ¹H NMR resonance for the hydride was clearly detected throughout the experiment; the concentration of **167a** could be monitored at the same time as the conversion of 1-octene to 2-octene. Negligible conversion of 1-octene occurred within *ca.* 4 hours; no 2-octene was detected by ¹H NMR spectroscopy, suggesting that species **167a** was a poor isomerisation catalyst at 298 K. The hydridocarbonyl complex was present at the same concentration throughout the reaction, so decomposition of the complex could be ruled out. It is possible that

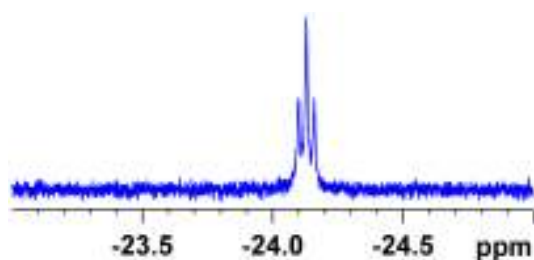


Figure 4.06. Partial ¹H NMR spectrum of hydridocarbonyl complex **167a**.

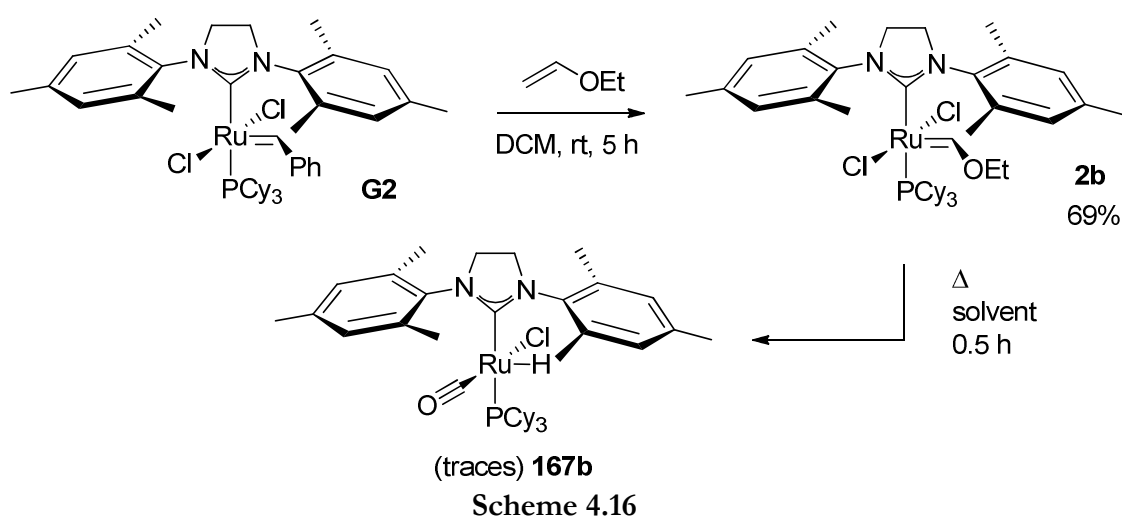
phosphane dissociation was too slow at 298 K to release the corresponding 14e complex into the reaction.

The preparation of the *N*-heterocyclic carbene-bearing analogue **167b** was less straightforward due to the documented low stability of this species, which is typically reported to be isolated as a yellow oil. Mol *et al.* obtained a complex mixture of products from the alcoholysis of **G2** (of which **167b** was a major constituent), so this was ruled out as a useful preparative route.⁷⁹ Two alternative routes were explored instead.

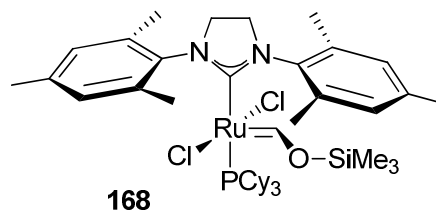
Thermolysis of the corresponding Fischer carbene was attempted, in a manner analogous to that used by Grubbs *et al.* to prepare bis(phosphine) ruthenium hydride **167a** from **2a** (Scheme 4.16).⁴⁴ The synthesis of Fischer carbene using the method of Grubbs *et al.* was straightforward,⁴⁴ with the orange/red product isolated in 69% yield. The identity of the product was confirmed by ¹H and ³¹P NMR spectroscopy; the characteristic ¹H NMR resonance was observed (δ_{H} (benzene-*d*₆) = 14.04 ppm, d ($^3J_{\text{H,P}}$ = 0.9 Hz)). The material was free of pre-catalyst and other phosphorus-containing compounds (as judged by ³¹P NMR spectroscopy).

Unfortunately, thermolysis of the Fischer carbene **2b** in toluene-*d*₈ (30 minutes at 383 K) was not successful; the concentration of Fischer carbene decreased significantly, but only small traces of **167b** were detected by ¹H NMR (δ_{H} (toluene-*d*₈) = -24.95 ppm, d ($^2J_{\text{H,P}}$ = 21.3 Hz)), with the remainder of the material unidentified. Given the known poor stability of **167b**,^{79,244} it is possible that the harsh conditions required to thermolyse Fischer carbene **2b** may have also destroyed any hydride that is formed.

The method of Nishida *et al.* was explored subsequently;²⁴³ when freshly distilled



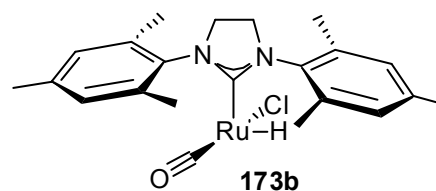
vinyloxytrimethylsilane (5 equiv.) was added to a solution of **G2** in toluene- d_8 . ^1H NMR analysis after 40 minutes at room temperature revealed partial conversion of **G2** to a new carbene species (δ_{H} (toluene- d_8) = 14.7 ppm, d ($^3J_{\text{H,P}}$ =



3.1 Hz)) which was tentatively assigned as Fischer carbene **168**. Heating the solution to 363 K in the magnet of the NMR spectrometer for 10 minutes led to complete consumption of **G2** and the generation of hydride **167b** (δ_{H} (toluene- d_8) = -24.9 ppm, d ($^2J_{\text{H,P}}$ = 21.5 Hz)). Conversion was judged to be *ca.* 70% by integrating the hydride signal *versus* the styrene present in solution, which should be equal to the original charge of **G2**. After a further 10 minutes at 363 K, the concentration decreased to 58% of the original charge of **G2**. After a ^{31}P spectrum was acquired and the sample was cooled to 298 K, the concentration present had decreased further, to 25% of the original charge. These results are in agreement with the known fragility of this species. While conversion was poor, the initial charge of **G2** was consumed and there was sufficient **167b** present to conduct an isomerisation experiment. The solution was cooled to 298 K and 1-octene was added to set the solution concentration to 0.5 mol L $^{-1}$; the loading of **167b** was therefore 1 mol%. The reaction was monitored over the course of 4 hours, during which time 8.5% conversion of 1-octene was obtained (**Figure 4.07**).

This degree of isomerisation was similar to that obtained in the 1,8-nonadiene RCM reaction in **Figure 4.04**, albeit with a detectable and quantifiable level of a known isomerisation agent. The concentration of hydride complex **167b** could be monitored throughout the reaction, and was found to decrease *via* an approximately first-order behaviour ($k_{\text{obs}} = 1.06 \times 10^{-4} \text{ s}^{-1}$) (**Figure 4.08**). This could be explained by rate limiting phosphane dissociation from **167b** to yield an active 14e complex **173b**. The dissociation rate is similar to that of tricyclohexylphosphane from **G2** ($9.2 \times 10^{-5} \text{ s}^{-1}$, see chapter 4), suggesting that the barriers to these two dissociation events are similar.

Subsequent attempts to reproduce this experiment were unsuccessful. Thermolysis of **G2** in the presence of vinyloxytrimethylsilane (5 equiv.) in toluene- d_8 (at 363 K in an oil bath for 15 minutes) led to the formation of a *different* species (*ca.* 7% conversion from **G2**) (δ_{H} (toluene- d_8) = -5.1 ppm, d ($^2J_{\text{H,P}}$ = 23.4 Hz)), consistent with



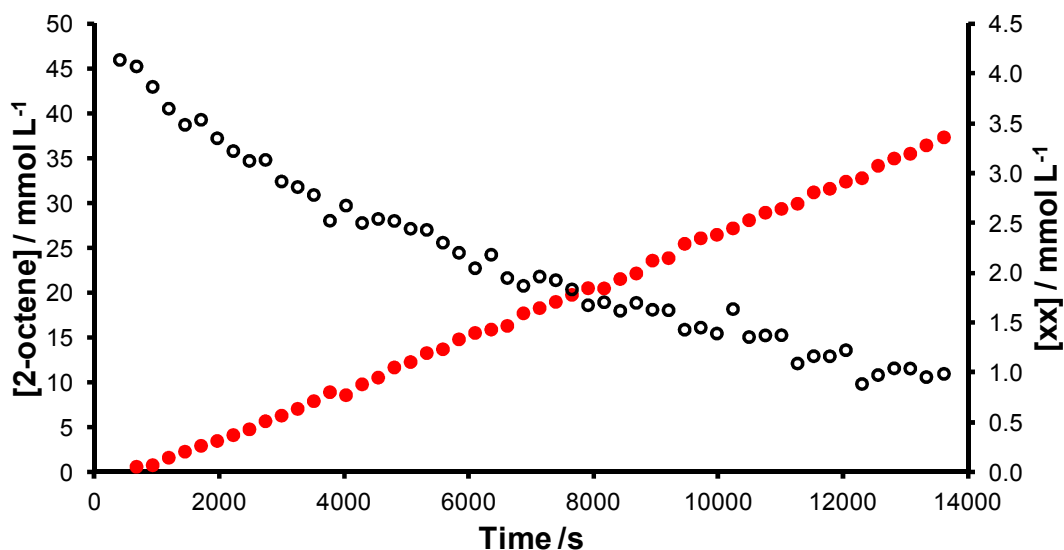


Figure 4.07. Concentration/time profiles from the isomerisation reaction of 1-octene (0.5 mol L^{-1} with *ca.* 1 mol% **167b** in toluene- d_8 at 298K) for (a) 2-octene (**red**, primary axis) and (b) ruthenium hydride complex **167b** (**black**, secondary axis).

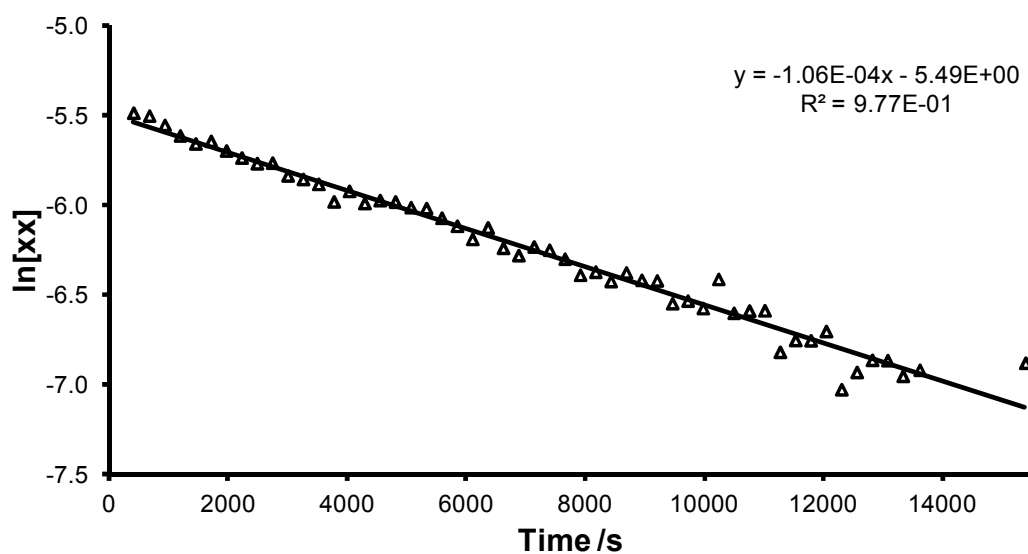


Figure 4.08. First-order treatment of the decay of hydride **167b** in the isomerisation reaction of 1-octene (0.5 mol L^{-1} in toluene- d_8) with **167b** (1 mol%).

the formation of a new ruthenium hydride complex. While the structure of the hydride complex with this chemical shift is unknown, the downfield chemical shift of this species (relative to **167b**) suggested that this new hydride complex was far less shielded than **167b**, yet still possessed one phosphane ligand as indicated by the single, large J -

coupling of 23.4 Hz. Although the identity of this species was unknown, the activity of this hydride complex (at *ca* 0.2 mol%) was tested in the same manner as for **167b** previously and found to result in less than 2% conversion to 2-octene after 3.5 hours. This species is therefore not a highly effective isomerisation catalyst. A third attempt to prepare **167b** for NMR kinetic experiments resulted in a mixture of **167b** and the unknown hydride complex (*ca.* 0.5 mmol L⁻¹ and 1.27 mmol L⁻¹, respectively); the lower concentration of **167b** resulted in correspondingly lower (5%) conversion of 1-octene to 2-octene after *ca.* 6 h at 298 K.

Diruthenium Hydride Complex

Grubbs *et al.* obtained **41** from the decomposition of methyldiene **3b** (see **Scheme 1.14** above; the crystal structure can be found in **Figure 4.09**).²⁷⁻²⁸ Importantly, it was shown that **41** could effect isomerisation, converting allylbenzene to 1-phenylpropene in 76% yield with 1.5 mol% **41** in DCM for 24 hours.²⁷ Complex **41** has also been suggested to be a potential cause of isomerisation in synthetic metathesis reactions.²⁵⁸ To date the observation of this complex in metathesis reaction mixtures has not been reported, but synthetic chemists do not tend to examine the high field region of the reaction mixture before work-up. Van Rensburg *et al.* looked for species **41** in their studies of the decomposition of methyldiene **3b** with ethene (at 313 K for 16 hours), but failed to identify it by ¹H NMR spectroscopic analysis.²⁴⁸

The isomerisation reaction of allylbenzene had a driving force that is not present for 1-octene metathesis: if the former substrate is isomerised, the alkene is brought into conjugation with the aromatic ring. In contrast, the isomerisation of 1-octene to 2-

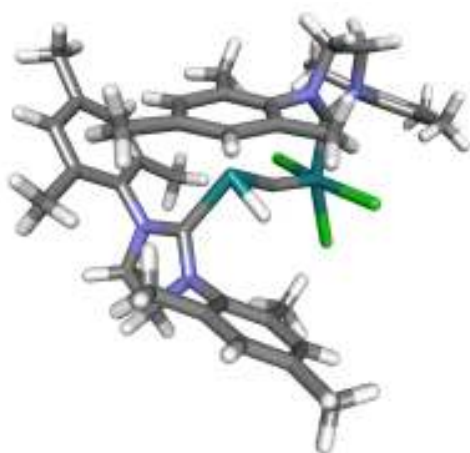


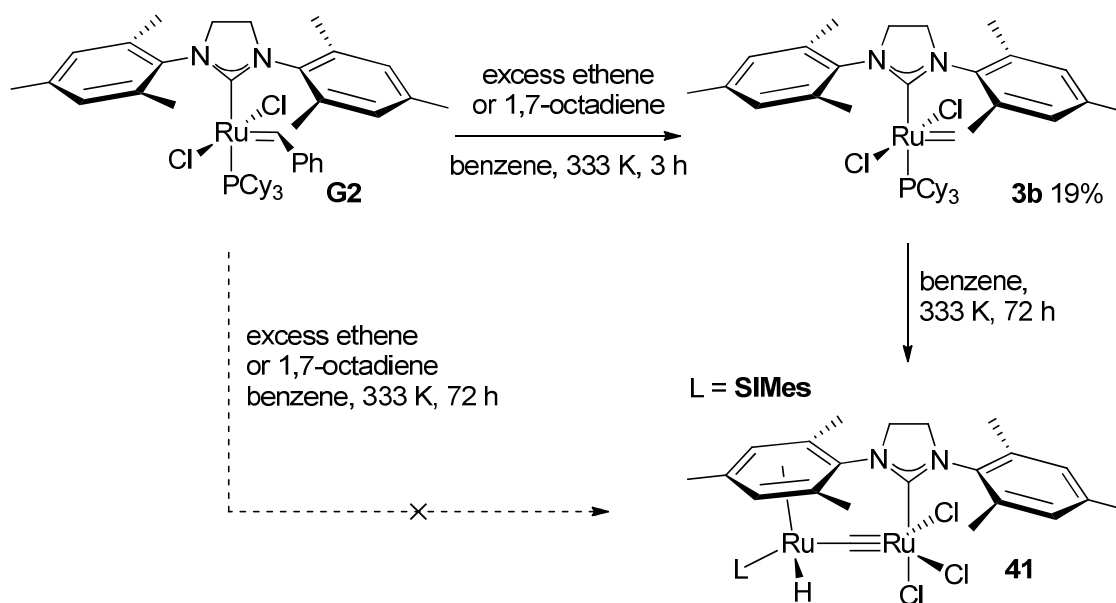
Figure 4.09. X-ray crystal structure of diruthenium hydride complex **41**, obtained by Grubbs *et al.*²⁷

octene is driven only by the conversion of an external alkene to an internal alkene.

Studies were conducted to expose complex **41** to the benchmark conditions used herein, to quantitatively compare complex **41** with hydridocarbonyl complex **167b**.

Grubbs *et al.* reported the synthesis of **41** from thermolysis of a purified sample of methyldiene **3b** for 72 h in benzene, during which the **41** precipitated from the reaction mixture. Initial attempts were made to obtain **41** *via* thermolysis of a metathesis reaction mixture. Pre-catalyst **G2** was dissolved in dry, ethene-sparged benzene and placed under an atmosphere of ethene. The reaction was heated at 333 K for 3 hours, during which time the reaction mixture turned from red to dark orange. The solvent was stripped from the reaction mixture and a fresh portion of dry benzene was added. The reaction was then heated (under nitrogen) for 3 days at 333 K, cooled, and the solvent was removed. Analysis of the residue by ^1H NMR did not reveal the presence of **41**. Therefore, a clean sample of methyldiene **3b** was sought instead (**Scheme 4.17**).

Three methods were explored for preparation of methyldiene **3b**. Reaction of pre-catalyst **G2** with 1,7-octadiene generates 1 equivalent of ethene (with respect to 1,7-octadiene) with the formation of cyclohexene as the only other hydrocarbon product.⁹⁰ Reaction of **G2** with 1,7-octadiene (60 equivalents) in dry benzene in a sealed (Ace) tube at 333 K for 3 hours yielded a brown solution containing a grey precipitate. Unfortunately, ^1H NMR analysis of the precipitate revealed it to be bis(mesityl)imidazolidinium chloride **IMes.HCl**; the quantity of this salt recovered



Scheme 4.17

suggested that *ca.* 50% of the original charge of pre-catalyst **G2** had lost the NHC ligand and a chloride ligand, therefore reducing the potential yield significantly. These conditions were therefore too forcing for methyldiene synthesis.

Reaction of **G2** with either *ca.* 50 equivalents of 1,7-octadiene or under an atmosphere of ethene, in a Schlenk tube for 3 hours at 333 K yielded methyldiene **3b** in 19% yield after column chromatography on silica gel (10-40% dry DCM/hexane). NMR spectroscopic analyses of the complex were consistent with the literature data for **3b**; in addition, the low field region of the spectrum contained signals consistent with those obtained during metathesis reactions that were attributed to methyldiene **3b**.⁹⁷ This clean sample of **3b** was thermolysed in dry benzene-*d*₆ at 338 K for three days in a septum-fitted NMR tube under an atmosphere of argon. The sample was analysed by ¹H NMR spectroscopy once it had cooled to room temperature, which revealed the presence of multiple hydride products, including **41** (δ_{H} (benzene-*d*₆) = -8.53 ppm, s) and hydridocarbonyl complex **167b** (δ_{H} (benzene-*d*₆) = -24.91 ppm, d ($^2J_{\text{H,P}}$ = 21.3 Hz)). In addition, weak signals were observed for three unidentified hydride complexes (δ_{H} (benzene-*d*₆) = -8.85 - -8.95 ppm, m; δ_{H} (benzene-*d*₆) = -9.22 ppm, br s; δ_{H} (benzene-*d*₆) = -12.85 ppm, dd (J = 16.5, 22.8)) (**Figure 4.10**); a precipitate was also observed in the NMR tube, consistent with reports of the poor solubility of **41** in benzene.²⁷ The formation of hydridocarbonyl complex **167b** was surprising given the lack of an obvious source of oxygen from which to form the carbon monoxide ligand. While the benzene-

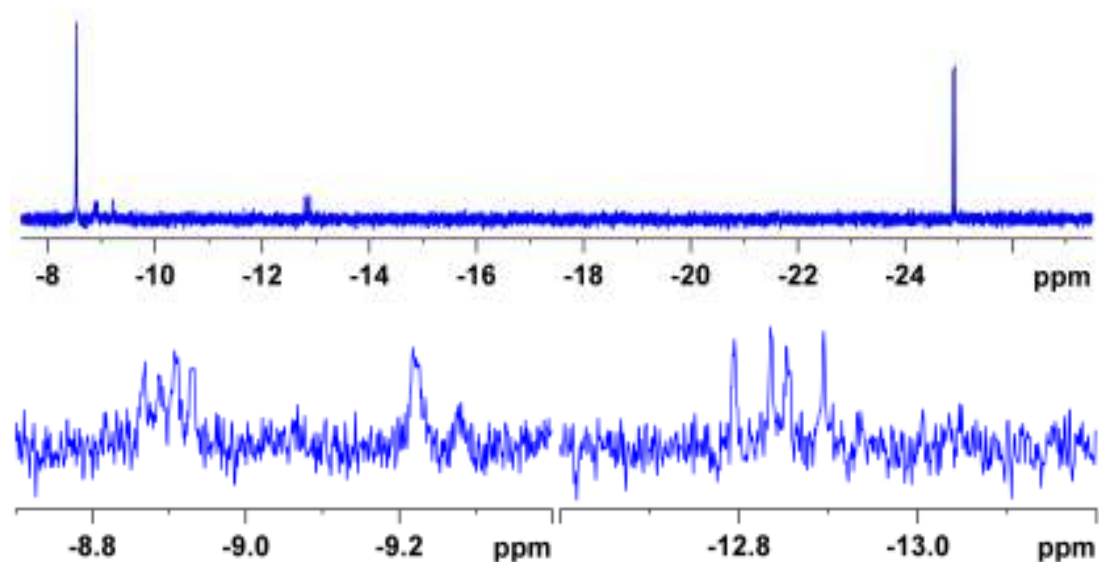


Figure 4.10. Partial ¹H NMR spectra from the thermolysis of methyldiene **3b**.

d_6 employed was dried over activated 4 Å molecular sieves and degassed with a stream of dry oxygen-free nitrogen before use, it was possible that traces of solubilised oxygen remained. The supernatant solution was carefully removed from the NMR tube to leave the solid residue, which was carefully washed with a small volume of benzene- d_6 . In addition, a small pale orange crystal was removed from the NMR tube and submitted for X-ray crystallographic analysis. Unfortunately, the isolated crystal was not diruthenium hydride **41**, but the hydrochloride salt of the NHC ligand (**Figure 4.11**).

The conditions required to generate **41** are clearly very forcing, and resulted in the decomposition of methylidene **3b** by loss of NHC and chloride. Mol *et al.* reported that alcoholysis of **G2** resulted in displacement of the NHC ligand by PCy₃; no *symmetrical* bis(phosphane)ruthenium hydride species were detected in the experiments reported here, which would appear on the ¹H NMR spectrum as a triplet. However, the doublet of doublets observed on the ¹H NMR spectrum at $\delta_{\text{H}} = -12.85$ could potentially indicate a bis(phosphane)ruthenium hydride with two different ²J_{H,P} coupling constants.

The residue in the NMR tube was dissolved in dry DCM- d_2 and analysed by ¹H NMR spectroscopy, which confirmed that only diruthenium hydride complex **41** was present in the high field region of the spectrum (δ_{H} (DCM- d_2 = -8.55 ppm, s), with no ruthenium carbene complexes evident at $\delta_{\text{H}} = ca.$ 20 ppm. A concentrated solution of 1-octene and internal standard was added (to a 1-octene concentration of 0.5 mol L⁻¹; the loading of **41** was *ca.* 0.2 mol%) and the reaction was monitored over the course of approximately 18 h at 294 K. The concentration/time profile shows that this species is

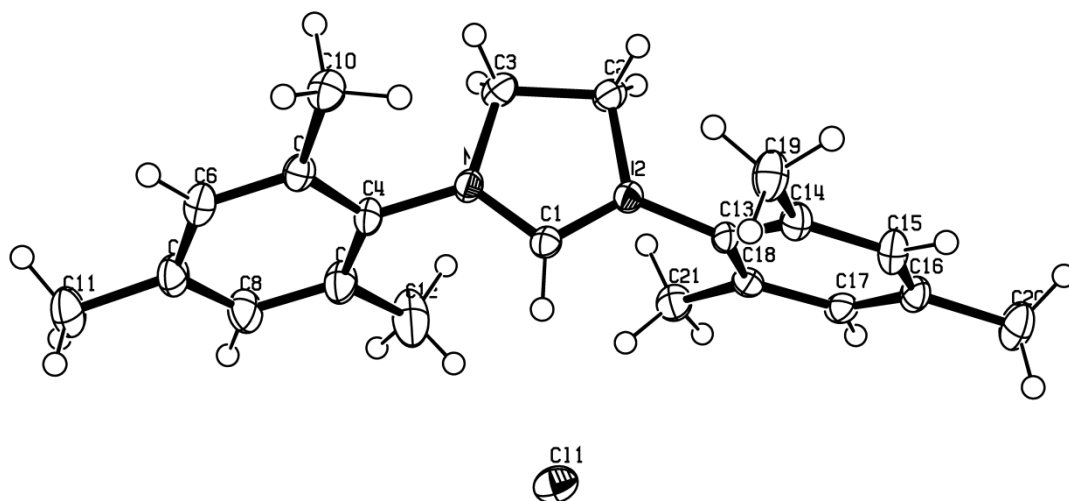


Figure 4.11. X-ray crystal structure of bis(mesityl)imidazolium hydrochloride.

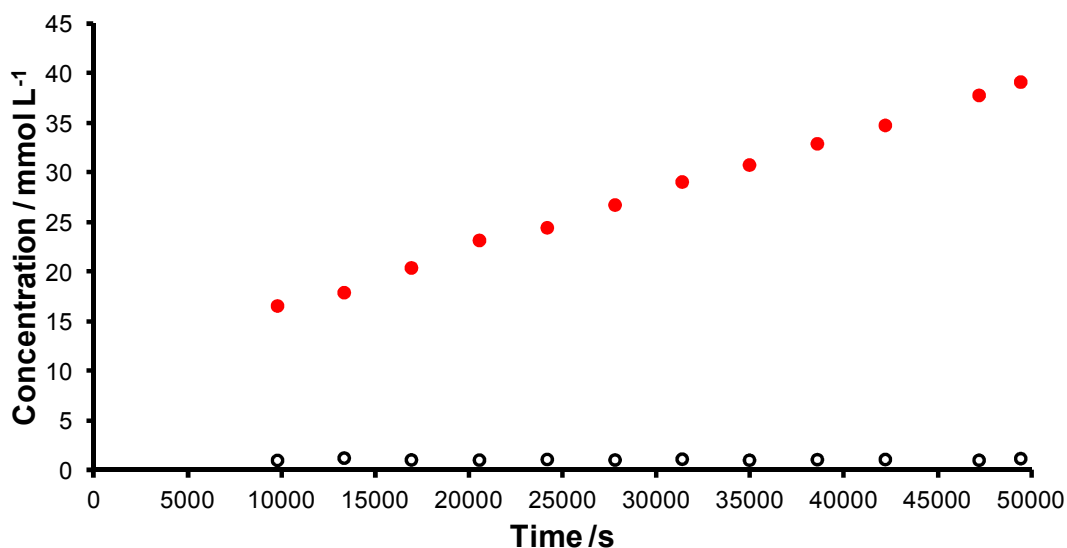


Figure 4.12. Concentration/time profiles from the reaction of 1-octene (0.5 mol L^{-1} in $\text{DCM-}d_2$) with **41** (*ca.* $0.2 \text{ mol}\%$) at 294 K for 2-octene (**red**) and complex **41** (**black**).

active for isomerisation, but could not account for the quantity of material generated in the RCM reaction (at this loading) (**Figure 4.12**).

Conclusions from Benchmarking Studies

The benchmarking of three key ruthenium hydride complexes has allowed their relative performance to be assessed for the isomerisation of simple alkenes. 1-Octene was an appropriate model substrate for this task, as it represented the behaviour of 1,8-nonadiene when exposed to the same isomerisation agents. The performance of the three ruthenium hydride complexes was assessed by overlaying the concentration/time profiles for 1-octene metathesis with the cyclohexene concentration/time profile from the aforementioned 1,8-nonadiene metathesis reaction (**Figure 4.13**). Notably, the profile from the metathesis reaction appears to feature a small induction period, whereas the reactions with the hydride complexes do not; this suggested that either a species was being formed *in situ* or that intermediates were building up to a level at which on-pathway isomerisation became kinetically competent *versus* metathesis.

Of the hydride complexes studied, two were found to be kinetically competent to isomerise alkenes at a rate comparable to that obtained from RCM reactions if present at loadings of *ca.* $0.5 \text{ mol}\%$ or greater. However, no ruthenium hydride complexes were observed in the ^1H NMR spectra from kinetic experiments with 1,8-

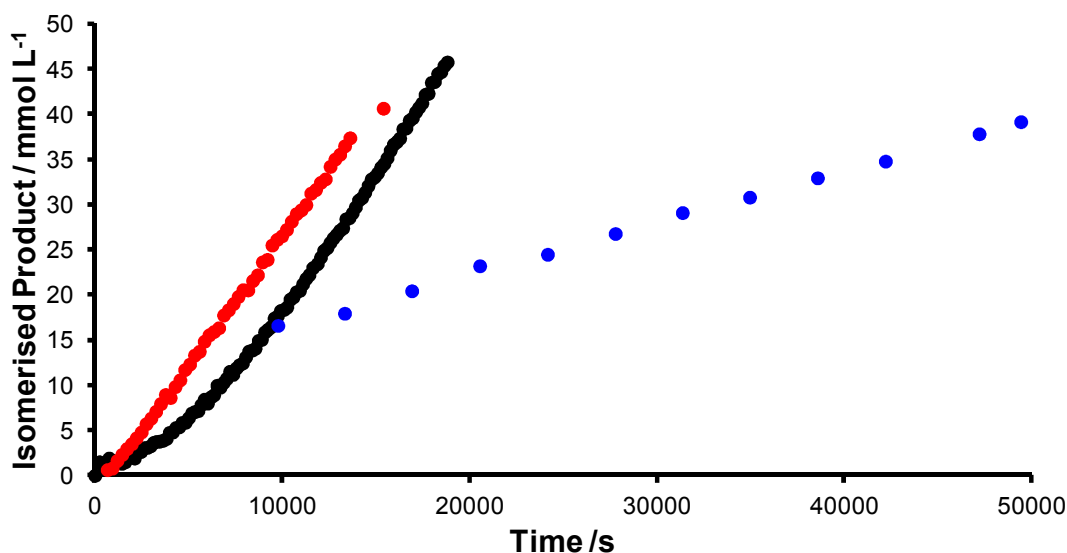


Figure 4.13. Concentration/time profiles for (a) cyclohexene in the metathesis reaction of 1,8-nonadiene (0.5 mol L^{-1} in benzene- d_6 , with 3 mol% **G2**, at 298 K) (**black**) and (b) 2-octene in the isomerisation reaction of 1-octene (0.5 mol L^{-1}) with (i) **167b** (1 mol% in toluene- d_8 at 298 K) (**red**) and (ii) **41** (0.2 mol% in DCM- d_2 at 294 K) (**blue**).

nonadiene RCM. Therefore, neither of these species was present at a loading of *ca.* 0.5 mol%. Secondly, it is not clear how these complexes might arise. The water content of the solvents used for these reactions was found to be less than 10 ppm (by Karl-Fischer titrimetry), which is equivalent to *ca.* 0.5 mmol L^{-1} ; however, a pathway involving the reaction of 14e ruthenium alkylidene species with water would require a bimolecular reaction between two species which are both present in trace quantities, to generate an undetectable quantity of a complex that is a remarkably efficient isomerisation catalyst. No alcohol or base was detected (by ^1H NMR) so this pathway cannot contribute significant quantities of ruthenium complexes (such as hydridocarbonyl complex **167b**).⁷⁹ Diruthenium hydride **41** was not detected in metathesis reactions, and could only be formed when *purified* methylidene complex **3b** was thermolysed for extended periods under rigorously controlled conditions. The harsh conditions required to generate known ruthenium hydride complexes contrast significantly with the mild conditions under which isomerisation side reactions appear in metathesis reactions.

Therefore, it appeared unlikely from these experiments that either of these two complexes are responsible for the isomerisation behaviour during metathesis.

‘On-pathway’ *versus* ‘Off-pathway’ Isomerisation

With the results of the ruthenium hydride benchmarking studies in hand, metathesis experiments were conducted with 1,8-nonadiene to understand if the isomerisation activity was a function of the reaction conditions. Importantly, evidence was sought that might allow identification of either an on-pathway isomerisation mechanism (*via* metathesis intermediates that then return to the catalytic cycle) or an off-pathway isomerisation mechanism (*via* irreversible formation of an isomerisation agent).

Kinetic Studies of Isomerisation in Metathesis Reactions

As discussed above, the metathesis reaction of 1,8-nonadiene was conducted with 0.5 mol L⁻¹ 1,8-nonadiene and 3 mol% pre-catalyst in an NMR tube fitted with a pierced cap. Isomerisation occurred at a rate fast enough to follow by kinetic experiments under these conditions, so these were used as the standard set of conditions around which other factors were varied in order to explore their effect on the reaction outcome.

Exploring the Effects of Solvent

A series of experiments were conducted to identify if the choice or quality of solvent affects the rate and degree of alkene isomerisation. While the majority of experiments described here were conducted in benzene-*d*₆ (for reasons of chemical shift resolution), chloroform-*d*, DCM-*d*₂ and toluene-*d*₈ were also tested. The reaction of 1,8-nonadiene (0.5 mol L⁻¹ with 3 mol% **G2** at 298 K) resulted in differing degrees of isomerisation in each solvent (**Figure 4.14**). These experiments showed that the isomerisation reaction was not indigenous to a specific solvent, or type of solvent (i.e. aromatic or chlorinated aliphatic, for example). The reaction in DCM-*d*₂ exhibited the most isomerisation, but close inspection of the high-field region of the ¹H NMR spectrum revealed the absence of hydride complexes. There was no clear relationship between solvent properties and the isomerisation rate. Benzene and toluene have similar dielectric constants and similar polarity,²⁰⁹ yet isomerisation occurs *ca.* 25% faster in benzene-*d*₆ than in toluene-*d*₈. There is a very approximate correlation between isomerisation rate and solvent boiling point, but isomerisation occurs at the same rate in benzene-*d*₆ and chloroform-*d* despite a *ca.* 20 K difference in boiling point, which may be related to the rate of ethene clearance from solution. The relative ratios of initiation rates for **G2** in these solvents

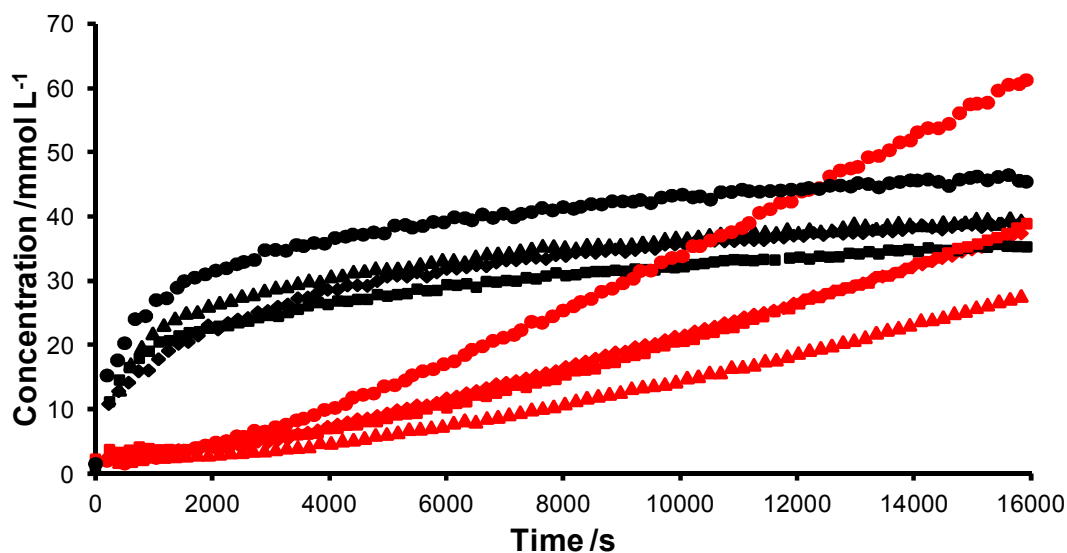


Figure 4.14. Concentration/time profiles for cycloheptene (**black**) and cyclohexene (**red**) in the RCM reaction of 1,8-nonadiene (0.5 mol L^{-1} with 3 mol% **G2** at 298 K) in benzene- d_6 (squares), chloroform- d (rhombi), DCM- d_2 (circles) and toluene- d_8 (triangles).

(see chapter 4) are *ca.* 2 : 1 : 3 : 2 for benzene- d_6 : chloroform- d : DCM- d_2 : toluene- d_8 , which does not reflect the relative rates of isomerisation exhibited in the 1,8-nonadiene RCM reactions. Therefore, while there was a solvent effect on this process, the precise origin of this effect was not clear.

Ruthenium hydride complexes have been reported to arise from the reaction of pre-catalysts **G1** and **G2** with alcohols, so more rigorous purification of the reaction solvents was undertaken, reasoning that isomerisation may be due to traces of alcohol in the solvents. The RCM reaction was repeated in chloroform- d which had been treated in two ways. One reaction was carried out in chloroform- d that had been shaken with an equal volume of distilled water and then separated, while the other was conducted in chloroform- d that had been percolated through a column of activated 4 Å molecular sieves and activated alumina. The water content of the solvents was quantified using Karl-Fischer titrometry: wet solvent contained water at *ca.* 300 ppm, the solvent dried over 4 Å sieves alone contained less than 10 ppm, and the solvent percolated through sieves and alumina before use also contained approximately 10 ppm. The concentration/time profiles were compared with those obtained in solvent dried over 4 Å molecular sieves alone (**Figure 4.15**). The rate of metathesis (i.e. the rate of formation of cycloheptene) was very similar in all three reactions. Remarkably, when the solvent

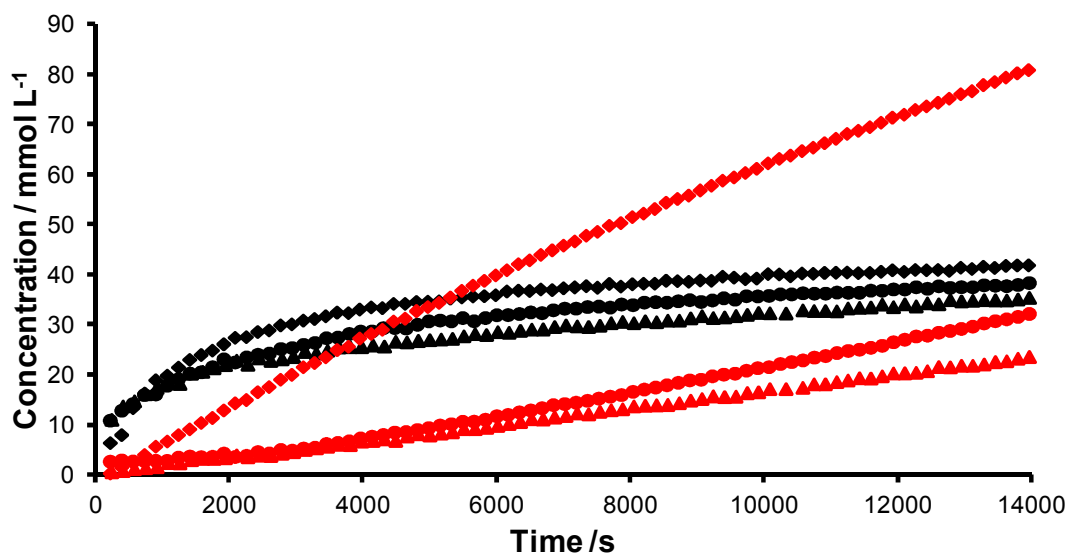


Figure 4.15. Concentration/time profiles for cycloheptene (black) and cyclohexene (red) from the reactions of 1,8-nonadiene with 3 mol% **G2** in (a) solvent dried overnight over activated 4 Å molecular sieves (circles), (b) solvent shaken with an equal volume of distilled water before use (triangles) and (c) solvent dried through a column of activated 4 Å molecular sieves and activated alumina before use (rhombi).

was dried through a column of molecular sieves and alumina, the rate of isomerisation in the reaction increased while deliberate wetting of the solvent *decreased* the rate of isomerisation. It is clear from this result that isomerisation *does not* arise from adventitious water in the solvent. Two possibilities arise from this result: either a water-sensitive species (responsible for off-pathway isomerisation) is formed *in situ*, or intermediates responsible for on-pathway isomerisation are water-sensitive.

If the latter case is true, then the rate of metathesis ought to decrease in the presence of water. 1,7-Octadiene is a useful substrate for measuring metathesis rate, as it cyclises rapidly and irreversibly and exhibits close to first-order (in diene) kinetic behaviour. The RCM of 1,7-octadiene (100 mmol L⁻¹) was therefore performed twice: one reaction was conducted in chloroform-*d* that had been dried over activated 4 Å molecular sieves overnight and the other in chloroform-*d* that had been shaken with an equal volume of distilled water. A low (1 mol%) loading of **G2** was employed, so that any significant decomposition of the metathesis intermediates should manifest in a difference in metathesis rate. The concentration/time profiles were obtained by ¹H NMR spectroscopy at 298 K (**Figure 4.16**). These results suggest that some

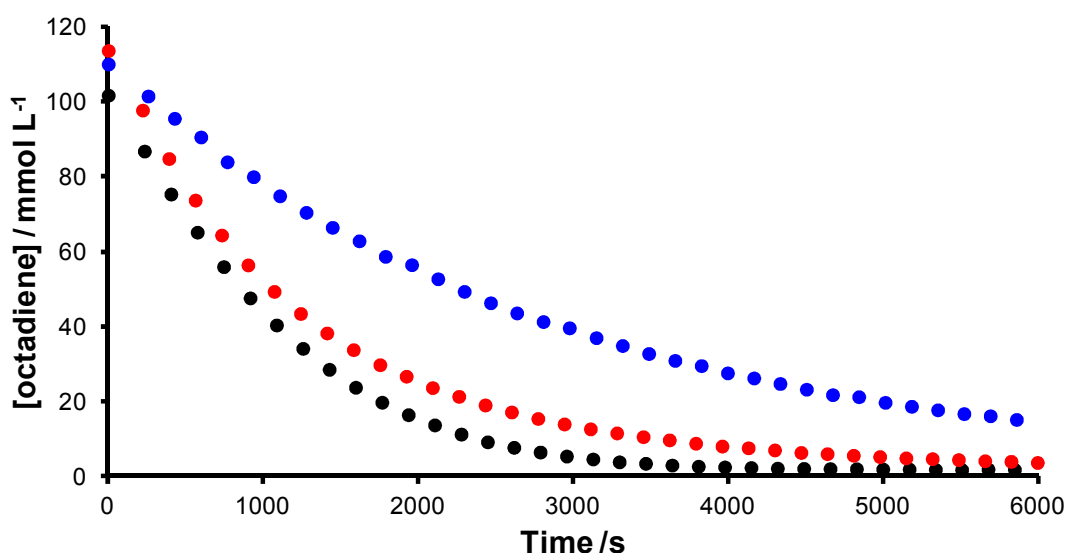


Figure 4.16. Concentration *versus* time profiles for the consumption of 1,7-octadiene in the RCM reaction of 1,7-octadiene (0.1 mol L^{-1} in chloroform-*d* at 298 K, with 1 mol% **G2**) in solvent (a) dried overnight on 4 \AA molecular sieves (**black**), (b) shaken with an equal volume of distilled water (**red**) or (c) containing 0.1 mol L^{-1} ethanol (**blue**).

intermediates are being decomposed by water present in the solvent, which could lead to a decrease in the rate of on-pathway metathesis. In contrast, the addition of one equivalent of ethanol (with respect to 1,7-octadiene) to the reaction yielded a significant decrease in metathesis rate (**Figure 4.16** above); treatment with activated alumina should have removed any traces of alcohol, however. A simple first-order treatment of the three datasets revealed that a small difference in rate was observed when the reaction solvent was treated with distilled water (*ca.* 30%), but that the presence of 1 equivalent of ethanol decreased the metathesis rate three-fold (**Figure 4.17**).

These results shows that alcohols can inhibit the rate of metathesis reactions; however, ethanol was present at *ca.* 0.1 mol L^{-1} while in the previous experiment water was present only at 300 ppm, so these experiments alone do not provide information about the relative inhibitive ability of water and ethanol. It is clear, however, that both substances should be avoided in metathesis reactions.

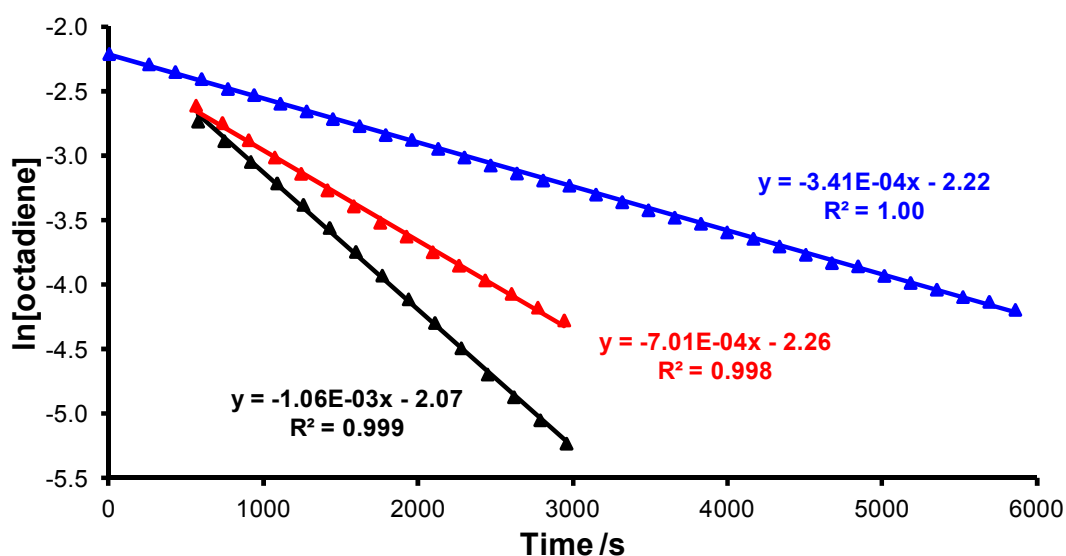


Figure 4.17. First order treatment of concentration/time data from the RCM reactions of 1,7-octadiene (0.1 mol L^{-1} in chloroform-*d* at 298 K with 1 mol% **G2**) in (a) dried overnight on 4 Å molecular sieves (**black**), (b) shaken with an equal volume of distilled water (**red**) or (c) containing 0.1 mol L^{-1} ethanol (**blue**).

Exploring the Effects of Pre-catalyst

A significant and growing number of metathesis pre-catalysts are known in the literature.¹⁵⁶ A number of pre-catalysts were studied in order to evaluate their influence on the isomerisation rate. The reaction of 1,8-nonadiene with 3 mol% **G2** in benzene-*d*₆ was used as the benchmark reaction for these studies; benzene-*d*₆ allowed resolution of the ethene ¹H NMR signal from that of the oligomers, and therefore reactions in this solvent allowed more detailed quantitative insights into the reaction profiles.

Studies were conducted with pre-catalyst **G1**, which features two PCy₃ ligands rather than an NHC ligand and a single PCy₃ ligand;⁹ it therefore exhibits quite different reactivity in metathesis reactions compared to **G2**.^{10,45,62} The concentration/time profile from the reaction of 1,8-nonadiene (at 0.5 mol L^{-1}) with **G1** revealed far slower production of cyclohexene than in the corresponding reaction with **G2** (**Figure 4.18**). Less than 0.5% conversion of 1,8-nonadiene to cyclohexene was obtained. The concentration of ethene peaked early in the reaction at *ca.* 120 mmol L^{-1} , suggesting that rapid metathesis occurred within the first few minutes of the experiment. The concentration of cycloheptene reached a maximum, decayed to *ca.* 50 mmol L^{-1} and then increased gradually to 60 mmol L^{-1} . Only traces of cyclic dimer **106d** were obtained. The

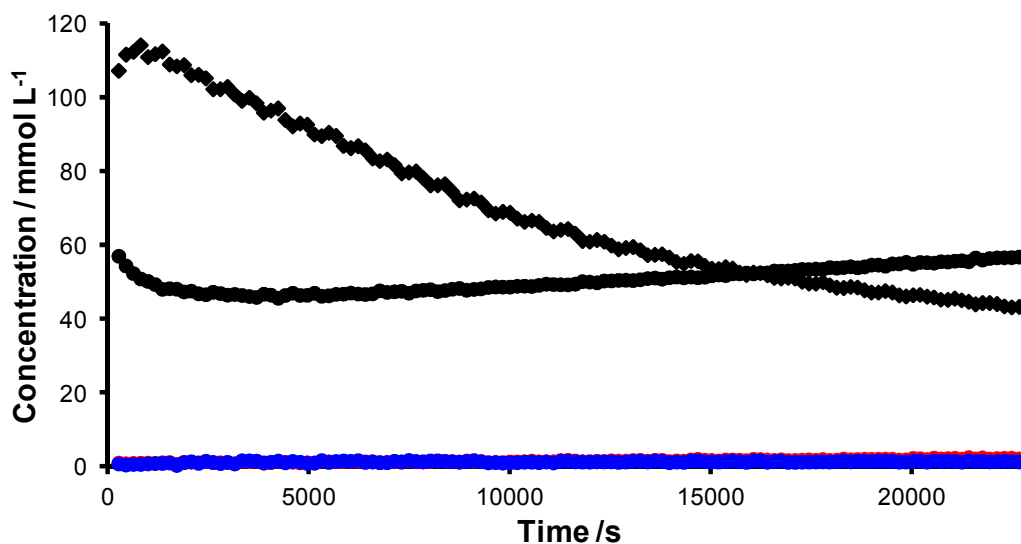
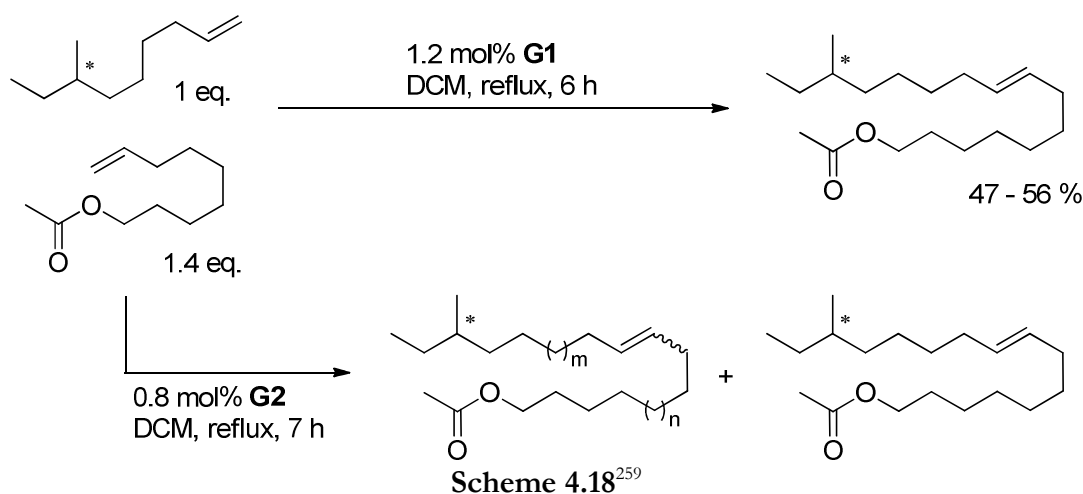


Figure 4.18. Concentration/time profiles from the reaction of 1,8-nonadiene with 3 mol% **G1** in benzene- d_6 at 298 K, showing (a) cycloheptene (**black circles**), (b) ethene (**black rhombi**), (c) cyclohexene (**red circles**) and (d) cyclic dimer **106d** (**blue circles**).

contrast between **G1** and **G2** was stark; the latter typically yields the thermodynamic product distribution, suggesting that cyclic dimer **106d** may be the product of oligomer back-biting processes (i.e. secondary metathesis), rather than simply dimerisation then RCM. Secondary metathesis processes are known to be slower with **G1** than with **G2**.⁴⁵

The very low rate of isomerisation in this experiment is in agreement with other literature reports of isomerisation processes in metathesis reactions. Mori used a key cross-metathesis step *en route* to pest insect pheromones (**Scheme 4.18**); both **G1** and **G2** were tested for this reaction.²⁵⁹ While **G1** furnished the desired cross-metathesis



products in moderate to good yields, significant quantities of products derived from isomerisation were obtained when **G2** was employed. Mori conducted GC-MS analyses of the reaction mixture, which detected a large number of species, including the starting materials, the desired product, homo-dimers of both starting materials, and many isomerised analogues thereof. In the latter products, numbers of CH₂ units were added or removed, leading to a complex distribution of signals in the chromatogram (**Figure 4.19**). While benchmarking studies with known ruthenium hydride complexes have established that such complexes that are structurally similar to **G1** (such as **167a**) are less active than those bearing NHCs (*vide supra*), the outcomes of the metathesis of 1,8-nonadiene with **G1** do not decisively distinguish between on-pathway and off-pathway mechanisms. The intermediates derived from **G1** and **G2** potentially behave very differently in both on-pathway mechanisms, in their propensity to generate hydride species *and* in the activity of those *in situ*-generated hydride complexes. The intermediates derived from **G1** are known to differ in reactivity from those derived from **G2**, for example, methyldiene **3a** can bind and dissociate phosphane reversibly, while the second-generation analogue **3b** is captured irreversibly by phosphane.²⁶ Van Rensburg *et al.* have calculated the barriers to β -hydride transfer in MCBs derived from both **G1** and **G2-unsat**.²⁴⁸ The barrier to hydride transfer is considerably *lower* for **G1**-

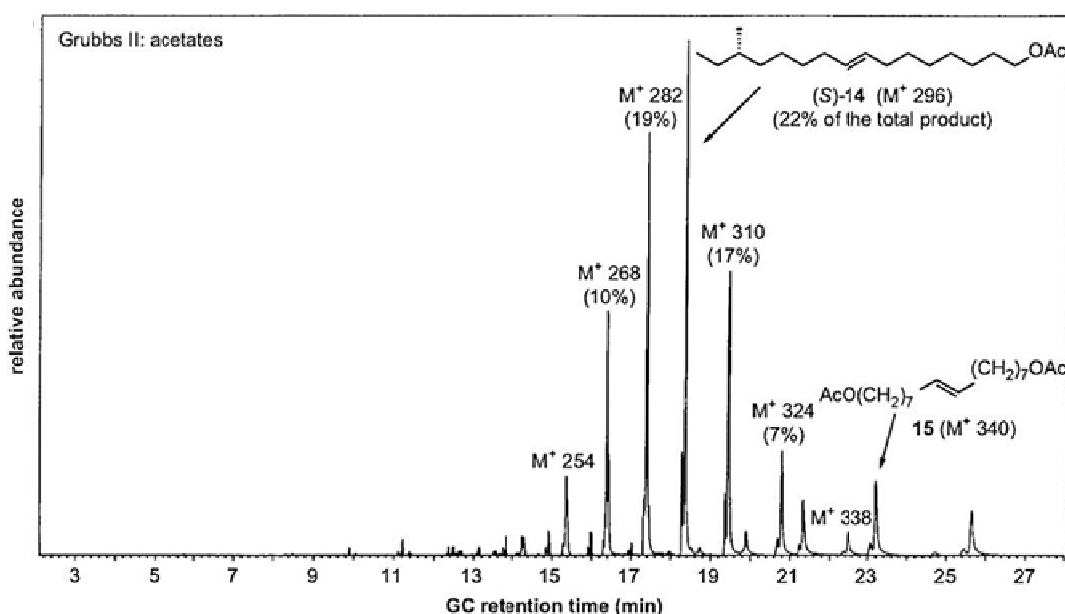


Figure 4.19. GC-MS trace from the metathesis reaction in **Scheme 4.18**, showing all reaction components that contain acetate functionality.²⁵⁹

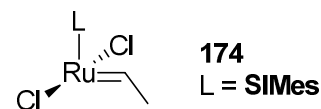
derived MCBs (16.9 kcal mol⁻¹ *versus* 24.3 kcal mol⁻¹), which would suggest that **G1** decomposition *via* this process ought to be considerably faster, as would an isomerisation mechanism based upon this process. However, MCBs are not as low in energy (with respect to the corresponding η^2 -complex, as determined by DFT calculations) for **G1**-catalysed metathesis reactions²⁶⁰⁻

²⁶¹ as in **G2**-catalysed metathesis reactions.⁵³ Piers *et al.* have observed and characterised MCB **53b**



spectroscopically, but could not generate analogue **53a**.³² Therefore the van Rensburg mechanism could be operating in **G2**-catalysed reactions, as the concentrations of MCB species are likely to be much higher than in **G1**-catalysed reactions.

Pre-catalyst **GH2** and analogues thereof were evaluated subsequently. This class of pre-catalyst initiates by a different mechanism from **G2** (as discussed in chapter 4),^{60-61,191} and typically initiates much faster than **G2** in the presence of high concentrations of alkene. In addition, no PCy₃ is present to recapture the ruthenium alkylidene species. The chelating alkoxy styrene ligand was initially believed to return to the metal centre once the metathesis reaction was complete,¹¹ but this has recently been shown to remain in solution and not return to the metal centre.¹⁹⁰ Therefore, once alkylidenes enter the catalytic cycle, they only exit *via* decomposition; in the corresponding reactions with **G2**, intermediate species such as alkylidene **119** and ethylidene **174** can be reversibly captured by phosphane, while methylidene **4b** can be removed from the catalytic cycle if it is captured by phosphane.²⁶



When a 0.5 mol L⁻¹ solution of 1,8-nonadiene in benzene-*d*₆ was exposed to **GH2** (3 mol%), the reaction outcome was dramatically different to that obtained from the corresponding reaction with **G2** (**Figure 4.20**). The equilibrium concentrations of cycloheptene and cyclic dimer **106d** were obtained within a few minutes of adding the 1,8-nonadiene solution to solid **GH2**, after which cyclohexene was produced rapidly. The corresponding pre-catalyst concentration/time profile confirmed that **GH2** entered the catalytic cycle more rapidly than **G2**, but this process was neither complete nor pseudo-first order in pre-catalyst (**Figure 4.21**). No new ruthenium carbene species were detected upon inspection of the low field region of the ¹H NMR spectra.

The ruthenium carbene species detected during **G2**-catalysed metathesis were all phosphane-bound, as ruthenium carbene species that are not phosphane-bound will be

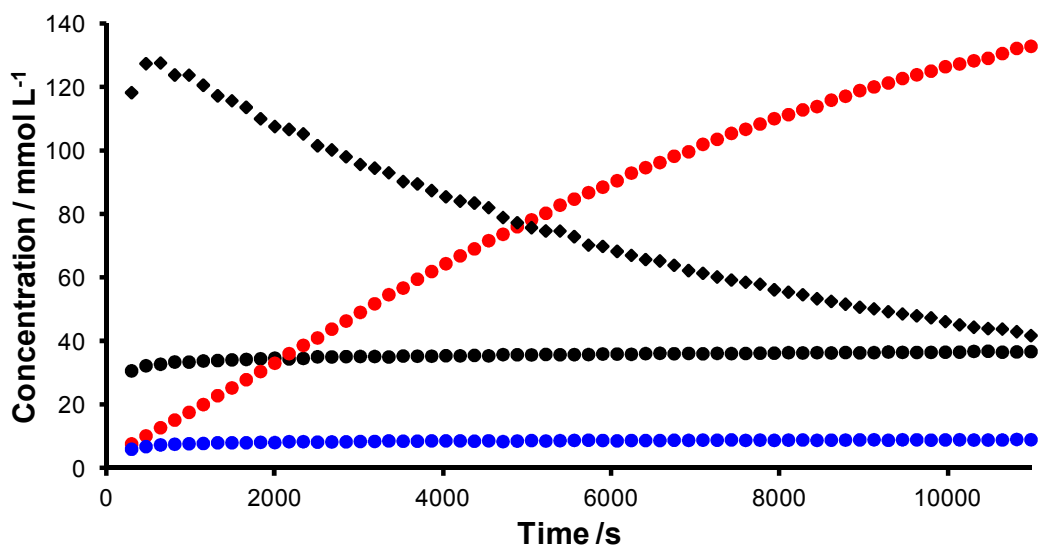


Figure 4.20. Concentration/time profiles, from the metathesis reaction of 1,8-nonadiene (0.5 mol L^{-1}) with 3 mol% **GH2** in benzene at 298 K, of (a) cycloheptene (**black circles**), (b) ethene (**black rhombi**), (c) cyclohexene (**red circles**) and (d) cyclic dimer **106d** (**blue circles**).

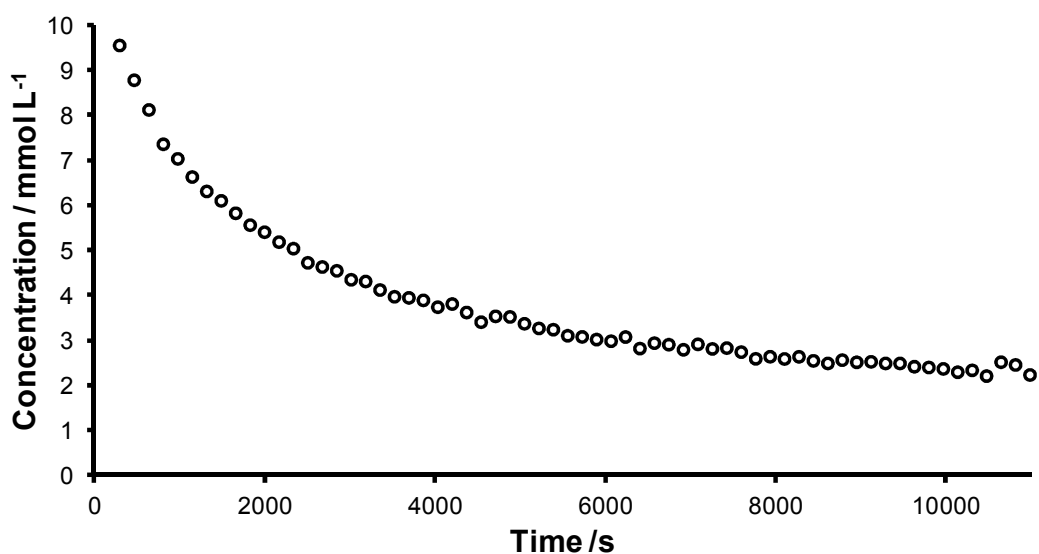


Figure 4.21. Concentration/time profile for **GH2** from the metathesis reaction of 1,8-nonadiene (0.5 mol L^{-1}) with 3 mol% **GH2** in benzene at 298 K.

rapidly interconverting between ruthenium carbene, η^2 -complexes and metallocyclobutanes, and therefore their ^1H NMR signals will be averaged across the spectrum, as discussed previously. Only at low ($< ca. 223 \text{ K}$) temperatures do species

such as MCBs undergo reaction on (or slower than) the NMR timescale, and therefore become spectroscopically observable.³²

The result from **GH2**-catalysed metathesis could indicate either an on-pathway or off-pathway process. If isomerisation was a result of on-pathway processes, the increased concentrations of intermediates (such as MCBs) would increase the rate of alkene isomerisation by these intermediates. If however the isomerisation was a result of off-pathway processes, the absence of phosphane could prevent hydride species such as **167b** becoming captured by phosphane. The isomerisation obtained in this experiment cannot be a result of complex **41**, as this is only formed from methylenide **3b**.²⁸

A large number of analogues of **GH2** have been reported, where substitution of the chelating alkoxy styrene ligand with electron-withdrawing groups typically leads to more rapid initiation. Two analogues of **GH2** were explored for the metathesis reaction of 1,8-nonadiene. Pre-catalysts **Zhan1B** and **Grela**¹⁵ have been found to initiate *ca.* 5-fold and 11-fold faster than **GH2**, respectively (see chapter 3), due to electronic activation from the dimethylsulfonamido- and nitro- substituents respectively. This results in the pre-catalyst entering the cycle more quickly, and a higher concentration of intermediates being generated more rapidly. Therefore, if the isomerisation reaction is an on-pathway process, these faster initiators would be expected to lead to more isomerisation in the reaction. The concentration/time profiles for pre-catalyst consumption and cycloheptene and cyclohexene formation in the RCM reactions of 1,8-nonadiene with 3 mol% of **GH2**, **Zhan1B**, and **Grela** (in benzene-*d*₆ at 298 K) were compared (**Figures 4.22** and **4.23**). The reaction profiles were found to be very similar, despite the marked differences in initiation rate. In all cases, cycloheptene quickly reached an equilibrium concentration of *ca.* 40 mmol L⁻¹, while cyclohexene formation was rapid. Notably, the degree of isomerisation was very similar with all three catalysts, which suggested that the source of the isomerisation was off-pathway, or that the rate-limiting step of the on-pathway isomerisation was much slower than the initiation rate.

Pre-catalyst **M8₅₃-SIPr** was also tested in the metathesis reaction of 1,8-nonadiene under the same conditions. This pre-catalyst initiates *ca.* 1.5-fold faster than **Grela** and possesses a different NHC ligand (**SIPr** rather than **SIMes**). The concentration *versus* time profile for this reaction showed rapid production of cyclohexene, faster even than the rate of cyclohexene formation in **GH2**-catalysed metathesis (**Figure 4.24**). This difference in activity is not due to the initiation rate, as

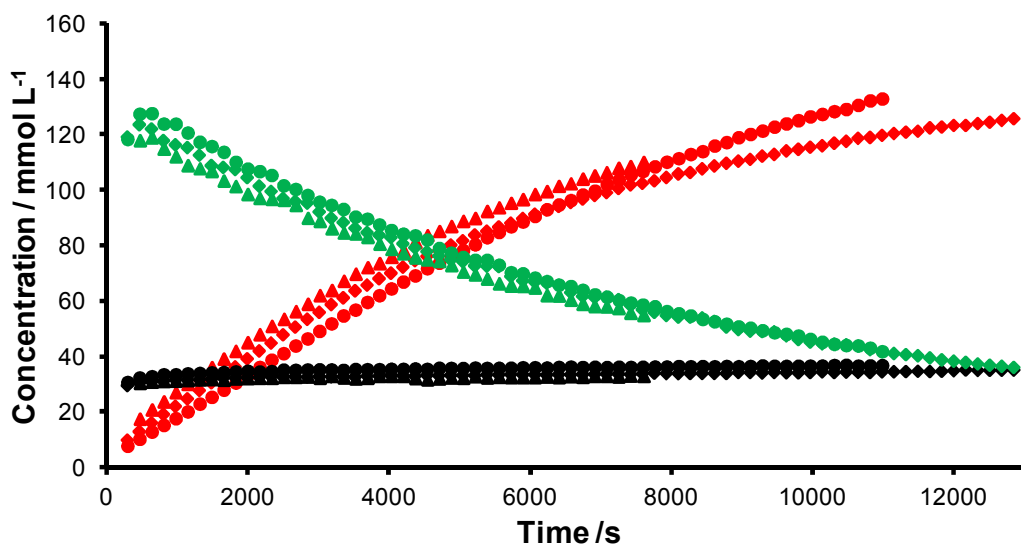


Figure 4.22. Concentration *versus* time profiles for cycloheptene (**black**), cyclohexene (**red**) and ethene (**green**) in the RCM of 1,8-nonadiene (0.5 mol L^{-1} in benzene- d_6 at 298 K) with 3 mol% of (i) **GH2** (circles), (ii) **Zhan1B** (triangles) and (iii) **Grela** (rhombi).

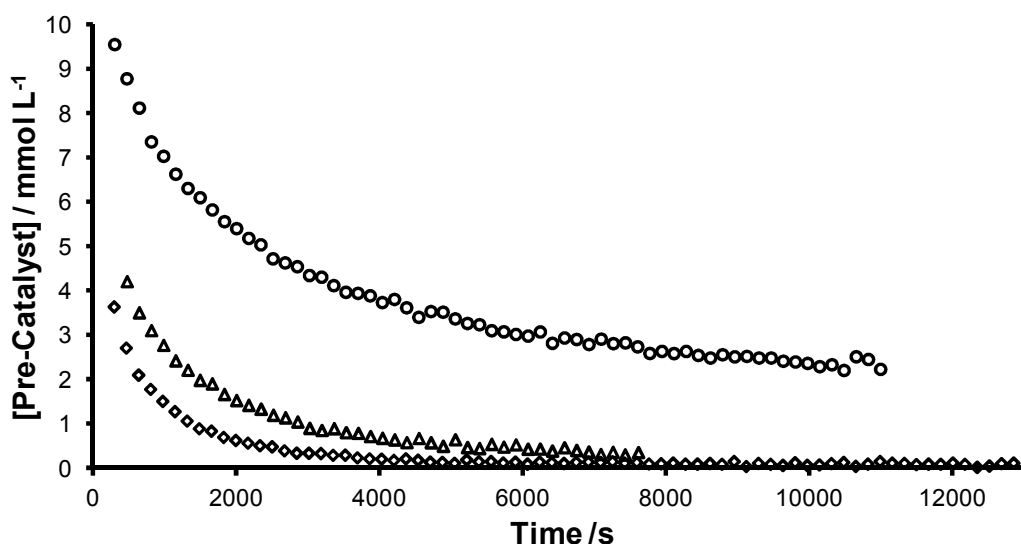


Figure 4.23. Concentration *versus* time profiles pre-catalyst in the RCM reactions of 1,8-nonadiene (0.5 mol L^{-1} in benzene- d_6 at 298 K) with 3 mol% of (i) **GH2** (circles), (ii) **Zhan1B** (triangles) and (iii) **Grela** (rhombi).

Grela and **Zhan1B** both initiate much faster than **GH2** but did not lead to an increased rate of isomerisation. The origin of the increased isomerisation rate must therefore be the different NHC; either the different ligand affects the barriers on the PES for on-

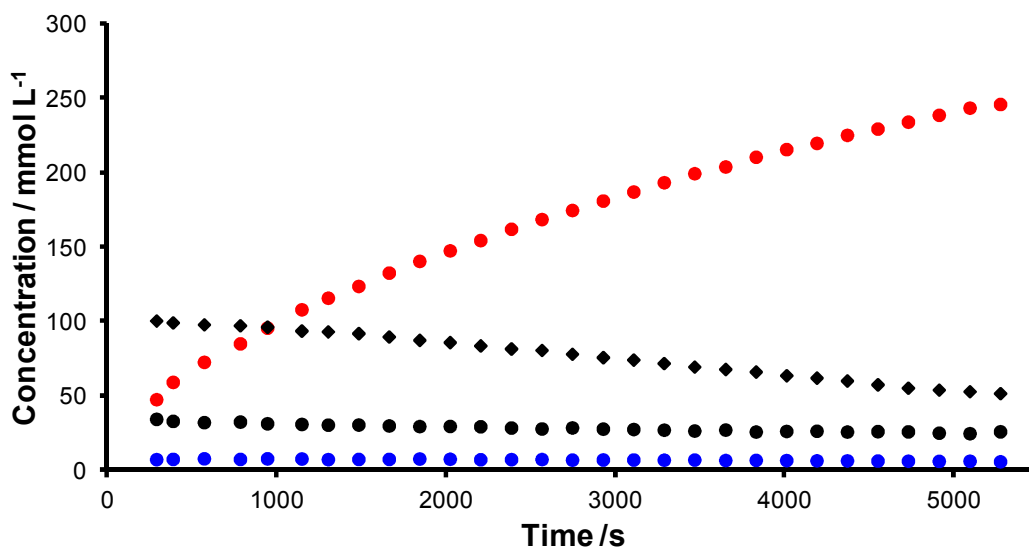


Figure 4.24. Concentration/time profiles, from the metathesis reaction of 1,8-nonadiene (0.5 mol L^{-1}) with 3 mol% **M853-SIPr** in benzene at 298 K, of (a) cycloheptene (**black circles**), (b) ethene (**black rhombi**), (c) cyclohexene (**red circles**) and (d) cyclic dimer **106d** (**blue circles**).

pathway isomerisation or *in situ* generated ruthenium hydride complexes bearing this NHC are more active than the corresponding **SIMes**-bearing analogues.

As discussed, it is not possible to identify and characterise the ruthenium carbene intermediates in **GH2**-catalysed metathesis reactions because phosphane is not present to capture the alkylidene intermediates and render them observable by ^1H NMR spectroscopy. In an attempt to overcome this limitation, the metathesis reaction of 1,8-nonadiene with **GH2** (3 mol%) was repeated and quenched with free phosphane at different time points. Three identical reactions were conducted in NMR tubes, each of which was quenched at a different time point ($t = 30 \text{ min}$, 1 h and 1.5 h) by the addition of a concentrated solution of PCy_3 (approx 10 mol% with respect to 1,8-nonadiene). The reactions were then analysed by NMR spectroscopy (**Figure 4.25**). A 400 MHz NMR spectrometer was employed, so two separate spectra were acquired due to the *ca.* 35 ppm spectrum width limitation; one spectrum covered the window from $\delta_{\text{H}} = 22$ to -2 ppm, while the second covered the window from $\delta_{\text{H}} = 0$ to -35 ppm. The spectra clearly showed a mixture of species consistent with the presence of methylidene **3b** (δ_{H} (benzene- d_6) = 18.33 ppm, s) and phosphane-captured **GH2** (δ_{H} (benzene- d_6) = 20.27, s; *lit.* δ_{H} (toluene- d_8) = 20.27, s).⁶¹ In addition, a complex signal was obtained that was

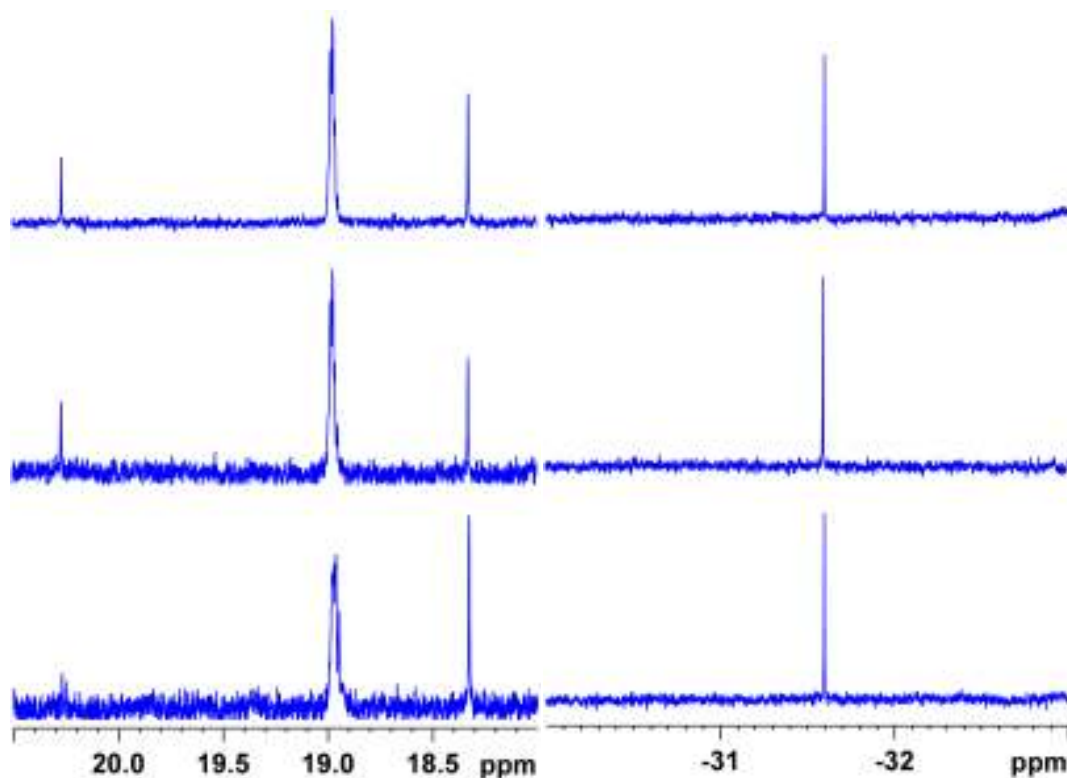


Figure 4.25. Partial ^1H NMR spectra of the tricyclohexylphosphane-quenched reaction mixture from the RCM of 1,8-nonadiene (0.5 mol L^{-1} in benzene- d_6) with **GH2** (3 mol%) (a) showing the low-field, ruthenium carbene region and (b) part of the high-field, ruthenium hydride region; reactions were quenched at (i) 0.5 hours, (ii) 1 hour and (iii) 1.5 hours.

consistent with a mixture of alkylidene **121c** and ethylidene **31b** ($\delta_{\text{H}} = ca. 19 \text{ ppm}$). The high field region of the ^1H NMR spectrum did not show the presence of hydridocarbonyl complexes **167a** or **167b**, or diruthenium hydride **41**.²⁸ However, a new and unidentified species (δ_{H} (benzene- d_6) = -31.60 ppm , s) was observed in all three samples. The chemical shift of this signal indicated that it represented a ruthenium hydride more shielded than hydridocarbonyl species **167**, while the singlet multiplicity revealed no $^2J_{\text{H,P}}$ coupling. This species therefore either did not feature a phosphane ligand, or was a multinuclear ruthenium complex where the $^nJ_{\text{H,P}}$ coupling was too small to observe; the line width of this signal at half-height was *ca.* 1.5 Hz. The possibility that the species was present in the pre-catalyst was ruled out by ^1H NMR spectroscopic analyses of **G2** and **GH2** in the absence of substrate.

The chemical shift of the unknown hydride species was 6 ppm further to the high field than that of hydridocarbonyl species **167**, so lay out with the spectrum width examined during the kinetic experiments. The reaction was repeated without a phosphane quench, and the high field of the ^1H NMR spectrum was inspected; the signal was not observed so must correspond to a phosphane-bound species, or a species that is formed in a process involving phosphane.

The results from these studies suggested that an off-pathway mechanism was most likely, as species consistent with a ruthenium hydride complexes were observed by ^1H NMR spectroscopy. However, the experiments provided little insight into the identity or origin of this species, as it was not clear from where these species arose.

Isomerisation in ROMP *versus* RCM

Extensive isomerisation was observed in all of the 1,8-nonadiene RCM reactions with second-generation pre-catalysts (those bearing an NHC ligand). The experiments documented above had ruled out diruthenium hydride complex **41** as the source of isomerisation. In addition, it was shown that wet solvents decreased the rate of isomerisation. Further insight was sought into the generality and source of the isomerisation processes.

ROMP, like RCM, proceeds *via* various η^2 -complexes and MCBs; many of the intermediates on each pathway are common to both classes of metathesis reaction. However, ethene is not present in ROMP reactions so this may result in differences in isomerisation behaviour; no isomerisation occurred in the ethene-free ROMP of cycloheptene discussed in chapter 2, for example. In order to explore the differences between RCM and ROMP reactions, the ROMP reaction of cycloheptene (0.5 mol L^{-1} in benzene- d_6) was carried out with **G2** (3 mol%) in the absence of ethene. The concentration/time profile (**Figure 4.26**) revealed very little isomerisation in this reaction mixture. The concentration of cycloheptene dropped rapidly from 0.5 mol L^{-1} to less than 0.1 mol L^{-1} within the first ten minutes of the experiment, while the cyclic dimer concentration peaked at *ca.* 45 mmol L^{-1} . Cyclohexene production was slow, with only *ca.* 2% conversion of cycloheptene to cyclohexene after *ca.* 4 hours. The remainder of the material balance consisted of larger oligomers as evidenced by the large, complex multiplet in the ^1H NMR spectrum at 5.5 ppm. The low field region of the ^1H NMR spectrum revealed only two ruthenium species: **G2** and a triplet signal assigned to

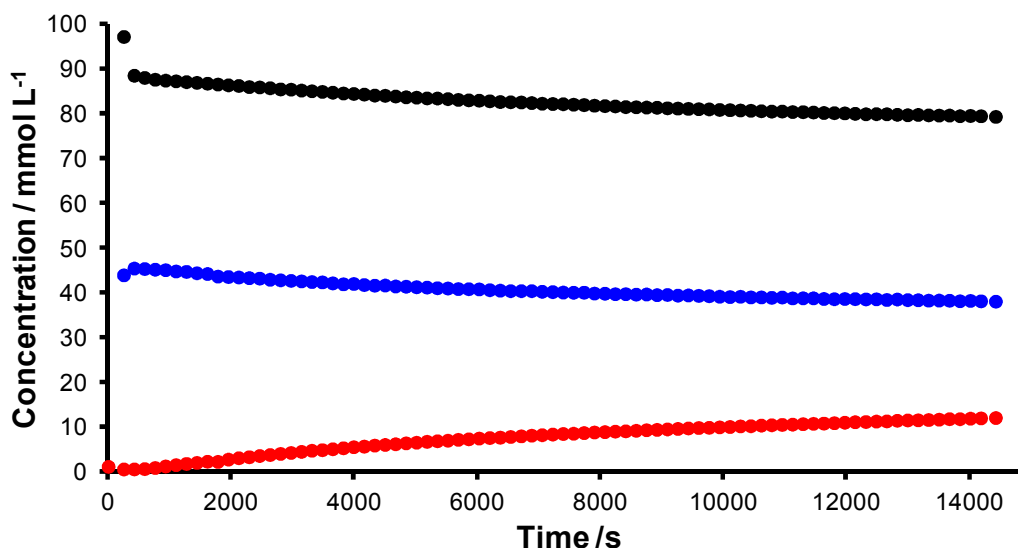


Figure 4.26. Concentration *versus* time profiles for (a) cycloheptene (**black**), (b) cyclohexene (**red**) and (c) cyclic dimer **106d** (**blue**) in the ROMP reaction of cycloheptene (0.5 mol L⁻¹ in benzene-*d*₆ with 3 mol% **G2** at 298K).

propagating carbene **121c** and longer chain analogues thereof; pre-catalyst **G2** was consumed in a first order reaction ($k_{obs} = 8.7 \times 10^{-5} \text{ s}^{-1}$, $R^2 = 0.9996$; *cf.* initiation rate in benzene-*d*₆ with ethyl vinyl ether $k_{mit} = 1.0 \times 10^{-4} \text{ s}^{-1}$) while the triplet signal was found to increase correspondingly during the course of the experiment (**Figure 4.27**). Material balance in the ruthenium carbene region was excellent, with only *ca.* 5% (0.7 mmol L⁻¹) of the initial charge of pre-catalyst unaccounted for after 4 hours. In this experiment, no ethene is present so the equilibrium exists between cycloheptene and cyclic dimer **106d**. In the ROMP experiment where the solvent is first sparged with ethene, 1,8-nonadiene and linear oligomers can also be formed. In addition, methyldiene **3b** is detected in the latter experiment, whereas it cannot form in ethene-free ROMP reactions.

According to **Equations 4.01** and **4.02**, ΔG for the ROMP of two molecules of cycloheptene to form one molecule of cyclic dimer can be calculated from the experimentally measured concentrations of cycloheptene and cyclic dimer. This value is approximately -1.1 kcal mol⁻¹ at 298 K ($K = 6$ at 14,000 seconds).

$$K = \frac{[\text{cyclic dimer } \mathbf{106d}]}{[\text{cycloheptene}]^2} \quad (4.01)$$

$$= \exp(-\Delta G/RT) = \exp(-(G_{\text{dimer}} - 2G_{\text{cycloheptene}})/RT) \quad (4.02)$$

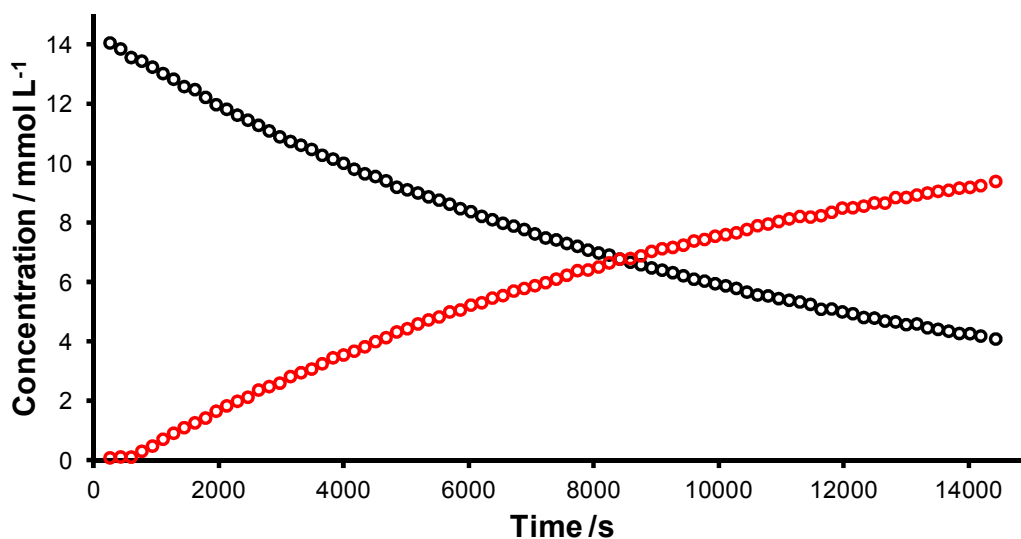


Figure 4.27. Concentration *versus* time profiles for pre-catalyst **G2** (black) and propagating carbenes (red) in the ROMP reaction of cycloheptene (0.5 mol L^{-1} in benzene- d_6) with 3 mol% **G2** at 298 K.

The ROMP experiment was repeated with *ca.* 0.1 equivalents of 1,7-octadiene added after 25 minutes. 1,7-Octadiene underwent RCM rapidly, producing cyclohexene plus ethene; the ethene that was generated was quickly consumed by the reaction and signals consistent with alkene end groups were observed throughout the remainder of the reaction. A small quantity (*ca.* 0.5 mmol L^{-1}) of methyldiene **3b** was detected in the low field region of the ^1H NMR spectra. After 1,7-octadiene was added, the isomerisation process was enabled, and quantities of cyclohexene (beyond those generated from the charge of 1,7-octadiene) were found to be produced (**Figure 4.28**). A similar level of isomerisation occurred when the reaction solvent was sparged with ethene *via* a fine-tipped pipette for 5 minutes (to *ca.* 50 mmol L^{-1} , therefore one equivalent) before the diene solution was added to the pre-catalyst (**Figure 4.29**). The charge of ethene was consumed entirely and alkene end-groups were observed *via* their characteristic signals at $\delta_{\text{H}} = \text{ca. } 5.8 \text{ ppm}$ and *ca.* 5.0 ppm ; the ethene concentration in RCM reactions in NMR tubes fitted with pierced caps decreased slowly over a number of hours; however the ethene consumption by reaction was far more rapid. These outcomes suggested that the methyldiene complex was the primary source of isomerisation, either as a source of ruthenium hydride complexes or *via* a MCB complex with a specific substitution pattern, for example.

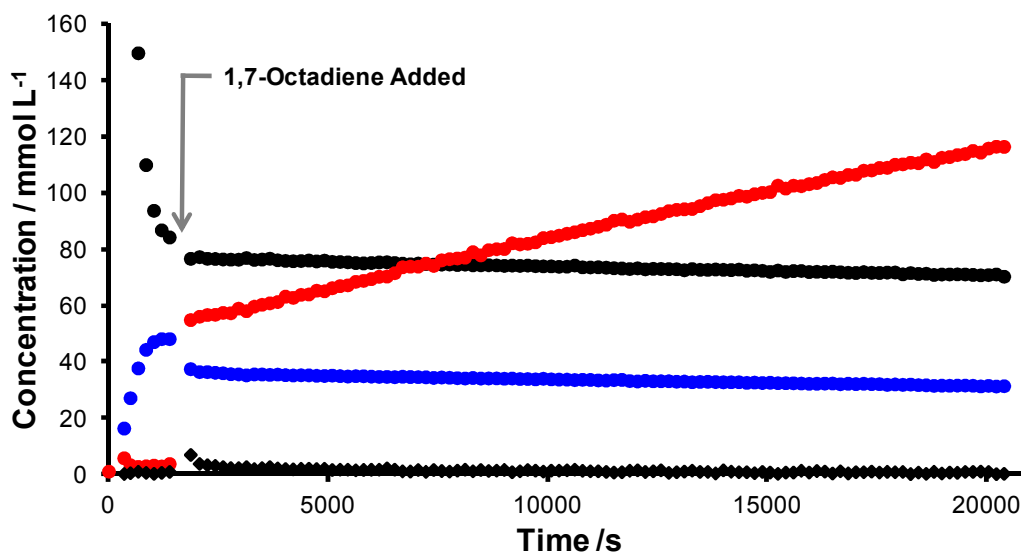


Figure 4.28. Concentration *versus* time profiles for cycloheptene (**black circles**), cyclohexene (**red circles**), cyclic dimer **106d** (**blue circles**) and ethene (**black rhombi**) in the ROMP reaction of cycloheptene (0.5 mol L^{-1} in benzene- d_6 with 3 mol% **G2** at 298 K) where *ca.* 0.1 equivalents of 1,7-octadiene were charged after 25 minutes.

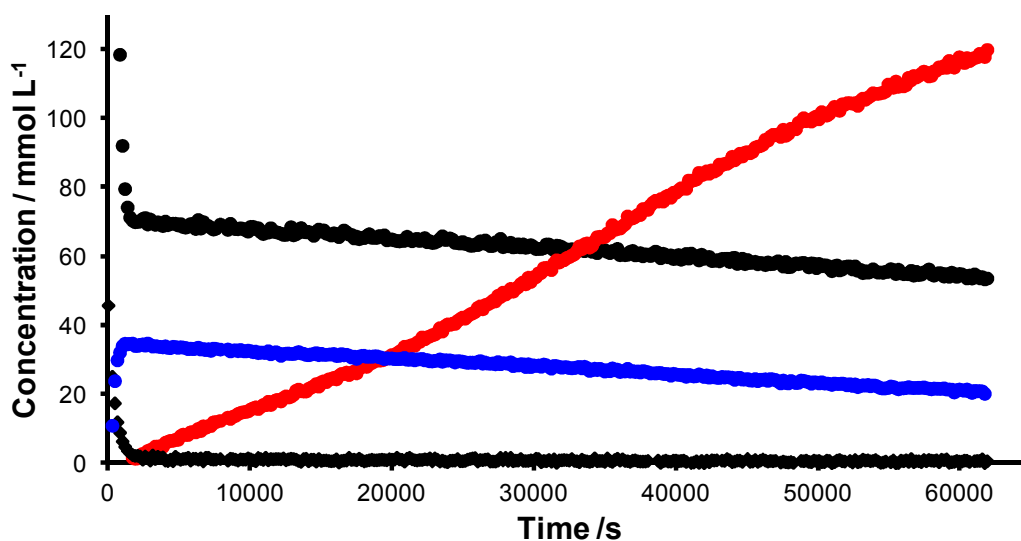


Figure 4.29. Concentration *versus* time profiles for cycloheptene (**black circles**), cyclohexene (**red circles**), cyclic dimer **106d** (**blue circles**) and ethene (**black rhombi**) in the ROMP reaction of cycloheptene (0.5 mol L^{-1} in ethene-sparged benzene- d_6 with 3 mol% **G2** at 298 K).

The low field region of the ^1H NMR spectra revealed the expected pre-catalyst decay, with a corresponding build up in alkylidene concentration which then decayed. Ethylidene **31b** and methylidene **3b** were produced in low (*ca.* 4 mmol L $^{-1}$ and 0.5 mmol L $^{-1}$, respectively) concentrations. Inspection of the high-field region of the ^1H NMR spectrum revealed traces of a signal consistent with hydridocarbonyl complex **167b**; while the signal to noise ratio did not permit quantification and profiling of the hydridocarbonyl complex throughout this reaction, the mere observation of this species in a metathesis reaction is exciting. To date, there have been no other reports of the observation of this ruthenium hydride complex in metathesis reaction mixtures, although Wagener *et al.* have detected traces of an unidentified complex ($\delta_{\text{H}} = -20.36$ ppm, d ($^2J_{\text{H,P}} = 17.8$ Hz)) in the metathesis reactions of 1-octene, and traces of other hydrides in the decomposition mixtures arising from analogues of **G2** and methylidene **3b**.²⁴⁵ Most literature reports of isomerisation in metathesis reactions infer (at best) or assume (at worst) the involvement of ruthenium hydride complexes. In these experiments, despite the poor signal to noise ratio, the chemical shift (δ_{H} (benzene- d_8) = -24.81 ppm) and proton-phosphorus coupling constant ($^2J_{\text{H,P}} = 21.0$ Hz) were both found to be consistent with the literature (δ_{H} (benzene- d_6) = -25.43 ppm, d ($^2J_{\text{H,P}} = 21.6$ Hz); δ_{H} (DCM- d_2) = -25.37 ppm, d ($^2J_{\text{H,P}} = 21.3$ Hz)).^{79,244}

A concentration/time profile for this species throughout the reaction was desired, so the ROMP experiment in ethene-sparged benzene- d_6 was repeated with a higher pre-catalyst loading (15 mol% **G2**) and with more scans per data point in order to increase the signal to noise ratio; 16 scans were acquired per spectrum, which should result in a *ca.* 2.8-fold increase in signal to noise over spectra acquired with 2 scans. The profile obtained was informative, clearly showing the production of **167b** over the course of the experiment (**Figures 4.30** and **4.31**). In addition, a new signal was observed to appear, peak (at *ca.* 0.4 mmol L $^{-1}$), and disappear during the course of the reaction (δ_{H} (benzene- d_6) = 14.08 ppm, s). The chemical shift of this species suggested that it possessed a π electron-donating α -substituent; Fischer carbene species such as **2b** exhibit a ^1H NMR signal at approximately 14 ppm. The signal was tentatively assigned to the hydroxymethylidene species **175b**, which it was thought could be generated by insertion of oxygen into the C-H bond of the methylidene (**Scheme 4.19**). The Fischer carbene resulting from oxygen insertion into the methylidene C-H bond could tautomerise to form the formyl complex, followed by insertion of the ruthenium into

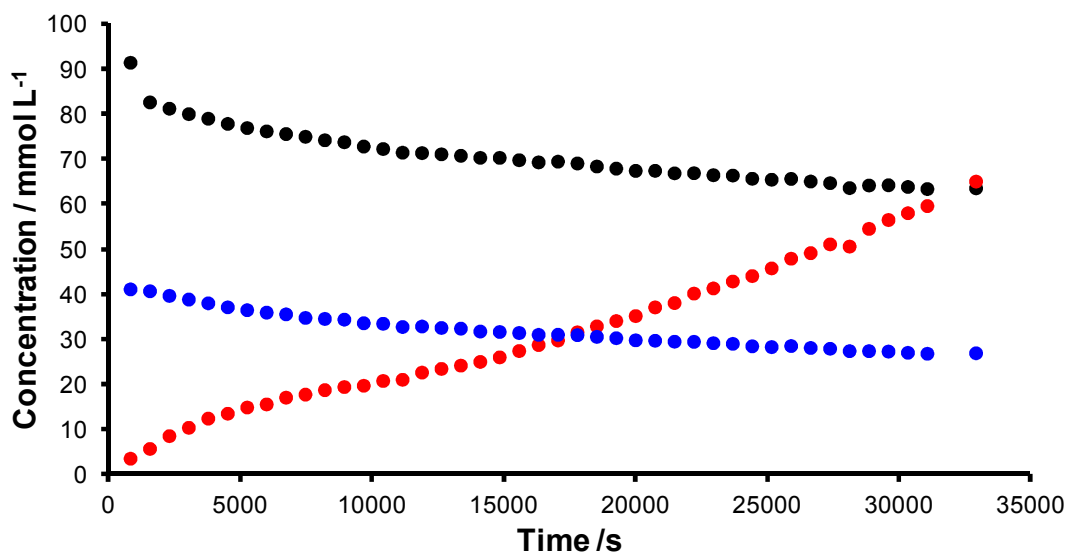


Figure 4.30. Concentration *versus* time profiles for cycloheptene (**black**), cyclohexene (**red**) and cyclic dimer (**blue**) in the ROMP reaction of cycloheptene (0.5 mol L^{-1} in benzene- d_6 at 298K) with **G2** (15 mol%).

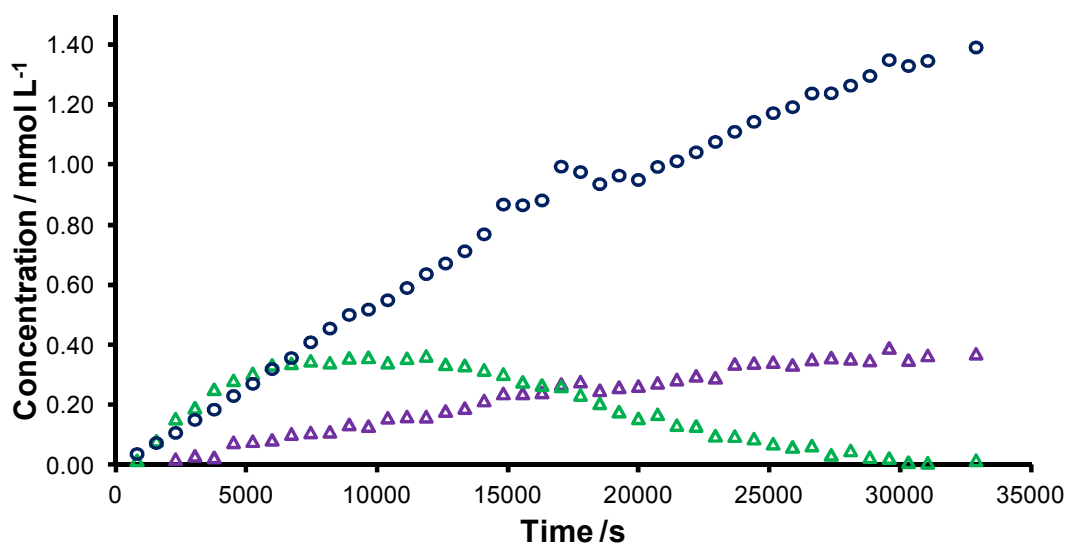
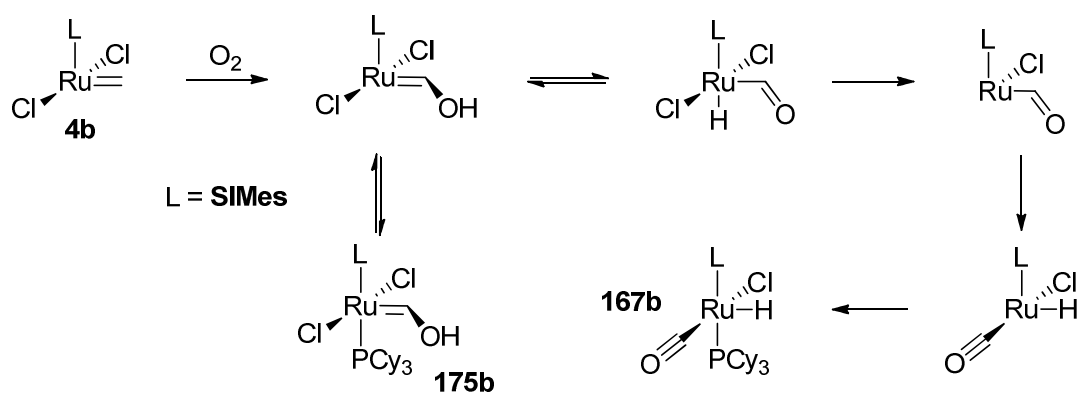


Figure 4.31. Concentration *versus* time profiles for methylenide (**blue circles**) and the signals at $\delta_{\text{H}} = -25 \text{ ppm}$ (**purple triangles**) and 14 ppm (**green triangles**) in the ROMP reaction of 1,8-nonadiene (0.5 mol L^{-1} in benzene- d_6 at 298K) with **G2** (15 mol%).

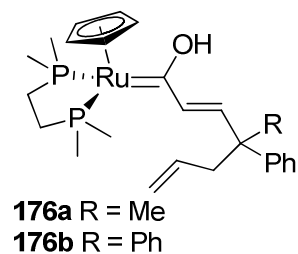
the C-H bond to yield hydridocarbonyl complex **167b**. Further theoretical and experimental studies would be necessary to fully explore this potential mechanism for hydridocarbonyl complex formation. However, this is the first observation of a known



Scheme 4.19

ruthenium hydride species in a metathesis reaction mixture where isomerisation occurs, and shows that isomerisation in this reaction is the result of an off-pathway process catalysed by an *in situ* generated catalyst.

This mechanism bears some similarities to that proposed by Mol *et al.*; the formyl complex is common to both pathways.⁸⁰ There are no precedents for this reaction in the literature; however, ruthenium hydroxycarbene complexes have been reported: species **176a** and **176b** have been isolated and characterised by ¹H NMR spectroscopy and X-ray crystallography.²⁶²



A source of oxygen in these reactions, other than traces of dissolved gaseous oxygen, is not obvious. The oxygen content of the solvents was investigated using a dissolved oxygen meter. The probe was submerged in commercial, untreated chloroform and stabilised at a reading of 0.11 mg/L. This is a concentration of approximately 3 nanomol L⁻¹, so could not account for the observed concentrations of ruthenium hydride complexes. The oxygen level decreased to 0.05 mg/L after sparging with nitrogen for 5 minutes.

The corresponding RCM reaction was conducted using a high (15 mol%) loading of pre-catalyst **G2**, in order to determine if the same ruthenium hydride complex was responsible for isomerisation during RCM (**Figure 4.32**). Over the course of *ca.* 14 hours, the concentrations of cycloheptene and cyclic dimer **106d** reached equilibrium then slowly decreased as material was consumed to generate cyclohexene. Conversion to cyclohexene reached *ca.* 50% over the course of the experiment. Inspection of the low field region revealed pre-catalyst decay accompanied by a build-up and then decay of

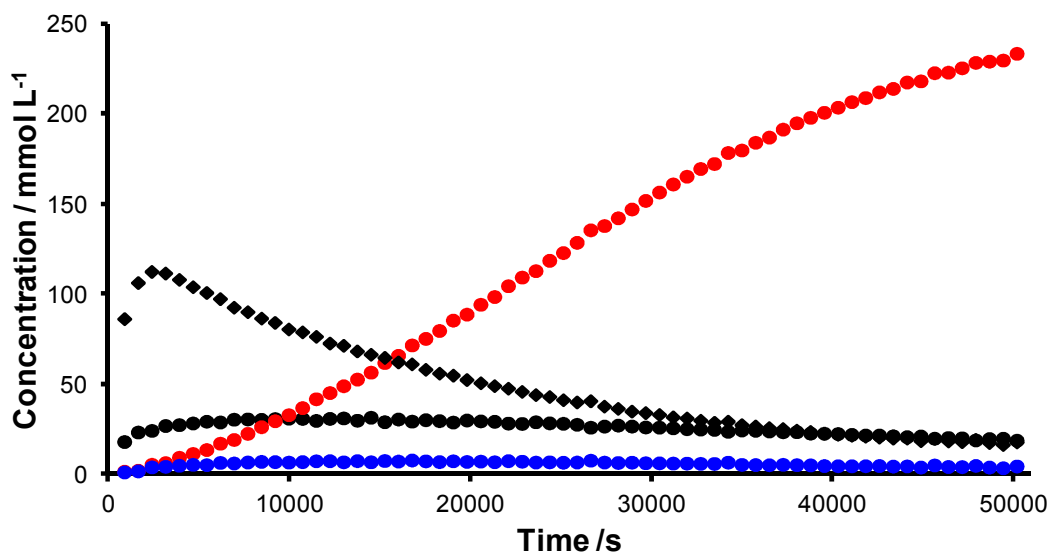


Figure 4.32. Concentration *versus* time profiles for cycloheptene (black circles), ethene (black rhombi) cyclohexene (red circles) and cyclic dimer (blue circles) in the RCM reaction of 1,8-nonadiene (0.5 mol L^{-1} in benzene- d_6 at 298 K) with **G2** (15 mol%).

alkylidene, plus gradual accumulation of methylidene **3b** and ethylidene **31b** (Figure 4.33). The ^1H NMR spectrum was inspected for the presence of ruthenium hydrides and Fischer carbene species. A species with a ^1H NMR chemical shift consistent with a

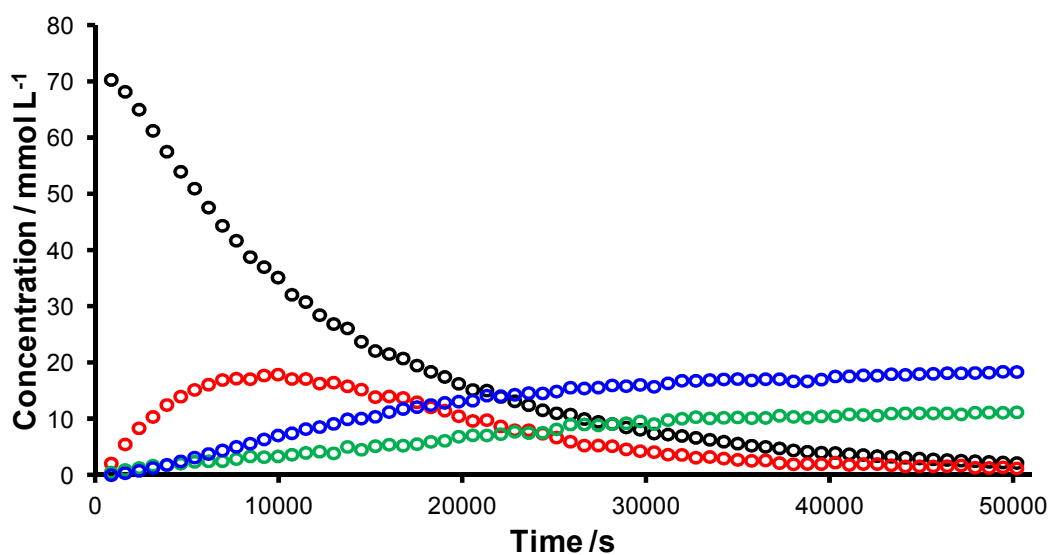


Figure 4.33. Concentration *versus* time profiles for pre-catalyst (black), alkylidene (red), methylidene (blue) and ethylidene (green) in the RCM reaction of 1,8-nonadiene (0.5 mol L^{-1} in benzene- d_6 at 298K) with **G2** (15 mol%).

Fischer carbene was detected ($\delta_{\text{H}} = 14.30$, $d(^2J_{\text{H,P}} = 4.6 \text{ Hz})$), but this differed from the species encountered in the ROMP reaction. Similarly, while traces of hydridocarbonyl complex **167b** were detected, a new hydride species was also observed ($\delta_{\text{H}} (\text{benzene-}d_6) = -20.37 \text{ ppm}$, $d(^2J_{\text{H,P}} = 17.1 \text{ Hz})$) (**Figures 4.34 and 4.35**). This species was most likely the same as that observed by Wagener *et al.* during their deuterium-labelling study,²⁴⁵ however this species has not yet been fully identified and characterised. Conducting the same reaction in air-sparged benzene- d_6 increased the concentration of the unknown species obtained (1.4 mmol L^{-1} after *ca.* 13.5 hours *versus* 0.7 mmol L^{-1} after 13.5 hour), but produced less of the hydridocarbonyl complex **167b** and less isomerised material (170 mmol L^{-1} after 13.5 hours *versus* 230 mmol L^{-1} after 13.5 hours).

The role of oxygen was further tested by conducting, in parallel, four reactions that differed only in the treatment of the solvent. All reactions contained 0.5 mol L^{-1} 1,8-nonadiene and 10 mol% **G2** in benzene- d_6 at 298 K for 14 hours. The solvent was sparged with oxygen, air, nitrogen or argon for five minutes before the reaction started. The treatment of the solvent made little difference to the reaction outcomes (**Figure 4.36**); similar quantities of isomerised material were obtained in each reaction. Inspection of the high field region of the ^1H NMR spectra revealed traces of the

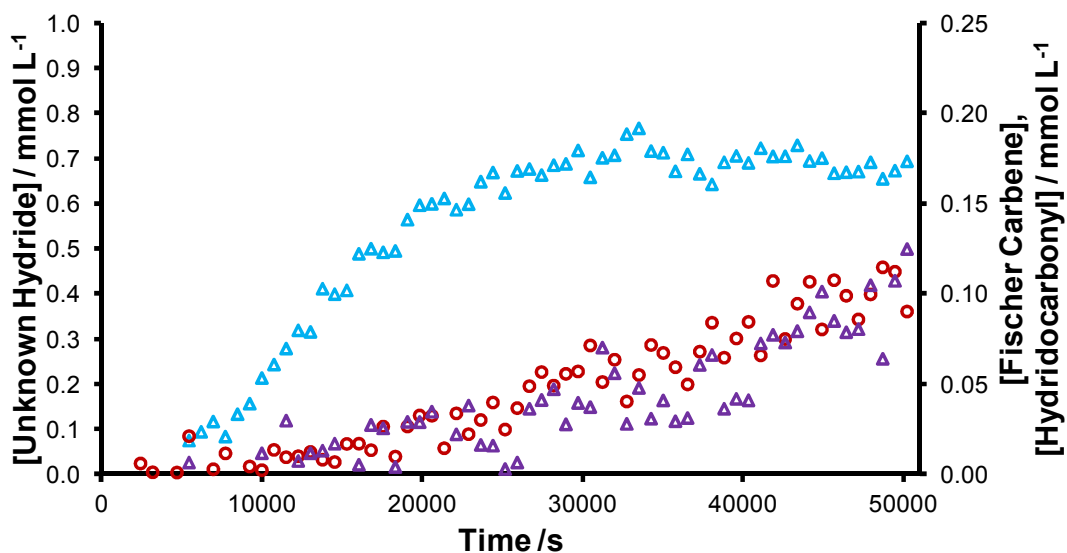


Figure 4.34. Concentration *versus* time profiles for an unknown Fischer carbene ($\delta_{\text{H}} (\text{benzene-}d_6) = 14.3 \text{ ppm}$) (**red**), hydridocarbonyl complex (**purple**) and unknown ruthenium hydride complex ($\delta_{\text{H}} = -20.4 \text{ ppm}$) (**blue**) in the RCM reaction of 1,8-nonadiene (0.5 mol L^{-1} in benzene- d_6 at 298K) with **G2** (15 mol%).

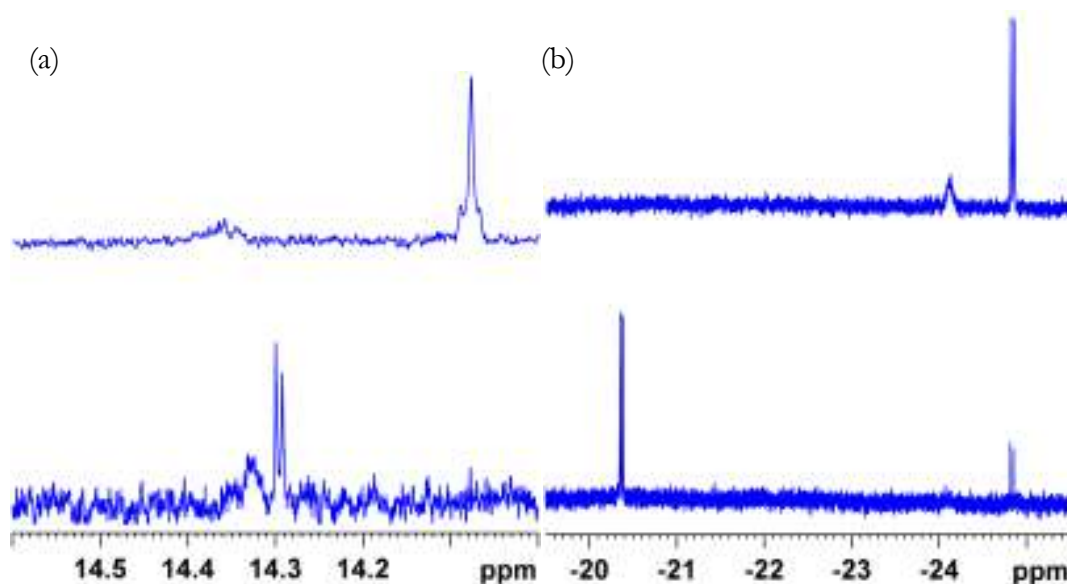


Figure 4.35. Partial ^1H NMR spectra (showing the *ca.* 13 – 15 ppm and *ca.* -19 to – 26 ppm regions) from (a) the ROMP reaction of cycloheptene (0.5 mol L^{-1} in ethene-sparged benzene- d_6) and (b) the RCM reaction of 1,8-nonadiene (0.5 mol L^{-1} in benzene- d_6); both reactions were conducted with 15 mol% **G2** at 298 K.

unknown hydride ($\delta_{\text{H}} = -20 \text{ ppm}$), hydridocarbonyl complex **167b**, and a third species ($\delta_{\text{H}} (\text{benzene-}d_6) = -31.60 \text{ ppm}$, s). The latter species was previously observed in the phosphane-quench experiments with **GH2**, and suggested that this species was a phosphane-bound hydride complex in which the $^nJ_{\text{H,P}}$ coupling constant was too small to observe.

Frustratingly, this new species could not be identified, although the experiments detailed here suggested that it was less active than complex **167b** for isomerisation. In addition, the identification of different Fischer carbene and ruthenium hydride species in reactions which formally involve the same intermediate ruthenium species suggests a degree of variability or a subtle dependence on reaction conditions. Isolation of these species from reaction mixtures was not attempted, as they formed only a fraction of the ruthenium complex population. Considerable further investigation would be required to identify the new ruthenium carbene species and their potential involvement in the formation of hydridocarbonyl and other ruthenium hydride complexes.

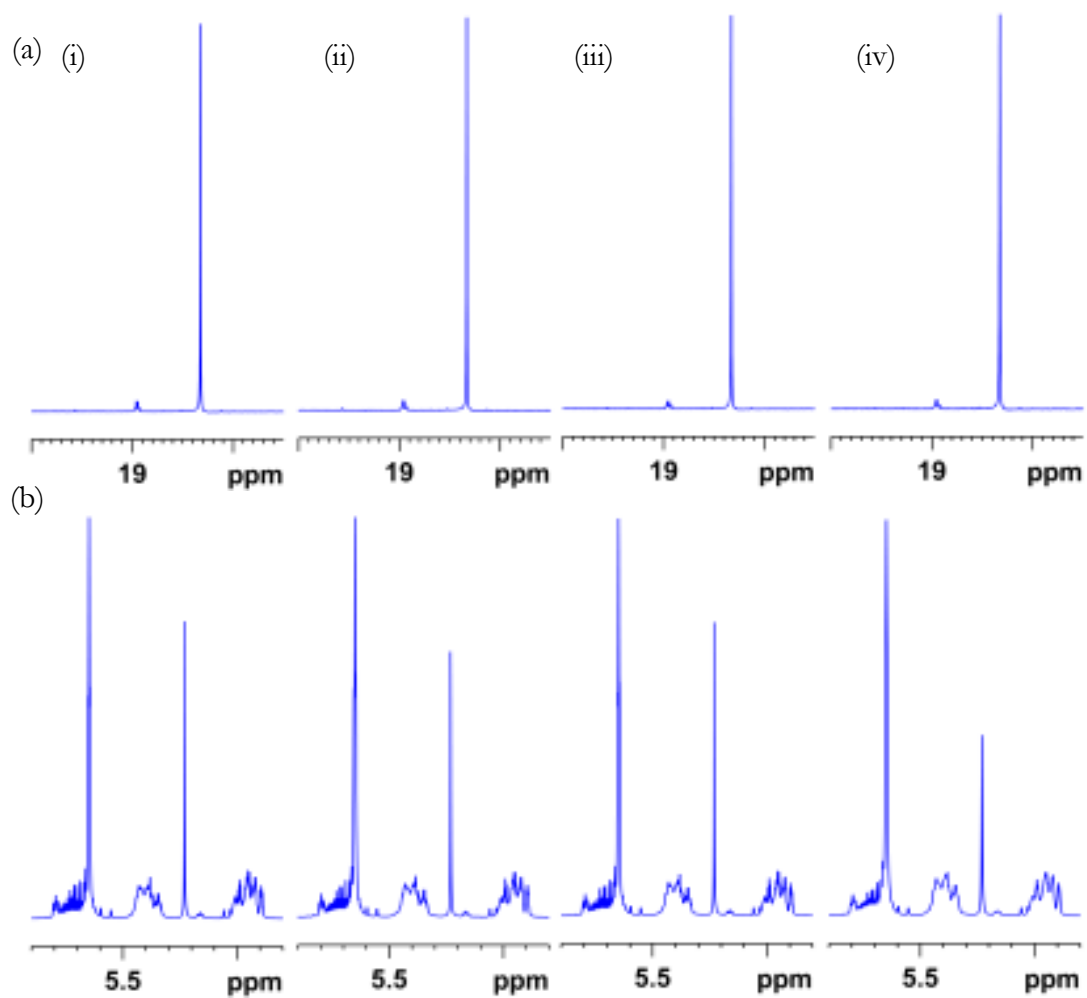
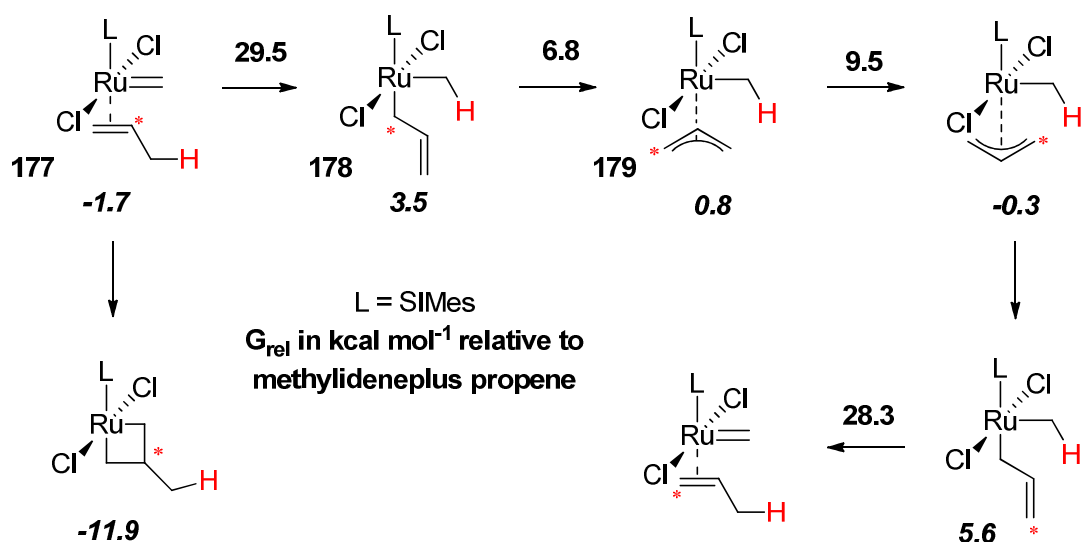


Figure 4.36. Partial ^1H NMR spectra from the reactions of 1,8-nonadiene (0.5 mol L^{-1} with 10 mol% **G2** at 298 K for 14 h) showing (a) the low field alkydene region and (b) the alkene region from reactions conducted in benzene- d_6 sparged with (i) oxygen, (ii) air, (iii) nitrogen or (iv) argon for five minutes.

Comparing Experimental Results with Density Functional Theory Calculations

The results of the experimental studies were compared to the results of *in silico* studies on three relevant pathways.¹⁸³ On-pathway isomerisation mechanisms proposed by Nolan and Prunet,²³⁶ and van Rensburg²⁴⁸ were considered, as well as isomerisation mediated by hydridocarbonyl complex **167b** according to the mechanism suggested by Grubbs.²³⁹ The isomerisation of 1-propene (as a model substrate) was considered for the Nolan-Prunet and ruthenium hydride mechanisms; the MCB derived from methylene plus ethene was considered when evaluating the van Rensburg mechanism. All calculations were carried out at the M06-L/6-311G* level of theory.⁵²

The Nolan-Prunet mechanism proceeds *via* η^2 -complex **177**, which was proposed to be stabilised by the agostic interaction of an allylic proton with the ruthenium centre.²³⁶ Formation of the η^2 -complex is favourable ($\Delta G = -1.7$ kcal mol⁻¹), but the transfer of the allylic proton which follows has a high barrier ($\Delta G^\ddagger = 31.2$ kcal mol⁻¹); this leads to the formation of dialkylruthenium complex **178** which then rearranges to (π -allyl)methylruthenium complex **179** ($\Delta G^\ddagger = 3.3$ kcal mol⁻¹). This species, after rotation of the allyl fragment ($\Delta G^\ddagger = 8.7$ kcal mol⁻¹) and rearrangement to the dialkylruthenium species, returns the hydride ($\Delta G^\ddagger = 22.7$ kcal mol⁻¹) to yield a new η^2 -complex and complete a formal isomerisation (**Scheme 4.20**). The hydride abstraction

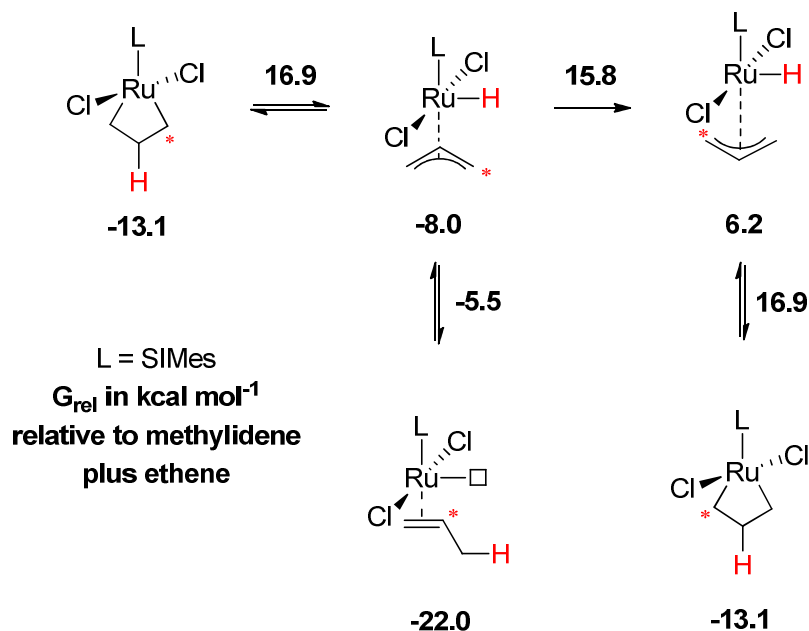


Scheme 4.20¹⁸³

event has a considerable barrier, and must compete with metallocyclobutanation ($\Delta G = -11.9 \text{ kcal mol}^{-1}$), rendering this an unattractive mechanism for isomerisation.

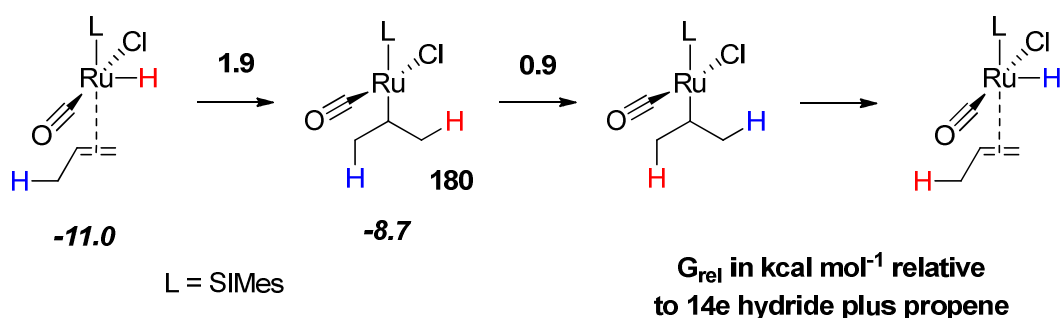
The van Rensburg pathway proceeds from a MCB,²⁴⁸ which makes this a more plausible pathway for isomerisation, as MCBs are known to be relatively low energy intermediates on the metathesis PES;¹⁵ MCB **53b** was calculated to be $13.1 \text{ kcal mol}^{-1}$ lower in energy than methyldene **4b** plus ethene. The β -hydride abstraction event ($\Delta G^\ddagger = 30.0 \text{ kcal mol}^{-1}$) yields a (π -allyl)ruthenium hydride complex, which then deposits the hydride on the unsubstituted terminus of the allyl fragment ($\Delta G^\ddagger = 2.5 \text{ kcal mol}^{-1}$) to yield a co-ordinatively unsaturated ruthenium η^2 - complex with propene, which is stabilised by an agostic CH-ruthenium interaction ($G = 8.9 \text{ kcal mol}^{-1}$ lower than metallocyclobutane **53b**). The reverse of this process (i.e. hydride abstraction ($\Delta G^\ddagger = 16.5 \text{ kcal mol}^{-1}$) followed by MCB formation ($\Delta G^\ddagger = 24.9 \text{ kcal mol}^{-1}$)) returns the ruthenium centre to the metathesis pathway (**Scheme 4.21**). As discussed previously, if an alkene larger than propene undergoes this series of steps, this could form the basis of an isomerisation mechanism. The barrier to β -hydride abstraction is still very large, but competes with retro-[2+2]-cycloaddition which typically has a larger barrier than MCB formation.⁵³

While the latter mechanism appears more favourable than the former, both PESs feature significant barriers to hydride abstraction. The PES for propene



Scheme 4.21¹⁸³

isomerisation by hydridocarbonyl complex **167b** is far smoother. There is a large initial barrier to phosphane dissociation ($\Delta G^\ddagger = 22.9 \text{ kcal mol}^{-1}$) which is comparable with the barrier to phosphane dissociation from **G2**,²⁶ in agreement with experimental observations when complex **167b** was exposed to 1-octene; the integral of the ^1H NMR resonance for the phosphane-bound hydride complex was found to decrease slowly over the course of the experiment, but at a similar rate to phosphane dissociation from **G2**. Binding of the alkene to the 14e hydridocarbonyl complex **173b** is highly exergonic ($\Delta G = -11.0 \text{ kcal mol}^{-1}$), which was attributed to the carbonyl ligand rendering the complex more Lewis acidic than methyldiene **4b**. The 14e hydride species **173b** can then hydrometallate the alkene ($\Delta G^\ddagger = 12.9 \text{ kcal mol}^{-1}$) to yield an alky ruthenium hydride complex **180**, which can then rotate ($\Delta G^\ddagger = 9.6 \text{ kcal mol}^{-1}$) and undergo β -hydride abstraction ($\Delta G^\ddagger = 9 \text{ kcal mol}^{-1}$) to complete the isomerisation reaction (**Scheme 4.22**). The potential energy surface for the isomerisation of alkenes by hydridocarbonyl complex **167b** is clearly more favourable than that of either of the on-pathway mechanisms. The latter surfaces feature *ca.* 30 kcal mol^{-1} barriers for hydride transfer while, once the phosphane ligand has dissociated, the largest barrier encountered by the hydridocarbonyl complex is only $12.9 \text{ kcal mol}^{-1}$ (**Figure 4.37**). However, the on-pathway mechanisms begin from intermediates on the metathesis pathway, so are known to be present in solution; the density functional theory calculations do not treat the *formation* of the hydridocarbonyl complex *in situ*, the mechanism of which is yet unknown. The experimental observation of hydridocarbonyl complex **167b** is therefore very important, as without this observation, it would not be possible to determine whether an on-pathway or off-pathway mechanism was in operation.



Scheme 4.22¹⁸³

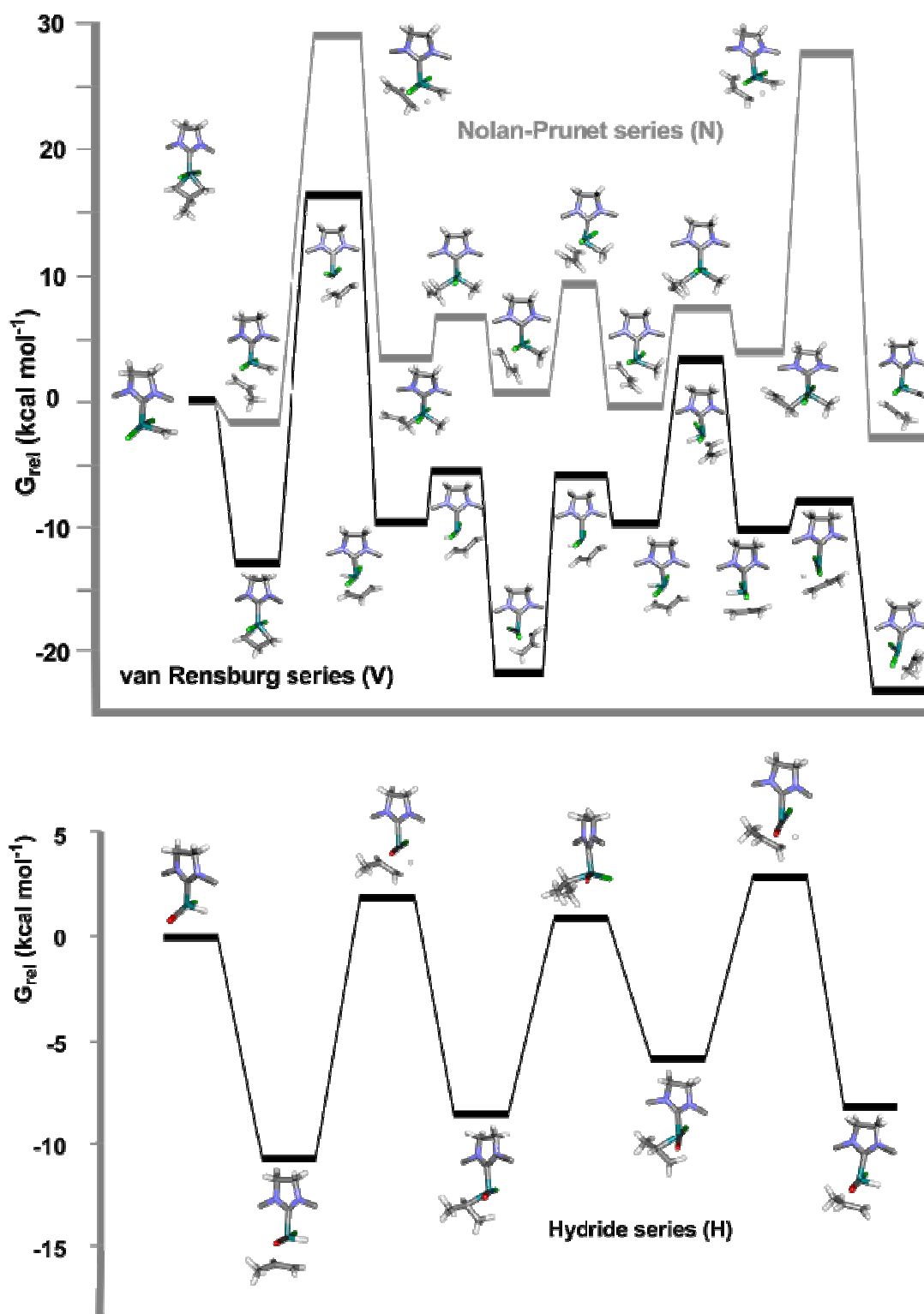


Figure 4.37. PESs for (a) the Nolan-Prunet and van Rensburg isomerisation mechanisms and (b) hydridocarbonyl-mediated isomerisation; calculations were performed at the M06-L/6-311G* level of theory.¹⁸³

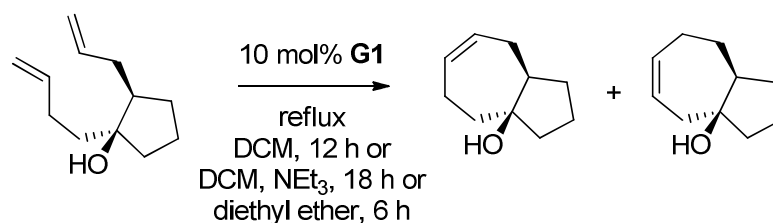
Benzoquinone as an Isomerisation Suppressant

Despite the lack of conclusive identification of some species in these reactions, the observation of known ruthenium hydride species was a significant outcome. This result suggested that the predominant source of isomerisation in these reactions was *in situ* generated ruthenium hydride species. DFT studies confirmed that isomerisation by a ruthenium hydride species, once this species is formed, is energetically more favourable than either of the literature on-pathway mechanisms. With this established, the role of benzoquinone and derivatives in suppressing this isomerisation was explored.

Suppressants for Isomerisation in Metathesis Reactions

Various agents have been proposed to suppress isomerisation in metathesis reactions; however, few solutions to the isomerisation problem have been rigorously explored, and few of these are complete solutions.

Taylor *et al.* encountered RCM product isomerisation in their synthesis of Laureatin natural products (**Scheme 4.23**).²⁶³ Isomerisation was a significant issue when the reaction was conducted in refluxing DCM. While an overall yield of 93% was obtained, almost 40% of this material consisted of the undesired isomer. This was attributed to the acidity of the solvent as the addition of triethylamine or a change of solvent to diethyl ether was found to suppress isomerisation and result in a yield of 83% or 98% respectively. The observation that base suppresses isomerisation suggests that the pathway characterised by Mol *et al.*, where base *accelerates* formation of hydridocarbonyl complex **167a** from **G1** plus primary alcohol, cannot in operation here.



Scheme 4.23²⁶³

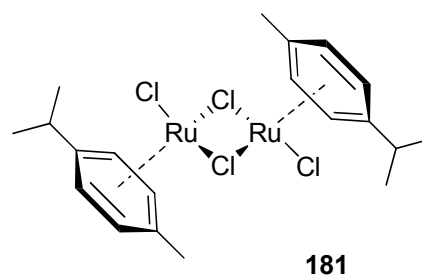
As discussed previously, Nolan and Prunet *et al.* have reported isomerisation of during metathesis reactions (**Scheme 4.01** above).²³⁶ Various potential isomerisation suppressants were screened (**Table 4.02**). Oxygen, water and PCy₃ were found to retard

Table 4.02. Potential isomerisation suppressants screened by Nolan and Prunet *et al.*²³⁶

Additive	Loading (mol%)	Time (h)	Product Ratios		
			Substrate	Cyclised	Isomerised
O ₂		15	90	10	
PCy ₃	5	60	40	60	
PCy ₃	0.5	72	10	70	20
H ₂ O	5	20	30	60	10
H ₂ O	traces ^a	12	10	80	10
Styrene	5	15	5	90	5
NEt ₃	5	72		50	50
NEt ₃	0.5	72		75	25
OPCy ₃	5	15		100	
OPCy ₃	0.5	15		100	
OPPh ₃	5	12	10	80	10
181	5	15	30	35	35

^a Glassware and solvents were used without drying beforehand.

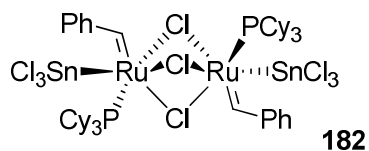
the RCM reaction significantly. PCy₃ would be expected to affect the phosphane dissociation equilibrium and therefore lower the concentration of active catalyst species present in solution. Oxygen and water may have caused catalyst decomposition, thereby leading to a reduced rate of metathesis, but did not significantly increase the rate of isomerisation, so any decomposition products may not be isomerisation active. This is in agreement with the results described above, where wet solvents did not increase the rate of isomerisation but did lead to a decrease in metathesis rate. Nolan and Prunet reported triethylamine or complex **181** were found to increase the degree of isomerisation, while only tricyclohexylphosphane oxide was found to suppress isomerisation without impeding the desired metathesis reaction. Triphenylphosphane oxide was not found to suppress isomerisation, which was attributed to ‘the subtlety of the effects’; the mechanism by which tricyclohexylphosphane oxide inhibits isomerisation is not known. However, the possibility that it co-ordinates weakly to the metal centre was discussed.



Meyer *et al.* have used Fe^{II} halogenides and Sn^{II} halogenides as additives for

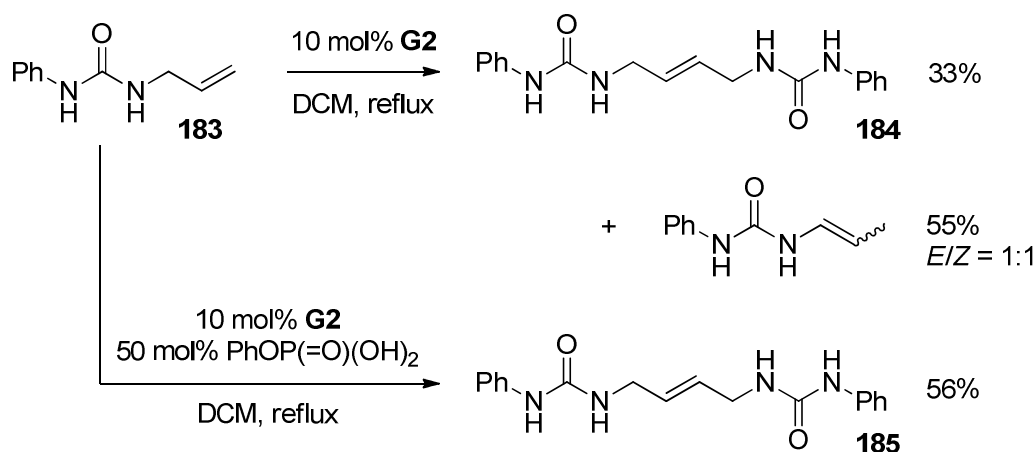
metathesis reactions.²⁶⁴ These additives were found to suppress isomerisation in the metathesis reactions of 1-octene, with the order of activity $\text{SnBr}_2 > \text{SnCl}_2 \approx \text{FeBr}_2 > \text{FeCl}_2$; Al^{III} , Sb^{III} , Ce^{III} , Ga^{II} , Fe^{III} and Yb^{III} salts were found to have no effect. Rate increases were observed with **G1** and **G2** when these salts were added (100 ppm pre-catalyst, with 20 eq. of the Fe^{II} or Sn^{II} salt). The authors proposed that the salts coordinated to the metal centre, preventing phosphane-reassociation and changing the electronic properties of the ruthenium centre.

Diruthenium species **182**, which contained two ruthenium centres bridged by three μ^2 -chloride ligands,



was isolated from the metathesis reaction with **G1** and SnCl_2 ; however, this does not necessarily reflect the solution state.

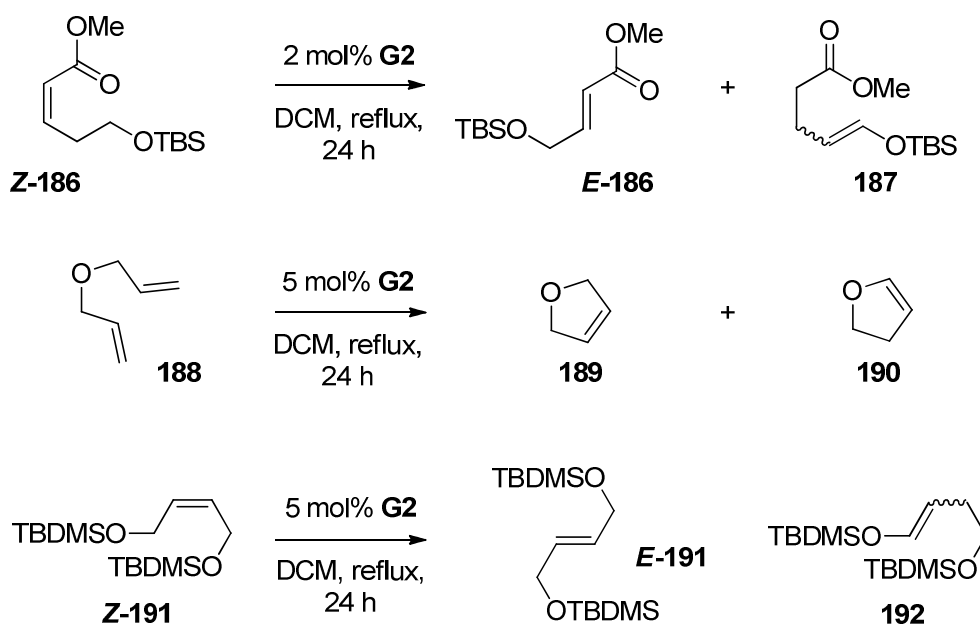
Steinke *et al.* has reported that phenylphosphoric acid (PPA) inhibited isomerisation processes during the synthesis of urea-based molecular receptors.²⁶⁵ Self-metathesis of **183** yielded a mixture of the desired dimeric product **184** and the unwanted isomerised substrate **185** (Scheme 4.24); when PPA was added to the reaction mixture, no isomerisation occurred. Benzoic acid and 2,6-dichloro-1,4-benzoquinone were also found to suppress isomerisation, but resulted in slightly lower yields (43% and 54% respectively) and significant quantities of starting material remaining. The corresponding triethylammonium salt ($[\text{PhOP}(=\text{O})(\text{OH})(\text{O})][\text{NHEt}_3]$) completely suppressed the metathesis reaction, while the tetraethylammonium salt ($[\text{PhOP}(=\text{O})(\text{OH})(\text{O})][\text{NEt}_4]$) resulted in an *increase* in isomerisation; the latter results are proposed to be a result of the release of free amine in solution which may have



Scheme 4.24²⁶⁵

promoted decomposition of the metathesis catalyst to form ruthenium hydride species.⁷⁹

Grubbs *et al.* conducted the most detailed assessment to date of potential isomerisation suppressants.²⁵⁸ Additives were screened using a series of test reactions: metathesis or isomerisation of *Z*- α,β -unsaturated ester **Z-186** to *E*-**186** or vinyl ether **187**; RCM or RCM-isomerisation of diallyl ether **188** to 1,4-dihydrofuran **189** or 1,2-dihydrofuran **190**; and metathesis or isomerisation of *Z*-1,4-but-2-ene diol derivative **Z-191** to *E*-**191** or vinyl ether **192** (Scheme 4.25). The widest variety of additives was screened in the first metathesis reaction. Trifluoroethanol, hexafluoro-*tert*-butanol and phenol all failed to reduce isomerisation; tricyclohexylphosphane oxide also did not suppress isomerisation, but this may simply have *slowed* isomerisation in the reaction that Nolan and Prunet *et al.* studied, in order to allow RCM to occur.²³⁶ 1,4-Benzoquinone, acetic acid and maleic anhydride were all found to decrease isomerisation. 1,4-Benzoquinone, acetic acid and radical scavengers galvinoxyl, TEMPO, 4-methoxyphenol and BHT were tested in the second metathesis reaction, but only benzoquinone and acetic acid were found to suppress isomerisation considerably. This result suggested that radicals were not involved in the isomerisation mechanism. Acetic acid and 1,4-benzoquinone were employed in the third metathesis reaction but only 1,4-benzoquinone was effective here, resulting in 92% conversion to *E*-**191** while the remaining 8% was starting material **Z-191**.



Scheme 4.25²⁵⁸

With 1,4-benzoquinone identified as an isomerisation inhibitor, different 1,4-benzoquinone analogues were tested for the metathesis reaction of diallyl ether **188**. Electron-deficient analogues such as 2,6-dichloro-1,4-benzoquinone and 2,3,5,6-tetrafluoro-1,4-benzoquinone performed best, with no isomerised product detected.

1,4-Benzoquinone, when added to a reaction containing diruthenium hydride complex **41** and allylbenzene, completely prevented isomerisation. Crucially, benzoquinone compounds also suppressed isomerisation in metathesis reactions catalysed by phosphane-free complex **GH2**, indicating that isomerisation processes and the suppression thereof were not dependent on the presence of phosphane. Grubbs *et al.* proposed that this isomerisation-suppressing behaviour arose because 1,4-benzoquinone could oxidise ruthenium hydride species generated *in situ* before such species could bind alkene and carry out isomerisation reactions. While 1,4-benzoquinone and its analogues appear to be efficient, simple and cost-effective isomerisation-suppressants, the exact mechanism of their action is not yet known.

Benzoquinone Applied to Simple Diene Metathesis

Experiments were carried out to assess if 1,4-benzoquinone could suppress isomerisation in 1,8-nonadiene metathesis reactions. The RCM reaction of 1,8-nonadiene (0.5 mol L⁻¹ in chloroform-*d* with 3 mol% **G2** at 298 K) was carried out in the presence of 10 mol% 1,4-benzoquinone (with respect to 1,8-nonadiene) and monitored by ¹H NMR spectroscopy. The concentration/time profiles for cycloheptene and cyclohexene in the reaction were compared with those from the corresponding reaction in the absence of 1,4-benzoquinone (**Figure 4.38**). The cycloheptene concentration/time profiles were similar, but the cyclohexene profiles were very different. The presence of 1,4-benzoquinone in the reaction suppressed isomerisation, but did not do so completely; conversion to cyclohexene was reduced from *ca.* 8% to less than 2%. In the context of synthetic chemistry, this level of reduction in side products would reduce waste and render purification of the desired product easier.

The 1,8-nonadiene RCM experiments discussed here underwent a series of colour changes, both in the absence and in the presence of 1,4-benzoquinone. Two experiments were conducted and profiled using UV/visible spectroscopy. Both contained 1,8-nonadiene at 0.5 mol L⁻¹ in chloroform (with 3 mol% **G2**), while only one contained 10 mol% 1,4-benzoquinone. The reactions were sampled at 1 hour intervals,

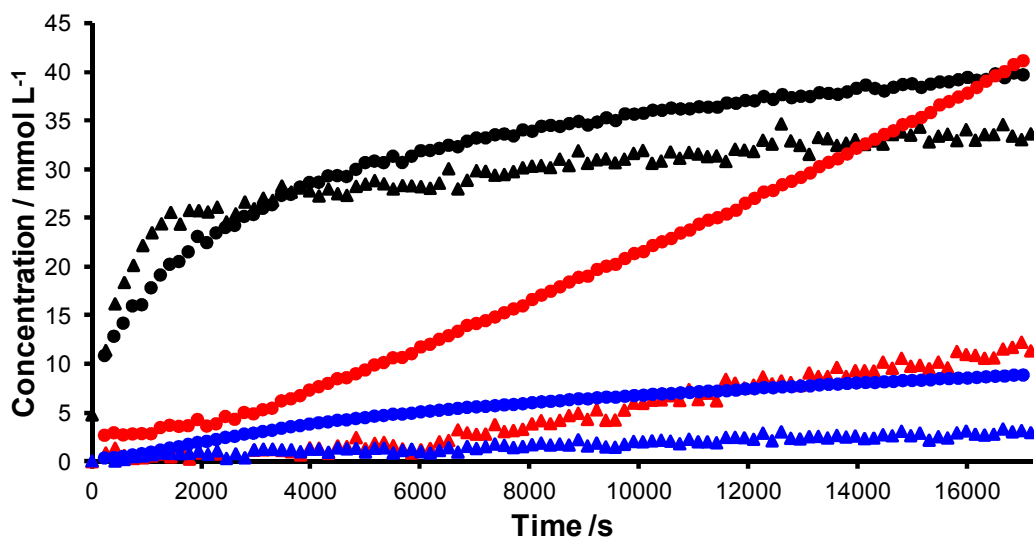


Figure 4.38. Concentration/time profiles for cycloheptene (**black**), cyclohexene (**red**) and cyclic dimer **106d** (**blue**) in the RCM of 1,8-nonadiene (0.5 mol L^{-1} in chloroform-*d* with 3 mol% **G2** at 298 K) (a) in the absence of 1,4-benzoquinone (circles) and (b) in the presence of 10 mol% (with respect to 1,8-nonadiene) 1,4-benzoquinone (triangles).

diluted 150-fold and analysed by UV/visible spectroscopy. Over the course of the experiment without additive the reaction mixture changed colour from red to orange; the same experiment with 1,4-benzoquinone changed colour from red to deep blue (**Figure 4.39**). The UV/visible spectra showed the decrease of the **G2** absorption ($\lambda_{\text{max}} = 335 \text{ nm}$) in both reactions. When no additive was present, a weak and broad absorption was observed at $\lambda = ca. 500 \text{ nm}$. However, when 1,4-benzoquinone was present in solution, a broad absorption ($\lambda_{\text{max}} = 600 \text{ nm}$) accounted for the relatively intense colour of the sample, which gradually increased as the reaction progressed.

Concentration *versus* time profile differences were also obtained from the analogous RCM mediated by **GH2** (**Figure 4.40**). Formation of the equilibrium concentration of cycloheptene was slower and the rate of cyclohexene formation was considerably lower in the presence of 1,4-benzoquinone. The concentration of cyclohexene in the RCM reaction without the additive reached *ca.* 0.2 mol L^{-1} after *ca.* 3 hours (40% conversion of 1,8-nonadiene) yet with the additive the cyclohexene concentration reached only 5 mmol L^{-1} (1% conversion) and did not increase further. The concentrations of cyclic dimer **106d** produced were similar in both reactions; alkylidene species are not observable in **GH2**-catalysed reactions (unless quenched by

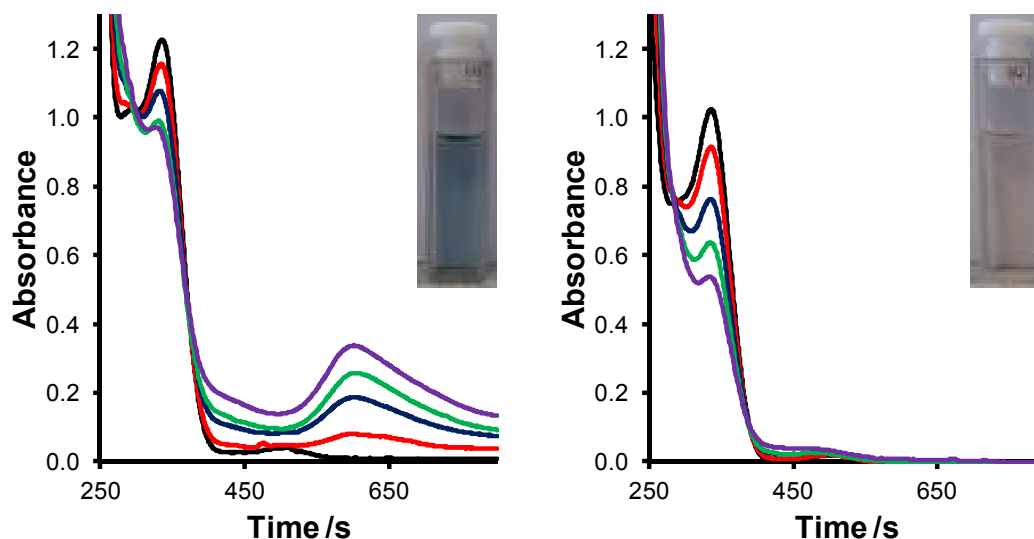


Figure 4.39. UV/visible spectra of the RCM reaction of 0.5 mol L^{-1} 1,8-nonadiene (with 3 mol% **G2** in chloroform at 298 K) initially (**black**) and after 1 hour (**red**), 2 hours (**blue**), 3 hours (**green**) and 4 hours (**purple**) (a) with 10 mol% benzoquinone and (b) without benzoquinone; insets show the diluted reaction mixtures after 3 hours.

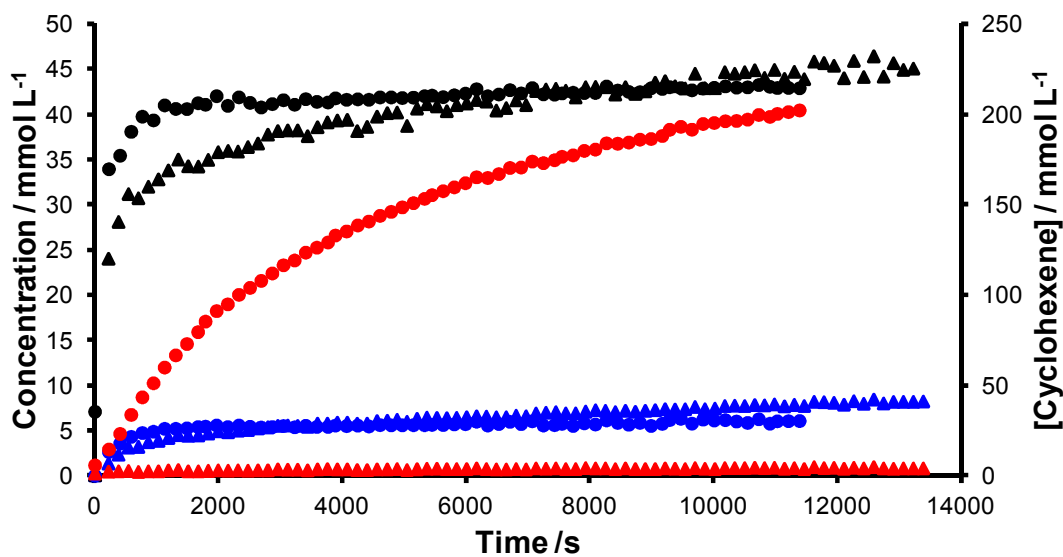


Figure 4.40. Concentration/time profiles for cycloheptene (**black**), cyclohexene (**red**, secondary axis) and cyclic dimer **106d** (**blue**) in the RCM of 1,8-nonadiene (0.5 mol L^{-1} in chloroform-*d* with 3 mol% **GH2** at 298 K) (a) in the absence of 1,4-benzoquinone and (b) in the presence of 10 mol% (with respect to 1,8-nonadiene) 1,4-benzoquinone.

phosphane, *vide supra*) so any differences in the alkylidene populations could not be probed by ^1H NMR spectroscopy.

Excluding the expected decrease in cyclohexene formation rate, three key differences in the presence of 1,4-benzoquinone raised questions about the mechanism by which this additive suppressed isomerisation in the reaction. Firstly, the appearance of the end group signals varied between reactions conducted with and without 10 mol% 1,4-benzoquinone, particularly in reactions conducted with **GH2** (Figure 4.41). While the peak shape in the absence of 1,4-benzoquinone was suggestive of a mixture of products, most likely diene and linear oligomer, when the additive was present the peak appeared to correspond to a single component only. Secondly, the concentration of cyclic dimer **106d** obtained was considerably less when 1,4-benzoquinone was present (*ca.* 3 mmol L⁻¹ versus *ca.* 9 mmol L⁻¹ after approximately 4.5 hours). Finally, the low field region of the ^1H NMR spectra was very different: no ruthenium carbene species other than pre-catalyst **G2** were detected. In the same reaction without 1,4-benzoquinone, alkylidene species and ethylidene **31b** were clearly observed during the experiment.

The differences between reactions with and without 1,4-benzoquinone could be explained by the destruction of the propagating carbene species. This species is common to cyclisation and oligomerisation pathways, and would explain the lower rate of cyclisation, the reduced degree of oligomerisation, and the absence of signals for species other than the pre-catalyst in the low field region. 1,4-Benzoquinone might be attacking the pre-catalyst or active catalyst alone, although this would not explain the marked decrease in linear oligomer yet only a slight decrease in cyclisation rate.

While 1,4-benzoquinone does suppress isomerisation, it does not do so

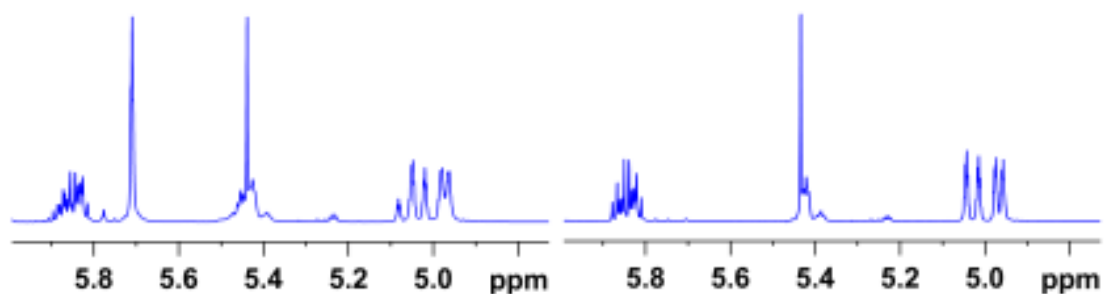


Figure 4.41. Partial ^1H NMR spectra of the reaction of 1,8-nonadiene (0.5 mol L⁻¹ in chloroform-*d*) with 3 mol% **GH2** at 298 K) after approximately 2.5 hours (a) without 1,4-benzoquinone and (b) with 10 mol% 1,4-benzoquinone.

completely and results in changes to the reaction mixture that have not been reported previously, such as the absence of ruthenium carbene species.

Probing the Mechanism of Action of Benzoquinone

Differences that were observed in the concentration/time profiles with and without 1,4-benzoquinone prompted further investigation of these reactions. Analysis of the low field region of the ^1H NMR spectra allowed insight into the behaviour of the pre-catalyst and related species. Concentration/time profiles for benzoquinone consumption and pre-catalyst decay were constructed for the two reactions conducted in the presence of 10 mol% 1,4-benzoquinone (one with **G2** and one with **GH2**) and compared to the pre-catalyst concentration/time profiles from the analogous experiments without 1,4-benzoquinone (**Figure 4.42**). Intriguingly, the shapes of the benzoquinone concentration *versus* time plots were very similar to those of the pre-catalyst concentration *versus* time plots; for **G2** the plots were slightly curved, while in **GH2**-catalysed reactions both profiles exhibited a steep initial slope, followed by a more gradual decrease in concentration. The decrease of pre-catalyst concentration was exactly the same in both experiments with **G2**, while with **GH2** more pre-catalyst was consumed when 1,4-benzoquinone was present.

The decrease of **GH2** concentration did not appear to follow a simple kinetic order, but initiation (*via* the interchange mechanism, *vide supra*)^{60-61,191} was fast due to the high concentrations of diene present. Due to the differences in the spectra discussed above, the concentration of 1,8-nonadiene could be profiled in this reaction; the diene concentration decreased quickly to *ca.* 0.3 mol L⁻¹ before then gradually decreasing (**Figure 4.43**); the shapes of the diene and **GH2** concentration *versus* time profiles did not appear to be the same, however.

The decrease of pre-catalyst and 1,4-benzoquinone concentrations in the **G2**-catalysed metathesis reactions of 1,8-nonadiene were approximately first order, allowing rate constants to be quantified (**Table 4.03**); however, only the first *ca.* 50% of pre-catalyst consumption and the first *ca.* 25% of 1,4-benzoquinone consumption was included in these treatments, so these rate constants must be considered approximate. These rate constants confirmed quantitatively that there was little difference in pre-catalyst consumption rate in the absence of and presence of 1,4-benzoquinone; both rate constants for pre-catalyst consumption are close to the rate constant measured

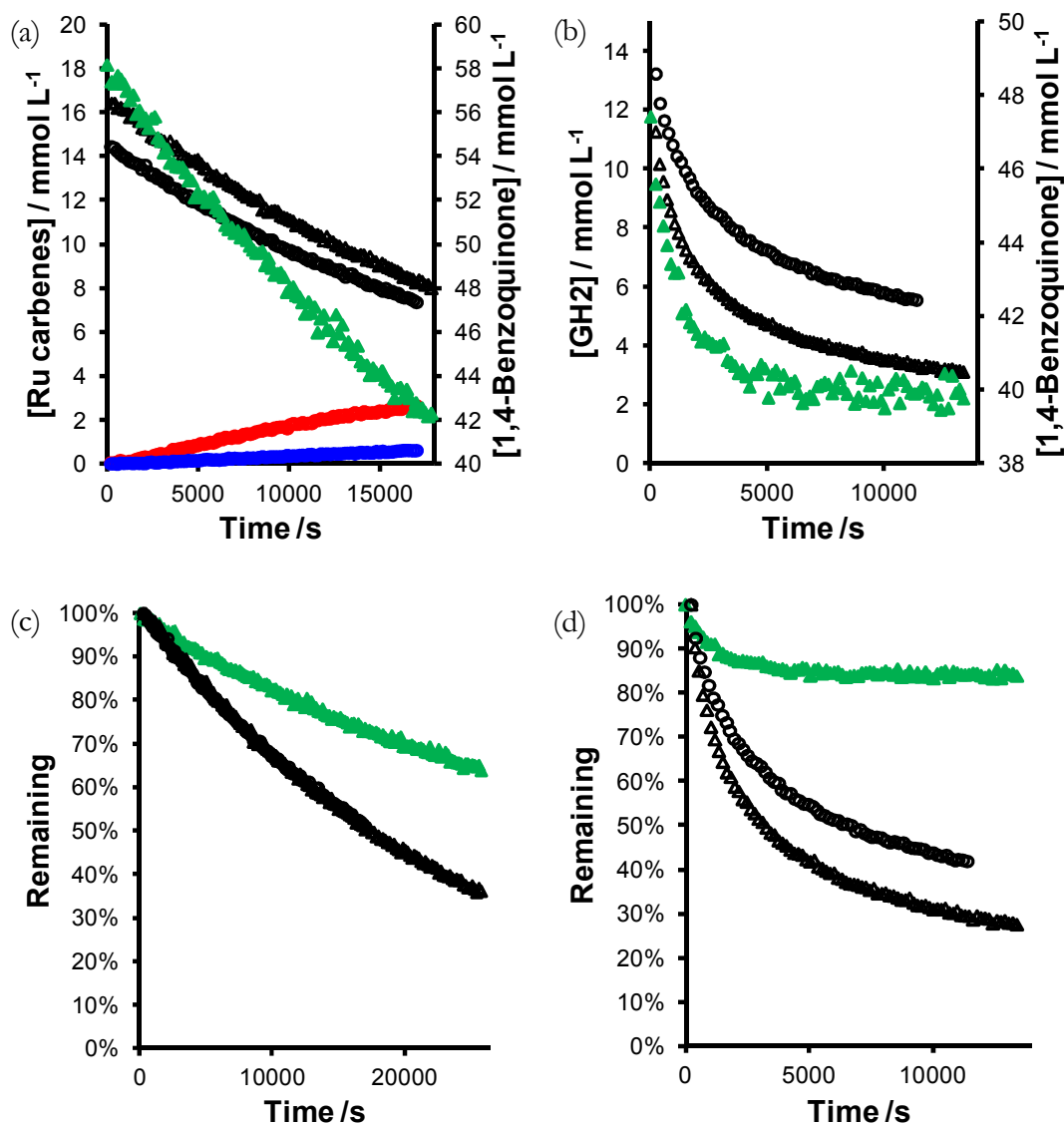


Figure 4.42. Concentration/time profiles for pre-catalyst (**black**), alkylidene (**red**), methylidene (**blue**) and 1,4-benzoquinone (**green**) in the RCM reactions of 1,8-nonadiene (0.5 mol L^{-1} in chloroform-*d* at 298 K) with (triangles) and without (circles) 10 mol% 1,4-benzoquinone; reactions were catalysed by (a) **G2** and (b) **GH2**; graphs (c) and (d) are plotted in % initial charge remaining for **G2** and **GH2** respectively.

experimentally with ethyl vinyl ether ($k_{\text{obs}} = 4.5 \times 10^{-5} \text{ s}^{-1}$).⁹⁷ Intriguingly, the rate of 1,4-benzoquinone consumption was approximately half the rate of pre-catalyst consumption. This trend continued even after the primary metathesis reaction was complete and the equilibrium concentrations of cycloheptene and cyclic dimer **106d** had been reached, suggesting that a reaction was occurring between 1,4-benzoquinone and

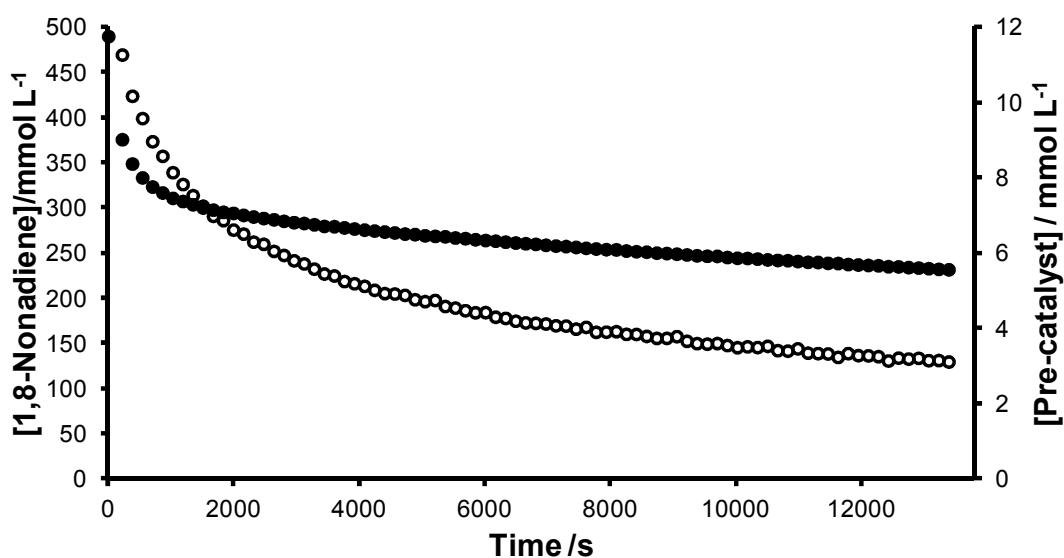
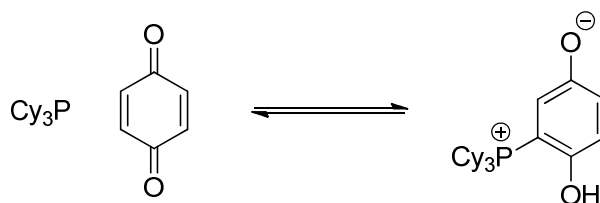


Figure 4.43. Concentration *versus* time profiles for 1,8-nonadiene and **GH2** in the metathesis reaction of 1,8-nonadiene (0.5 mol L^{-1} in chloroform-*d* with 3 mol% **GH2** and 10 mol% 1,4-benzoquinone at 298 K).

Table 4.03. Pseudo-first order rate constants for the consumption of **G2** and 1,4-benzoquinone in the RCM reactions of 1,8-nonadiene (in chloroform-*d* at 298 K with 3 mol% **G2**) without (Entry 1) and with (Entry 2) 1,4-benzoquinone.

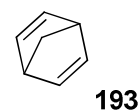
Entry	1,4-Benzoquinone Loading	k_{obs} for G2 consumption	k_{obs} for 1,4-benzoquinone consumption
1	-	$3.98 \times 10^{-5} \text{ s}^{-1}$	-
2	10 mol%	$4.04 \times 10^{-5} \text{ s}^{-1}$	$1.70 \times 10^{-5} \text{ s}^{-1}$

either 14e benzylidene **1b** or tricyclohexylphosphane. Two possibilities for this correlation were considered. Firstly, it is known that 1,4-benzoquinone can act as a Michael acceptor for phosphanes (**Scheme 4.26**). The reaction of PPh_3 with 1,4-benzoquinone has been found to occur on the same timescale as the metathesis reactions studied here;²⁶⁶ the products of PMe_3 and PEt_3 addition to benzoquinone have been isolated and characterised.²⁶⁷ PCy_3 is known to be more nucleophilic than PPh_3 ; these two species have N parameters²⁶⁸ of 14.64 and 14.33 respectively.²⁶⁹ The reaction mixture turned a deep orange-red colour almost instantly when (colourless) PCy_3 was added to a yellow solution of 1,4-benzoquinone, in agreement with the literature



Scheme 4.26

However, it was the second possibility, that the 14e complex was reacting with 1,4-benzoquinone, that could best account for the reaction mixture turning *blue* in colour as time progressed. Harding *et al.* have reported the formation of radical species when **G1** and **G2** are exposed to 1,4-benzoquinone, documenting specifically that the reaction mixtures were found to turn a deep blue colour.²⁷⁰⁻²⁷¹ Radical species were also found to be formed when **G1** and **G2** were exposed to alkenes such as cyclopentene and norbornadiene **193**. Spectroscopic analyses (using IR and Raman spectroscopies) suggested that co-ordination of 1,4-benzoquinone and analogues to the ruthenium species occurred *via* the oxygen of benzoquinone (Figure 4.44). However, Grubbs *et al.* have isolated complex **194** from the reaction of pre-catalyst **195** with 1,4-benzoquinone (Scheme 4.27), demonstrating that 1,4-benzoquinone can act as an η^4 -ligand to ruthenium.²⁷²



Grubbs *et al.* have shown that 1,4-benzoquinone (and some analogues) suppress the isomerisation of allylbenzene with diruthenium hydride complex **41**,²⁵⁸ however, the observations of Harding *et al.* that 1,4-benzoquinone undergoes reaction with 14e ruthenium carbene species, plus the observation documented above that reactions catalysed by **G2** with 1,4-benzoquinone present do not produce phosphane-bound ruthenium carbene species, suggested that 1,4-benzoquinone might react with ruthenium *carbene* species as well as ruthenium *hydride* species. Methylidene **4b** has already been implicated in the isomerisation side-reactions (*vide supra*), therefore 1,4-benzoquinone might suppress isomerisation in metathesis reactions *via* capture of the ruthenium carbene species that lead to the active ruthenium hydride complexes, rather

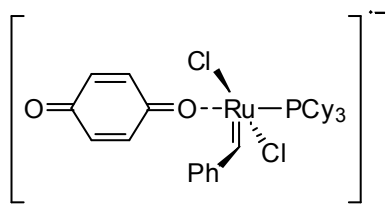
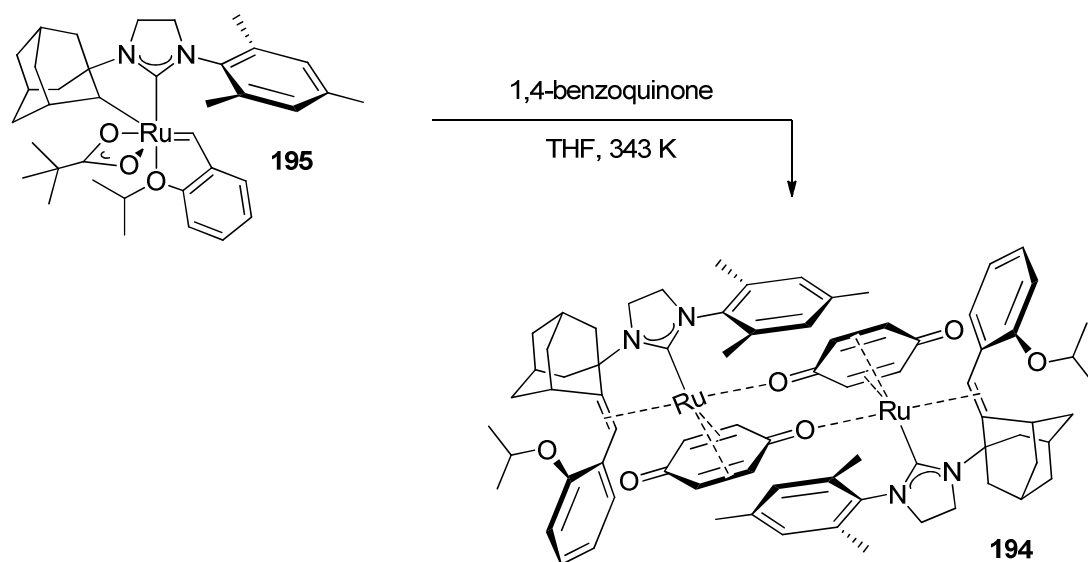


Figure 4.44. Co-ordination of 1,4- benzoquinone to the 14e complex generated by **G1**.²⁷¹



Scheme 4.27²⁷²

than exclusively through oxidation of the ruthenium hydride species directly.

The metathesis reaction of 1,7-octadiene was used to test this hypothesis; this reaction occurs smoothly without the formation of oligomers, even at very high (*ca.* 4 mol L⁻¹) concentrations.^{90,187} The RCM of 1,7-octadiene (0.5 mol L⁻¹ in chloroform-*d* with 3 mol% **G2** at 298 K) was carried out in the absence of 1,4-benzoquinone, and then in the presence of 10 mol% 1,4-benzoquinone. The resulting concentration *versus* time profiles for each reaction were quite different (**Figure 4.45**). The reaction in the absence of additive exhibited a smooth decay of 1,7-octadiene concentration and a corresponding smooth profile for cyclohexene production, but the profile collected in the presence of 1,4-benzoquinone was of a completely different shape. The latter profile consisted of an initial rapid turnover of 1,7-octadiene at a rate similar to that in the experiment without 1,4-benzoquinone, followed by a much slower rate of diene consumption after *ca.* 2000 s.

The corresponding pre-catalyst concentration *versus* time profiles revealed the same rate of **G2** consumption in both reactions ($k_{obs} = 3.75 \times 10^{-5} \text{ s}^{-1}$ without 1,4-benzoquinone; $k_{obs} = 3.83 \times 10^{-5} \text{ s}^{-1}$ with 10 mol% 1,4-benzoquinone). Methylidene complex **3b** was only detected in the reaction without 1,4-benzoquinone. Once again, the rate of benzoquinone consumption was *ca.* half that of pre-catalyst decrease ($k_{obs} = 1.68 \times 10^{-5} \text{ s}^{-1}$).

If the reaction of 1,4-benzoquinone with PCy₃ was the primary process taking

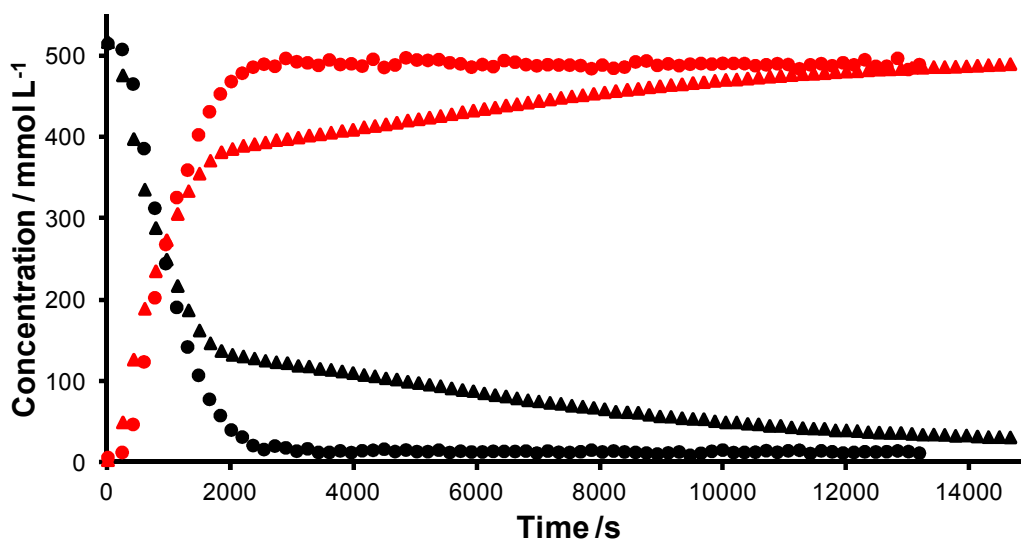


Figure 4.45. Concentration *versus* time profiles for cyclohexene (red) and 1,7-octadiene (black) in the RCM reactions of 1,7-octadiene (0.5 mol L^{-1} in chloroform-*d* with 3 mol% **G2** at 298 K) (a) in the absence of 1,4-benzoquinone (circles) and (b) in the presence of 10 mol% 1,4-benzoquinone (triangles).

place, then the rate of metathesis would be expected to *increase* as phosphane would be prevented from re-capturing ruthenium carbene species, resulting in a higher concentration of metathesis-active 14e species. However, as the reaction rate is *decreased* in the presence of 10 mol% 1,4-benzoquinone and all ruthenium carbene species other than **G2** are absent, it is most likely that 1,4-benzoquinone is undergoing reaction with the 14e complexes responsible for metathesis, thereby slowing the rate of metathesis. In this case, 1,4-benzoquinone and 1,7-octadiene would compete for 14e complexes, which would explain the initial rapid metathesis followed by a change in the rate of 1,7-octadiene consumption. At the point of this change in slope, the concentrations of 1,4-benzoquinone and 1,7-octadiene present were *ca.* 50 mmol L^{-1} and *ca.* 140 mmol L^{-1} , which suggested that 14e complexes such as **1b** and **4b** are approximately 3-fold more selective for 1,4-benzoquinone than for 1,7-octadiene.

Data-fitting approaches were explored to try to model this behaviour. The RCM reaction of 1,7-octadiene has been described using a simple kinetic model (see chapter 4),⁹⁷ so a term was added to the model to model the reaction of the active catalyst with 1,4-benzoquinone; **Equations 4.03** to **4.08** describe this model. First, attempts were made to fit all parameters except k_7 (which was fixed to $4.5 \times 10^{-5} \text{ s}^{-1}$ as measured

$$d/dt [\mathbf{G2}] = -k_1 \cdot [\mathbf{G2}] \quad (4.03)$$

$$d/dt [\text{cat}] = k_1 \cdot [\mathbf{G2}] - k_{BQ} \cdot [\text{cat}] \cdot [\text{BQ}] - k_1 \cdot [\text{cat}] \cdot [\text{PCy}_3] \quad (4.04)$$

$$d/dt [\text{phosphane}] = k_1 \cdot [\mathbf{G2}] - k_1 \cdot [\text{cat}] \cdot [\text{PCy}_3] \quad (4.05)$$

$$d/dt [\text{BQ}] = -k_{BQ} \cdot [\text{cat}] \cdot [\text{BQ}] \quad (4.06)$$

$$d/dt [\mathbf{103c}] = -k_2 \cdot [\text{cat}] \cdot [\mathbf{103c}] + k_2 \cdot [\text{cat}] \cdot [\mathbf{104c}] \quad (4.07)$$

$$d/dt [\mathbf{103c}] = k_2 \cdot [\text{cat}] \cdot [\mathbf{103c}] - k_2 \cdot [\text{cat}] \cdot [\mathbf{104c}] \quad (4.08)$$

previously) simultaneously by fitting both datasets (i.e. data from the reaction without 1,4-benzoquinone and the reaction with 10 mol% 1,4-benzoquinone); concentration/time data for 1,7-octadiene, cyclohexene and 1,4-benzoquinone were fitted, and initial values of 0.01 and 100 were used in the data fitting. Values for each rate constant were obtained (**Table 4.04**) but these did not result in a simulation that correctly described the concentration/time data (**Figure 4.46**). While the concentration *versus* time profile for the reaction in the absence of additive agreed well with the experimental profile, the simulation did not describe the reaction with 1,4-benzoquinone well. The shapes of the 1,7-octadiene (not shown) and cyclohexene concentration/time profiles were not correct, while the 1,4-benzoquinone consumption rate was vastly underestimated.

An alternative approach to the fitting was attempted. First, the concentration/time profiles from the additive-free reaction were fitted, to generate values for k_1 , k_2 and k_2 . Then, these values were fixed and the concentration/time data from the reaction in the presence of 1,4-benzoquinone was fitted, allowing only k_{BQ} to change. The fit to the additive-free reaction was, as expected, better. However, the fit to the reaction in the presence of 1,4-benzoquinone was poor (**Figure 4.47**). The intriguing shape of the concentration/time profile in the presence of 1,4-benzoquinone therefore cannot simply be explained by capture of the active catalyst by benzoquinone.

Table 4.04. Rate constants obtained from fitting the concentration/time data from the RCM reactions of 1,7-octadiene (0.5 mol L⁻¹ in chloroform-*d* at 298 K) in the absence of and in the presence of 10 mol% 1,4-benzoquinone.

Entry	k_1 (L mol ⁻¹ s ⁻¹)	k_2 (L mol ⁻¹ s ⁻¹)	k_2 (L mol ⁻¹ s ⁻¹)	k_{BQ} (L mol ⁻¹ s ⁻¹)
1	25.0	7.48	0.319	0.0368
2	0.418	2.68	0.100	0.0451

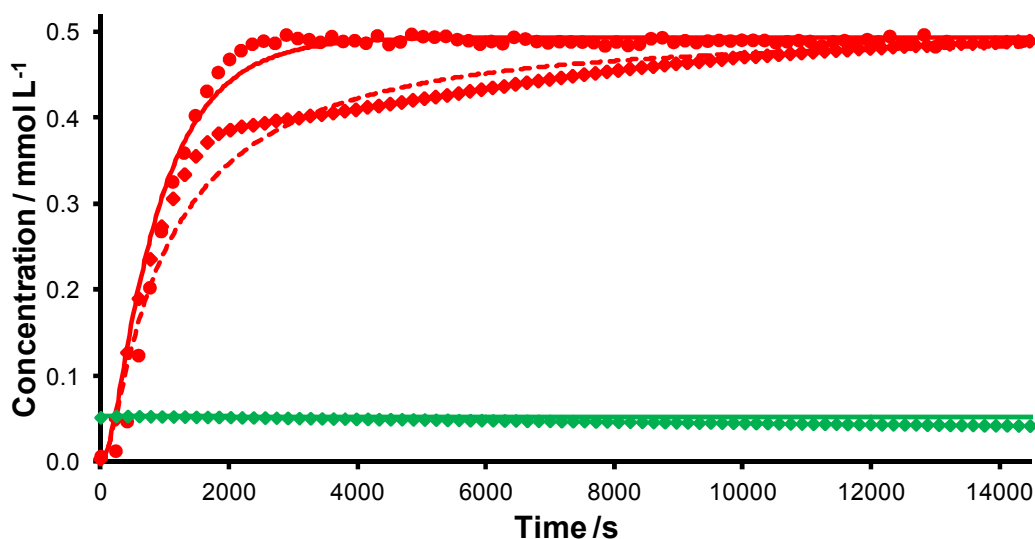


Figure 4.46. Experimental (points) and simulated (lines) concentration *versus* time profiles for (a) cyclohexene (**red**) and (b) 1,4-benzoquinone (**green**) in the RCM of 0.5 mol L⁻¹ 1,7-octadiene (with 3 mol% **G2** in chloroform-*d* at 298 K); obtained from fitting both datasets simultaneously to the model described by **Equations 4.03** to **4.08**.

It was noted previously that 1,4-benzoquinone was consumed at half the rate that pre-catalyst was consumed. Therefore, a second model was tested, in which benzoquinone captures two molecules of catalyst sequentially (**Equations 4.09 – 4.15**).

$$d/dt [\mathbf{G2}] = -k_i \cdot [\mathbf{G2}] \quad (4.09)$$

$$d/dt [\text{cat}] = k_i \cdot [\mathbf{G2}] - k_i \cdot [\text{cat}] [\text{PCy}_3] - k_{\text{BQ}} \cdot [\text{cat}] \cdot [\text{BQ}] - k_{\text{BQ}2} \cdot [\text{cat}] [\text{BQ-cat}] \quad (4.10)$$

$$d/dt [\text{phosphane}] = k_i \cdot [\mathbf{G2}] - k_i \cdot [\text{cat}] [\text{PCy}_3] \quad (4.11)$$

$$d/dt [\text{BQ}] = -k_{\text{BQ}} \cdot [\text{cat}] \cdot [\text{BQ}] \quad (4.12)$$

$$d/dt [\mathbf{103c}] = -k_2 \cdot [\text{cat}] \cdot [\mathbf{103c}] + k_2 \cdot [\text{cat}] \cdot [\mathbf{104c}] \quad (4.13)$$

$$d/dt [\mathbf{104c}] = k_2 \cdot [\text{cat}] \cdot [\mathbf{103c}] - k_2 \cdot [\text{cat}] \cdot [\mathbf{104c}] \quad (4.14)$$

$$d/dt [\text{BQ-cat}] = k_{\text{BQ}1} \cdot [\text{cat}] \cdot [\text{BQ}] - k_{\text{BQ}2} \cdot [\text{BQ-cat}] \cdot [\text{cat}] \quad (4.15)$$

Initially, all rate constants were obtained from fitting both datasets simultaneously; initial values of 0.01 and 100 were used for k_i , k_2 , k_2 , $k_{\text{BQ}1}$ and $k_{\text{BQ}2}$. A poor fit to the experimental concentration/time data was obtained, with K_2 underestimated and the 1,4-benzoquinone concentration/time profile not reproduced (**Table 4.05**, Entry 1 and

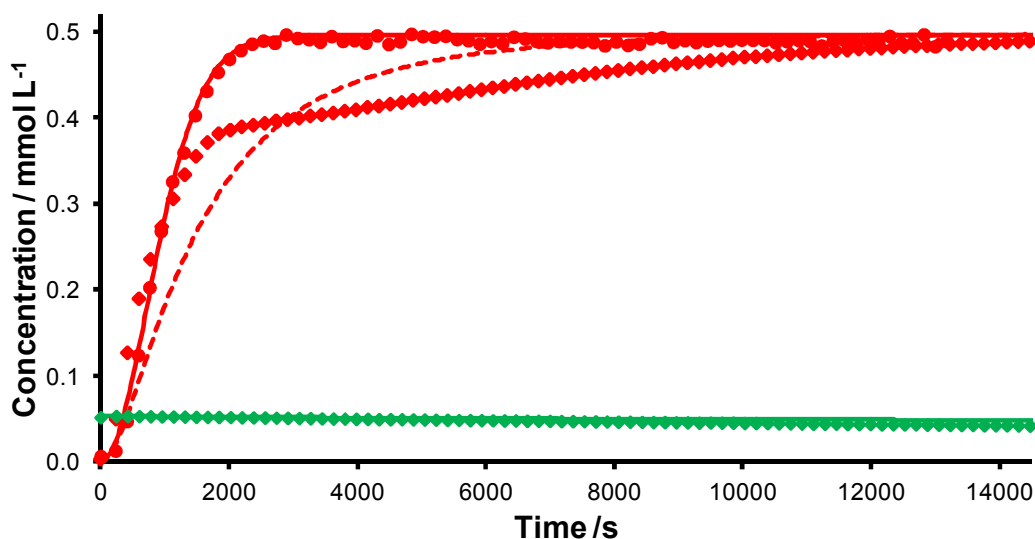


Figure 4.47. Experimental (points) and simulated (lines) concentration *versus* time profiles for the (a) cyclohexene (**red**) and (b) 1,4-benzoquinone (**green**) in the RCM of 0.5 mol L^{-1} 1,7-octadiene (with 3 mol% **G2** in chloroform-*d* at 298 K); obtained from fitting the two datasets sequentially to the model described by **Equations 4.03** to **4.08**.

Table 4.05. Rate constants obtained from fitting the concentration/time data from the RCM reactions of 1,7-octadiene (0.5 mol L^{-1} in chloroform-*d* at 298 K) in the absence of and in the presence of 10 mol% 1,4-benzoquinone; units are $\text{L mol}^{-1} \text{ s}^{-1}$.

Entry	k_1	k_2	k_2	k_{BQ1}	k_{BQ2}
1	42.3	36.5	3.64	0.349	1.01×10^{-6}
2	0.418	2.68	0.100	0.0325	2.94

Figure 4.48). Subsequent attempts to fit the additive-free dataset first, and then fit k_{BQ1} and k_{BQ2} yielded a better fit to the additive-free dataset, but did still not model the distinctive shape of the cyclohexene concentration/time profile when 1,4-benzoquinone was present (**Table 4.05**, Entry 2 and **Figure 4.49**).

Further investigations would be necessary in order to understand better how this shape of concentration/time profile arose, and thereby to understand how 1,4-benzoquinone exerts an effect on metathesis reactions. However, the fact that 1,4-benzoquinone acts upon catalytic species is clear from the data presented here.

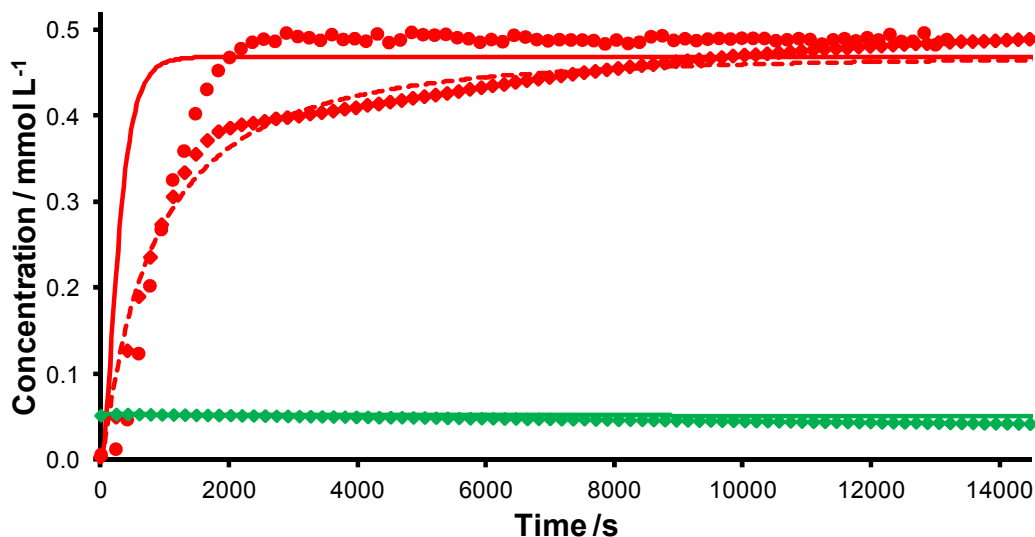


Figure 4.48. Experimental (points) and simulated (lines) concentration *versus* time profiles for the (a) cyclohexene (**red**) and (b) 1,4-benzoquinone (**green**) in the RCM reactions of 0.5 mol L^{-1} 1,7-octadiene (with 3 mol% **G2** in chloroform-*d* at 298 K) ; obtained from fitting both datasets simultaneously to the model described by Equations 4.09 to 4.15.

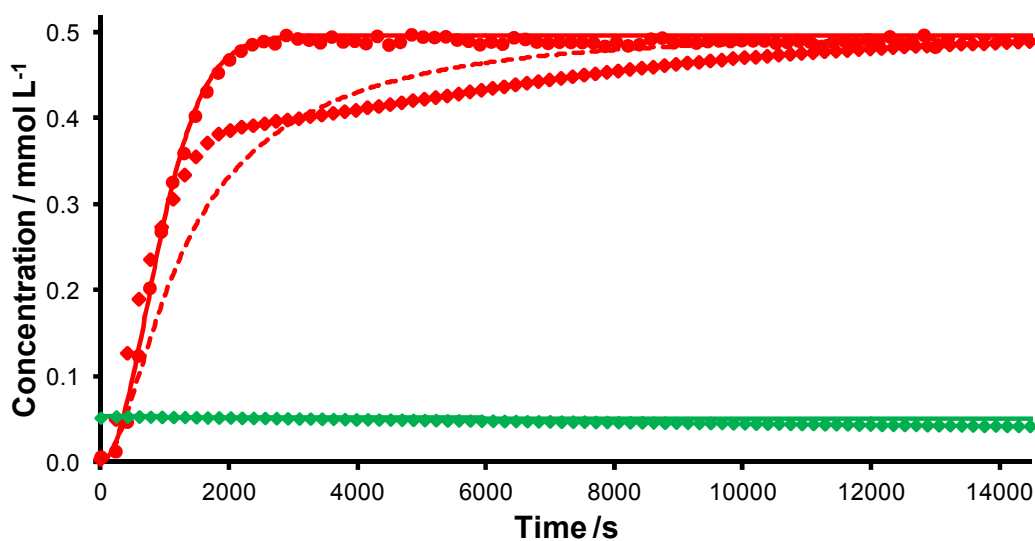


Figure 4.49. Experimental (points) and simulated (lines) concentration *versus* time profiles for the (a) cyclohexene (**red**) and (b) 1,4-benzoquinone (**green**) in the RCM reactions of 0.5 mol L^{-1} 1,7-octadiene (with 3 mol% **G2** in chloroform-*d* at 298 K); obtained from fitting the two datasets sequentially to the model described by Equations 4.09 to 4.15.

Conclusions

The experiments documented and discussed in this chapter have been conducted in order to better understand the source of isomerisation in metathesis reactions of 1,8-nonadiene at 298 K, which represented very mild conditions. While definitive answers have not yet been obtained, some interesting preliminary results have been found.

Initial kinetic experiments allowed isomerisation reactions to be profiled, but did not reveal the presence of ruthenium hydride complexes; no characteristic signals in the otherwise empty high field region that might indicate the presence of ruthenium hydride complexes were detected.

The possibility that undetectable concentrations of ruthenium hydride complexes were responsible was considered. A series of potential isomerisation agents were prepared (at known and measured concentrations) and tested in the isomerisation reaction of 1-octene at 298 K. Bis(tricyclohexylphosphane)-ligated complex **167a** was found to be kinetically incompetent for the isomerisation reaction; the *N*-heterocyclic carbene-bearing analogue **167b** and diruthenium hydride complex **41** were found to be catalytically active, but only at loadings of *ca.* 1 mol%, which would be clearly visible on the ¹H NMR spectrum if present in metathesis reactions.

Further metathesis experiments were conducted in different solvents (benzene-*d*₆, chloroform-*d*, DCM-*d*₂ and toluene-*d*₈) but the isomerisation was not specific to one solvent. Wet solvent was also ruled out as a potential cause of isomerisation in the metathesis reaction; wet solvents were found to *reduce* the isomerisation rate in these reactions.

Different pre-catalysts were tested for the metathesis reaction. First-generation pre-catalyst **G1** produced only very small quantities of isomerised product, while phosphane-free (and rapidly initiating) Hoveyda-type pre-catalysts resulted in considerably more isomerisation. Hoveyda-type pre-catalysts with different initiation rates were found to lead to the same rate of isomerisation, ruling out the possibility that these two rates were correlated. These results began to suggest that the isomerisation processes were due to a ruthenium-hydride species generated *in situ*, rather than an on pathway isomerisation mechanism.

ROMP reactions in the absence of ethene led to very little isomerisation, while the introduction of ethene (*via* a charge of 1,7-octadiene or sparging of the solvent with

ethene before the reaction) stimulated the isomerisation activity. In addition, a signal consistent with known ruthenium hydride complex **167b** was detected in the high field region of the ^1H NMR spectrum. A repeat of this experiment with a higher (15 mol% rather than 3 mol%) pre-catalyst loading allowed the concentration of this complex to be measured throughout the reaction, and also led to the identification of a complex with a ^1H NMR signal consistent with a Fischer carbene-like species.

It was concluded therefore that ruthenium hydride complexes, generated *in situ* are the cause of isomerisation in the metathesis reaction of 1,8-nonadiene. Further, the dependence of the formation of ruthenium hydride species on the presence of methylidene was established. This is consistent with the observation that Hoveyda-type pre-catalysts lead to increased isomerisation activity; the solution concentration of methylidene is increased because phosphane is not present to capture it. In reactions where phosphane is present, the concentration of alkene is typically much higher, and so reaction with alkene is favoured over phosphane capture to yield complex **167b**, which is observable by ^1H NMR spectroscopy. However, other unidentified ruthenium hydride complexes have also been detected in these metathesis reactions. Further work is necessary to probe the mechanism of formation of ruthenium hydride complexes in metathesis reactions. Oxidation of methylidene complex **4b** by traces of oxygen in the solvent might account for the isomerisation activity, *via* insertion into the methylidene C-H bond.

Density functional theory calculations are consistent with these experimental observations. Barriers on the potential energy surfaces for mechanisms proposed by van Rensburg *et al.* and Nolan and Prunet *et al.* are often considerable ($> 30 \text{ kcal mol}^{-1}$) while the 14e hydridocarbonyl complex **173b** encounters barriers of $12.9 \text{ kcal mol}^{-1}$ at most.

The use of 1,4-benzoquinone to suppress isomerisation in these metathesis reactions was also explored. While this additive reduced the rate of isomerisation, it did not suppress it entirely. Close inspection of the low field region of the ^1H NMR spectra revealed that no other alkylidenes were detected. In addition, the concentration/time profiles from the RCM reactions of 1,7-octadiene with and without 1,4-benzoquinone suggested that 1,4-benzoquinone was reacting with 14e ruthenium carbene complexes, thereby reducing their solution concentration and therefore the rate of their decomposition to form ruthenium hydride complexes. As discussed, further studies

would be required to fully interrogate the pathways leading to ruthenium hydride complexes during metathesis reactions.

In conclusion, these results contribute to our understanding of isomerisation during metathesis reactions; isomerisation results from generation of 14e hydride complexes *in situ* from methyldiene complex **4b**. Further studies may yield insight into how this reaction occurs, and perhaps lead to the development of methods to suppress isomerisation without incurring a decrease in metathesis activity.

Chapter 5:

Conclusions

Conclusions from Studies of Alkene Ring-closing Metathesis Reactions

The results documented in this thesis have contributed to the quantitative understanding of alkene metathesis on a number of levels, from the fundamental processes that catalyst species participate in, to the interplay of substrate structure and reactivity.

A key decision during the course of this work was the choice of prototypical system with which to explore the effect of target ring size on the reaction outcome. Synthetic chemists prefer to work with functionalised systems which are close in structure to those employed in target synthesis; however, during the course of this work 1,6-heptadiene, 1,7-octadiene, 1,8-nonadiene, 1,9-decadiene, 1,10-undecadiene and 1,11-dodecadiene were studied (see **Scheme 2.06** in chapter 2). These substrates contain no additional functionality and therefore differences in reactivity are a function of the chain length alone. These substrates were employed at every stage of this work, from kinetic studies to understand the effect of target ring size on RCM rate, to the simulation of metathesis reaction concentration/time profiles *in silico* and the study of isomerisation side reactions that were found to occur.

Robust and reproducible kinetic studies, monitored by ¹H NMR spectroscopy, were designed that allowed detailed and accurate concentration/time profiles to be constructed for a number of RCM reactions. The interpulse delay was increased so that all nuclei could fully relax between the acquisition of each scan. An internal standard was present so that the concentrations of reactants and products could be quantified, including those of side products that were present at low concentrations. Widening the spectral window observed during kinetic experiments allowed various catalyst-related species to be observed and their concentrations quantified, providing detailed insight into the processes occurring during reactions. In contrast, most kinetic studies of RCM in the literature were not conducted with an internal standard, monitored only the

substrate and product, and typically relied upon simple conversion *versus* time profiles to draw only qualitative comparisons.²⁷³

Our approach was successfully employed to investigate various themes in RCM chemistry. It was shown that, when substrates possess minimal functionality, six-membered rings (i.e. cyclohexene) form fastest by RCM, followed closely by five-membered rings (cyclopentene) which form faster than seven-membered rings (cycloheptene). Formation of eight-membered rings is slower again; the formation of *cis*-cyclooctene could not be monitored using kinetic experiments. In addition, oligomeric by-products formed during the metathesis of 1,8-nonadiene and 1,9-decadiene, even at concentrations of 10 mmol L⁻¹. The order of reactivity was therefore qualitatively in agreement with known *thermodynamic* effective molarities, but the rate differences were found to be very modest compared to the EM_T differences.⁹⁶ Comparison of these prototypical systems with those used in the literature revealed interesting results: diethyl diallylmalonate was found to undergo RCM at approximately half of the rate of the RCM of 1,6-heptadiene, despite the presence of bulky *gem*-diester functionality which would be expected to accelerate cyclisation. This difference in reactivity was ascribed to the unfavourable equilibrium between the chain carrier (i.e. methyldiene complex **4b**) and propagating carbene (see **Scheme 2.24** in chapter 2).¹⁸¹

Unfortunately, attempts to quantify kinetic effective molarities were not successful. The measurement of an appropriate rate constant from a prototypical cross-metathesis reaction could not be achieved. However, the cyclisations studied were shown to be under *thermodynamic* control, and so the partitioning between cycloalkene and oligomer would approach the thermodynamic ratio during each reaction. Interestingly, 1,5-hexadiene was shown to be a metathesis inhibitor during the course of these experiments: the rate of RCM of 1,6-heptadiene and 1,7-octadiene was found to be decreased by the presence of 1,5-hexadiene. The inhibitory behaviour of 1,5-hexadiene was explored using DFT calculations, which showed that the chelated η^2 -complex **120a** was low on the PES.

While kinetic studies had yielded interesting information about relative rates of reaction, the outcomes were unfortunately still primarily qualitative, or only semi-quantitative. The use of reaction simulation approaches (using numerical integration software) was explored for RCM reactions. Only one communication discussing this approach for RCM had been published, but was not followed up by the original authors.

Using this model as a starting point, the RCM reactions of diethyl diallylmalonate were studied. Unfortunately, it was found that the literature results could not be reproduced. Further investigation showed that the model was too flexible and that a number of sets of rate constants could yield concentration/time profiles that were consistent with the experimental data. Therefore, several conclusions from the original publication were not consistent with what is known about alkene metathesis.

Work was carried out in order to improve this model, so that it could be reliably applied to applications in RCM chemistry. The model was constrained by measuring the pre-catalyst initiation rate, as this process was best modelled in the reaction simulation (i.e. the simulated step corresponded best with the actual physical reaction). The decomposition term was dropped from the model, as the pathway was not observed to occur in solution at an appreciable rate.

Constraint of the model in this way allowed various aims to be achieved. The relative rates of RCM of 1,6-heptadiene, 1,7-octadiene and diethyl diallylmalonate were quantified, achieving the primary aim of the work. In addition, the effect of pre-catalyst structure was explored; isolation of the initiation and metathesis rates allowed the effects of the NHC ligand and chelating alkoxy styrene ligand on RCM activity to be identified. These results provide a framework for rationalising and predicting the RCM activity of new pre-catalysts. Preliminary experiments suggest that solvent effects on the reactions of 1,7-octadiene in chloroform and DCM are limited to the initiation event alone, which could potentially allow for the informed choice of solvent for metathesis reactions; initiation rates for **G2** and **GH2** were measured in a range of solvents, providing a rather narrow range of values.

During the course of these reactions, it was noted that metathesis of 1,8-nonadiene (and larger α,ω -dienes) often led to formation of cycloalkene products one CH_2 unit shorter than the target cycloalkene, which arose from isomerisation-RCM processes occurring during reactions. Further investigation of the effects of the reaction conditions established that the isomerisation was not specific to certain solvents or pre-catalysts. Ruthenium-hydrides were detected in solution, suggesting that isomerisation was not due to the 'on-pathway' reactions of metathesis intermediates, but was due instead to the irreversible formation of these ruthenium hydride complexes. Kinetic experiments allowed these species to be profiled during a metathesis reaction for the first time. These ruthenium hydride complexes were only observed in reactions in which

ethene was generated and ruthenium methyldiene complex **3b** was present, implicating these species in the pathway from ruthenium carbene to ruthenium hydride. Benchmarking of some known ruthenium hydride complexes suggested that the need to dissociate phosphane renders the 16e species far less efficient than the 14e species; however, *in situ* formation of a 14e ruthenium hydride complex, which only becomes visible by ^1H NMR when captured by phosphane (due to reactions occurring faster than the NMR timescale), would explain the observations.

The effects of 1,4-benzoquinone as an isomerisation suppressant were investigated briefly, making use of the kinetic approach. It was shown that 1,4-benzoquinone reacts with intermediate ruthenium carbene complexes, slowing the productive metathesis reaction. These results suggested that the ruthenium hydride complexes responsible for isomerisation arose from ruthenium carbene intermediates that, in the presence of 1,4-benzoquinone, were removed from solution before they could form ruthenium hydride complexes.

Several key themes permeated the work reported in this thesis. Thermodynamic control initially complicated the experimental study of the RCM of the simple α,ω -diene substrates, necessitating the use of low (10 mmol L^{-1}) concentrations in order to avoid the formation of oligomeric by-products. Isomerisation side reactions were prolific in reactions which reached an equilibrium concentration of cycloalkene which was far below the initial charge of diene; for example, the RCM reactions of 1,8-nonadiene at 0.5 mol L^{-1} at 298 K rapidly formed isomerisation-RCM side products.

Accurate kinetic studies and careful analysis of reaction mixtures and products were invaluable in achieving the aims of this thesis at all stages. Density functional theory studies, carried out primarily by collaborators at the University of Manchester, have informed and supported work at various points.

The work in this thesis not only achieved many of the aims at the outset, but has laid the foundation for future studies of alkene metathesis. The kinetic methods, reaction simulation models and accumulated knowledge of the interplay of structure and reactivity in these simple systems provide a useful starting point for further studies in this area.

Future Directions for Quantitative Studies

Various future directions can be envisioned based on this work. While several important aims were achieved, work on other topics is at a relatively early stage.

The reaction simulation approach has the most scope for elaboration. At present, the model can describe only reactions that yield a single target cycloalkene. By splitting the RCM event into formation of a new alkylidene and then cyclisation or cross-metathesis of that alkylidene, the model could be used to describe reactions in which oligomeric by-products arise. Such a model would then allow the calculation of kinetic *and* thermodynamic effective molarities. Further changes to the model might also take into account non-productive cycles, or isomerisation processes. By splitting the model in to a larger number of more detailed processes, the steps in the simulation will better match the actual physical processes, which may make it easier to link experiment and theory with the simulations.

Detailed experimental and computational studies would be required to inform more elaborate reaction simulation models, as many processes are difficult to study. The use of rapidly-initiating pre-catalysts such as **Piers2** or **G2-3BrPy** might allow the rapid build-up of key intermediates and careful measurement of key rate constants, although extrapolation to room temperature would be necessary. The availability of various analogues of **GH2** and **G2** would effectively allow systematic variation of the initiation rate (to form the same active species) during exploration of the processes in metathesis.

During the course of this work, it was only possible to qualitatively or semi-quantitatively link the outcomes from reaction simulation with results from DFT. For example, in the studies in chapter 3 on the initiation of Hoveyda-type pre-catalysts, the energetic parameters for the initiation step were measured experimentally; however, it was difficult to then link these with DFT calculations on the initiation pathway; two large barriers were present (the interchange step to form the η^2 -complex and the reaction of this complex to form an MCB) and it was not clear which barrier the experimental measurements reflected. Similarly, while high quality data on the RCM of simple dienes was obtained, linking the rate data to the corresponding PES calculations was difficult. It was not clear which barrier was controlling the rate of cycloalkene formation, while the energetic span model predicted the wrong order of rates. In more detailed models, the simulated steps will better reflect the actual chemical processes.

Four key areas would benefit from further exploration of the reaction simulation approach for metathesis chemistry: the quantitative assessment of the effects of substrate structure on reactivity; the effect of reaction conditions on the rate and efficiency of metathesis; pre-catalyst design and selection; and mechanistic studies on key processes in metathesis.

The initial aims of the work conducted in this thesis were to quantitatively assess the effects of substrate structure on reactivity. While the current model can only assess substrates that yield only cyclic product, a logical extension of the model would cover the alternative (intermolecular) pathway which can produce oligomeric material. Various substrate structural features could then be evaluated, from allylic functionality to backbone substituents that may exert an influence *via* the Thorpe-Ingold and/or reactive rotamer effects.

Investigations into solvent effects on RCM have been started, but further kinetic data is necessary to identify if any solvents exert strong effects on steps other than pre-catalyst initiation. The issue of solvent choice has considerable implications on large-scale chemical synthesis, so this topic is worthwhile pursuing. Further studies could be conducted with a more detailed model for RCM. If, as initial results suggest, solvent effects are limited to the initiation event, this would have implications for solvent selection for industrial-scale metathesis reactions. Similarly, the use of additives such as $\text{Ti}(\text{O}^i\text{Pr})_4$ could be studied and their effects on different stages of the reaction could be elucidated.

Results presented in this thesis show that the reaction simulation approach has potential applications in pre-catalyst design and evaluation. While it was shown that differences in initiation rate alone accounted for the differences in metathesis activity (for pre-catalysts bearing the same NHC), only a limited number of pre-catalysts were assessed. There is considerable scope for evaluating other pre-catalysts with the current model and, once decomposition can be accounted for, further studies in pre-catalyst evaluation could be conducted.

Development of a model to achieve the aims set out above would require mechanistic studies of alkene metathesis. Processes such as substrate and product isomerisation could also be studied using a simulation approach. The mechanism of the inhibition of isomerisation by 1,4-benzoquinone warrants further study. Preliminary results suggest that this compound reacts with 14e ruthenium alkylidenes, in which case

the complex between alkylidene and 1,4-benzoquinone may be isolable; Grubbs *et al.* have isolated complex **194** from the reaction of cyclometallated metathesis pre-catalyst **195** with 1,4-benzoquinone. Unwanted isomerisation during metathesis reactions is a problem in many applications that has still not been completely solved.

Further development of the reaction simulation approach would allow studies of alkene metathesis at a number of levels, with the development of accurate models as the central theme tying the research together. In the same way that much has been achieved with the tools developed during the course of the last few years, further development of these tools would potentially allow further interesting and relevant investigations into the interplay of structure and reactivity in RCM.

Experimental

Equipment

All manipulations of solid pre-catalysts and solutions thereof were conducted under a gentle flow of oxygen-free nitrogen or argon. Manipulation of solutions was performed using oven-dried volumetric glassware and gastight syringes that had been dried in a vacuum dessicator.

NMR kinetics experiments were conducted using either a Bruker Avance II (400 MHz ^1H observation) with a BBFO- ζ -ATMA probe or a Bruker Avance II+ (600 MHz ^1H observation) with either a BBO- ζ -ATMA or TBI- ζ probe. A Bruker Avance DRX (500 MHz ^1H observation) with $^1\text{H}/^{13}\text{C}$ -DUL probe, Bruker Avance DPX (400 MHz ^1H observation) with $^1\text{H}/^{13}\text{C}/^{19}\text{F}/^{31}\text{P}$ -QNP- ζ probe and Bruker Avance III (400 MHz ^1H observation) with $^1\text{H}/^{13}\text{C}/^{19}\text{F}/^{31}\text{P}$ -QNP- ζ probe were also used to acquire NMR spectra. Data was processed using Bruker Topspin version 2.1 or version 3.0 software. All spectrometers except the Avance DPX and Avance III were equipped with temperature control units.

UV/visible spectra were obtained using a Varian Cary 50 UV/visible spectrophotometer equipped with a peltier-cooled cuvette holder. Quartz cuvettes were dried in an oven before use.

Materials

Pre-catalysts **G2**, **GH2**, **G2-SIPr**, **GH2-SIPr**, **G2-CHCMe2** and **G1** were purchased from Sigma-Aldrich. **Grela** was purchased from Apeiron. **Zhan1B**, **Indenyl-SIMes** and **Indenyl-SIPr** were purchased from Strem. Pre-catalysts **M71-SIMes**, **M71-SIPr**, **M8₃₂-SIPr**, **M8₅₃-SIPr** and **Grela-SIPr** were gifts from Omega Cat. System. $(\text{PCy}_3)_2\text{RuCl}_2(\text{CHOEt})$ and $(\text{SIMes})(\text{PCy}_3)\text{RuCl}_2(\text{CHOEt})$ were prepared according to the literature procedure.⁴⁴

Benzene- d_6 , chloroform- d and toluene- d_8 were purchased from Sigma-Aldrich and DCM- d_2 was purchased from Goss Scientific. All deuterated solvents were dried overnight over activated 4 Å molecular sieves before use and degassed with a flow of

nitrogen, unless otherwise stated. Karl-Fischer analysis showed the water content of these solvents to be *ca.* 5 – 9 ppm.

DCM, hexane and toluene were obtained as anhydrous from the in-house solvent purification system; regular Karl-Fischer analysis of these solvents recorded a water content of *ca.* 5 ppm or less. Chloroform was purchased from Sigma-Aldrich and dried by passage through a column of activated alumina. Benzene, dimethyl carbonate, methyl *tert*-butyl ether and trifluorotoluene were purchased as anhydrous from Sigma-Aldrich. 1,2-Difluorobenzene and hexafluorobenzene were purchased from Fluorochem and distilled under argon from calcium hydride onto freshly activated 4 Å molecular sieves. Methanol was purchased from Sigma-Aldrich and dried by distillation from calcium hydride onto freshly activated 3 Å molecular sieves.

1,5-Hexadiene, 1,6-heptadiene, 1,7-octadiene, 1,8-nonadiene and 1,9-decadiene were purchased from Sigma-Aldrich, while 1,10-undecadiene and 1,11-dodecadiene were purchased from Fluorochem. Cyclopentene, cyclohexene, cycloheptene, *cis*-cyclooctene and *cis*- and *trans*-cyclodecene were purchased from Sigma-Aldrich. All dienes and cycloalkenes were passed through a column of activated alumina before use. Ethyl vinyl ether was purchased from Alfa Aesar and freshly distilled to remove stabilisers before use. Trimethoxybenzene and 1,4-benzoquinone were purchased from Sigma-Aldrich and used as supplied. Diethyl diallylmalonate **102** was purchased from Sigma-Aldrich and used as supplied, or prepared according to the literature procedure¹¹⁶ and purified by distillation under reduced pressure.

Preparations of Ruthenium Complexes

Ruthenium Alkylidene Complexes

(SIMes)(PCy₃)RuCl₂(CH₂) 3b

Synthesis using 1,7-octadiene. **G2** (228.7 mg, 0.269 mmol) was dissolved in a solution of 1,7-octadiene (2 mL) and dry benzene (6 mL) and stirred under argon for 2.5 h at 50°C. The volatiles were then removed *in vacuo* and the residue loaded onto silica. Elution with 0-50% DCM/hexane (dry) yielded 39.4 mg of an orange-yellow solid (0.051 mmol, 19%) with a ¹H NMR spectrum consistent with that of **3b**.

Ruthenium Hydride Complexes

(PCy₃)₂RuCl(CO)H 167a

G1 (126.9 mg, 0.154 mmol) was suspended in dry methanol (4 mL) containing a few drops of dry triethylamine in a microwave vial fitted with cap. The suspension was heated with stirring at 70°C for 4 h, filtered, washed with dry methanol and dry hexane and dried on a frit under a flow of argon to yield a yellow powder (84.1 mg). Analysis of a sample by ¹H NMR suggested that the material was *ca.* 25% (PCy₃)₂RuCl(CO)H (*via* integration of the characteristic signal at δ_{H} (benzene-*d*₆) = -24.12 ppm (t, ³J_{HP} = 18.0 Hz) *versus* an internal standard), with the remainder of the material unidentified, but neither ruthenium carbene nor hydride. This solution was used for kinetic experiments after addition of a portion of neat 1-octene, such that the initial 1-octene concentration was *ca.* 500 mmol L⁻¹; absolute concentrations were obtained by integration *versus* the internal standard.

(SIMes)(PCy₃)RuCl(CO)H 167b

Attempted thermolysis of Fischer carbene. (PCy₃)₂RuCl₂(CHOEt) (12.6 mg, 0.015 mmol) was dissolved in toluene-*d*₈ (0.6 mL) with 1,3,5-trimethoxybenzene (10.2 mg, 0.061 mmol) in a septum-fitted NMR tube and heated in an oil bath to 110°C for 30 minutes, before analysis by ¹H NMR. Only traces of the desired complex were observed.

From reaction with vinyloxytrimethylsilane. A solution of vinyloxytrimethylsilane (11.4 mg, 0.098 mol) was prepared in toluene-*d*₈ (1 mL, 98 mmol L⁻¹). 0.5 mL was added to **G2** (7.6 mg, 8.95 μmol, thus 5.5 equiv. vinyloxytrimethylsilane) in an NMR tube.

Analysis after *ca.* 40 minutes at rt revealed the presence of unreacted **G2**, plus a new species ($\delta_{\text{H}} = 14.68$ ppm, d, $^3J_{\text{H,P}} = 3.1$ Hz) attributed to (SIMes)(PCy₃)RuCl₂(CHOTMS). Heating to 90°C for *ca.* 10 minutes in the NMR magnet led to complete consumption of **G2** and the new carbene species, and formation of **167b** (*ca.* 70% conversion from **G2**). Further heating led to decomposition of **167b**. The solution containing **167b** was used for kinetics experiments, after addition of a concentrated solution containing 1-octene and internal standard (1,3,5-trimethoxybenzene), such that the 1-octene concentration was *ca.* 500 mmol L⁻¹.

Attempted repeat 1. A solution of vinyloxytrimethylsilane (11.3 mg, 0.097 mmol) was prepared in toluene-*d*₈ (1 mL, 97 mmol L⁻¹). 0.3 mL was added to **G2** (7.5 mg, 8.83 μmol, thus 3.3 equiv. vinyloxytrimethylsilane) in an NMR tube. The solution was heated to 90°C in an oil bath for 15 minutes before ¹H NMR analysis, which revealed the presence of an unidentified hydride complex (δ_{H} (toluene-*d*₈) = -5.11 ppm, d ($^3J_{\text{HP}} = 23.4$ Hz)).

Attempted repeat 2. A solution of vinyloxytrimethylsilane (24.8 mg, 0.213 mmol) was prepared in toluene-*d*₈ (2 mL, 107 mmol L⁻¹). 1 mL was added to **G2** (15.6 mg, 18.37 μmol, thus 5.8 equiv. vinyloxytrimethylsilane) in an NMR tube. The solution was heated to 90°C in an oil bath for 15 minutes before ¹H NMR analysis, which revealed the presence of an unidentified hydride complex plus the desired complex **167b**.

Diruthenium hydride 41

Attempted one-pot procedure without ethene removal. **G2** (15 mg, 17.67 μmol) was dissolved in benzene-*d*₆ (0.6 mL), sparged with ethene, and heated to 55°C in a septum-fitted NMR tube under an atmosphere of ethene for 72 h. ¹H NMR analysis revealed no ruthenium hydride complexes.

Attempted one-pot procedure with ethene removal. **G2** (273.0 mg, 0.322 mmol) was dissolved in anhydrous benzene (10 mL) in a Schlenk flask. The atmosphere was removed and replaced with ethene twice. The reaction was stirred at 50°C for 1.5 h, after which the solvent was removed under vacuum. The solid was washed with dry hexane, and a portion was analysed by ¹H NMR, which showed (SIMes)(PCy₃)RuCl₂(CH₂) **3b** plus *ca.* 20% styrene. The solid was redissolved in dry benzene and heated to 50°C under argon for 72 h. The solvent was removed *in vacuo*

and a portion was dissolved in DCM- d_2 for analysis by NMR spectroscopy, which revealed no hydride **41**.

Attempted preparation from reaction of G2 with 1,7-octadiene. **G2** (450.6 mg, 0.531 mmol) was dissolved in degassed (by three freeze-pump-thaw cycles) dry benzene (15 mL) in an Ace tube. The solution was frozen in liquid nitrogen, 1,7-octadiene (3 mL) was layered on the top, the tube was closed and allowed to thaw. The solution was heated for 3 h at 55°C during which time a grey precipitate formed. The solution was allowed to cool, and carefully decanted. The solid precipitate was found to be **SIMes.HCl** by ^1H NMR analysis.

Preparation from methyldene complex. A solution of methyldene **3b** was heated to 50°C in an oil bath for 72 h, during which time a precipitate formed. ^1H NMR analysis showed the presence of various hydride complexes (see Chapter 4). The solution was carefully removed *via* syringe, and the precipitate taken up in DCM- d_2 ; this sample was used for the kinetic studies, by adding a solution of 1-octene and 1,3,5-trimethoxybenzene and monitoring the reaction by periodic ^1H NMR analyses.

Unidentified hydride from **GH2**-catalysed reactions

A stock solution containing 1,8-nonadiene (189 mg, 1.524 mmol) and 1,3,5-trimethoxybenzene (127.7 mg, 0.759 mmol) in 3 mL benzene- d_6 was prepared (thus 508 mmol L $^{-1}$ /253 mmol L $^{-1}$). Three NMR tubes were charged with **GH2** (5.5 – 6.2 mg, 8.8 – 9.9 μmol) and 600 μL of the stock solution. A concentrated solution of PCy $_3$ (94.6 mg, 0.337 mmol) in benzene- d_6 (0.4 mL, thus 843 mmol L $^{-1}$) was prepared, and 100 μL were added to each tube at a different time point (*ca.* 0.5 h, 1 h and 1.5 h). The solutions were then analysed by ^1H NMR spectroscopy. A signal at $\delta_{\text{H}} = -31.6$ ppm (s) was attributed to an unknown ruthenium hydride complex. Analysis of a reaction in the absence of tricyclohexylphosphane revealed no ruthenium hydride complexes.

Typical Procedures

Metathesis Kinetics by ^1H NMR Spectroscopy

Substrate Concentration of 10 mmol L^{-1}

A clean and dry volumetric flask was flushed with inert gas and charged with an appropriate mass of 1,3,5-trimethoxybenzene and an appropriate mass of diene. The flask was made up to volume with dry solvent, under a flow of inert gas. This concentrated stock solution (typically approximately 100 mmol L^{-1} total diene concentration) was then diluted to an appropriate concentration in a second volumetric flask, using a clean and dry gastight syringe. The flask was made up to volume using dry solvent. This solution (typically 10 mM total diene concentration) was used as a stock solution. A clean, oven-dried NMR tube was flushed with inert gas using a balloon. The 10 mM stock solution ($600\text{ }\mu\text{L}$) was added and the tube capped. The tube was inserted into the magnet and the instrument internal temperature was set to 298K and allowed to equilibrate. ^1H NMR analysis was carried out before pre-catalyst addition to confirm the absence of impurities and check that the sample contained the correct concentration of diene with respect to the internal standard. A dry volumetric flask was flushed with inert gas and charged with an appropriate mass of pre-catalyst. The flask was made up to volume using dry solvent approximately 5 minutes before charging the solution to the NMR tube. This catalyst solution was charged to the NMR tube *via* a dry glass syringe and the time was noted. The tube was shaken vigorously for approx. 15 seconds before the solid cap was exchanged for a pierced cap. The sample was then analysed at appropriate intervals using a Bruker Topspin automated script, *multi_zgvd2b*. Samples were automatically shimmed using *topshim 1dfast* between acquisitions. The sample was held at the appropriate temperature for the duration of the experiment.

Substrate Concentration of 0.5 mol L^{-1}

A clean and dry volumetric flask was flushed with inert gas and charged with an appropriate mass of 1,3,5-trimethoxybenzene and an appropriate mass of diene. The flask was made up to volume with dry solvent, under a flow of inert gas. This stock solution was approximately 0.5 mol L^{-1} in diene. This solution ($600\text{ }\mu\text{L}$) was added to an NMR tube. An appropriate mass of solid pre-catalyst was added to a second clean and

dry NMR tube. The first sample was used to tune, match, lock and shim the instrument, check the stock solution for impurities, and quantify the initial concentration of diene. A 600 μL portion of the stock solution was then added to the solid pre-catalyst, the tube was shaken for 15 seconds, and the solid cap was exchanged for a pierced cap. The NMR tube was then inserted into the magnet and the reaction was monitored.

Initiation Kinetics by UV/Visible Spectroscopy

Ethyl Vinyl Ether Concentrations of *ca.* 25 to 300 mmol L^{-1}

A 4 mol L^{-1} solution of distilled ethyl vinyl ether in dry solvent was prepared in a dry volumetric flask which had been flushed with inert gas. An appropriate mass of pre-catalyst was dissolved in dry solvent in volumetric glassware to give a stock solution with a concentration of *ca.* 8 mmol L^{-1} . This stock solution was diluted to 0.3 mmol L^{-1} in volumetric glassware, and 1 mL of this dilute solution was added to each cuvette, plus 1.6 to 2 mL of dry solvent. Each cuvette was allowed to equilibrate at the desired temperature in the spectrometer before an appropriate volume of ethyl vinyl ether solution was added and acquisitions were started.

Ethyl Vinyl Ether Concentrations of *ca.* 0.2 to 3 mol L^{-1}

A 4 mol L^{-1} solution of distilled ethyl vinyl ether in dry solvent was prepared in a dry volumetric flask which had been flushed with inert gas. This solution was added, with appropriate volumes of dry solvent, to the cuvettes, so that the ethyl vinyl ether concentration in each cuvette was as required. A *ca.* 6 mmol L^{-1} solution of pre-catalyst in dry solvent was prepared. Each cuvette was allowed to equilibrate in the spectrometer before the addition of an appropriate volume of pre-catalyst solution, from which point the reaction was monitored.

Appendix A:

Peer-Reviewed Publications

The following publications are derived, either in part or in full, from work presented in this thesis.

Chemical Physics Letters 2009

Shanthi Pandian, Ian H. Hillier, Mark A. Vincent, Neil A. Burton, Ian W. Ashworth, David J. Nelson, Jonathan M. Percy and Giuseppe Rinaudo, *Chem. Phys. Lett.* **2009**, *476*, 37. Early work on the determination of effective molarities was contributed to this publication, which sought to estimate effective molarity using density functional theory calculations.

Tetrahedron 2009

Ian W. Ashworth, Jonathan A. Miles, David J. Nelson, Jonathan M. Percy and Kuldip Singh, *Tetrahedron* **2009**, *65*, 9637. The effective molarity was measured for the challenging RCM of an intermediate *en route* to difluorinated sugar analogues.

Chemical Communications 2010

Ian W. Ashworth, Davide Carboni, Ian H. Hillier, David J. Nelson, Jonathan M. Percy, Guiseppe Rinaudo and Mark A. Vincent, *Chem. Commun.* **2010**, *46*, 7145. The order of reactivity of the simple dienes in kinetic experiments was detailed, as well as the inhibitive effect of 1,5-hexadiene (see chapter 2 of this thesis).

Chemical Communications 2011

Ian W. Ashworth, Ian H. Hillier, D. J. Nelson, J. M. Percy and Mark A. Vincent, *Chem. Commun.* **2011**, *47*, 5428. UV/visible kinetics and density functional theory were used to explore the initiation mechanism of Hoveyda-type metathesis pre-catalysts (see chapter 4 of this thesis).

The Journal of Organic Chemistry 2011

David J. Nelson, Davide Carboni, Ian W. Ashworth and Jonathan M. Percy, *J. Org. Chem.* **2011**, *76*, 8386. The simulation approach to interpreting RCM kinetic data was explored, improved, and applied (see chapter 4 of this thesis).

Chemistry – A European Journal 2011

David J. Nelson, Ian W. Ashworth, Ian H. Hillier, Sara H. Kyne, Shanthi Pandian, John A. Parkinson, Jonathan M. Percy, Giuseppe Rinaudo and Mark A. Vincent, *Chem. Eur. J.* **2011**, *17*, 13087. Thermodynamic effective molarities for RCM obtained from empirical data, solution experiments, and density functional theory were presented and discussed.

European Journal of Organic Chemistry 2012

Ian W. Ashworth, Ian H. Hillier, David J. Nelson, Jonathan M. Percy, and Mark A. Vincent, *Eur. J. Org. Chem.* **2012**, DOI: 10.1002/ejoc.201201036. Thermodynamic effective molarities for RCM obtained from empirical data, solution experiments, and density functional theory were presented and discussed.

References

- (1) Banks, R. L.; Bailey, G. C. *I&EC Product Research and Development* **1964**, *3*, 170.
- (2) Hoveyda, A. H.; Zhugralin, A. R. *Nature* **2007**, *450*, 243.
- (3) Nicolaou, K. C.; Bulger, P. G.; Sarlah, D. *Angew. Chem. Int. Ed.* **2005**, *44*, 4490.
- (4) Chauvin, Y. *Angew. Chem. Int. Ed.* **2006**, *45*, 3740.
- (5) Grubbs, R. H. *Angew. Chem. Int. Ed.* **2006**, *45*, 3760.
- (6) Schrock, R. R. *Angew. Chem. Int. Ed.* **2006**, *45*, 3748.
- (7) Trnka, T. M.; Grubbs, R. H. *Acc. Chem. Res.* **2001**, *34*, 18.
- (8) Marinescu, S. C.; Schrock, R. R.; Müller, P.; Takase, M. K.; Hoveyda, A. H. *Organometallics* **2011**, *30*, 1780.
- (9) Schwab, P.; France, M. B.; Ziller, J. W.; Grubbs, R. H. *Angew. Chem. Int. Ed.* **1995**, *34*, 2039.
- (10) Scholl, M.; Ding, S.; Lee, C. W.; Grubbs, R. H. *Org. Lett.* **1999**, *1*, 953.
- (11) Kingsbury, J. S.; Harrity, J. P. A.; Bonitatebus, P. J.; Hoveyda, A. H. *J. Am. Chem. Soc.* **1999**, *121*, 791.
- (12) Garber, S. B.; Kingsbury, J. S.; Gray, B. L.; Hoveyda, A. H. *J. Am. Chem. Soc.* **2000**, *122*, 8168.
- (13) Michrowska, A.; Bujok, R.; Harutyunyan, S.; Sashuk, V.; Dolgonos, G.; Grell, K. *J. Am. Chem. Soc.* **2004**, *126*, 9318.
- (14) Love, J. A.; Morgan, J. P.; Trnka, T. M.; Grubbs, R. H. *Angew. Chem. Int. Ed.* **2002**, *41*, 4035.
- (15) van der Eide, E. F.; Piers, W. E. *Nature Chem.* **2010**, *2*, 571.
- (16) Agrawal, D.; Schröder, D. *Organometallics* **2011**, *30*, 32.
- (17) Conrad, J. C.; Amoroso, D.; Czechura, P.; Yap, G. P. A.; Fogg, D. E. *Organometallics* **2003**, *22*, 3634.
- (18) Blacquiere, J. M.; McDonald, R.; Fogg, D. E. *Angew. Chem. Int. Ed.* **2010**, *49*, 3807.
- (19) Schmid, T. E.; Bantreil, X.; Citadelle, C. A.; Slawin, A. M. Z.; Cazin, C. S. J. *Chem. Commun.* **2011**, *47*, 7060.
- (20) Bantreil, X.; Schmid, T. E.; Randall, R. A. M.; Slawin, A. M. Z.; Cazin, C. S. J. *Chem. Commun.* **2010**, *46*, 7115.
- (21) Fürstner, A.; Thiel, O. R.; Lehmann, C. W. *Organometallics* **2002**, *21*, 331.
- (22) Denk, K.; Fridgen, J.; Herrmann, W. A. *Adv. Synth. Catal.* **2002**, *344*, 666.
- (23) Kost, T.; Sigalov, M.; Goldberg, I.; Ben-Asuly, A.; Lemcoff, N. G. *J. Organomet. Chem.* **2008**, *693*, 2200.
- (24) Vidavsky, Y.; Anaby, A.; Lemcoff, N. G. *Dalton Trans.* **2012**, *41*, 32.
- (25) Monsaert, S.; Lozano Vila, A.; Drozdak, R.; Van Der Voort, P.; Verpoort, F. *Chem. Soc. Rev.* **2009**, *38*, 3360.
- (26) Sanford, M. S.; Love, J. A.; Grubbs, R. H. *J. Am. Chem. Soc.* **2001**, *123*, 6543.
- (27) Hong, S. H.; Day, M. W.; Grubbs, R. H. *J. Am. Chem. Soc.* **2004**, *126*, 7414.
- (28) Hong, S. H.; Wenzel, A. G.; Salguero, T. T.; Day, M. W.; Grubbs, R. H. *J. Am. Chem. Soc.* **2007**, *129*, 7961.

- (29) Romero, P. E.; Piers, W. E.; McDonald, R. *Angew. Chem. Int. Ed.* **2004**, *43*, 6161.
- (30) Dubberley, S. R.; Romero, P. E.; Piers, W. E.; McDonald, R.; Parvez, M. *Inorg. Chim. Acta* **2006**, *359*, 2658.
- (31) Leitao, E. M.; Eide, E. F. v. d.; Romero, P. E.; Piers, W. E.; McDonald, R. *J. Am. Chem. Soc.* **2010**, *132*, 2784.
- (32) Romero, P. E.; Piers, W. E. *J. Am. Chem. Soc.* **2005**, *127*, 5032.
- (33) Romero, P. E.; Piers, W. E. *J. Am. Chem. Soc.* **2007**, *129*, 1698.
- (34) Rowley, C. N.; van der Eide, E. F.; Piers, W. E.; Woo, T. K. *Organometallics* **2008**, *27*, 6043.
- (35) van der Eide, E. F.; Romero, P. E.; Piers, W. E. *J. Am. Chem. Soc.* **2008**, *130*, 4485.
- (36) Wenzel, A. G.; Grubbs, R. H. *J. Am. Chem. Soc.* **2006**, *128*, 16048.
- (37) Wenzel, A. G.; Blake, G.; VanderVelde, D. G.; Grubbs, R. H. *J. Am. Chem. Soc.* **2011**, *133*, 6429.
- (38) Keitz, B. K.; Grubbs, R. H. *J. Am. Chem. Soc.* **2011**, *133*, 16277.
- (39) Herrmann, W. A. *Angew. Chem. Int. Ed.* **2002**, *41*, 1290.
- (40) Liu, M.; Yang, I.; Buckley, B.; Lee, J. K. *Org. Lett.* **2010**, *12*, 4764.
- (41) Kelly Iii, R. A.; Clavier, H.; Giudice, S.; Scott, N. M.; Stevens, E. D.; Bordner, J.; Samardjiev, I.; Hoff, C. D.; Cavallo, L.; Nolan, S. P. *Organometallics* **2007**, *27*, 202.
- (42) Huang, J.; Stevens, E. D.; Nolan, S. P.; Petersen, J. L. *J. Am. Chem. Soc.* **1999**, *121*, 2674.
- (43) Sanford, M. S.; Ulman, M.; Grubbs, R. H. *J. Am. Chem. Soc.* **2001**, *123*, 749.
- (44) Louie, J.; Grubbs, R. H. *Organometallics* **2002**, *21*, 2153.
- (45) Ritter, T.; Hejl, A.; Wenzel, A. G.; Funk, T. W.; Grubbs, R. H. *Organometallics* **2006**, *25*, 5740.
- (46) Fürstner, A.; Ackermann, L.; Gabor, B.; Goddard, R.; Lehmann, C. W.; Mynott, R.; Stelzer, F.; Thiel, O. R. *Chem. Eur. J.* **2001**, *7*, 3236.
- (47) Getty, K.; Delgado-Jaime, M. U.; Kennepohl, P. *J. Am. Chem. Soc.* **2007**, *129*, 15774.
- (48) Fey, N.; Ridgway, B. M.; Jover, J.; McMullin, C. L.; Harvey, J. N. *Dalton Trans.* **2011**, *40*, 11184.
- (49) Zhao, Y.; Truhlar, D. G. *Org. Lett.* **2007**, *9*, 1967.
- (50) Poater, A.; Ragone, F.; Correa, A.; Cavallo, L. *Dalton Trans.* **2011**, *40*, 11066.
- (51) Sliwa, P.; Handzlik, J. *Chem. Phys. Lett.* **2010**, *493*, 273.
- (52) Zhao, Y.; Truhlar, D. G. *J. Chem. Phys.* **2006**, *125*, 194101.
- (53) Hillier, I. H.; Pandian, S.; Percy, J. M.; Vincent, M. A. *Dalton Trans.* **2011**, *40*, 1061.
- (54) Zhao, Y.; Truhlar, D. G. *J. Chem. Theory Comput.* **2009**, *5*, 324.
- (55) Benitez, D.; Tkatchouk, E.; Goddard, W. A. *Organometallics* **2009**, *28*, 2643.
- (56) Torker, S.; Merki, D.; Chen, P. *J. Am. Chem. Soc.* **2008**, *130*, 4808.
- (57) Minenkov, Y.; Occhipinti, G.; Heyndrickx, W.; Jensen, V. R. *Eur. J. Inorg. Chem.* **2011**, 1507.
- (58) Love, J. A.; Sanford, M. S.; Day, M. W.; Grubbs, R. H. *J. Am. Chem. Soc.* **2003**, *125*, 10103.
- (59) Vougioukalakis, G.; Grubbs, R. *Chem. Eur. J.* **2008**, *14*, 7545.
- (60) Vorfalt, T.; Wannowius, K. J.; Plenio, H. *Angew. Chem. Int. Ed.* **2010**, *49*, 5533.
- (61) Thiel, V.; Hendann, M.; Wannowius, K.-J.; Plenio, H. *J. Am. Chem. Soc.* **2011**, *134*, 1104.
- (62) Chatterjee, A. K.; Choi, T.-L.; Sanders, D. P.; Grubbs, R. H. *J. Am. Chem. Soc.* **2003**, *125*, 11360.
- (63) Luján, C.; Nolan, S. P. *J. Organomet. Chem.* **2011**, *696*, 3935.
- (64) Luján, C.; Nolan, S. P. *Cat. Sci. Technol.* **2012**, *2*, 1027.

- (65) Smith, A. B.; Adams, C. M.; Kozmin, S. A. *J. Am. Chem. Soc.* **2001**, *123*, 990.
- (66) Yamamoto, K.; Biswas, K.; Gaul, C.; Danishefsky, S. J. *Tetrahedron Lett.* **2003**, *44*, 3297.
- (67) Hoye, T. R.; Jeffrey, C. S.; Tennakoon, M. A.; Wang, J.; Zhao, H. *J. Am. Chem. Soc.* **2004**, *126*, 10210.
- (68) Yee, N. K.; Farina, V.; Houpis, I. N.; Haddad, N.; Frutos, R. P.; Gallou, F.; Wang, X.-j.; Wei, X.; Simpson, R. D.; Feng, X.; Fuchs, V.; Xu, Y.; Tan, J.; Zhang, L.; Xu, J.; Smith-Keenan, L. L.; Vitous, J.; Ridges, M. D.; Spinelli, E. M.; Johnson, M.; Donsbach, K.; Nicola, T.; Brenner, M.; Winter, E.; Kreye, P.; Samstag, W. *J. Org. Chem.* **2006**, *71*, 7133.
- (69) Wagner, J.; Martin Cabrejas, L. M.; Grossmith, C. E.; Papageorgiou, C.; Senia, F.; Wagner, D.; France, J.; Nolan, S. P. *J. Org. Chem.* **2000**, *65*, 9255.
- (70) Zeng, X.; Wei, X.; Farina, V.; Napolitano, E.; Xu, Y.; Zhang, L.; Haddad, N.; Yee, N. K.; Grinberg, N.; Shen, S.; Senanayake, C. H. *J. Org. Chem.* **2006**, *71*, 8864.
- (71) Gallenkamp, D.; Fürstner, A. *J. Am. Chem. Soc.* **2011**, *133*, 9232.
- (72) Straub, B. F. *Angew. Chem. Int. Ed.* **2005**, *44*, 5974.
- (73) Yang, H.-C.; Huang, Y.-C.; Lan, Y.-K.; Luh, T.-Y.; Zhao, Y.; Truhlar, D. G. *Organometallics* **2011**, *30*, 4196.
- (74) Fernández, I.; Lugan, N.; Lavigne, G. *Organometallics* **2012**, *31*, 1155.
- (75) Ulman, M.; Grubbs, R. H. *J. Org. Chem.* **1999**, *64*, 7202.
- (76) Hong, S. H.; Chlenov, A.; Day, M. W.; Grubbs, R. H. *Angew. Chem. Int. Ed.* **2007**, *46*, 5148.
- (77) Poater, A.; Cavallo, L. *J. Mol. Catal. A: Chem.* **2010**, *324*, 75.
- (78) Trnka, T. M.; Morgan, J. P.; Sanford, M. S.; Wilhelm, T. E.; Scholl, M.; Choi, T.-L.; Ding, S.; Day, M. W.; Grubbs, R. H. *J. Am. Chem. Soc.* **2003**, *125*, 2546.
- (79) Dinger, M. B.; Mol, Johannes C. *Eur. J. Inorg. Chem.* **2003**, *2003*, 2827.
- (80) Dinger, M. B.; Mol, J. C. *Organometallics* **2003**, *22*, 1089.
- (81) Banti, D.; Mol, J. C. *J. Organomet. Chem.* **2004**, *689*, 3113.
- (82) Macnaughtan, M. L.; Johnson, M. J. A.; Kampf, J. W. *J. Am. Chem. Soc.* **2007**, *129*, 7708.
- (83) Macnaughtan, M. L.; Gary, J. B.; Gerlach, D. L.; Johnson, M. J. A.; Kampf, J. W. *Organometallics* **2009**, *28*, 2880.
- (84) White, D. E.; Stewart, I. C.; Grubbs, R. H.; Stoltz, B. M. *J. Am. Chem. Soc.* **2007**, *130*, 810.
- (85) Gatti, M.; Drinkel, E.; Wu, L.; Pusterla, I.; Gaggia, F.; Dorta, R. *J. Am. Chem. Soc.* **2010**, *132*, 15179.
- (86) Yu, M.; Ibrahim, I.; Hasegawa, M.; Schrock, R. R.; Hoveyda, A. H. *J. Am. Chem. Soc.* **2012**, *134*, 2788.
- (87) Galan, B. R.; Gembicky, M.; Dominiak, P. M.; Keister, J. B.; Diver, S. T. *J. Am. Chem. Soc.* **2005**, *127*, 15702.
- (88) Galan, B. R.; Kalbarczyk, K. P.; Szczepankiewicz, S.; Keister, J. B.; Diver, S. T. *Org. Lett.* **2007**, *9*, 1203.
- (89) Stewart, I. C.; Keitz, B. K.; Kuhn, K. M.; Thomas, R. M.; Grubbs, R. H. *J. Am. Chem. Soc.* **2010**, *132*, 8534.

- (90) Pandian, S.; Hillier, I. H.; Vincent, M. A.; Burton, N. A.; Ashworth, I. W.; Nelson, D. J.; Percy, J. M.; Rinaudo, G. *Chem. Phys. Lett.* **2009**, *476*, 37.
- (91) Thomas, R. M.; Keitz, B. K.; Champagne, T. M.; Grubbs, R. H. *J. Am. Chem. Soc.* **2011**, *133*, 7490.
- (92) Deiters, A.; Martin, S. F. *Chem. Rev.* **2004**, *104*, 2199.
- (93) McReynolds, M. D.; Dougherty, J. M.; Hanson, P. R. *Chem. Rev.* **2004**, *104*, 2239.
- (94) Fürstner, A. *Chem. Commun.* **2011**, *47*, 6505
- (95) Prunet, J. *Eur. J. Org. Chem.* **2011**, *2011*, 3634.
- (96) Nelson, D. J.; Ashworth, I. W.; Hillier, I. H.; Kyne, S. H.; Pandian, S.; Parkinson, J. A.; Percy, J. M.; Rinaudo, G.; Vincent, M. A. *Chem. Eur. J.* **2011**, *17*, 13087
- (97) Nelson, D. J.; Carboni, D.; Ashworth, I. W.; Percy, J. M. *J. Org. Chem.* **2011**, *76*, 8386.
- (98) Ruzicka, L. *Chem. Ind. (London)* **1935**, *54*, 2.
- (99) Wagener, K. B.; Boncella, J. M.; Nel, J. G. *Macromolecules* **1991**, *24*, 2649.
- (100) Ashworth, I. W.; Miles, J. A. L.; Nelson, D. J.; Percy, J. M.; Singh, K. *Tetrahedron* **2009**, *65*, 9637.
- (101) Hudlicky, T.; Wernerova, M. *Synlett* **2010**, 2701.
- (102) Kirby, A. J. *Adv. Phys. Org. Chem.* **1980**, *17*, 183.
- (103) Galli, C.; Mandolini, L. *Eur. J. Org. Chem.* **2000**, *2000*, 3117.
- (104) Ercolani, G.; Mandolini, L.; Mencarelli, P.; Roelens, S. *J. Am. Chem. Soc.* **1993**, *115*, 3901.
- (105) Forbes, M. D. E.; Patton, J. T.; Myers, T. L.; Maynard, H. D.; Smith, D. W.; Schulz, G. R.; Wagener, K. B. *J. Am. Chem. Soc.* **1992**, *114*, 10978.
- (106) Page, M. I.; Jencks, W. P. *Proc. Natl. Acad. Sci. USA* **1971**, *68*, 1678.
- (107) Casadei, M. A.; Galli, C.; Mandolini, L. *J. Am. Chem. Soc.* **1984**, *106*, 1051.
- (108) Mitchell, L.; Parkinson, J. A.; Percy, J. M.; Singh, K. *J. Org. Chem.* **2008**, *73*, 2389.
- (109) Nicola, T.; Brenner, M.; Donsbach, K.; Kreye, P. *Org. Proc. Res. Dev.* **2005**, *9*, 513.
- (110) Shu, C.; Zeng, X.; Hao, M.-H.; Wei, X.; Yee, N. K.; Busacca, C. A.; Han, Z.; Farina, V.; Senanayake, C. H. *Org. Lett.* **2008**, *10*, 1303.
- (111) Farina, V.; Shu, C.; Zeng, X.; Wei, X.; Han, Z.; Yee, N. K.; Senanayake, C. H. *Org. Process Res. Dev.* **2009**, *13*, 250.
- (112) Skinner, H. A.; Pilcher, G. *Quat. Rev. Chem. Soc.* **1963**, *17*, 264.
- (113) Gradillas, A.; Castells, J. P. *Angew. Chem. Int. Ed.* **2006**, *45*, 6086.
- (114) Fu, G. C.; Nguyen, S. T.; Grubbs, R. H. *J. Am. Chem. Soc.* **1993**, *115*, 9856.
- (115) Nguyen, S. T.; Grubbs, R. H.; Ziller, J. W. *J. Am. Chem. Soc.* **1993**, *115*, 9858.
- (116) Kirkland, T. A.; Grubbs, R. H. *J. Org. Chem.* **1997**, *62*, 7310.
- (117) Vo Thanh, G.; Loupy, A. *Tetrahedron Lett.* **2003**, *44*, 9091.
- (118) Meylemans, H. A.; Quintana, R. L.; Goldsmith, B. R.; Harvey, B. G. *ChemSusChem* **2011**, *4*, 465.
- (119) Lloyd-Jones, G. C.; Purser, S. *Chem. Eur. J.* **2011**, *17*, 4724.
- (120) Hoye, T. R.; Jeon, J.; Tennakoon, M. A. *Angew. Chem. Int. Ed.* **2011**, *50*, 2141.
- (121) Fürstner, A.; Thiel, O. R.; Ackermann, L.; Schanz, H.-J.; Nolan, S. P. *J. Org. Chem.* **2000**, *65*, 2204.
- (122) Maier, M. E. *Angew. Chem. Int. Ed.* **2000**, *39*, 2073.

- (123) Michaut, A.; Rodriguez, J. *Angew. Chem. Int. Ed.* **2006**, *45*, 5740.
- (124) Hammer, K.; Undheim, K. *Tetrahedron* **1997**, *53*, 2309.
- (125) Miller, S. J.; Kim, S.-H.; Chen, Z.-R.; Grubbs, R. H. *J. Am. Chem. Soc.* **1995**, *117*, 2108.
- (126) Linderman, R. J.; Siedlecki, J.; O'Neil, S. A.; Sun, H. *J. Am. Chem. Soc.* **1997**, *119*, 6919.
- (127) Miles, J. A. L.; Mitchell, L.; Percy, J. M.; Singh, K.; Uneyama, E. *J. Org. Chem.* **2007**, *72*, 1575.
- (128) Mitchell, L., PhD Thesis, University of Leicester, 2008.
- (129) Banfi, L.; Basso, A.; Guanti, G.; Riva, R. *Tetrahedron Lett.* **2003**, *44*, 7655.
- (130) Sukkari, H. E.; Gesson, J.-P.; Renoux, B. *Tetrahedron Lett.* **1998**, *39*, 4043.
- (131) Inoue, M.; Miyazaki, K.; Uehara, H.; Maruyama, M.; Hiram, M. *Proc. Natl. Acad. Sci. USA* **2004**, *101*, 12013.
- (132) Kaliappan, K. P.; Kumar, N. *Tetrahedron Lett.* **2003**, *44*, 379.
- (133) Crimmins, M. T.; Choy, A. L. *J. Org. Chem.* **1997**, *62*, 7548.
- (134) Dalgard, J. E.; Rychnovsky, S. D. *Org. Lett.* **2004**, *6*, 2713.
- (135) Nevalainen, M.; Koskinen, A. M. P. *Angew. Chem. Int. Ed.* **2001**, *40*, 4060.
- (136) Kress, J. J. *Mol. Catal. A: Chem.* **1995**, *102*, 7.
- (137) Sutthasupa, S.; Shiotsuki, M.; Sanda, F. *Polym J* **2010**, *42*, 905.
- (138) Ulman, M.; Grubbs, R. H. *Organometallics* **1998**, *17*, 2484.
- (139) Hoye, T. R.; Zhao, H. *Org. Lett.* **1999**, *1*, 1123.
- (140) Hoveyda, A. H.; Lombardi, P. J.; O'Brien, R. V.; Zhugralin, A. R. *J. Am. Chem. Soc.* **2009**, *131*, 8378.
- (141) Courchay, F. C.; Baughman, T. W.; Wagener, K. B. *J. Organomet. Chem.* **2006**, *691*, 585.
- (142) Schmidt, B.; Nave, S. *Chem. Commun.* **2006**, 2489.
- (143) Lin, Y. A.; Davis, B. G. *Beilstein J. Org. Chem.* **2010**, *6*, 1219.
- (144) BouzBouz, S.; Cossy, J. *Org. Lett.* **2001**, *3*, 1451.
- (145) Quinn, K. J.; Isaacs, A. K.; Arvary, R. A. *Org. Lett.* **2004**, *6*, 4143.
- (146) Conrad, J. C.; Eelman, M. D.; Silva, J. A. D.; Monfette, S.; Parnas, H. H.; Snelgrove, J. L.; Fogg, D. E. *J. Am. Chem. Soc.* **2007**, *129*, 1024.
- (147) Monfette, S.; Blacquiere, J. M.; Fogg, D. E. *Organometallics* **2011**, *30*, 36.
- (148) Guo, X.; Basu, K.; Cabral, J. A.; Paquette, L. A. *Org. Lett.* **2003**, *5*, 789.
- (149) Basu, K.; Cabral, J. A.; Paquette, L. A. *Tetrahedron Lett.* **2002**, *43*, 5453.
- (150) Crowe, W. E.; Goldberg, D. R. *J. Am. Chem. Soc.* **1995**, *117*, 5162.
- (151) Roe, S. J.; Legeay, J.-C.; Robbins, D.; Aggarwal, P.; Stockman, R. A. *Chem. Commun.* **2009**, 4399.
- (152) Collins, S. K.; El-Azizi, Y. *Pure Appl. Chem.* **2006**, *78*, 783.
- (153) Clive, D. L. J.; Wickens, P. L.; Sgarbi, P. W. M. *J. Org. Chem.* **1996**, *61*, 7426.
- (154) Warwel, S.; Katker, H.; Rauenbusch, C. *Angew. Chem.* **1987**, *99*, 714.
- (155) Warwel, S.; Katker, H. *Synthesis* **1987**, *10*, 935.
- (156) Vougioukalakis, G. C.; Grubbs, R. H. *Chem. Rev.* **2009**, *110*, 1746.
- (157) Kuhn, K. M.; Bourg, J.-B.; Chung, C. K.; Virgil, S. C.; Grubbs, R. H. *J. Am. Chem. Soc.* **2009**, *131*, 5313.
- (158) Blacquiere, J. M.; Jurca, T.; Weiss, J.; Fogg, D. E. *Adv. Synth. Catal.* **2008**, *350*, 2849.

- (159) Galan, B. R.; Giessert, A. J.; Keister, J. B.; Diver, S. T. *J. Am. Chem. Soc.* **2005**, *127*, 5762.
- (160) Ding, F.; Yu, B.; Monsaert, S.; Sun, Y.-g.; Gao, E.; Dragutan, I.; Dragutan, V.; Verpoort, F. *Spectrochim. Acta, Part A* **2010**, *77*, 170.
- (161) Adlhart, C.; Volland, Martin A. O.; Hofmann, P.; Chen, P. *Helv. Chim. Acta* **2000**, *83*, 3306.
- (162) Adlhart, C.; Chen, P. *Helv. Chim. Acta* **2000**, *83*, 2192.
- (163) Adlhart, C.; Hinderling, C.; Baumann, H.; Chen, P. *J. Am. Chem. Soc.* **2000**, *122*, 8204.
- (164) Wang, H.; Metzger, J. O. *Organometallics* **2008**, *27*, 2761.
- (165) Wang, H.-Y.; Yim, W.-L.; Kluner, T.; Metzger, J. O. *Chem. Eur. J.* **2009**, *15*, 10948.
- (166) Adjiman, C. S.; Clarke, A. J.; Cooper, G.; Taylor, P. C. *Chem. Commun.* **2008**, 2806.
- (167) Topspin 2.1 ed.; Brüker: Billerica, MA, 2007.
- (168) Bain, G., Personal Communication: Karl-Fischer titrometry of dried and undried deuterated solvents.
- (169) Lee, L.-s.; Ou, H.-j.; Hsu, H.-l. *Fluid Phase Equilib.* **2005**, *231*, 221.
- (170) Henderson, R. K.; Jimenez-Gonzalez, C.; Constable, D. J. C.; Alston, S. R.; Inglis, G. G. A.; Fisher, G.; Sherwood, J.; Binks, S. P.; Curzons, A. D. *Green Chem.* **2011**, *13*, 854.
- (171) Mandolini, L. *Adv. Phys. Org. Chem.* **1986**, *22*, 1.
- (172) Schmidt, B.; Nave, S. *Adv. Synth. Catal.* **2007**, *349*, 215.
- (173) Wang, H.-Y.; Yim, W.-L.; Guo, Y.-L.; Metzger, J. O. *Organometallics* **2012**, *31*, 1625
- (174) Kozuch, S.; Shaik, S. *Acc. Chem. Res.* **2011**, *44*, 101.
- (175) Cramer, C. J.; Truhlar, D. G. *Acc. Chem. Res.* **2008**, *41*, 760.
- (176) Dias, E. L.; Nguyen, S. T.; Grubbs, R. H. *J. Am. Chem. Soc.* **1997**, *119*, 3887.
- (177) Beesley, R. M.; Ingold, C. K.; Thorpe, J. F. *J. Chem. Soc., Trans.* **1915**, *107*, 1080.
- (178) Ingold, C. K.; Sako, S.; Thorpe, J. F. *J. Chem. Soc., Trans.* **1922**, *121*, 1177.
- (179) Jung, M. E.; Piizzi, G. *Chem. Rev.* **2005**, *105*, 1735.
- (180) Jung, M. E.; Gervay, J. *J. Am. Chem. Soc.* **1991**, *113*, 224.
- (181) Lane, D. R.; Beavers, C. M.; Olmstead, M. M.; Schore, N. E. *Organometallics* **2009**, *28*, 6789.
- (182) Spartan '10 1.1.0 ed.; Wavefunction: 2010.
- (183) Hillier, I. H.; Vincent, M. A.; Percy, J. M., Personal Communication: DFT calculations on ruthenium metathesis.
- (184) Brzezinska, K.; Wolfe, P. S.; Watson, M. D.; Wagener, K. B. *Macromol. Chem. Phys.* **1996**, *197*, 2065.
- (185) Wagener, K. B.; Brzezinska, K.; Anderson, J. D.; Younkin, T. R.; Steppe, K.; DeBoer, W. *Macromolecules* **1997**, *30*, 7363.
- (186) Tallarico, J. A.; Bonitatebus, P. J.; Snapper, M. L. *J. Am. Chem. Soc.* **1997**, *119*, 7157.
- (187) Ashworth, I. W.; Carboni, D.; Hillier, I. H.; Nelson, D. J.; Percy, J. M.; Rinaudo, G.; Vincent, M. A. *Chem. Commun.* **2010**, *46*, 7145.
- (188) Monfette, S.; Fogg, D. E. *Chem. Rev.* **2009**, *109*, 3783.
- (189) Lehman, S. E.; Schwendeman, J. E.; O'Donnell, P. M.; Wagener, K. B. *Inorg. Chim. Acta* **2003**, *345*, 190.
- (190) Vorfalt, T.; Wannowius, K. J.; Thiel, V.; Plenio, H. *Chem. Eur. J.* **2010**, *16*, 12312.

- (191) Ashworth, I. W.; Hillier, I. H.; Nelson, D. J.; Percy, J. M.; Vincent, M. A. *Chem. Commun.* **2011**, 47, 5428.
- (192) Dekker, F. H. M.; Spronk, R.; Mol, J. C. *Fluid Phase Equilib.* **1993**, 84, 321.
- (193) Zahnley, T.; Macey, R.; Oster, G. In *Berkeley Madonna*; 8.3.18 ed.; University of California at Berkeley: Berkeley, California, 2010.
- (194) In *Micromath Scientist*; 3.0 ed.; Micromath: St. Louis, Missouri, 2011.
- (195) Kamlet, M. J.; Abboud, J. L. M.; Taft, R. W. In *Progress in Physical Organic Chemistry*; John Wiley & Sons, Inc.: 2007, p 485.
- (196) Hildebrand, J. H. *J. Soc. Chem. Ind.* **1936**, 55, 665.
- (197) Miao, X.; Fischmeister, C.; Bruneau, C.; Dixneuf, P. H. *ChemSusChem* **2008**, 1, 813.
- (198) Wilson, G.; Porter, K.; Weissman, H.; White, S.; Sottos, N.; Moore, J. *Adv. Synth. Catal.* **2009**, 351, 1817.
- (199) Nelson, D. J.; Ashworth, I. W.; Hillier, I. H.; Kyne, S. H.; Pandian, S.; Parkinson, J. A.; Percy, J. M.; Rinaudo, G.; Vincent, M. A. *Chem. Eur. J.* **2011**, 17, 13087
- (200) Bieniek, M.; Michrowska, A.; Usanov, D. L.; Grela, K. *Chem. Eur. J.* **2008**, 14, 806.
- (201) Jafarpour, L.; Schanz, H.-J.; Stevens, E. D.; Nolan, S. P. *Organometallics* **1999**, 18, 5416.
- (202) Clavier, H.; Nolan, Steven P. *Chem. Eur. J.* **2007**, 13, 8029.
- (203) Dinger, M. B.; Mol, J. C. *Adv. Synth. Catal.* **2002**, 344, 671.
- (204) Cordier, P.; Aubert, C.; Malacria, M.; Lacôte, E.; Gandon, V. *Angew. Chem. Int. Ed.* **2009**, 48, 8757.
- (205) Mammen, M.; Shakhnovich, E. I.; Whitesides, G. M. *J. Org. Chem.* **1998**, 63, 3168.
- (206) Solans-Monfort, X.; Pleixats, R.; Sodupe, M. *Chem. Eur. J.* **2010**, 16, 7331.
- (207) Ashworth, I. W., Personal Communication: Rate law derivations for the initiation of the Grubbs-Hoveyda pre-catalyst.
- (208) Atkins, P.; de Paula, J. *Atkins' Physical Chemistry*; W. H. Freeman and Company: New York, 2006.
- (209) Smallwood, I. M. *Handbook of organic solvent properties*; Arnold: London, 1996.
- (210) O'Toole, T. R.; Younathan, J. N.; Sullivan, B. P.; Meyer, T. J. *Inorganic Chemistry* **1989**, 28, 3923.
- (211) Menard, D.; Chabanel, M. *J. Phys. Chem. A* **1975**, 79.
- (212) Baur, M. E.; Horsma, D. A.; Knobler, C. M.; Perez, P. *J. Phys. Chem. A* **1969**, 73.
- (213) Borovikov, J. J. *Zh. Obshch. Khim.* **1969**, 39.
- (214) Abboud, J. L. M.; Notari, R. *Pure Appl. Chem.* **1999**, 71, 645.
- (215) Hunter, C. A.; Sanders, J. K. M. *J. Am. Chem. Soc.* **1990**, 112, 5525.
- (216) Díez-González, S.; Marion, N.; Nolan, S. P. *Chem. Rev.* **2009**, 109, 3612.
- (217) Keitz, B. K.; Endo, K.; Herbert, M. B.; Grubbs, R. H. *J. Am. Chem. Soc.* **2011**, 133, 9686.
- (218) Thomas, R. M.; Fedorov, A.; Keitz, B. K.; Grubbs, R. H. *Organometallics* **2011**, 30, 6713.
- (219) Endo, K.; Grubbs, R. H. *J. Am. Chem. Soc.* **2011**, 133, 8525.
- (220) Teo, P.; Grubbs, R. H. *Organometallics* **2010**, 22, 6045.
- (221) Clavier, H.; Nolan, S. P. *Chem. Commun.* **2010**, 46.
- (222) Tolman, C. A. *Chem. Rev.* **1977**, 77, 313.

- (223) Poater, A.; Cosenza, B.; Correa, A.; Giudice, S.; Ragone, F.; Scarano, V.; Cavallo, L. *Eur. J. Inorg. Chem.* **2009**, 2009, 1759.
- (224) Dorta, R.; Stevens, E. D.; Scott, N. M.; Costabile, C.; Cavallo, L.; Hoff, C. D.; Nolan, S. P. *J. Am. Chem. Soc.* **2005**, 127, 2485.
- (225) Gusev, D. G. *Organometallics* **2009**, 28, 6458.
- (226) Mathew, J.; Suresh, C. H. *Inorg. Chem.* **2010**, 49, 4665.
- (227) Samojłowicz, C.; Bieniek, M.; Zarecki, A.; Kadyrov, R.; Grela, K. *Chem. Commun.* **2008**, 6282.
- (228) Samojłowicz, C.; Bieniek, M.; Pazio, A.; Makal, A.; Woźniak, K.; Poater, A.; Cavallo, L.; Wójcik, J.; Zdanowski, K.; Grela, K. *Chem. Eur. J.* **2011**, 17, 12981.
- (229) Katritzky, A. R.; Fara, D. C.; Yang, H.; Tamm, K.; Tamm, T.; Karelson, M. *Chem. Rev.* **2004**, 104, 175.
- (230) Reichardt, C. *Chem. Rev.* **1994**, 94, 2319.
- (231) Johnson, B. P.; Gabrielsen, B.; Matulenko, M.; Dorsey, J. G.; Reichardt, C. *Anal. Lett.* **1986**, 19, 939.
- (232) Skrzypczak, A.; Neta, P. *Int. J. Chem. Kinet.* **2004**, 36, 253.
- (233) Gumbel, G.; Elias, H. *Inorg. Chim. Acta* **2003**, 342, 97.
- (234) Schmidt, B. *Eur. J. Org. Chem.* **2004**, 2004, 1865.
- (235) Schmidt, B. *J. Mol. Catal. A: Chem.* **2006**, 254, 53.
- (236) Bourgeois, D.; Pancrazi, A.; Nolan, S. P.; Prunet, J. *J. Organomet. Chem.* **2002**, 643-644, 247.
- (237) Sutton, A. E.; Seigal, B. A.; Finnegan, D. F.; Snapper, M. L. *J. Am. Chem. Soc.* **2002**, 124, 13390.
- (238) De Bo, G.; Markó, I. E. *Eur. J. Org. Chem.* **2011**, 2011, 1859.
- (239) McGrath, D. V.; Grubbs, R. H. *Organometallics* **1994**, 13, 224.
- (240) Hanessian, S.; Giroux, S.; Larsson, A. *Org. Lett.* **2006**, 8, 5481.
- (241) Schmidt, B. *Eur. J. Org. Chem.* **2003**, 2003, 816.
- (242) Schmidt, B. *J. Org. Chem.* **2004**, 69, 7672.
- (243) Arisawa, M.; Terada, Y.; Nakagawa, M.; Nishida, A. *Angew. Chem. Int. Ed.* **2002**, 41, 4732.
- (244) Arisawa, M.; Terada, Y.; Takahashi, K.; Nakagawa, M.; Nishida, A. *J. Org. Chem.* **2006**, 71, 4255.
- (245) Courchay, F. C.; Sworen, J. C.; Ghiviriga, I.; Abboud, K. A.; Wagener, K. B. *Organometallics* **2006**, 25, 6074.
- (246) Paquette, L. A.; Efremov, I. *J. Am. Chem. Soc.* **2001**, 123, 4492.
- (247) Kotha, S.; Mandal, K. *Tetrahedron Lett.* **2004**, 45, 1391.
- (248) Janse van Rensburg, W.; Steynberg, P. J.; Meyer, W. H.; Kirk, M. M.; Forman, G. S. *J. Am. Chem. Soc.* **2004**, 126, 14332.
- (249) Moers, F. G.; Langhout, J. P. *Recl. Trav. Chim. Pays-Bas* **1972**, 91, 591.
- (250) Esteruelas, M. A.; Werner, H. *J. Organomet. Chem.* **1986**, 303, 221.
- (251) Beach, N. J.; Dharmasena, U. L.; Drouin, S. D.; Fogg, D. E. *Adv. Synth. Catal.* **2008**, 350, 773.
- (252) Yi, C. S.; Lee, D. W.; Chen, Y. *Organometallics* **1999**, 18, 2043.
- (253) Lee, H. M.; Smith, D. C.; He, Z.; Stevens, E. D.; Yi, C. S.; Nolan, S. P. *Organometallics* **2001**, 20, 794.
- (254) Yi, C. S.; Lee, D. W. *Organometallics* **1999**, 18, 5152.

- (255) Gao, R.; Yi, C. S. *ACS Catalysis* **2011**, *1*, 544.
- (256) Yi, C. S.; He, Z.; Lee, D. W.; Rheingold, A. L.; Lam, K.-C. *Organometallics* **2000**, *19*, 2036.
- (257) Yi, C. S. *J. Organomet. Chem.* **2011**, *696*, 76.
- (258) Hong, S. H.; Sanders, D. P.; Lee, C. W.; Grubbs, R. H. *J. Am. Chem. Soc.* **2005**, *127*, 17160.
- (259) Mori, K. *Tetrahedron* **2009**, *65*, 3900.
- (260) Piacenza, M.; Hyla-Kryspin, I.; Grimme, S. *J. Comput. Chem.* **2007**, *28*, 2275.
- (261) Cavallo, L. *J. Am. Chem. Soc.* **2002**, *124*, 8965.
- (262) Yang, H.; Chung, C.-P.; Lin, Y.-C.; Liu, Y.-H. *Dalton Trans.* **2011**, *40*, 3703.
- (263) Edwards, S. D.; Lewis, T.; Taylor, R. J. K. *Tetrahedron Lett.* **1999**, *40*, 4267.
- (264) Meyer, W. H.; McConnell, A. E.; Forman, G. S.; Dwyer, C. L.; Kirk, M. M.; Ngidi, E. L.; Blignaut, A.; Saku, D.; Slawin, A. M. Z. *Inorg. Chim. Acta* **2006**, *359*, 2910.
- (265) Gimeno, N.; Formentin, P.; Steinke, J. H. G.; Vilar, R. *Eur. J. Org. Chem.* **2007**, *2007*, 918.
- (266) Nori-Shargh, D.; Farahani, N. S. *Int. J. Chem. Kinet.* **2004**, *36*, 472.
- (267) Moiseev, D. V.; Patrick, B. O.; James, B. R.; Hu, T. Q. *Inorg. Chim. Acta* **2010**, *363*, 3569.
- (268) Mayr, H.; Ofial, A. R. *J. Phys. Org. Chem.* **2008**, *21*, 584.
- (269) Kempf, B.; Mayr, H. *Chem. Eur. J.* **2005**, *11*, 917.
- (270) Amir-Ebrahimi, V.; G. Hamilton, J.; Nelson, J.; J. Rooney, J.; M. Thompson, J.; J. Beaumont, A.; Rooney, A. D.; J. Harding, C. *Chem. Commun.* **1999**, 1621.
- (271) Amir-Ebrahimi, V.; Hamilton, J. G.; Nelson, J.; Rooney, J. J.; Rooney, A. D.; Harding, C. J. *J. Organomet. Chem.* **2000**, *606*, 84.
- (272) Herbert, M. B.; Lan, Y.; Keitz, B. K.; Liu, P.; Endo, K.; Day, M. W.; Houk, K. N.; Grubbs, R. H. *J. Am. Chem. Soc.* **2012**, *134*, 7861.
- (273) Ritter, T.; Day, M. W.; Grubbs, R. H. *J. Am. Chem. Soc.* **2006**, *128*, 11768.